Dominik Tabak

Synteza wybranych pochodnych kwasu 8-hydroksy-2-metylochinolino-7-karboksylowego oraz jego analogów jako potencjalnych inhibitorów integrazy wirusa HIV oraz herbicydów

Praca doktorska wykonana
w Zakładzie Chemii Organicznej
Instytutu Chemii
Uniwersytetu Śląskiego

Promotor: prof. dr hab. inż. Jarosław Polański

Katowice 2013

Składam serdeczne podziękowania wszystkim
osobom, dzięki którym powstała niniejsza praca.

Spis treści

1. Cel pracy

Niniejsza praca stanowi kontynuację badań podjętych w Zakładzie Chemii Organicznej Uniwersytetu Śląskiego, dotyczących syntezy związków zawierających fragment chinolinowy jako potencjalnych inhibitorów integrazy wirusa HIV oraz potencjalnych leków przeciwnowotworowych.

Celem pracy była synteza wybranych pochodnych amidowych kwasu 8-hydroksy-2-metylochinolino-7-karboksylowego (**Rys. 1**) oraz zbadanie aktywności biologicznej uzyskanych połączeń w zakresie zdolności do hamowania integrazy wirusa HIV, właściwości przeciwnowotworowych i przeciwgrzybicznych.

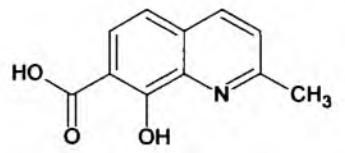

Rys. 1. Kwas 8-hydroksy-2-metylochinolino-7-karboksylowy

W zakres pracy wchodziła również próba syntezy kwasu 2-metylo-5,8-diokso-5,8-dihydrochinolino-7-karboksylowego (**Rys. 2**) oraz jego pochodnych zawierających w swojej strukturze fragment 5,8-chinolinodionowy, o znanych właściwościach przeciwnowotworowych.

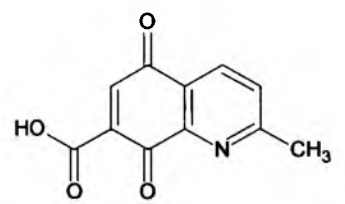

Rys. 2. Kwas 2-metylo-5,8-diokso-5,8-dihydrochinolino-7-karboksylowy

W trakcie realizacji pracy, zakres poszerzył się o wykorzystanie syntezowanych związków jako ligandów kompleksujących niektóre metale przejściowe (Ru, Re, Cu). W szczególności zainteresowałem się wykorzystaniem otrzymanych kompleksów do badań pozwalających na ustalenie struktur ligandów organicznych.

2. Forma pracy

Niniejsza praca przedstawiona została w postaci tematycznego zbioru publikacji, patentów oraz materiałów konferencyjnych P1 - P25.

Wykaz publikacji podstawowych:

[P1] Polanski J., Niedbala H., Musiol R., Podeszwa B., Tabak D., Palka A., Mencel A., Finster J., Mouscadet J. F., Le Bret M., *5-hydroxy-6-quinaldic acid as a novel molecular scaffold for HIV-1 integrase inhibitors*, Lett. Drug Des. Discov., 2006, **3**, 175-178

[P2] Niedbala H., Polanski J., Gieleciak R., Musiol R., Tabak D., Podeszwa B., Bak A., Palka A., Mouscadet J. F., Gasteiger J., Le Bret M., *Comparative molecular surface analysis (CoMSA) for virtual combinatorial library screening of styrlquinoline HIV-1 blocking agents*, Comb. Chem. High Throughput Screen, 2006, **9**, 753-770

[P3] Polanski J., Niedbala H., Musiol R., Podeszwa B., Tabak D., Palka A., Mencel A., Mouscadet J. F., Le Bret M., *Fragment based approach for the investigation of HIV-1 integrase inhibition*, Lett. Drug Des. Discov., 2007, **4**, 99-105

[P4] Podeszwa B., Niedbala H., Polanski J., Musiol R., Tabak D., Finster J., Serafin K., Milczarek M., Wietrzyk J., Boryczka S., Mol W., Jampilek J., Dohnal J., Kalinowski D. S., Richardson D. R., *Investigating the Antiproliferative Activity of Quinoline-5,8-diones and Styrylquinolinecarboxylic Acids on Tumour Cell Lines*, Bioorg. Med. Chem. Lett., 2007, **17**, 6138-6141

[P5] Malecki J. G., Kruszynski R., Tabak D., Kusz J., *The reactions between [RuHCl(CO)(PPh$_3$)$_3$ and quinoline carboxylic acids*, Polyhedron, 2007, **26** , 5120-30

[P6] Musiol R., Tabak D., Niedbala H., Podeszwa B., Jampilek J., Kralova K., Dohnal J., Finster J., Mencel A., Polanski J., *Investigating biological activity spectrum for novel quinoline analogues 2: hydroxyquinolinecarboxamides with photosynthesis inhibiting activity*, Bioorg. Med. Chem., 2008, **16**, 4490-4499

[P7] Machura B., Milek J., Kusz J., Nycz J., Tabak D., *Reactivity of oxorhenium(V) complexes towards quinoline carboxylic acids. X-ray structure of [ReOCl$_2$(hquin-7-COOH)(PPh$_3$)]·PPh$_3$, [ReOBr$_2$(hquin-7-COOH)(PPh$_3$)] and [ReOX$_2$(hmquin-7-COOH)(PPh$_3$)]. DFT and TD-DFT calculations for [ReOCl$_2$(hquin-7-COOH)(PPh$_3$)]*, Polyhedron, 2008, **27**, 1121-1130

[P8] Malecki J. G., Kusz J., Kruszynski R., Tabak D., Mazurak Z., *The reaction between [RuCl$_2$(PPh$_3$)$_3$] and hydroxyquinoline carboxylic acid*, Structural Chemistry, 2008, **19**, 257-263.

[P9] Machura B., Kusz J., Tabak D., *Synthesis, spectroscopic characterization, X-ray structure, and DFT calculations of [ReOBr$_2$(hmquin-7-COOH)(AsPh$_3$)]*, Structural Chemistry, 2009, **20**, 361-368

[P10] Musiol R., Jampilek J., Podeszwa B., Finster J., Tabak D., Dohnal J., Polanski J., *RP-HPLC determination of lipophilicity in series of quinoline derivatives*, Cent. Eur. J. Chem., 2009, **7**, 586-597

[P11] Machura B., Kusz J., Tabak D., Kruszynski R., *Synthesis, spectroscopic characterization, crystal and molecular structure of [ReOBr(hmquin-7-COOH)$_2$] and [ReOCl(hmquin-7-COOH)$_2$]·MeCN complexes. DFT and TD-DFT calculations for [ReOBr(hmquin-7-COOH)$_2$]*, Polyhedron, 2009, **28**, 493-500

[P12] Machura B., Świtlicka A., Mroziński J., Kłak J., Kruszynski R., Kusz J., Tabak D., *Synthesis, spectroscopic characterization, X-ray structure and magnetic properties of [Cu(hmquin-7-COOH)$_2$(MeOH)] complex*, Polyhedron, 2009, **28**, 3774-3780

[P13] Majerz-Maniecka K., Musiol R., Skórska-Stania A., Tabak D., Mazur P., Oleksyn B.J., Polański J. *X-ray and molecular modelling in fragment-based design of three small quinoline scaffolds for HIV integrase inhibitors*, Bioorg. Med. Chem., 2011, **19**, 1606-12

[P14] Machura B., Świtlicka A., Wolff M., Tabak D., Musioł R., Polański J., Kruszyński R., *Novel tricarbonyl rhenium complexes of 5,8-quinolinedione derivatives - synthesis, spectroscopic characterisation, X-ray structure and DFT calculations*, Journal of Organometallic Chemistry, 2011, **696**, 731-738.

[P15] Niedbała H., Musioł R., Pałka A., Podeszwa B., Mencel A., Tabak D., Polański J., Finster J., *Sposób oczyszczania amidów kwasów chinaldynokarboksylowych*, PL 374130, 2006-10-16, PL 207140, 2010-11-30

[P16] Musiol R., Jampilek J., Kralova K., Tabak D., Podeszwa B., Finster J., Polanski J., *Substituted amides of quinoline derivatives: preparation and their photosynthesis-inhibiting activity*, ECSOC-10, 2006

Wykaz publikacji uzupełniających:

[P17] Polanski J., Niedbala H., Musiol R., Tabak D., Podeszwa B., Gieleciak R., Bak A., Palka A., Magdziarz T., *Analogues of the styryquinoline and styrylquinazoline HIV-1 integrase inhibitors: Design and synthetic problems*, Acta Poloniae Pharm. Drug Res., 2004, **61**, 3-4

[P18] Jampilek J., Musiol R., Pesko M., Kralova K., Vejsova M., Carroll J., Coffey A., Finster J., Tabak D., Niedbala H., Kozik V., Polanski J., Csollei J., Dohnal J., *Ring-substituted 4-hydroxy-1H-quinolin-2-ones: Preparation and biological activity*, Molecules, 2009, **14**, 1145-1159

[P19] Machura B., Wolff M., Tabak D., Ikeda Y., Hasegawa K., *Novel trans-dioxorhenium complex with imidazo[1,2a]pyridine ligand – Synthesis, spectroscopic and electrochemical characterization, X-ray crystal structure and DFT calculations*, Polyhedron, 2012, **39**, 76-84

[P20] Machura B., Wolff M., Tabak D., Schachner J. A., Mosch-Zanetti N. C., *Oxidorhenium(V) complexes with phenolate- and carboxylate-based ligands: Structure and catalytic epoxidation*, Eur. J. Inorg. Chem, 2012, **23**, 3764-3773

[P21] Musioł R., Niedbała H., Pałka A., Podeszwa B., Finster J., Mencel A., Serafin K., Tabak D., Polański J., *Amidy heterocykliczne hamujące działanie integrazy HIV oraz ich zastosowanie*, PL 379432, 2007-10-15, PL 210315, 2012-01-31

[P22] Podeszwa B., Musioł R., Tabak D., Finster J., Polański J., Niedbała H., Pałka A., *2-oksoamidy jako inhibitory integrazy HIV, ich prekursory oraz ich zastosowanie*, PL 380818, 2008-04-14, PL 210314, 2012-01-31

[P23] Musioł R., Podeszwa B., Tabak D., Finster J., Niedbała H., Polański J., *Nowe związki o działaniu antyproliferacyjnym, ich prekursory oraz ich zastosowanie do hamowania rozwoju komórek nowotworowych*, PL 382828, 2009-01-05, PL 213476, 2013-03-29

[P24] Musiol R., Jampilek J., Kralova K., Tabak D., Finster J., Podeszwa B., Kozik V., Dohnal J., Polanski J., *Preparation and herbicidal activities of substituted amides of quinoline derivatives*, ECSOC-11, 2007

[P25] Musiol R., Jampilek J., Kralova K., Finster J., Tabak D., Niedbala H., Csollei J., Dohnal J., Polanski J., *Ring-substituted 4-hydroxy-1H-quinolin-2-ones: Preparation and their photosynthesis-inhibiting activity*, ECSOC-12, 2008

W części literaturowej krótko przedstawiłem wprowadzenie do tematyki pracy. W rozdziale 4 opisałem metody syntezy, struktury oraz aktywności badanych pochodnych, zarówno związków opisanych w publikacjach P1 - P16, jak również dotychczas nieopublikowanych.

3. Część literaturowa

Wirus ludzkiego niedoboru odporności (HIV) należy do grupy retrowirusów. Tak jak pozostałe wirusy nie może on namnażać się poza komórką gospodarza i aby powielić swój materiał genetyczny wykorzystuje enzymy oraz inne substancje obecne w zakażonych komórkach [1-3]. Strategie poszukiwania odpowiedniej chemoterapii zakażeń HIV zogniskowane są obecnie na poszukiwaniu związków hamujących wirusa poprzez blokowanie kluczowych dla jego cyklu replikacyjnego [4,5] receptorów i białek, zaangażowanych we wniknięcie wirusa do komórki oraz specyficznych enzymów, niezbędnych do jego replikacji (odwrotnej transkryptazy, integrazy i proteazy) [6].

Ze względu na mechanizm działania można wyróżnić kilka grup aktywnych związków [6,7]:

- modyfikatory receptorów CD4
- leki wiążące wirusową glikoproteinę gp 120
- antagoniści receptorów CXCR4 i CCR5
- inhibitory fuzji wirusa z komórką
- nukleozydowe inhibitory odwrotnej transkryptazy (NRTI)
- nukleotydowe inhibitory odwrotnej transkryptazy (NtRTI)
- nienukleozydowe inhibitory odwrotnej transkryptazy (NNRTI)
- inhibitory integrazy
- inhibitory transkrypcji
- inhibitory proteazy

Skuteczność terapii antywirusowej aktualnie stosowanymi lekami, pomimo ich znacznej aktywności przeciwko HIV okazała się niewystarczająca. Dodatkowe komplikacje w leczeniu powodują mutacje wirusa odporne na podawane związki. Częściowym rozwiązaniem problemu okazała się terapia multilekowa HAART (Highly Active Antiretroviral Therapy), polegająca na podawaniu przynajmniej dwóch inhibitorów odwrotnej transkryptazy i jednego inhibitora proteazy [5]. Także ta terapia nie jest jednak w pełni skuteczna. Obecnie sądzi się, iż rozwiązaniem może okazać się odkrycie nowych inhibitorów integrazy wirusa HIV, enzymu nie mającego odpowiednika w ludzkim organizmie.

3.1. Budowa integrazy wirusa HIV

Integraza (IN) jest enzymem katalizującym decydujący etap replikacji HIV - wbudowanie wirusowego DNA do genomu zainfekowanej komórki. W strukturze tego białka można wyróżnić trzy domeny, niezbędne do jego pełnej aktywności: katalityczną, C - terminalną i N - terminalną [4-5,8]. Domena katalityczna, kluczowa dla procesu integracji, posiada charakterystyczną triadę aminokwasów (**Rys. 3**) [9]. Tworzą ją dwie reszty kwasu asparaginowego D64 i D116 oraz jedna kwasu glutaminowego E152 (tzw. motyw DDE) [5,10-12].

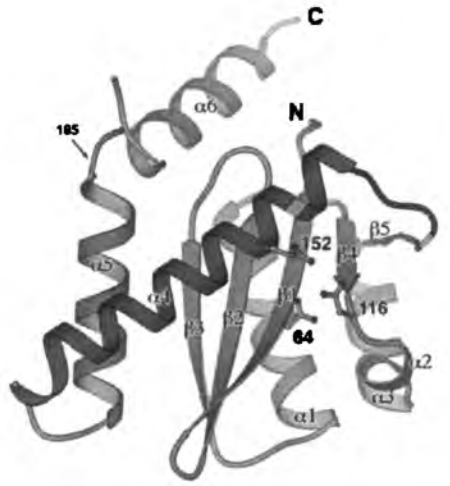

Rys. 3. Model domeny katalitycznej IN HIV [9]

Aktywność enzymatyczna integrazy ściśle uzależniona jest od obecności dwuwartościowych kationów metali. Przyjmuje się, że w warunkach fizjologicznych kompleksuje ona dwa jony Mg^{2+}. Pierwszy jon wiązany jest przez reszty D64 i D116, natomiast drugi może być kompleksowany przez D64 i E152 podczas wiązania integrazy z DNA (**Rys. 4**) [5,10,12-15].

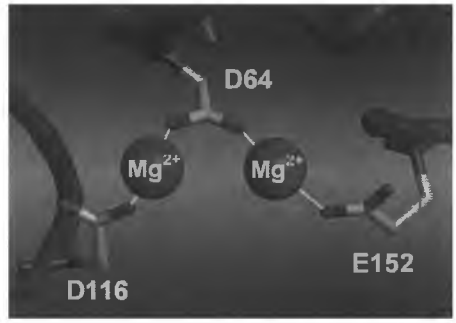

Rys. 4. Model domeny katalitycznej IN kompleksującej dwa jony Mg^{2+} [13]

Proces integracji wirusowego DNA do genomu komórki gospodarza jest złożoną reakcją i obejmuje następujące etapy [4-5,10,13]:

- 3' - processing, czyli reakcja hydrolizy, w której integraza usuwa dwa nukleotydy z każdego końca 3' wirusowego DNA i w to miejsce formuje wolne grupy 3' - OH (**Rys. 5**) [13]
- strand transfer (ST) - reakcja transestryfikacji, w której wolne grupy OH zostają użyte jako czynnik nukleofilowy do ataku na wiązanie fosfodiestrowe przeciwległych nici docelowego DNA (**Rys. 6**) [13]

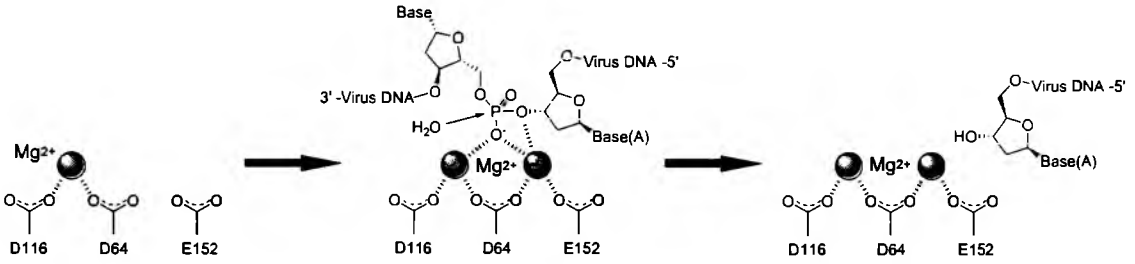

Rys. 5 Mechanizm reakcji 3' – processing [13]

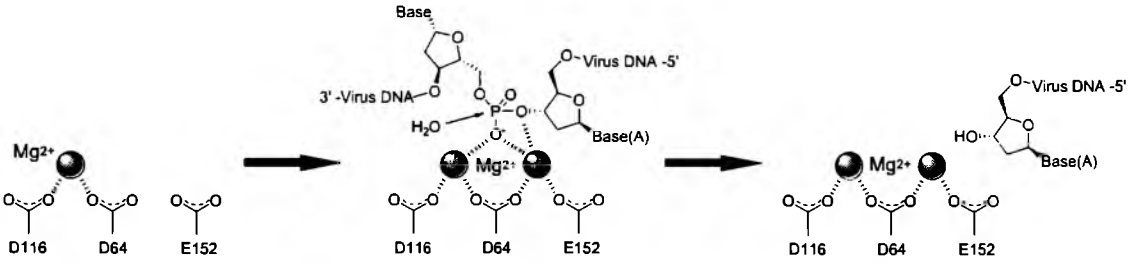

Rys. 6 Mechanizm reakcji strand transfer [13]

3.2. Inhibitory integrazy HIV

Potencjalne leki wykazujące aktywność hamującą działanie IN HIV poprzez oddziaływanie z jej domeną katalityczną należą do różnych klas związków organicznych [5,6,16-20,]. Obiecującymi inhibitorami integrazy wydają się polifenole np. kwas L-cykoriowy (**LCA**) i jego pochodne [16], czy też piranodipirydyny (PDP), np. **V-165** [6,16,21].

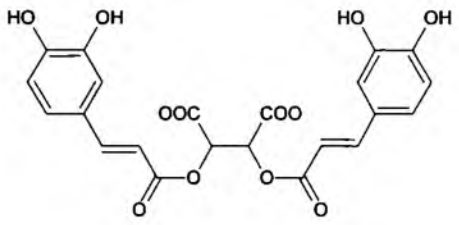

LCA

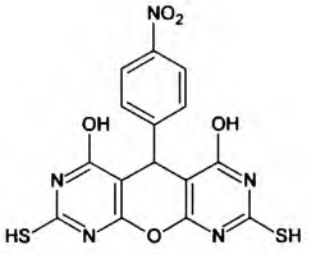

V-165

IC_{50} = 8,9 mM

Znaczącą grupą aktywnych związków są także styrylochinoliny (**SQ**) [16,22-31], których badania doprowadziły do otrzymania **FZ-41**, inhibitora skierowanego do badań przedklinicznych [5,16].

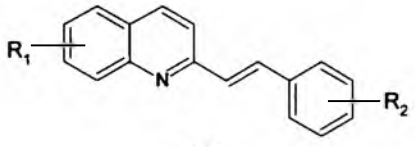

SQ

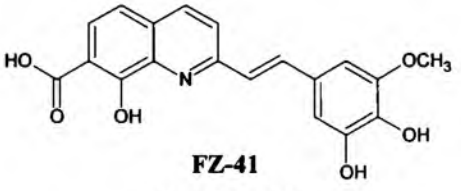

FZ-41

IC_{50} = 0,7 mM

Wysoką aktywność anty-HIV wykazały strukturalne analogi styrylochinolin - styrylochinazoliny **1**. Fragment chinolinowy zawierają także inhibitory oparte na pochodnych 8-hydroksychinoliny oraz kwasu 8-hydroksy-7-chinolinowego **2** [16].

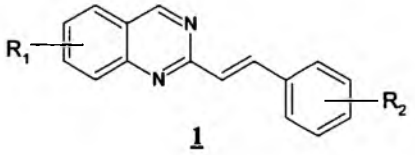

1

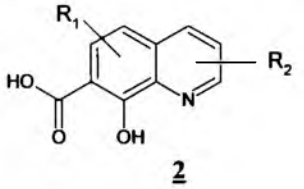

2

Wykorzystanie fragmentu chinolonowego doprowadziło z kolei do opracowania **Elvitegraviru (JTK-303)**, leku zaaprobowanego przez FDA w 2012 r. [16,20,32].

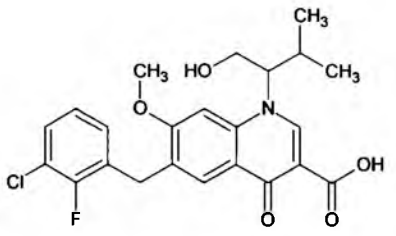

Elvitegravir (JTK-303, GS-9137)

IC_{50} = 1,7 nM

Szeroką grupę inhibitorów integrazy HIV stanowią diketokwasy (DKA) [10,15-17,33-39]. Wykazują one wysoką aktywność zarówno w badaniach in vitro, jak i w hodowlach komórkowych, a szczególne zainteresowanie badaczy zawdzięczają dzięki selektywności wobec etapu strand transfer [16-17,35]. Strukturę DKA tworzy najczęściej podstawiony fragment aromatyczny lub heteroaromatyczny połączony z fragmentem α,γ-diketokarboksylowym. Przyjmuje się, że związki tego typu najchętniej występują w formach enolowych (**Rys. 7**).

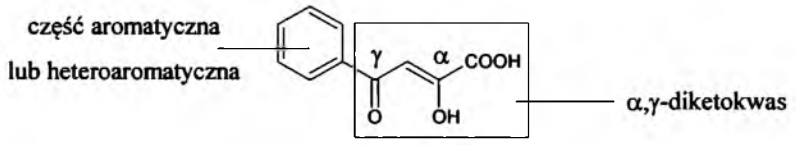

Rys. 7. Budowa diketokwasów (DKA)

Typowymi przykładami takiej budowy mogą być **L-708,906** i **L-731,988** [16], a także **MA-DKA** [40].

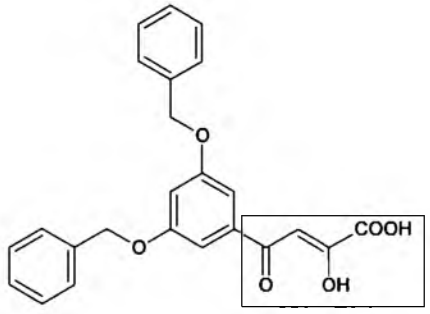

L - 708,906

IC_{50} = 100 nM

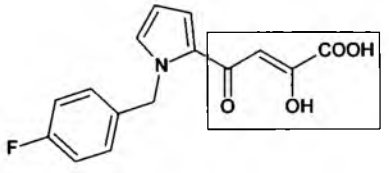

L - 731,988

IC_{50} = 50 nM

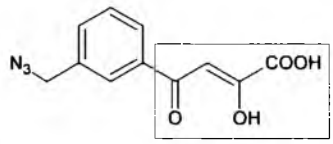

MA-DKA

Wymagania strukturalne związane z aktywnością diketokwasów nie są rygorystyczne. Badania SAR ujawniły, że grupa karboksylowa DKA może być zastąpiona przez grupy bioizosteryczne, zwłaszcza pierścienie heterocykliczne [16,41]. Wymiana grupy karboksylowej na grupę triazolową doprowadziła do opracowania **S-1360**, pierwszego inhibitora integrazy skierowanego do badań klinicznych [6,16]. Badania tego związku zostały jednak zatrzymane w II fazie badań klinicznych ze względu na niekorzystny metabolizm [16]. Izosteryczna grupa tetrazolowa jest z kolei obecna w **5-CITEP**. Poznanie struktury krystalograficznej kompleksu tego inhibitora z domeną katalityczną IN, w znacznym stopniu przyczyniło się do poznania mechanizmu działania diketokwasów oraz ich dalszego rozwoju [42].

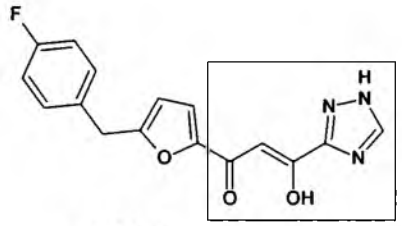

S-1360

IC_{50} = 20 nM

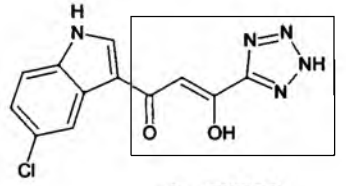

5 - CITEP

IC_{50} = 2,3 mM

Wysoce aktywne są również pochodne 1,6-naftyrydyny, w których cały fragment diketokwasu został wbudowany w pierścień heterocykliczny [43]. Z tej grupy wywodzą się takie inhibitory jak **L-870,810** (ze względu na toksyczność badania zatrzymano w I fazie badań klinicznych), **L-870,812** (w badaniach przedklinicznych) oraz związek **3** [6,16].

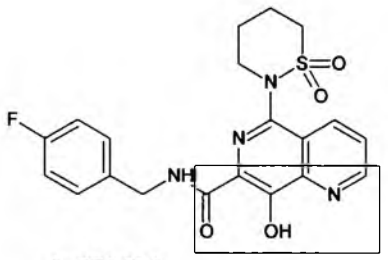

L-870,810

IC_{50} = 10 nM

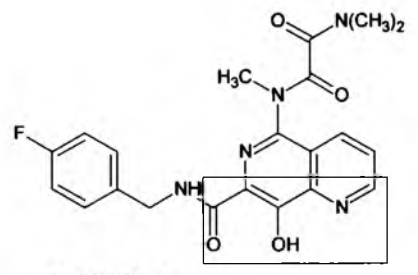

L-870,812

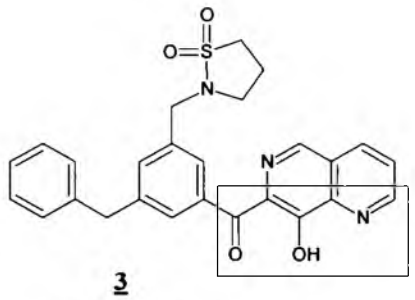

3

IC_{50} = 10 nM

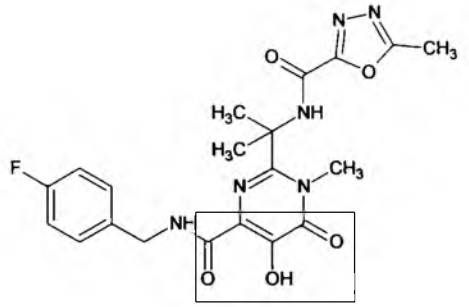

Raltegravir (MK-0518)

IC_{50} = 10 nM

Szczególnym osiągnięciem wykorzystania wysokiej aktywności fragmentu diketokwasowego była synteza pochodnej 5-hydroksypirymidynonu - **Raltegraviru (Isentres™, MK-0518)**, pierwszego inhibitora integrazy wprowadzonego do terapii anty-HIV (zatwierdzony przez FDA w 2007 r.) [44].

Mechanizm hamowania integrazy HIV przez diketokwasy polega prawdopodobnie na chelatowaniu dwóch jonów Mg^{2+}, zawartych w domenie katalitycznej (**Rys. 8a i 8b**) [4-6,10,13-14], co uniemożliwia przyłączenie wirusowego DNA do DNA gospodarza [14]. Hipotezę tą potwierdzają badania kompleksowania jonów metali przez DKA oraz badania aktywności anty-HIV otrzymanych kompleksów [10].

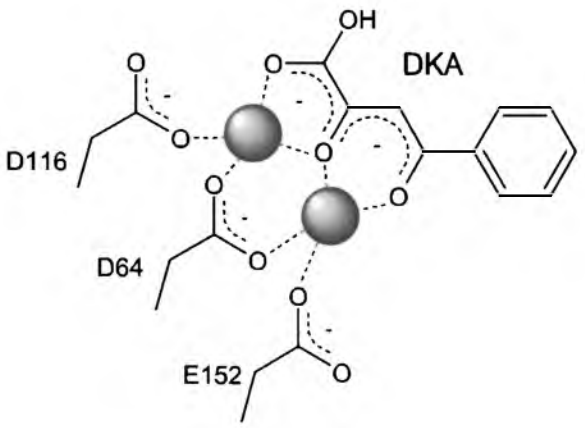

Rys. 8a. Prawdopodobna struktura kompleksu DKA z domena katalityczna integrazy [5]

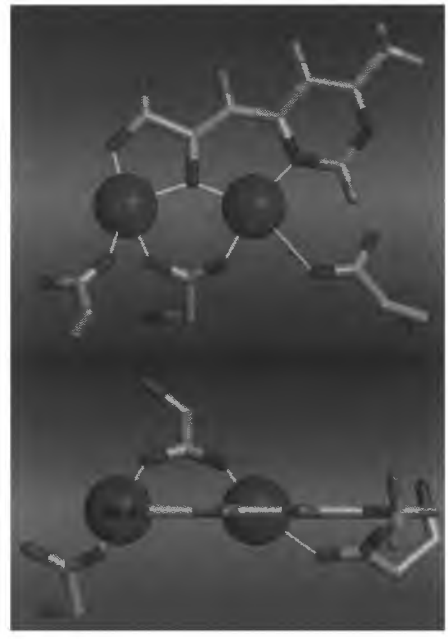

Rys. 8b. Model wiązania inhibitora w domenie katalitycznej IN [13]

Istotnym czynnikiem dla selektywności DKA wobec reakcji ST jest charakter i podstawienie fragmentu aromatycznego diketokwasu [34,36,38]. Najczęściej spotykaną grupą jest podstawnik p-fluorobenzylowy. Wysoka czułość na modyfikacje tego fragmentu wskazuje na to, że pierścień aromatyczny dostarcza dodatkowego wiązania hydrofobowego z IN [39].

Badania niedawno otrzymanych pochodnych kwasu 2-hydroksy-3-heteroaryloakrylowego (HHAA) **4** doprowadziły do określenia prawdopodobnego farmakofora [13,41]. Składa się on z domeny hydrofilowej i hydrofobowej. Domenę hydrofilową stanowi grupa karboksylowa lub jej bioizoster, zawierający heteroatom z wolną parę elektronową, za pomocą której może koordynować jony Mg^{2+}. Domenę hydrofobową tworzy natomiast podstawnik aromatyczny, którego usytuowanie przestrzenne jest niezwykle ważne, ze względu na oddziaływanie hydrofobowe z integrazą (**Rys.9**) [13,41].

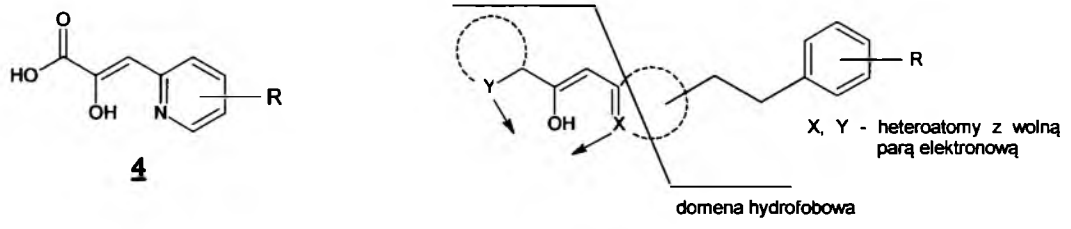

Rys. 9. Model farmakofora diketokwasowego [41]

4. Badania własne

Fragment chinolinowy jest obecny w wielu biologicznie aktywnych związkach. Zarówno sama 8-hydroksychinolina, jak i jej pochodne wykazują szerokie spektrum działania [45]. Badania tych związków ujawniły ich właściwości przeciwgrzybiczne [46-51], antybakteryjne, przeciwpierwotniakowe [52], przeciwgruźlicze [53-54], a także przeciwnowotworowe [55-58] i herbicydowe [46-47,58]. Znane są także chinolinowe inhibitory integrazy np. **5** [59-60].

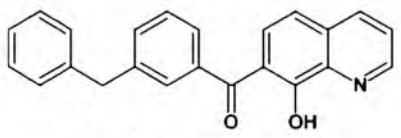

5

IC_{50} = 0,37 mM

Kwas 8-hydroksy-2-metylochinolino-7-karboksylowy **6** może stanowić dobry punkt wyjścia do projektowania nowych inhibitorów integrazy HIV. Pochodne tego kwasu zawierają bowiem fragment α,γ-diketokwasu, w którym grupa karboksylowa jest maskowana układem heterocyklicznym chinoliny (**Rys. 10**).

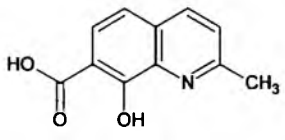

6

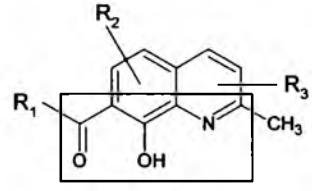

Rys. 10. Fragment diketokwasowy pochodnych kwasu 8-hydroksy-7-chinaldynokarboksylowego

4.1. Synteza amidowych pochodnych kwasu 8-hydroksychinaldyno-7-karboksylowego

Kwas 8-hydroksychinaldyno-7-karboksylowy **6** , stanowiący substrat do dalszych syntez otrzymano w reakcji Kolbego - Schmidta jak opisano w [22]. Synteza ta przebiega w dwóch etapach (**Schemat 1**). Pierwszy etap polegający na utworzeniu soli potasowej 8-hydroksychinaldyny prowadzono w suchym toluenie. W drugim etapie przez roztwór wygenerowanej soli w suchym DMF przepuszczano dwutlenek węgla.

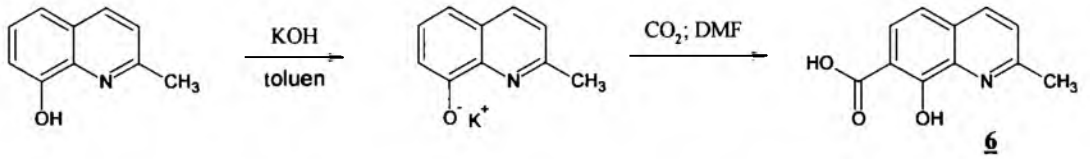

Schemat 1. Synteza kwasu 8-hydroksychinaldyno-7-karboksylowego

Syntezę kwasu 8-hydroksy-2-metylo-5-nitrochinolino-7-karboksylowego **7** (**Schemat 2**) przeprowadzono według standardowej procedury nitrowania mieszaniną stężonych kwasów H_2SO_4 i HNO_3 w temp. 0 – 5°C.

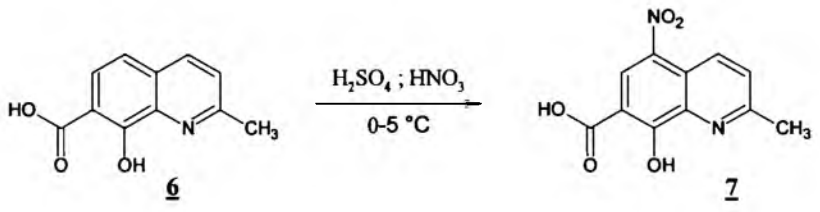

Schemat 2. Synteza kwasu 8-hydroksy-2-metylo-5-nitrochinolino-7-karboksylowego

Pochodne amidowe kwasów **6** i **7** otrzymano w reakcji z odpowiednimi aminami (**Schemat 3**). Syntezy prowadzono w bezwodnym dichlorometanie, w obecności 1,3-dicykloheksylokarbodiimidu (**DCC**) lub 1-etylo-3-(3'-dimetyloaminopropylo)-karbodiimidu (**EDCI**, EDAC), jako odczynników katalizujących bezpośrednią reakcję amin z kwasami karboksylowymi [15].

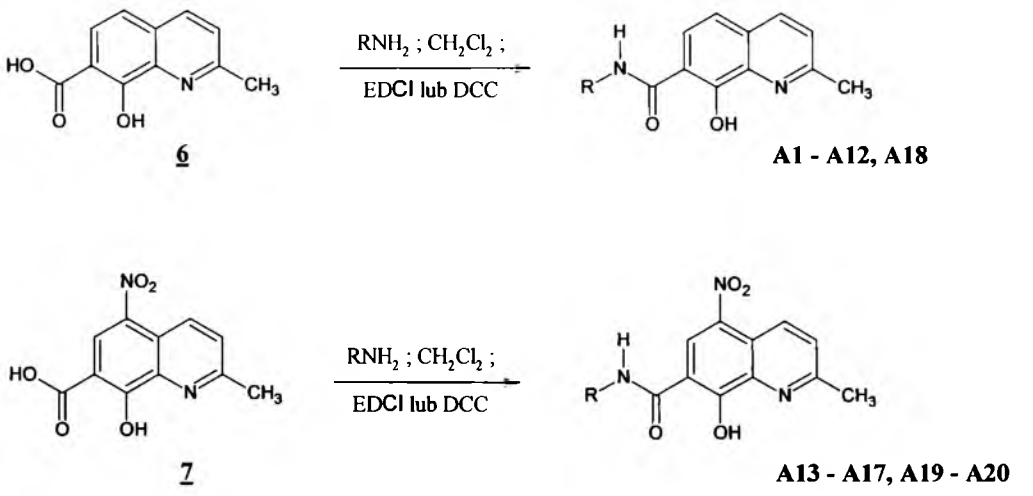

Schemat 3. Synteza amidowych pochodnych kwasu 8-hydroksychinaldyno-7-karboksylowego

Wzory otrzymanych pochodnych, ich temperatury topnienia oraz wydajności przeprowadzonych reakcji zebrane zostały w **Tabeli 1**.

Tabela 1. Pochodne amidowe kwasów 6 i 7

Nr	Struktura	t.topn. [°C]	Wydajność [%]	Publikacja
6	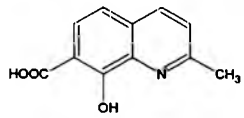	229 - 230	39,0	P1
7	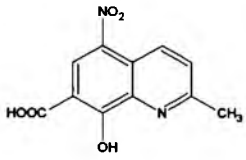	>260	58,2	P1

A1	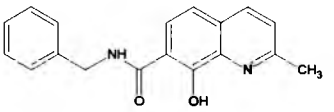	215 - 218	86,4	P6, P10
A2	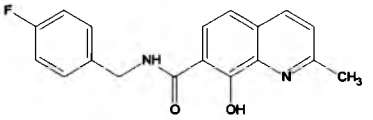	190 - 196	26,3	P3, P6, P10
A3	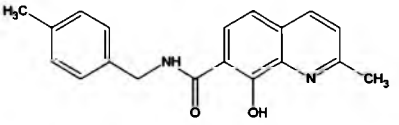	192 - 200 (rozkład)	36,4	P6, P10
A4	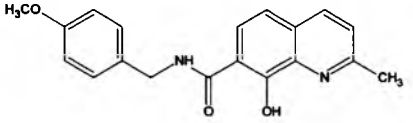	180 - 190 (rozkład)	34,6	P6, P10
A5	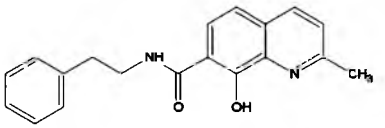	228 - 236	61,7	P6, P10
A6	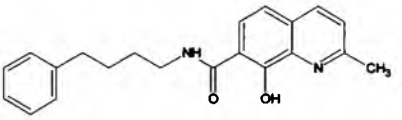	196 - 201	73,2	P6, P10
A7	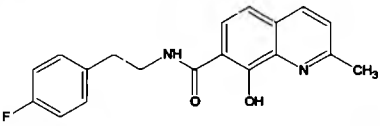	189 - 193	52,1	P10
A8	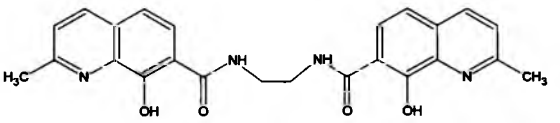	254 - 257	6,9	P3, P6, P10
A9	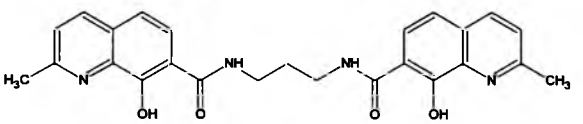	293 - 297	22,9	P3, P6, P10
A10	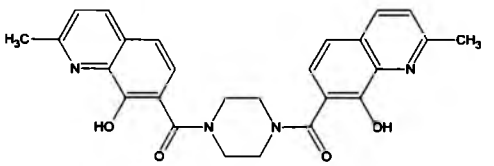	284 - 286	10.0	P3
A11	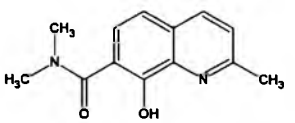	228 - 232	10,4	NP*

A12	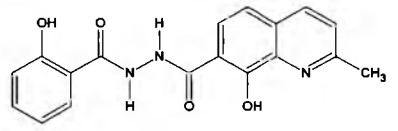	147 - 150	37,6	P6
A13	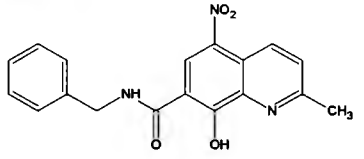	219 - 228 (rozkład)	60,8	P6
A14	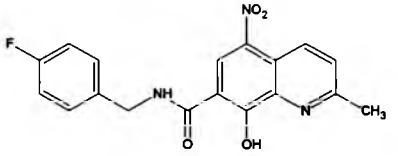	202 - 206	43,9	P6
A15	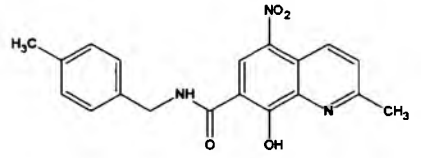	228 - 232	78,3	P6
A16	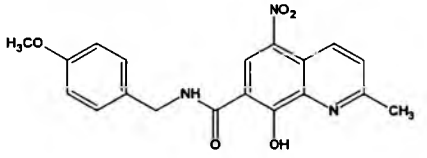	211 - 214	63,1	P6
A17	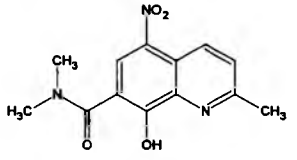	rozkład około 340	81,9	NP*
A18	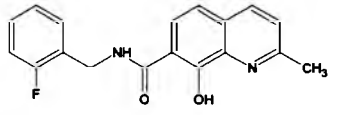	221 - 224 (rozkład)	23,7	NP*
A19	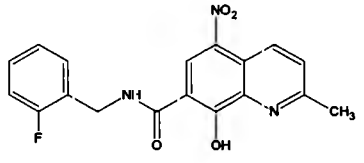	231 - 233	84,1	NP*
A20	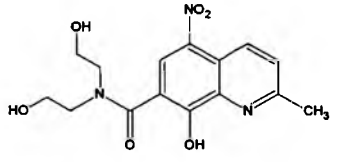	208 - 212	92,4	NP*

*NP – związek niepublikowany

Struktury otrzymanych związków zostały potwierdzone za pomocą widm ^{1}H NMR, ^{13}C NMR oraz analizy elementarnej (**Tabela 2**).

Tabela 2. Charakterystyka amidowych pochodnych kwasów **6** i **7**

Nr	Wzór sumaryczny	^{1}H NMR, ^{13}C NMR, AE
6	$C_{11}H_9NO_3$	**^{1}H NMR** (400 MHz, DMSO-d_6): δ 2.80 (s, 3H), 7.19 (d, J = 8.6 Hz, 1H), 7.70 (d, J = 8.5 Hz, 1H), 7.86 (d, J = 8.6 Hz, 1H), 8.53 (d, J = 8.5 Hz, 1H); **^{13}C NMR** (100 MHz, DMSO-d_6): δ 22.2, 112.5, 112.9, 124.9, 127.4, 130.4, 135.2, 140.8, 156.2, 160.8, 170.7
7	$C_{11}H_8N_2O_5$	**^{1}H NMR** (400 MHz, DMSO-d_6): δ 2.94 (s, 3H), 8.14 (d, J = 9.0 Hz, 1H), 9.20 (s, 1H), 9.66 (d, J = 9.0 Hz, 1H); **^{13}C NMR** (100 MHz, DMSO-d_6): δ 19.8, 122.5, 124.9, 128.9, 129.2, 130.8, 137.4, 141.1, 154.9, 161.6, 171.6
A1	$C_{18}H_{16}N_2O_2$	**^{1}H NMR** (400 MHz, DMSO-d_6): δ 2.61 (s, 3H), 4.07 (s, 2H), 6.97 (d, J = 8.5 Hz, 1H), 7.33 (d, J = 8.4 Hz, 1H), 7.37-7.43 (m, 3H), 7.49 (dd, J = 8.0 Hz, 1.5 Hz, 2H), 7.77 (d, J = 8.4 Hz, 1H), 8.04 (d, J = 8.4 Hz, 1H), 8.45 (bs, 2H); **^{13}C NMR** (100 MHz, DMSO-d_6): δ 24.6, 42.3, 112.5, 115.6, 122.6, 126.7, 128.4, 128.6, 128.8, 129.1, 134.2, 135.9, 140.1, 155.4, 162.0, 171.9; **AE** calc: 73.95 C, 5.52 H, found: 74.12 C, 5.68 H
A2	$C_{18}H_{15}FN_2O_2$	**^{1}H NMR** (400 MHz, DMSO-d_6): δ 2.61 (s, 3H), 4.09 (s, 2H), 6.98 (d, J = 8.4 Hz, 1H), 7.25 (t, J = 8.9 Hz, 2H), 7.34 (d, J = 8.4 Hz, 1H), 7.54 (dd, J = 8.5 Hz, 5.6 Hz, 2H), 7.77 (d, J = 8.4 Hz, 1H), 8.05 (d, J = 8.4 Hz, 1H), 8.46 (bs, 2H); **^{13}C NMR** (100 MHz, DMSO-d_6): δ 24.6, 41.6, 112.7, 115.4 (d, $^{2}J_{C\text{-}F}$ = 21.5 Hz), 115.5, 122.7, 126.6, 129.2, 130.5 (d, $^{4}J_{C\text{-}F}$ = 3.1 Hz), 131.2 (d, $^{3}J_{C\text{-}F}$ = 8.4 Hz), 135.9, 140.0, 155.6, 161.9, 162.0 (d, $^{1}J_{C\text{-}F}$ = 244.6 Hz), 172.1; **AE** calc: 69.67 C, 4.87 H, found: 70.01 C, 4.80 H
A3	$C_{19}H_{18}N_2O_2$	**^{1}H NMR** (400 MHz, DMSO-d_6): δ 2.30 (s, 3H), 2.61 (s, 3H), 4.02 (s, 2H), 6.97 (d, J = 8.4 Hz, 1H), 7.21 (d, J = 7.8 Hz, 2H), 7.33 (d, J = 8.5 Hz, 1H), 7.35 (d, J = 8.2 Hz, 2H), 7.76 (d, J = 8.4 Hz, 1H), 8.04 (d, J = 8.4 Hz, 1H), 8.43 (bs, 2H); **^{13}C NMR** (100 MHz, DMSO-d_6): δ 20.7, 24.6, 42.1, 112.5, 115.6, 122.6, 126.7, 128.8, 129.0, 129.1, 131.1, 135.8, 137.8, 140.1, 155.4, 162.0, 171.9; **AE** calc: 74.49 C, 5.92 H, found: 74.32 C, 6.10 H
A4	$C_{19}H_{18}N_2O_3$	**^{1}H NMR** (400 MHz, DMSO-d_6): δ 2.61 (s, 3H), 3.75 (s, 3H), 3.99 (s, 2H), 6.95-6.98 (m, 3H), 7.33 (d, J = 8.4 Hz, 1H), 7.40 (d, J = 8.7 Hz, 2H), 7.76 (d, J = 8.4 Hz, 1H), 8.04 (d, J = 8.4 Hz, 1H), 8.28 (bs, 2H); **^{13}C NMR** (100 MHz, DMSO-d_6): δ 24.6, 41.8, 55.2, 112.5, 113.9, 115.6, 122.6, 126.0, 126.7, 129.1, 130.4, 135.9, 140.1, 155.5, 159.4, 162.0, 171.9; **AE** calc: 70.79 C, 5.63 H, found: 70.65 C, 5.49 H
A5	$C_{19}H_{18}N_2O_2$	**^{1}H NMR** (400 MHz, DMSO-d_6): δ 2.62 (s, 3H), 2.90 (t, 2H), 3.09 (t, 2H), 6.97 (d, J = 8.4 Hz, 1H), 7.22-7.35 (m, 5H), 7.77 (d, J = 8.4 Hz, 1H), 8.03 (d, J = 8.4 Hz, 1H), 8.11 (bs, 2H); **^{13}C NMR** (100 MHz, DMSO-d_6): δ 24.7, 33.1, 40.0, 112.6, 115.6, 122.5, 126.6, 126.7, 128.5, 128.6, 129.1, 135.8, 137.3, 140.2, 155.5, 162.0, 172.0; **AE** calc: 74.49 C, 5.93 H, found: 74.63 C, 6.05 H

A6	$C_{21}H_{22}N_2O_2$	**^{1}H NMR** (400 MHz, DMSO-d_6): δ 1.54-1.65 (m, 4H), 2.58 (t, J = 7.2 Hz, 2H), 2.62 (s, 3H), 2.84 (t, J = 7.2 Hz, 2H), 6.96 (d, J = 8.4 Hz, 1H), 7.13-7.30 (m, 5H), 7.32 (d, J = 8.4 Hz, 1H), 7.76 (d, J = 8.4 Hz, 1H), 7.96 (bs, 2H), 8.03 (d, J = 8.4 Hz, 1H); **^{13}C NMR** (100 MHz, DMSO-d_6): δ 24.7, 26.6, 27.6, 34.5, 38.7, 112.5, 115.7, 122.5, 125.7, 126.6, 128.2, 128.3, 129.1, 135.8, 140.2, 141.6, 155.4, 162.1, 171.9; **AE** calc: 75.42 C, 6.63 H, found: 75.36 C, 6.78 H
A7	$C_{19}H_{17}FN_2O_2$	**^{1}H NMR** (400 MHz, DMSO-d_6): δ 2.62 (s, 3H), 2.87 (t, 2H), 3.08 (t, 2H), 6.96 (d, J = 8.4 Hz, 1H), 7.15 (t, J = 8.9 Hz, 2H), 7.27-7.31 (m, 2H), 7.33 (d, J = 8.3 Hz, 1H), 7.76 (d, J = 8.4 Hz, 1H), 8.03 (d, J = 8.4 Hz, 1H), 8.08 (bs, 2H); **^{13}C NMR** (100 MHz, DMSO-d_6): δ 24.6, 32.2, 39.9, 112.5, 115.3 (d, $^2J_{C\text{-}F}$ = 21.2 Hz), 115.7, 122.5, 126.7, 129.1, 130.6 (d, $^3J_{C\text{-}F}$ = 8.1 Hz), 133.5 (d, $^4J_{C\text{-}F}$ = 3.1 Hz), 135.8, 140.2, 155.4, 161.1 (d, $^1J_{C\text{-}F}$ = 242.4 Hz), 162.0, 171.9; **AE** calc: 70.36 C, 5.28 H, found: 70.23 C, 4.56 H
A8	$C_{24}H_{22}N_4O_4$	**^{1}H NMR** (400 MHz, DMSO-d_6): δ 2.64 (s, 6H), 3.14 (s, 4H), 7.00 (d, J = 8.5 Hz, 2H), 7.36 (d, J = 8.4 Hz, 2H), 7.78 (d, J = 8.4 Hz, 2H), 8.08 (d, J = 8.4 Hz, 2H); **^{13}C NMR** (100 MHz, DMSO-d_6): δ 24.5, 36.9, 112.8, 115.3, 122.8, 126.6, 129.2, 136.2, 139.7, 155.6, 161.7, 172.1; **AE** calc: 66.97 C, 5.15 H, found: 66.74 C, 5.22 H
A9	$C_{25}H_{24}N_4O_4$	**^{1}H NMR** (400 MHz, DMSO-d_6): δ 1.82-1.87 (m, 2H), 2.64 (s, 6H), 2.90 (t, 4H), 6.97 (d, J = 8.4 Hz, 2H), 7.36 (d, J = 8.3 Hz, 2H), 7.77 (d, J = 8.4 Hz, 2H), 7.89 (bs, 2H), 8.07 (d, J = 8.4 Hz, 2H); **AE** calc: 67.55 C, 5.44 H, found: 67.34 C, 5.62 H
A10	$C_{26}H_{24}N_4O_4$	**^{1}H NMR** (400 MHz, DMSO-d_6): δ 2.67 (s, 6H), 2.97 (s, 8H), 7.01 (d, J = 8.4 Hz, 2H), 7.42 (d, J = 8.4 Hz, 2H), 7.78 (d, J = 8.5 Hz, 2H), 8.16 (d, J = 8.8 Hz, 2H); **AE** calc: 68.41 C, 5.30 H, found: 68.26 C, 5.19 H
A11	$C_{13}H_{14}N_2O_2$	**^{1}H NMR** (400 MHz, DMSO-d_6): δ 2.62 (s, 3H), 3.18 (bs, 6H), 6.94 (d, J = 8.4 Hz, 1H), 7.32 (d, J = 8.4 Hz, 1H), 7.75 (d, J = 8.4 Hz, 1H), 7.66 (bs, 1H), 8.02 (d, J = 8.3 Hz, 1H); **AE** calc: 67.81 C, 6.13 H, found: 68.03 C, 6.17 H
A12	$C_{18}H_{15}N_3O_4$	**^{1}H NMR** (400 MHz, DMSO-d_6): δ 2.76 (s, 3H), 6.96-7.03 (m, 2H), 7.37 (d, J = 8.8 Hz, 1H), 7.46(ddd, J = 8.4 Hz, 7.2 Hz, 1.7 Hz, 1H), 7.60 (d, J = 8.4 Hz, 1H), 7.97 (dd, J = 7.9 Hz, 1.6 Hz, 1H), 7.97 (d, J = 8.7 Hz, 1H), 8.34 (d, J = 8.4 Hz, 1H), 11.07 (bs, 1H), 11.44 (bs, 1H); **^{13}C NMR** (100 MHz, DMSO-d_6): δ 23.9, 112.1, 115.2, 115.7, 117.2, 119.3, 124.6, 125.2, 129.0, 129.2, 133.9, 137.4, 137.6, 155.8, 157.2, 158.2, 164.7, 164.8; **AE** calc: 64.09 C, 4.48 H, found: 63.92 C, 4.38 H
A13	$C_{18}H_{15}N_3O_4$	**^{1}H NMR** (400 MHz, DMSO-d_6): δ 2.58 (s, 3H), 4.07 (s, 2H), 7.35-7.47 (m, 5H), 7.53 (d, J = 8.7 Hz, 1H), 8.25 (bs, 2H), 9.08 (d, J = 8.7 Hz, 1H), 9.14 (s, 1H); **^{13}C NMR** (100 MHz, DMSO-d_6): δ 24.0, 42.4, 122.5, 123.8, 125.3, 128.2, 128.5, 128.6, 128.8, 131.0, 132.5,133.9, 146.5, 155.2, 155.3, 168.3; **AE** calc: 64.09 C, 4.48 H, found: 63.95 C, 4.42 H
A14	$C_{18}H_{14}FN_3O_4$	**^{1}H NMR** (400 MHz, DMSO-d_6): δ 2.59 (s, 3H), 4.04 (s, 2H), 7.27 (t, J = 8.8 Hz, 2H), 7.50 (t, J = 8.8 Hz, 2H), 7.51 (d, J = 8.7 Hz, 1H), 8.09 (bs, 2H), 9.08 (d, J = 8.7 Hz, 1H), 9.14 (s, 1H); **^{13}C NMR** (100 MHz, DMSO-d_6): δ 24.0, 41.6, 115.4 (d, $^2J_{C\text{-}F}$ = 21.5 Hz), 122.3, 123.8, 125.3, 128.3, 130.3, 131.0, 131.2 (d, $^3J_{C\text{-}F}$ = 8.5 Hz), 132.5, 146.5, 155.2, 162.1 (d, $^1J_{C\text{-}F}$ = 244.8 Hz), 162.7, 168.3; **AE** calc: 60.84 C, 3.97 H, found: 60.68 C, 3.80 H
A15	$C_{19}H_{17}N_3O_4$	**^{1}H NMR** (400 MHz, DMSO-d_6): δ 2.30 (s, 3H), 2.58 (s, 3H), 4.00 (s, 2H), 7.21 (d, J = 8.0 Hz, 2H), 7.33 (d, J = 8.0 Hz, 2H), 7.52 (d, J = 8.7 Hz, 1H), 8.16 (bs, 2H), 9.08 (d, J = 8.7 Hz, 1H), 9.14 (s, 1H); **^{13}C NMR** (100 MHz, DMSO-d_6): δ 20.7, 24.0, 42.1, 122.3, 123.8, 125.3, 128.3, 128.8, 129.1, 130.9, 131.0, 132.5, 134.5, 137.0, 146.5, 155.2, 168.3; **AE** calc: 64.95 C, 4.88 H, found: 65.12 C, 4.96 H

A16	$C_{19}H_{17}N_3O$	**^{1}H NMR** (400 MHz, DMSO-d_6): δ 2.59 (s, 3H), 3.75 (s, 3H), 3.98 (s, 2H), 6.96 (d, J = 8.6 Hz, 2H), 7.37 (d, J = 8.6 Hz, 2H), 7.54 (d, J = 8.7 Hz, 1H), 8.11 (bs, 2H), 9.09 (d, J = 8.7 Hz, 1H), 9.14 (s, 1H); **^{13}C NMR** (100 MHz, DMSO-d_6): δ 23.9, 41.9, 55.2, 114.0, 122.3, 123.8, 125.4, 125.8, 128.3, 130.4, 131.0, 132.8, 146.2, 155.2, 159.4, 168.1; **AE** calc: 62.12 C, 4.66 H, found: 61.83 C, 4.71 H
A17	$C_{13}H_{13}N_3O_4$	**^{1}H NMR** (400 MHz, DMSO-d_6): δ 2.59 (s, 3H), 2.60 (bs, 6H), 7.53 (d, J = 8.7 Hz, 1H), 8.41 (bs, 2H), 9.08 (d, J = 8.7 Hz, 1H), 9.14 (s, 1H); **^{13}C NMR** (100 MHz, DMSO-d_6): δ 24.1, 34.4, 122.5, 123.8, 125.4, 128.2, 131.0, 132.6, 146.5, 155.3, 168.3; **AE** calc: 56.72 C, 4.75 H, found: 56.55 C, 4.87 H
A18	$C_{18}H_{15}FN_2O_2$	**^{1}H NMR** (400 MHz, DMSO-d_6): δ 2.62 (s, 3H), 4.12 (s, 2H), 6.96 (d, J = 8.3 Hz, 1H), 7.28 (dd, J = 13.0 Hz, 6.2 Hz, 2H), 7.33 (d, J = 8.3 Hz, 1H), 7.45 (dd, J = 13.5 Hz, 7.4 Hz, 1H), 7.56 (t, J = 7.3 Hz, 1H), 7.76 (d, J = 8.4 Hz, 1H), 8.04 (d, J = 8.2 Hz, 1H); **^{13}C NMR** (100 MHz, DMSO-d_6): δ 24.5, 35.9 (d, $^3J_{C\text{-}F}$ = 4.4 Hz), 112.4, 115.5 (d, $^2J_{C\text{-}F}$ = 21.2 Hz), 115.6, 121.1, 121.3, 122.5, 124.7 (d, $^4J_{C\text{-}F}$ = 3.6 Hz), 126.7, 129.1, 130.9 (d, $^3J_{C\text{-}F}$ = 8.3 Hz), 131.2 (d, $^3J_{C\text{-}F}$ = 3.4 Hz), 135.9, 140.0, 155.4, 160.3 (d, $^1J_{C\text{-}F}$ = 246.5 Hz), 171.8; **AE** calc: 69.67 C, 4.87 H, found: 69.81 C, 5.01 H
A19	$C_{18}H_{14}FN_3O_4$	**^{1}H NMR** (400 MHz, DMSO-d_6): δ 2.58 (s, 3H), 4.13 (s, 2H), 7.22-7.30 (m, 2H), 7.40-7.49 (m, 1H), 7.53 (d, J = 8.7 Hz, 1H), 7.53-7.57 (m, 1H), 8.39 (bs, 2H), 9.08 (d, J = 8.7 Hz, 1H), 9.14 (s, 1H); **^{13}C NMR** (100 MHz, DMSO-d_6): δ 23.9, 35.9 (d, $^3J_{C\text{-}F}$ = 4.4 Hz), 112.4, 115.5 (d, $^2J_{C\text{-}F}$ = 21.2 Hz), 120.9, 121.0, 122.6, 123.8 124.6 (d, $^4J_{C\text{-}F}$ = 3.6 Hz), 125.4, 128.2, 131.0 (d, $^3J_{C\text{-}F}$ = 8.3 Hz), 131.2 (d, $^3J_{C\text{-}F}$ = 3.4 Hz), 132.6, 146.3, 155.3, 160.3 (d, $^1J_{C\text{-}F}$ = 246.6 Hz), 168.3; **AE** calc: 60.84 C, 3.97 H, found: 60.95 C, 4.12 H
A20	$C_{15}H_{17}N_3O_6$	**^{1}H NMR** (400 MHz, DMSO-d_6): δ 2.60 (s, 1H), 3.03 (t, J = 5.3 Hz, 4H), 3.66 (bs, 4H), 5.19 (bs, 2H), 7.53 (d, J = 8.7 Hz, 1H), 8.43 (bs, 2H), 9.08 (d, J = 8.7 Hz, 1H), 9.14 (s, 1H); **^{13}C NMR** (100 MHz, DMSO-d_6): δ 24.0, 48.8, 56.3, 122.3, 123.8, 125.3, 128.3, 131.1, 132.5, 146.5, 155.2, 168.3; **AE** calc: 53.73 C, 5.11 H, found: 53.82 C, 5.27 H

4.2.Próby syntezy pochodnych kwasu 2-metylo-5,8-chinolinodiono-7-karboksylowego

Ze względu na silne właściwości przeciwnowotworowe obszernie badaną grupą związków są pochodne 7-amino-5,8-chinolinodionu **8**. Fragment ten występuje w wielu związkach pochodzenia naturalnego, np. w lawendamycynie **9** [57,61]. Dalsze badania analogów 5,8-chinolinodionu ujawniły także ich wysoką aktywność antybakteryjną i antywirusową [62].

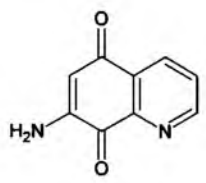

8

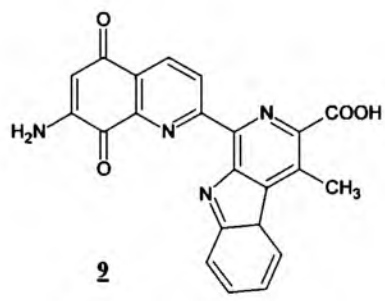

9

Substratem syntezy kwasu 2-metylo-5,8-chinolinodiono-7-karboksylowego **12** był wcześniej otrzymany kwas 8-hydroksy-2-metylo-5-nitrochinolino-7-karboksylowy **7**. Pierwszy etap syntezy obejmował redukcję grupy nitrowej za pomocą ditionianu sodu, a następnie zabezpieczenie grupy aminowej w postaci pochodnej acetamidowej **11**. W drugim etapie przeprowadzono utlenianie związku **11** za pomocą dichromianu(VI) potasu (**Schemat 4**). Reakcję prowadzono w lodowatym kwasie octowym wg procedury opisanej w [63].

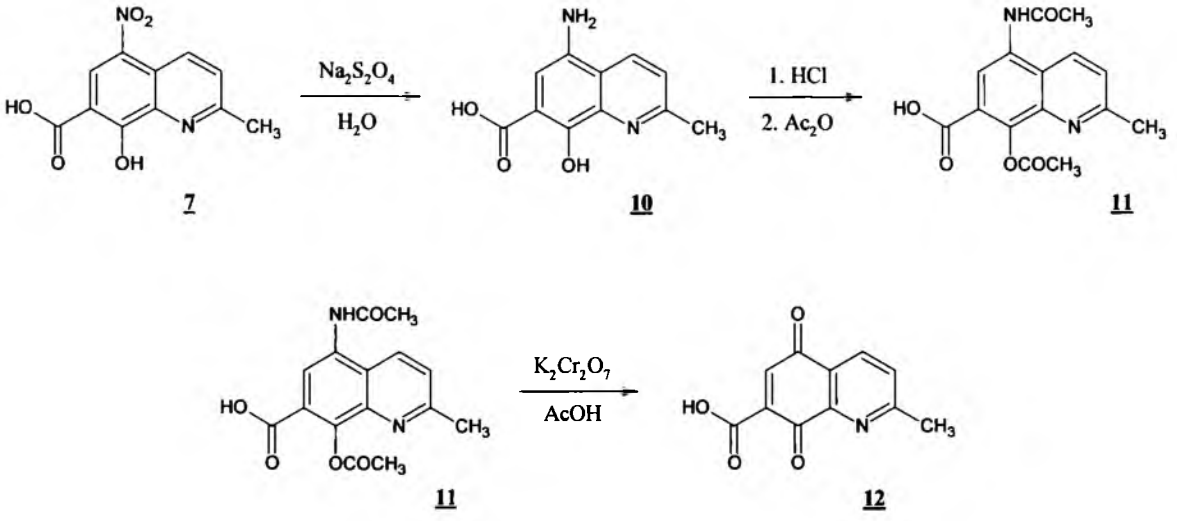

Schemat 4. Synteza kwasu 2-metylo-5,8-chinolinodiono-7-karboksylowego

Celem dokładnego ustalenia struktury otrzymaną pochodną poddano badaniom spektroskopowym. W szczególności analiza widm ^{13}C NMR oraz ^{14}N NMR ujawniła, że na skutek dekarboksylacji nieoczekiwanym produktem reakcji jest 7-acetamido-2-metylo--5,8-chinolinodion **13** (**Tabela 3**). Definitywnym potwierdzeniem budowy związku **13** było otrzymanie przez pracowników Zakładu Krystalografii UŚ jego struktury krystalograficznej (**Rys. 11**) [P14].

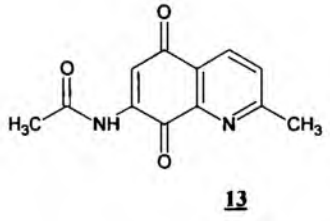

Tabela 3. Charakterystyka 7-acetamido-2-metylo-5,8-chinolinodionu **13**

Nr	Struktura	^{1}H NMR, ^{13}C NMR, ^{14}N NMR, IR, EI-MS, AE
13	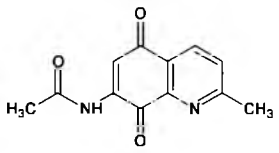	**Mp.** 244 - 247 (rozkład); **^{1}H NMR** (400 MHz, DMSO-d_6): δ 2.24 (s, 3H), 2.64 (s, 3H), 7.69 (s, 1H), 7.70 (d, J = 8.1 Hz, 1H), 8.20 (d, J = 8.1 Hz, 1H), 10.00 (bs, 1H); **^{13}C NMR** (100 MHz, DMSO-d_6): δ 24.5, 24.6, 115.0, 126.5, 128.1, 133.7, 142.0, 145.8, 163.4, 171.4, 178.6, 184.8; **^{14}N NMR** (400 MHz, $CDCl_3$ + 90% CH_3NO_2 w $CDCl_3$): δ 80 (aminowy), 310 (pirydynowy); **IR** (KBr, cm^{-1}): ν 3332 (s), 1719 (s), 1687 (vs), 1641 (vs), 1618 (s), 1589 (s), 1510 (vs), 1373 (m), 1317 (s), 1216 (s), 1137 (s); **EI-MS** (70 eV): m/z 230 (M^+), 188, 161 (100), 132, 119, 104, 93, 68, 43; **AE** calc. for $C_{12}H_{10}N_2O_3$: 62.80 C, 4.38 H, 12.17 N; found: 62.91 C, 4.06 H, 12.30 N

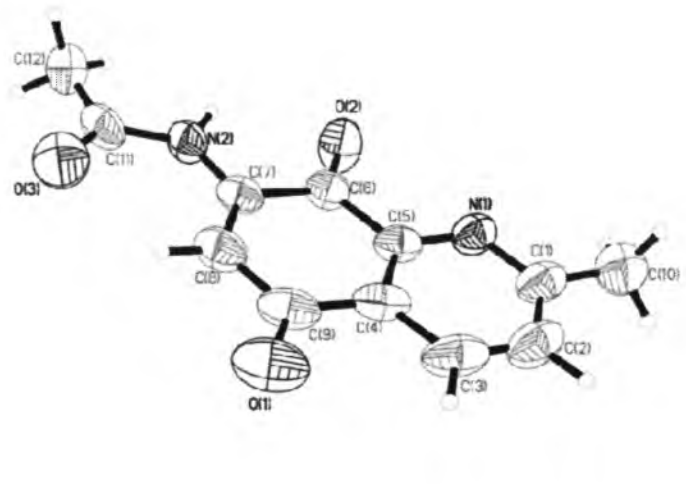

Rys. 11. Struktura krystalograficzna 7-acetamido-2-metylo-5,8-chinolinodionu **13** [P14]

4.3. Oznaczenia aktywności anty-HIV

Oznaczenia aktywności otrzymanych pochodnych względem integrazy HIV zostały przeprowadzone w jednostce współpracującej - CNRS UMR 8532, LBPA, Ecole Normale Superieure de Cachan, Francja. Wyniki aktywności (IC_{50}) zostały zebrane w **Tabeli 4**. Większość związków okazała się nieaktywna, tylko jeden z nich (**A12**) wykazał umiarkowaną aktywność rzędu 50 μM [P3].

Tabela 4. Aktywność anty-HIV amidowych pochodnych kwasów **6** i **7** [P3]

Nr	IC_{50} [μM]	Nr	IC_{50} [μM]	Nr	IC_{50} [μM]	Nr	IC_{50} [μM]
6	>100	**A5**	>100	**A11**	>100	**A17**	>100
7	>100	**A6**	>100	**A12**	50	**A18**	>100
A1	>100	**A7**	>100	**A13**	>100	**A19**	>100
A2	>100	**A8**	>100	**A14**	>100	**A20**	>100
A3	>100	**A9**	>100	**A15**	>100		
A4	>100	**A10**	>100	**A16**	>100		

Pochodne kwasu 8-hydroksy-2-metylochinolino-7-karboksylowego **6** okazały się związkami nieaktywnymi, pomimo strukturalnego podobieństwa do aktywnych pochodnych naftyrydyny. Fakt ten wynika prawdopodobnie z istnienia uprzywilejowanej konformacji amidów naftyrydynowych, stabilizowanych przez utworzenie wewnątrzcząsteczkowego wiązania wodorowego (**Rys. 12**). Hipotezę tą potwierdzają badania pochodnych salicylamidu, łatwo tworzących planarne konformacje, stabilizowane przez wiązanie wodorowe [64-66]. Zmiana położenia wiązania wodorowego jest spowodowana deprotonowaniem grupy fenolowej (**Rys. 13**) [64,67-69].

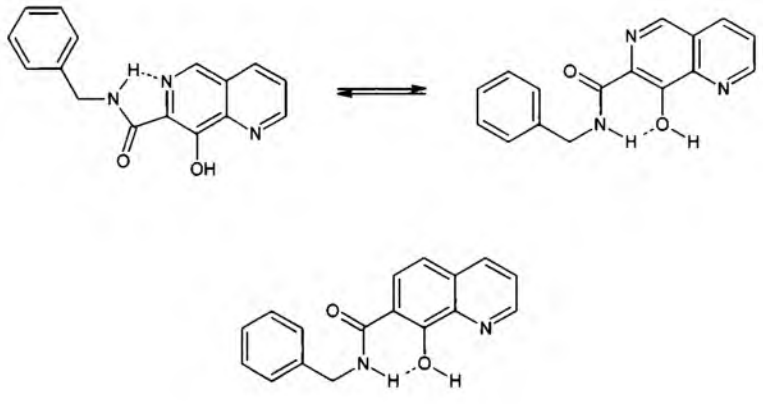

Rys. 12. Konformacje pochodnych naftyrydyny i chinoliny

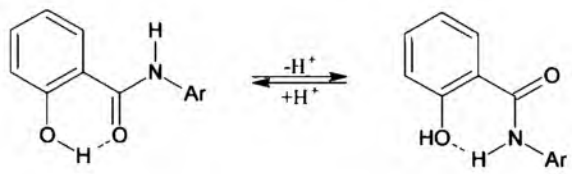

Rys. 13. Amidy kwasu salicylowego

Zmiany konformacyjne wywołane istnieniem wiązania wodorowego mogą powodować mniejszą zdolność do kompleksowania dwóch jonów Mg^{2+}, a tym samym zmniejszać aktywność wobec IN HIV [13]. W przypadku prostych amidowych pochodnych kwasu 8-hydroksy-7-chinaldynokarboksylowego grupa NH nie może uczestniczyć w wiązaniu Mg^{2+}, gdyż jest zbyt słabą zasadą Lewisa (**Rys. 14**).

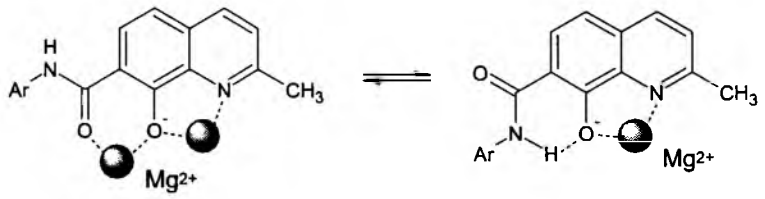

Rys. 14. Zmiana zdolności kompleksującej jony Mg^{2+} na skutek zmiany konformacji

W ciągu dalszych badań przeprowadzono dokowanie molekularne kwasu 8-hydroksy-2-metylochinolino-7-karboksylowego **6** do domeny katalitycznej integrazy HIV-1, zawierającej dwa jony Mg^{2+}[P13]. Badany związek wykazuje uprzywilejowaną konformację, wiążąc się z dwoma kationami magnezu, natomiast nie wiąże się bezpośrednio z resztami aminokwasowymi Asp 116, Asp 64 i Glu 152 (**Rys. 15a**). W przeciwieństwie do kwasu **6**, jego aktywny izomer kwas 5-hydroksy-2-metylochinolino-6-karboksylowy **6a**, nie wiąże dwóch jonów Mg^{2+}, natomiast silnie oddziaływuje z resztami aminokwasowymi za pośrednictwem wiązań wodorowych (**Rys. 15b**).

W ramach współpracy z Zakładem Krystalochemii i Krystalofizyki UJ udało się także wyznaczyć strukturę krystalograficzną kwasu 8-hydroksy-2-metylochinolino-7--karboksylowego (**Rys. 16**) [P13].

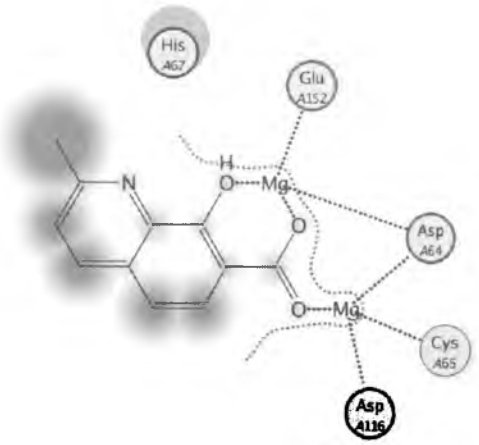

Rys. 15a. Dokowanie molekularne kwasu 8-hydroksychinaldyno-7-karboksylowego do integrazy HIV-1 [P13]

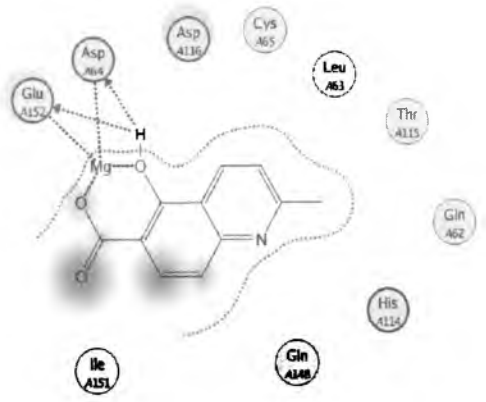

Rys. 15b. Dokowanie molekularne kwasu 5-hydroksychinaldyno-6-karboksylowego do integrazy HIV-1 [P13]

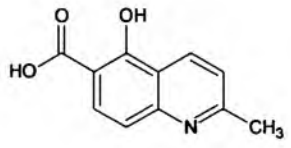

6a

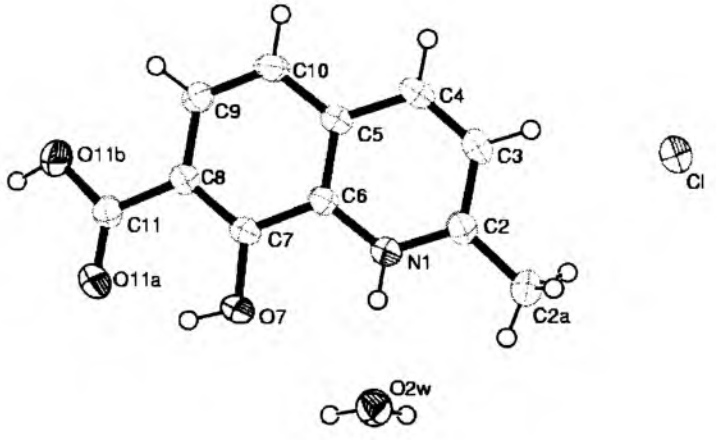

Rys. 16. Struktura krystalograficzna kwasu 8-hydroksy-2-metylochinolino-7-karboksylowego **6** [P13]

4.4. Synteza N-podstawionych pochodnych pirolo[3,4-g]chinolino-6,8-dionu

Ostatnio przeprowadzone badania potwierdzają, że usztywnienie struktury diketokwasu np. poprzez wprowadzenie do cząsteczki trzeciego pierścienia może prowadzić do pochodnych typu **14**, o wysokiej aktywności [70]. Szczególnie obiecujące wydają się być N-podstawione pochodne pirolo[3,4-g]chinolino-6,8-dionu **15** i **16** [71-73].

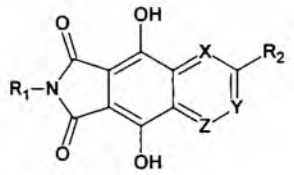

14

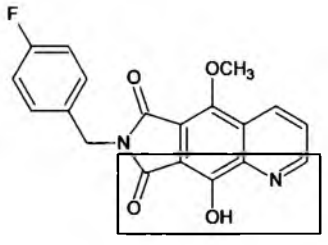

15

IC_{50} = 80 nM

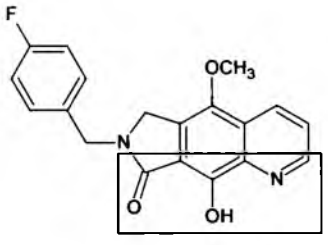

16

IC_{50} = 60 nM

Pierwszym etapem syntezy analogów związku **15** było otrzymanie N-podstawionych pochodnych 2,5-pirolidynodionu. W reakcji bezwodnika kwasu bursztynowego **17** z odpowiednimi aminami otrzymano związki **B1 - B5** (**Schemat 5**). Syntezy prowadzono według procedury opisanej w [74]. Kolejnym etapem było przeprowadzenie kwasu 2,3-pirydynodikarboksylowego **18** w jego ester dimetylowy **19** [75] w wyniku metanolizy powstającego w warunkach reakcji chlorku kwasowego (**Schemat 5**).

Otrzymany 2,3-pirydynodikarboksylan dimetylu **19** poddano następnie kondensacji Dieckmanna z uzyskanymi wcześniej imidowymi pochodnymi 2,5-pirolidynodionu **B1 - B5**, w wyniku czego zsyntezowano związki **C1 - C5** (**Schemat 5**). Reakcje prowadzono w bezwodnym tetrahydrofuranie w obecności metanolanu sodu [72].

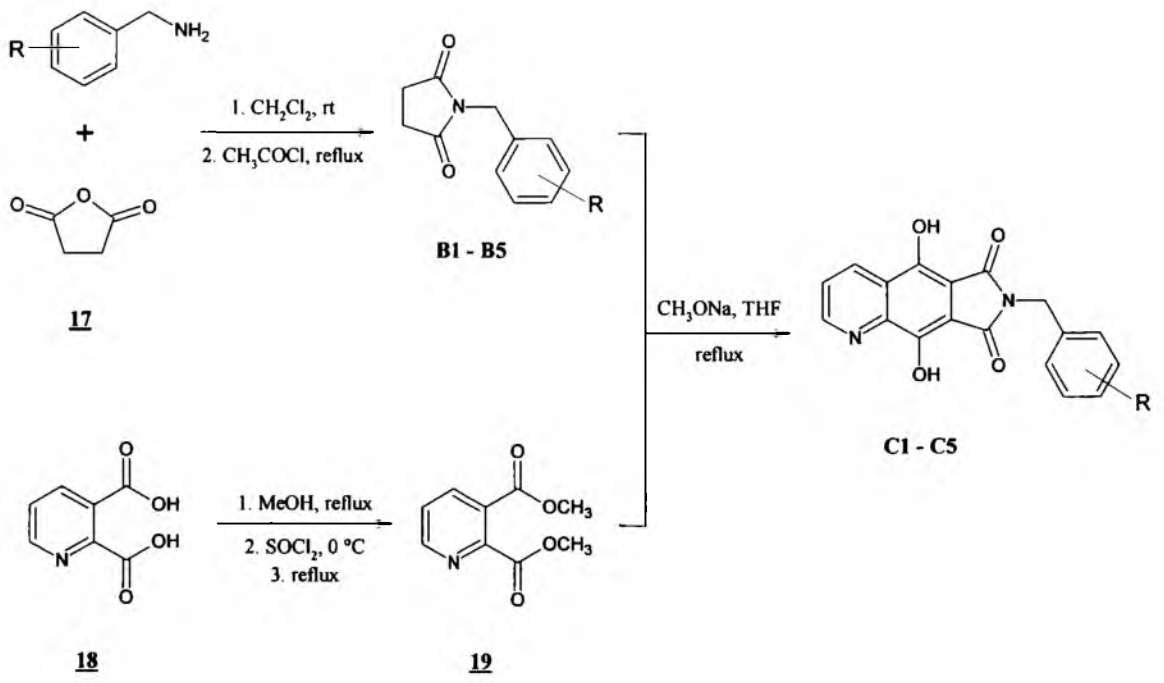

Schemat 5. Synteza N-podstawionych pochodnych pirolo[3,4-g]chinolino-6,8-dionu

Wzory otrzymanych pochodnych, ich temperatury topnienia oraz wydajności przeprowadzonych reakcji zebrane zostały w **Tabeli 5.**

Tabela 5. Pochodne 2,5-pirolidynodionu **B1 - B5** i pirolo[3,4-g]chinolino-6,8-dionu **C1 - C5**

Nr	Struktura	t.topn. [°C]	Wydajność [%]	Uwagi, literatura
19	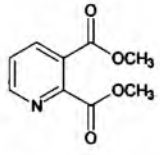	51-52	41,3	lit. t.topn. 53 - 55 °C [75]
B1	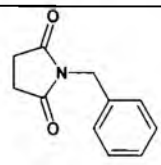	85-87	68,0	lit. t.topn. 102 - 103 °C [76]
B2	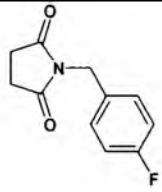	117-120	82,5	^{1}H NMR [77]

B3	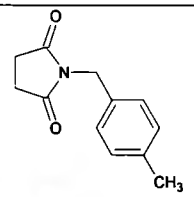	84-85	74,3	[70]
B4	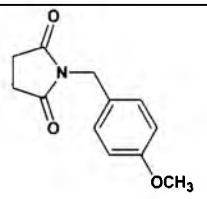	126-128	49,2	[77]
B5	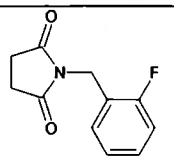	66-70	55,7	NP*
C1	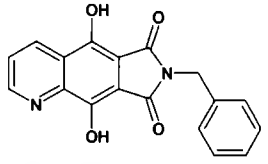	242-246	84,6	NP*
C2	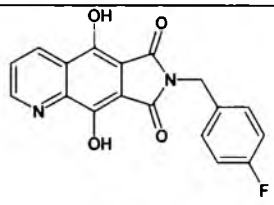	255-260	75,4	lit. t.topn. 282 - 284 °C [78]
C3	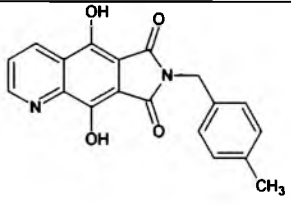	241-245	91,7	NP*
C4	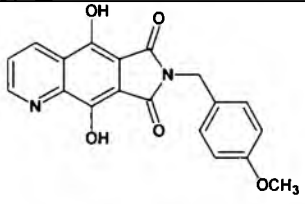	269-272	50,9	NP*
C5	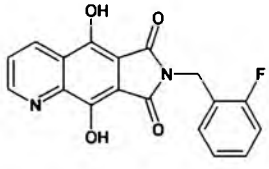	230-233	72,0	NP*

*NP – związek niepublikowany

Struktury otrzymanych związków zostały potwierdzone za pomocą widm ^{1}H NMR, ^{13}C NMR oraz spektrometrii mas (**Tabela 6**).

Tabela 6. Charakterystyka pochodnych **B1 - B5** oraz **C1 - C5**

Nr	Wzór sumaryczny	^{1}H NMR, ^{13}C NMR, ESI-MS
19	$C_9H_9NO_4$	**^{1}H NMR** (400 MHz, DMSO-d_6): δ 3.86 (s, 3H), 3.87 (s, 3H), 7.71 (dd, J = 8.0 Hz, 4.8 Hz, 1H), 8.30 (dd, J = 8.0 Hz, 1.6 Hz, 1H), 8.81 (dd, J = 4.8 Hz, 1.6 Hz, 1H); **^{13}C NMR** (100 MHz, DMSO-d_6): δ 52.8, 53.0, 124.9, 125.6, 137.9, 150.6, 152.3, 165.1, 166.4; **ESI-MS** (+20V): m/z 196.24 $[M+H]^+$, 218.23 $[M+Na]^+$, 391.50 $[2M+H]^+$, 413.48 $[2M+Na]^+$
B1	$C_{11}H_{11}NO_2$	**^{1}H NMR** (400 MHz, DMSO-d_6): δ 2.69 (s, 4H), 4.54 (s, 2H), 7.24-7.33 (5H); **^{13}C NMR** (100 MHz, DMSO-d_6): δ 28.3, 41.3, 127.3, 127.5, 128.4, 136.3, 177.6; **ESI-MS** (+20V): m/z 190.19 $[M+H]^+$, 212.18 $[M+Na]^+$, 379.38 $[2M+H]^+$, 401.35 $[2M+Na]^+$
B2	$C_{11}H_{10}FNO_2$	**^{1}H NMR** (400 MHz, DMSO-d_6): δ 3.18 (s, 4H), 5.03 (s, 2H), 7.51 (t, J = 8.9 Hz, 2H), 7.81 (dd, J = 8.8 Hz, 5.4 Hz, 2H); **^{13}C NMR** (100 MHz, DMSO-d_6): δ 28.1, 40.6 (d, $^5J_{C\text{-}F}$ = 0.6 Hz), 115.2 (d, $^2J_{C\text{-}F}$ = 21.5 Hz), 129.8 (d, $^3J_{C\text{-}F}$ = 8.3 Hz), 132.6 (d, $^4J_{C\text{-}F}$ = 3.2 Hz), 161.5 (d, $^1J_{C\text{-}F}$ = 243.2 Hz), 177.6; **ESI-MS** (+20V): m/z 208.12 $[M+H]^+$, 230.13 $[M+Na]^+$, 415.40 $[2M+H]^+$, 437.21 $[2M+Na]^+$
B3	$C_{12}H_{13}NO_2$	**^{1}H NMR** (400 MHz, DMSO-d_6): δ 2.26 (s, 3H), 2.67 (s, 4H), 4.49 (s, 2H), 7.05-7.18 (m, 4H) **^{13}C NMR** (100 MHz, DMSO-d_6): δ 20.7, 28.1, 41.0, 127.6, 129.0, 133.4, 136.6, 177.6; **ESI-MS** (+20V): m/z 204.30 $[M+H]^+$, 226.29 $[M+Na]^+$, 407.61 $[2M+H]^+$, 429.58 $[2M+Na]^+$
B4	$C_{12}H_{13}NO_3$	**^{1}H NMR** (400 MHz, DMSO-d_6): δ 2.66 (s, 4H), 3.72 (s, 3H), 4.46 (s, 2H), 6.86 (d, J = 8.6 Hz, 2H), 7.19 (d, J = 8.7 Hz, 2H); **^{13}C NMR** (100 MHz, DMSO-d_6): δ 28.1, 40.8, 55.1, 113.8, 128.4, 129.2, 158.6, 177.6; **ESI-MS** (+20V): m/z 220.39 $[M+H]^+$, 242.38 $[M+Na]^+$, 439.81 $[2M+H]^+$, 461.84 $[2M+Na]^+$
B5	$C_{11}H_{10}FNO_2$	**^{1}H NMR** (400 MHz, DMSO-d_6): δ 2.70 (s, 4H), 4.59 (s, 2H), 7.10-7.38 (m, 4H); **^{13}C NMR** (100 MHz, DMSO-d_6): δ 28.1, 35.1 (d, $^3J_{C\text{-}F}$ = 4.9 Hz), 115.2 (d, $^2J_{C\text{-}F}$ = 21.0 Hz), 122.9 (d, $^2J_{C\text{-}F}$ = 14.5 Hz), 124.3 (d, $^4J_{C\text{-}F}$ = 3.5 Hz), 129.4 (d, $^3J_{C\text{-}F}$ = 4.0 Hz), 129.4 (d, $^3J_{C\text{-}F}$ = 8.0 Hz), 159.8 (d, $^1J_{C\text{-}F}$ = 245.5 Hz), 177.4; **ESI-MS** (+20V): m/z 208.28 $[M+H]^+$, 230.31 $[M+Na]^+$, 415.55 $[2M+H]^+$, 437.61 $[2M+Na]^+$
C1	$C_{18}H_{12}N_2O_4$	**^{1}H NMR** (400 MHz, DMSO-d_6): δ 4.75 (s, 2H), 7.22-7.38 (m, 5H), 7.80 (dd, J = 8.4 Hz, 4.2 Hz, 1H), 8.73 (dd, J = 8.5 Hz, 1.2 Hz, 1H), 9.05 (dd, J = 4.0 Hz, 1.2 Hz, 1H), 10.74 (bs, 2H); **^{13}C NMR** (100 MHz, DMSO-d_6): δ 40.5, 107.6, 108.0, 123.8, 125.8, 127.3, 127.4, 128.6, 133.2, 137.0, 143.4, 144.0, 146.2, 150.9, 165.3, 166.5; **ESI-MS** (+20V): m/z 321.39 $[M+H]^+$, 343.38 $[M+Na]^+$, 642.10 $[2M+H]^+$, 664.75 $[2M+Na]^+$
C2	$C_{18}H_{11}FN_2O_4$	**^{1}H NMR** (400 MHz, DMSO-d_6): δ 4.73 (s, 2H), 7.16 (t, J = 8.9 Hz, 2H), 7.38 (dd, J = 8.4 Hz, 5.6 Hz, 2H), 7.80 (dd, J = 8.4 Hz, 4.3 Hz, 1H), 8.73 (dd, J = 8.4 Hz, 1.3 Hz, 1H), 9.05 (dd, J = 4.2 Hz, 1.3 Hz, 1H), 10.75 (bs, 2H); **^{13}C NMR** (100 MHz, DMSO-d_6): δ 40.3, 107.6, 108.0, 115.3 (d, $^2J_{C\text{-}F}$ = 21.4 Hz), 123.9, 125.7, 129.7 (d, $^3J_{C\text{-}F}$ = 8.3 Hz), 133.2, 133.3 (d, $^4J_{C\text{-}F}$ = 3.1 Hz), 143.4, 144.0, 146.2, 150.9, 161.4 (d, $^1J_{C\text{-}F}$ = 243.2 Hz), 165.2, 166.5; **ESI-MS** (+20V): m/z 339.27$[M+H]^+$, 361.30 $[M+Na]^+$, 677.54 $[2M+H]^+$, 699.62 $[2M+Na]^+$

C3	$C_{19}H_{14}N_2O_4$	**^{1}H NMR** (400 MHz, DMSO-d_6): δ 2.26 (s, 3H), 4.70 (s, 2H), 7.14 (d, J = 7.6 Hz, 2H), 7.21 (d, J = 7.5 Hz, 2H), 7.80 (dd, J = 8.2 Hz, 4.2 Hz, 1H), 8.73 (dd, J = 8.2 Hz, 1.0 Hz, 1H), 9.05 (dd, J = 3.9 Hz, 1.5 Hz, 1H), 10.72 (bs, 2H); **^{13}C NMR** (100 MHz, DMSO-d_6): δ 20.7, 40.3, 107.7, 108.1, 123.9, 125.8, 127.5, 129.1, 133.3, 134.1, 136.6, 143.5, 144.1, 146.2, 151.0, 165.4, 166.6; **ESI-MS** (+20V): m/z 335.40$[M+H]^+$, 358.03 $[M+Na]^+$, 669.38 $[2M+H]^+$, 691.50 $[2M+Na]^+$
C4	$C_{19}H_{14}N_2O_5$	**^{1}H NMR** (400 MHz, DMSO-d_6): δ 2.66 (s, 3H), 4.67 (s, 2H), 6.82-6.92 (m, 4H), 7.80 (dd, J = 8.4 Hz, 4.3 Hz, 1H), 8.72 (dd, J = 8.4 Hz, 1.6 Hz, 1H), 9.05 (dd, J = 4.3 Hz, 1.6 Hz, 1H), 10.72 (bs, 1H); **^{13}C NMR** (100 MHz, DMSO-d_6): δ 40.5, 55.2, 107.6, 108.0, 123.9, 125.7, 128.4, 129.1, 133.2, 134.1, 136.8, 143.4, 144.0, 146.2, 151.0, 165.3, 166.5; **ESI-MS** (+20V): m/z 351.10$[M+H]^+$, 373.09 $[M+Na]^+$, 701.22 $[2M+H]^+$, 723.19 $[2M+Na]^+$
C5	$C_{18}H_{11}FN_2O_4$	**^{1}H NMR** (400 MHz, DMSO-d_6): δ 4.80 (s, 2H), 7.12-7.25 (m, 2H), 7.28-7.36 (m, 2H), 7.81 (dd, J = 8.4 Hz, 4.3 Hz, 1H), 8.74 (dd, J = 8.4 Hz, 1.6 Hz, 1H), 9.06 (dd, J = 4.3 Hz, 1.6 Hz, 1H), 10.77 (bs, 1H); **^{13}C NMR** (100 MHz, DMSO-d_6): δ 34.5 (d, $^3J_{C\text{-}F}$ = 4.2 Hz), 107.6, 108.0, 115.3 (d, $^2J_{C\text{-}F}$ = 21.0 Hz), 123.6 (d, $^2J_{C\text{-}F}$ = 14.5 Hz), 123.8, 124.5 (d, $^4J_{C\text{-}F}$ = 3.4 Hz), 125.7, 129.4 (d, $^3J_{C\text{-}F}$ = 8.3 Hz), 129.5 (d, $^3J_{C\text{-}F}$ = 4.1 Hz), 133.2, 143.4, 144.0, 146.2, 150.9, 159.9 (d, $^1J_{C\text{-}F}$ = 245.4 Hz), 165.1, 166.3; **ESI-MS** (+20V): m/z 338.95 $[M+H]^+$, 360.91 $[M+Na]^+$, 676.95 $[2M+H]^+$, 698.94 $[2M+Na]^+$

4.5. Synteza N-podstawionych pochodnych pirolo[3,4-b]pirydyno-5,7-dionu

W ramach pracy otrzymano także krótką serię imidowych pochodnych pirolo[3,4-b]pirydyno-5,7-dionu. Pierwszy etap syntezy związków **D1** - **D5** polegał na reakcji bezwodnika kwasu pirydyno-2,3-dikarboksylowego **20** z podstawionymi benzyloaminami. W drugim etapie niewydzielane ze środowiska reakcji pochodne amidowe poddane zostały ogrzewaniu w polu mikrofalowym w obecności bezwodnika octowego (**Schemat 6**) [79].

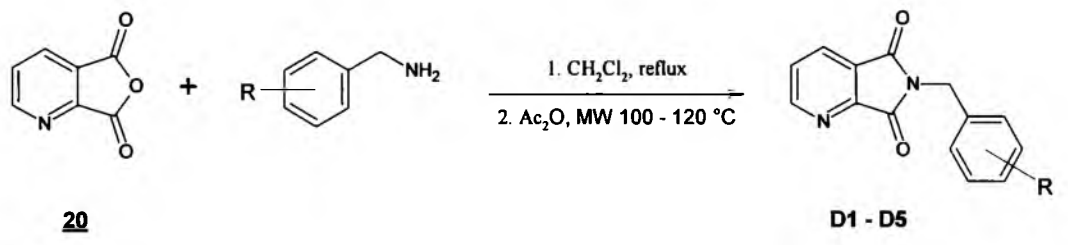

20 **D1 - D5**

Schemat 6. Synteza N-podstawionych pochodnych pirolo[3,4-b]pirydyno-5,7-dionu

W **Tabeli 7** podane zostały wzory otrzymanych pochodnych, ich temperatury topnienia oraz wydajności przeprowadzonych reakcji.

Tabela 7. Pochodne pirolo[3,4-b]pirydyno-5,7-dionu **D1 - D5**

Nr	Struktura	t.topn. [°C]	Wydajność [%]	Uwagi, literatura
D1	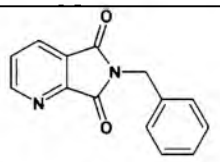	161-162	82,4	lit. t.topn. 162 °C [79]
D2	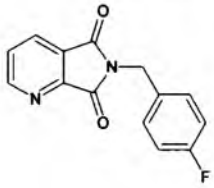	164-167	93,8	NP*
D3	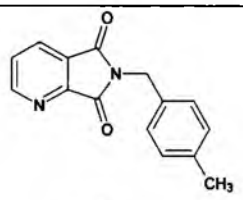	164-165	90,1	NP*
D4	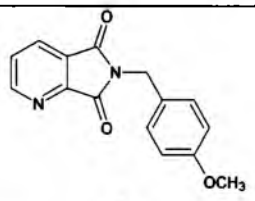	144-149	67,5	lit. t.topn. 130 °C [80]
D5	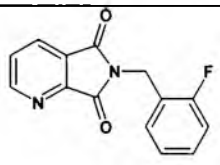	232-236	84,6	NP*

*NP – związek niepublikowany

Struktury otrzymanych związków zostały potwierdzone za pomocą widm ^{1}H NMR, ^{13}C NMR oraz spektrometrii mas (**Tabela 8**).

Tabela 8. Charakterystyka imidowych pochodnych **D1 - D5**

Nr	Wzór sumaryczny	^{1}H NMR, ^{13}C NMR, ESI-MS
D1	$C_{14}H_{10}N_2O_2$	**^{1}H NMR** (400 MHz, DMSO-d_6): δ 4.81 (s, 2H), 7.22-7.38 (m, 5H), 7.79 (dd, J = 7.7 Hz, 5.0 Hz, 1H), 8.32 (dd, J = 7.6 Hz, 1.5 Hz, 1H), 8.99 (dd, J = 5.0 Hz, 1.5 Hz, 1H); **^{13}C NMR** (100 MHz, DMSO-d_6): δ 40.9, 127.3, 127.4, 127.5, 127.9, 128.5, 131.4, 136.3, 151.4, 154.9, 166.1, 166.2; **ESI-MS** (+20V): m/z 238.93 $[M+H]^+$, 260.86 $[M+Na]^+$, 476.84 $[2M+H]^+$, 498.73 $[2M+Na]^+$
D2	$C_{14}H_9FN_2O_2$	**^{1}H NMR** (400 MHz, DMSO-d_6): δ 4.79 (s, 2H), 7.15 (t, J = 8.9 Hz, 2H), 7.40 (dd, J = 8.5 Hz, 5.6 Hz, 2H), 7.79 (dd, J = 7.6 Hz, 5.0 Hz, 1H), 8.31 (dd, J = 7.6 Hz, 1.3 Hz, 1H), 8.98 (dd, J = 4.9 Hz, 1.3 Hz, 1H); **^{13}C NMR** (100 MHz, DMSO-d_6): δ 40.3, 115.3 (d, $^2J_{C\text{-}F}$ = 21.4 Hz), 127.3, 127.9, 129.7 (d, $^3J_{C\text{-}F}$ = 8.3 Hz), 131.4, 132.6 (d, $^4J_{C\text{-}F}$ = 3.1 Hz), 151.5, 154.9, 161.5 (d, $^1J_{C\text{-}F}$ = 243.3 Hz), 166.1, 166.2; **ESI-MS** (+20V): m/z 257.26 $[M+H]^+$, 279.25 $[M+Na]^+$, 513.55 $[2M+H]^+$, 535.52 $[2M+Na]^+$
D3	$C_{15}H_{12}N_2O_2$	**^{1}H NMR** (400 MHz, DMSO-d_6): δ 2.25 (s, 3H), 4.76 (s, 2H), 7.12 (d, J = 7.9 Hz, 2H), 7.22 (d, J = 8.0 Hz, 2H), 7.79 (dd, J = 7.7 Hz, 5.0 Hz, 1H), 8.31 (dd, J = 7.7 Hz, 1.4 Hz, 1H), 8.98 (dd, J = 5.0 Hz, 1.4 Hz, 1H); **^{13}C NMR** (100 MHz, DMSO-d_6): δ 20.6, 40.7, 127.2, 127.5, 127.9, 129.0, 131.4, 133.4, 136.6, 151.4, 154.9, 166.0, 166.1; **ESI-MS** (+20V): m/z 252.89 $[M+H]^+$, 274.87 $[M+Na]^+$, 504.77 $[2M+H]^+$, 526.76 $[2M+Na]^+$
D4	$C_{15}H_{12}N_2O_3$	**^{1}H NMR** (400 MHz, DMSO-d_6): δ 3.71 (s, 3H), 4.73 (s, 2H), 6.88 (d, J = 8.3 Hz, 2H), 7.27 (d, J = 8.3 Hz, 2H), 7.78 (dd, J = 7.3 Hz, 5.1 Hz, 1H), 8.30 (d, J = 7.4 Hz, 1H), 8.97 (d, J = 4.4 Hz, 1H); **^{13}C NMR** (100 MHz, DMSO-d_6): δ 40.5, 55.1, 113.9, 127.3, 127.9, 128.4, 129.1, 131.4, 151.4, 154.9, 158.6, 166.1, 166.2; **ESI-MS** (+20V): m/z 269.40 $[M+H]^+$, 291.37 $[M+Na]^+$, 538.10 $[2M+H]^+$, 559.83 $[2M+Na]^+$
D5	$C_{14}H_9FN_2O_2$	**^{1}H NMR** (400 MHz, DMSO-d_6): δ 4.86 (s, 2H), 7.13-7.23 (m, 2H), 7.30-7.44 (m, 2H), 7.80 (dd, J = 7.7 Hz, 5.0 Hz, 1H), 8.33 (dd, J = 7.7 Hz, 1.5 Hz, 1H), 8.99 (dd, J = 5.0 Hz, 1.5 Hz, 1H); **^{13}C NMR** (100 MHz, DMSO-d_6): δ 35.1(d, $^3J_{C\text{-}F}$ = 4.9 Hz), 115.3 (d, $^2J_{C\text{-}F}$ = 21.1 Hz), 123.0 (d, $^2J_{C\text{-}F}$ = 14.4 Hz), 124.5 (d, $^4J_{C\text{-}F}$ = 3.5 Hz), 127.3, 128.0, 129.7 (d, $^3J_{C\text{-}F}$ = 8.2 Hz), 129.9 (d, $^3J_{C\text{-}F}$ = 3.8 Hz), 131.5, 151.4, 155.0, 159.9 (d, $^1J_{C\text{-}F}$ = 245.4 Hz), 165.9, 166.0; **ESI-MS** (+20V): m/z 257.48 $[M+H]^+$, 279.35 $[M+Na]^+$, 513.79 $[2M+H]^+$, 535.66 $[2M+Na]^+$

4.6. Badania krystalograficzne

W ramach współpracy z Zakładem Krystalografii UŚ przeprowadzono syntezy kilku związków kompleksowych kwasu 8-hydroksy-2-metylochinolino-7-karboksylowego **6** oraz 7-acetamido-2-metylo-5,8-chinolinodionu **13**, zawierających metale przejściowe: Ru, Re, Cu. Wzory strukturalne oraz struktury krystalograficzne otrzymanych kompleksów zamieszczone są w **Tabeli 9** [P5,P7-12,P14].

Tabela 9. Kompleksy metali przejściowych z ligandami **6** i **13**

Nr	Wzór strukturalny	Struktura krystalograficzna	Publikacja
E1	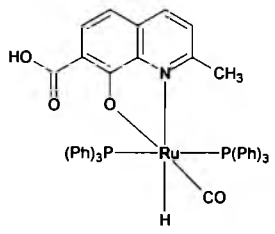	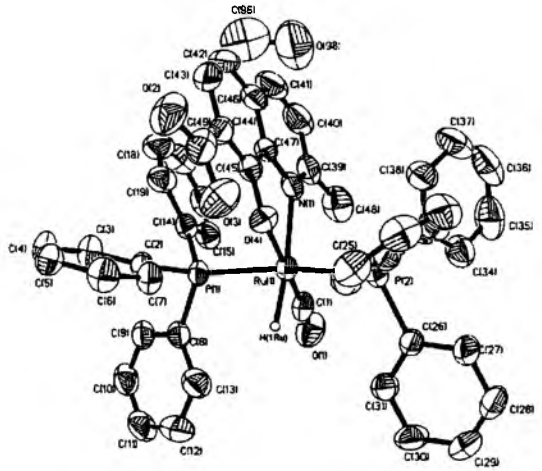	[P5]
E2	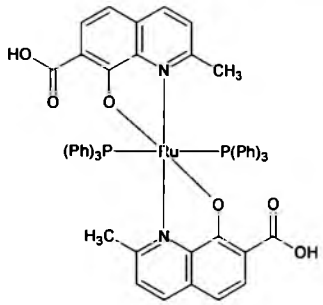	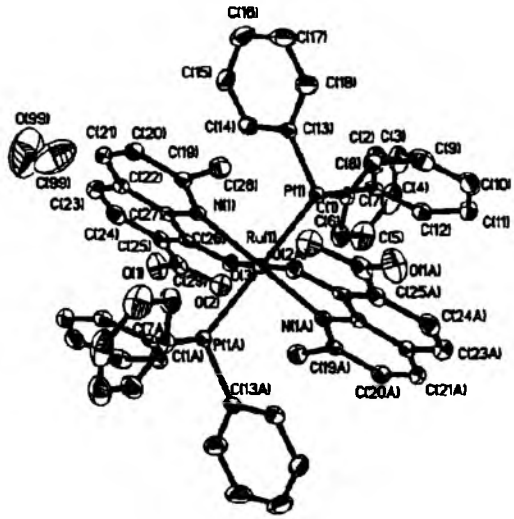	[P8]
E3	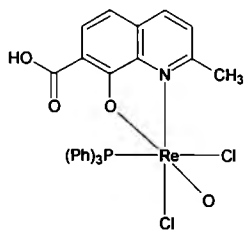	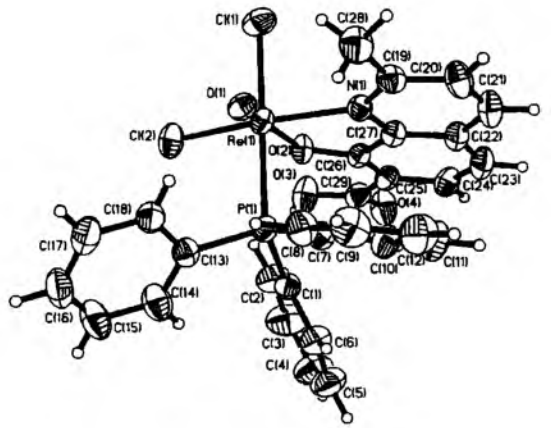	[P7]

E4	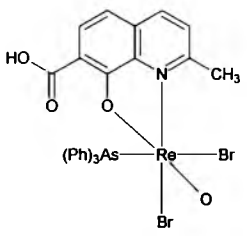	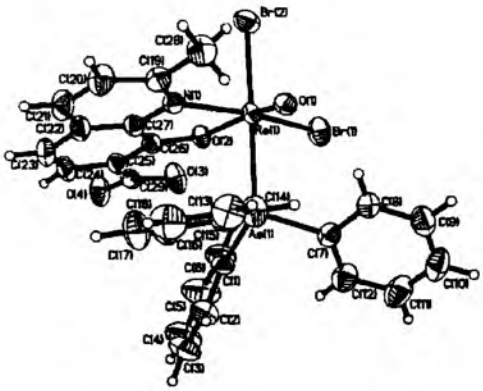	[P9]
E5	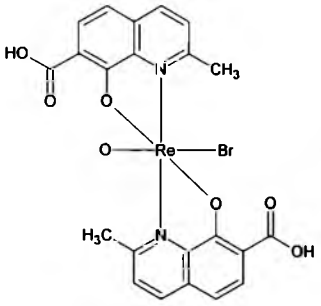	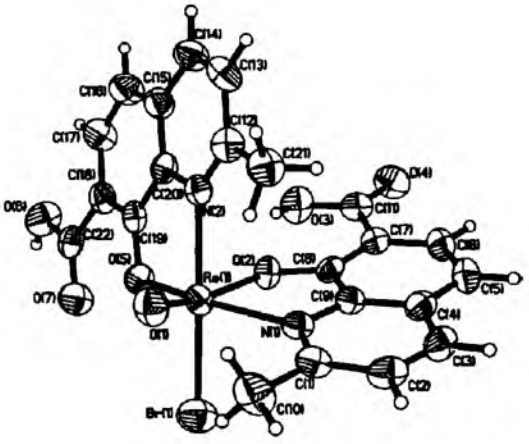	[P11]
E6	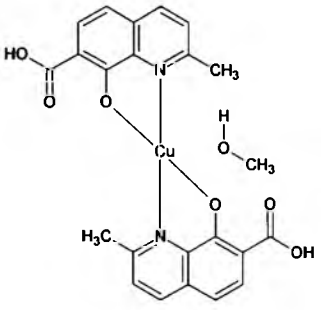	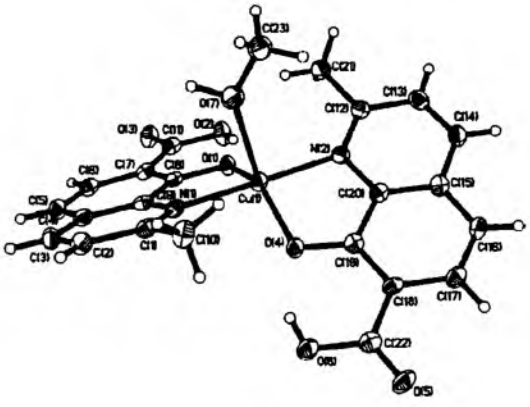	[P12]
E7	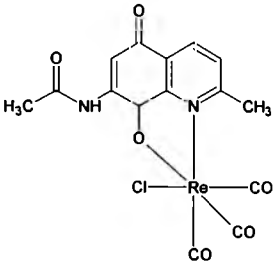	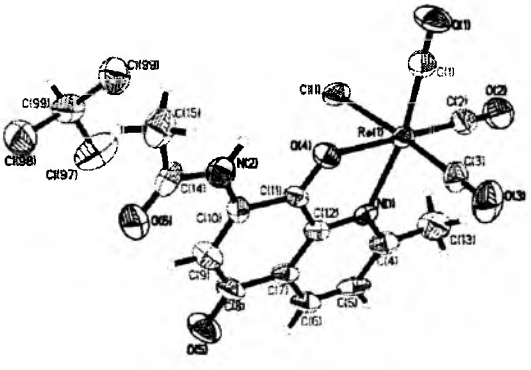	[P14]

4.7. Oznaczenia aktywności hamowania fotosyntezy

Otrzymane pochodne amidowe **A1 - A9, A12 - A16** zostały poddane badaniom hamowania procesów fotosyntezy u *Chlorella vulgaris Beij.* Oznaczenia wykonano w jednostkach współpracujących: Zentiva a.s., U Kabelovny 130, 102 37 Prague 10, Czechy oraz Institute of Chemistry, Faculty of Natura Sciences, Comenius University, Mlynska Dolina CH - 2,84215 Bratislava, Słowacja, zgodnie z procedurą opisaną w [81-82].

Wyniki przeprowadzonych badań przedstawia **Tabela 10.** Trzy spośród otrzymanych połączeń (**A3, A4, A6**) hamują fotosyntezę w stopniu porównywalnym z aktywnością wzorcowego herbicydu **DCMU** (diuronu) [P6].

Tabela 10. Aktywność hamowania fotosyntezy pochodnych **A1 - A9 i A12 - A16** [P6]

Nr	log K*	czystość [%]*	IC_{50} [µM/L]
A1	0,2812	91,17	17,2
A2	0,3389	91,48	158
A3	0,3793	91,30	7,2
A4	0,2843	91,22	4,8
A5	0,2404	90,81	b
A6	0,5075	93,31	8,5
A7	0,3342	91,56	15,9
A8	0,1109	91,47	93,7
A9	0,1168	92,06	149
A12	0,6361	94,17	n/a
A13	0,4021	99,37	n/a
A14	0,4136	96,22	n/a
A15	0,4304	99,30	n/a
A16	0,4087	98,74	n/a
DCMU	—	—	7.3

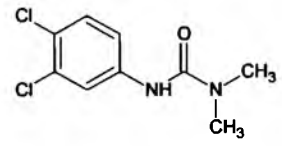

DCMU

* - oznaczono metodami HPLC

b - aktywność nie została oznaczona ze względu na słabą rozpuszczalność

W **Tabeli 10** podano również wartości log K, czyli miarę hydrofobowości badanych pochodnych. Wartość ta wyznaczona została metodami RP - HPLC, na podstawie uzyskanych czasów retencji [48,83-84]. Zależności pomiędzy strukturą, a aktywnością otrzymanych połączeń opisałem w publikacji [P6].

5. Podsumowanie

W ramach przeprowadzonych prac P1 - P16 oraz badań do tej pory nieopublikowanych zsyntezowałem i scharakteryzowałem 20 amidowych pochodnych kwasu 8-hydroksy-2-metylochinolino-7-karboksylowego, 5 N-podstawionych pochodnych 2,5-pirolidynodionu, 5 N-podstawionych pochodnych pirolo[3,4-g]chinolino-6,8-dionu oraz 5 pochodnych pirolo[3,4-b]pirydyno-5,7-dionu. Budowę wszystkich otrzymanych związków potwierdziłem za pomocą metod spektroskopowych ^{1}H NMR, ^{13}C NMR, IR oraz za pomocą spektrometrii mas (ESI-MS) lub też analizy elementarnej. Większość otrzymanych związków nie została wcześniej opisana w literaturze chemicznej.

Uzyskane pochodne amidowe kwasu 8-hydroksychinaldyno-7-karboksylowego zostały poddane badaniom na aktywność antywirusową in vitro. Jeden z otrzymanych związków wykazał umiarkowaną aktywność wobec integrazy HIV. Trzy inne okazały się inhibitorami procesów fotosyntezy u *Chlorella vulgaris Beij.*

W trakcie wykonywanych syntez, po stwierdzeniu trudności z charakteryzacją spektroskopową powstałych produktów reakcji, wykorzystałem badania krystalograficzne kompleksów otrzymanych związków z niektórymi metalami przejściowymi jako źródło danych o strukturach nowych ligandów.

6. Literatura

[1] Stryer L. *Biochemia*, Wydawnictwo Naukowe PWN, Warszawa, 1999, 410-412

[2] Stryer L. *Biochemia*, Wydawnictwo Naukowe PWN, Warszawa, 1999, 888-892

[3] Virella G. *Mikrobiologia i choroby zakaźne*, Wydawnictwo Medyczne Urban & Partner, Wrocław, 2000, 252-253

[4] Marchand C., Johnson A. A., Semenova E., Pommier Y. *Mechanisms and inhibition of HIV integration,* Drug Discovery Today: Disease Mechanisms, 2006, **3**, 253-260

[5] Pommier Y., Johnson A. A., Marchand C. *Integrase inhibitors to treat HIV / AIDS,* Nature Reviews Drug Discovery, 2005, **4**, 236-248

[6] De Clercq E., *Anti-HIV chemotherapy: current state of the art*, Med. Chem. Res., 2004, **13**, 439-478

[7] De Clercq E., *HIV - chemotherapy and - prophylaxis: new drugs, leads and approaches*, The International Journal of Biochemistry & Cell Biology, 2004, **36**, 1800-1822

[8] Chiu T. K., Davies D. R., *Structure and Function of HIV-1 Integrase: An Update*, Frontiers in Medicinal Chemistry, 2006, **3**, 1-19

[9] Greenwald J., Le V., Butler S. L., Bushman F. D., Choe S., *Mobility of the HIV-1 integrase active site loop is important for catalytic activity*, Biochemistry, 1999, **38**, 8892-8898

[10] Sechi M., Bacchi A., Carcelli M., Compari C., Duce E., Fisicaro E., Rogolino D., Gates P., Derudas M., Al - Mawsawi L. Q., Neamati N., *From Ligand to Complexes: Inhibition of Human Immunodeficiency Virus Type 1 Integrase by β - Diketo Acid Metal Complexes*, J. Med. Chem., 2006, **49**, 4248-4260

[11] Esposito D., Craigie R., *HIV integrase structure and function*, Adv. Virus Res., 1999, **52**, 319-333

[12] Chiu T. K., Davies D. R., *Structure and function of HIV-1 integrase*, Curr. Top. Med. Chem., 2004, **4**, 671-686

[13] Kawasuji T., Fuji M., Yoshinaga T., Sato A., Fujiwara T., Kiyama R., *A platform for designing HIV integrase inhibitors. Part 2: A two - metal binding model as a potential mechanism of HIV integrase inhibitors*, Bioorganic & Medicinal Chemistry, 2006 **14**, 8420-8429

[14] Grobler J. A., Stillmock K., Hu B., Witmer M., Felock P., Espeseth A. S., Wolfe A., Egbertson M., Bourgeois M., Melamed J., Wai J. S., Young S., Vacca J., Hazuda D. J., *Diketo acid inhibitor mechanism and HIV-1 integrase: Implications for metal binding in the active site of phosphotransferase enzymes*, Proc. Natl. Acad. Sci. U.S.A., 2002, **99**, 6661-6666

[15] Long Y. Q., Jiang X. H., Dayam R., Sanchez T., Shomaker R., Sei S., Neamati N., *Rational design and synthesis of novel dimeric diketoacid - containing inhibitors of HIV-1 integrase: Implication for binding to two metal ions on the active site of integrase*, J. Med. Chem., 2004, **47**, 2561-2573

[16] Cotelle P., *Patented HIV-1 Integrase Inhibitors (1998 - 2005)*, Recent Patents on Anti - Infective Drug Discovery, 2006, **1**, 1-15

[17] Hazuda D. J., Felock P., Witmer M., Wolfe A., Stillmock K., Grobler J. A., Espeseth A., Gabryelski L., Schleif W., Blau C., Miller M. D., *Inhibitors of strand transfer that prevent integration and inhibit HIV-1 replication in cells*, Science, 2000, **28**, 7646-7650

[18] Johnson A. A., Marchand C., Pommier Y., *HIV-1 integrase inhibitors: A decade of research and two drugs in clinical trial*, Curr. Top. Med. Chem., 2004, **4**, 1059-1067

[19] Nair V., Chi G., *HIV integrase inhibitors as therapeutic agents in AIDS*, Rev. Med. Virol. 2007, **17**, 277-295

[20] Marchand C., Maddali K., Metifiot M., Pommier Y., *HIV-1 IN inhibitors : 2010 update and perspectives*, Curr. Top. Med. Chem., 2009, **9**, 1016-1037

[21] Pannecouque C., Pluymers W., Van Maele B., Tetz V., Cherepanov P., De Clercq E., Witvrouw M., Debyser Z., *New class of HIV integrase inhibitors that block viral replication in cell culture*, Curr. Biol., 2002, **12**, 1169-1177

[22] Mekouar K., Mouscadet J. F., Desmaële D., Subra F., Leh H., Savouré D., Auclair C., d'Angelo J., *Styrylquinoline Derivatives: A New Class of Potent HIV-1 Integrase Inhibitors That Block HIV - 1 Replication in CEM Cells*, J. Med. Chem., 1998, **41**, 2846-2857

[23] Ouali M., Laboulais C., Leh H., Gill D., Desmaële D., Mekouar K., Zouhiri F., d'Angelo J., Auclair C., Mouscadet J.F., Le Bret M., *Modeling of the Inhibition of Retroviral Integrases by Styrylquinoline Derivatives*, J. Med. Chem., 2000, **43**, 1949-1957

[24] Zouhiri F., Mouscadet J. F., Mekouar K., Desmaële D., Savouré D., Leh H., Subra F., Le Bret M., Auclair C., d'Angelo J., *Structure - Activity Relationships and Binding Mode of Styrylquinolines as Potent Inhibitors of HIV - 1 Integrase and Replication of HIV-1 in Cell Culture*, J. Med. Chem., 2000, **43**, 1533-1540

[25] Zouhiri F., Desmaële D., d'Angelo J., Ourevitch M., Mouscadet J.F., Leh H., Le Bret M., *HIV-1 replication inhibitors of the styrylquinoline class: incorporation of a masked diketo acid pharmacophore*, Tetrahedron Lett., 2001, **42**, 8189-8192

[26] Polanski J., Zouhiri F., Jeanson L., Desmaele D., d'Angelo J., Mouscadet J. F., Gieleciak R., Gasteiger J., Le Bret M., *Use of the Kohonen neural network for rapid screening of ex vivo anti-HIV acivity of styrquinolines*, J. Med. Chem., 2002, **45**, 4647-4654

[27] Deprez E., Barbe S., Kolaski M., Leh H., Zouhiri F., Auclair C., Brochon J. C., Le Bret M., Mouscadet J. F., *Mechanism of HIV - 1 integrase inhibition by styrylquinoline derivatives in vitro*, Mol. Pharmacol., 2004, **65**, 85-98

[28] Benard Ch., Zouhiri F., Normand - Bayle M., Danet M., Desmaele D., Leh H., Mouscadet J. F., Mbemba G., Thomas C. M., Bonnenfant S., Le Bret M., d'Angelo J., *Linker - modified quinoline derivatives targeting HIV-1 integrase: Synthesis and biological activity*, Bioorg. Med, Chem. Lett., 2004, **14**, 2473-2476

[29] d'Angelo J., Mouscadet J. F., Desmaele D., Zouhiri F., Leh H., *HIV-1 integrase: The next target for AIDS therapy?*, Pathol. Biol., 2001, **49**, 237-246

[30] Normand - Bayle M., Benard Ch., Zouhiri F., Mouscadet J. F., Leh H., Thomas C. M., Mbemba G., Desmaele D., d'Angelo J., *New HIV-1 replication inhibitors of the styrylquinoline class bearing aroyl/acyl groups at the C-7 position: Synthesis and biological activity*, Bioorg. Med, Chem. Lett., 2005, **15**, 4019-4022

[31] Zouhiri F., Danet M., Benard Ch., Normand – Bayle M., Mouscadet J. F., Leh H., Thomas C. M., Mbemba G., d'Angelo J., Desmaele D., *New HIV-1 replication inhibitors of the styrylquinoline class: Intoduction of an additional carboxyl group at the C-5 position of the quinoline*, Tetrahedron Lett., 2005, **46**, 2201-2205

[32] Sato M., Motomura T., Aramaki H., Matsuda T., Yamashita M., Ito Y., Kawakami H., Matsuzaki Y., Watanabe W., Yamataka K., Ikeda S., Kodama E., Matsuoka M., Shinkai H., *Novel HIV-1 Integrase Inhibitors Derrived from Quinolone Antibiotics*, J. Med. Chem. 2006, **49**, 1506-1508

[33] Pais G. C. G., Burke T. R., *Novel aryl diketo - containing inhibitors of HIV-1 integrase*, Drugs Future, 2002, **27**, 1101-1111

[34] Wai J. S., Egbertson M. S., Payne L. S., Fisher T. E., Embrey M. W., Tran L. O., Melamed J. Y., Langford H. M., Guare J. P., Zhutang L., Grey V. E., Vacca J. P., Holloway M. K., Naylor - Olsen A. M., Hazuda D. J., Felock P. J., Wolfe A. L., Stillmock K. A., Schleif W. A., Gabryelski L. J., Young S. D., *4 - Aryl - 2,4 - dioksobutanoic acid inhibitors of HIV-1 integrase and viral replication in cells*, J. Med. Chem., 2000, **43**, 4923-4926

[35] Pluymers W., Pais G., Van Maele B., Pannecouque C., Fikkert V., Burke T. R., De Clercq E., Witvrouw M., Neamati N., Debyser Z., *Inhibition of HIV-1 integration by diketo derivatives*, Antimicrob. Agents Chemother., 2002, **46**, 3292-3297

[36] Pais G. C. G., Zhang X., Marchand C., Neamati N., Cowansage K., Svarovskaia E. S., Pathak V. K., Tang Y., Nicklaus M., Pommier Y., Burke T. R., *Structure activity of 3 - aryl - 1,3 - diketo containing compounds as HIV-1 integrase inhibitors*, J. Med. Chem., 2002, **45**, 3184-3194

[37] Marchand C., Zhang X., Pais G. C. G., Cowansage K., Neamati N., Burke T. R., Pommier Y., *Structural determinants for HIV-1 integrase inhibition by β - diketo acids*, J. Biol. Chem., 2002, **277**, 12596-12603

[38] Sechi M., Derudas M., Dallocchio R., Dessi A., Bacchi A., Sannia L., Carta F., Palomba M., Ragab O., Chan C., Shoemaker R., Sei S., Dayam R., Neamati N., *Design and synthesis of novel indole β - diketo acid derivatives as HIV-1 integrase inhibitors*, J. Med. Chem., 2004, **47**, 5298-5310

[39] Walker M. A., Johnson T., Ma Z., Zhang Y., Banville J., Remillard R., Plamondon S., Pendri A., Wong H., Smith D., Torri A., Samanta H., Lin Z., Demine C., Terry B., Krystal M., Meanwell N., *Exploration of the diketoacid integrase inhibitor chemotype leading to the discovery of the anilide – ketoacids chemotype*, Bioorg. & Med. Chem. Lett., 2006, **16**, 5818-5821

[40] Zhang X., Pais G. C. G., Svarovskaia S., Marchand C., Johnson A. A., Karki R. G., Nicklaus M. C., Pathak V. K., Pommier Y., Burke T. R., *Azido containing Aryl β - Diketo Acid HIV-1 Integrase Inhibitors*, Bioorg. & Med. Chem. Lett., 2003, **13**, 1215-1219

[41] Kawasuji T., Yoshinaga T., Sato A., Yodo M., Fujiwara T., Kiyama R., *A platform for designing HIV integrase inhibitors. Part 1: 2-hydroxy-3-heteroaryl acrylic acid derivatives as novel HIV integrase inhibitor and modeling of hydrophilic and hydrophobic pharmacophores*, Bioorg. & Med. Chem., 2006 **14**, 8430-8445

[42] Goldgur Y., Craigie R., Cohen G. H., Fujiwara T., Yoshinaga T., Fujishita T., Sugimoto H., Endo T., Murai H., Davies D. R., *Structure of the HIV-1 integrase catalytic domain complexed with an inhibitor: A platform for antivirial drug design*, Proc. Natl. Acad. Sci. USA., 1999, **96**, 13040-13043

[43] Guare J. P., Wai J. S., Gomez R. P., Anthony N. J., Jolly S. M., Cortez A. R., Vacca J. P., Felock P. J., Stillmock K. A., Schleif W. A., Moyer G., Gabryelski L. J., Jin L., Chen I. W., Hazuda D. J., Young S. D., *A series of 5 - amino substituted 4 - fluorobenzyl - 8 - hydroxy - [1,6] naphthyridine - 7 - carboxamide HIV-1 integrase inhibitors*, Bioorg. & Med. Chem. Lett. 2006, **16**, 2900-2904

[44] Li H., Wang C., Sanchez T., Tan Y., Jiang C., Neamati N., Zhao G., *Amide-containing diketoacids as HIV-1 integrase inhibitors: Synthesis, structure-activity relationship analysis, and biological activity*, Bioorg. & Med. Chem., 2009, **17**, 2913-2919

[45] *Chemia Leków*, pod red. A. Zejca i M. Gorczycy, wyd II, PZWL, Warszawa, 2002

[46] Jampilek J., Dolezal M., Kunes J., Buchta V., Karlova K., *Quinaldine derivatives: Preparation and biological* activity, Med. Chem., 2005, **1**, 591-599

[47] Harris C. R., Thorarensen A., *Advances in the discovery of novel antibacterial agents during the year 2002*, Curr. Med. Chem., 2004, **11**, 2213-2243

[48] Musioł R., Jampilek J., Buchta V., Silva L., Niedbała H., Podeszwa B., Pałka A., Majerz - Maniecka K., Oleksyn B., Polański J., *Antifungal properties of new series of quinoline derivatives*, Bioorg. & Med. Chem., 2006, **14**, 3592-3598

[49] Gershon H., Gershon M., Clarke D. D., *Synergistic mixtures of fungitoxic monochloro and dichloro-8-quinolinols against five fungi*, Mycopathologia, 2004, **158**, 131-135

[50] Dardari Z., Lemrani M., Bahloul A., Sebban A., Hassar M., Kitane S., Berrada M., Boudouma M., *Antileishmanial activity of a new 8-hydroxyquinoline derivative designed 7-[5'-(3'-phenylisoxazolino)methyl]-8-hydroxyquinoline: preliminary study*, Farmaco 2004, **59**, 195-199

[51] Musioł R., Serda M., Hensel-Bielówka S., Polański J., *Quinoline-based antifungals*, Curr. Med. Chem., 2010, **17**, 1960-1973

[52] Franck X., Fournet A., Prina E., Mahieux R., Hocquemiller R., Figadere B., *Biological evaluation of substituted quinolines*, Bioorg. & Med. Chem. Lett., 2004, **14**, 3635-3638

[53] Andries K., Verhasselt P., Guillemont J., Gohlmann H. W., Neefs J. M., Winkler H., Van Gestel J., Timmerman P., Zhu M., Lee E., Williams P., de Chaffoy D., Huitric E., Hoffner S., Cambau E., Truffot - Pernot C., Lounis N., Jarlier V., *A Diarylquinoline Drug Active on the ATP Synthase of Mycobacterium tuberculosis*, Science, 2005, **307**, 223-227

[54] Vangapandu S., Jain M., Jain R., Kaur S., Singh P. P., *Ring-substituted quinolines as potential anti-tuberculosis agents*, Bioorg. Med. Chem., 2004, **12**, 2501-2508

[55] Montgomery G. J., McKeown P., McGown A. T., Robins D. J., *Synthesis and antiproliferative activity of unsaturated quinoline derivatives*, Anti-Cancer Drug Design, 2000, **15**, 171-181

[56] Sissi C., Palumbo M., *The quinolone family: from antibacterial to anticancer agents*, Curr. Med. Chem. Anti-Canc. Agents, 2003, **3**, 439-450

[57] Podeszwa B., Niedbala H., Polanski J., Musiol R., Tabak D., Finster J., Serafin K., Milczarek M., Wietrzyk J., Boryczka S., Mol W., Jampilek J., Dohnal J., Kalinowski D. S., Richardson D. R., *Investigating the Antiproliferative Activity of Quinoline-5,8-diones and Styrylquinolinecarboxylic Acids on Tumour Cell Lines*, Bioorg. Med. Chem. Lett., 2007, **17**, 6138-6141

[58] Musioł R., Jampilek J., Kralova K., Richardson D. R., Kalinowski D., Podeszwa B., Finster J., Niedbała H., Pałka A., Polański J., *Investigating biological activity spectrum for novel quinoline analogues*, Bioorg. Med. Chem., 2007, **15**, 1280-1288

[59] Polański J., Niedbała H., Musioł R., Podeszwa B., Tabak D., Pałka A., Mencel A., Finster J., Mouscadet J. F., Le Bret M., *5 - hydroxy - 6 - quinaldic acid as a novel molecular scaffold for HIV-1 integrase inhibitors*, Lett. Drug. Des. Discov., 2006, **3**, 175-178

[60] Zhuang L., Wai J. S., Embrey M. W., Fisher T. E., Egbertson M. S., Payne L. S., Guare J. P., Vacca J. P., Hazuda D. J., Felock P. J., Wolfe A. L., Stillmock K. A., Witmer M. V., Moyer G., Schleif W. A., Gabryelski L. J., Leonard Y. M., Lynch J. J., Michelson S. R., Young S. D. J., *Design and synthesis of 8-hydroxy - [1,6] naphthyridines as novel inhibitors of hiv-1 integrase in vitro and in infected cells*, Med. Chem., 2003, **46**, 453-456

[61] Boger D. L., Yasuda M., Mitscher L. A., Drake S. D., Kitos P. A., Thompson S. C., *Streptonigrin and lavendamycin partial structures. Probes for the minimum, potent pharmacophore of streptonigrin, lavendamycin, and synthetic quinoline-5,8-diones*, J. Med. Chem., 1987, **30**, 1918-1928

[62] Behforouz M., Behforouz N. C., *Lavendamycin analogs, quinoline-5,8-diones and methods of using them*, US 6,444,684 B1, 2002

[63] Podeszwa B., *Synteza wybranych pochodnych 7-amino-2-metylo-5,8-chinolinodionu w poszukiwaniu nowych inhibitorów integrazy HIV*, praca doktorska UŚ, Katowice 2006

[64] Kanamori D., Okamura T., Yamamoto H., Ueyama N., *Linear - to - turn conformational switching induced by deprotonation of usymmetrically linked phenolic oligoamides*, Angew. Chem. Int. Ed., 2005, **44**, 969-972

[65] Steinwender E., Mikenda W., *OH...O(S) Hydrogen Bonds in 2-hydroxy(thio)benzamides. Survey of spectroscopic and structural* data, Monatsh. Chem., 1990, **121**, 809-820

[66] Kondo M., *The nuclear magnetic resonance study of several o-disubstituted* benzenes, Bull. Chem. Soc. Jpn., 1972, **45**, 2790-2793

[67] Kanamori D., Furukawa A., Okamura T., Yamamoto H., Ueyama N., *Contribution of the intramolecular hydrogen bond to the shift of the pKa value and the oxidation potential of phenols and phenolate anions*, Org. Biomol. Chem., 2005, **3**, 1453-1459

[68] Mock W. L., Chua D. C. Y., *Exceptional active site H-bonding in enzymes? Significance of the oxyanion hole in the serine proteases from a model study*, J. Chem. Soc. Perkin Trans., 1995, **2**, 2069-2074

[69] Kanamori D., Okamura T., Yamamoto H., Shimizu S., Tujimoto Y., Ueyama N., *Structures of the Small-Molecule Bcl-2 Inhibitor (BH3I-2) and Its Related Simple Model in Protonated and Deprotonated Forms*, Bull. Chem. Soc. Jpn., 2004, **77**, 2057-2064

[70] Verschueren W. G., Dierynck I., Amssoms K. I. E., Hu L., Boonants P. M. J. G., Pille G. M. E., Daeyaert F. F. D., Hertogs K., Surleraux D. L. N. G., Wigerinck P. B. T. P., *Design and optimization of tricyclic phtalimide analogues as novel inhibitors of HIV-1 integrase*, J. Med. Chem., 2005, **48**, 1930-1940

[71] Metobo S. E., Jin H., Tsiang M., Kim C. U., *Design, synthesis and biological evaluation of novel tricyclic HIV-1 integrase inhibitors by modification of its pyridine ring*, Bioorg. & Med. Chem. Lett., 2006, **16**, 3985-3988

[72] Jin H., Cai R. Z., Schacherer L., Jabri S., Tsiang M., Fardis M., Chen X., Chen J. M., Kim C. U., *Design, synthesis and SAR studies of novel and highly active tri - cyclic HIV integrase inhibitors,* Bioorg. & Med. Chem. Lett., 2006, **16**, 3989-3992

[73] Fardis M., Jin H., Jabri S., Cai R. Z., Mish M., Tsiang M., Kim C. U., *Effect of substitution of novel tricyclic HIV-1 integrase inhibitors*, Bioorg. & Med. Chem. Lett., 2006, **16**, 4031-4035

[74] Burnett D. A., Hart D. J., *Conformational effects on the oxidative coupling of benzyltetrahydroisoquinolines to morphinane and aporphine alkaloids*, J. Org. Chem., 1987, **52**, 5662-5667

[75] Murray W. M., Semple J. E., *Facile access to novel 1,4-dihydroxynaphtalene 2,3-dicarboximides and heterofused analogs*, Synthesis, 1996, **10**, 1180-1182

[76] Jaśkowska J. Kowalski P., N-*Alkylation of imides using phase transfer catalysts under solvent-free conditions*, J. Heterocyclic Chem., 2008, **45**, 1371-1375

[77] Zhang J., Senthilkumar M., Ghosh S. C., Hong S. H., *Synthesis of cyclic imides from simple diols*, Angew. Chem. Int. Ed., 2010, **49**, 6391-6395

[78] Cai Z.R., Chen X., Fardis M., Jabri S. Y., Jin H., Kim C. U., Metobo S. E., Mish M. R., Pastor R. M., *Phosphonate analogs of HIV integrase inhibitor compounds*, WO2005/117904 A2, 2005

[79] Blanco M. M., Levin G. J., Schapira C. B., Perillo I. A., *Improved synthesis of N-substituted 2,3-pyridine-dicarboximides with microwave irradiation*, Heterocycles, 2002, **57**, 1881-1890

[80] Pin F., Comesse S., Garrigues B., Marchalin S., Daich A., *Intermolecular and Intramolecular α-Amidoalkylation Reactions Using Bismuth Triflate as the Catalyst*, J. Org. Chem., 2007, **72**, 1181-1191

[81] Kralowa K., Sersen F., Mielnik M., *Inhibition of photosynthesis in Chlorella vulgaris by Cu(II) complexes with biologically active ligands*, J. Trace Microprobe Techn., 1998, **16**, 491-500

[82] Wellburn A. R., *The spectral determination of chlorophylls with spectrophotometers of different resolution,* J. Plant. Phsiol., 1994, **144**, 307-313

[83] Valko K., *Application of high-performance liquid chromatography based measurements of lipophilicity to model biological distribution*, J. Chromatogr. A., 2004, **1037**, 299-310

[84] Gocan S., Cimpan G., Comer J., *Lipophilicity measurements by liquid chromatography*, J., Adv. Chromatogr., 2006, **44**, 79-176

7. Dorobek naukowy

7.1. Wykaz publikacji

1. Polanski J., Niedbala H., Musiol R., Tabak D., Podeszwa B., Gieleciak R., Bak A., Palka A., Magdziarz T., *Analogues of the styryquinoline and styrylquinazoline HIV-1 integrase inhibitors: Design and synthetic problems*, Acta Poloniae Pharm. Drug Res., 2004, **61**, 3-4
2. Polanski J., Niedbala H., Musiol R., Podeszwa B., Tabak D., Palka A., Mencel A., Finster J., Mouscadet J. F., Le Bret M., *5-hydroxy-6-quinaldic acid as a novel molecular scaffold for HIV-1 integrase inhibitors*, Lett. Drug Des. Discov., 2006, **3**, 175-178
3. Niedbala H., Polanski J., Gieleciak R., Musiol R., Tabak D., Podeszwa B., Bak A., Palka A., Mouscadet J. F., Gasteiger J., Le Bret M., *Comparative molecular surface analysis (CoMSA) for virtual combinatorial library screening of styrlquinoline HIV-1 blocking agents*, Comb. Chem. High Throughput Screen, 2006, **9**, 753-770
4. Polanski J., Niedbala H., Musiol R., Podeszwa B., Tabak D., Palka A., Mencel A., Mouscadet J. F., Le Bret M., *Fragment based approach for the investigation of HIV-1 integrase inhibition*, Lett. Drug Des. Discov., 2007, **4**, 99-105
5. Podeszwa B., Niedbala H., Polanski J., Musiol R., Tabak D., Finster J., Serafin K., Milczarek M., Wietrzyk J., Boryczka S., Mol W., Jampilek J., Dohnal J., Kalinowski D. S., Richardson D. R., *Investigating the Antiproliferative Activity of Quinoline-5,8-diones and Styrylquinolinecarboxylic Acids on Tumour Cell Lines*, Bioorg. Med. Chem. Lett., 2007, **17**, 6138-6141.
6. Malecki J. G., Kruszynski R., Tabak D., Kusz J., *The reactions between $[RuHCl(CO)(PPh_3)_3$ and quinoline carboxylic acids*, Polyhedron, 2007, **26** , 5120-30
7. Musiol R., Tabak D., Niedbala H., Podeszwa B., Jampilek J., Kralova K., Dohnal J., Finster J., Mencel A., Polanski J., *Investigating biological activity spectrum for novel quinoline analogues 2: hydroxyquinolinecarboxamides with photosynthesis inhibiting activity*, Bioorg. Med. Chem., 2008, **16**, 4490-4499
8. Machura B., Milek J., Kusz J., Nycz J., Tabak D., *Reactivity of oxorhenium(V) complexes towards quinoline carboxylic acids. X-ray structure of $[ReOCl_2$(hquin-7-COOH)$(PPh_3)]\cdot PPh_3$, $[ReOBr_2$(hquin-7-COOH)$(PPh_3)]$ and $[ReOX_2$(hmquin-7-COOH)$(PPh_3)]$. DFT and TD-DFT calculations for $[ReOCl_2$(hquin-7-COOH)$(PPh_3)]$*, Polyhedron, 2008, **27**, 1121-1130
9. Malecki J. G., Kusz J., Kruszynski R., Tabak D., Mazurak Z., *The reaction between $[RuCl_2(PPh_3)_3]$ and hydroxyquinoline carboxylic acid*, Structural Chemistry, 2008, **19**, 257-263.

10. Jampilek J., Musiol R., Pesko M., Kralova K., Vejsova M., Carroll J., Coffey A., Finster J., Tabak D., Niedbala H., Kozik V., Polanski J., Csollei J., Dohnal J., *Ring-substituted 4-hydroxy-1H-quinolin-2-ones: Preparation and biological activity*, Molecules, 2009, **14**, 1145-1159

11. Machura B., Kusz J., Tabak D., *Synthesis, spectroscopic characterization, X-ray structure, and DFT calculations of [$ReOBr_2$(hmquin-7-COOH)($AsPh_3$)]*, Structural Chemistry, 2009, **20**, 361-368

12. Musiol R., Jampilek J., Podeszwa B., Finster J., Tabak D., Dohnal J., Polanski J., *RP-HPLC determination of lipophilicity in series of quinoline derivatives*, Cent. Eur. J. Chem., 2009, **7**, 586-597

13. Machura B., Kusz J., Tabak D., Kruszynski R., *Synthesis, spectroscopic characterization, crystal and molecular structure of [ReOBr(hmquin-7-COOH)$_2$] and [ReOCl(hmquin-7-COOH)$_2$]·MeCN complexes. DFT and TD-DFT calculations for [ReOBr(hmquin-7-COOH)$_2$]*, Polyhedron, 2009, **28**, 493-500

14. Machura B., Świtlicka A., Mroziński J., Kłak J., Kruszynski R., Kusz J., Tabak D., *Synthesis, spectroscopic characterization, X-ray structure and magnetic properties of [Cu(hmquin-7-COOH)$_2$(MeOH)] complex*, Polyhedron, 2009, **28**, 3774-3780

15. Majerz-Maniecka K., Musiol R., Skórska-Stania A., Tabak D., Mazur P., Oleksyn B.J., Polański J. *X-ray and molecular modelling in fragment-based design of three small quinoline scaffolds for HIV integrase inhibitors*, Bioorg. Med. Chem., 2011, **19**, 1606-12

16. Machura B., Świtlicka A., Wolff M., Tabak D., Musioł R., Polański J., Kruszyński R., *Novel tricarbonyl rhenium complexes of 5,8-quinolinedione derivatives - synthesis, spectroscopic characterisation, X-ray structure and DFT calculations*, Journal of Organometallic Chemistry, 2011, **696**, 731-738.

17. Machura B., Wolff M., Tabak D., Ikeda Y., Hasegawa K., *Novel trans-dioxorhenium complex with imidazo[1,2a]pyridine ligand – Synthesis, spectroscopic and electrochemical characterization, X-ray crystal structure and DFT calculations*, Polyhedron, 2012, **39**, 76-84

18. Machura B., Wolff M., Tabak D., Schachner J. A., Mosch-Zanetti N. C., *Oxidorhenium(V) complexes with phenolate- and carboxylate-based ligands: Structure and catalytic epoxidation*, Eur. J. Inorg. Chem, 2012, **23**, 3764-3773

7.2. Wykaz patentów i zgłoszeń patentowych

1. Niedbała H., Musioł R., Pałka A., Podeszwa B., Mencel A., Tabak D., Polański J., Finster J., *Nowe inhibitory integrazy HIV, ich prekursory oraz ich stosowanie*, PL 371824, 2006-06-26
2. Niedbała H., Musioł R., Pałka A., Podeszwa B., Mencel A., Tabak D., Polański J., Finster J., *Sposób oczyszczania amidów kwasów chinaldynokarboksylowych*, PL 374130, 2006-10-16, PL 207140, 2010-11-30
3. Musioł R., Jampilek J., Buchta V., Kralova K., Finster J., Podeszwa B., Tabak D., Polański J., *Analogi chinazoliny jako fungicydy i herbicydy oraz ich zastosowanie*, PL 379252, 2007-10-01
4. Musioł R., Mrozek A., Finster J., Tabak D., Szurko A., Polański J., Ratuszna A., *Pochodne chinazoliny i ich zastosowanie*, PL 388641, 2011-01-31
5. Musioł R., Niedbała H., Pałka A., Podeszwa B., Finster J., Mencel A., Serafin K., Tabak D., Polański J., *Amidy heterocykliczne hamujące działanie integrazy HIV oraz ich zastosowanie*, PL 379432, 2007-10-15, PL 210315, 2012-01-31
6. Podeszwa B., Musioł R., Tabak D., Finster J., Polański J., Niedbała H., Pałka A., *2-oksoamidy jako inhibitory integrazy HIV, ich prekursory oraz ich zastosowanie*, PL 380818, 2008-04-14, PL 210314, 2012-01-31
7. Musioł R., Podeszwa B., Tabak D., Finster J., Niedbała H., Polański J., *Nowe związki o działaniu antyproliferacyjnym, ich prekursory oraz ich zastosowanie do hamowania rozwoju komórek nowotworowych*, PL 382828, 2009-01-05, PL 213476, 2013-03-29

7.3. Udział w konferencjach

1. Niedbała H., Polański J., Tabak D., *Synteza nowych potencjalnych inhibitorów integrazy wirusa HIV*, XVIII Ogólnopolska Szkoła Chemii Wiosna 2003, Kudowa Zdrój, 29 04 - 04 05 2003, poster
2. Tyman – Szram B., Niedbała H., Musioł R., Sajewicz M., Rompalski P., Karczmarek M., Tabak D., Polański J., *Determination of pK_a of Quinaldic AIDS by TLC*, The XXVIIth Symphosium Chromatographic Methods of Investigating the Organic Compounds, Katowice, Szczyrk, 4 - 6 06 2003, poster
3. Tyman – Szram B., Niedbała H., Musioł R., Sajewicz M., Lubańska W., Karczmarek M., Tabak D., Polański J., *Investigation of Methods of Determination pK_a Values for Novel HIV Integrase Inhibitors*, The XXVIIth Symphosium Chromatographic Methods of Investigating the Organic Compounds, Katowice, Szczyrk, 4 - 6 06 2003, poster

4. Niedbała H., Polański J., Tabak D., *Synteza potencjalnych inhibitorów integrazy wirusa HIV*, XLVI Zjazd PTCh i SITPCh, Lublin, 15 - 18 09 2003, poster
5. Polański J., Niedbała H., Musioł R., Tabak D., Podeszwa B., Bąk A., Pałka A., Magdziarz T., *Analogues of the styryquinoline and styrylquinazoline HIV-1 integrase inhibitors: Design and synthetic problems*, IV Multidyscyplinarna Konferencja Nauki o Leku, 17 - 19 05 2004, komunikat
6. Polański J., Niedbała H., Musioł R., Podeszwa B., Tabak D., Pałka A., Mouscadet J. F., Gieleciak R., Bąk A., Magdziarz T., Gasteiger J., Le Bret M., *Comparative molecular surface analysis (CoMSA): application for diketoacid DKA pharmacophore mapping HIV integrase inhibitors*, World Conference on Dosing Antiinfectives, Nurnberg, 2004, komunikat
7. Tabak D., Niedbała H., Mencel A., Pałka A., Podeszwa B., Polański J., Musioł R., *Optymalizacja syntezy amidów kwasów chinolinokarboksylowych*, XLVIII Zjazd PTChem I SITPChem, Poznań, 18 - 22 09 2005, poster
8. Musioł R., Jampilek J., Podeszwa B., Finster J., Tabak D., Polański J., *Structure – lipophilicity relationship in serie of quinoline derivatives*, 18th International Conference on Physical Organic Chemistry, Warszawa, 20 - 25 08 2006, poster
9. Musiol R., Jampilek J., Kralova K., Tabak D., Podeszwa B., Finster J., Polanski J., *Substituted amides of quinoline derivatives: preparation and their photosynthesis-inhibiting activity*, ECSOC-10, 2006, c007
10. Musiol R., Jampilek J., Kralova K., Tabak D., Finster J., Podeszwa B., Kozik V., Dohnal J., Polanski J., *Preparation and herbicidal activities of substituted amides of quinoline derivatives*, ECSOC-11, 2007, a011
11. Musiol R., Jampilek J., Kralova K., Finster J., Tabak D., Niedbala H., Csollei J., Dohnal J., Polanski J., *Ring-substituted 4-hydroxy-1H-quinolin-2-ones: Preparation and their photosynthesis-inhibiting activity*, ECSOC-12, 2008, c0012
12. Kusz J., Kruszynski R., Malecki J. G., Tabak D., *Struktura molekularna i elektronowa kompleksu [Ru(PPh3)2(C10H8NO3)2]*, 50 Konwersatorium Krystalograficzne, Wrocław 26-28.06.2008, str 182, poster

Curriculum Vitae

Dominik Tabak

Data urodzenia: 03. 10. 1978

Stan cywilny: żonaty

Adres: Al. J. Piłsudskiego 20 / 128
41 – 303 Dąbrowa Górnicza

Wykształcenie:

- 2003 – 2007: Studia Doktoranckie Instytutu Fizyki Uniwersytetu Śląskiego
- 1997 – 2003: Uniwersytet Śląski w Katowicach, Wydział Matematyki, Fizyki i Chemii, kierunek Chemia, specjalność Chemia Organiczna
- 1993 – 1997: I Prywatne Liceum Ogólnokształcące w Sosnowcu

Doświadczenie zawodowe:

- 08. 10. 2012 – obecnie: Uniwersytet Śląski w Katowicach, Instytut Chemii, chemik
- 01. 04. 2011 – 30. 09. 2012: Uniwersytet Śląski w Katowicach, Instytut Chemii, Zakład Chemii Nieorganicznej, Metaloorganicznej i Katalizy, asystent naukowo-dydaktyczny
- 01. 10. 2003 - 31. 03. 2011: Uniwersytet Śląski w Katowicach, Instytut Chemii, Zakład Chemii Organicznej, asystent naukowo-dydaktyczny

Znajomość języków obcych:

- język angielski - zaawansowany

Przebyte kursy i szkolenia:

- Praktyczny kurs nowoczesnych metod analizy instrumentalnej współfinansowany przez Unię Europejską z Europejskiego Funduszu Społecznego

Dodatkowe informacje:

- umiejętność obsługi ESI/APCI-LC-MS (Varian 500-MS IT Mass Spectrometer)
- prawo jazdy kategorii B

Dane naukometryczne (Scopus):

- liczba publikacji: 18
- liczba cytowań: 161
- liczba cytowań bez samocytowań: 70
- indeks *h*: 8

Załączniki

Oświadczenie o wkładzie pracy

W przedstawionym cyklu publikacji P1-P25 wykonałem syntezy, w szczególności:

- kwasu 5-hydroksy-2-metylochinolino-6-karboksylowego [P1]
- kwasu 2-metylochinolino-8-karboksylowego [P2]
- kwasu 8-hydroksy-2-metylochinolino-7-karboksylowego [P1,P4,P13] oraz jego pochodnych amidowych [P3,P6,P10,P15,P16]
- kwasu 8-hydroksy-2-metylochinolino-7-karboksylowego - ligandu kompleksującego [P5,P7,P8,P9,P11,P12]
- kwasu 8-hydroksy-2-metylo-5-nitrochinolino-7-karboksylowego [P3] oraz jego pochodnych amidowych [P3,P6]
- kwasu 2-metylochinolino-5,8-dikarboksylowego [P4]
- 7-acetamido-2-metylo-5,8-chinolinodionu [P14]
- innych związków [P17-P18, P21-25]

W ramach publikacji P19-P20 wykonałem oraz zinterpretowałem widma ESI-MS otrzymanych związków kompleksowych.

Katowice, 11.06.2013

Prof. dr hab. Jarosław Polański
Zakład Chemii Organicznej
Instytut Chemii
ul. Szkolna 9
40-006 Katowice

OŚWIADCZENIE

Jako kierownik Zakładu Chemii Organicznej oświadczam, że udział mgra Dominika Tabaka w w/w publikacjach jest kluczowy dla tematu opisanego tytułem rozprawy doktorskiej.
Uważam ponadto, że zakres prac badawczych wykonanych przez Doktoranta z dużą nadwyżką spełnia wymogi stawiane rozprawom doktorskim.

Publikacje

5-Hydroxy-6-Quinaldic Acid as a Novel Molecular Scaffold for HIV-I Integrase Inhibitors

J. Polanski*,[1], H. Niedbala[1], R. Musiol[1], B. Podeszwa[1], D. Tabak[1], A. Palka[1], A. Mencel[1], J. Finster[1], J.-F. Mouscadet[2], M. Le Bret[2]

[1]*Department of Organic Chemistry, Institute of Chemistry, University of Silesia, PL-40-006 Katowice, Poland*

[2]*CNRS UMR 8113, LBPA, Ecole Normale Supérieure de Cachan, 94235 Cachan, France*

Received December 12, 2006: Revised February 02, 2006: Accepted February 20, 2006

Abstract: 8-Hydroxy-7-quinaldic acid can be considered as a basic scaffold for all reported styrylquinoline HIV-1 integrase inhibitors. However, when tested *in vitro*, this compound appeared to be inactive against the enzyme. We have designed and synthesized an improved molecular fragment, i.e. 5-hydroxy-8-nitro-6-quinaldic acid, which appeared to inhibit HIV-1 integrase *in vitro*.

Keywords: Molecular scaffold, HIV integrase inhibitors, styrylquinolines.

Discovering drugs is a complex issue that lacks general approach. A so-called fragment design that insists on the importance of the certain two-dimensional molecular frameworks for the drug-likeness and lead generation has appeared in recent years[1-3]. In such an approach, we try to develop drugs starting from the search of the specific low-molecular weight fragments capable of binding a target receptor. Although the affinity of such fragments is too low to ensure effective drugs, they appear useful for a further construction of leads. NMR, MS and crystallography-based techniques have been reported among possible methods for the identification of such fragments or molecular scaffolds [3].

Diketoacid DKA **1** compounds are potent HIV IN inhibitors with *in vivo* antiviral activity [4, 5]. It has also been found that DKAs inhibit RNAse-H [5] and HCV NS5b polymerase [6]. Moreover, similar compounds are effective antiviral agents against influenza [7]. In HIV therapy however, DKAs needed heterocyclic modifications to give S-1360 (**2**) or L-870810 (**3**), the first IN targeted drugs under clinical testing [8]. Styrylquinolines (**4**) are another recently discovered powerful IN inhibitors that inhibit HIV-1 replication in cell cultures, probably by preventing the binding of DNA to IN [9-14].

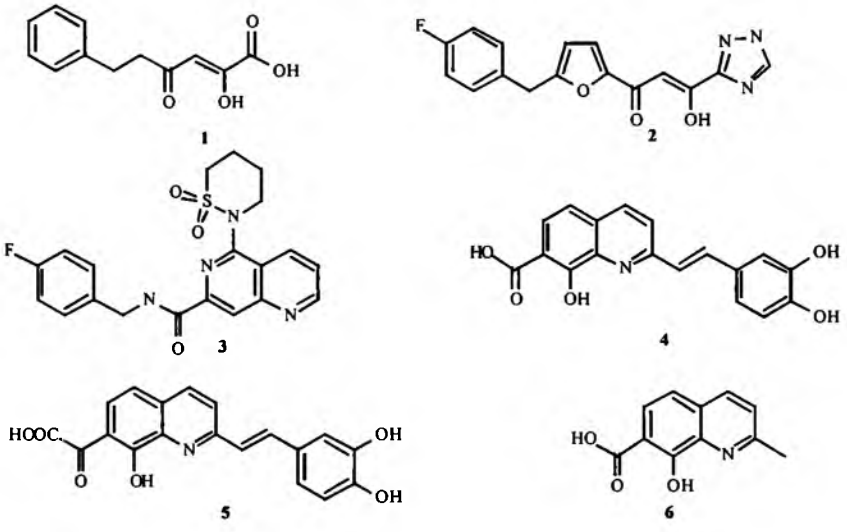

Fig. (1). Some DKA and styrylquinoline compounds reported.

Despite some structural similarities, the mechanism of HIV inhibition seems to be different for DKAs and

*Address correspondence to this author at the Department of Organic Chemistry, Institute of Chemistry, University of Silesia, PL-40-006 Katowice, Poland; E-mail: Polanski@us.edu.pl

1570-1808/06 $50.00+.00

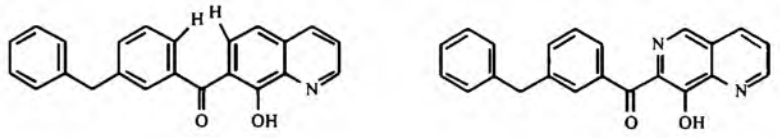

7 IC_{50}=0.37uM 7a IC_{50}=0.04uM

Fig. (2). Structure of quinoline and diazine based HIV integrase inhibitors [16].

styrylquinolines [15] and an effort to mimic the DKA pharmacophore in the styrylquinoline series resulted in compound **5**, which appeared to be inactive *in vitro* against IN. On the other hand, this compound exhibited a significant antiviral activity *in vivo* [13].

8-Hydroxy-7-quinaldic acid **6**, which can be considered as a basic scaffold for all reported styrylquinoline HIV-1 inhibitors, contains a basic hydroxyketo moiety found both in DKAs and styrylquinolines. However, if tested *in vitro*, this compound appeared to be inactive against integrase [10]. The aim of this study was to search for quinaldine scaffolds that can possess an improved affinity to HIV-I integrase.

Using Kohonen neural network, we have shown previously that the distribution of the electrostatic potential within quinoline moiety is of crucial importance for *ex vivo* activity of styrylquinoline compounds [12]. In the same context, the significantly different integrase inhibitions by diazine **7a** (IC_{50} = 0.04 μM) and quinoline **7** (IC_{50} = 0.37 μM) [16] analogs should also be mentioned here (Figure2). Although the latter was explained by speculating that steric hindrance prevents molecule **7** from taking coplanar conformation [16], a nitrogen atom, located in position 6, significantly influences the distribution of electrostatic potential, e.g., increasing the hydroxyl acidity, which offers an alternative explanation for the activity differences.

The distribution of electrostatic potential in hydroxyquinaldic acids depends upon the arrangement of hydroxyl and carboxyl substituents. Therefore, we obtained several different quinaldine scaffolds **9-10** and **12-14** and tested their HIV-1 inhibition.

Compound **9** was obtained in Skraup reaction from 4-amino-2-hydroxybenzoic acid **8** and crotonaldehyde. Direct nitration of **9** resulted in 5-hydroxy-8-nitro-6-quinaldic acid **10** with 53% yield (Fig. **3**). The direct sulfonation of commercially available 8-hydroxyquinoline or 8-hydroxyquinaldine **11** gave **12**, which reacted further to yield **13** [17]. Nitration of compound **11** gave **14** [17]. 8-hydroxy-7-quinaldic acid was obtained according to known procedure (Fig. **4**) [10].

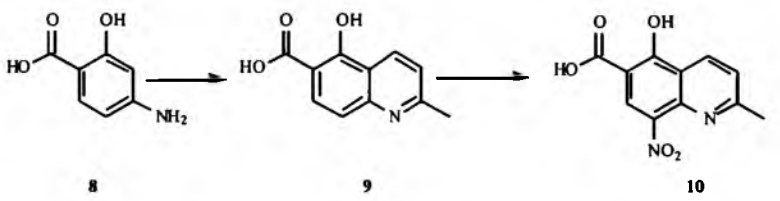

8 **9** **10**

Fig. (3). Synthesis of 5-hydroxy-8-nitro-6-quinaldic acid.

Anti-integrase inhibition was evaluated in a 96-wells plate assay measuring INs overall activity using short blunt-

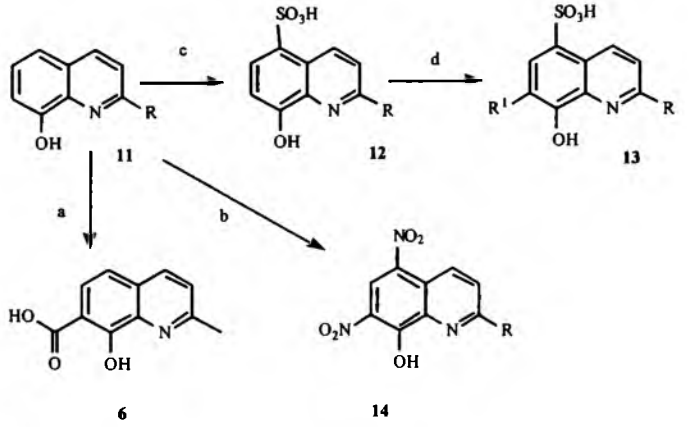

Fig. (4). a) KOH, CO_2, b) HNO_3\$H_2SO_4$ (0-5°C), c) H_2SO_4, 0-5°C, d) Br_2 or HNO_3\$H_2SO_4$ (0-5°C).

ended oligonucleotides mimicking viral U5 DNA extremity in the presence of 150nM recombinant HIV-1 integrase and 10 mM Mg^{2+} ions. IC_{50} were obtained from nonlinear regression fitting of dose-response curves using Prism software.

The HIV inhibition of the new compounds is shown in Table 1. In contrast to the inactivity of 8-hydroxy-7-quinaldic acid **6**, isosteric 5-hydroxy-6-quinaldic acid **9** was found to have IC_{50} value of 47 μm. The introduction of a nitro group into position 8 provided compound **10** of the IC_{50} value amounting to 42 μm. Other tested scaffolds **12-14** appeared to have IC_{50} values higher than 100 μm. Thus, 5-hydroxy-6-quinaldic acid **9** and its nitrated analog **10** that mimic the distribution of electrostatic potential in high active compounds **3** or **7a**, appeared to indicate the highest integrase inhibition among the scaffolds tested.

Table 1. HIV-1 Integrase Inhibition Data

Compound	R	R^1	IC_{50} [μM]
6	-	-	>100[a]
9	-	-	47
10	-	-	42
12a	CH_3	-	>100
12b	H	-	>100
13a	H	NO_2	>100
13b	CH_3	NO_2	>100
13c	H	Br	>100
13d	CH_3	Br	>100
14a	CH_3	-	>100
14b	H	-	>100

[a]as described previously [9].

In conclusion, we developed 5-hydroxy-6-quinaldic acid as a novel promising scaffold for the design of the HIV-1 integrase inhibitors. We believe this compound can be converted into novel lead structures.

EXPERIMENTAL SECTION

8-Hydroxyquinaldine-7-carboxylic acid (6), was obtained in Kolbe-Schmidt reaction as described in reference [9].

5-Hydroxy-6-quinaldic acid (9). To a refluxing solution of 1.0 equiv of 4-amino-2-hydroxybenzoic acid, (**8**) was added dropwise over three hour period 1.2 equiv of crotonaldehyde. The resulting mixture was heated under reflux for 2 hour. After being cooled aqueous ammonia was added to pH 3 and the mixture was extracted with CH_2Cl_2. The organic layer was washed with brine, dried over magnesium sulfate and concentrated under vacuum. The crude product was recrystallized from ethanol (31%). ^1H NMR ($DMSO_{-d6}$, 500MHz) δ(ppm): 2.82 (s, 3H); 7.32 (d, J=8.85Hz, 1H); 7.58 (d, J= 8.55Hz, 1H); 8.2 (d, J= 8.9Hz, 1H); 8.9 (d, J= 8.55 Hz, 1H). A.E. calcd $C_{11}H_9NO_3*H_2O$: C=59.73, H=5.01; Found C=59.80, H=5.44.

5-Hydroxy-8-nitro-6-quinaldic acid (10). Compound **9** was added slowly to nitration mixture (1/3 H_2SO_4/HNO_3) while cooling and stirring. After the period of four hours, the resulting mixture was poured onto 100 g of crushed ice. Yellow solid was separated, crystallized and dried to afford pure product in 53%. ^1H NMR ($DMSO_{-d6}$, 500 MHz) δ(ppm): 2.95 (s, 3H); 7.91 (d, J= 8.45Hz, 1H), 9.01 (d, J=8.3 Hz, 1H); 9.06 (s, 1H). A.E. calcd $C_{11}H_8N_2O_5*H_2O$: C=49.62, H=3.79; Found C=49.18, H=3.17.

8-Hydroxyquinaldine-5-sulfonic acid and **8-Hydroxyquinoline-5-sulfonic acid (12a, 12b)**. Compounds were obtained according to described procedures [17]. Direct nitration of **12a,b** afforded in **13a-d** compounds were identified by their melting points and their purity was checked by TLC.

5,7-Dinitro-8-hydroxyquinaldine and 5,7-dinitro-8-hydroxyquinoline **14a, 14b** were obtained according to known procedure [17c].

ACKNOWLEDGEMENTS

This study is supported by KBN, Warsaw 3T09A 01127. Anti-integrase screening program is supported by the French agency for research against AIDS (ANRS) and by the European program TRIoH (FP6 503480).

REFERENCES

[1] Fattori, D. D. *Drug Discov. Today*, **2004**, *9*, 229.
[2] Erlanson, D. A.; McDowell, R. S.; O'Brien, T. *J. Med. Chem.*, **2004**, *47*, 3463.
[3] Shuker, S. B.; Hajduk, P. J.; Meadows, R. P.; Fesik, S. W. *Science*, **1996**, *274*, 1531.
[4] Hazuda, D. J.; Felock, P.; Witmer, M.; Wolfe, A.; Stillmock, K.; Grobler, J. A.; Espeseth, A.; Gabryelski, L.; Schleif, W.; Blau, C.; Miller, M. D. *Science*, **2000**, *28*, 7646.
[5] Long, Y. Q.; Jiang, X-H.; Dayam, R.; Sanchez, T.; Shoemaker, R.; Sei, S.; Neamati, N. *J. Med. Chem.*, **2004**, *47*, 2561.
[6] Shaw-Reid, C. A.; Munshi, V.; Graham, P.; Wolfe, A.; Witmer, M.; Danzeisen, R.; Olsen, D. B.; Carroll, S. S.; Embrey, M.; Wai, J. S.; Miller, M. D.; Cole, J. L.; Hazuda, D. J. *J. Biol. Chem.*, **2003**, *278*, 2777.
[7] Hastings, J. C.; Selnick, H.; Wolanski, B.; Tomassini, J. E. *Antimicrob. Agents Chemother.*, **1996**, *40*, 1304.
[8] Johnson, A. A.; Marchand, C.; Pommier, Y. *Curr. Topics Med. Chem.*, **2004**, *4*, 671.
[9] Mekouar, K.; Mouscadet, J. F.; Desmaele, D.; Subra, F.; Leh, H.; Savoure, D.; Auclair, C.; d'Angelo, J. *J. Med. Chem.*, **1998**, *41*, 2846.
[10] Ouali, M.; Laboulais, C.; Leh, H.; Gill, D.; Desmaele, D.; Mekouar, K.; Zouhiri, F.; d'Angelo, J.; Auclair, C.; Mouscadet, J. F.; Le Bret, M. *J. Med. Chem.*, **2000**, *43*, 1949.
[11] Zouhiri, F.; Mouscadet, J. F.; Mekouar, K.; Desmaele, D.; Savoure, D.; Leh, H.; Subra, F.; Le Bret, M.; Auclair, Ch.; d'Angelo, J. *J. Med. Chem.*, **2000**, *43*, 1533.
[12] Polanski, J.; Zouhiri, F.; Jeanson, L.; Desmaële, D.; d'Angelo, J.; Mouscadet, J.-F.; Gieleciak, R.; Gasteiger, J.; Le Bret, M. *J. Med. Chem.*, **2002**, *45*, 4647.
[13] Zouhiri, F.; Desmaele, D.; d'Angelo, J.; Ourevitch, M.; Mouscadet, J.-F.; Leh, H.; Le Bret, M. *Tetrahedron Lett.*, **2001**, *42*, 8189.
[14] Benard, Ch.; Zouhiri, F.; Normand-Bayle, M.; Danet, M.; Desmaele, D.; Leh, H.; Mouscadet, J.-F.; Mbemba, G.; Thomas, C.-M.; Bonnenfant, S.; Le Bret, M.; d'Angelo, J. *Bioorg. Med. Chem. Lett.*, **2004**, *14*, 2473.
[15] Pommier, Y.; Johnson, A. A.; Marchand, C. *Nat. Rev. Drug Discov.*, **2005**, *4*, 236.
[16] Zhuang, L.; Wai, J. S.; Embrey, M. W.; Fisher, T. E.; Egbertson, M. S.; Payne, L. S.; Guare, J. P.; Vacca, J.P.; Hazuda, D. J.;

Felock, P. J.; Wolfe, A. L.; Stillmock, K. A.; Witmer, M. V.; Moyer, G.; Schleif, W. A.; Gabryelski, L. J.; Leonard, Y. M.; Lynch, J. J.; Michelson, S. R.; Young, S. D. *J. Med. Chem.*, **2003**, *46*, 453.

[17] (a) Gershon, H.; McNeil, M. W. *J. Heterocycl. Chem.*, **1972**, *9*, 659; (b) Gershon, H.; McNeil, M. W.; Grefig A. T. *J. Org. Chem.*, **1969**, *34*, 3268; (c) Behforouz, M.; Haddad, J.; Cai, W.; Arnold, M. B.; Mohammadi, F.; Sousa, A. C.; Horn, M. A. *J. Org. Chem.*, **1996**, *61*, 6552.

Comparative Molecular Surface Analysis (CoMSA) for Virtual Combinatorial Library Screening of Styrylquinoline HIV-I Blocking Agents

Halina Niedbala[1], Jaroslaw Polanski[*,1], Rafal Gieleciak[1], Robert Musiol[1], Dominik Tabak[1], Barbara Podeszwa[1], Andrzej Bak[1], Anna Palka, Jean-Francois Mouscadet[3], Johann Gasteiger[2] and Marc Le Bret[3]

[1]*Department of Organic Chemistry, Institute of Chemistry, University of Silesia, PL-40-006 Katowice, Poland*

[2]*Computer-Chemie-Centrum, Institute of Organic Chemistry, University of Erlangen-Nürnberg, D-91052 Erlangen, Germany*

[3]*CNRS UMR 8532, LBPA, Ecole Normale Supérieure de Cachan, 94235 Cachan, France*

Abstract: We used comparative molecular surface analysis to design molecules for the synthesis as part of the search for new HIV-1 integrase inhibitors. We analyzed the virtual combinatorial library (VCL) constituted from various moieties of styrylquinoline and styrylquinazoline inhibitors. Since imines can be applied in a strategy of dynamic combinatorial chemistry (DCC), we also tested similar compounds in which the -C=N- or -N=C- linker connected the heteroaromatic and aromatic moieties. We then used principal component analysis (PCA) or self-organizing maps (SOM), namely, the Kohonen neural networks to obtain a clustering plot analyzing the diversity of the VCL formed. Previously synthesized compounds of known activity, used as molecular probes, were projected onto this plot, which provided a set of promising virtual drugs. Moreover, we further modified the above mentioned VCL to include the single bond linker –C-N- or –N-C-. This allowed increasing compound stability but expanded also the diversity between the available molecular probes and virtual targets. The application of the CoMSA with SOM indicated important differences between such compounds and active molecular probes. We synthesized such compounds to verify the computational predictions.

INTRODUCTION

The HIV genome encodes the enzyme integrase (IN) that catalyzes the insertion of reverse transcribed viral DNA into the host cell genome. This enzyme therefore plays a key role in the viral replication cycle. IN is a 32-kDa protein (288 amino acids) that consists of three functional domains. The central domain (or core domain, residues 50-210) contains the catalytic triad (DDE) that is essential for enzymatic activity. This domain is flanked by the N-terminal domain (which has a role in the assembly of an active multimeric form of the enzyme) and the C-terminal domain (which has the role in the nonspecific DNA-binding activity). These three domains, protein oligomerization the integrity of the catalytic triad, and a cationic cofactor such as magnesium is necessary for IN activity [1]. The integration process requires two distinct catalytic steps. During the first step, termed 3'-processing, IN specifically removes two nucleotides from each end of the linear viral DNA. The second step, called strand transfer, occurs after the translocation of the viral DNA into the nucleus. During this step, IN transfers both extremities of the viral DNA into the target DNA by a one step transesterification reaction, resulting in full-site integration.

Recently discovered powerful inhibitors of IN may have important medical applications. Most styrylquinoline derivatives inhibit IN *in vitro* [1-6]. Computer simulations have shown that these drugs bind in the immediate vicinity of the Mg^{2+} ion, which appears to be essential for the enzymatic activity, at a probable DNA-binding site, suggesting a competitive mechanism for inhibition [3-6]. IN is the probable *ex vivo* target of the HIV-blocking effect of most stryrylquinoline derivatives. Styrylquinolines inhibit HIV-1 replication in cell cultures, probably by preventing the binding of DNA to IN. This series of molecules has been extended to include styrylquinazolines, which have also been shown to inhibit HIV-1 IN [7]. The identification of a common critical feature should make it possible to find new powerful inhibitors in this series. The Kohonen network has been used for a rapid qualitative screening of the *ex vivo* activity of styrylquinoline compounds [6]. In the current publication we investigated the possibility for quantitative modeling of the compound activity.

This study had three aims. The first was to determine whether a quantitative relationship of the 3D-QSAR-model type could be constructed for styrylquinoline inhibitors on the basis of a pharmacophore mapping strategy. We used novel, recently developed robust 3D-QSAR and 4D-QSAR techniques and comparative molecular surface analysis in particular — to address this issue [8-10]. The second was to use this approach for the analysis of molecular diversity in the virtual combinatorial library (VCL) of styrylquinolines, with the aim of designing new synthetic drugs. Our third aim was to carry out synthesis experiments, especially to assess the prospects for practical applications of the dynamic combinatorial approach for the development of such inhibitors. By synthesizing novel compounds we also enlarge the molecular diversity of the compounds investigated, which is needed for the efficient design of novel drugs.

*Address correspondence to this author at the Department of Organic Chemistry, Institute of Chemistry, University of Silesia, PL-40-006 Katowice, Poland; E-mail: Polanski@us.edu.pl

1386-2073/06 $50.00+.00

THEORETICAL BACKGROUND

Self-Organizing Neural Networks

A self-organizing neural network is a data processing unit designed for data projection into a space defined in terms of a small number of dimensions. It generally consists of neurons arranged in a one- or two-dimensional map. The network distributes vectors arriving at the input among output neurons. In this process, a weight vector of the same size as the input must be defined for each output neuron. Individual inputs and weights are then compared to determine the signal distribution. This so-called Kohonen competitive strategy makes it possible to identify a single neuron obtaining a most similar input vector. The learning process of the network can start from random values of neuron weights, going on to present weights to each neuron with the aim of locating the designation of individual inputs within the map. Technically, this can be achieved by identifying the neuron that minimizes the Euclidean distance between these vectors. If an individual neuron obtains (or wins) a certain input, then its weight must be modified to resemble this particular input more closely, which also implies that the geometric distance between a weight and an input neuron decreases during iterative learning. So-called neighborhood relations between neurons define the arrangement of neurons on a two-dimensional map. In the Kohonen WTM (winner take most) strategy, learning involves not only the correction of the winner weights but also of the weights of the neighboring neurons. A more detailed description of SOM algorithms can be found elsewhere [11, 12]. The practical application of the SOM method to chemistry, drug design and bioinformatics has been described in several reviews [12-19].

Feature Maps of the Molecular Electrostatic Potential

Zupan and Gasteiger designed a scheme for applying the SOM algorithm for the projection of molecular surface properties into a two-dimensional feature map, such as an electrostatic potential map [12, 20, 21]. In his technique, the SOM network is fed with the Cartesian coordinates (inputs to the network take the form of a three-element vector consisting of x, y, and z coordinates) of the points sampled from the molecular surfaces. As a result, 10,000-30,000 points sampled at the surface are mapped to about 400-2500 (*20x20* to *50x50*) neurons arranged into a two-dimensional map of electrostatic potential or another molecular feature. This technique has been used for the comparison of individual maps of bioactive compounds [12] or bioisosteric moieties [22, 23]. Although the robust neuron technique is considered to be an efficient comparison tool, the rules for this comparison are actually very unclear. The problem lies essentially in the difficulties involved in normalizing the surface area enclosed in any single neuron of the individual maps of two independent molecules. If we retain the same map size for two different molecules, then the larger the surface area of a given molecule, the greater will be the proportion enclosed in a single output neuron. We therefore decided to make use of the memorizing ability of the neural network to design a comparison scheme based on the SOM network [24-26]. A template molecule was used to train a template network. The knowledge concerning surface geometry encoded in the weights of the network was then used to simulate a comparative map of the second molecule. This principle is explained in more detail in Fig. **1a**, which illustrates the idea of comparative mapping of a compound series c_1-c_n using alternatively three different templates: **Ta**, **Tb** and **Tc**. Fig. **1b** shows particular structures **Ta**, **Tb** and **Tc**, that we applied in this study. This process generates a series of comparative maps: M1, M2 and M3. This forms a kind of molecular superimposition tool, illustrating the electrostatic potential profile desired. QSAR [27-31] and high-throughput screening [23, 32] investigations have demonstrated the efficiency of this method in drug discovery. An interesting innovation of the method is that by the different adjustment of the SOM neuron parameters, molecular objects can be compared with different tolerances (Fig. **2**). This issue has been discussed in more detail elsewhere [13, 33].

CoMSA FOR MOLECULAR DIVERSITY STUDIES

Recent developments in combinatorial library design have been reviewed by Schneider [34] and Bajorath [35]. This includes clustering techniques based on molecular similarity, structure-based docking and scoring, as well as fragment-based *de novo* design. Mathematically, molecular diversity studies are based on the analysis of multidimensional problems. Furthermore, the solutions for molecular library objects, most of which are virtual objects, are *a priori* unknown. The unsupervised SOM technique is potentially useful in such cases because, in contrast to supervised methods, it is not necessary to have any of the answers available in advance. Indeed, Gasteiger *et al.* described the application of Kohonen networks for clustering and data mining in molecular diversity studies [36]. Since differences in the size of the molecules in the dataset preclude direct comparisons, autocorrelation functions are used to transform the molecular data into vectors of equal length, standardizing the size of the objects to be compared. In the example that follows, the Kohonen network is used as a tool for normalizing the size of molecular data. We showed previously that comparative mapping can be used in molecular diversity studies [32], and recently, Schneider published an interesting example of the application of SOM for the analysis of a small virtual combinatorial library [37].

EXPERIMENTAL

Methods

Activity Tests

All the activity tests were performed as reported precisely previously [6].

Model Building

The experimental data for the HIV-1 blocking agents have been measured or extracted from previous publications [2, 3, 5] and are given in Tables **1** and **2**. The 3D-coordinates of the molecules were obtained with the 3D structure generator CORINA [38-40]. Partial atomic charges were calculated by the partial equalization of orbital electronegativity (PEOE) method [41, 42], and the SURFACE program was used to calculate the Coulombic electrostatic potential on the molecular surface.

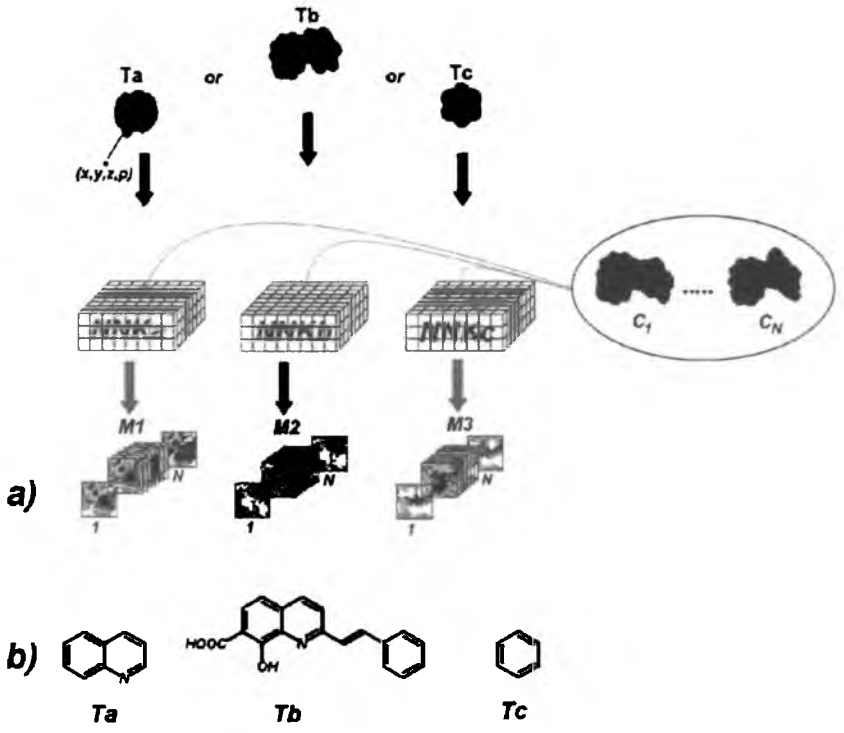

Fig. (1). (**a**) Comparative molecular surface analysis with an alternative mapping strategy. The molecular data (Cartesian coordinates x,y,z) of three different molecules, templates T1-T3, were sequentially used to train three different Kohonen network that processed molecular data from the compound series c_1-c_n, generating three series of comparative maps: M1, M2 and M3. (**b**) Molecular formulas giving the structures of the templates Ta, Tb and Tc.

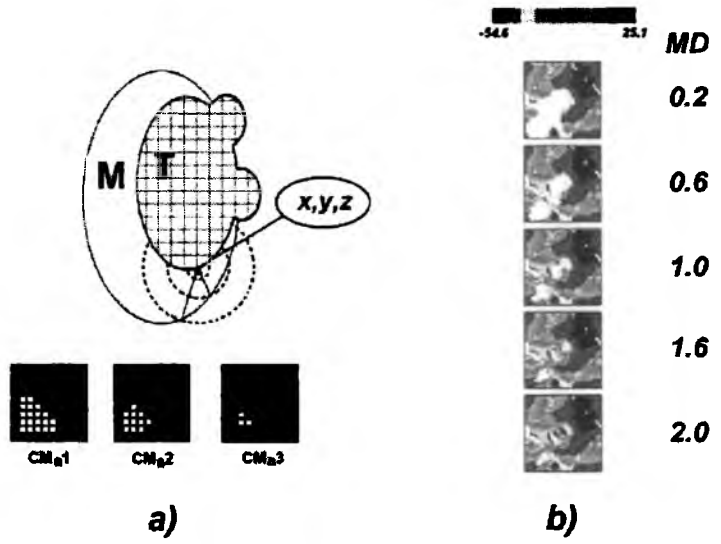

Fig. (2). (**a**) Comparative mapping of two given molecules **M** and **T** facilitating the generation of fuzzy molecular surface patterns (CMa1 to CMa3) by adjustment of the diameter of a sphere defining the winning distance (**MD**) of a SOM neuron. (**b**) Five possible comparative maps of the styrylquinoline molecule **M** obtained using the **T** template. Since these molecules differ in structure (the H atoms in **M** replaced for COOH and OH in molecule **T**), the network records this difference by white areas (empty neurons) for MD =0.2 Å. However, increasing the **MD** "neutralizes" this difference, such that the network records molecules **M** and **T** as two congruent structures (MD=2 Å).

Table 1. Structures and Three Different Types of Anti-HIV Activity of Styrylquinoline Compounds According to [2, 3, 6]

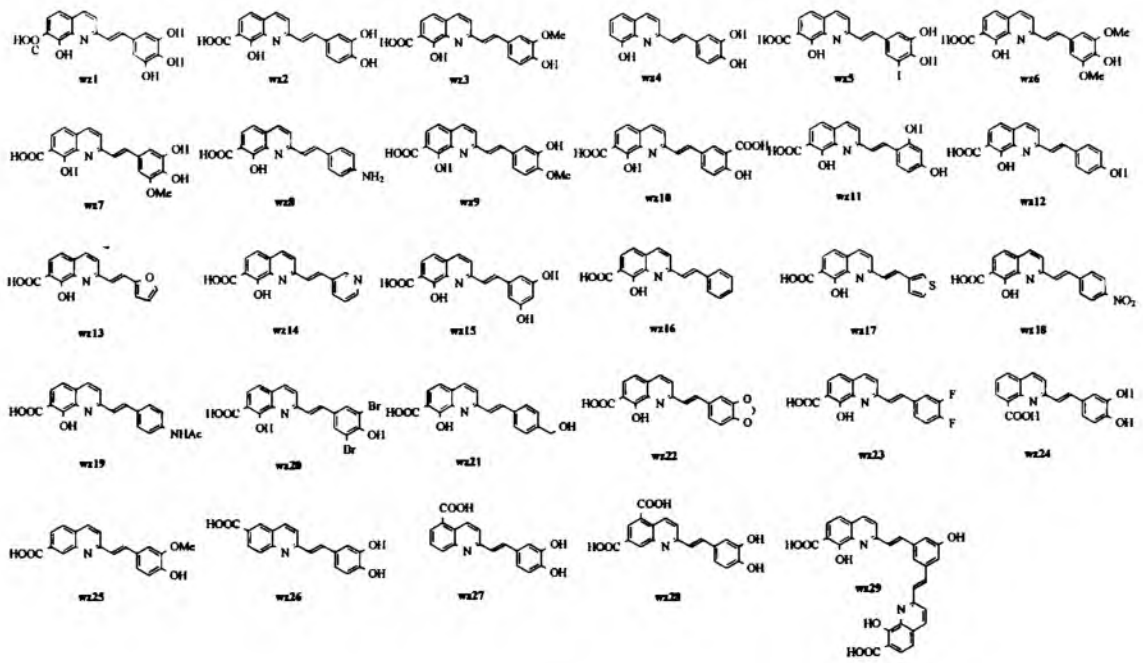

Cmpnd	Integra[a)]	Process[b)]	IC_{50}[c)]	Cmpnd	Integra[a)]	Process[b)]	IC_{50}[c)]
wz1	0.3	0.4	1.2	**wz16**	5.3	2.1	-
wz2	2.4	1.0	1.3	**wz17**	3.4	3.0	-
wz3	2.8	3.7	3	**wz18**	1.2	1.7	-
wz4	7.4	2.4	-	**wz19**	1.4	1.2	-
wz5	4.0	4.9	6.8	**wz20**	1.3	1.2	30
wz6	4.9	4.5	9	**wz21**	-	-	110
wz7	0.7	1.7	12	**wz22**	-	-	10
wz8	3.5	2.2	50	**wz23**	-	-	30
wz9	0.9	3.3	54	**wz24**	-	-	12
wz10	2.7	0.6	80	**wz25**	-	-	20
wz11	3.7	2.8	80	**wz26**	-	-	20
wz12	1.6	1.6	95	**wz27**	-	-	50
wz13	1.9	5.1	NR[d)]	**wz28**	-	-	15
wz14	4.1	11	NR	**wz29**	-	-	NR
wz15	3.2	3.2	NR		-	-	-

[a)]Inhibitory activity against HIV-1 IN in *strand transfer* reaction.
[b)]Inhibitory activity against HIV-1 IN in *3'-end-processing* reaction.
[c)]Concentration (μM) at which 50% of the viruses are killed in *ex vivo* experiment.
[d)]NR-not reached, means that IC_{50} is expected to be much larger than 100 μM.

CoMFA, CoMSA and 4D QSAR

The CoMFA method is the first complex 3-D QSAR method that was developed [43]. CoMFA and related grid techniques analyze molecular field for a series of molecules superimposed within the grid constructed. The nodes of this grid define the points for which electrostatic or van der Waals potential is calculated. Usually, because of the large number of nodes, these methods generate large datasets that must be transformed and analyzed further by the Partial Least Squares (PLS) method.

Table 2. The Performance of 3D and 4D QSAR Modeling of Anti-HIV Activity

	Integra[a]	Process[b]	IC_{50}[c]
CoMFA	-0.002 (2)[d]	-0.34 (2)	0.43 (3)
COMSA (Ta)[e]	-0.25-0.67	-0.18-0.71	-0.58-0.46
COMSA (Tb)	0.09-0.67	-0.27-0.11	-0.09-0.68
COMSA (Tc)	-0.28-0.36	-0.41-0.52	-0.14-0.32
4D-QSAR	-0.05 (1)	-0.08 (1)	0.36 (7)
SOM-4D-QSAR	-0.15 (3)	-0.15 (3)	0.45 (7)

[a]Inhibitory activity against HIV-1 IN in *strand transfer* reaction.
[b]Inhibitory activity against HIV-1 IN in *3'-end-processing* reaction.
[c]Concentration required to achieve a 50% reduction of the viral load in the cell supernatant.
[d]Number of PLS components.
[e]Template acc. to Fig. 1b.

Similarly, a series of comparative patterns yielded by comparative Kohonen mapping can also be processed by PLS to form a 3-D QSAR model. This scheme outlines the precise quantitative version of the *Comparative Molecular Surface Analysis* (*CoMSA*). This method is discussed in references [8-10, 18, 28,30, 32, 44].

Multidimensional QSAR, namely, Hopfinger's 4D-QSAR [45] is a new idea that can improve QSAR modeling performance concentrating on the conformational space of the molecular series. In this method a spatial rectangular grid is constructed over molecular configurations. This grid defines spatial cubics that are used to calculate descriptors characterizing the pattern of the occupancy of each cell (cubic) by the molecule atoms during molecular dynamics simulations. Moreover, a new 4D-QSAR scheme involving a self-organizing neural network was designed [46].

Data Analysis

Kohonen mapping: The competitive Kohonen strategy [11] was used to construct a two-dimensional topographic map based on signals from randomly sampled points on the surface of the molecule. Each neuron, j, was then defined by three weights, w_{ji}. The competitive training of the network was based on the rule that each point, s, of the molecular surface was projected into that neuron, sc, the weights of which, w_{ci}, were closest to the Cartesian coordinates, x_{si}, of this point, s, (eq. 1).

$$out_{sc} \leftarrow \min\left[\sum_{i=1}^{3}(x_{si} - w_{ji})^2\right] \qquad (1)$$

The feature map was produced by projecting the molecular electrostatic potential (MEP) from the surface points, s, into a two-dimensional arrangement of neurons, after calculating the mean MEP value within a particular neuron and color-coding it.

The comparative scheme used in this work is illustrated in Fig. **1**. In this method, the Kohonen network, trained on data describing the template molecule, processed signals from the surfaces of other molecules. The electrostatic potential of each input vector was then projected through the network to obtain a series of simultaneous comparative maps for the template molecule and for each molecule analyzed. The respective MEP values from the surfaces of the processed molecules were then projected into the network, making it possible to compare the parts of the molecule surfaces that could be superimposed. If the surfaces could not be superimposed on the reference molecule (template), then the respective output neurons obtained no signal from the molecules processed. This is illustrated by white areas on the comparative maps. The tolerance of this comparison can be adjusted as explained in Fig. **2**.

All the molecules were superimposed before calculation of the molecular surfaces. We used the Match3D program [47] for this operation. The KMAP 3.0 program [48] was used for the simulation of Kohonen networks. The output of this program was used to calculate mean MEP values for each neuron and respective feature maps were transformed into respective vectors.

Partial Least Squares Analysis: The vectors obtained were processed by the PLS method, with a leave-one-out cross-validation procedure. The PLS procedures were programmed within the MATLAB environment (MATLAB ver. 5.1). A PLS model was constructed for the centered data, and its complexity was estimated based on the leave-one-out cross-validation (CV) procedure. The data were centered (but not rescaled) for each cross-validation run. In the leave-one-out CV method, the calibration is repeated m times, with a different object (the i-th object) left out each time, the i-th object being treated as the prediction object. The dependent variable for each left-out object is calculated based on the model with one, two, three factors etc. The root mean square error of CV for the model with j factors is defined as:

$$\mathrm{RMSECV} = \sqrt{\frac{\sum(obs - pred)^2}{m}} \qquad (2)$$

where, *obs* is the assayed value; *pred* –is the predicted value of the dependent variable and i refers to the object index, which ranges from 1 to m. Models with k factors, for which RMSECV reaches a minimum, are considered optimal.

We used the performance metrics accepted and widely used in 3D QSAR studies, including CoMFA analyses in particular — cross-validated q^2_{cv}

$$q^2_{CV} = 1 - \frac{\sum (obs - pred)^2}{\sum (obs - mean(obs))^2} \qquad (3)$$

where, *obs* is the assayed value; *pred* is the predicted value, *mean* is the mean value of *obs* and i refers to the object index, which ranges from 1 to m.

We ran the CORINA, PETRA, SURFACE and KMAP programs to generate 3D molecular representations, to calculate partial atomic charges and molecular surfaces, and to generate 2D Kohonen maps of molecular electrostatic potential on an O2 SGI workstation. PLS scripts were programmed in MATLAB and run on a PC.

Chemistry

Melting points were recorded on a Boetius apparatus and are uncorrected. The ^{1}H NMR spectra were obtained on

Inova 300 MHz and Bruker 500 MHz instruments. When diffuse, easily exchangeable protons were not listed. Analytical thin-layer chromatography was performed on Merck silica gel $60F_{254}$ alumina precoated plates (0.25 mm layer). All liquid chromatography separations were performed using Merck silica gel 50-100 mesh. For all microwave assisted synthesis, a monomode microwave reactor with temperature control from Plazmatronika was applied [49]. Solvents such as ether and chloroform were dried and purified according to standard procedures. Chemicals obtained from commercial suppliers were used without further purification.

Microwave-Assisted Condensation of Amine and Aldehyde

2[(2-Hydroxyphenylimino)methyl]-8-hydroxyquinoline 2 (Scheme **1**). Commercial 8-hydroxy-2-carbaldehyde (0.17 g, 0.1 mmol) and 2-aminophenol (0.1 g, 0.1 mmol) were mixed thoroughly with montmorillonite K10 (0.5 g) and irradiated in a domestic microwave oven (750 W for 3.5 min). The resulting product was extracted in dichloromethane (2x10 mL). The solvent was removed under reduced pressure and crystallization from ethanol gave compound 2 (65%) as a light yellow solid; m.p. 168-169°C lit. m.p. 168-169°C [50].

2-(Hydroxyethoxymethyl)-8-quinolinecarboxylic acid 6 (Scheme **2**). A solution of *o*-nitrosotoluene (0.61 g, 0.005 M) in 50 mL ethanol was added dropwise to a refluxing solution of (0.94 g, 0.005 M) of 8-quinaldinecarboxylic acid **3a** (prepared as previously described [6]) and 20 drops of piperidine in 100 mL ethanol over 3 h period. The resulting mixture was refluxed for 13 h under argon and then concentrated under vacuum. The solution was cooled and filtered to give a brown-red precipitate. Crystallization from 2–propanol gave product **6** in 6.2 % yield; m.p. 203-207°C. ^{1}H NMR (DMSO-D_6): δ (ppm) 15.9 (s, 1H), 8.94 (d, 1H, J=8.5 Hz), 8.67 (d, 1H, J=7.9 Hz), 8.49 (d, 1H, J=7.9 Hz), 8.35 (d, 1H, J=8.5 Hz), 7.98 (t, 1H), 4.49 (q, 2H), 1.42 (t, 3H). Anal. Calcd. for $C_{13}H_{13}O_4N$: C, 63.15; H, 5.26; N, 5.66. Found: C, 64.01; H, 4.33; N, 5.83.

Styrylquinolines 7a, 7b, 7c (Scheme **3**). Application of microwave assisted chemistry in styrylquinoline synthesis was highlighted recently [49]. Quinaldic acid (1,0 equiv.) was added to aldehyde (2 equiv.) and thoroughly mixed. The resulting mixture was heated in a microwave reactor with temperature and microwave control. The detailed procedures as well as analysis of compounds have been reported elsewhere [49].

2-[2-(3-Chlorophenyl)ethenyl]-7-quinolinecarboxylic acid (7a). Reaction of 7-quinolinecarboxylic acid with 3-chlorobenzaldehyde gave **7a** in 55% yield as a yellow solid; mp: 325°C. **2-[2-(2-Hydroxyphenyl)ethenyl]-7-quinolinecarboxylic acid (7a)**. A red solid was obtained in 62% yield; mp: 325-328°C. **2-[2-(2-Hydroxyphenyl)ethenyl]-5-quinolinecarboxylic acid (7c)**. A red solid was obtained with 58% yield; mp: 338-345°C (decomp.).

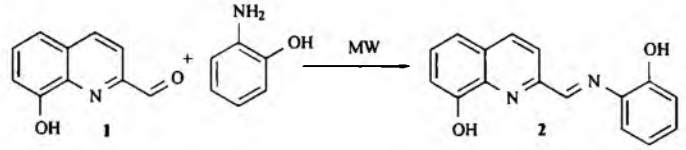

Scheme 1.

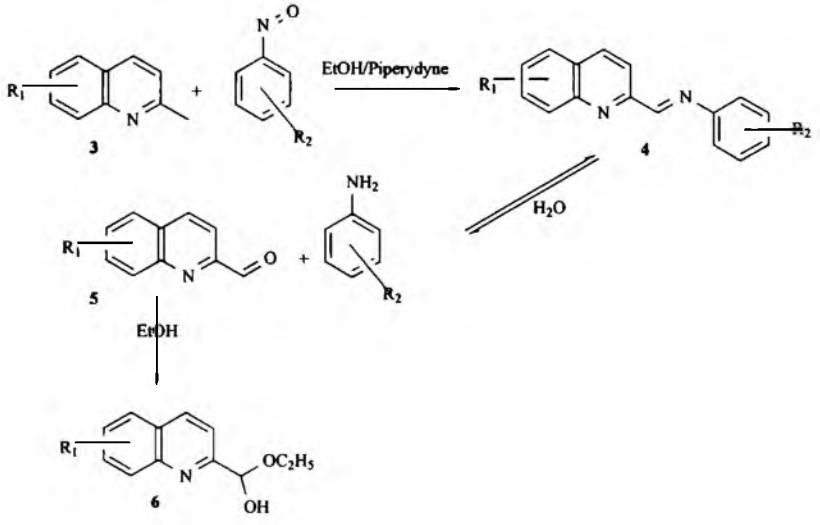

Scheme 2.

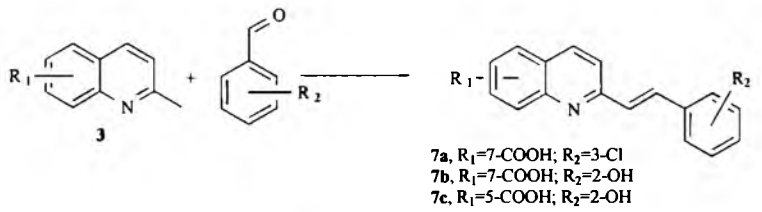

Scheme 3.

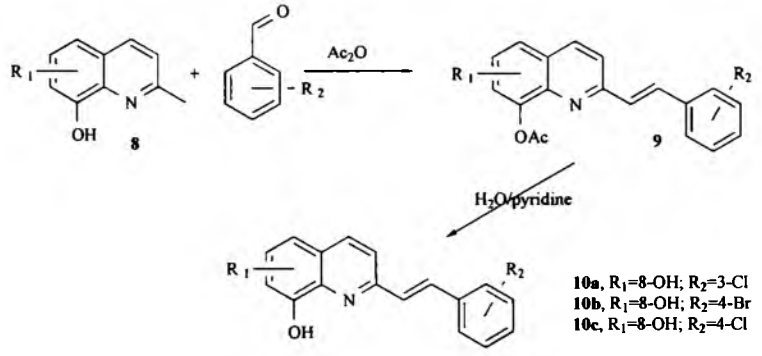

Scheme 4.

Styrylquinolines 10a, 10b, 10c (Scheme 4). These compounds were obtained under microwave irradiation of substrates on alumina carrier during 6 min at temperature and power level control. All experiments and compounds **10a-c** were described previously in references [51, 52].

2-[2-(3-Chlorophenyl)ethenyl]-8-hydroxyquinoline (10a). The product was obtained in 45% yield as a yellow solid mp: 150°C; **2-[2-(4-Bromophenyl)ethenyl]-8-hydroxyquinoline (10b).** Light yellow needles were obtained in 31% yield; mp: 145°C.

2-[2-(4-Chlorophenyl)ethenyl]-8-hydroxyquinoline (10c). A light yellow solid was obtained in 35% yield; mp: 120-123°C.

Compounds **12a** and **12b** (Scheme 5) were obtained by the condensation of 1 mmol 8-hydroxy-2-aminoquinoline with the appropriate aldehyde in dry benzene (30 mL) using the Dean-Stark apparatus. The reaction mixture was refluxed for 2 h. The resulting mixture was concentrated, cooled and the precipitate was filtered and purified by crystallization from benzene to give:

2-(2-Hydroxybenzylideneimino)-8-hydroxyquinoline (12a). Orange needles were obtained in yield 30%; mp: 184-186°C [52]. **2-(2,3-Dihydroxy-benzylideneimino)-8-hydroxyquinoline (12b).** Red-orange needles were obtained in 32% yield; mp: 170-172°C; ^{1}H NMR (DMSO-$_{d6}$, 500MHz) δ: 6.91 (m, 1H), 7.03 (d, 1H, *J*=9.3Hz), 7.36 (t, 1H), 7.44 (d, 1H, *J*=5.4Hz), 7.63 (d, 1H, *J*=8.4Hz), 7.9 (m, 1H), 8.42 (s,

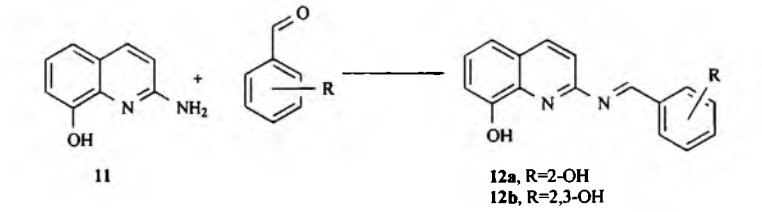

Scheme 5.

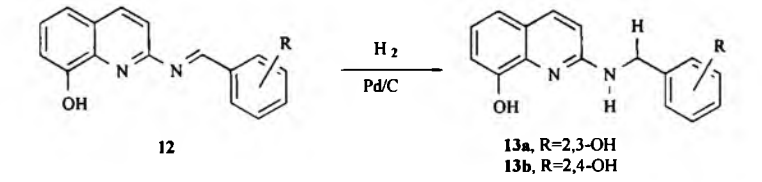

Scheme 6.

1H), 9.93 (s, 1H), 8.1 (d, 1H, *J*=16.2Hz), 8.27 (d, 1H, *J*=8.53). Anal. Calcd. for $C_{16}H_{12}N_2O_3 \cdot 2H_2O$: C, 60.76; H, 5.10; N, 8.86. Found: C, 60.92; H, 5.03; N, 8.69.

Compounds 13a and 13b (Scheme 6)

The imine obtained in the previous step was reduced with hydrogen in the presence of Pd on charcoal (5%) during 18 h at room temperature. Then, the precipitate was filtered off, and the product was purified by crystallization from benzene to give:

2-[(2,3-Dihydroxy-benzylidene)-amino]-8-hydroxyquinoline (13a) as brown needles, melting point: 250°C (decomp). ^{1}H NMR (DMSO-$_{d6}$, 500MHz) δ: 4.5 (s, 2H), 7.0 (m, 1H), 7.05 (d, 1H, *J*=9.3Hz), 7.36 (t, 1H), 7.4 (d, 1H, *J*=5.4Hz), 7.65 (d, 1H, *J*=8.5Hz), 7.9 (m, 1H), 8.45 (m, 2H), 8.1 (d, 1H, *J*=7.2Hz), 8.3 (d, 1H, *J*=8.5Hz). Anal. Calcd. for $C_{16}H_{12}N_2O_3$: C, 68.08; H, 5.00; N, 9.92. Found: C, 68.12; H, 5.08; N, 9.71.

2-[(2,4-Dihydroxy-benzylidene)-amino]-8-hydroxyquinoline (13b). Yellow crystals were obtained in 30% yield; mp 140-143°C. ^{1}H NMR (DMSO-$_{d6}$, 500MHz) δ: 6.4 (s, 2H), 6.76 (d, 1H, *J*=8.9Hz), 6.85 (d, 1H, *J*=7.5Hz), 6.98 (t, 1H), 7.08 (d, 1H, *J*=7.95Hz), 7.35 (s, 1H), 7.85 (d, 1H, *J*=8.8Hz), 8.42 (bs). Anal. Calcd. for $C_{16}H_{12}N_2O_3$: C, 68.08; H, 5.00; N, 9.92. Found: C, 68.34; H, 4.98; N, 10.01.

RESULTS AND DISCUSSION

The so-called predictive ability is a basic parameter calculated in QSAR modeling. However, current QSAR or molecular diversity studies generally work in the factual chemical compounds space. It means that both modeling QSAR relationships and testing predictive ability or validating this is performed by the application of the compounds of the known activity that were synthesized *a priori*. Thus, QSAR predictability does not apply to novel compounds (virtual chemical space) that are to be synthesized in the next step of the investigation. Below we describe the results of the approach aimed at the practical design of novel HIV inhibitors by means of a molecular diversity study.

Chemical Compounds

Table **1** gives the experimental integrase inhibition data for the HIV-1 blocking agents that have been measured in previous publications [2, 3, 6]. The imine analog **2** (Scheme **1**) were basically elaborated in the condensation of the respective aldehyde **1** and commercially available amines. In this particular case, microwave assisted organic synthesis (MAOS) appeared to be especially efficient. Alternatively, the reaction of the quinaldine **3** (known starting quinaldine subunits were obtained by the Scraup reaction) with aromatic nitroso compound also yields the respective quinoline–C=N–aryl compound. The reactions of similar heteroaromatic systems with nitrosocompounds have been described in a previous study [53]. However the reaction of *o*-nitrosotoluene with 8-quinaldinecarboxylic acid performed in ethanol gives **6** instead of imine **4** (Scheme **2**). This result indicated that imine **4** was formed in the reaction and then hydrolyzed to the respective amine and aldehyde which then reacted with ethanol to form the hemiacetal **6**. We performed condensation of aldehydes with quinaldines for the preparation of the styrylquinolines **7a**, **7b** and **7c** (Scheme **3**). This method provides low yields for the quinaldine moiety containing a hydroxyl group, giving a mixture which was difficult to purify. Accordingly, compounds **10a**, **10b** and **10c** were obtained using MAOS with solid phase (Scheme **4**) [51]. Imines containing –N=C– linker **12a** and **12b** were synthesized, as shown in Scheme **5**, by condensation of 2-amino-quinaldine with an appropriate aldehyde in a similar way as the analogs described above. These compounds were reduced to corresponding amines **13a** or **13b** with hydrogen and Pd on charcoal (Scheme **6**).

3D QSAR and 4D QSAR Modeling of Styrylquinoline Anti-HIV Activity

Table **2** compares the results obtained in complex 3D and 4D QSAR studies of styrylquinoline anti-HIV activity, giving the performances of the models correlating the three different anti-HIV activities with the molecular descriptors generated by the CoMFA, CoMSA, Hopfinger's, and SOM 4D-QSAR methods. The values of q^2 ranged from –0.41 to 0.71. We did not stop at a single relationship. Instead, by controlling a number of parameters we generated hundreds of 3D QSAR models.

In particular, we optimized the Kohonen map size and the neuron maximal distance (MD) parameter. This ranged from *5x5, 10x10, 20x20 and 30x30.* (map size) and 0.3 to 2.1 (MD). It resulted in 28 different CoMSA models. The weights of the Kohonen neural network are initialized randomly, therefore generation of each comparative map set was carried out 50 times with fixed map size and MD parameter in order to obtain statistically reliable results. Thus, for each template and activity 1400 CoMSA models were examined.

This is illustrated in Fig. **3**, which shows fluctuations in q^2 values for the selected CoMSA models obtained with different templates and anti-HIV activity types. Only three selected examples are illustrated, but similar distributions were obtained in the experiments for other models. Generally, irrespective of the anti-HIV activity type, biological behavior can be modeled with moderate efficiency. It would therefore probably be unreasonable to expect highly predictive 3D and 4D QSAR models for this series. However, the results in Table **2** indicate that CoMFA and 4D-QSAR analyses generated comparable results, whereas CoMSA performed slightly better. In the CoMSA procedure, we used the alternative mapping strategy [18] with different templates (**Ta**, **Tb** or **Tc**) to investigate the contributions of the various parts of the molecules.

By analysis of numerous CoMSA models, one could point out optimal network parameters. For **Ta** and **Tb** templates, optimal results were obtained by using networks of size *20x20* or *30x30* and MD parameter less than 1.0. Whereas for the **Tc** template, optimal results were obtained by using networks *10x10* and higher MD values. In fact, q^2 depended on the template selected (Table **2**). The results obtained, together with the efficiency of comparative mapping observed during the qualitative screening of anti-HIV activity [6], suggest that this technique can be an interesting option for the ligand-based design of the new drugs of this type.

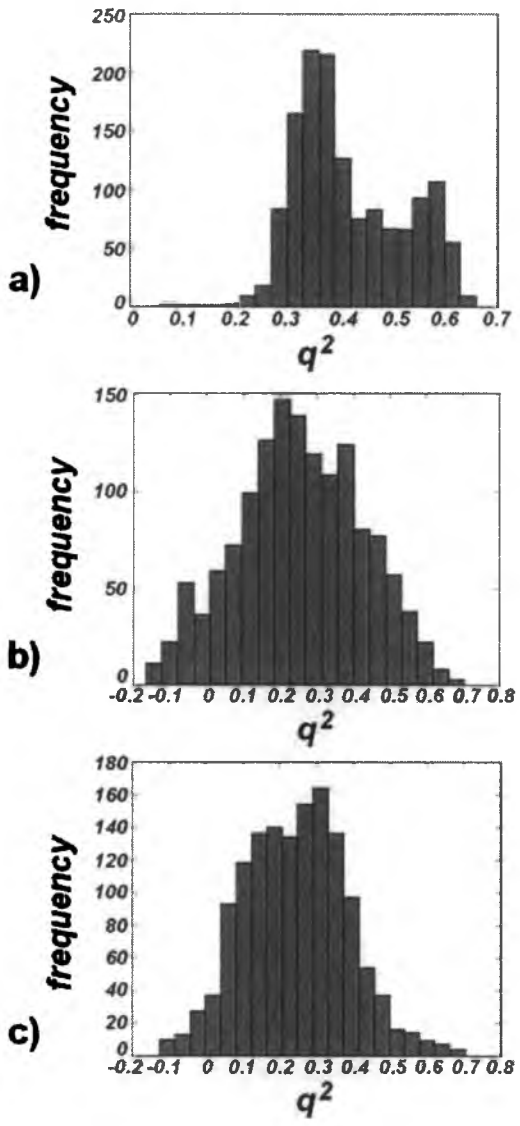

Fig. (3). Histograms illustrating the q^2 performance of the 1400 CoMSA runs analyzing (**a**) the inhibitory activity against HIV-1 integrase in strand transfer reaction; (**b**) process activity using $\mathbf{T_a}$ with comparative electrostatic potential matrices preprocessed to eliminate all empty neurons; and (**c**) IC_{50} activity using the $\mathbf{T_b}$ template.

CoMSA for the Studies of the Molecular Diversity of Virtual Drug Molecules

In this study, we applied the CoMSA technique to the search for new synthetic drugs inhibiting HIV-1 integrase, namely, promising molecules resembling parent compounds but including the -N=C- or -C=N- bond linker and/or a quinazoline moiety. Although the imine group is probably not stable enough for the construction of commercial drugs, this substitution provides insight into similar but more stable compounds, and into possibilities for application of the dynamic combinatorial approach [54, 55]. Since quinazolines have also been shown to inhibit integrase, we used the quinazoline skeleton to generate a possible variation within the basic series. Fig. **4** indicates the molecular formulae of the molecules constituting the virtual combinatorial library (VCL) analyzed in this study. We designed molecules with variations in three main areas. The heteroaromatic ring may take one of three forms — A1, A2 and A3 —the linker may also take one of three forms — B1(-C=C-), B2 (-N=C-) to aromatic ring unit could have either a hydrogen atom or one of 8 substituents, generating $(9^5+9^3)/2= 29889$ variants. However, as the combinations of these different types of variation resulted in a virtual library containing 269001 different compounds, which was considered too large for practical application, we imposed further limits, such that the aromatic ring had a maximum of three substituents different from the hydrogen atom, which generated a VCL consisting of 26784 molecules. We then used the CORINA, PETRA, SURFACE and KMAP drug design program packages to generate 3D molecular representations, to calculate partial atomic charges and molecular surfaces and to generate 2D Kohonen maps of molecular electrostatic potential for the template molecules (**Ta**, **Tb**, and **Tc**, Fig. **2**). This approach generated three independent comparative map series using a Kohonen network of size (*10x10*) suitable for this purpose.

The calculation of the electrostatic potential on the molecular surface was the part of the program sequence requiring the largest amount of CPU time. The comparative patterns obtained were analyzed further either by Principal Component Analysis (PCA) or by means of a second Kohonen network. Fig. **5** illustrates the results obtained for PCA clustering of the comparative patterns resulting from CoMSA with the **Ta** template. In particular, we analyzed the distribution of virtual molecules including different B units (i.e. B1, B2 or B3, Fig. **5a**), or A units (A1, A2 or A3, Fig. **5b**), indicated by different colors. Moiety A, in particular, clearly differentiated the library into three independent VCL object clusters, with VCL objects having different A substructures being classified to different clusters (Fig. **5b**). The structure of the central linker did not determine the clustering pattern of the virtual molecules with respect to the three main clusters (Fig. **5a**). Comparative mapping with the **Tb** template generated similar results (data not shown). These results are quite surprising, because higher similarity between the -C=N- and -C=C- linker could be expected. Although, an inspection of the modeled 3D structures indicates that quinoline-C=C-Ar, and quinoline-C=N-(or -N=C)-Ar molecules are planar, in fact, the investigated benzylideneanilines appeared to have nonplanar structures [56]. This makes an important difference in respect not only to the

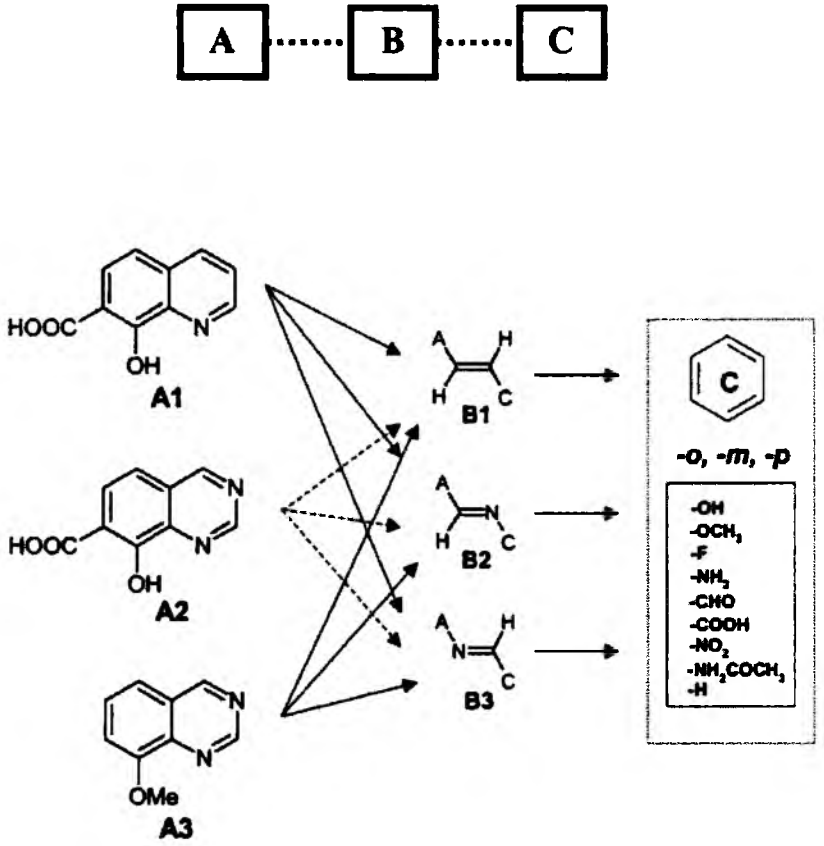

Fig. (4). Scheme illustrating a virtual combinatorial library (VCL) constituted of the A, B and C parts (details in text).

molecular geometry but also to the resonance connection between the quinoline and Ar moieties.

In Fig. **6**, we illustrate the use of a similar technique for clustering the patterns obtained by comparative mapping with the template **Tc**. In contrast to what was observed with the **Ta** and **Tb** templates, the compounds were evenly distributed and with no evident clustering for this template. The clouds of points representing molecules of the different series penetrate into each other. This situation maximizes the chances of finding potential drugs from another group. Thus,

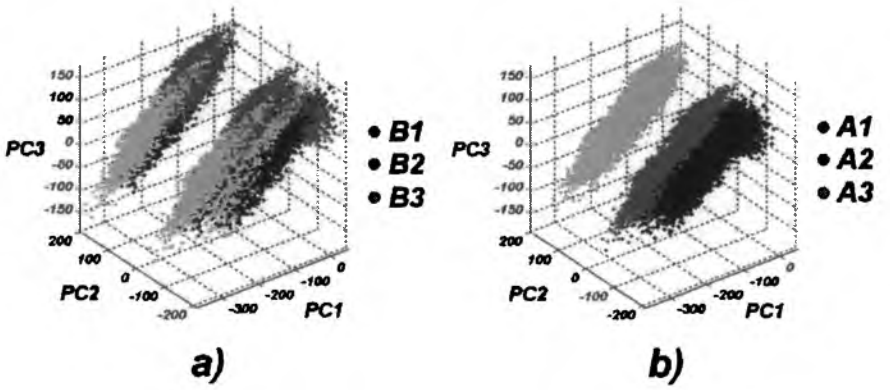

Fig. (5). The plot of the first three PC scores, PC1-PC2-PC3, used for classification of the comparative maps obtained with the Ta template. Shades of black and white indicate the constitution of the respective moieties of the A-B-C VCL.

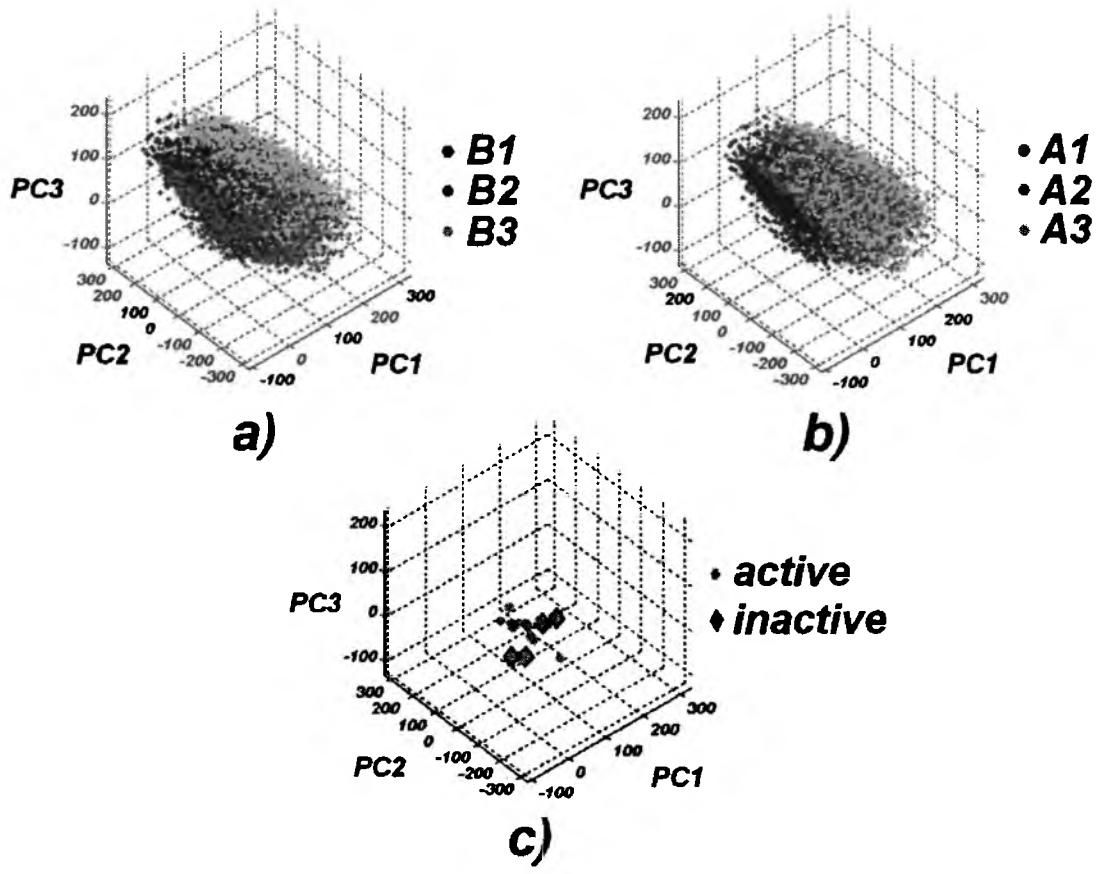

Fig. (6). The plot of the first three PC scores, PC1-PC2-PC3, used for classification of the comparative maps obtained with the Tc template. Shades of black and white in (**a**) and (**b**) indicate the constitution of the respective moieties of the A-B-C VCL. The destination of the molecular probes — VCL members representing real known compounds is indicated in (**c**).

we used the PCA plot for identification of potentially useful compounds in our VCL (Fig. **6c**). However, as several molecules included in VCL have been synthesized and described in previous publications as real compounds, they can be used as molecular probes, identifying promising domains within the PCA plots, and we can now use the scheme for the identification of virtual molecules. The **Tc** template provided 3D-QSAR CoMSA models of similar or even higher quality for some activity types than **Ta** or **Tb** (Table **2**). This scheme is therefore likely to be as predictive as the others. However, unless we convert these virtual molecules into real ones by synthesizing them, it is not possible to check real predictability of the method. The PCA method clusters the objects analyzed in a continuous space. We can, however, classify them using the Kohonen network, which generates discrete clustering by distributing the objects among individual neurons defined as separate units. Since all comparative maps are of the same size, the Kohonen network can process a whole series of such maps presented at the input level. This method constitutes a clear scheme for the identification of potential drugs. Virtual molecules occupying neurons that also contain known active compounds may have potential as inhibitors.

Fig. **7** illustrates two possible applications of Kohonen networks for clustering VCL. The network can learn the data for the whole VCL (Fig. **7a**) or for certain sublibraries (Fig. **7b**). Molecular probes can then be located within the network, making it possible to identify potential drugs. Figs. **8** and **9** illustrate the application of this method for two different templates. The colors used in the map indicate the numbers arbitrarily assigned to compounds. The closer the num-

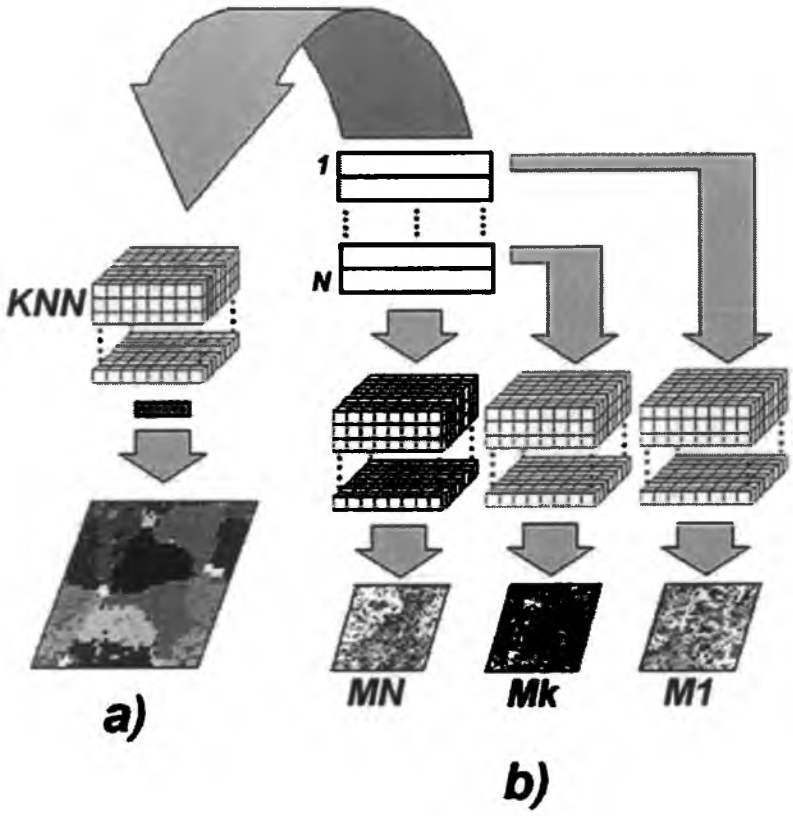

Fig. (7). Two possible strategies for classification of VCL. The whole VCL is processed by a single Kohonen network (**a**), or a series of Kohonen networks is used to process VCL sublibraries (**b**).

bers, the greater is the similarity between moieties constituting the VCL member.

As previously reported, Kohonen networks can be used to generate fuzzy molecular surface representations [33]. Thus, the larger the winning or maximal distance (MD) of the SOM neuron, the greater is the tolerance of the comparison that can be achieved. Figs. **2**, **8** and **9** show clearly that clustering pattern depends upon the tolerance of the comparative Kohonen network used during the first CoMSA step: the higher the value of MD (greater tolerance) the more compact are the clusters formed. This is because a more tolerant comparison (Fig. **2**) facilitates the classification of a larger number of virtual individuals as similar, resulting in their assignment to the same neurons. Greater tolerance also results in more distinct clustering. This makes it possible to adjust the molecular similarity rules according to the level desired. Table **3** indicates the results of a search for promising targets based on the strategy shown in Fig. **7b**. Similarity level is controlled so as to differentiate different sublibrary types. Thus, Table **3** identifies certain VCL compounds projected into the same neuron as potential inhibitors. Furthermore, the A1-B3 type sublibrary seems to be more promising than the A1-B2 sublibrary, because no virtual A1-B2 targets are co-clusterized with active probes. Molecular probes with positive activity profiles tend to be isoneuronal (Fig. **10**). Similarly, inactive molecular probes also clustered together. We used such plots to adjust the similarity level desired for positive molecular probing, as shown in Table **3**.

VCL Modifications Due to Synthetic Availability of Real Compounds

Since CoMSA-VCL analysis identified imine analogs of styrylquinolines as potentially interesting virtual drugs, we conducted a synthetic study to determine the optimal conditions for obtaining such compounds. The -C=N- bond is formed during the reaction between amine and aldehyde and similar systems have been set up in the past [50]. In fact, the imine is formed; however, it appeared to be hydrolyzed, giving product **5** and after reactions with solvent hemiacetal **6**. Similar problems in synthesis of imines were described recently [57]. Although searching the Beilstein database indicated that similar benzylideneaniline having carboxylic group has been obtained [58] we should conclude that carboxylic function is probably acidic enough to catalyze this hydrolysis. This suggests that further structural modification will be required to obtain molecules of the desired stability. This modification might consist of the imine reduction [54] or the carboxylic group replacement. Consequently, we con-

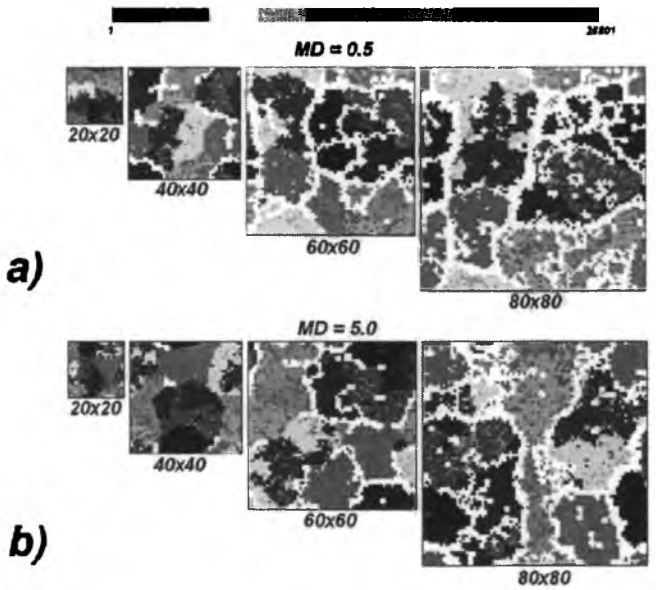

Fig. (8). Clustering of the comparative maps (obtained for template **Ta**) by the second Kohonen network of a different size. Differences in tolerance of the comparison of the molecular surfaces modified by the MD parameter of the network (MD=0.5 Å for the upper line and MD=5 Å for the lower line) make it possible to adjust the similarity scale. Two different comparisons for two arbitrary scales are shown in (**a**) and (**b**). Shades of black and white indicate the numbers of VCL members-the closer the numbers, the greater the similarity between the molecular structures.

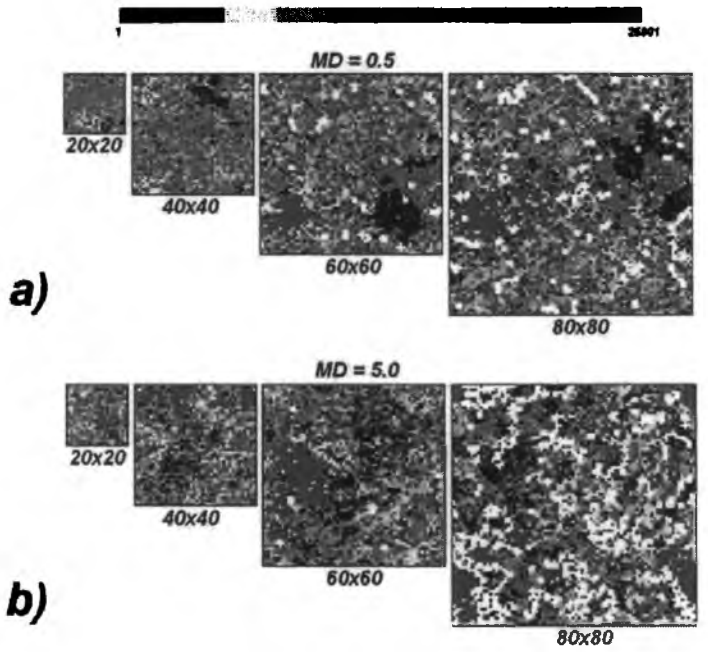

Fig. (9). Clustering of the comparative maps (obtained for template **Tc**) by the second Kohonen network of a different size. Differences in the tolerance of comparison of the molecular surfaces modified by the MD parameter of the network (MD=0.5 Å for the upper line and MD=5 Å for the lower line) make it possible to adjust the similarity scale. Two different comparisons for two arbitrary scales are shown in (**a**) and (**b**). Shades of black and white indicate the numbers of VCL members-the closer the numbers, the greater the similarity between the molecular structures.

structed a novel VCL, as shown in Fig. **11**, that includes some of such modified molecules. Diversity evaluation by clustering method similar to that applied previously indicates, however, that such modifications will significantly influence the clustering scheme of the compounds. We obtained no hits co-clusterized with active molecular probes. Table **4** reports the results obtained for 11 molecules of the modified VCL series, which were synthesized in the current study, in order to compare the results of the calculation with the IN inhibition. Actually, the IN inhibition of all molecules given in Table **4** appeared to be relatively low.

Table 3. The Results of the Molecular Probing of VCL With Real Actives (*In Vivo* Activity)

Some of Virtual Targets Clustered Together With Active Molecular Probes	
VCL Sublibrary Type	
	C
A1B1	3,5-OH, 4-F 3,4-OCH_3, 5-$NHOCOCH_3$ 3-OH, 4-OCH_3, 5-NH_2 3-NH_2, 4-OH 3,5-NH_2, 4-OCH_3
A1B2	a)
A1B3	3-OH,4-OCH_3,5-NH_2 3-OH,4-OH,5-NH_2 3,5-NH_2,4-OCH_3, 4-OH,5-NH_2 3-NH_2,5-CHO
A2B1	3-F,4-OCH_3,5-OH 3-F,4-OH,5-NH_2 2-$NHOCOCH_3$, 3-OH 2-OCH_3,3-OH, 5-NH_2 3-F,4-OCH_3,5-NH_2 3-OH,4-OCH_3,5-NH_2 3-OH,4-OH,5-OCH_3

Structure Activity Relationships for the Novel Compounds

The inhibition of the integrase by imines **2**, **12a** and **12b** or amines **13a** and **13b**, that do not contain a carboxylic function is relatively low. It appeared that quinoline-C=N-aryl compound **2** has much higher affinity to integrase than quinoline-N=C-aryl ones **12a** and **12b**. This information provides an important hint for the activity rules. If the planarity of the quinoline–C=N-aryl, quinoline–N=C-aryl system is distorted on the nitrogen atom similarly to the imines described previously [56], then unlike quinoline–N=C-aryl, quinoline–C=N-aryl preserves resonance of the quinoline moiety with the double bond C=N. As we have found previously, electro-donating groups in the *para* position of the aryl styrylquinoline moiety are of crucial importance for the *ex vivo* activity [6]. Therefore, the above mentioned regularity extends this rule, indicating that the presence of the conjugated double bond increases integrase affinity. Furthermore, amines **13a** and **13b** are more active than their imine analogues, e.g., **12a**. This can be attributed to the dif-

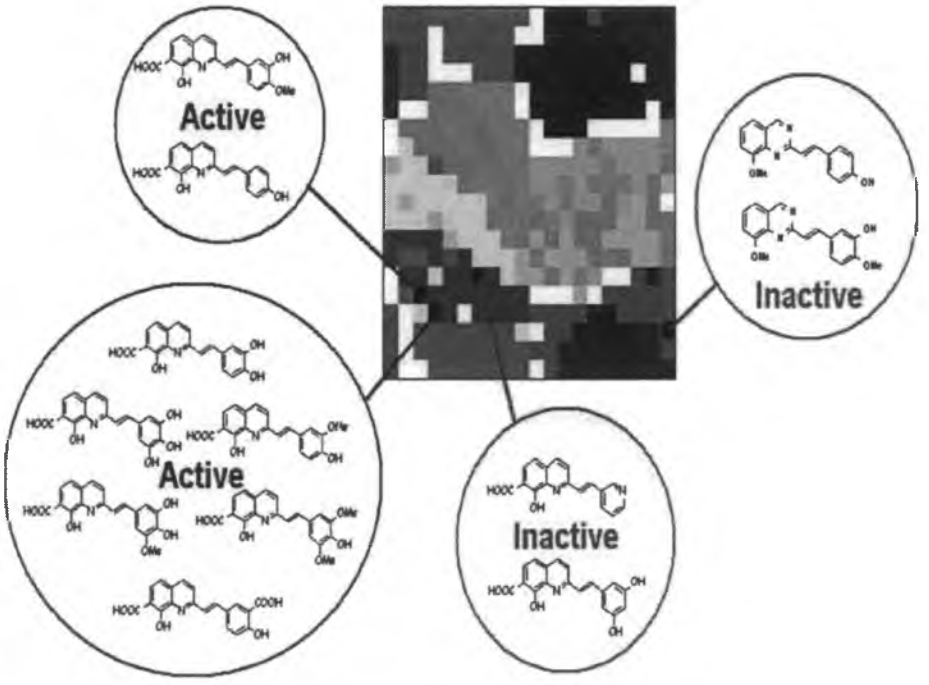

Fig. (10). Some molecular probes located within the same neuron in the Kohonen network Clusterization. For styrylquinoline compounds, activity data refer to the concentration required to achieve a 50% decrease in viral load in the cell supernatant for styrylquinazoline [6].

(Table 3) contd.....

VCL Sublibrary Type	
A2B2	2-OH,3-CHO,5-OCH_3 3-OCH_3,4-OH, 5-COOH 3-OCH_3,5-COOH 3,5-OCH_3, 4-F 2,5-$NHOCOCH_3$, 3CHO
A2B3	3-OH 3-OH, 4-OCH_3 3-OH, 4F
A3B1	3-OH, 4OCH_3, 5-NH_2 3-F, 4-$NHOCOCH_3$ 3-F, 4-OH 3,4-OH, 4-$NHOCOCH_3$ 3-OCH_3, 4-OH, 5-COOH
A3B2	a)
A3B3	a)

[a]No compounds co-classified with active molecular probes.

ferences in the electronic effect of the different nitrogen hybridization states of sp^3 (amines), less electroacceptor than sp^2 (imines). Thus, similarly to the previous results [6] the electrodonor substitution in position 2 tends to enhance the activity. On the other hand, our results show that synthetic chemistry determining the boundaries of the availability of the potential drugs is still a bottleneck in drug discovery.

CONCLUSIONS

Completely new possibilities for drug discovery have been added to traditional methods in recent years. Genomics and combinatorial chemistry are two impressive examples of these new methods. Some of these methods are sophisticated enough to include information on the target macromolecular structures to which possible drugs bind. Dynamic combinatorial chemistry makes possible to use macromolecular target directly to shape the most suitable ligand in an equilibrium process [54, 55]. The reversible chemistry of imine bond formation provides an important illustration of the dynamic combinatorial concept [54].

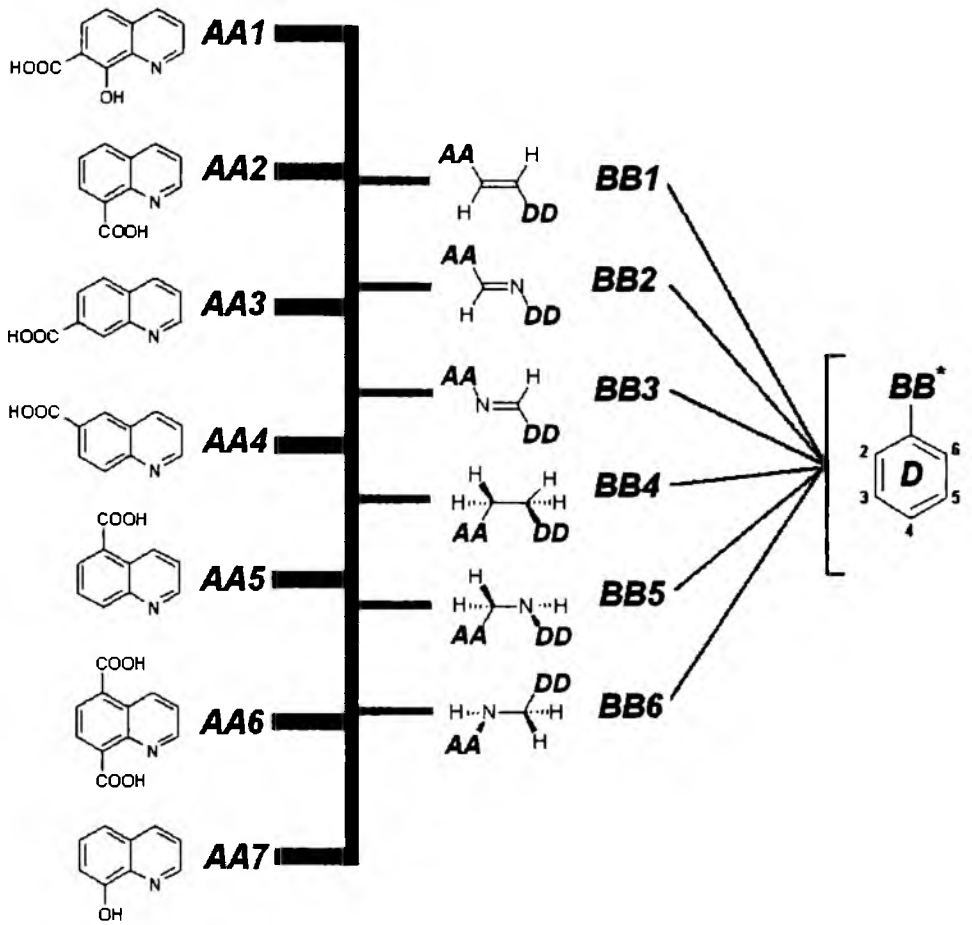

Fig. (11). Three counter-part VCL modified to meet synthetically available molecules (details in text).

Table 4. The Activities of the Obtained Compounds Towards 3'-Processing Step (*In Vitro* Experiment [6])

No.	VCL Structure [a]		IC_{50}
2	AA7-BB2-DD[2-OH]	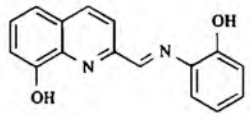	148
7a	AA3-BB1-DD[3-Cl]	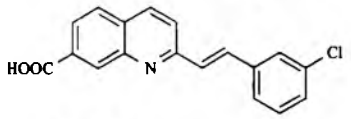	236
10a	AA7-BB1-DD[3-Cl]	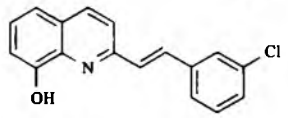	251
13a	AA7-BB6-DD[2-OH; 3-OH]	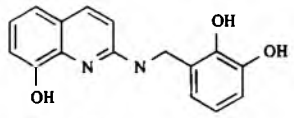	260
10b	AA7-BB1-DD[4-Cl]	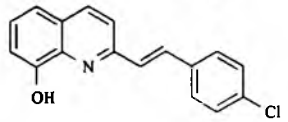	320
13b	AA7-BB6-DD[2-OH; 4-OH]	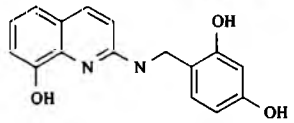	335
7c	AA5-BB1-DD[2-OH]	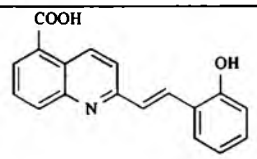	344
12a	AA7-BB3-DD[2-OH]	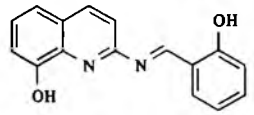	385
12b	AA7-BB3-DD[2-OH; 3-OH]	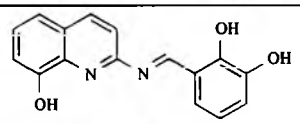	547
7b	AA3-BB1-DD[2-OH]	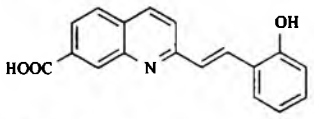	no. inhibit.
10c	AA7-BB1-DD[4-Br]	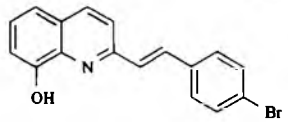	no. inhibit.

[a]Compare Fig. 11.

Although predictability is usually tested in QSAR or molecular diversity studies, this does not apply to novel compounds (virtual chemical space) that are to be synthesized in the next step of the investigation. Instead, this verifies the statistical reliability of the model. In the current study, we described the results of the approach aimed at the practical design of novel HIV inhibitors by a molecular diversity study. Thus, the reported performance does not rely to the factual but to virtual chemical space, testing the *a priori* method predictability.

Although currently only at the initial design stages, this work is likely to open up new interesting possibilities for the discovery of new styrylquinoline-type HIV inhibitors using this method. In the search for promising targets for the DCC imine library, we obtained a series of novel quinoline analogues and determined their activity towards HIV integrase. For high throughput screening of a combinatorial library of styrylquinoline and styrylquinazoline analogues, we applied comparative molecular surface analysis (CoMSA), PCA and Kohonen neural networks for obtaining classification plot onto which known active compounds were projected. In the synthetic part of these studies, we obtained several of the analogues that were predicted using the MAOS method [51]. In conclusion, we show how CoMSA analysis and the SOM neural network can be used for rapid screening of combinatorial libraries. On the other hand, our results indicate that the synthetic chemistry determining the boundaries of the availability of the potential drugs is still a bottleneck in drug discovery.

ACKNOWLEDGEMENTS

This study is supported by KBN, Warsaw 3T09A 01127. Anti-integrase screening program is supported by the French agency for research against AIDS (ANRS) and by the European program TRIoH (FP6 503480).

REFERENCES

[1] Craigie, R *J. Biol. Chem.*, **2001**, *276*, 23213.
[2] Mekouar, K.; Mouscadet, J.-F.; Desmaele, D.; Subra, F.; Leh, H.; Savoure, D.; Auclair, Ch.; d'Angelo, J. *J. Med. Chem.*, **1998**, *41*, 2846.
[3] Ouali, M.; Laboulais, C.; Leh, H.; Gill, D.; Desmaele, D.; Mekouar, K.;Zouhiri, F.; d'Angelo, J.; Auclair, Ch.; Mouscadet, J.-F.; Le Bret, M. *J. Med. Chem.*, **2000**, *43*, 1949.
[4] Zouhiri, F.; Mouscadet, J.-F.; Mekouar, K.; Desmaele, D.; Savoure, D.; Leh, H.; Subra, F.; Le Bret, M.; Auclair, Ch.; d'Angelo, J. *J. Med. Chem.*, **2000**, *43*, 1533.
[5] Deprez, E.; Barbe, S; Kolaski, M.; Leh, H; Zouhiri, F.; Auclair, C., Brochon, J.C.; Le Bret, M.; Mouscadet, J.-F. *Mol. Pharmacol.*, **2004**, *65*, 85.
[6] Polanski, J.; Zouhiri, F.; Jeanson, L.; Desmaële, D.; d'Angelo, J.; Mouscadet, J.-F.; Gieleciak, R.; Gasteiger, J.; Le Bret, M. *J. Med. Chem.*, **2002**, *45*, 4647.
[7] Lee, J.Y.; Park, J.H.; Lee, S.J.; Park, H.; Lee, Y. S. *Arch. Pharm. Pharm. Med. Chem.*, **2002**, *6*, 277.
[8] Polanski, J.; Gieleciak, R.; Bak, A. *J. Chem. Inf. Comput. Sci.*, **2002**, *42*, 184.
[9] Polanski, J.; Walczak, B. *Comput. Chem.*, **2000**, *24*, 615.
[10] Polanski, J.; Gieleciak, R. *J. Chem. Inf. Comput. Sci.*, **2003**, *43*, 656.
[11] Kohonen, T. *Self-Organization and Associative Memory*, 3rd. Ed., Springer Verlag, Berlin, **1989**.
[12] Zupan, J.; Gasteiger, J. *Neural Networks in Chemistry and Drug Design*, Wiley-VCH, Weinheim, **1999**.
[13] Anzali, S.; Gasteiger, J.; Holzgrabe, U.; Polanski, J.; Teckentrup, A.; Wagener, M. *Persp. Drug Discov. Des.*, **1998**, *9/10/11*, 273.
[14] Manallack. D.T.; Livingstone, D.J. *Eur. J. Med. Chem.*, **1999**, *34*, 195.
[15] Gerstein, M.; Greenbaum, D.; Luscombe, M. N. *Method Inform. Med.*, **2001**, *40*, 346.
[16] Brazma, A.; Vilo, J. *FEBS Lett.*, **2000**, *480*, 17.
[17] Toronen, P.; Kolehmainen, M.; Wong, G.; Castren, E. *FEBS Lett.*, **1999**, *451*, 142.
[18] Polanski, J. *Adv. Drug. Deliv. Rev.*, **2003**, *55*, 1149.
[19] Schneider, G.; Wrede, *Prog. Biophys. Mol. Biol.*, **1998**, *70*, 175.
[20] Gasteiger, J.; Zupan, J. *Angew. Chem. Int. Ed. Engl.*, **1993**, *32*, 503.
[21] Gasteiger, J.; Li, X.; Rudolph, Ch.; Sadowski, J.; Zupan, J. *J. Am. Chem. Soc.*, **1994**, *116*, 4608.
[22] Anzali, S.; Maderski, W. K. R.; Osswald, M.; Dorsch, D. *Bioorg. Med. Chem. Lett.*, **1998**, *8*, 11.
[23] Polanski, J.; Gasteiger, J.; Jarzembek, K. *Comb. Chem. High Throughput Screen.*, **2000**, *3*, 481.
[24] Polanski, J.; Gasteiger, J. *The comparison of molecular surfaces by an assembly of self organizing neural network, "Computers in Chemistry '94"*, Technical University of Wroclaw, National Institute of Standards and Technology, Gaithersburg, MD, USA; Wroclaw **1994**, pp. 88.
[25] Anzali, S.; Barnickel, G.; Krug, M.; Sadowski, J.; Wagener, M.; Gasteiger, J.; Polanski, J. *J. Comput.-Aided Mol. Des.*, **1996**, *10*, 521.
[26] Barlow, T.W. *J. Mol. Graphics*, **1995**, *13*, 24.
[27] Polanski, J. Gasteiger, J.; Wagener, M.; Sadowski, J. *Quant. Struct. Act. Relat.*, **1998**, *17*, 27.
[28] Polanski, J. *SAR QSAR Env. Res.*, **2000**, *11*, 245.
[29] Polanski, J.; Gasteiger, J. *Acta Pol. Pharm.*, **1999**, *56*, 112.
[30] Polanski, J. *Acta Biochim. Pol.*, **2000**, *47*, 37.
[31] Anzali, S.; Barnickel, G.; Krug, M.; Sadowski, J.; Wagener, M.; Gasteiger, J. In: Devillers, J., (Ed.), *Neural Networks in QSAR and Drug Design*, Academic Press, London, **1996**, pp. 209.
[32] Polanski, J.; Gieleciak, R. *Mol. Divers.*, **2003**, *7*, 45.
[33] Polanski, J. In: Gasteiger, J., (Ed.), *Chemoinformatics From Data to Knowledge*, Wiley-VCH, Weinheim, BRD, **2003**, pp. 302-319.
[34] Schneider, G. *Curr. Med. Chem.*, **2002**, *9*, 2095.
[35] Bajorath, J. *Curr. Drug Discov.*, **2002**, *3*, 24.
[36] Sadowski, J.; Wagener, M.; Gasteiger, J. *Angew. Chem. Int. Ed. Engl.*, **1995**, *34*, 2674.
[37] Schneider, G.; Nettekoven, M. *J. Comb. Chem.*, **2003**, *5*, 233.
[38] Sadowski, J.; Gasteiger J. *Chem. Rev.*, **1993**, *93*, 2567.
[39] Sadowski, J.; Gasteiger, J.; Klebe, G. *J. Chem. Inf. Comput. Sci.*, **1994**, *34*, 1000.
[40] CORINA (MATCH3D, SONNIA) are available from Molecular Networks GmbH, Erlangen Germany; see http://www.molecular-networks.com.
[41] Gasteiger, J.; Marsili, M. *Tetrahedron*, **1998**, *36*, 3219.
[42] Gasteiger, J.; Saller H. *Angew. Chem. Int. Engl. Ed.*, **1985**, *24*, 687.
[43] Cramer, R.D.; Petterson, D.E.; Bunce, J.D. *J. Am. Chem. Soc.*, **1988**, *110*, 5959.
[44] Hasegawa, K.; Matsuoka, S.; Arakawa, M.; Funatsu, K. *Comput. Chem.*, **2002**, *26*, 583.
[45] Hopfinger, A.J.; Wang, S.; Tokarski, J.S.; Jin, B.; Albuquerque, M.; Madhav, P.J.; Duraiswami, C. *J. Am. Chem. Soc.*, **1997**, *119*, 10509.
[46] Polanski, J.; Bak, A. *J. Chem. Inf. Comput. Sci.*, **2003**, *43*, 2081.
[47] CORINA (MATCH3D, SONNIA) are available from Molecular Networks GmbH, Erlangen Germany; see http://www.molecular-networks.com
[48] CORINA (MATCH3D, SONNIA) are available from Molecular Networks GmbH, Erlangen Germany; see http://www.molecular-networks.com
[49] Musiol, R.; Podeszwa, B.; Finster, J.; Niedbala, H.; Polanski, J. *Mon. Chem.*, **2006**, *137*, 1211-1217.
[50] Hata, T.; Uno, T. S. *Bull Chem. Soc. Jpn.*, **1972**, *45*, 477.
[51] Polanski, J.; Niedbala, H.; Musiol, R.; Tabak, D.; Podeszwa, B.; Gieleciak, R.; Bak, A.; Palka, A.; Magdziarz, T. *Acta Pol. Pharm.*, **2004**, *61*, 3.
[52] Musiol, R.; Jampilek, J.; Buchta, V.; Silva, L.; Niedbala, H.; Podeszwa, B.; Palka, A.; Majerz-Maniecka, K.A; Oleksyn, B. *Bioorg. Med. Chem.*, **2006**, *14*, 3592.

[53] De Clercq, E. *Med. Res. Rev.*, **2002**, *22*, 531.
[54] Huc, I.; Lehn, J.-M. *Proc. Natl. Acad. Sci. USA*, **1997**, *94*, 2106.
[55] Otto, S.; Furlan, R.L.E.; Sanders, J.M. *Drug Discov. Today*, **2002**, *7*, 117.
[56] Burgi, H.B.; Dunitz, J.D. *Chem. Commun.*, **1969**, *9*, 472.
[57] Majerz-Maniecka, K.A.; Musiol, R.; Nitek, W.; Oleksyn, B.J.; Polanski, J. *Bioorg. Med. Chem. Lett.*, **2006**, *16*, 1005.
[58] Manchot, W.; Furlong, E.N. *Chem. Ber.*, **1909**, *42*, 4389.

Received: February 25, 2006 **Revised: October 2, 2006** **Accepted: October 11, 2006**

Fragment Based Approach for the Investigation of HIV-1 Integrase Inhibition

J. Polanski*,[a], H. Niedbala[a], R. Musiol[a], B. Podeszwa[a], D. Tabak[a], A. Palka[a], A. Mencel[a], J.-F. Mouscadet[b] and M. Le Bret[b]

[a]*Department of Organic Chemistry, Institute of Chemistry, University of Silesia, PL-40-006 Katowice, Poland;* [b]*CNRS UMR 8532, LBPA, Ecole Normale Supérieure de Cachan, 94235 Cachan, France*

Received September 07, 2006: Revised October 24, 2006: Accepted November 14, 2006

Abstract: HIV-1 integrase (IN) inhibition of a novel series of quinoline derivatives was investigated. The compounds were designed on the basis of quinoline molecular scaffolds that attempt to mimic the basic naphtyridine motif of the L-870810 HIV-1 IN inhibitor. It appeared that the IN inhibition of the novel compounds was limited by the electroacceptor substitution within quinoline. Although the compounds studied here indicate structural similarity to L-870810, they are much less efficient than this compound. This can be explained by differences in conformations and apparent magnesium complexing ability in the naphtyridine and quinoline based amides.

Keywords: Quinoline derivatives;HIV-1 integrase inhibition; Structure-activity relationships.

1. INTRODUCTION

The HIV genome encodes an enzyme – integrase (IN) that catalyzes the insertion of reverse transcribed viral DNA into the host cell genome. This enzyme, therefore, plays a key role in the viral replication cycle. IN is a 32-kDa protein (288 amino acids) that consists of three functional domains. The central domain (or core domain, residues 50-210) contains the catalytic triad (DDE) that is essential for enzymatic activity. This domain is flanked by the N-terminal domain, which plays a role in the assembly of an active multimeric form of the enzyme, and the C-terminal domain, which is involved in nonspecific DNA-binding activity. IN activity requires these three domains, protein oligomerization, the integrity of the catalytic triad, and a cationic cofactor such as magnesium [1]. The integration process involves two distinct catalytic steps. During the first step, termed 3'-processing, IN specifically removes two nucleotides from each 3' end of the linear double-stranded viral DNA. The second step, called strand transfer, occurs after the translocation of the viral DNA into the nucleus. During this step, IN transfers both extremities of the viral DNA into the target DNA by a one step trans-esterification reaction, resulting in full-site integration.

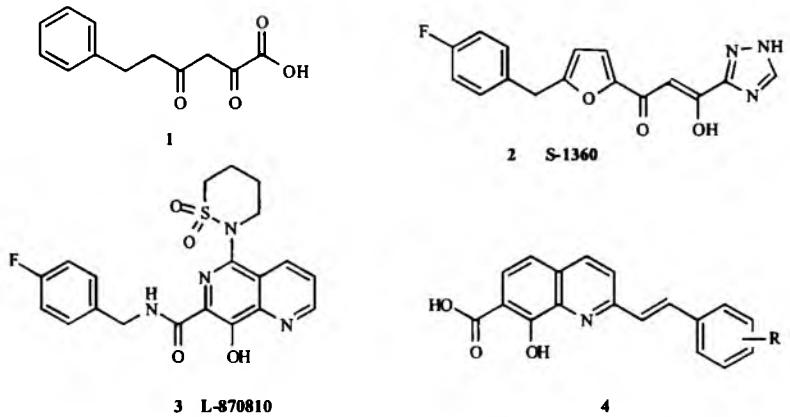

Fig. (1).

Diketoacid **1** compounds (DKA) shown in Fig. (**1**) are potent HIV IN inhibitors with *in vivo* antiviral activity [2, 3]. It also has been found that DKAs inhibit RNAse-H and HCV NS5b polymerase [4, 5]. Moreover, similar compounds are effective antiviral agents against influenza [6]. In HIV therapy, the DKA pharmacophore required heterocyclic replacement of the carboxylic function to obtain

*Address correspondence to this author at the Department of Organic Chemistry, Institute of Chemistry, University of Silesia, PL-40-006 Katowice, Poland; Tel: +48-32-3591128; Fax: +48-32-2599978; E-mail: polanski@us.edu.pl

1570-1808/07 $50.00+.00

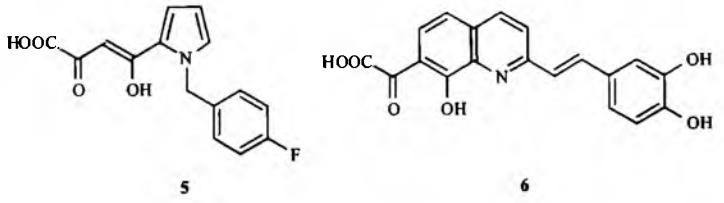

5 6

Fig. (2).

S-1360 **2** or L-870,810 **3**, the first IN targeted drugs under clinical testing [7]. Styrylquinolines (SQ) **4** are another recently discovered class of powerful IN inhibitors that inhibit HIV-1 replication in cell cultures, probably by preventing the binding of DNA to IN [8-14]. Unfortunately, these potent compounds are no longer under clinical trials or further development due to their unexpected side effects. In particular, the research on L-870810 has been stopped due to its toxicity toward liver and kidney cells [15]. However, just recently a novel promising drug candidate MK-0518 has appeared [16]. In this study we attempted to develop new active compounds that could mimic the potent scaffold of L-870810 and S-1360. A different molecular skeleton of novel compounds could be essential in searching for new integrase inhibitors.

Although structural similarities between the heterocyclic systems of naphtyridine in **3** and quinoline in **4** can be observed, the mechanism of inhibition for these compounds is different [14]. An effort to mimic the DKA pharmacophore **5** in the SQ series resulted in compound **6**, as shown in Fig. (2), which appeared to be inactive *in vitro* against IN. However, this compound exhibited significant antiviral activity *in vivo* [12].

Fragment design, an approach whereby drugs are screened from specific low-molecular weight fragments capable of binding to a target receptor, has been developed in recent years [17-19]. Although the affinity of such fragments is too low to ensure drug effectiveness, they appear useful for further construction of leads. In the current publication we synthesized new compounds with improved HIV-1 IN inhibition based on novel quinoline scaffolds [20]. These scaffolds were linked by amide function to aryl moieties similar to the p-fluorophenylmethyl group of compound **3**.

2. RESULTS AND DISCUSSION

8-Hydroxy-7-quinaldic acid **7**, which can be considered a basic scaffold for all reported SQ HIV-1 inhibitors, contains a basic hydroxycarbonyl moiety found in both DKAs and SQs. However, if tested *in vitro*, this compound appeared to be inactive against IN [10].

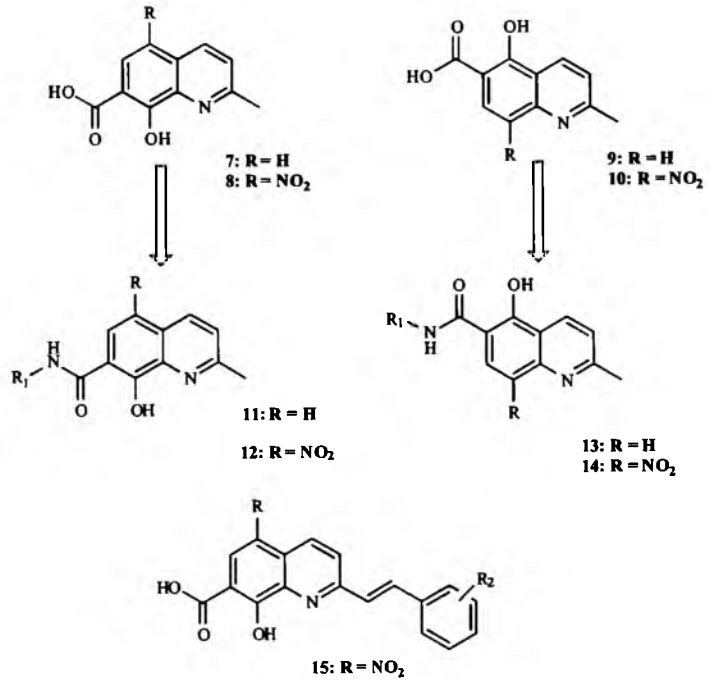

Fig. (3).

Fig. (3) illustrates scaffolds **8-10**, relevant to **7**, which were designed for the improvement of HIV-1 IN inhibition. Table (1) reports inhibition data for scaffolds **7-10** and amides **11-15**. Actually, compounds **9** and **10** appeared to inhibit IN better than compound **7**, with the IC_{50} amounting for 47 and 42 μM [20], respectively. Scaffolds **8** and **8a** appeared to have IC_{50} values higher than 100 μM. However, inhibition measured for these compounds was not completely reliable due to insufficient solubility in the testing medium, in particular with regard to compound **8a**. Scaffolds **7-10** can be used both for the construction of potential drugs related to L-870810, **11-14**, or SQ compounds, such as **15**.

The inhibition data reported here indicate an interesting difference between the IN inhibition values of newly synthesized compounds. Compounds **14** and the SQ-type compound **15** based on novel scaffolds **8** and **10** appeared to have IC_{50} values in the range of 30-50 μM. In contrast, the IC_{50} values for amide **11**, based on scaffold **7**, and amide **13**, based on scaffold **9**, are higher than 100 μM.

Because the main heterocyclic system of scaffold **7** and **9** is isosteric, electronic factors should account for the differences in the IN inhibition of these compounds. In fact, regarding electronic factors, **9** should be a better mimic of the naphtyridine system of L-870810, compound **3**. The increased OH acidity differentiates, for example, compound **3** from the quinoline type cycles. The increased OH acidity favors lower IC_{50} values (compare compound **14a** with **13c**), also according to our previous results [20, 21]. The amidation of **10** yields compounds having IC_{50} values similar to that of scaffold **10**. In contrast, the amidation of **9** results in compounds with an IC_{50} value evidently higher than that of scaffold **9**. Since amidation should decrease the OH acidity, this seems to suggest that a powerful electroacceptor, namely 8-NO_2,, which is capable of increasing the OH acidity, is a group that balances this decrease and creates a higher inhibition of IN by amide **14**.

Further explanation is needed for the fact that the addition of a hydrophobic group to L-870810 does not improve the IC_{50} values of amide **14** in comparison to the original scaffold acid **10**. Essentially the same IC_{50} values are obtained for compounds **10** and **14**. In Fig. (4) we explained this effect by intramolecular hydrogen bonding that favors a different conformation for the naphtyridine L-870 810 and quinoline-like compounds. Thus, two different hydrogen bond stabilized conformations, **Ia** and **Ib** (schematically indicated by the different phenyl moiety position), are available for naphtyridine, while a single conformation **IIb** is available for quinoline. Accordingly, the hydrophobic moiety in **Ia** and **IIb** extends to different spatial locations and cannot enhance IN inhibition for the quinoline-type amides. In addition, Mg^{2+} complexing, which is believed to be an important factor limiting the activity of IN inhibitors [14], will also be preferred in **Ic** and not **IIc**. This would ensure formation of a double oxygen anchor, capable of Mg^{2+} complexing, of a similar structure to the one existing in **Ic**. An alternative Mg^{2+} complexing, due directly to **IIb** and involving the nitrogen-oxygen anchor **IIc**, is less probable due to the low basicity of the nitrogen electron lone pair. Thus, the quinoline system mimics the parent naphtyridine to only some extent both due to the substantial differences in the location of the carbocyclic aromatic group and due to the different Mg^{2+} complexing ability.

Thus, it appeared that a substitution pattern for quinoline is critical for the obtained IN inhibition by amides. Compounds **15** and **16**, having IC_{50} values in a range similar to that of scaffolds **9** and **10**, can further illustrate this rule. The IC_{50} value of SQ **15** is not enhanced by linking to p-metoxystyryl, since, as previously discovered, hydroxystyryl fragments are needed in the non-quinoline moiety for the efficient inhibition of the SQ compound **1** [13]. Similarly, **16a** and **16b**, which include scaffold **8a** derived from **8** by nitro-replacement of the 7-carboxylic function but not including the hydroxystyryl moiety, appeared to have IC_{50} values similar to compound **15**. Thus, the reported compounds demonstrate the maximal IN inhibition level that is provided by the appropriately substituted quinoline moiety, which is, however, not enhanced by additional fragments capable of binding IN.

3. CHEMISTRY

Scheme (1) depicts the synthesis of new compounds based on 8-hydroxyquinaldine scaffolds. Commercially available 8-hydroxyquinaldine undergoes Kolbe-Schmidt reaction to give **7** which was used to obtain appropriate

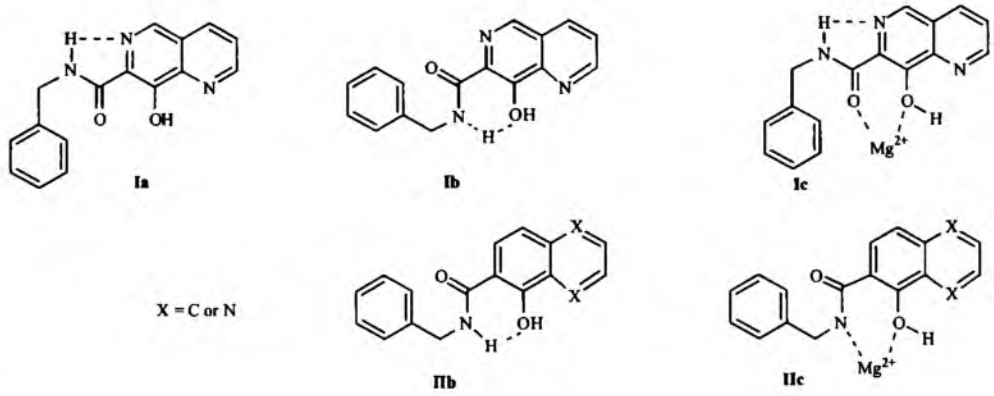

Fig. (4).

Table 1. The IN Inhibition of the Novel Compounds

No.	Structure	IC_{50} [μM]	No	Structure	IC_{50} [μM]
7	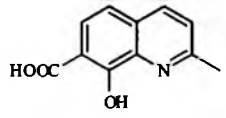	>100[a]	13a	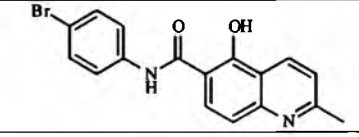	>100
8	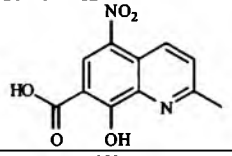	>100[c]	13b	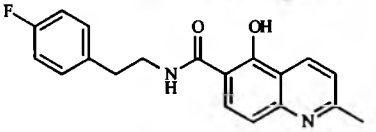	>100
8a	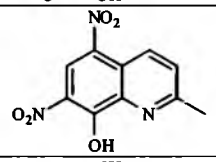	>100[c]	13c	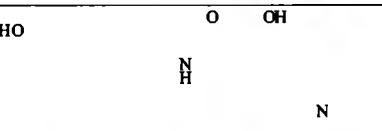	>100
9	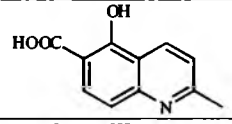	47[b]	13d	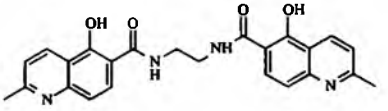	>100
10	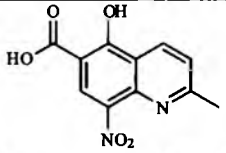	42[b]	14a	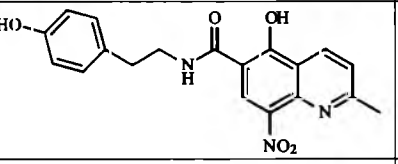	48
11a	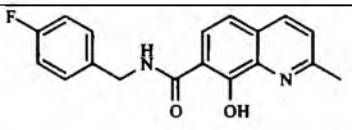	>100	14b	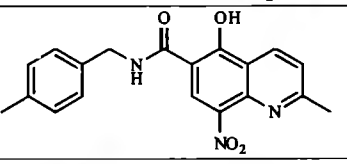	51
11b	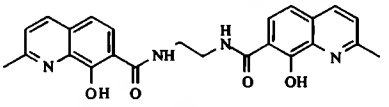	>100	15	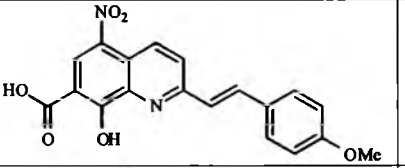	32
11c	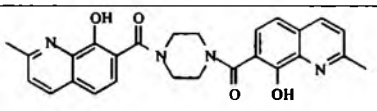	>100	16a	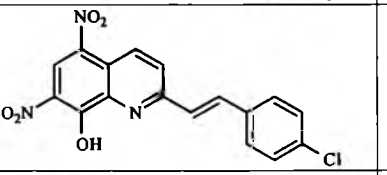	30
11d	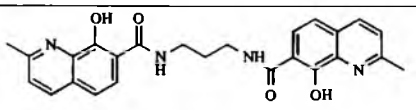	>100	16b	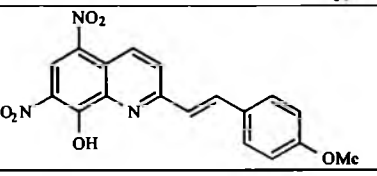	64

[a]according to [8]
[b]according to [20]
[c]cannot be determined accurately, for compound 8a due to its very low solubility

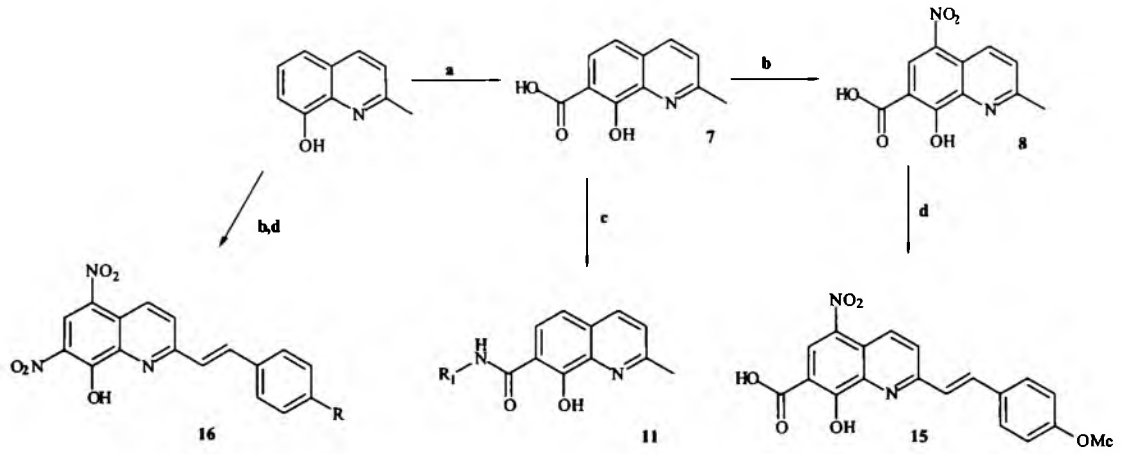

Scheme 1. Synthesis of 8-hydroxyquinaldine: (a) KOH, CO_2; (b) H_2SO_4/HNO_3, 5°C; (c) DCC, amine; (d) aldehyde, microwave irradiation.

amides [19, 20]. Direct nitration of **7** yields **8** which was further reacted to yield **15**. Nitration of 8-hydroxyquinaldine gives known 5,7-dinitroquinaldine which was reacted to yield **16** under microwave irradiation [22].

The derivatives of 5-hydroxyquinaldine-6-carboxylic acid shown in Scheme (**2**) were prepared in a multistep process, as showed above. Commercially available 4-aminosalicylic acid was used in Scraup reaction to obtain **9**. This scaffold was used directly in synthesis of appropriate amides **13**, or **14**.

4. EXPERIMENTAL

Anti-IN inhibition was evaluated in a 96-wells plate assay measuring IN overall activity using short blunt-ended oligonucleotides mimicking viral U5 DNA extremity in the presence of 150 nM recombinant HIV-1 IN and 10 mM Mg^{2+} ions. IC_{50} were obtained from nonlinear regression fitting of dose-response curves using Prism software.

All proton NMR spectra were recorded on Bruker 500 MHz spectrometer. The chemical shifts were expressed in ppm relative to tetramethylsilane as internal standard. When diffuse, easily exchangeable protons were not listed.

General Procedure for the Synthesis of Amides 11, 13 and 14 is as follows

To 10 cm^3 of DCC in dichloromethane 1.5 mmol of quinaldic acid was added and the resulted mixture was stirred at ambient temperature during 30 min. Mixture was cooled to 0°C and 1.5 mmol of appropriate amine (0.75 mmol diamine) was added dropwise. After 30 min. the resulted solid was filtered off and recrystallized from propanol.

8-Hydroxy-2-methylquinoline-7-carboxylic acid 4-fluorobenzylamide (**11a**) white solid, yield 26%, mp 190-196°C. ^1H NMR (DMSO-d_6) δ: 2.59 (s, 3H), 4.08 (s, 2H), 6.98 (d, *J*=8.3 Hz, 1H), 7.24 (d, *J*=8.6 Hz, 2H), 7.3 (d,

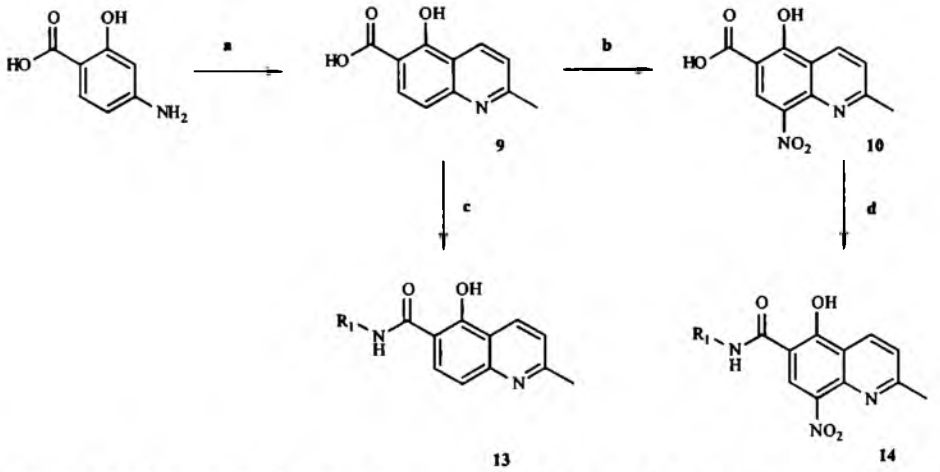

Scheme 2. Synthesis of 5-hydroxyquinoline derivatives: (a) crotonaldehyde, HCl; (b) H_2SO_4/HNO_3, 5°C; (c, d) DCC, amine.

J=8.3 Hz, 1H), 7.5 (d, *J*=5.3 Hz, 2H), 7.75 (d, *J*=8.3 Hz, 1H), 8.03 (d, *J*=8.3H, 1H), 8.51 (bs, 1H), 17.5 (bs, 1H). Anal. calcd for $C_{18}H_{15}FN_2O_2$: C, 69.67; H, 4.87. Found: C, 70.01; H, 4.80.

N,N-di(8-hydroxy-2-methylquinoline-7-carbonyl)ethane-1,2-diamine (**11b**) white solid, yield 7%, mp 254-257°C. ^{1}H NMR (DMSO-d_6) δ: 2.6 (s, 6H), 3.14 (s, 4H), 7.0 (d, *J*=8.3Hz, 2H), 7.33 (d, *J*=8.3Hz, 1H), 7.76 (d, *J*=8.3Hz, 2H), 8.04 (d, *J*=8.3Hz, 2H), 8.5 (bs, 1H). Anal. calcd for $C_{24}H_{22}N_4O_4$: C, 66.97; H, 5.15. Found C, 66.74; H, 5.22.

N,N-di(-8-hydroxy-2-methylquinoline-7-carbonyl)piperazine (**11c**) white solid, yield 10%, mp 284-286°C. ^{1}H NMR (DMSO-d_6) δ: 2.66 (s, 6H); 3.1 (s, 8H), 7.03 (d, *J*=8.4Hz, 2H); 7.43 (d, *J*=8.4Hz, 2H); 7.78 (d, *J*=8.4Hz, 2H); 8.15 (d, *J*=8.4Hz, 2H). Anal. calcd for $C_{26}H_{24}N_4O_4$: C, 68.41; H, 5.30. Found: C, 68.26; H, 5.19.

N,N-Di(8-hydroxy-2-methylquinoline-7-carbonyl)propane-1,3-diamine (**11d**) white solid, yield 23%, mp 293-297°C. ^{1}H NMR (DMSO-d_6) δ: 1.82-1.87(m, 2H), 2.6 (s, 6H); 2.9 (t, 4H), 6.9 (d, *J*=8.4Hz, 2H), 7.32(d, *J*=8.4Hz, 2H); 7.75 (d, *J*=8.4Hz, 2H), 7.93 (bs, 2H); 8.34 (d, *J*=8.4Hz, 2H). Anal. calcd for $C_{25}H_{24}N_4O_4$: C, 67.56; H, 5.44. Found C, 67.34; H, 5.62.

5-Hydroxy-2-methylquinoline-6-carboxylic acid 4-bromoanilide (**13a**) beige solid, yield 30%, mp185°C. ^{1}H NMR (DMSO-d_6) δ: 2.34 (s, 3H); 7.3 (d, *J*=8,8 Hz, 1H); 7.53(d, *J*=8.8 Hz, 1H); 7.6 (d, J = 14,8 Hz, 2H); 7.72 (d, J = 14.8 Hz, 2H); 8.36 (d, *J*=8,8 Hz, 1H); 8,75 – 8,77 (d, *J*=8.4 Hz, 1H). Anal. calcd for $C_{17}H_{13}BrN_2O_2$*$2H_2O$: C, 51.77; H, 3.96. Found C, 51.91; H, 4.33.

5-Hydroxy-2-methylquinoline-6-carboxylic acid 4-fluorobenzylamide (**13b**) brown solid, yield 21%, mp 225°C. ^{1}H NMR (DMSO-d_6) δ: 2.74 (s, 3H); 4.00 (s, 2H); 7.11 (d, *J*=8.3Hz, 1H); 7.21 (d, *J*=8.5Hz, 1H); 7.3 (d, *J*=8,6 Hz, 2H); 7.38 (d, *J*= 8,25 Hz, 1H); 7.5 (d, *J*= 14,05 Hz, 2H); 8.05 (d, *J*=7,4 Hz, 1H); Anal. calcd for $C_{18}H_{15}FN_2O_2$*$2H_2O$: C, 62.09; H, 6.08. Found C, 62.43; H, 5.49.

5-Hydroxy-2-methylquinoline-6-carboxylic acid 2-(4-hydroxyphenyl)ethylamide (**13c**) beige solid, yield 32%, mp 178-182°C. ^{1}H NMR (DMSO-d_6) δ: 2.60 (s, 3H); 2.7 (t, 2H); 2.89 (t, 2H); 6.65 (d, *J*=7.6Hz, 2H); 6.98 (d, *J*=8,2 Hz, 1H); 7.03 (d, *J*=7.6Hz, 2H); 7.20 (d, *J*=8.25 Hz, 1H); 7.85 (d, *J*=8.65 Hz, 1H); 8.35 (d, *J*=8.5 Hz, 1H). Anal. calcd for $C_{19}H_{18}N_2O_3$*1/$2H_2O$: C, 68.34; H, 6.39. Found C, 68.88; H, 6.44.

N,N-di(5-hydroxy-2-methylquinoline-6-carbonyl) ethane-1,2-diamine (**13d**) beige solid, yield 15%, mp 198°C.

^{1}H NMR (DMSO-d_6) δ: 2.71 (s, 6H); 3.08 (t, 4H); 7.1 (d, *J*=8.7 Hz, 2H); 7.4 (d, *J*=8.4 Hz, 2H); 7.98 (d, *J*=8.75 Hz, 2H); 8.62 (d, *J*=8.3Hz, 2H); 16.05 (bs, 2H). Anal. calcd for $C_{24}H_{22}N_4O_4$*3/$2H_2O$: C, 60.74; H, 5.56. Found C, 60.63; H, 5.68.

5-Hydroxy-2-methyl-8-nitroquinoline-6-carboxylic acid 2-(4-hydroxyphenyl)ethylamide (**14a**) yellow solid, 47%, mp 114-117°C. ^{1}H NMR (DMSO-d_6) δ: 2.20 (s, 3H); 2.5 (t, 2H); 2.97 (t, 2H); 6.67 (d, *J*= 7.6Hz, 2H); 7.0 (d, *J*=7.6Hz, 2H); 7.26 (d, *J*=8.2Hz, 1H); 8.49 (d, *J*=7.1Hz, 1H), 8.96 (s, 1H). Anal. calcd for $C_{19}H_{17}N_3O_5$ *$2.5H_2O$: C, 55.23; H, 5.05. Found C, 55.34; H, 5.34.

5-Hydroxy-2-methyl-8-nitroquinoline-6-carboxylic acid 4-methylbenzylamide (**14b**) yellow solid, yield 23%, mp168-172°C. ^{1}H NMR (DMSO-d_6) δ: 2.3 (s, 3H); 2.56 (s, 3H); 3.97 (s, 2H); 7.21 (d, *J*=7.1Hz, 2H); 7.26 (d, *J*=8.1Hz, 1H); 7.31 (d, *J*=7.2Hz, 2H); 8.06 (bs, 1H); 8.49 (d, *J*=7.8Hz, 1H); 8.95 (s, 1H). Anal. calcd for $C_{19}H_{17}N_3O_4$ *$2H_2O$: C, 58.79; H, 4.95. Found C, 58.91; H, 5.42.

General Procedure for Synthesis Of Styrylquinolines 15, 16

1 mmol of quinaldine derivative was thoroughly mixed with 2 mmol of aromatic aldehyde and exposed to microwave irradiation for 6 min as described previously [22]. After the reaction was completed the crude product was washed with hot ether and recrystallized from ethanol.

8-Hydroxy-2-[2-(4-methoxyphenyl)vinyl]-5-nitroquinoline-7-carboxylic acid (**15**) brown solid, yield 24%, mp228-230°C. ^{1}H NMR (DMSO-d_6) δ: 3.8 (s, 3H); 7.05 (d, *J*=8.6Hz, 2H), 7.6 (d, *J*=8.2Hz, 2H); 7.9 (d, *J*=16.1Hz, 1H); 8.1 (d, *J*=16.5Hz, 1H); 8.5 (d, *J*=9.15Hz, 1H); 9.1 (s, 1H); 9.53 (d, *J*=9.1Hz, 1H). Anal. calcd for $C_{19}H_{14}N_2O_6$: C, 62.30; H, 3.85. Found C, 62.48; H, 3.52.

2-[2-(4-Chlorophenyl)vinyl]-5,7-dinitro-8-hydroxyquinoline (**16a**) Brown solid, yield 19%, mp 255-260°C. ^{1}H NMR (DMSO-d_6) δ: 7,5 (m,2H); 7,92-8,4 (m,3H); 8,62-8,65 (m 2H); 9,2 (s,1H); 9,55 (d, J=9Hz, 1H), Anal. calcd for $C_{17}H_{10}N_3O_5Cl$*$2H_2O$: C, 50.07; H, 3.46. Found C, 50.12; H, 3.37.

2-[2-(4-Methoxyphenyl)vinyl]-5,7-dinitro-8-hydroxyquinoline (**16b**) brown solid, yield 54%, mp 230°C. ^{1}H NMR (DMSO-d_6) δ: 2.48 (s, 3H), 6.73 (d, *J*=10.3 Hz, 2H), 6.86 (d, *J*=10.3 Hz, 2H), 7.3 (d, *J*=8.3 Hz, 1H), 8.35 (d, *J*=8.3 Hz, 1H), 9.24 (d, *J*=15.8 Hz, 1H), 11.4 (s, 1H), 12.15 (d, *J*=15.8 Hz, 1H). Anal. calcd for $C_{18}H_{13}N_3O_6$ C, 58.86; H, 3.57. Found C, 59.17; H, 4.08.

5. CONCLUSION

We investigated the HIV IN inhibition of a novel series of quinoline derivatives based on molecular scaffolds related to those present in L-870810 and SQ inhibitors. The IN inhibition of the novel compounds was limited by the electroacceptor substitution within quinoline. Although the compounds studied here indicate some structural similarity to L-870810, they are much less efficient than this compound. This can probably be explained by conformational differences in the naphtyridine and quinoline based amides. It appeared that quinoline mimicked the parent naphtyridine only to some extent. This is due to both the substantial conformational differences resulting from the intramolecular hydrogen bond formation and due to the different Mg^{2+} complexing ability. Thus, the electroacceptor NO_2 substitution that makes the breaking of hydrogen bonds easier and enhances Mg^{2+} complexing ability also favors HIV integrase inhibition.

ACKNOWLEDGMENT

This work is supported in part by a KBN grant KBN 3T09A 01127, Anti-IN screening program is supported by

the French agency for research against AIDS (ANRS) and by the European program TRIoH (FP6 503480).

REFERENCES

[1] Deprez, E.; Barbe, S.; Kolaski, M.; Leh, H.; Zouhiri, F.; Auclair, C.; Brochon, J.C.; Le Bret, M.; Mouscadet, J.F. *Mol. Pharmacol.*, **2004**, *65*, 85.

[2] Hazuda, D.J.; Felock P.; Witmer, M.; Wolfe, A.; Stillmock, K.; Grobler, J.A.; Espeseth, A.; Gabryelski, L.; Schleif, W.; Blau, C.; Miller, M.D. *Science*, **2000**, *287*, 646.

[3] Long, Y-Q.; Jiang, X-H.; Dayam, R.; Sanchez, T.; Shoemaker, R.; Sei, S.; Neamati, N. *J. Med. Chem.*, **2004**, *47*, 2561.

[4] Shaw-Reid, C. A.; Munshi, V.; Graham, P.; Wolfe, A.; Witmer, M.; Danzeisen, R.; Olsen, D. B.; Carroll, S. S.; Embrey, M.; Wai, J. S.; Miller, M. D.; Cole, J. L.; Hazuda, D. J. *J. Biol. Chem.*, **2003**, *278*, 2777.

[5] Summa, V.; Petrocchi, A.; Pace, P.; Matassa, V.G.; De Francesco, R.; Altamura, S.; Tomei, L.; Koch, U.; Neuner, P. *J. Med. Chem.*, **2004**, *47*, 14.

[6] Hastings, J. C.; Selnick, H.; Wolanski, B.; Tomassini, J. E. *Antimicrob. Agents Chemother.*, **1996**, *40*, 1304.

[7] Johnson, A.A.; Marchand, Ch.; Pommier, Y. *Curr. Topics in Med. Chem.*, **2004**, *4*, 1059.

[8] Mekouar, K.; Mouscadet, J.-F.; Desmaele, D.; Subra, F.; Leh, H.; Savoure, D.; Auclair, Ch.; d'Angelo, J. *J. Med. Chem.*, **1998**, *41*, 2846.

[9] Ouali, M.; Laboulais, C.; Leh, H.; Gill, D.; Desmaele, D.; Mekouar, K.; Zouhiri, F.; d'Angelo, J.; Auclair, Ch.; Mouscadet, J.-F.; Le Bret, M. *J. Med. Chem.*, **2000**, *43*, 1949.

[10] Zouhiri, F.; Mouscadet, J.-F.; Mekouar, K.; Desmaele, D.; Savoure, D.; Leh, H.; Subra, F.; Le Bret, M.; Auclair, Ch.; d'Angelo, J. *J. Med. Chem.*, **2000**, *43*, 1533.

[11] Polanski, J.; Zouhiri, F.; Jeanson, L.; Desmaële, D.; d'Angelo, J.; Mouscadet, J.-F.; Gieleciak, R.; Gasteiger, J.; Le Bret, M. *J. Med. Chem.*, **2002**, *45*, 4647.

[12] Zouhiri, F.; Desmaele, D.; d'Angelo, J.; Ourevitch, M.; Mouscadet, J.-F.; Leh, H.; Le Bret, M. *Tetrahedron Lett.*, **2001**, *42*, 8189.

[13] Benard, Ch.; Zouhiri, F.; Normand-Bayle, M.; Danet, M.; Desmaele, D.; Leh, H.; Mouscadet, J.-F.; Mbemba, G.; Thomas, C.-M.; Bonnenfant, S.; Le Bret, M.; d'Angelo, J. *Bioorg. Med. Chem. Lett.*, **2004**, *14*, 2473.

[14] Pommier, Y.; Johnson, A.A.; Marchand, C. *Nat. Rev. Drug Discov.*, **2005**, *4*, 236.

[15] Little, S.; Drusano, G.; Schooley, R.; Haas, D.; Kumar, P.; Hammer, S.; McMahon, D.; Squires, K.; Asfour, R.; Richman, D.; Chen, J.; Saah, A.; Leavitt, R.; Hazuda, D.; Nguyen, B.Y. *Antiretroviral effect of L-000870810, a novel HIV-1 integrase inhibitor, in HIV-1 infected patients.* abstract 161, XII CROI, Boston, **2005**.

[16] Lataillade, M.; Kozal, M.J. *AIDS Patients Care STD*, **2006**, *20*, 489.

[17] Fattori, D. D. *Drug. Discov. Today*, **2004**, *9*, 229.

[18] Erlanson, D. A.; McDowell, R. S.; O'Brien, T. *J. Med. Chem.*, **2004**, *47*, 3463.

[19] Shuker, S. B.; Hajduk, P. J.; Meadows, R. P.; Fesik, S. W. *Science*, **1996**, *274*, 1531.

[20] Polanski, J.; Niedbala, H.; Musiol, R.; Podeszwa, B.;. Tabak, D.; Palka, A.; Mencel, A.; Finster, J.; Mouscadet, J. F.; Le Bret, M. *Lett. Drug Des. Discov.*, **2006**, *3*, 175.

[21] Majerz-Maniecka, K.A.; Musiol, R.; Nitek, W.; Oleksyn, B.J.; Polanski, J. *Bioorg. Med. Chem. Lett.*, **2005**, *16*, 1005.

[22] Musiol, R.; Podeszwa B., Finster J., Niedbala, H.; Polanski, J. *Monatsh. Chem.*, **2006** *137*, 1211.

Available online at www.sciencedirect.com
ScienceDirect
Bioorganic & Medicinal Chemistry Letters 17 (2007) 6138–6141
Bioorganic & Medicinal Chemistry Letters

Investigating the antiproliferative activity of quinoline-5,8-diones and styrylquinolinecarboxylic acids on tumor cell lines

B. Podeszwa,[a] H. Niedbala,[a] J. Polanski,[a,*] R. Musiol,[a] D. Tabak,[a] J. Finster,[a] K. Serafin,[a] M. Milczarek,[b] J. Wietrzyk,[b] S. Boryczka,[c] W. Mol,[c] J. Jampilek,[d,e] J. Dohnal,[d,e] D. S. Kalinowski[f] and D. R. Richardson[f]

[a]*Department of Organic Chemistry, Institute of Chemistry, University of Silesia, PL-40006 Katowice, Poland*
[b]*Department of Experimental Oncology, Ludwik Hirszfeld, Institute of Immunology and Experimental Therapy, Polish Academy of Sciences, PL-53114 Wroclaw, Poland*
[c]*Department of Organic Chemistry, Medical University of Silesia, PL-41200 Sosnowiec, Poland*
[d]*Zentiva a.s., CZ-10237 Prague 10, Czech Republic*
[e]*Department of Chemical Drugs, Faculty of Pharmacy, University of Veterinary and Pharmaceutical Sciences, CZ-61242 Brno, Czech Republic*
[f]*Department of Pathology, Iron Metabolism and Chelation Program, University of Sydney, Sydney, New South Wales 2006, Australia*

Received 25 July 2007; revised 7 September 2007; accepted 8 September 2007
Available online 14 September 2007

Abstract—The structure–activity relationships of new quinoline based compounds were investigated. Quinoline-5,8-dione and styrylquinoline scaffolds were used for the design of potentially active compounds. The novel analogues had comparable antiproliferative activity to cisplatin when evaluated in a bioassay against the P388 leukemia cell line. However, these compounds appeared far less efficient against SK-N-MC neuroepithelioma cells. Analogues without the 5,8-dione structure but containing the 8-carboxylic acid group were also found to induce antiproliferative activity. Hydrophobicity as measured by HPLC did not correlate with antiproliferative activity.

Quinoline-5,8-dione is a substantial molecular fragment of lavendamycin (**1**) and related compounds (**2**, **3**). Lavendamycin was originally isolated from the fermented broth of *Streptomyces lavendulae* and this class of compounds were identified in the 1970s as anti-tumor agents.[1]

The efficient synthesis of compound **2** made a number of analogues available and revealed interesting biological activity.[2–5] Their antiproliferative effects on cancer cells, including leukemia cells[6,7] and A549 carcinoma cells, have been reported.[8]

Although the toxicity of lavendamycin makes it unsuitable for clinical use, the activity of this compound has inspired several investigations.[9–12] Recently, the syntheses of a series of quinoline-5,8-diones and lavendamycin derivatives have been described. The evaluation of their antiproliferative activity against transformed cells and a normal rat kidney epithelial cell line validates their importance as potential anti-tumor agents.[3] In the current study, we investigated the potential anti-tumor activity of several known and novel quinoline-5,8-dione analogues and derivatives.

As reported recently, structural modification of lavendamycin to quinoline-5,8-diones having H or Me substitutions at position 2 retains high cytotoxicity. However, the resulting drugs are unselective and do not differentiate between tumor and normal cells, making their pharmaceutical use as anti-cancer agents problematic. On the other hand, the unmodified lavendamycin molecule showed improved selectivity against cancer cells. The highest selective toxicity being observed for analogues having a carboxylic acid group or its derivative at the C-2′ position (see **1**, **2** in Fig. 1).[3]

Keywords: Antiproliferative activity; Quinoline-5,8-diones; Quinolinecarboxylic acid.
* Corresponding author. E-mail: Polanski@us.edu.pl

0960-894X/$ - see front matter © 2007 Elsevier Ltd. All rights reserved.
doi:10.1016/j.bmcl.2007.09.040

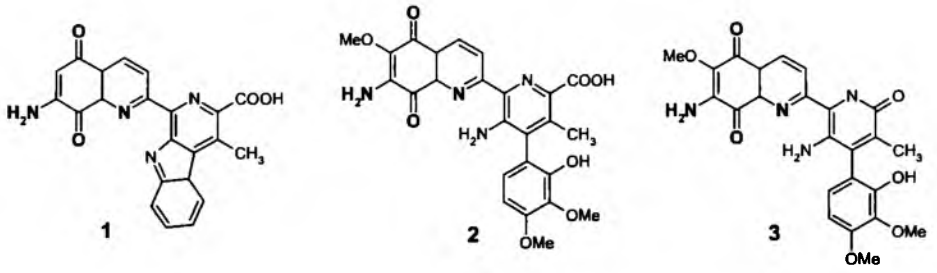

Figure 1. Structures of: lavendamycin (**1**), streptonigrin (**2**), and streptonigrone (**3**). In bold, the 7-aminoquinoline-5,8-dione moiety is shown.

In the current investigation, we examined the antiproliferative activity of a series of quinoline-5,8-diones against the mouse leukemia P388 line and human SK-N-MC cancer cell type. This includes both the analogues previously described and novel compounds **7**, **9** and **10**. Moreover, the effectiveness of the carboxylic substitution within the non-quinoline moiety of lavendamycin inspired us to investigate the importance of the carboxylic substitution by itself. Therefore, we synthesized a series of quinoline analogues **12–32** having carboxylic substitution(s) in the carbocyclic ring.

As shown in Figure 2, quinolines containing the carboxylic group were obtained according to Skraup protocol from appropriate aminobenzoic acids. Styrylquinolines were synthesized from 8-hydroxyquinaldine or quinaldic acids by the Skraup reaction, employing a microwave-assisted protocol.[13,14] Multi-step reactions lead us to **4** and **5**. Acylation with appropriate chlorides afforded amides **6–10**.

The antiproliferative activity of the synthesized compounds was tested against the P388 mouse leukemia and SK-N-MC human neuroblastoma cell lines.[15] Results are shown in Table 1. The clinically used cytotoxic agent, cisplatin, was used as a reference compound in this examination. Generally, the antiproliferative activity of the quinolinediones on P388 cells (Table 1, compounds **6–10**) was similar to that of cisplatin. The level of antiproliferative activity of compounds **6–10** against P388 cells was similar, irrespective of the individual 7-**R**(CO)N-substitution pattern. The N-unsubstituted compound **4** was also an efficient cytotoxic agent, although the activity of this compound was lower. It is noteworthy that the 7-methoxy substitution in compound **5** preserves the activity of analogue **4**. This indicates that although the 7-amido substitution (compounds **6–10**) is necessary for high cytotoxicity, the potent activity of the quinolinedione scaffold is not limited to the 7-amine substitution. The antiproliferative activity of the two quinoline-5,8-dione compounds, **5** and **6**, tested against SK-N-MC cells, was far less potent than that seen in P388.

We investigated if further modification of the quinoline scaffold by the removal of the 5,8-quinone function would retain activity. Therefore, 8-hydroxy-5,7-dinitroquinoline **11** was obtained. The presence of the nitro-

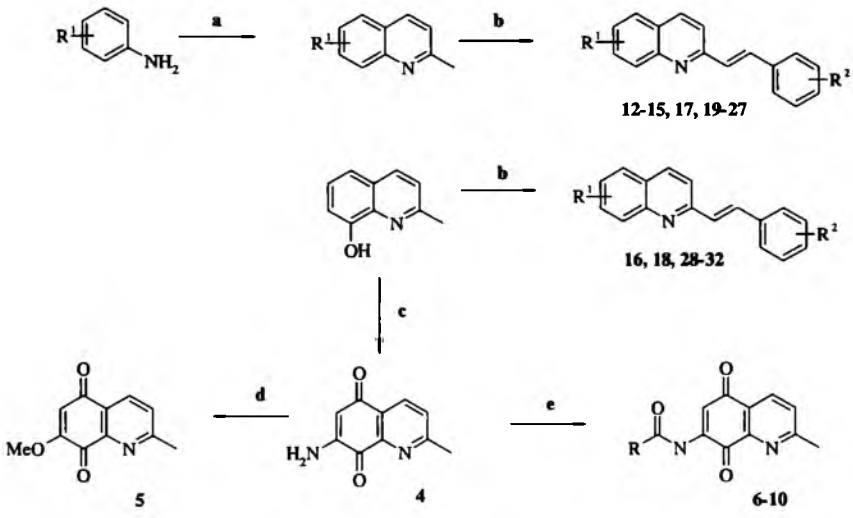

Figure 2. (a) Skraup synthesis, crotonaldehyde; (b) microwave irradiation[13] and aromatic aldehyde; (c) multi-step synthesis described earlier[2]; (d) MeOH; (e) Py/acid chlorides.

Table 1. Log K determinations using HPLC and antiproliferative activity assay results of the compounds examined in this study

Compound[a]	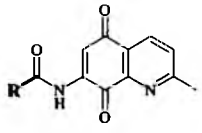	Log K	Antiproliferative activity	
			P388	SK-N-MC
	R		IC_{50} (μM)	IC_{50} (μM)
4	See Figure 2	ND	10.31 ± 6.80	ND
5	See Figure 2	0.0907	6.10 ± 2.80	4.26
6	CH_3–	0.2227	1.61 ± 0.87	> 6.25
7	CH_3CH_2–	ND	1.43 ± 1.06	ND
8	$CH_3CH_2CH_2$–	ND	1.51 ± 0.85	ND
9	$PhCH_2CH_2$–	ND	1.44 ± 0.28	ND
10	(*E*)-PhCH=CH–	ND	2.39 ± 0.34	ND
11	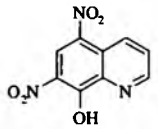	0.7154	7.14 ± 3.78	> 6.25
	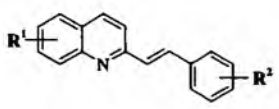			
	R^1	R^2		
12	8-COOH	2-OH	1.6787	13.56 ± 1.24	ND
13	5,8-COOH	2-Cl	1.2047	113.72 ± 14.70	ND
14	5,8-COOH	4-Cl	1.2107	109.68 ± 10.54	ND
15	5,8-COOH	3-Cl	1.2163	113.81 ± 32.42	ND
16	5,7-NO_2-8-OH	4-OMe	ND	79.11 ± 10.64	ND
17	6-COOH	4-Cl	1.6043	116.29 ± 46.91	ND
18	8-OH	3-Cl	1.5395	15[b]	ND
19	6-COOH	2-OH	1.3842	51.15 ± 31.44	ND
20	5,8-COOH	2-Br	1.2062	89.40 ± 30.43	ND
21	5-COOH	3-OMe	1.2263	100.02 ± 24.3	ND
22	8-COOH	4-Cl	1.8165	15.33 ± 1.26	ND
23	6-COOH	3-Cl	1.6315	109.77 ± 53.91	ND
24	5-COOH	2-OH	1.2550	30[b]	ND
25	5,8-COOH	3-OMe	1.1811	25[b]	ND
26	5-COOH	4-Br	1.4397	109.12 ± 18.21	ND
27	7-COOH	2-OH	1.3678	30[b]	ND
28	5,7-NO_2-8-OH	4-Cl	ND	7.14 ± 3.78[c]	ND
29	5,7-NHAc-8-OAc	2,4-OMe	ND	20[b]	ND
30	5-NO_2-7-COOH-8-OH	2-Cl	ND	158.38 ± 45.53	ND
31	5-NO_2-7-COOH-8-OH	4-OMe	ND	147.63 ± 49.44	ND
32	5,7-NHAc-8-OAc	2-Br	ND	6.58 ± 4.43	ND
	cisplatin			**3.39 ± 1.54**	ND

The results are means ± standard deviation of 3–7 experiments. ND, not determined.

[a] Compounds **4–6** and **11** were described previously in Ref. 2, compound **8** in Ref. 4, compounds **12, 15, 16, 18, 19, 21, 24, 27** in Ref. 3, **28, 29, 31** in Ref. 16, **23** in Ref. 17.

[b] Antiproliferative activity could be measured only as percent of inhibition of cancer cells proliferation at 0.1 μM.

[c] Under poor solubility in the test medium.

substituents makes the 8-hydroxy group highly acidic which should mimic the 8-quinolinone structure. In fact, it appeared that this compound was an efficient antiproliferative agent against P388 cells, having activity similar to that of the unsubstituted 7-aminequinaldine-5,8-dione (compound **4**). The SAR observed in compounds **6–10** indicated that the cytotoxic activity of these analogues depended only to a limited extent upon the individual structure of the amide group. It is of interest to note that there is a marked difference in the antiproliferative activity of compounds **5**, **6**, and **11** when comparing P388 leukemia cells and the SK-N-MC neuroepithelioma line. Similarly to compound **6**, analogue **11** showed very limited activity against the SK-N-MC line, while compound **5** was active against both line types.

In the styrylquinoline series (compounds **12–32**), some interesting relationships between structural properties and P388 cell line activity were observed. Compound **28** having the 8-OH function of the acidity enhanced by 5,7-dinitro substitution showed the activity similar to that of compounds **4** and **11**, which can be probably explained by the effect similar to that discussed for compound **11**.

The carboxylic group located at the C-8 position was found to induce antiproliferative effects, as observed in compounds **12** and **22**. If we compare the activity of compounds **12** and **22** to the high activity of compound **11**, where the 8-hydroxy group mimics the C=O through nitro substitution, the antiproliferative efficacy was probably due to the close proximity of the C=O and the heterocyclic nitrogen. This explanation is thought to be more probable to explain the activity rather than implicating the ionizable properties of the 8-COOH group. This feature is reminiscent of the original lavendamycin **1** structure, featuring a carbonyl with a neighboring heterocyclic nitrogen.

On the other hand, the CO/N proximity rule was no longer true if an additional COOH group was present within the quinoline moiety, e.g., the activity of compounds **13–15** was much lower than that observed for compound **12** or the activity of compounds **30** and **31** was much lower than that observed for **22**.

The same effect was observed for all compounds having the COOH substitution accompanied by an additional electroaccepting group. Thus, compound **32** having high activity (CO/N proximity can be here identified by the heterocyclic N and 8-O(CO)Me substitution) can be compared to low activity compounds **30–31** which have an additional 5-COOH/7-NO_2 system. Since such a substitution increases the ionization of COOH, this suggests that this effect is disadvantageous for antiproliferative activity.

The attempt to explain the antiproliferative activity of this series of compounds by hydrophobicity measured by HPLC (column 3, Table 1) was unsuccessful. This parameter did not closely correlate with antiproliferative activity.

Acknowledgments

This study has been supported by Polish Ministry of Science Grant No. 3T09A 01127 and by the Ministry of Education of the Czech Republic MSM 6215712403. D.R.R. thanks the National Health and Medical Research Council (NHMRC) of Australia for Fellowship and Project Grant funding and the Australian Research Council (ARC) for a Discovery Grant. D.S.K. appreciates the support of an Australian Post-Graduate Award.

References and notes

1. Rao, K. V. *Cancer Chemother. Rep.* Part 2 **1974**, *4*, 11.
2. Behforouz, M.; Haddad, J.; Cai, W.; Arnold, M. B.; Mohammadi, F.; Sousa, A. C.; Horn, M. A. *J. Org. Chem.* **1996**, *61*, 6552.
3. Behforouz, M.; Cai, W.; Mohammadi, F.; Stocksdale, M. G.; Gu, Zh.; Ahmadian, M.; Baty, D. E.; Etling, M. R.; Al-Anzi, Ch. H.; Swiftney, T. M.; Tanzer, L. R.; Merriman, R. L.; Behforouz, N. C. *Bioorg. Med. Chem.* **2007**, *15*, 495.
4. Behforouz, M.; Cai, W.; Stocksdale, M. G.; Lucas, J. S.; Jung, J. Y.; Briere, D.; Wang, A.; Katen, K. S.; Behforouz, N. C. *J. Med. Chem.* **2003**, *46*, 5773.
5. Behforouz, M.; Gu, Z.; Cai, W.; Horn, M. A.; Ahmadian, M. *J. Org. Chem.* **1993**, *58*, 7089.
6. Balitz, D. M.; Bush, J. A.; Bradner, W. T.; Doyle, T. W.; O'Herron, F. A.; Nettleton, D. E. *J. Antibiot. (Tokyo)* **1982**, *35*, 259.
7. Abe, N.; Nakakita, Y.; Nakamura, T.; Enoki, N.; Uchida, H.; Takeo, S.; Munekata, M. *J. Antibiot. (Tokyo)* **1993**, *46*, 1672.
8. Fang, Y.; Linardic, C. M.; Richardson, D. A.; Cai, W.; Behforouz, M.; Abraham, R. T. *Mol. Cancer Ther.* **2003**, *2*, 517.
9. Doyle, T. W.; Balitz, D. M.; Grulich, R. E.; Nettleton, D. E.; Gould, S. J.; Tann, C.-H.; Meows, A. E. *Tetrahedron Lett.* **1981**, *22*, 4595.
10. Hackethal, C. A.; Golbey, R. B.; Tan, C. T. C.; Karnofsky, D. A.; Burchenal, J. H. *Antibiot. Chemother.* **1961**, *11*, 178.
11. Boger, D. L.; Yasuda, M.; Mitscher, L. A.; Drake, S. D.; Kitos, P. A.; Thompson, S. C. *J. Med. Chem.* **1987**, *30*, 1918.
12. Wilson, W. L.; Labra, C.; Barrist, E. *Antibiot. Chemother.* **1961**, *11*, 147.
13. Musiol, R.; Podeszwa, B.; Finster, J.; Niedbala, H.; Polanski, J. *Monatsh. Chem.* **2006**, *137*, 1211.
14. Musiol, R.; Jampilek, J.; Kralova, K.; Richardson, D. R.; Kalinowski, D. S.; Podeszwa, B.; Finster, J.; Niedbala, H.; Palka, A.; Polanski, J. *Bioorg. Med. Chem.* **2007**, *15*, 1280.
15. The mouse P388 leukemia cell line and human SK-N-MC neuroepithelioma cell type were obtained from the American Type Culture Collection (Rockville, MD, U.S.A.). The P388 cell line was cultured in RPMI 1640 medium with 2 mM L-glutamine adjusted to contain 1.5 g/L sodium bicarbonate, 4.5 g/L glucose, and 1.0 mM sodium pyruvate, 10% fetal bovine serum (FBS) at 37 °C in 5% CO_2. The SK-N-MC cell type was cultured in minimum essential medium (MEM; Gibco, Melbourne Australia) containing 10% (v/v) FBS, 1.0 mM sodium pyruvate (Gibco), 1% (v/v) non-essential amino acids (Gibco), 2 mM L-glutamine (Gibco), 100 U/mL penicillin (Gibco), streptomycin (Gibco), and 0.28 μg/mL fungizone (Squibb Pharmaceuticals, Montreal, Canada). Twenty-four hours before addition of the tested compounds, the cells were plated in 96-well plates. The assay was performed after 72 h exposure to varying concentrations of the tested agents. The results were calculated as IC_{50} values. Each concentration of each individual compound was tested in triplicate in a single experiment, with each experiment being repeated 3–7 times. After 72 h of incubation with tested compounds, 20 μL of MTT solution (MTT: stock solution: 5 mg/mL) was added to each well and incubated for 4 h at 37 °C. After this incubation, 80 μL of the lysis mixture was added to each well (lysis mixture: 225 mL dimethylformamide, 67.5 g sodium dodecyl sulphate, and 275 mL of distilled water). The optical densities of the samples were read after an incubation of 24 h at 570 nm.
16. Polanski, J.; Niedbala, H.; Musiol, R.; Podeszwa, B.; Tabak, D.; Palka, A.; Mencel, A.; Mouscadet, J.-F.; Le Bret, M. *Lett. Drug Des. Discov.* **2007**, *4*, 99.
17. Polanski, J.; Niedbala, H.; Musiol, R.; Tabak, D.; Podeszwa, B.; Gieleciak, R.; Bak, A.; Palka, A.; Magdziarz, T. *Acta Pol. Pharm., Drug Res.* **2004**, *61*, 3.

Available online at www.sciencedirect.com
ScienceDirect
Polyhedron 26 (2007) 5120–5130
POLYHEDRON
www.elsevier.com/locate/poly

The reactions between $[RuHCl(CO)(PPh_3)_3]$ and quinoline carboxylic acids

J.G. Małecki [a,*], R. Kruszyński [b], D. Tabak [c], J. Kusz [d]

[a] *Department of Crystallography, Institute of Chemistry, University of Silesia, 9th Szkolna St., 40-006 Katowice, Poland*
[b] *Department of X-Ray Crystallography and Crystal Chemistry, Institute of General and Ecological Chemistry, Łódź University of Technology, 116 Żeromski St., 90-924 Łódź, Poland*
[c] *Department of Organic Chemistry, Institute of Chemistry, University of Silesia, 9th Szkolna St., 40-006 Katowice, Poland*
[d] *Institute of Physics, University of Silesia, 4th Uniwersytecka St., 40-006 Katowice, Poland*

Revised 11 July 2007; accepted 12 July 2007
Available online 24 August 2007

Abstract

The reactions of $[RuHCl(CO)(PPh_3)_3]$ with 8-hydroxy-2-methyl-quinoline-7-carboxylic acid and quinoline-2-carboxylic acid have been examined, and two novel ruthenium(II) complexes – $[(PPh_3)_2RuH(CO)(C_{10}H_8NO_3)]$ and $[(PPh_3)_2RuCl(CO)(C_9H_6O_2)]$ – have been obtained. The compounds have been studied by IR and UV–Vis spectroscopy, and X-ray crystallography. The molecular orbital diagrams of the complexes have been calculated with the density functional theory (DFT) method. The spin-allowed singlet–singlet electronic transitions of the compounds have been calculated with the time-dependent DFT method, and the UV–Vis spectra of the compounds have been discussed on this basis.

Keywords: Ruthenium; Quinoline carboxylic acid; Hydride and carbonyl complexes; X-ray structure; TDDFT method

1. Introduction

The quinoline moiety is present in many classes of biologically active compounds. A number of them have been clinically used as antifungal, antibacterial and antiprotozoic drugs [1,2] as well as antituberculotic agents [3,4]. Some quinoline-based compounds show antineoplastic activity [5]. Quinoline derivatives reveal also antiasthmatic and antiplatelet activity [6–10] and due to acetylcholinesterase inhibition, these compounds are potential drugs for treatment of nervous diseases [11]. Recently strong attention has been focused on styrylquinoline derivatives because of their activity as prospective HIV integrase inhibitors [12–16]. The study dealing with styrylquinoline derivatives showed that they could also possess strong antifungal activity [17], thus the compounds containing 8-hydroxyquinoline pharmacophore seem especially interesting. According to the results reported recently, some new 8-hydroxyquinoline derivatives possess interesting antifungal and herbicidal activities [18–20].

On the other hand ruthenium carbonyl and hydride complexes are very interesting due to their catalytic and structural properties. As it was shown for the complex with quinoline 2-carboxylic acid, the formation of *cis*-coordinated metal complexes is often a leading step in the cytostatic processes involving metal based drugs [21].

In this paper we present the synthesis and characterisations of two novel ruthenium(II) complexes containing the quinoline moiety.

2. Experimental

2.1. Physical measurements

Infrared spectra were recorded on a Nicolet Magna 560 spectrophotometer in the spectral range 4000–400 cm^{-1}

* Corresponding author.
E-mail addresses: gmalecki@us.edu.pl (J.G. Malecki), kruszyna@p.lodz.pl (R. Kruszyński), tapcio@interia.pl (D. Tabak).

0277-5387/$ - see front matter © 2007 Elsevier Ltd. All rights reserved.
doi:10.1016/j.poly.2007.07.023

Table 1
Crystal data and structure refinement details of $[(PPh_3)_2RuH(CO)(C_{10}H_8NO_3)]\cdot 0.5CH_3OH$ (1) and $[(PPh_3)_2RuCl(CO)(C_9H_6O_2)]$ (2)

	1	2
Empirical formula	$C_{49.50}H_{45}NO_{5.50}P_2Ru$	$C_{47}H_{36}ClNO_3P_2Ru$
Formula weight	904.88	861.23
Temperature (K)	293(2)	293(2)
Crystal system	monoclinic	monoclinic
Space group	$P2_1/n$	$P2_1/n$
Unit cell dimensions		
a (Å)	12.3516(5)	10.9441(5)
b (Å)	15.1962(5)	21.2302(11)
c (Å)	22.7646(9)	16.8572(8)
β	97.205(4)	92.153(4)
Volume (Å^3)	4239.1(3)	3913.9(3)
Z	4	4
D_{calc} (Mg/m^3)	1.418	1.462
Absorption coefficient (mm^{-1})	0.496	0.595
$F(000)$	1868	1760
Crystal dimensions (mm)	0.08 × 0.08 × 0.28	0.04 × 0.12 × 0.38
θ Range for data collection (°)	2.83–25.00	2.91–25.00
Index ranges	$-14 \leqslant h \leqslant 14$, $-8 \leqslant k \leqslant 18$, $-27 \leqslant l \leqslant 26$	$-7 \leqslant h \leqslant 13$, $-25 \leqslant k \leqslant 25$, $-20 \leqslant l \leqslant 20$
Reflections collected	26145	24198
Independent reflections [R_{int}]	7333 [0.0371]	6860 [0.0467]
Data/restraints/parameters	7333/0/543	6860/0/496
Goodness-of-fit on F^2	0.915	0.977
Final R indices [$I > 2\sigma(I)$]	$R_1 = 0.0338$ $wR_2 = 0.0746$	$R_1 = 0.0267$ $wR_2 = 0.0627$
R indices (all data)	$R_1 = 0.0669$, $wR_2 = 0.0793$	$R_1 = 0.0467$, $wR_2 = 0.0652$
Largest difference in peak and hole (e Å^{-3})	0.857 and −0.508	0.516 and −0.357

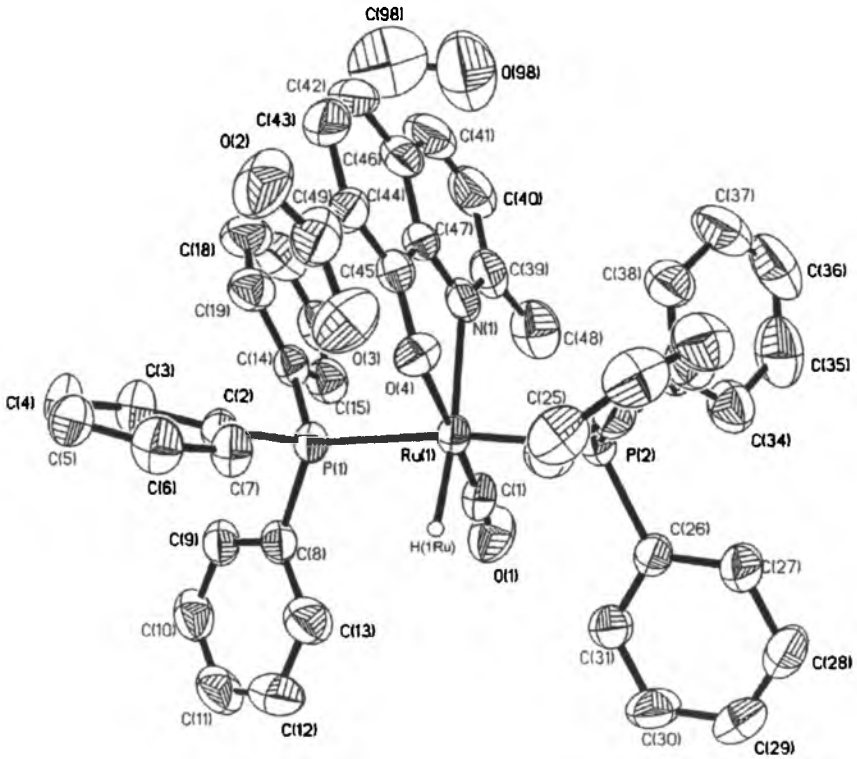

Fig. 1. Drawing of $[(PPh_3)_2RuH(CO)(C_{10}H_8NO_3)]\cdot 0.5CH_3OH$ with 50% probability displacement ellipsoids. The hydrogen atoms except H(1Ru) are omitted.

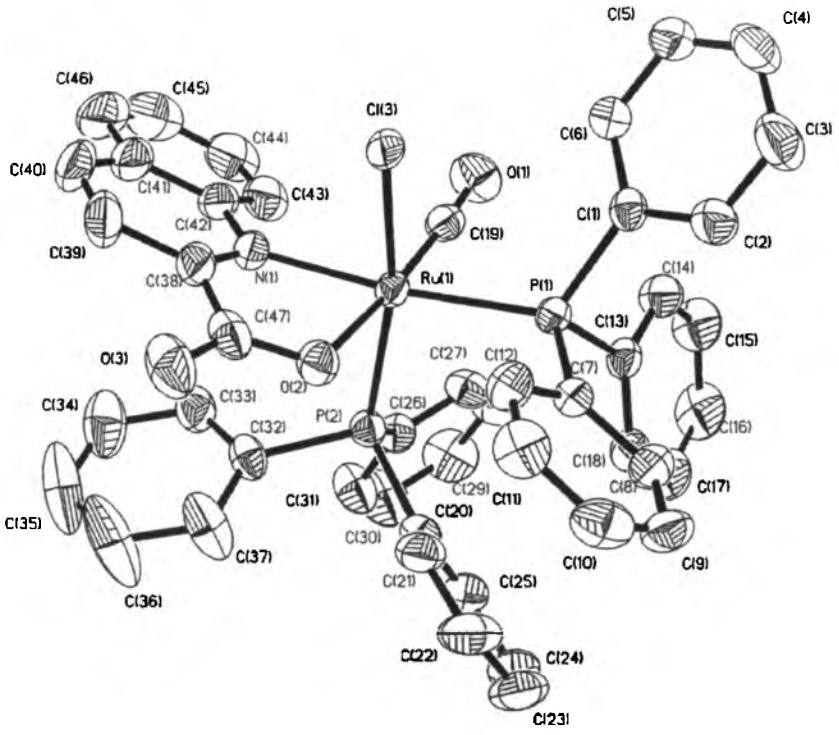

Fig. 2. Drawing of $[(PPh_3)_2RuCl(CO)(C_9H_6O_2)]$ with 50% probability displacement ellipsoids. The hydrogen atoms are omitted for clarity.

with the samples in the form of KBr pellets. Electronic spectra were measured on a Lab Alliance UV–Vis 8500 spectrophotometer in the range 800–200 nm in dichloromethane solution. Elemental analyses (C, H, N) were performed on a Perkin–Elmer CHN–2400 analyzer.

All reagents, except the 8-hydroxy-2-methylquinoline-7-carboxylic acid, used for the synthesis of the complexes are commercially available and were used without further purification. The $[RuHCl(CO)(PPh_3)_3]$ complex was synthesised using a literature method [22]. The 8-hydroxy-2-methylquinoline-7-carboxylic acid was synthesised as described in the literature [13].

2.2. Synthesis of $[(PPh_3)_2RuH(CO)(C_{10}H_8NO_3)]$ (1) and $[(PPh_3)_2RuCl(CO)(C_9H_6O_2)]$ (2)

A suspension of $[RuHCl(CO)(PPh_3)_3]$ (0.95 g, 1×10^{-3} mol) and 8-hydroxy-2-methyl-quinoline-7-carboxylic acid (0.21 g) or quinoline-2-carboxylic acid (0.18 g) in methanol (100 cm^{-3}) was refluxed until the solid dissolved, then the solution was cooled and filtered. Crystals suitable for X-ray crystal analysis were obtained by slow evaporation of the reaction mixture. Yield 78% (1) and 82% (2).

Anal. Calc. for 1: $C_{47}H_{36}ClNO_3P_2Ru$: C, 63.94; H, 4.58; N, 3.64. Found: C, 64.01; H, 4.53; N, 3.66%.

2: $C_{50}H_{42}ClNO_3P_2Ru$: C, 66.48; H, 4.69; N, 1.55. Found: C, 66.28; H, 4.59; N, 1.51%.

IR (KBr, cm^{-1}): 1: 3055 ν_{CH}; 2925 $\nu_{CH\text{-phenyl}}$; 1945 ν_{Ru-H}; 1918 ν_{CO}; 1610 ν_{CN}; 1590 asν_{COO}; 1482 $\delta_{(C-CH\text{ in the plane})}$; 1436 $\nu_{Ph(P-Ph)}$; 1378 sν_{COO}; 1121 $\delta_{(C-CH\text{ in the plane})}$; 996 $\delta_{(C-C\text{ out of the plane})}$; 756 $\delta_{(C-C\text{ out of the plane})}$; 697 $\delta_{(C-C\text{ in the plane})}$.

2: 3060 ν_{CH}; 1938 ν_{CO}; 1650 ν_{CN}; 1596 asν_{COO}; 1482 $\delta_{(C-CH\text{ in the plane})}$; 1434 $\nu_{Ph(P-Ph)}$; 1348 sν_{COO}; 1089 $\delta_{(C-CH\text{ in the plane})}$; 750 $\delta_{(C-C\text{ out of the plane})}$; 696 $\delta_{(C-C\text{ in the plane})}$.

UV–Vis [nm] in CH_3OH (logε): 1: 400 (3.48); 357 sh (3.59); 332 (3.77); 281 (4.31); 210 (4.40).

2: 350 (3.01); 283 (3.38); 238 (4.20); 206 (4.32).

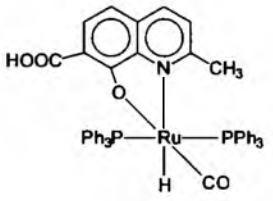

Fig. 3. Structural drawing of $[(PPh_3)_2RuH(CO)(C_{10}H_8NO_3)]$.

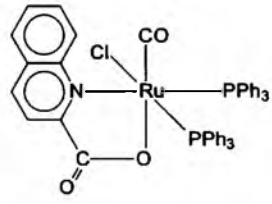

Fig. 4. Structural drawing of $[(PPh_3)_2RuCl(CO)(C_9H_6O_2)]$.

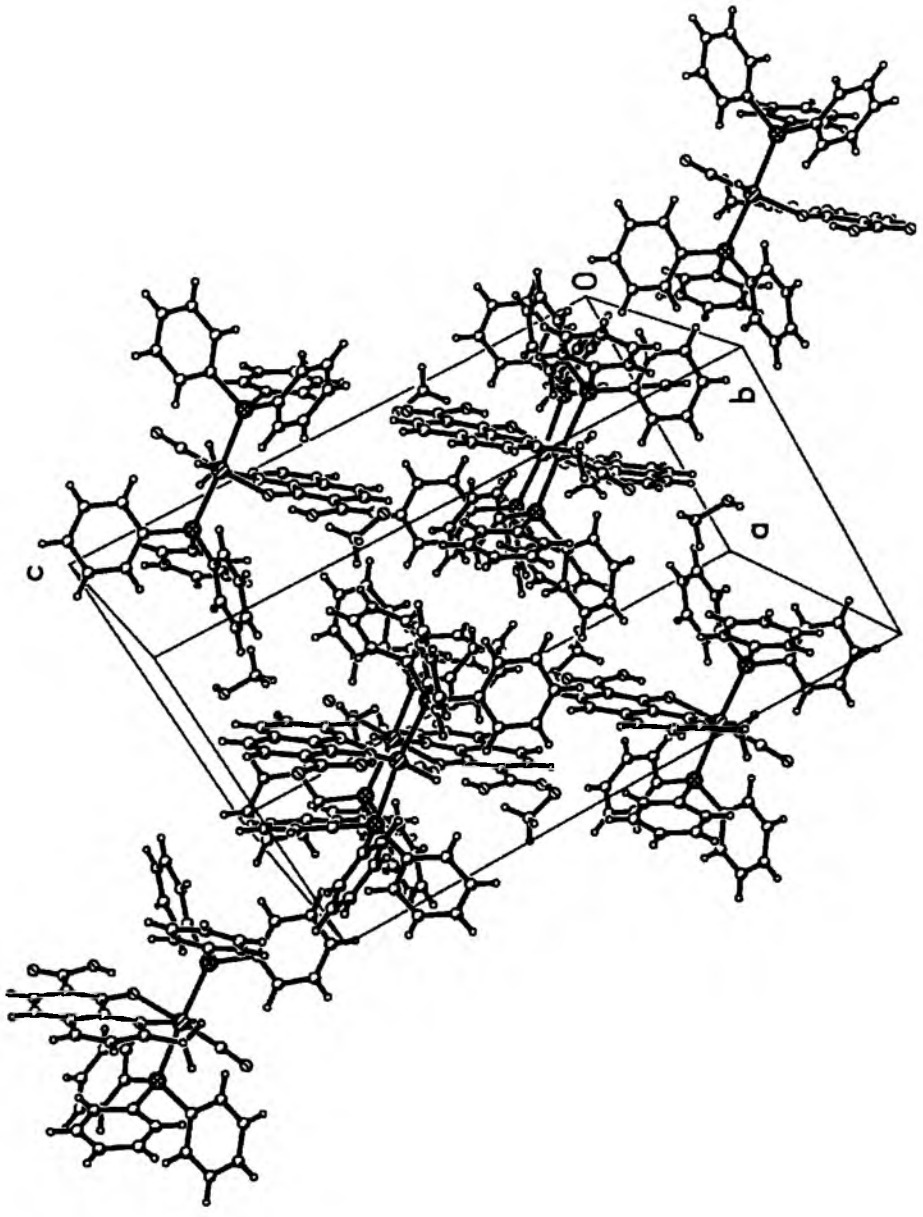

Fig. 5. Part of the molecular packing of $[(PPh_3)_2RuH(CO)(C_{10}H_8NO_3)]$.

2.3. DFT calculations

The GAUSSIAN-03 program [23] was used for the calculations. The geometry optimisation was carried out using the DFT method with the B3LYP functional [24,25]. The electronic transitions were calculated with the PCM model [26] with dichloromethane as the solvent. The calculation was performed using the DZVP basis set [27] with f functions and with exponents 1.94722036 and 0.748930908 on the ruthenium atom and polarisation functions for all other atoms: 6–31g(2d,p) – chlorine, 6–31g** – carbon, nitrogen, oxygen, and 6–31g(d,p) – hydrogen. Natural bond orbital (NBO) calculations were performed using the NBO code [28] included in GAUSSIAN-03.

2.4. Crystal structure determination and refinement

A green prism of complex **1** and a white prism of **2** were mounted in turn on a KM-4-CCD automatic diffractometer equipped with a CCD detector, and were used for data

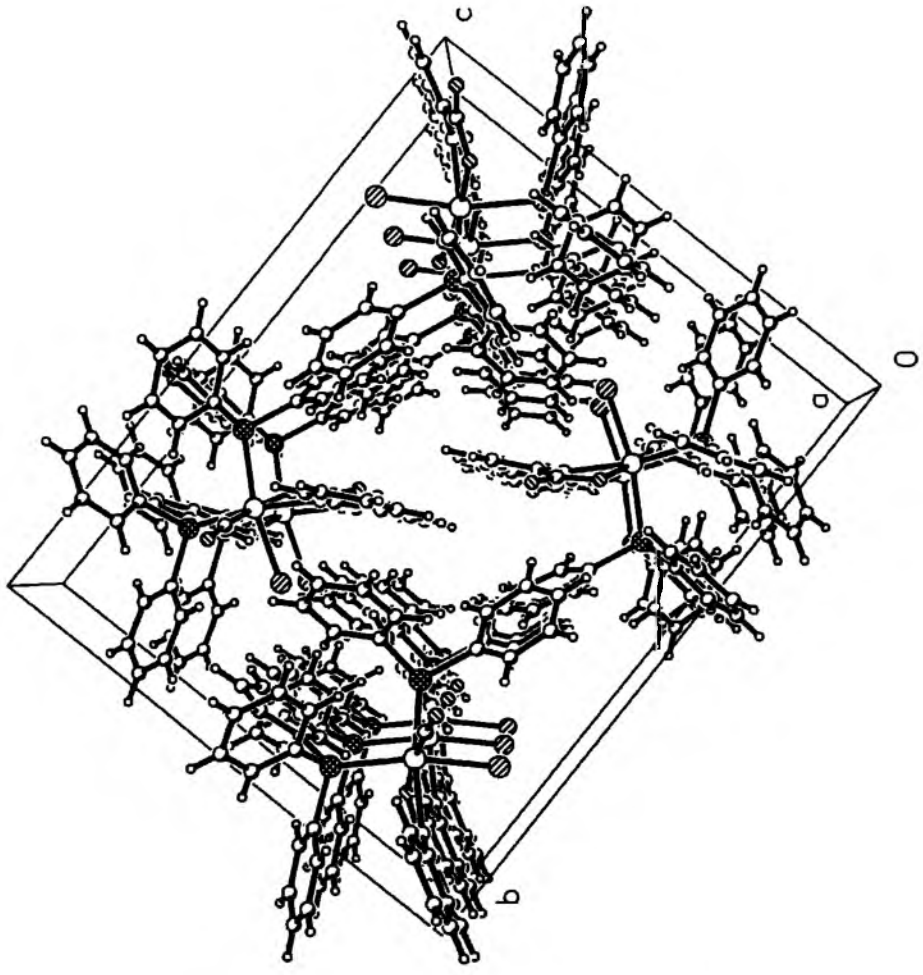

Fig. 6. Part of the molecular packing $[(PPh_3)_2RuCl(CO)(C_9H_6O_2)]$.

collection. X-ray intensity data were collected with graphite monochromated Mo Kα radiation ($\lambda = 0.71073$ Å) at the temperature 295.0(3) K, with the ω scan mode. The Ewald sphere reflections were collected up to $2\theta = 50.0°$ for both complexes. The unit cell parameters were determined from least-squares refinement of the setting angles of 7333 and 6860 strongest reflections for complexes **1** and **2**, respectively. Details concerning the crystal data and refinement are gathered in Table 1. The reference frames, monitored every 40 measurement frames, show 1.01% decay for the crystal of compound **1** and no decay for the crystal of compound **2**. During the data reduction of compound **1** a decay correction was taken into account. Lorentz, polarisation and numerical absorption [29] corrections were applied. The structures were solved using the Patterson method combined with a partial structure expansion procedure. All the non-hydrogen atoms were refined anisotropically using the full-matrix, least-squares technique on F^2. The hydrogen atoms were found from difference Fourier synthesis after four cycles of anisotropic refinement, and refined as "riding" on the adjacent atom with an individual isotropic temperature factor equal to 1.2 times the value of the equivalent temperature factor of the parent atom. The H(1Ru) atom in complex **1** was placed in a calculated position (Ru–H distance 1.6 Å) according to similar compounds [30–36]. SHELXS97 [37], SHELXL97 [38] and SHELXTL [39] programs were used for all calculations. Atomic scattering factors had values incorporated in the computer programs.

3. Results and discussion

The reaction between the $[RuHCl(CO)(PPh_3)_3]$ complex and 8-hydroxy-2-methyl-quinoline-7-carboxylic acid or quinoline-2-carboxylic acid in methanolic solution gives the mononuclear ruthenium(II) compounds $[(PPh_3)_2RuH-$

$(CO)(C_{10}H_8NO_3)]$ (green, air-stable, crystalline solid) and $[(PPh_3)_2RuCl(CO)(C_9H_6O_2)]$ (white solid). Infrared spectra of the complexes exhibit characteristic bands of coordinated ligands – quinoline carboxylic acid, CO, PPh_3 and the hydride group.

The strong bands at 1938 and 1918 cm^{-1} for complex **1** and **2**, respectively, are assigned to the ν_{CO} stretching vibrations of the ruthenium bonded carbonyl group, and the band at 1945 cm^{-1} corresponds to ν_{Ru-H} of the hydride ligand (complex **1**). The ν_{CO} and ν_{Ru-H} stretching vibrations in the $[RuHCl(CO)(PPh_3)_3]$ complex are at 2020 and 1903 cm^{-1}, respectively. The bands at 1610 and 1650 cm^{-1} are attributed to the CN stretching vibration of the quinoline ligand. The asymmetric and symmetric ν_{COO} stretching bands are at 1590, 1596 cm^{-1} and 1378, 1348 cm^{-1} for compounds **1** and **2**, respectively.

The positions of the ν_{CO} and ν_{Ru-H} bands in the IR spectrum of complex **1** indicate a decrease of the metal–carbonyl carbon interaction and an increase of the Ru–H bond order. Taking into account the IR spectra of both complexes, the quinoline type ligand is a σ-donor that induces a large Ru–CO back-bonding.

3.1. Crystal structure

Both obtained complexes crystallise in the monoclinic space group $P2_1/n$. The crystal data of complexes **1** and **2** are given in Table 1. The molecular structures of **1** and **2** are presented in Figs. 1 and 2 (see Figs. 3, 4), respectively, and molecular packing is depicted, receptively, in Figs. 5 and 6. The ruthenium atom in the complex $[(PPh_3)_2RuH(CO)(C_{10}H_8NO_3)]$ is in a distorted octahedral environment with *trans*-triphenylphosphine ligands (angle P(1)–Ru(1)–P(2) 172.19(3)°). The carbonyl ligand is in a *trans*-position to the O donor atom (C(1)–Ru(1)–O(4) 178.12(11)°) and the hydrido ion lies *trans* to the coordinated nitrogen from the quinoline ligand – with an angle of 170.0°. The Ru–N bond distance is longer in complex **1** than in complex **2** due to the *trans* effect of the hydride ligand. The interatomic distances in the carbonyl and triphenylphosphine ligands are normal.

In the structure of compound **I** one very weak intramolecular O(4)–HO(3) hydrogen bond (D···A distance 2.554(3) Å and D–H···A angle 151.7°) and one very weak intermolecular C(40)–H(40)O(98) hydrogen bond (D···A distance 3.290(10) Å and D–H···A angle 139.5°) can be found.

The ruthenium atom of complex **2**, $[(PPh_3)_2RuCl(CO)(C_9H_6O_2)]$, is also in a distorted octahedral environment with *cis*-triphenylphosphine ligands (angle P–Ru–P 99.28(2)°). The carbonyl ligand is in a *trans* position to the carboxylic O donor atom (O(2)–Ru–C(19) 174.95(9)°) and the chloride ion is *trans* to the P(2) atom −166.11(2)°. All Ru–ligand distances, namely Ru–Cl 2.4250(6), Ru–P 2.3763(7), 2.3861(7), Ru–N 2.169(2), Ru–C 1.826(3) and Ru–O 2.1035(16) Å, are normal and comparable with distances in other ruthenium complexes containing heterocyclic ligands.

Table 2
Selected bond lengths (Å) and angles (°) for $[(PPh_3)_2RuH(CO)(C_{10}H_8NO_3)]$ (**1**) and $[(PPh_3)_2RuCl(CO)(C_9H_6O_2)]$ (**2**)

	1			2	
	Experimental	Calculated		Experimental	Calculated
Bond lengths (Å)					
Ru(1)–C(1)	1.805(4)	1.806	Ru(1)–C(19)	1.826(3)	1.865
Ru(1)–O(4)	2.127(19)	2.126	Ru(1)–O(2)	2.1035(16)	2.108
Ru(1)–N(1)	2.221(3)	2.225	Ru(1)–N(1)	2.169(2)	2.243
Ru(1)–P(2)	2.355(8)	2.354	Ru(1)–P(2)	2.3861(7)	2.456
Ru(1)–P(1)	2.360(8)	2.361	Ru(1)–P(1)	2.3763(7)	2.438
Ru(1)–H(1Ru)	1.6042	1.604	Ru(1)–Cl(3)	2.4250(6)	2.458
C(1)–O(1)	1.231(4)	1.159	C(19)–O(1)	1.155(3)	1.164
Angles (°)					
C(1)–Ru(1)–O(4)	178.12(11)	178.14	C(19)–Ru(1)–O(2)	174.95(9)	178.18
C(1)–Ru(1)–N(1)	103.76(12)	103.67	N(1)–Ru(1)–C(19)	98.15(10)	101.67
O(4)–Ru(1)–N(1)	75.66(9)	75.83	O(2)–Ru(1)–N(1)	77.43(7)	76.57
C(1)–Ru(1)–P(2)	92.83(10)	92.87	P(1)–Ru(1)–C(19)	84.89(8)	87.79
O(4)–Ru(1)–P(2)	89.02(6)	88.97	P(1)–Ru(1)–O(2)	99.05(5)	94.03
N(1)–Ru(1)–P(2)	97.25(6)	97.33	N(1)–Ru(1)–P(1)	169.76(6)	163.87
C(1)–Ru(1)–P(1)	86.66(10)	86.68	C(19)–Ru(1)–P(2)	99.86(8)	97.02
O(4)–Ru(1)–P(1)	91.55(6)	91.53	O(2)–Ru(1)–P(2)	82.70(5)	82.57
N(1)–Ru(1)–P(1)	90.44(6)	90.44	N(1)–Ru(1)–P(2)	89.87(6)	90.77
P(2)–Ru(1)–P(1)	172.19(3)	172.10	P(2)–Ru(1)–P(1)	99.28(2)	101.11
C(1)–Ru(1)–H(1Ru)	85.4	85.30	C(19)–Ru(1)–Cl(3)	92.45(8)	93.27
O(4)–Ru(1)–H(1Ru)	95.1	95.09	O(2)–Ru(1)–Cl(3)	84.56(5)	86.92
N(1)–Ru(1)–H(1Ru)	170.0	170.21	N(1)–Ru(1)–Cl(3)	81.98(6)	80.28
P(2)–Ru(1)–H(1Ru)	86.1	85.99	P(1)–Ru(1)–Cl(3)	88.14(2)	86.21
P(1)–Ru(1)–H(1Ru)	86.1	86.12	P(2)–Ru(1)–Cl(3)	166.11(2)	167.56

The molecules in the crystal are connected by four very weak C–H···O intramolecular hydrogen bonds: C(12)–H(12)···O(2) (D···A distance 3.059(3) Å, D–H···A angle 120.0°), C(21)–H(21)···O(2) (D···A distance 3.074(3) Å, D–H···A 145.6°), C(6)–H(6)···Cl(3) (D···A distance 3.208(3) Å, D–H···A angle 108.90°) and C(43)–H(43)···O(1) (D···A distance 3.267(4) Å, D–H···A angle 132.6°).

3.2. Geometry optimisation

The geometries of the studied complexes were optimised by the DFT method with the B3LYP functional. The geometry parameters for the optimised complexes are gathered in Table 2. In general, the predicted bond lengths and angles are in agreement with the X-ray structural data. The largest difference is found for the C(1)–O(1) bond (~0.072 Å) (compound **1**). The maximum differences between the optimised and experimental geometry of compound **2** are exhibited in the Ru(1)–N(1) distance (0.074 Å) and N(1)–Ru(1)–P(1) angle (5.9°).

3.3. Charge distribution and NBO analysis

The calculated charges on the ruthenium atom in the studied complexes are considerable lower than the formal charge of +2 and are close to −0.01 and 0.26 for **1** and **2**, respectively. The charges on the P atoms are positive and close to 1.15 (1.20); the charge on the chloride ligand in $[(PPh_3)_2RuCl(CO)(C_9H_6O_2)]$ is larger than −1 (−0.55), the charge on the quinoline carboxylic acid ligands is close to −0.64 for **1** and −0.52 for **2**. The occupancies of the ruthenium d orbitals, obtained from the NBO analysis, are as follow: d_{xy} – 1.73; d_{xz} – 1.84; d_{yz} – 1.21; $d_{x^2-y^2}$ – 1.23; d_{z^2} – 1.61 for $[(PPh_3)_2RuH(CO)(C_{10}H_8NO_3)]$ and d_{xy} – 1.80; d_{xz} – 1.74; d_{yz} – 1.75; $d_{x^2-y^2}$ – 1.13; d_{z^2} – 0.96 for $[(PPh_3)_2RuCl(CO)(C_9H_6O_2)]$.

The Ru–C bond orbitals in the two studied complexes are polarised towards the carbon atom, and the C≡O bond orbitals are polarised towards the oxygen end. The oxygen atoms of the carbonyl ligands have one lone pair (LP) orbital. The occupancies of the Ru–C bonds are (*anti*-bonding NBOs are given in round brackets)

Table 3
The energy and character of selected occupied and virtual MOs for $[(PPh_3)_2RuH(CO)(C_{10}H_8NO_3)]$ (**1**) and $[(PPh_3)_2RuCl(CO)(C_9H_6O_2)]$ (**2**)

	$[(PPh_3)_2RuH(CO)(C_{10}H_8NO_3)]$ (**1**)		$[(PPh_3)_2RuCl(CO)(C_9H_6O_2)]$ (**2**)	
	E (eV)	Character	*E* (eV)	Character
HOMO – 20	−7.902	$\pi_{qu} + n_P$	−7.728	$\pi_{Cl} + n_P$
HOMO – 19	−7.788	π_{qu}	−7.510	π_{Cl}
HOMO – 18	−7.393	$\pi_{qu} + \sigma_H$	−7.282	π_{Ph}
HOMO – 17	−7.306	$\pi_{phosphine}$	−7.219	π_{Ph}
HOMO – 16	−7.249	$\pi_{phosphine}$	−7.203	$\pi_{qu} + \pi_{Cl}$
HOMO – 15	−7.200	π_{COOH}	−7.099	$\pi_{Ph} + \pi_{COO}$
HOMO – 14	−7.067	π_{Ph}	−7.061	$\pi_{Cl} + \pi_{Ph}$
HOMO – 13	−6.999	π_{Ph}	−7.040	$\pi_{COO} + d$
HOMO – 12	−6.983	π_{Ph}	−6.949	π_{Ph}
HOMO – 11	−6.966	π_{Ph}	−6.931	π_{Ph}
HOMO – 10	−6.893	π_{Ph}	−6.865	π_{Ph}
HOMO – 9	−6.860	π_{Ph}	−6.838	π_{Ph}
HOMO – 8	−6.787	π_{Ph}	−6.819	π_{Ph}
HOMO – 7	−6.776	$\pi_{Ph} + d + \pi_{CO}$	−6.770	π_{Ph}
HOMO – 6	−6.708	$\pi_{Ph} + d + \pi_{CO}$	−6.721	π_{Ph}
HOMO – 5	−6.669	$\pi_{Ph} + d$	−6.675	$\pi_{Ph} + d + \pi_{CO}$
HOMO – 4	−6.615	π_{Ph}	−6.596	π_{Ph}
HOMO – 3	−6.400	$d + \pi_{CO} + n_P$	−6.588	$\pi_{Ph} + d + \pi_{CO}$
HOMO – 2	−6.313	$d + \pi^*_{CO}$	−6.487	$\pi_{Cl} + \pi_{qu}$
HOMO – 1	−5.886	$d + n_P$	−6.248	$d + \pi^*_{Cl}\pi_{Co}$
HOMO	−5.255	$d + \pi^*_{qu}$	−6.119	$d + \pi^*_{Cl}$
LUMO	−1.567	π^*_{qu}	−2.025	π^*_{qu}
LUMO + 1	−0.838	$d_{z^2} + \pi^*_{qu}$	−1.518	$d - \sigma_{Cl} - n_p$
LUMO + 2	−0.759	$\pi^*_{qu} + \pi^*_{Ph}$	−0.999	π^*_{qu}
LUMO + 3	−0.631	$d + \pi^*_{Ph}$	−0.882	$d + \pi^*_{qu}$
LUMO + 4	−0.571	$d + \pi^*_{Ph}$	−0.811	$d + \pi^*_{Ph}$
LUMO + 5	−0.484	π^*_{Ph}	−0.713	π^*_{Ph}
LUMO + 6	−0.272	π^*_{Ph}	−0.555	π^*_{Ph}
LUMO + 7	−0.179	π^*_{Ph}	−0.539	π^*_{Ph}
LUMO + 8	−0.160	π^*_{Ph}	−0.433	$d + \pi^*_{CO} + \pi^*_{Ph}$
LUMO + 9	−0.098	π^*_{Ph}	−0.248	$d + \pi^*_{CO} + \pi^*_{Ph}$
LUMO + 10	0.041	π^*_{Ph}	−0.218	$\pi^*_{Ph} + \pi^*_{CO}$
LUMO + 11	0.065	π^*_{Ph}	−0.174	$d + \pi^*_{CO} + \pi^*_{Ph}$
LUMO + 12	0.201	$d + \pi^*_{CO} + \pi^*_{Ph}$	−0.063	π^*_{Ph}
LUMO + 13	0.234	$d + \pi^*_{CO} + \pi^*_{Ph}$	−0.052	π^*_{Ph}

for complex **1**: 1.976 (0.398) and for complex **2**: 1.938 (0.272).

3.4. Electronic structure

The energies and characters of several highest occupied and lowest unoccupied molecular orbitals of the studied complexes are presented in Table 3. The HOMO–LUMO gaps of complexes **1** and **2** are 3.69 and 4.09 eV, respectively. In both cases, the ruthenium atom possesses a d^6 configuration. The highest MO is d_{xz} with a contribution of the p_π antibonding orbitals from the quinoline ligand in the case of complex **1** and from the chlorine ligands of compound **2**. The π_{Ru-CO} bonding interaction contribute in the H-2 and H-3 orbitals of compounds **1** and **2**. The π^*_{Ru-CO} orbitals are also distributed among several unoccupied molecular orbitals. They contribute in L + 12, L + 13 (complex **1**) and L + 9, L + 11 for **2**. The LUMO orbitals are localised on the quinoline ring. The d_{z^2} orbital of the Ru atom

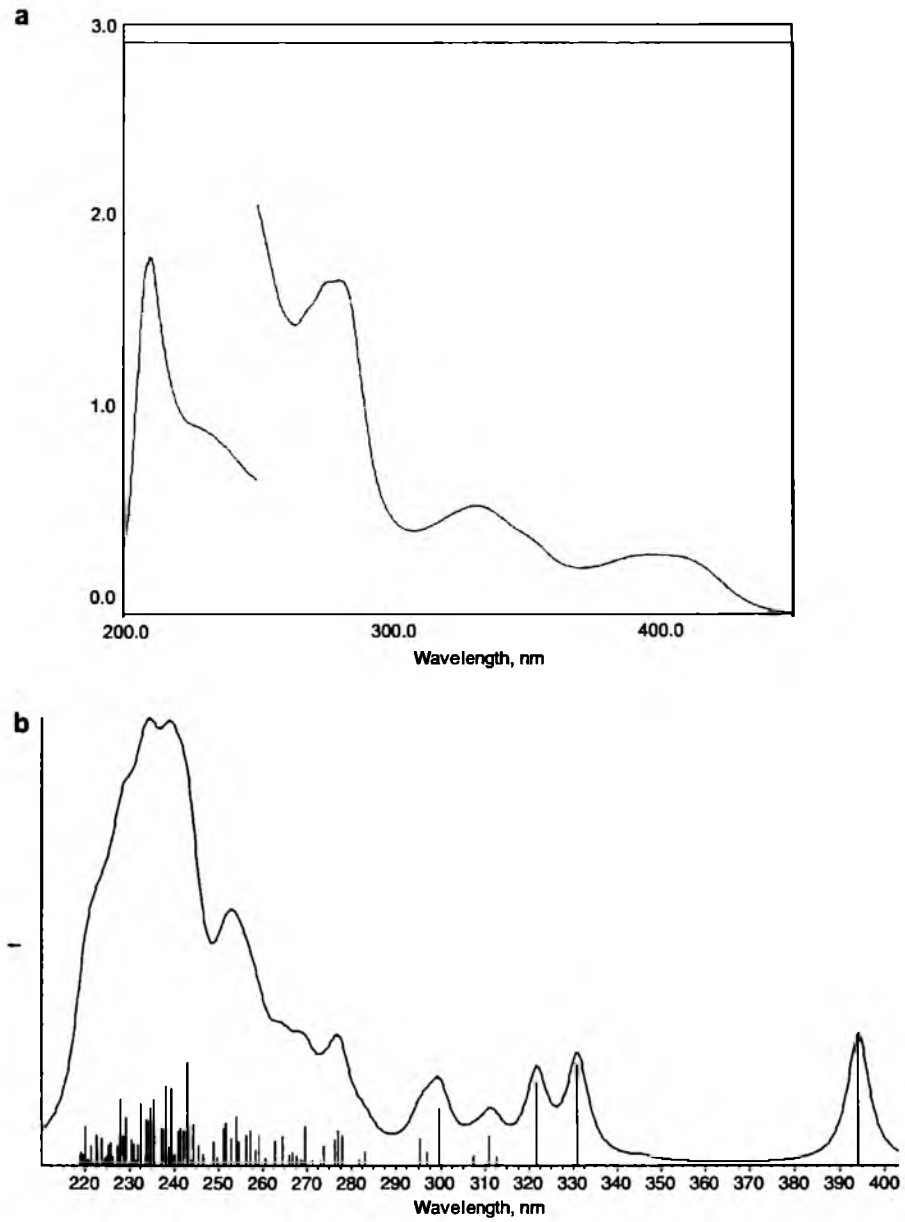

Fig. 7. The UV–Vis spectra of $[(PPh_3)_2RuH(CO)(C_{10}H_8NO_3)]$: (a) experimental; (b) calculated.

makes the largest contribution into L + 3, whereas the L + 4 molecular orbital has $d_{x^2-y^2}$ character in the studied complexes.

3.5. Electronic spectrum

The experimental and calculated electronic spectra of allowed singlet transitions, calculated with the TDDFT method, are presented in Figs. 7 and 8, respectively, for complexes **1** and **2**. The contour of the calculated spectrum was broadening by the Lorentzian function, calculated by the equation:

$$I = \frac{I_0}{1 + \left(\frac{\nu - \nu_0}{\gamma}\right)^2}; \quad \text{where}$$

$\gamma = 1/2$ the spectral width at 1/2 height.

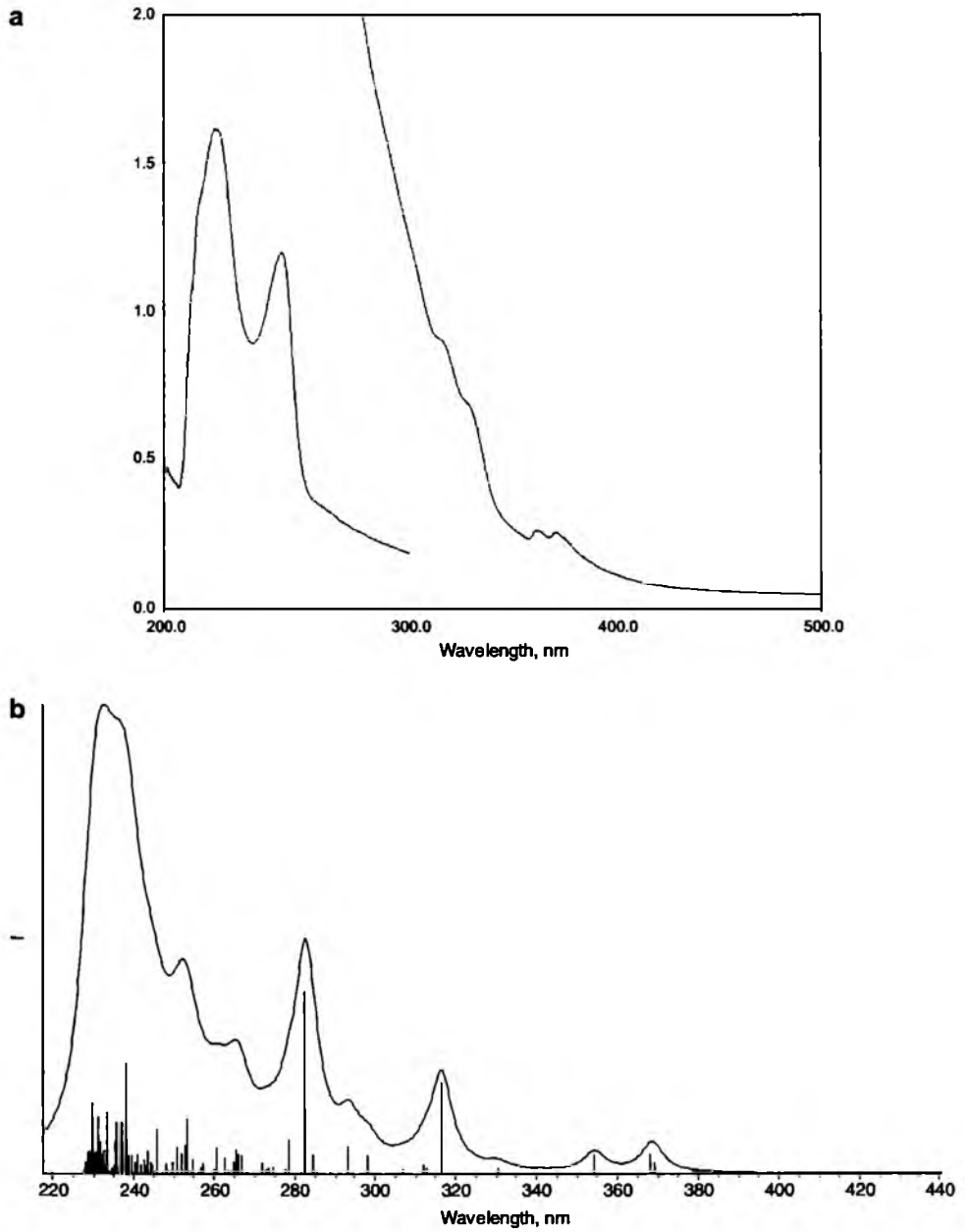

Fig. 8. The UV–Vis spectra of $[(PPh_3)_2RuCl(CO)(C_9H_6O_2)]$: (a) experimental; (b) calculated.

Hundred electronic transitions were calculated for the studied complexes using the DZVP with the f functions basis set on the ruthenium atom, and they do not comprise all the experimental absorption bands. The UV–Vis spectra were calculated up to ~225 nm, so the shortest wavelength experimental bands cannot be assigned to calculated transitions. However, considering that the solution spectra of PPh_3 and quinoline type ligands exhibit intense absorption bands in the 260–200 nm region, some additional intraligand and interligand transitions are expected to be found at higher energies in the calculations.

The assignments of the calculated transitions to the experimental bands are based on the criterion of the energy and oscillator strength of the calculated transitions. In the description of the electronic transitions only the main components of the molecular orbitals are taken into consideration.

The first experimental bands at 400 and 357 nm in $[(PPh_3)_2RuH(CO)(C_{10}H_8NO_3)]$ (**1**) and at 350.0 nm in $[(PPh_3)_2RuCl(CO)(C_9H_6O_2)]$ (**2**) consist of $d \rightarrow \pi^*_{qu}$ MLCT (Metal–Ligand Charge Transfer) transitions (HOMO/H-1 → LUMO). The next bands with maxima at 332 and 280 nm for complex **1** and 283 nm for **2** were calculated as the d → d LF (Ligand Field) transitions with contributions of MLCT excitation between *d* ruthenium and $\pi^*_{phosphine/qu}$ orbitals. For the higher energy band (maximum at 238 nm) of complex **2**, mainly intra- and interligand transitions are observed ($\pi_{qu} \rightarrow \pi^*_{Ph}$; $\pi_{qu} \rightarrow \pi^*_{qu}$; $\pi_{Cl} \rightarrow \pi^*_{Ph}$; $\pi_{CO} \rightarrow \pi^*_{Ph}$; $\pi_{CO} \rightarrow \pi^*_{qu}$). The bands at 210 and 206 nm for complexes **1** and **2**, respectively, were not calculated but in the energy region some additional intraligand and interligand transitions are expected.

Acknowledgement

The crystallographic part was financed by funds allocated by the Ministry of Science and Higher Education to the Department of X-ray Crystallography and Crystal Chemistry, Institute of General and Ecological Chemistry, Technical University of Łódź.

Appendix A. Supplementary material

CCDC 649418 and 649903 contain the supplementary crystallographic data for **1** and **2**. These data can be obtained free of charge via http://www.ccdc.cam.ac.uk/conts/retrieving.html, or from the Cambridge Crystallographic Data Centre, 12 Union Road, Cambridge CB2 1EZ, UK; fax: (+44) 1223-336-033; or e-mail: deposit@ccdc.cam.ac.uk.

References

[1] H.J. Roth, H. Fenner, in: Arzneistoffe, third ed., Deutscher Apotheker Verlag, Stuttgart, 2000, pp. 51–114.
[2] C.R. Harris, A. Thorarensen, Curr. Med. Chem. 11 (2004) 2213.
[3] K. Andries, P. Verhasselt, J. Guillemont, H.W. Gohlmann, J.M. Neefs, H. Winkler, J. Van Gestel, P. Timmerman, M. Zhu, E. Lee, P. Williams, D. de Chaffoy, E. Huitric, S. Hoffner, E. Cambau, C. Truffot-Pernot, N. Lounis, V. Jarlier, Science 307 (2005) 223.
[4] S. Vangapandu, M. Jain, R. Jain, S. Kaur, P.P. Singh, Bioorg. Med. Chem. 12 (2004) 2501.
[5] C. Sissi, M. Palumbo, Curr. Med. Chem. Anti-Canc. Agents 3 (2003) 439.
[6] E. Bossu, A.M. Agliano, N. Desideri, I. Sestili, R. Porra, M. Grandilone, M.G. Quaglia, J. Pharm. Biomed. Anal. 19 (1999) 539.
[7] T.C. Ko, M.J. Hour, J.C. Lien, C.M. Teng, K.H. Lee, S.C. Kuo, L.J. Huang, Bioorg. Med. Chem. Lett. 11 (2001) 279.
[8] J. Jampilek, M. Dolezal, J. Kunes, P. Vichova, D. Jun, I. Raich, R. O'Connor, M. Clynes, J. Pharm. Pharmacol. 56 (2004) 783.
[9] J. Jampilek, M. Dolezal, J. Kunes, P. Vichova, D. Jun, I. Raich, R. O'Connor, M. Clynes, Curr. Org. Chem. 8 (2004) 1235.
[10] J. Jampilek, M. Dolezal, V. Opletalova, J. Hartl, Curr. Med. Chem. 13 (2006) 117.
[11] J.L. Marco, C.M. Carmo, Mini Rev. Med. Chem. 3 (2003) 518.
[12] K. Mekouar, J.F. Mouscadet, D. Desmaele, F. Subra, H. Leh, D. Savoure, C. Auclair, J. d'Angelo, J. Med. Chem. 41 (1998) 2846.
[13] J. Polanski, F. Zouhiri, L. Jeanson, D. Desmaele, J. d'Angelo, J. Mouscadet, R. Gieleciak, J. Gasteiger, M. Le Bret, J. Med. Chem. 45 (2002) 4647.
[14] J. Polanski, H. Niedbala, R. Musiol, D. Tabak, B. Podeszwa, R. Gieleciak, A. Bak, A. Palka, T. Magdziarz, Acta Pol. Pharm. Drug Res. 61 (2004) 3.
[15] Y. Pommier, A.A. Johnson, C. Marchand, Nat. Rev. Drug. Discov. 4 (2005) 236.
[16] F. Zouhiri, M. Danet, C. Bernard, M. Normand-Bayle, J.F. Mouscadet, H. Leh, C.M. Thomas, G. Mbemba, J. d'Angelo, D. Desmaele, Tetrahedron Lett. 46 (2005) 2201.
[17] R. Musiol, J. Jampilek, V. Buchta, L. Silva, H. Niedbala, B. Podeszwa, A. Palka, K.A. Majerz-Maniecka, B. Oleksyn, J. Polanski, Bioorg. Med. Chem. 14 (2006) 3592.
[18] J. Jampilek, M. Dolezal, J. Kunes, V. Buchta, K. Kralova, Med. Chem. 1 (2005) 591.
[19] R. Musiol, J. Jampilek, K. Kralova, B. Podeszwa, J. Finster, H. Niedbala, A. Palka, J. Polanski. ECSOC-9 2005, November 1–30, http://www.usc.es/congresos/ecsoc/9/BOCNP/c005/index.htm.
[20] R. Musiol, J. Jampilek, K. Kralova, D.R. Richardson, D. Kalinowski, B. Podeszwa, J. Finster, H. Niedbala, A. Palka, J. Polanski. Bioorg. Med. Chem. 15 (2007) 1280.
[21] A.H. Velders, A.C.G. Hotze, G.A. van Albada, J.G. Haasnoot, J. Reedijk, Inorg. Chem. 39 (2000) 4073.
[22] N. Ahmad, J.J. Levinson, S.D. Robinson, M.F. Uttely, Inorg. Synth. 15 (1974) 48.
[23] M.J. Frisch, G.W. Trucks, H.B. Schlegel, G.E. Scuseria, M.A. Robb, J.R. Cheeseman, J.A. Montgomery Jr., T. Vreven, K.N. Kudin, J.C. Burant, J.M. Millam, S.S. Iyengar, J. Tomasi, V. Barone, B. Mennucci, M. Cossi, G. Scalmani, N. Rega, G.A. Petersson, H. Nakatsuji, M. Hada, M. Ehara, K. Toyota, R. Fukuda, J. Hasegawa, M. Ishida, T. Nakajima, Y. Honda, O. Kitao, H. Nakai, M. Klene, X. Li, J.E. Knox, H.P. Hratchian, J.B. Cross, C. Adamo, J. Jaramillo, R. Gomperts, R.E. Stratmann, O. Yazyev, A.J. Austin, R. Cammi, C. Pomelli, J.W. Ochterski, P.Y. Ayala, K. Morokuma, G.A. Voth, P. Salvador, J.J. Dannenberg, V.G. Zakrzewski, S. Dapprich, A.D. Daniels, M.C. Strain, O. Farkas, D.K. Malick, A.D. Rabuck, K. Raghavachari, J.B. Foresman, J.V. Ortiz, Q. Cui, A.G. Baboul, S. Clifford, J. Cioslowski, B.B. Stefanov, G. Liu, A. Liashenko, P. Piskorz, I. Komaromi, R.L. Martin, D.J. Fox, T. Keith, M.A. Al-Laham, C.Y. Peng, A. Nanayakkara, M. Challacombe, P.M.W. Gill, B. Johnson, W. Chen, M.W. Wong, C. Gonzalez, J.A. Pople, GAUSSIAN 03, Revision B.03, Gaussian, Inc., Pittsburgh, PA, 2003.
[24] D. Becke, J. Chem. Phys. 98 (1993) 5648.
[25] W. Lee, R. Yang, G. Parr, Phys. Rev. B 37 (1988) 785.
[26] J. Mennucci, J. Tomasi, Chem. Phys. 106 (1997) 5151.

[27] K. Eichkorn, F. Weigend, O. Treutler, R. Ahlrichs, Theor. Chim. Acc. 97 (1997) 119.
[28] D. Glendening, A.E. Reed, J.E. Carpenter, F. Weinhold, NBO (version 3.1).
[29] D. Becke, J. Chem. Phys. 98 (1993) 5648.
[30] M.V. Ovchinnikov, A.M. Ellern, I.A. Guzei, R.J. Angelici, Inorg. Chem. 40 (2001) 7014.
[31] S.M. Boniface, G.R. Clark, T.J. Collins, W.R. Roper, J. Organomet. Chem. 206 (1981) 109.
[32] H. Werner, W. Stuer, B. Weberndorfer, J. Wolf, Eur. J. Inorg. Chem. (1999) 1707.
[33] P.C. Junk, J.W. Steed, J. Organomet. Chem. 587 (1999) 191.
[34] A. Romero, A. Vegas, A. Santos, A.M. Cuadro, J. Chem. Soc., Dalton Trans (1987) 183.
[35] J.G. Haasnoot, W. Hinrichs, O. Weir, J.G. Vos, Inorg. Chem. 25 (1986) 4140.
[36] E. Bonfada, C. Maichle-Mossmer, J. Strahle, U. Abram, Z. Anorg. Allg. Chem. 625 (1999) 1327.
[37] G.M. Sheldrick, Acta Cryst. A46 (1990) 467.
[38] G.M. Sheldrick, SHELXL97, Program for the Solution and Refinement of Crystal Structures, University of Göttingen, Germany, 1997.
[39] G.M. Sheldrick, shelxtl: Release 4.1 for Siemens Crystallographic Research Systems, 1990.

Available online at www.sciencedirect.com
ScienceDirect
Bioorganic & Medicinal Chemistry
ELSEVIER
Bioorganic & Medicinal Chemistry 16 (2008) 4490–4499

Investigating biological activity spectrum for novel quinoline analogues 2: Hydroxyquinolinecarboxamides with photosynthesis-inhibiting activity

Robert Musiol,[a] Dominik Tabak,[a] Halina Niedbala,[a] Barbara Podeszwa,[a] Josef Jampilek,[b,c] Katarina Kralova,[d] Jiri Dohnal,[b,c] Jacek Finster,[a] Agnieszka Mencel[a] and Jaroslaw Polanski[a,*]

[a]*Institute of Chemistry, University of Silesia, Szkolna 9, 40006 Katowice, Poland*
[b]*Zentiva a.s., U kabelovny 130, 102 37 Prague 10, Czech Republic*
[c]*Department of Chemical Drugs, Faculty of Pharmacy, University of Veterinary and Pharmaceutical Sciences, Palackeho 1/3, 61242 Brno, Czech Republic*
[d]*Institute of Chemistry, Faculty of Natural Sciences, Comenius University, Mlynska dolina Ch-2, 84215 Bratislava, Slovakia*

Received 3 October 2007; revised 9 February 2008; accepted 19 February 2008
Available online 23 February 2008

Abstract—Two series of amides based on quinoline scaffold were designed and synthesized in search of photosynthesis inhibitors. The compounds were tested for their photosynthesis-inhibiting activity against *Spinacia oleracea* L. and *Chlorella vulgaris* Beij. The compounds lipophilicity was determined by the RP-HPLC method. Several compounds showed biological activity similar or even higher than that of the standard (DCMU). The structure–activity relationships are discussed.

1. Introduction

Designing new drugs is extremely complicated problem that attract much attention in current drug discovery strategies. With the novel methods and software tools for molecular modeling more and more molecular descriptors are available.[1,2] This does not always correspond to the number of biological data available. From the medicinal chemist point of view the availability of such data should significantly improve the performance of molecular design.

Quinoline is a system present in many classes of biologically active compounds. Recently, we have reported active herbicides based on such a scaffold.[3,4] A number of quinoline related compounds have been clinically used as antifungal, antibacterial, and antiprotozoic drugs[3,5–8] as well as antituberculotic agents.[9–11] Some quinoline analogues showed also antineoplastics activity.[12] Recently styrylquinoline derivatives have gained remarkable attention due to their activity as potential HIV integrase inhibitors.[13–17] Similar compounds could also possess strong antifungal activity.[7] The compounds containing 8-hydroxyquinoline pharmacophore seem to be especially interesting.[3,4,7]

Various compounds possessing an amide –NHCO– functionality were found to inhibit photosynthetic electron transport. Although this was discovered more than 50 years ago,[18] there are still many unanswered questions about the structural requirements for the activity of these compounds. In this particular case, a better understanding of the SAR trends are not only important for the design of the modern agricultural agents but can also give the remarkable insight into the photosynthesis mechanisms of the green cells. It has been reported recently that the amides of substituted pyridine-4-carboxylic acids[19] as well as anilides of the substituted pyrazine-2-carboxylic acids[20–24] inhibited oxygen evolution rate in spinach chloroplasts and they showed some antialgal properties. In the current research, we designed quinoline series containing the –NHCO– functionality

Keywords: Quinoline derivatives; Lipophilicity; PET inhibition; Spinach chloroplasts; Chlorophyll; *Chlorella vulgaris*.
* Corresponding author. Tel.: +48 32 3591206; fax: +48 32 2599978; e-mail: polanski@us.edu.pl

0968-0896/$ - see front matter © 2008 Elsevier Ltd. All rights reserved.
doi:10.1016/j.bmc.2008.02.065

in a hope to improve herbicidal activity. Figure 1 illustrates the design of the new analogues (**1–25**) that are based on structural analogies to active herbicides (**I–III**) having photosynthesis-inhibiting activity. New compounds contain (heterocyclic N)—C(=O)—N molecular fragment included in the quinoline moiety. In compounds **1–17**, two nitrogen atoms were separated by four carbon atoms to imitate a structure of **I** (four carbon atoms) or **II** (three carbon atoms). The nitro substitution in quinolines **III** is modified to the amide function.

2. Results and discussion

2.1. Chemistry

Compounds investigated in this work can be divided into two main series, as shown in Figure 1. The comparison of 8-hydroxyquinoline-7-carboxyamides **1–17** to the second series, that is, 8-hydroxyquinoline-7-carboxyamides **18–25**, indicates the reversed arrangement of heterocyclic nitrogen vs. the carboxyamide and hydroxyl functionality. The synthetic pathways of all discussed quinoline derivatives **1–25** are shown in Scheme 1.

The Kolbe–Schmidt reaction leads to 8-hydroxy-2-methylquinoline-7-carboxylic acid, whereas the Skraup synthesis gave 5-hydroxy-2-methylquinoline-6-carboxylic acid. These compounds were further reacted with the appropriate amine in the presence of ethyldimethylaminopropyl carbodiimid (EDCI) or dicyclohexyl carbodiimid (DCC) to afford an amide.

In the case of compounds **15**, **16**, **17**, and **24** diamine and salicylic acid or a twofold excess of quinaldic acid were used. Compound **25** was prepared by the reaction of a twofold excess of 5-hydroxy-2-methyl-quinoline-6-carboxylic acid with urea.

2.2. Lipophilicity

The drugs cross biological barriers most frequently through passive transport, which strongly depends on their lipophilicity; therefore lipophilicity of the drug molecules plays an important role in drug absorption, permeation, and disposition.[27] The lipophilicity of molecules is usually measured by their octanol/water partition coefficients (log*P*) since the pioneering work of Hansch, Fujita and Leo.[28] Log*P* is the logarithm of the partition coefficient in a biphasic system (e.g. *n*-octanol/water), defined as the ratio of a compound concentration in phase 1 and in phase 2. The log*P* is determined for the uncharged species of the drug. Note that it may exist preferably in the ionic or zwitterionic form(s).

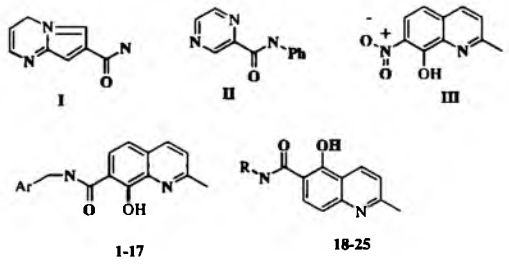

Figure 1. Design of compounds **1–25** on the basis of structural analogy to ALS (**I**),[25] heterocyclic amides (**II**)[20–24] and 8-hydroxy-7-nitroquinoline derivative (**III**).[4,26] In bold important molecular fragments included in **I–III** and in **1–25** are shown.

It has long been recognized that the retention of a compound in reversed-phase liquid chromatography is governed by its lipophilicity/hydrophobicity, and thus shows correlation with an octanol–water partition coefficient.[29] In reversed phase chromatography hydrophobic forces govern the retention, and it has been long recognized as a potential method for lipophilicity determination.[30] High performance liquid chromatography (HPLC) provides an excellent platform for computer controlled automated measurements with computerized data acquisition for a large number of research compounds. The other advantages in the use of the HPLC retention data for lipophilicity determination are that there is no need for concentration determination and method validation, small impurities are separated from the main component, a small amount of material is needed for the measurements, and the procedure can be completely automated. Therefore, the investigation of the true potential of this method is of great importance.[31]

An excellent review on the effect of stationary and mobile phase selection has been published by Pliska et al. and by Claessens et al.[27a,32] Reversed phase-high performance liquid chromatography (RP-HPLC) methods have become popular and widely used for lipophilicity measurement. The general procedure is the measurement of the directly accessible retention time under isocratic conditions with varying amounts of an organic modifier in the mobile phase using RP columns and calculating the logarithm of the capacity factors (log*K*). Log*K* is the logarithm of the capacity factors in chromatographic approaches, which is related to the partitioning of a compound between a mobile and a (pseudo-)stationary phase. Log*K* is used as the lipophilicity index converted to log*P* scale.[27a,31–33]

Lipophilicity computing software can usually calculate log*P* and *C*log*P*. *C*log*P* values present the logarithm of *n*-octanol/water partition coefficient based on established chemical interactions. The software calculates log*P* values as lipophilicity contributions/increments of individual atoms, fragments, and the pairs of interacting fragments in the chemical structure, that is, increments of carbon and hetero atoms, aromatic systems, and functional groups. The software calculates lipophilicity contributions according to different internal databases/libraries. Therefore, the values of calculated lipophilicities are dependent on the used software, and the values for individual compounds may be different. This fact as well as various ionic/zwitterionic forms and intramolec-

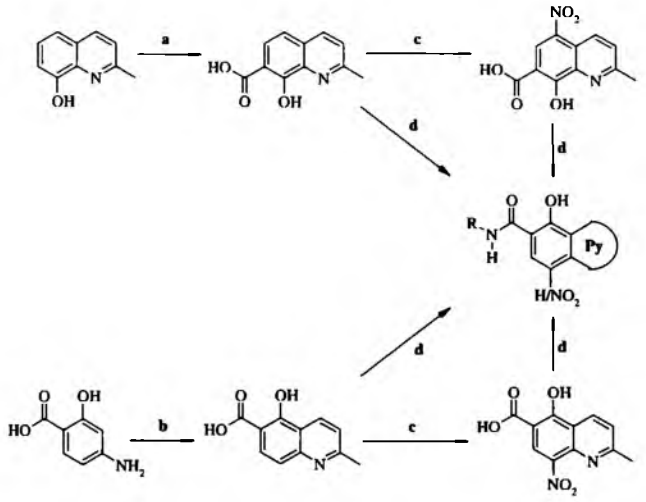

Scheme 1. Synthesis of compounds **1–25**. Reagents and condition: (a) KOH, CO_2; (b) Skraup synthesis; (c) HNO_3/H_2SO_4 5 °C; (d) amine, EDCI or DCC.

ular interactions may cause differences between calculated and experimentally determined lipophilicities.[34]

Log*P*/*C*log*P* values were measured by means of the RP-HPLC and calculated using two commercially available programs. The RP-HPLC was performed under isocratic conditions with methanol as an organic modifier in the mobile phase using end-capped nonpolar C_{18} stationary RP column. The capacity factors *K* were determined and subsequent log*K* values were calculated. The results are shown in Tables 1 and 2; Figure 2.

The overall correlation between the calculated and experimentally determined log*K* values is rather poor. The ACD/log*P* calculated data correlate relatively better with the measured values. In particular, log*P*/*C*log*P* values calculated by ChemOffice software do not agree well with the log*K* values measured for compounds **1–17**, see Figure 2.

This disagreement could be probably attributed to the presence of ionisable fragments in the molecules of hydroxyquinolines, which enhance intramolecular interactions. The commercially available chemical software (ChemOffice and ACD/log*P*) is not suitable for calculating the lipophilicity of similar highly functionalized molecules. The significant differences between the experimental and calculated parameters could be observed for compounds **6**, **7**, and **15–17**. This effect is caused probably by the interactions of the salicylamide hydroxyl and carboxamide functionalities as well as the interaction of this system with heterocyclic nitrogen.[35] Both dimers **16** and **17** showed the lowest log*K* value and compound **15** has the highest one within the series **1–17**, as expected.

Compounds **10–14** substituted in the $C_{(5)}$ position of quinoline by nitro functionality showed higher experimental log*K* than the calculated log*P* values. In comparison to the unsubstituted compounds nitro group increases log*K*, see **1–5/10–14**. Moreover, the substitution pattern of the phenyl moiety can further explain the log*K* increase. This complied with the sequence $H < OCH_3 < F < CH_3$. The log *K* data followed also the aliphatic linker increase indicating the length-dependence of the chains: $C_2H_4Ph < CH_2Ph < C_4H_8Ph$.[36] Chain branching caused also the increase in lipophilicity, see **1/3** and **11/12**.

Similarly to the calculated log*P* data for compounds **1–17**, the overall data calculated for compounds **18–25** also do not agree well enough with the experimentally determined parameters (log *K* values correlate relatively better with calculated *C*log*P* values), see Figure 2. As expected, dimer **24** showed the lowest lipophilicity, the same as compound **17**. Compound **25** possessed the highest log*K* that was unexpected. Acid **18** showed also high hydrophobicity contrary to all the results of the lipophilicity calculated softwares. The comparison of compounds **3–21**, **7–23**, **4–20**, and **17–25** indicated a higher log*K* values within the series of **18–25** than those observed within **1–17**. This fact can be explained by hydrogen bond between phenolic and carbonyl group[37] and/or hydrogen bond between phenolic and quinoline–nitrogen[3,4,7] due to their opposite positions.[35]

2.3. Biological activities

All compounds were tested for their in vitro herbicidal susceptibility. The results obtained are shown in Tables 1 and 2. 8-Hydroxy-2-methyl-quinoline-7-carboxylic acid (2-hydroxyethyl)-amide (**6**) was found to be inactive in both tests, which seems to indicate the importance of the phenyl moiety.

Table 1. The PET inhibition in spinach chloroplasts and reduction of chlorophyll content in *C. vulgaris* of compounds **1–17** compared to that of the standard DCMU compound

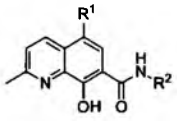

Compound	R^1	R^2	Log*K*	Log*P*/C log*P* ChemOffice	Log*P* ACD/log*P*	PET inhibition IC_{50} (μmol/L)	Chlorophyll reduction IC_{50} (μmol/L)
1	H	$-CH_2Ph$	0.2812	3.31/4.840	3.75 ± 0.80	[b]	17.2
2	H	$-CH_2Ph$–4-F	0.3389	3.47/4.983	3.80 ± 0.85	[b]	158
3	H	$-CH(CH_3)Ph$–4-F	0.3720	3.78/5.292	4.15 ± 0.85	[b]	83.3
4	H	$-CH_2Ph$–4-CH_3	0.3793	3.79/5.339	4.21 ± 0.80	[b]	7.2
5	H	$-CH_2Ph$–4-OCH_3	0.2843	3.18/4.759	3.67 ± 0.81	[b]	4.8
6	H	$-C_2H_4OH$	0.2629	1.06/1.076	1.35 ± 0.81	[b]	[b]
7	H	$-C_2H_4Ph$	0.2404	3.59/4.969	4.17 ± 0.80	[b]	77.7 ± 6.3[a]
8	H	$-C_2H_4Ph$–4-F	0.3342	3.74/5.112	4.22 ± 0.84	[b]	15.9
9	H	$-C_4H_8Ph$	0.5075	4.00/5.348	5.06 ± 0.79	[b]	8.5
10	NO_2	$-CH_2Ph$	0.4021	2.96/3.531	4.07 ± 0.82	32.0	[b]
11	NO_2	$-CH_2Ph$–4-F	0.4136	3.10/3.674	4.12 ± 0.86	95.0	[b]
12	NO_2	$-CH(CH_3)Ph$–4-F	0.4283	3.42/5.224	4.47 ± 0.86	8.7	43.6
13	NO_2	$-CH_2Ph$–4-CH_3	0.4304	3.38/4.030	4.53 ± 0.82	107.0	[b]
14	NO_2	$-CH_2Ph$–4-OCH_3	0.4087	3.09/3.450	3.98 ± 0.82	137.0	[b]
15	H	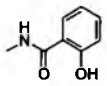	0.6361	2.31/4.755	3.60 ± 0.87	[b]	[b]
16	H	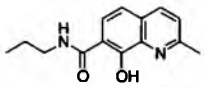	0.1109	2.91/5.991	4.04 ± 1.13	[b]	93.7
17	H	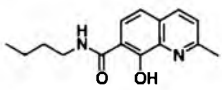	0.1168	3.01/6.303	4.26 ± 1.12	[b]	149
DCMU	—	—	—	2.76/2.691	2.78 ± 0.38	1.9	7.3

The measured log*K* and calculated log*P*/C log*P* data are shown to illustrate lipophilicity.

[a] IC_{50} was not determined, a value referring to an average decrease of Chl content related to the control determined for the concentration range of 0.83–100 μmol/L ([%] ± SD) is indicated.

[b] Inactive compound.

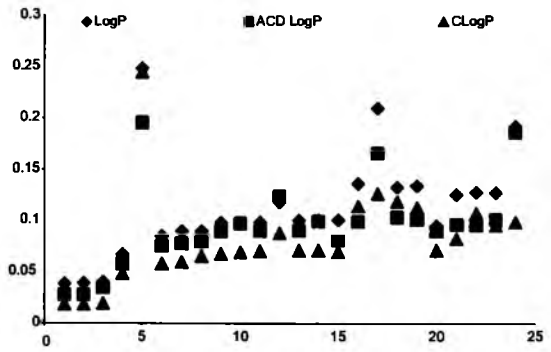

Figure 2. Comparison of the computed log*P*/C log*P* values using the two programs with the log*K* values of the compounds **1–25**.

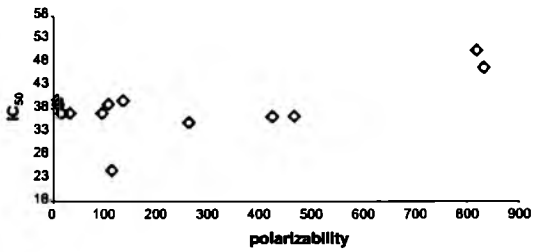

Figure 3. Activity (IC_{50}) of PET activity versus polarizability of studied compounds.

2.3.1. PET inhibition activity in spinach chloroplasts. An interesting activity rules can be deduced for the derivatives of 8-hydroxy-2-methylquinoline-7-carboxylic acid tested. Compounds lacking 5-NO_2 functionality are inactive if tested for the inhibition of oxygen evolution rate in spinach chloroplasts. This rule makes active compounds **10–14** that shows the PET inhibition activity ranging from 8.7 (**12**) to 137.0 μmol/L (**14**). The activity of compound **12** is comparable to that of DCMU. Thus, the most important requirement for high PET activity is the $C_{(5)}$ substitution by nitro moiety. Moreover, the activity increases with the electron accepting power of

Table 2. The PET inhibition in spinach chloroplasts and reduction of chlorophyll content in *C. vulgaris* of compounds **18–25** compared to that of the standard DCMU compound

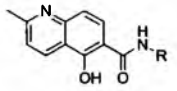

Compound	R	Log *K*	log *P*/*C*log *P* ChemOffice	Log *P* ACD/log *P*	PET inhibition IC_{50} (μmol/L)	Chlorophyll reduction IC_{50} (μmol/L)
18	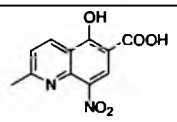	0.4072	1.95/3.235	2.47 ± 0.36	114.0	108.6 ± 11.3[a]
19	–Ph–4–Cl	0.3812	3.80/5.464	4.73 ± 0.42	265.0	23.8
20	$-CH_2Ph-4-CH_3$	0.3800	3.79/5.339	3.84 ± 0.41	468.0	97.2 ± 3.8
21	$-CH(CH_3)Ph-4-F$	0.3663	3.78/5.292	3.78 ± 0.47	426.0	100.0 ± 5.9[a]
22	$-C_2H_4Ph-4-OH$	0.3775	3.20/4.302	3.06 ± 0.40	16.0	102.5 ± 8.9[a]
23	$-C_4H_8Ph$	0.4173	4.42/5.877	4.68 ± 0.39	7.2	10.9
24	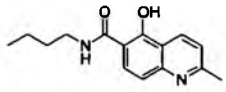	0.1203	3.01/6.303	3.51 ± 0.51	819.0	19.5
25	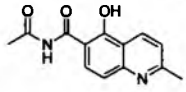	0.6120	3.20/6.223	3.31 ± 0.65	833.0	5.5
DCMU	—	—	2.76/2.691	2.78 ± 0.38	1.9	7.3

The measured log *K* and calculated log *P*/*C*log *P* data are shown to illustrate lipophilicity.

[a] IC_{50} was not determined, a value referring to an average decrease of Chl content related to the control for the concentration range of 0.83–100 μmol/L is indicated.

the $C_{(4)}$ substituent. However, only a poor correlation can be observed between the activity and polarizability as shown in Figure 3, or molar refractivity that was not shown here.

Among the amides of 5-hydroxy-2-methylquinoline-6-carboxylic acid **18–25** two compounds showed interesting IC_{50} values, compound **23** (IC_{50} = 7.2 μmol/L) and compound **22** (IC_{50} = 16.0 μmol/L). Moreover, the activity level of compound **23** was comparable to that of DCMU activity. Both dimers **24** and **25** possessed only very low activity. No simple structure–activity rule explaining the activity changes within the series **18–25** was revealed.

2.3.2. Reduction of chlorophyll content in *Chlorella vulgaris*. The derivatives of 8-hydroxy-2-methylquinoline-7-carboxylic acid indicated a high selectivity of herbicidal effect. Amides **1–9**, **15–17** inhibited selectively chlorophyll production in *C. vulgaris*, whereas amides possessing nitro functionality in the $C_{(5)}$ position, that is, compounds **10–14** are practically inactive against *C. vulgaris*. Compound **12** is the only exception in this trend.

Among the first series three compounds **1**, **8**, and **9** inhibited chlorophyll production in *C. vulgaris* comparable to DCMU. The inhibitory activity of compounds **4**, **5** even exceeded the activity of DCMU. In particular, IC_{50} values varied in the range from 4.8 (**5**) to 17.2 μmol/L (**1**), which makes compound **5** the most efficient inhibitor.

The inhibitory activity of 8-hydroxy-2-methylquinoline-7-carboxamides having the benzylamide functionality, compounds **1**,**2**, **4**, **5**, clearly depended on the electron-accepting properties of the benzyl substituent, which is illustrated in Figure 4.[38] This trend is contrary to that previously described for the PET activity.

Lipophilicity can be the second important factor affecting the activity of the compounds investigated. Compound **3** differed from **2** by linker branching to carboxamido group and phenyl moiety. The log *K* value of **3** was higher than that of **2** and the activity of **3** was much higher than **2**. Compounds **1**, **7**, **9**, and **2**, **8** as well as **16**, **17** differed from each other in the linker length connecting two aromatic moieties within the molecule, that is, a number of CH_2 groups in this linker. The comparison of compounds **1** and **9** having similar unsubstitued aromatic group showed that the increase of the compound lipophilicity caused by the prolongation of the linker by two CH_2 groups led to a moderate increase

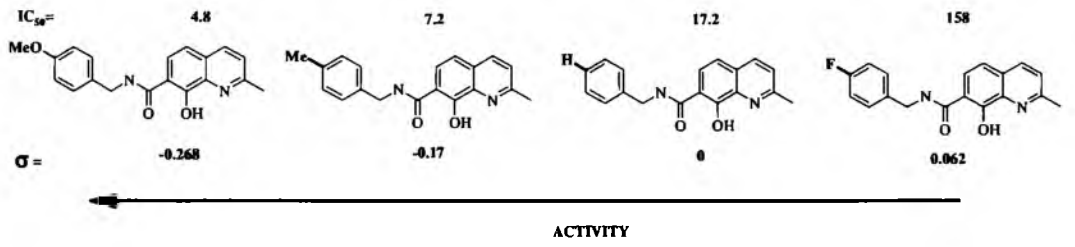

Figure 4. The IC_{50} ([μmol/L]) values decreases with the increase of the Hammett σ constant of the benzyl substituent of 8-hydroxy-2-methylquinoline-7-carboxyamides (**1**,**2**, **4**, and **5**).

of inhibitory activity. On the other hand, the prolongation of the linker in compound **1** by a single CH_2 group decreased the activity of compound **7** and the similar prolongation of the linker in compound **2** (4-fluorobenzylamide derivative) increased the activity of compound **8**. Moreover, the addition of a single CH_2 group to the linker of bis-[8-hydroxy-2-methylquinoline-7-carboxylic acid]-1,2-ethylamide (**16**) slightly decreased the activity of **17**. This indicates that lipophilicity alone cannot explain the activity changes within the first series of compounds **1–17**. Thus, the distance between the quinoline nucleus and the $C'_{(4)}$-hydrogen substituent in phenyl ring is probably also an important parameter influencing the activity.

The derivatives of 5-hydroxy-2-methylquinoline-6-carboxylic acid did not show similar selectivity as compounds **1–17**. The activity of 5-hydroxy-2-methylquinoline-6-carboxamides **19–25** is relatively high. Compounds **19**, **23–25** have advantageous IC_{50} values in the range of 5.5–23.8 μmol/L, and compound **25** is the most active analogue (IC_{50} = 5.5 μmol/L). Compound **24** showed higher activity than **17** and **23** was comparable to **9**. The comparison of the individual values listed in Table 2 indicates that the relationships between log*K* and the activity of the series **18–25** are slightly better than that for compounds **1–17**. Improved antialgal activity correlated with increased lipophilicity.

3. Conclusion

The comparison of antialgal activity to the oxygen evolution rate in spinach chloroplasts for the novel quinoline compounds indicated that the derivatives of 8-hydroxy-2-methylquinoline-7-carboxylic acid showed selective antialgal activity, whereas the derivatives of 8-hydroxy-2-methyl-5-nitroquinoline-7-carboxylic acid inhibited a better PET in spinach chloroplasts. 5-Hydroxy-2-methylquinoline-6-carboxamides showed unselective activity in both tests.

As we presented here quinoline based scaffolds can be successfully used for the design of new active electron transfer inhibitors. High to moderate activity of compounds **4**, **5**, **12**, and **23** makes these molecular fragments valuable for further study and modifications. Although there is no clear structure activity relationship for the series, we have shown some trends. Lipophilicity and the electron-accepting or electron-withdrawing power of the substituents are probably the most important among molecular features discussed. The inactivity of compound **18** suggests that the carboxamide function is the attribute that limits the activity.

4. Experimental

4.1. General

All reagents were purchased from Aldrich. Kieselgel 60, 0.040–0.063 mm (Merck, Darmstadt, Germany) was used for column chromatography. TLC experiments were performed on alumina-backed silica gel 40 F254 plates (Merck, Darmstadt, Germany). The plates were illuminated under UV (254 nm) and evaluated in iodine vapour. Melting points were determined on Boetius PHMK 05 (VEB Kombinat Nagema, Radebeul, Germany) and are uncorrected. Elemental analyses were carried out on an automatic Perkin-Elmer 240 microanalyser (Boston, USA). The purity of the final compounds was checked by HPLC, see Section 4.3. The detection wavelength 210 nm was chosen. Peaks in the chromatogram of the solvent (blank) were deducted from peaks in the chromatogram of the sample solution. A purity of the individual compounds was determined from area peaks in the chromatogram of the sample solution. UV spectra (λ, nm) were determined on a Waters Photodiode Array Detector 2996 (Waters Corp., Milford, MA, USA) in ca 6×10^{-4} mol methanolic solution and logϵ (the logarithm of molar absorption coefficient ϵ) was calculated for the absolute maximum λ_{max} of individual target compounds. All ^{1}H NMR spectra were recorded on a Bruker AM-500 (499.95 MHz for ^{1}H), Bruker BioSpin Corp., Germany. Chemical shifts are reported in ppm (δ) to internal $Si(CH_3)_4$, when diffused easily exchangeable signals are omitted.

4.2. Synthesis

4.2.1. General procedure of substituted amides of quinoline derivatives 1–25 syntheses. To the solution prepared hydroxyquinaldinecarboxylic acids (1.02 g, 5.0 mmol) in dry CH_2Cl_2 with EDCI or DCC (0.6 mmol) was added appropriate amine (5.3 mmol) in dry CH_2Cl_2 during 4 h. After the reaction was completed, solid was filtered, washed with 5% $NaHCO_3$, water, and diethyl ether.

4.2.2. 8-Hydroxy-2-methylquinoline-7-carboxylic acid benzylamide (1). A white crystalline compound. Yield 86%. Mp 215–218 °C. Anal. calcd for $C_{18}H_{16}N_2O_2$ (292.34): C 73.95%, H 5.52%; found: C 74.12%, H 5.68%. HPLC purity 91.17%. UV (nm), $\lambda_{max}/\log\epsilon$: 258.3/3.62. ^{1}H NMR (DMSO-d_6, 500 MHz) δ: 2.57 (s, 3H), 4.06 (s, 2H), 6.94 (d, 1H, J = 8.4 Hz), 7.3 (d, 1H, J = 8.4 Hz), 7.35–7.37 (m, 3H), 7.45 (d, 2H, J = 7.3 Hz), 7.73 (d, 1H, J = 8.4 Hz), 8.0 (d, 1H, J = 8.4 Hz), 8.58 (bs, 2H).

4.2.3. 8-Hydroxy-2-methylquinoline-7-carboxylic acid 4-fluorobenzylamide (2). Product was obtained according to the described procedure.[26] Yield 26%. Mp 190–196 °C. HPLC purity 91.48%. UV (nm), $\lambda_{max}/\log\epsilon$: 258.3/3.60.

4.2.4. 8-Hydroxy-2-methylquinoline-7-carboxylic acid [1-(4-fluorophenyl)-ethyl]-amide (3). A white crystalline compound. Yield 36%. Mp 208–210 °C. Anal. calcd for $C_{19}H_{17}FN_2O_2$+2H_2O (360.36): C 63.32%, H 5.87%; found: C 63.55%, H 5.61%. HPLC purity 98.91%. UV (nm), $\lambda_{max}/\log\epsilon$: 258.4/3.55. ^{1}H NMR (DMSO-d_6, 500 MHz) δ: 1.47 (d, 3H, J = 6.7 Hz), 2.6 (s, 3H), 4.46 (q, 1H), 5.59 (d, 1H, J = 7.8 Hz), 7.95 (d, 1H, J = 8.3 Hz), 7.22–7.33 (m, 3H), 7.50–7.57 (m, 2H), 7.75 (d, 1H, J = 8.4 Hz), 8.01 (d, 1H, J = 8.4 Hz), 8.37 (s, 1H).

4.2.5. 8-Hydroxy-2-methylquinoline-7-carboxylic acid 4-methylbenzylamide (4). Product A white crystalline compound. Yield 36.4%. Mp 192–200 °C (dec). Anal. calcd for $C_{19}H_{18}N_2O_2$ (306.37): C 74.49%, H 5.92%; found: C 74.32%, H 6.10%. HPLC purity 91.30%. UV (nm), $\lambda_{max}/\log\epsilon$: 258.3/3.59. ^{1}H NMR (DMSO-d_6, 500 MHz) δ: 2.3 (s, 3H), 2.6(s, 3H), 4.02 (s, 2H), 6.9 (d, 1H, J = 8.4 Hz), 7.2 (d, 2H, J = 7.5 Hz), 7.31–7.35 (m, 3H), 7.75 (d, 1H, J = 8.3 Hz), 8.04 (d, 1H, J = 8.3 Hz), 8.43 (bs, 2H).

4.2.6. 8-Hydroxy-2-methylquinoline-7-carboxylic acid 4-methoxybenzylamide (5). A white crystalline compound. Yield 34.5%. Mp 180–190 °C (dec). Anal. calcd for $C_{19}H_{18}N_2O_3$ (322.37): C 70.79%, H 5.63%; found: C 70.65%, H 5.49%. HPLC purity 91.22%. UV (nm), $\lambda_{max}/\log\epsilon$: 258.3/3.64. ^{1}H NMR (DMSO-d_6, 500 MHz) δ: 2.59 (s, 3H), 3.73 (s, 3H), 4.00 (s, 2H), 6.94 (d, 2H, J = 8.4 Hz), 6.97 (d, 1H, J = 8.3 Hz), 7.32 (d, 1H, J = 8.3 Hz), 7.40 (d, 2H,J = 8.4 Hz), 7.75 (d, 1H, J = 8.3 Hz), 8.03 (d, 1H, J = 8.3 Hz), 8.4 (bs, 2H).

4.2.7. 8-Hydroxy-2-methyl-quinoline-7-carboxylic acid (2-hydroxyethyl)-amide (6). A white crystalline compound. HPLC purity 99.59%. Yield 78.5%. Mp 228–229 °C. UV (nm), $\lambda_{max}/\log\epsilon$: 258.7/3.59.[39]

4.2.8. 8-Hydroxy-2-methylquinoline-7-carboxylic acid phenethylamide (7). A white crystalline compound. Yield 62%. Mp 228–235 °C. Anal. calcd for $C_{19}H_{18}N_2O_2$ (306.37): C 74.49%, H 5.93%; found: C 74.63%, H 6.05%. HPLC purity 90.81%. UV (nm), $\lambda_{max}/\log\epsilon$: 258.3/3.62. ^{1}H NMR (DMSO-d_6, 500 MHz) δ: 2.61 (s, 3H), 2.89 (t, 2H), 3.09 (t, 2H), 6.98 (d, 1H, J = 8.4 Hz), 7.21–7.25 (m, 3H), 7.29–7.33 (m, 3H), 7.77 (d, 1H, J = 8.3 Hz), 8.03 (d, 1H, J = 8.3 Hz), 8.19 (bs, 2H).

4.2.9. 8-Hydroxy-2-methylquinoline-7-carboxylic acid [2-(4-fluorophenyl)-ethyl]-amide (8). A white crystalline compound. Yield 52%. Mp 189–193 °C. Anal. calcd for $C_{19}H_{17}FN_2O_2$ (324.36): C 70.36%, H 5.28%; found: C 70.23%, H 5.46%. HPLC purity 91.56%. UV (nm), $\lambda_{max}/\log\epsilon$: 258.3/3.61. ^{1}H NMR (DMSO-d_6, 500 MHz) δ: 2.61 (s, 3H), 2.88 (t, 2H), 3.09 (t, 2H), 6.98 (d, 1H, J = 8.2 Hz), 7.12 (t, 2H), 7.28 (t, 2H), 7.33 (d, 1H, J = 8.3 Hz), 7.77 (d, 1H, J = 8.2 Hz), 8.03 (d, 1H, J = 8.2 Hz), 8.21 (bs, 2H).

4.2.10. 8-Hydroxy-2-methylquinoline-7-carboxylic acid (3-phenylbuthyl)-amide (9). A white crystalline compound. Yield 73%. Mp 196–201 °C. Anal. calcd for $C_{21}H_{22}N_2O_2$ (334.42): C 75.42%, H 6.63%; found: C 75.36%, H 6.78%. HPLC purity 93.31%. UV (nm), $\lambda_{max}/\log\epsilon$: 258.3/3.61. ^{1}H NMR (DMSO-d_6, 500 MHz) δ: 1.61 (s, 4H), 2.55 (s, 2H), 2.64 (s, 3H), 2.83 (s, 2H), 6.96 (d, 1H, J = 8.4 Hz), 7.10 (d, 3H, J = 6.7 Hz), 7.18 (t, 2H), 7.26 (d, 1H, J = 8.2 Hz), 7.81 (d, 1H, J = 8.3 Hz), 7.94 (d, 1H, J = 8.2 Hz), 8.15 (bs, 2H).

4.2.11. 8-Hydroxy-2-methyl-5-nitroquinoline-7-carboxylic acid benzylamide (10). A yellow crystalline compound. Yield 61%. Mp 219–228 °C. Anal. calcd for $C_{18}H_{15}N_3O_4$ (337.33): C 64.09%, H 4.48%; found: C 63.95%, H 4.42%. HPLC purity 99.37%. UV (nm), $\lambda_{max}/\log\epsilon$: 427.7/3.64. ^{1}H NMR (DMSO-d_6, 500 MHz) δ: 2.58 (s, 3H); 4.05 (s, 2H); 7.37–7.45 (m, 5H); 7.52 (d, 1H, J = 8.6 Hz); 8.18 (bs, 2H); 9.07 (d, 1H, J = 8.6 Hz); 9.13 (s, 1H).

4.2.12. 8-Hydroxy-2-methyl-5-nitroquinoline-7-carboxylic acid 4-flourobenzylamide (11). A yellow crystalline compound. Yield 44%. Mp 202–206 °C. Anal. calcd for $C_{18}H_{14}FN_3O_4$ (355.34): C 60.84%, H 3.97%; found: C 60.68%, H 3.80%. HPLC purity 96.22%. UV (nm), $\lambda_{max}/\log\epsilon$: 427.7/3.66. DMSO-$d_6$, 500 MHz) δ: 2.57 (s, 3H); 4.05 (s, 2H); 7.25 (t, 2H); 7.50 (t, 2H); 7.51 (d, 1H); 8.21 (bs, 2H); 9.07 (d, 1H, J = 8.6 Hz); 9.13 (s, 1H).

4.2.13. 8-Hydroxy-2-methyl-5-nitroquinoline-7-carboxylic acid [1-(4-fluorophenyl)-ethyl]-amide (12). An orange crystalline compound. Yield 54%. Mp 220–222 °C (dec). Anal. calcd for $C_{19}H_{16}FN_3O_4$+2H_2O (405.36): C 56.29%, H 4.97%; found: C 55.92%, H 5.06%. HPLC purity 99.09%. UV (nm), $\lambda_{max}/\log\epsilon$: 427.7/3.58. ^{1}H NMR (DMSO-d_6, 500 MHz) δ: 1.49 (d, 3H, J = 6.8 Hz), 2.56 (s, 3H), 4.46 (q, 1H), 7.18–7.27 (m, 2H), 7.49–7.56 (m, 3H), 8.3 (d, 1H, J = 8.7 Hz), 9.12 (s, 1H).

4.2.14. 8-Hydroxy-2-methyl-5-nitroquinoline-7-carboxylic acid 4-methylbenzylamide (13). A yellow crystalline compound. Yield 78%. Mp 228–232 °C. Anal. calcd for $C_{19}H_{17}N_3O_4$ (351.35): C 64.95%, H 4.88%; found: C 65.12%, H 4.96%. HPLC purity 99.30%. UV (nm), $\lambda_{max}/\log\epsilon$: 427.7/3.65. ^{1}H NMR (DMSO-d_6, 500 MHz) δ: 2.28 (s, 3H); 2.57 (s. 3H); 3.99 (s, 2H); 7.20 (d, 2H,

J = 7.7 Hz); 7.31 (d, 2H, J = 7.7 Hz); 7.51 (d, 1H, J = 8.6 Hz); 8.16 (bs, 2H); 9.06 (d, 1H, J = 8.7 Hz); 9.13 (s, 1H).

4.2.15. 8-Hydroxy-2-methyl-5-nitroquinoline-7-carboxylic acid 4-methoxybenzylamide (14). A yellow crystalline compound. Yield 63%. Mp 211–214 °C. Anal. calcd for $C_{19}H_{17}N_3O$ (367.35): C 62.12%, H 4.66%; found: C 61.83%, H 4.71%. HPLC purity 98.74%. UV (nm), λ_{max}/log ϵ: 430.2/3.58. ^{1}H NMR (DMSO-d_6, 500 MHz) δ: 2.58 (s, 3H); 3.74 (s, 3H); 3.96 (s, 2H); 6.96 (d, 2H, J = 8.6 Hz); 7.36 (d, 2H, J = 8.6 Hz); 7.52 (d, 1H, J = 8.7 Hz); 8.05 (bs, 2H); 9.08 (d, 1H, J = 8.7 Hz); 9.13 (s, 1H).

4.2.16. 2-Hydroxybenzoic acid *N'*-(8-hydroxy-2-methylquinoline-7-carbonyl)-hydrazide (15). A yellow crystalline compound. Yield 37.6%. Mp 147–150 °C. Anal. calcd for $C_{18}H_{15}N_3O_4$ (337.33): C 64.09%, H 4.48%; found: C 63.92%, H 4.38%. HPLC purity 94.17%. UV (nm), λ_{max}/log ϵ: 290.3/3.56. ^{1}H NMR (DMSO-d_6, 500 MHz) δ: 2.75 (s, 3H); 6.96–7.00 (m, 2H); 7.36 (d, 1H, J = 8.6 Hz); 7.46 (t, 1H); 7.60 (d, 1H, J = 8.4 Hz); 7.95–7.97 (m, 2H); 8.34 (d, 1H, J = 8.4 Hz); 11.07 (bs, 1H); 11.44 (bs, 1H).

4.2.17. Bis-[8-hydroxy-2-methylquinoline-7-carboxylic acid]-1,2-ethylamide (16). Product was obtained according to the described procedure.[26] Yield 7%. Mp 254–257 °C. HPLC purity 91.47%. UV (nm), λ_{max}/log ϵ: 258.3/3.60.

4.2.18. Bis-[8-hydroxy-2-methylquinoline-7-carboxylic acid]-1,3-propylamide (17). Product was obtained according to the described procedure.[26] Yield 23%. Mp 293–297 °C. HPLC purity 92.06%. UV (nm), λ_{max}/log ϵ: 258.3/3.60.

4.2.19. 5-Hydroxy-2-methyl-8-nitroquinoline-6-carboxylic acid (18). Product was obtained according to the described procedure.[26] Yield 53%. Mp 280°C (dec). HPLC purity 94.25%. UV (nm), λ_{max}/log ϵ: 284.4/3.67.

4.2.20. 5-Hydroxyquinaldine-6-carboxylic acid 4-chlorophenylamide (19). An orange crystalline compound. Yield 35%. Mp 176–178 °C. Anal. calcd for $C_{17}H_{13}ClN_2O_2$+2H_2O (348.76): C 61.82%, H 4.55%; found: C 61.79%, H 4.21%. HPLC purity 94.13%. UV (nm), λ_{max}/log ϵ: 265.5/3.57. ^{1}H NMR (DMSO-d_6, 500 MHz) δ: 2.76 (s, 3H), 7.46 (d, 1H, J = 8.4 Hz), 7.45 (d, 2H, J = 7.5 Hz), 7.58 (d, 1H, J = 8.4 Hz), 7.75 (d, 2H, J = 7.5 Hz), 8.37 (d, 1H, J = 9.2 Hz), 8.56 (d, 1H, J = 8.8 Hz).

4.2.21. 5-Hydroxyquinaldine-6-carboxylic acid 4-methylbenzylamide (20). A beige crystalline compound. Yield 50%. Mp 184–186 °C. Anal. calcd for $C_{18}H_{18}N_2O_2$+2H_2O (342.37): C 65.80%, H 6.49%; found: C 65.85%, H 6.77%. HPLC purity 98.95%. UV (nm), λ_{max}/log ϵ: 257.2/3.57. ^{1}H NMR (DMSO-d_6, 500 MHz) δ: 2.28 (s, 3H), 2.65 (s, 3H), 3.95 (s, 2H), 7.10 (d, 1H, J = 7.5 Hz), 7.20 (d, 1H, J = 8.5 Hz), 7.30 (d, 1H, J = 8.5 Hz), 7.40 (d, 2H, J = 7.6 Hz), 7.90 (d, 2H, J = 7.6 Hz), 8.0 (bs, 1H), 8.60 (d, 1H, J = 8.2Hz).

4.2.22. 5-Hydroxy-2-methylquinoline-6-carboxylic acid [1-(4-fluorophenyl)-ethyl]-amide (21). A bright brown solid. Yield 31%. Mp 240 °C (dec). Anal. calcd for $C_{19}H_{17}FN_2O_2$+H_2O (342.36): C 66.66%, H 5.59%; found: C 67.02%, H 5.39%. HPLC purity 81.13%. UV (nm), λ_{max}/log ϵ: 260.7/3.56. ^{1}H NMR (DMSO-d_6, 500 MHz) δ: 1.65 (d, 3H), 2.7 (s, 3H), 4.6 (q, 1H), 7.35–7.5 (m, 8H).

4.2.23. 5-Hydroxyquinaldine-6-carboxylic acid 2-(4-hydroxyphenyl)-ethylamide (22). Product was obtained according to the described procedure.[26] Yield 47%. Mp 114–117 °C. HPLC purity 95.83%. UV (nm), λ_{max}/log ϵ: 258.4/3.54.

4.2.24. 5-Hydroxyquinaldine-6-carboxylic acid (4-phenylbuthyl)-amide (23). A beige crystalline compound. Yield 52%. Mp 156–159 °C. Anal. calcd for $C_{21}H_{22}N_2O_2$+H_2O (352.42): C 71.60%, H 6.82%; found: C 71.38%, H 7.34%. HPLC purity 98.63%. UV (nm), λ_{max}/log ϵ: 257.2/3.52. ^{1}H NMR (DMSO-d_6, 500 MHz) δ: 1.48–1.60 (m, 4H), 2.60 (m, 5H); 2.75 (t, 2H), 6.95 (d, 1H, J = 8.5 Hz), 7.15 (d, 1H, J = 7.9 Hz), 7.20–7.30 (m, 5H), 7.60 (bs, 1H); 7.88 (d, 1H, J = 8.5 Hz), 8.48 (d, 1H, J = 8.6 Hz).

4.2.25. Bis-(5-hydroxy-2-methylquinoline-6-carboxylic acid)-1,3-propylamide (24). A light brown crystalline compound. Yield 24%. Mp 226 °C. Anal. calcd for $C_{25}H_{24}N_4O_4$+2H_2O (480.49): C 61.35%, H 5.93%; found: C 61.65%, H 6.05%. HPLC purity 92.56%. UV (nm), λ_{max}/log ϵ: 248.9/3.56. ^{1}H NMR (DMSO-d_6, 500 MHz) δ: 1.85 (s, 2H), 2.35 (s, 6H), 2.90 (t, 4H), 6.95 (d, 2H, J = 8,65 Hz), 7.10 (d, 2H, J = 9.35 Hz), 7.85 (d, 2H, J = 8.6 Hz), 7.94 (bs, 2H), 8.55 (d, 2H, J = 7.5 Hz), 18.15 (s, 2H).

4.2.26. 1,3-Bis-(5-hydroxyquinaldine-6-carboxyl)-urea (25). A yellow crystalline compound. Yield 29%. Mp 206 °C. Anal. calcd for $C_{23}H_{18}N_4O_5$+H_2O (448.42): C 60.99%, H 4.53; found: C 60.84%, H 4.95%.HPLC purity 94.75%. UV (nm), λ_{max}/log ϵ: 263.1/3.55. ^{1}H NMR (DMSO-d_6, 500 MHz) δ: 2.63 (s, 6H), 7.15 (d, 2H, J = 8.1 Hz), 7.35 (d, 2H, J = 8.15 Hz), 8.05 (d, 2H, J = 8.75 Hz), 8.70 (d, 2H, J = 8.65 Hz).

4.3. Lipophilicity

HPLC determination (capacity factor K/calculated log K).

The HPLC separation module Waters Alliance 2695 XE and Waters Photodiode Array Detector 2996 (Waters Corp., Milford, MA, USA) were used. The chromatographic column Symmetry® C_{18} 5 μm, 4.6 × 250 mm, Part No. WAT054275, (Waters Corp., Milford, MA, USA) was used. The HPLC separation process was monitored by Millennium32® Chromatography Manager Software, Waters 2004 (Waters Corp., Milford, MA, USA). The mixture of MeOH p.a. (55.0%) and

H_2O-HPLC—Mili-Q Grade (45.0%) was used as a mobile phase. The total flow of the column was 0.9 mL/min, injection 30 μL, column temperature 30 °C, and sample temperature 10 °C. The detection wavelength 210 nm was chosen. The KI methanolic solution was used for the dead time (T_D) determination. Retention times (T_R) were measured in minutes.

The capacity factors K were calculated using the Millennium32® Chromatography Manager Software according to the formula $K = (T_R - T_D)/T_D$, where T_R is the retention time of the solute, whereas T_D denotes the dead time obtained via an unretained analyte. Log K, calculated from the capacity factor K, is used as the lipophilicity index converted to log P scale. The log K values of the individual compounds are shown in Tables 1 and 2.

4.4. Lipophilicity and physicochemical calculations

Log P, that is, the logarithm of the partition coefficient for n-octanol/water, was calculated using the programs CS ChemOffice Ultra ver. 9.0 (CambridgeSoft, Cambridge, MA, USA) and ACD/log P ver. 1.0 (Advanced Chemistry Development Inc., Toronto, Canada). Clog P values (the logarithm of n-octanol/water partition coefficient based on established chemical interactions) were generated by means of CS ChemOffice Ultra ver. 9.0 (CambridgeSoft, Cambridge, MA, USA) software. The results are shown in Tables 1 and 2.

Molar refractivity, polarizability, and other simple physicochemical constants were calculated using ACD labs software. The Hammett constants were taken from Hansh and Leo.[38] Polarizabilty was calculated according to Lorentz–Lorenz equation.

$$\text{Polarizability} = 0.3964308 \cdot \frac{(n^2 - 1)}{(n^2 + 2)} \cdot \frac{M_W}{d}$$

4.5. Biological activities

4.5.1. PET inhibition in spinach chloroplasts. Chloroplasts were prepared by the procedure of Walker from spinach (*Spinacia oleracea* L.).[40] The inhibition of photosynthetic electron transport (PET) in spinach chloroplasts was determined spectrophotometrically (Kontron Uvikon 800, Kontron, Muenchen, Germany) using an artificial electron acceptor 2,6-dichlorophenol-indophenol (DCIPP) according to Kralova et al.[41–43] and the rate of photosynthetic electron transport was monitored as a photoreduction of DCPIP. The measurements were carried out in phosphate buffer (0.02 mol/L, pH 7.2) containing sucrose (0.4 mol/L), $MgCl_2$ (0.005 mol/L) and NaCl (0.015 mol/L). The chlorophyll content was 30 mg/L in these experiments and the samples were irradiated (~100 W/m^2) from 10 cm distance with a halogen lamp (250 W) using a 4 cm water filter to prevent warming of the samples (suspension temperature 22 °C). The studied compounds were dissolved in DMSO due to their limited water solubility. The applied DMSO concentration (up to 4%) did not affect the photochemical activity in spinach chloroplasts (PET). The inhibitory efficiency of the studied compounds has been expressed by IC_{50} values, that is, by molar concentration of the compounds causing a 50% decrease in the oxygen evolution relative to the untreated control. The comparable IC_{50} value for a selective herbicide 3-(3,4-dichlorophenyl)-1,1-dimethylurea, DCMU (Diurone®) was about 1.9 μmol/L.[42] The results are summarized in Tables 1 and 2.

4.5.2. Reduction of chlorophyll content in the green algae *C. vulgaris* Beij. The green algae *C. vulgaris* Beij was cultivated statically at room temperature according to Kralova et al.[43] (photoperiod 16 h light/8 h dark; photosynthetic active radiation 80 μmol/m^{2}s; pH 7.2). The effect of the compounds on algal chlorophyll (Chl) content was determined after 7-day cultivation in the presence of the tested compounds. The Chl content in the algal suspension was determined spectrophotometrically (Kontron Uvikon 800, Kontron, Muenchen, Germany) after extraction into methanol according to Wellburn.[44] The Chl content in the suspensions at the beginning of the cultivation was 0.01 mg/L. The applied compound concentrations were as follows: 100, 75. 50, 25, 8.3, 4.2, and 0.83 μmol/L. Because of the low solubility of the studied compounds in water, these were dissolved in DMSO. DMSO concentration in the algal suspensions did not exceed 0.25% and the control samples contained the same DMSO amount as the suspensions treated with the tested compounds. The antialgal activity of the compounds was expressed as IC_{50} (the concentration of the inhibitor causing a 50% decrease in content of chlorophyll as compared with the control sample) or as percentage of the control determined for the studied concentration range (100–0.83 μmol/L) with the corresponding standard deviation (SD). Comparable IC_{50} value for a selective herbicide 3-(3,4-dichlorophenyl)-1,1-dimethylurea, DCMU (Diurone®) was about 7.3 μmol/L.[42] The results are summarized in Tables 1 and 2.

Acknowledgments

This study was supported by KBN Warsaw 3T09A01127, by the Ministry of Education of the Czech Republic MSM 6215712403, and by the Slovak Scientific Grant Agency VEGA 1/0089/03.

References and notes

1. Anzali, S.; Barnickel, G.; Cezanne, B.; Krug, M.; Filimonov, D.; Poroikov, V. *J. Med. Chem.* **2001**, *44*, 2432.
2. Kos, A., PASS Prediction of Activity Spectra for Substances, http://www.akosgmbh.de/pass/index.htm.
3. Jampilek, J.; Dolezal, M.; Kunes, J.; Buchta, V.; Kralova, K. *Med. Chem.* **2005**, *1*, 591.
4. Musiol, R.; Jampilek, J.; Kralova, K.; Richardson, D. R.; Kalinowski, D.; Podeszwa, B.; Finster, J.; Niedbala, H.; Palka, A.; Polanski, J. *Bioorg. Med. Chem.* **2007**, *15*, 1280.
5. Jampilek, J.; Dolezal, M.; Kunes, J.; Buchta, V. ECSOC-8 **2004**, November 1–30, http://www.lugo.usc.es/%7Eqoseijas/ECSOC-8/BOCNP/005/index.htm.

6. Roth, H. J.; Fenner, H. In *Arzneistoffe*, 3rd ed.. In *Deutscher Apotheker*; Verlag: Stuttgart, 2000; pp 51–114.
7. Musiol, R.; Jampilek, J.; Buchta, V.; Silva, L.; Niedbala, H.; Podeszwa, B.; Palka, A.; Majerz-Maniecka, K.; Oleksyn, B.; Polanski, J. *Bioorg. Med. Chem.* **2006**, *14*, 3592.
8. Harris, C. R.; Thorarensen, A. *Curr. Med. Chem.* **2004**, *11*, 2213.
9. Vangapandu, S.; Jain, M.; Jain, R.; Kaur, S.; Singh, P. P. *Bioorg. Med. Chem.* **2004**, *12*, 2501.
10. Andries, K.; Verhasselt, P.; Guillemont, J.; Gohlmann, H. W.; Neefs, J. M.; Winkler, H.; Van Gestel, J.; Timmerman, P.; Zhu, M.; Lee, E.; Williams, P.; de Chaffoy, D.; Huitric, E.; Hoffner, S.; Cambau, E.; Truffot-Pernot, C.; Lounis, N.; Jarlier, V. *Science* **2005**, *307*, 223.
11. Vinsova, J.; Imramovsky, A.; Jampilek, J.; Monreal-Ferriz, J.; Dolezal, M. *Anti-infective Agents Med. Chem.* **2008**, *7*, 12.
12. Sissi, C.; Palumbo, M. *Curr. Med. Chem. Anti-Canc. Agents* **2003**, *3*, 439.
13. Mekouar, K.; Mouscadet, J. F.; Desmaele, D.; Subra, F.; Leh, H.; Savoure, D.; Auclair, C.; d'Angelo, J. *J. Med. Chem.* **1998**, *41*, 2846.
14. Polanski, J.; Zouhiri, F.; Jeanson, L.; Desmaele, D.; d'Angelo, J.; Mouscadet, J.; Gieleciak, R.; Gasteiger, J.; Bret, M. L. *J. Med. Chem.* **2002**, *45*, 4647.
15. Polanski, J.; Niedbala, H.; Musiol, R.; Tabak, D.; Podeszwa, B.; Gieleciak, R.; Bak, A.; Palka, A.; Magdziarz, T. *Acta Poloniae Pharm. Drug Res.* **2004**, *61*, 3.
16. Pommier, Y.; Johnson, A. A.; Marchand, C. . *Nat. Rev. Drug. Discov.* **2005**, *4*, 236.
17. Zouhiri, F.; Danet, M.; Bernard, C.; Normand-Bayle, M.; Mouscadet, J. F.; Leh, H.; Thomas, C. M.; Mbemba, G.; d'Angelo, J.; Desmaele, D. *Tetrahedron Lett.* **2005**, *46*, 2201.
18. Roberts, D.H.; Hutson, T.R. (Eds.), *Herbicides*, 1987, Vol. 6.
19. Miletin, M.; Hartl, J.; Dolezal, M.; Odlerova, Z.; Kralova, K.; Machacek, M. *Molecules*, **2000**, *5*, 208 (http://www.mdpi.org/molecules/papers/50300208.pdf).
20. Dolezal, M.; Vicik, R.; Miletin, M.; Kralova, K. *Chem. Pap.* **2000**, *54*, 245.
21. Dolezal, M.; Miletin, M.; Kunes, J.; Kralova, K. *Molecules* **2002**, *7*, 363 (http://www.mdpi.net/molecules/papers/70300363.pdf).
22. Jampilek, J.; Dolezal, M.; Osicka, Z.; Kunes, J.; Kralova, K. ECSOC-7 2003, November 1–30, http://www.mdpi.net/ec/ec_article.php?id=81&file=papers/ecsoc-7/C001/C001.htm.
23. Dolezal, M.; Cmedlova, P.; Palek, L.; Kunes, J.; Buchta, V.; Jampilek, J.; Kralova, K. ECSOC-9 2005, November 1–30, http://www.usc.es/congresos/ecsoc/9/BOCNP/c010/index.htm.
24. Dolezal, M.; Palek, L.; Vinsova, J.; Buchta, V.; Jampilek, J.; Kralova, K. *Molecules* **2006**, *11*, 242, http://www.mdpi.org/molecules/papers/11040242.pdf.
25. Liu, J.; Li, Z.; Yan, H.; Wang, L.; Chen, J. . *Bioorg. Med. Chem. Lett.* **1999**, *9*, 1927.
26. Polanski, J.; Niedbala, H.; Musiol, R.; Podeszwa, B.; Tabaka, D.; Palka, A.; Mencel, A.; Mouscadet, J. F.; Le Bret, M. *Lett. Drugs Des. Disc.* **2007**, *4*, 99.
27. (a) Pliska, V.; Testa, B.; van de Waterbeemd, H. *Lipophilicity in Drug Action and Toxicology*; Wiley-VCH: Weinheim, 1996; (b) Avdeef, A. *Curr. Top. Med. Chem.* **2001**, *1*, 277; (c) Nasal, A.; Siluk, D.; Kaliszan, R. *Curr. Med. Chem.* **2003**, *10*, 381; (d) Toropov, A. A.; Benfenati, E. *Curr. Drug Disc. Technol.* **2007**, *4*, 77.
28. (a) Hansch, C.; Mahoney, P. P.; Fujita, T.; Muir, R. M. *Nature* **1962**, *194*, 178; (b) Hansch, C.; Fujita, T. *J. Am. Chem. Soc.* **1964**, *86*, 1616; (c) Leo, A.; Hansch, C.; Elkins, D. *Chem. Rev.* **1971**, *71*, 525.
29. Valko, K. J. *Chromatography A* **2004**, *1037*, 299.
30. (a) Haggerty, W. J.; Murill, E. A. *Res. Dev.* **1974**, *25*; (b) Carlson, R. M.; Carlson, R. E.; Kopperman, H. L. *J. Chromatogr.* **1975**, *107*, 219; (c) Mirrlees, M. S.; Moulton, S. J.; Murphy, C. T.; Taylor, P. *J. Med. Chem.* **1976**, *19*, 619; (d) Unger, S. H.; Cook, J. R.; Holenberg, J. S. *J. Pharm. Sci.* **1978**, *67*, 1364; (e) Braumann, Th.; Weber, G.; Grimme, L. H. *J. Chromatogr.* **1983**, *261*, 329.
31. Valko, K.; Du, C. M.; Bevan, C.; Reynolds, D. P.; Abraham, M. H. *Curr. Med. Chem* **2001**, *8*, 1137.
32. Cimpan, G.; Irimie, F.; Gocan, S.; Claessens, H. A. *J. Chromatogr. A.* **1998**, *714*, 247.
33. (a) Hartmann, T.; Schmitt, J. *Drug Disc. Today Technol.* **2004**, *1*, 431; (b) Gocan, S.; Cimpan, G.; Comer, J. *Adv. Chromatogr.* **2006**, *44*, 79.
34. Meylan, W. M.; Howard, P. H. *J. Pharm. Sci.* **1995**, *84*, 83.
35. Palmer, M. H. *The Structure and Reactions of Heterocyclic Compounds*; Edward Arnold Publisher Ltd.: London, 1967.
36. Jampilek, J.; Vinsova, J.; Grafnetterova, T.; Dohnal, J. ECSOC-9 2005, November 1–30, http://www.usc.es/congresos/ecsoc/9/GOS/a008/index.htm.
37. Dolezal, M.; Jampilek, J.; Osicka, Z.; Kunes, J.; Buchta, V.; Vichova, P. *Farmaco* **2003**, *58*, 1105.
38. Hansch, C.; Leo, A. J. *Substituent Constants for Correlation Analysis in Chemistry and Biology*; John Wiley: New York, 1979.
39. Detailed information on this group of amides will be published elsewhere.
40. Walker, D. A. In *Methods in Enzymology Part C*; Colowick, S. P., Kaplan, N. O., Eds.; Academic Press: New York, 1980; Vol. 69, pp 94–104.
41. Kralova, K.; Sersen, F.; Sidoova, E. *Chem. Pap.* **1992**, *46*, 348.
42. Fedke, C. *Biochemistry and Physiology of Herbicide Action*; Springer Verlag: Berlin-Heidelberg-New York, 1982.
43. Kralova, K.; Sersen, F.; Melnik, M. *J. Trace Microprobe Techn.* **1998**, *16*, 491.
44. Wellburn, A. R. *J. Plant. Physiol.* **1994**, *144*, 307.

Available online at www.sciencedirect.com
ScienceDirect
Polyhedron 27 (2008) 1121–1130
POLYHEDRON
www.elsevier.com/locate/poly

Reactivity of oxorhenium(V) complexes towards quinoline carboxylic acids. X-ray structure of $[ReOCl_2(hquin\text{-}7\text{-}COOH)(PPh_3)] \cdot OPPh_3$, $[ReOBr_2(hquin\text{-}7\text{-}COOH)(PPh_3)]$ and $[ReOX_2(hmquin\text{-}7\text{-}COOH)(PPh_3)]$. DFT and TD-DFT calculations for $[ReOCl_2(hquin\text{-}7\text{-}COOH)(PPh_3)]$

B. Machura [a,*], J. Miłek [a], J. Kusz [b], J. Nycz [c], D. Tabak [c]

[a] *Department of Crystallography, Institute of Chemistry, University of Silesia, 9th Szkolna Street, 40-006 Katowice, Poland*
[b] *Institute of Physics, University of Silesia, 4th Uniwersytecka Street, 40-006 Katowice, Poland*
[c] *Department of Organic Chemistry, Institute of Chemistry, University of Silesia, 9th Szkolna Street, 40-006 Katowice, Poland*

Received 24 October 2007; accepted 11 December 2007
Available online 28 January 2008

Abstract

The reactions of $[ReOX_3(PPh_3)_2]$ (X = Cl, Br) with 8-hydroxyquinoline-7-carboxylic acid (Hhquin-7-COOH) and 8-hydroxy-2-methylquinoline-7-carboxylic acid (Hhmquin-7-COOH) have been examined and $[ReOX_2(hquin\text{-}7\text{-}COOH)(PPh_3)]$ and $[ReOX_2(hmquin\text{-}7\text{-}COOH)(PPh_3)]$ complexes have been obtained. All the complexes were characterized by IR, UV–Vis spectroscopy and elemental analysis. The crystal and molecular structures have been determined for $[ReOCl_2(hquin\text{-}7\text{-}COOH)(PPh_3)] \cdot OPPh_3$, $[ReOBr_2(hquin\text{-}7\text{-}COOH)(PPh_3)]$ and $[ReOX_2(hmquin\text{-}7\text{-}COOH)(PPh_3)]$. The electronic structure of $[ReOCl_2(hquin\text{-}7\text{-}COOH)(PPh_3)]$ has been calculated with the density functional theory (DFT) method, and TDDFT/PCM calculations have been employed to produce a hundred of singlet excited-states starting from the ground-state geometry optimized in the gas phase.

Keywords: Rhenium oxo complexes; 8-Hydroxyquinoline-7-carboxylic acid; 8-Hydroxy-2-methylquinoline-7-carboxylic acid; X-ray and electronic structure; DFT calculations; NBO analysis

1. Introduction

For many years inorganic compounds containing an oxygen atom multiply bonding to a transition metal have been in the center of interest to those scientists engaged in basic research and to those trying to employ these complexes in catalytic processes. Oxygen atom transfer chemistry has been implicated in various reactions of industrial and biological importance, including olefin epoxidation and catalysis by cytochrome P-450 [1–3].

The chemistry of oxo rhenium complexes arouses particular interest among these compounds. Methyltrioxorhenium and its derivatives are among the most versatile oxidation catalysts known to date [4]. The oxorhenium(V) chelates $[ReOCl_2(O\text{–}N)(PPh_3)]$ with pyridinecarboxylate ligands exhibit a remarkable catalytic activity for the conversion of ethane, under relatively mild conditions, to a mixture of propionic and acetic acids in a single-pot process with various advantages over the industrial ones [5].

Furthermore, the favorable nuclear properties of ^{186}Re and ^{188}Re nuclides make the compounds with these radioisotopes useful for applications in radioimmunotheraphy [6,7]. Consequently, the inorganic chemistry studies with

* Corresponding author.
E-mail address: basia@ich.us.edu.pl (B. Machura).

0277-5387/$ - see front matter © 2007 Elsevier Ltd. All rights reserved.
doi:10.1016/j.poly.2007.12.006

the naturally occurring non-radioactive rhenium isotopes are very attractive to clearly establish the molecular structure of ^{99m}Tc- and $^{186/188}$Re-based radiopharmaceuticals. In this context, the design, synthesis and reactivity of novel rhenium oxocomplexes has become the aim of several laboratories, including ours.

Previously, we investigated the reactivity of oxorhenium(V) species – $[ReOX_3(PPh_3)_2]$ and $[ReOX_3(AsPh_3)_2]$ (X = Cl or Br) – towards 8-hydroxyquinoline (Hhqn) and quinoline-2-carboxylic acid [8,9]. As an extension of this work, we were keen to examine the reactivity of $[ReOX_3(PPh_3)_2]$ towards quinoline ligands containing both hydroxy and carboxylate fragments. 8-Hydroxyquinoline-7-carboxylic acid (Hhquin-7-COOH) and 8-hydroxy-2-methylquinoline-7-carboxylic acid (Hhmquin-7-COOH) are such ligands. Additionally, presented here and in previous work [8,9] quinoline derivatives are structural fragments of styryloquinolines, which are important class of compounds in the search for the potential inhibitors of HIV-1 integrase [10].

Here we present synthesis of $[ReOCl_2$(hquin-7-COOH)$(PPh_3)] \cdot OPPh_3$ (**1** · $OPPh_3$), $[ReOBr_2$(hquin-7-COOH)$(PPh_3)]$ (**2**), $[ReOCl_2$(hmquin-7-COOH)$(PPh_3)]$ (**3**) and $[ReOBr_2$(hmquin-2-COOH)$(PPh_3)]$ (**4**) complexes. X-ray studies have been performed for **1** · $OPPh_3$, **2** and **3** and they confirm bidentate coordination mode of the quinoline carboxylic acids. The COOH group of the quinoline carboxylic acids in the examined complexes is potentially available for further conjugation.

The electronic structure of **1** has been calculated with the density functional theory (DFT), and TDDFT/PCM calculations have been employed to produce a hundred of singlet excited-states starting from the ground-state geometry optimized in the gas phase.

Currently density functional theory (DFT) is commonly used to examine the electronic structure of transition metal complexes. It meets with the requirements of being accurate, easy to use and fast enough to allow the study of relatively large molecules of transition metal complexes [11]. Recent calculations with TD-DFT method for open- and closed-shell of 5d-metal complexes (including rhenium complexes) have also supported the TD-DFT method to be applicable for such systems giving good assignment of experimental spectra [12,13].

Some theoretical investigations have been carried out on the rhenium compounds. The electronic structures of nitrido, oxo, carbonyl, nitrosyl and nitrile rhenium complexes, as well as their spectroscopic properties, bonding and reactivity have been theoretically studied at the HF, MP2, EHT and DFT levels of theory using various basis sets [14–22]. Gancheff et al. [16] have performed extended tests of the ability of the B3LYP method in LANL2DZ basis set for rhenium compounds in a geometry optimization and calculation of spectral properties. Although this is not a very extended basis set, its use with DFT has shown to be sufficient for the geometry optimization and calculation of spectral properties. The correctness of B3LYP method with LANL2DZ basis set for rhenium complexes has been also proven in this paper. The experimental geometry of $[ReOCl_2$(hquin-7-COOH)$(PPh_3)]$ is well reproduced and the calculated electronic spectrum is in good accordance with the experimental one.

2. Experimental

2.1. General procedure

The $[ReOX_3(PPh_3)_2]$ complexes were prepared as reported previously [23]. 8-Hydroxyquinoline-7-carboxylic acid and 8-hydroxy-2-methylquinoline-7-carboxylic acid were synthesized according to the literature methods [24]. All the other reagents used to the synthesis were commercially available and were used without further purification.

IR spectra were recorded on a Nicolet Magna 560 spectrophotometer in the spectral range 4000–400 cm^{-1} with the samples in the form of KBr pellets. Electronic spectra were measured on a spectrophotometer Lab Alliance UV–Vis 8500 in the range 1000–180 nm in acetonitrile solution. Elemental analyses (C H N) were performed on a Perkin–Elmer CHN-2400 analyzer. The ^{1}H NMR spectrum was recorded with a Bruker AM 400 spectrometer at room temperature using $CDCl_3$ as a solvent.

2.2. Preparation of $[ReOCl_2$(hquin-7-COOH)$(PPh_3)] \cdot OPPh_3$ (1 · $OPPh_3$)

A mixture of $[ReOCl_3(PPh_3)_2]$ (0.50 g, 0.60 mmol), 8-hydroxyquinoline-7-carboxylic acid (0.13 g, 0.69 mmol) and acetonitrile (50 ml) was stirred at room temperature for 3 h. The resulting red-brown solution was left to slow evaporation and dark red crystals were obtained after few days. Yield 75%.

Anal. Calc. for $C_{46}H_{36}Cl_2NO_5P_2Re$: C, 55.15; H, 3.62; N, 1.40. Found: C, 55.70; H, 3.66; N, 1.45%.

IR (KBr; ν/cm^{-1}): 1707(s) $\nu_{C=O}$(COOH); 1616(m), 1588(m), 1567(m), ν_{CN} and $\nu_{C=C}$; 978(vs) $\nu_{Re=O}$.

^{1}H NMR (400 MHz; $CDCl_3$) δ = 12.47 (s, 1 H, COOH), 8.17 (dd, 1H), 8.02 (d, 1H), 7.91 (dd, 1H), 7.70–7.25 (m, 31H), 7.16 (d, 1H).

2.3. Preparation of $[ReOBr_2$(hquin-7-COOH)$(PPh_3)]$ (2)

A procedure similar to that for $[ReOCl_2$(hquin-7-COOH)$(PPh_3)] \cdot OPPh_3$ was used with $[ReOBr_3(PPh_3)_2]$ (0.50 g, 0.52 mmol) and 8-hydroxyquinoline-7-carboxylic acid (0.12 g, 0.63 mmol). Dark red crystals of $[ReOBr_2$(hquin-7-COOH)$(PPh_3)]$ were collected in 80% yield.

Anal. Calc. for $C_{28}H_{21}Br_2NO_4PRe$: C, 41.39; H, 2.61; N, 1.72. Found: C, 40.90; H, 2.68; N, 1.70%.

IR (KBr; ν/cm^{-1}): 1718(s) $\nu_{C=O}$(COOH); 1612(m), 1592(m), 1570(m), ν_{CN} and $\nu_{C=C}$; 981(vs) $\nu_{Re=O}$.

^{1}H NMR (400 MHz; $CDCl_3$) δ = 12.46 (s, 1H, COOH), 8.15 (dd, 1H), 8.04 (d, 1H), 7.93 (dd, 1H), 7.57 (br, 1H), 7.42–7.28 (m, 15H), 7.20 (d, 1H).

2.4. Preparation of [$ReOCl_2$(hmquin-7-COOH)(PPh_3)] (3)

A procedure similar to that for [$ReOCl_2$(hquin-7-COOH)(PPh_3)] · $OPPh_3$ was used with [$ReOCl_3(PPh_3)_2$] (0.50 g, 0.60 mmol) and 8-hydroxy-2-methylquinoline-7-carboxylic acid (0.14 g, 0.69 mmol). Crystalline precipitate of [$ReOCl_2$(hmquin-7-COOH)(PPh_3)] was collected in 70% yield.

Anal. Calc. for $C_{29}H_{23}Cl_2NO_4PRe$: C, 47.22; H, 3.14; N, 1.90. Found: C, 47.50; H, 3.10; N, 1.85%.

IR (KBr; ν/cm^{-1}): 1718(s) $\nu_{C=O}$(COOH); 1616(m), 1550(m), 1513(m), ν_{CN} and $\nu_{C=C}$; 983(vs) $\nu_{Re=O}$.

^1H NMR (400 MHz; $CDCl_3$) $\delta = 12.42$ (s, 1H, COOH), 7.91 (d, 1H), 7.84 (d, 1H), 7.55 (d, 1H), 7.44–7.26 (m, 15H), 7.15 (d, 1H), 2.89 (s, 3H).

2.5. Preparation of [$ReOBr_2$(hmquin-7-COOH)(PPh_3)] (4)

A procedure similar to that for [$ReOCl_2$(hquin-7-COOH)(PPh_3)] · $OPPh_3$ was used with [$ReOBr_3(PPh_3)_2$] (0.50 g, 0.52 mmol) and 8-hydroxy-2-methylquinoline-7-carboxylic acid (0.13 g, 0.64 mmol). Crystalline precipitate of [$ReOBr_2$(hmquin-7-COOH)(PPh_3)] was collected in 65% yield.

Anal. Calc. for $C_{29}H_{23}Br_2NO_4PRe$: C, 42.14; H, 2.80; N, 1.69. Found: C, 42.37; H, 2.73; N, 1.65%.

IR (KBr; ν/cm^{-1}): 1710(s) $\nu_{C=O}$(COOH); 1620(m), 1559(m), 1513(m), ν_{CN} and $\nu_{C=C}$; 982(vs) $\nu_{Re=O}$.

2.6. Crystal structures determination and refinement

The X-ray intensity data of 1 · $OPPh_3$, 2 and 3 were collected on a KM-4-CCD automatic diffractometer equipped with CCD detector and graphite monochromated Mo Kα radiation ($\lambda = 0.71073$ Å) at room temperature. Details concerning crystal data and refinement are given in Table 1. Lorentz, polarization and empirical absorption correction using spherical harmonics implemented in SCALE3 ABSPACK scaling algorithm [25] were applied. The structures were solved by the Patterson method and subsequently completed by the difference Fourier recycling. All the non-hydrogen atoms were refined anisotropically using full-matrix, least-squares technique. The hydrogen atoms were treated as "riding" on their adjacent atoms and assigned isotropic temperature factors equal 1.2 times the value of equivalent temperature factor of the aromatic parent atoms and equal 1.5 times the value of equivalent temperature factor of the methyl parent carbon atom and oxygen atom (OH). SHELXS97 [26], SHELXL97 [27] and SHELXTL [28] programs were used for all the calculations.

Table 1
Crystal data and structure refinement for 1 · $OPPh_3$, 2 and 3 complexes

	1 · $OPPh_3$	2	3
Empirical formula	$C_{46}H_{36}Cl_2NO_5P_2Re$	$C_{28}H_{21}Br_2NO_4PRe$	$C_{29}H_{23}Cl_2NO_4PRe$
Formula weight	1001.80	812.45	737.55
Temperature (K)	293(2)	293(2)	293(2)
Wavelength (Å)	0.71073	0.71073	0.71073
Crystal system	monoclinic	monoclinic	monoclinic
Space group	$P2_1/c$	$P2_1/n$	$P2_1/c$
Unit cell dimensions			
a (Å)	10.0349(3)	10.5930(3)	16.6364(9)
b (Å)	20.9077(7)	15.1539(3)	10.4172(4)
c (Å)	20.0326(5)	17.0501(5)	17.5480(9)
β (°)	94.851(2)	104.627(3)	116.327(7)
Volume (Å^3)	4187.9(2)	2648.27(12)	2725.7(2)
Z	4	4	4
D_{calc} (Mg/m^3)	1.589	2.038	1.797
Absorption coefficient (mm^{-1})	3.153	7.702	4.749
F(000)	1992	1552	1440
Crystal size (mm)	0.12 × 0.16 × 0.34	0.07 × 0.14 × 0.14	0.01 × 0.14 × 0.32
θ Range for data collection (°)	2.94–25.00	2.92–25.00	2.81–25.05
Index ranges	$-11 \leqslant h \leqslant 11$, $-24 \leqslant k \leqslant 24$, $-19 \leqslant l \leqslant 23$	$-12 \leqslant h \leqslant 12$, $-18 \leqslant k \leqslant 10$, $-20 \leqslant l \leqslant 20$	$-19 \leqslant h \leqslant 19$, $-12 \leqslant k \leqslant 12$, $-20 \leqslant l \leqslant 12$
Reflections collected	25758	16435	16679
Independent reflections (R_{int})	7351 (0.0217)	4639 (0.0223)	4823 (0.0417)
Completeness to $2\theta = 50°$ (%)	99.6	99.7	99.7
Data/restraints/parameters	7351/0/515	4639/0/335	4823/0/345
Goodness-of-fit on F^2	1.024	0.989	0.979
Final R indices [$I > 2\sigma(I)$]	$R_1 = 0.0207$, $wR_2 = 0.0456$	$R_1 = 0.0151$, $wR_2 = 0.0350$	$R_1 = 0.0236$, $wR_2 = 0.0463$
R indices (all data)	$R_1 = 0.0324$, $wR_2 = 0.0474$	$R_1 = 0.0194$, $wR_2 = 0.0356$	$R_1 = 0.0344$, $wR_2 = 0.0479$
Largest difference in peak and hole (e Å^{-3})	0.909 and −0.435	0.679 and −0.520	1.096 and −1.065

Atomic scattering factors were those incorporated in the computer programs.

3. Computational details

The gas phase geometry of **1** was optimized in the singlet ground-state with the DFT method using the hybrid B3LYP [29,30] functional of · GAUSSIAN-03 [31]. The LANL2DZ with additional *d* function with exponent $\alpha = 0.3811$ and *f* function with exponent $\alpha = 2.033$ basis set [32,33] was chosen for the rhenium atom and the standard 6-31G basis set for all the other atoms [34,35]. TDDFT calculations were employed to produce a hundred singlet excited-states starting from the ground-state geometry optimized in the gas phase The solvent (acetonitrile) effect was simulated using the polarizable continuum model (PCM) [36].

Natural bond orbital (NBO) calculations were performed with the NBO code [37,38] included in GAUSSIAN03.

4. Results and discussion

4.1. Preparation and infrared data

The $[ReOX_2(hquin\text{-}7\text{-}COOH)(PPh_3)]$ and $[ReOX_2(hmquin\text{-}7\text{-}COOH)(PPh_3)]$ (X = Cl, Br) complexes were prepared in good yields by ligand exchange reactions starting from $[ReOX_3(PPh_3)_2]$ complexes and 8-hydroxyquinoline-7-carboxylic acid or 8-hydroxy-2-methylquinoline-7-carboxylic acid.

$$[ReOX_3(PPh_3)_2] + Hhquin\text{-}7\text{-}COOH \rightarrow [ReOX_2(hquin\text{-}7\text{-}COOH)(PPh_3)] + HX + PPh_3$$

X = Cl, Br

$$[ReOX_3(PPh_3)_2] + Hhmquin\text{-}7\text{-}COOH \rightarrow [ReOX_2(hmquin\text{-}7\text{-}COOH)(PPh_3)] + HX + PPh_3$$

The complexes are air stable and soluble in common organic solvents. The $[ReOCl_2(hquin\text{-}7\text{-}COOH)(PPh_3)]$ complex crystallizes as the $[ReOCl_2(hquin\text{-}7\text{-}COOH)(PPh_3)] \cdot OPPh_3$ adduct. The starting oxo complexes are synthesized by the reduction of ammonium perrhenate:

$$ReO_4^- + 3X^- + 4H^+ + 3PPh_3 \rightarrow [ReOX_3(PPh_3)_2] + OPPh_3 + 2H_2O$$

and $[ReOX_3(PPh_3)_2]$ compounds can be impure with $OPPh_3$.

The selected frequencies observed in the IR spectra of $[ReOX_2(hquin\text{-}7\text{-}COOH)(PPh_3)]$ and $[ReOX_2(hmquin\text{-}7\text{-}COOH)(PPh_3)]$ complexes are given in Section 2. The carboxylic acid group of the *hquin-7-COOH* and *hmquin-7-COOH* ligand is characterized by the $\nu_{C=O}$ absorption observed in the range 1700–1720 cm^{-1} [39,40].

The strong $\nu(Re{=}O)$ stretching bands of $[ReOX_2(hquin\text{-}7\text{-}COOH)(PPh_3)]$ and $[ReOX_2(hmquin\text{-}7\text{-}COOH)(PPh_3)]$ compounds are in the higher end of the range observed for $\{ReO\}^{3+}$ core complexes. Similar to the reported previously $[ReOX_2(hqn)(PPh_3)]$ and $[ReOX_2(quin\text{-}2\text{-}c)(PPh_3)]$ complexes, the Re–hydroxy bond *trans* to the oxo ligand does not compete effectively for the d_{Re} orbitals. Moreover,

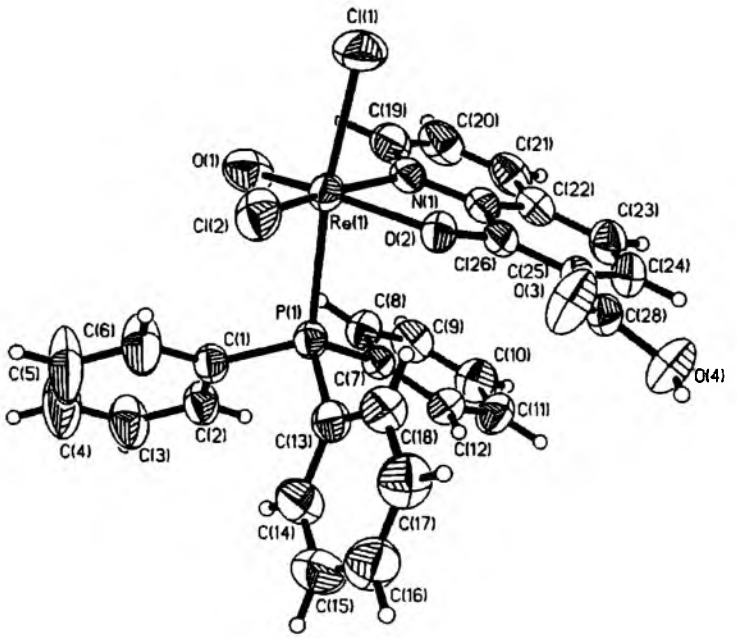

Fig. 1. The molecular structure of **1**. Displacement ellipsoids are drawn at 50% probability.

the narrow range in which the ν(Re=O) bands appear is very similar to those observed for Re(V)-oxo complexes with 8-quinolinolato or quinoline-2-carboxylate ligands [8,9].

4.2. Crystal structures

The crystallographic data for **1** · $OPPh_3$, **2** and **3** are given in Table 1, and molecular structures of the $ReOCl_2$(hquin-7-COOH)(PPh_3)] and [$ReOCl_2$(hmquin-7-COOH)(PPh_3)] complexes are presented in Figs. 1 and 2, respectively. The intermolecular interactions found in the examined structures are shown in Table 2 [41,42]. Additionally in the examined structures exist $\pi\cdots\pi$ stacking interactions between the rings of the *hquin-7-COOH* or *hmquin-7-COOH* ligands and one of the triphenylphospine rings. (Table 3) [43]. Presence of the methyl group in the quinoline ring significantly decreases $\pi\cdots\pi$ stacking interactions.

The geometry of [$ReOX_2$(hquin-7-COOH)(PPh_3)] and [$ReOX_2$(hmquin-7-COOH)(PPh_3)] compounds reveal typical features of quasi-octahedral oxorhenium(V)complexes with oxygenated bidentate ligands. The deformation of the octahedron is caused by the presence multiple bonding ligand (terminal oxo) and narrow bite angle of the chelating ligand. The high concentration of electronic density along the Re–O_t axis strongly influences the positions of the adjacent halogen atoms, which are pushed away. The presence of the methyl group attached to the quinoline ring in **3** seems to be responsible for significant increase in the Cl(1)–Re(1)–P(1) angle and decrease in the O(1)–Re(1)–P(1) one. In each complex, the rhenium atom is coordinated by a terminal oxygen atom (O_t), two halide ions in *cis* arrangement, the phosphorus atom of PPh_3 molecule, and the bidentate N,O donors of the *hquin-7-COOH* or *hmquin-7-COOH* ligand. The oxygen atom of the quinoline derivative lies in *trans* position to the terminal oxo ion.

Table 2
Hydrogen bonds for **1** · $OPPh_3$, **2** and **3** complexes

D	A	H···A (Å)	D···A (Å)	D–H···A (°)
1 · $OPPh_3$				
O(4)	O(5)	1.83	2.629(3)	165.9
C(32)	O(3)	2.57	3.489(4)	169.6
C(18)	O(2)	2.32	3.084(3)	139.4
C(24)	O(4)	2.41	2.735(4)	100.4
Complex 2				
C(16)	Br(1)#1	2.82	3.747(3)	171.8
O(4)	Br(2)#2	2.57	3.377(2)	166.9
C(4)	O(1)#3	2.47	3.314(3)	151.0
C(14)	O(2)	2.49	3.243(3)	137.9
C(19)	O(1)	2.49	2.913(3)	107.8
C(24)	O(4)	2.38	2.720(3)	101.3
Complex 3				
C(2)	O(2)	2.52	3.067(5)	117.7
C(18)	O(1)	2.40	3.066(4)	129.0

#1 $0.5+x$, $1.5-y$, $-0.5+z$; #2 $-0.5+x$, $1.5-y$, $-0.5+z$; #3: $-x+2$, $-y+1$, $-z+1$.

The selected bond distances and angles of [$ReOX_2$(hquin-7-COOH)(PPh_3)] and [$ReOX_2$(hmquin-7-COOH)(PPh_3)] complexes are collected in Tables 4 and 5.

The Re–O_t bond lengths of [$ReOX_2$(hquin-7-COOH)-(PPh_3)] and [$ReOX_2$(hmquin-7-COOH)(PPh_3)] fall in the range 1.639–1.76 Å, typical of mononuclear complexes of rhenium(V) having $[ReO]^{3+}$ core, and indicate the presence of a triple bond Re≡O [44]. The elongation of Re–O_t distance in **1** · $OPPh_3$ seems to be results of the crystal packing

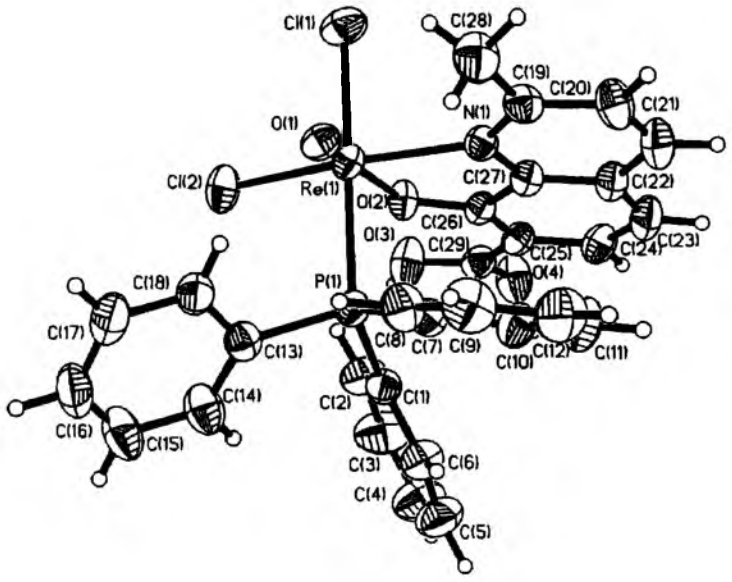

Fig. 2. The molecular structure of 4. Displacement ellipsoids are drawn at 50% probability.

Table 3
Analysis of short contacts between the *hquin-7-COOH* and *hmquin-7-COOH* rings and triphenylphospine ring (distances in Å and angles in °)

R(I)	R(J)	Cg···Cg	α	β	d_p
1·OPPh₃					
Cg(2)	Cg(1)	3.5208	10.74	18.27	3.264
Cg(3)	Cg(1)	3.6021	9.68	21.25	3.385
Complex 2					
Cg(2)	Cg(1)	3.6675	16.42	22.00	3.084
Cg(3)	Cg(1)	3.6123	16.19	19.58	3.591
Complex 3					
Cg(2)	Cg(1)	4.0621	21.21	24.36	3.075
Cg(3)	Cg(1)	5.3487	17.81	47.74	2.282

R1, R2, R3 indicates the centroids of aromatic rings containing C(7), N(1), C(24) atoms, respectively, α is a dihedral angle between planes *I* and *J*, β is an angle between Cg(I)–Cg(*J*) vector and normal to plane *I* and d_p is a perpendicular distance of Cg(*I*) on ring *J* plane.

caused by the presence of triphenylphosphine oxide in the lattice. The interatomic distances between the rhenium atom and the oxygen atom of bidentate ligand are somewhat shorter than an ideal single Re–O bond length (*ca.* 2.04 Å) [45], and indicates small delocalization in the O(2)–Re(1)–O(1) moiety. The similar trend is observed for many Re(V)-oxo complexes with an monoanionic oxygen *trans* to the oxo group [46].

The Re1–X(1) distances *trans* to the phosphorus atom of PPh_3 molecule are slightly longer than the Re1–X(1) bonds *trans* to the nitrogen atom of the *hquin-7-COOH* or *hmquin-7-COOH* ligand. It is a consequence of *structural trans* effect of the phosphine ligand.

4.3. Geometry optimization, charge distribution, electronic structure and NBO analysis

The geometry of **1** was optimized in a singlet state by the DFT method with the B3LYP functional. The optimized geometric parameters of **1** are gathered in Table 4. In general, the predicted bond lengths and angles are in agreement with the values based upon the X-ray crystal structure data, and the general trends observed in the experimental data (discussed above) are well reproduced in the calculations.

Table 4
The experimental and optimized bond lengths (Å) and angles (°) for **1**

Bond lengths	Experimental	Optimized	Bond angles	Experimental	Optimized
Re(1)–O(1)	1.7197(19)	1.678	O(1)–Re(1)–O(2)	161.91(9)	157.88
Re(1)–O(2)	2.0106(16)	2.043	O(1)–Re(1)–N(1)	89.34(9)	86.23
Re(1)–N(1)	2.139(2)	2.170	O(2)–Re(1)–N(1)	75.00(8)	74.26
Re(1)–Cl(1)	2.3816(7)	2.436	O(1)–Re(1)–Cl(1)	98.96(7)	101.76
Re(1)–Cl(2)	2.3325(8)	2.396	O(2)–Re(1)–Cl(1)	89.49(5)	86.91
Re(1)–P(1)	2.4891(7)	2.541	N(1)–Re(1)–Cl(1)	87.45(6)	84.59
			O(1)–Re(1)–Cl(2)	104.03(8)	105.24
			O(2)–Re(1)–Cl(2)	92.11(5)	95.19
			N(1)–Re(1)–Cl(2)	166.47(6)	167.64
			Cl(1)–Re(1)–Cl(2)	88.37(3)	88.49
			O(1)–Re(1)–P(1)	89.37(7)	91.07
			O(2)–Re(1)–P(1)	82.29(5)	81.50
			N(1)–Re(1)–P(1)	91.92(6)	97.62
			Cl(1)–Re(1)–P(1)	171.63(3)	167.09
			Cl(2)–Re(1)–P(1)	90.35(2)	86.93

Table 5
The experimental bond lengths (Å) and angles (°) for **2** and **3**

Bond lengths	**2** X = Br	**3** X = Cl	Bond angles	**2**	**3**
Re(1)–O(1)	1.6742(17)	1.673(2)	O(1)–Re(1)–O(2)	160.60(7)	163.62(10)
Re(1)–O(2)	2.0044(17)	1.986(2)	O(1)–Re(1)–N(1)	87.02(8)	92.07(10)
Re(1)–N(1)	2.139(2)	2.183(3)	O(2)–Re(1)–N(1)	75.39(7)	75.58(9)
Re(1)–X(1)	2.5444(3)	2.3922(10)	O(1)–Re(1)–X(1)	99.16(6)	100.26(9)
Re(1)–X(2)	2.4950(3)	2.3393(9)	O(2)–Re(1)–X(1)	87.61(5)	90.28(7)
Re(1)–P(1)	2.4702(7)	2.4773(9)	N(1)–Re(1)–X(1)	85.12(5)	88.46(8)
			O(1)–Re(1)–X(2)	103.88(6)	104.24(8)
			O(2)–Re(1)–X(2)	94.28(4)	88.29(7)
			N(1)–Re(1)–X(2)	168.51(5)	163.68(8)
			X(1)–Re(1)–X(2)	89.502(9)	89.17(4)
			O(1)–Re(1)–P(1)	90.68(6)	81.05(8)
			O(2)–Re(1)–P(1)	82.09(5)	88.58(7)
			N(1)–Re(1)–P(1)	92.40(6)	92.12(8)
			X(1)–Re(1)–P(1)	169.694(17)	178.55(3)
			X(2)–Re(1)–P(1)	91.100(16)	89.90(3)

Table 6
Atomic charges from the Natural Population Analysis (NPA) for 1

Atom	Charge
Re(1)	1.012
O(1)	−0.440
O(2)	−0.659
N(1)	−0.466
Cl(1)	−0.391
Cl(2)	−0.337
P(1)	1.270

Table 6 presents the atomic charges from the Natural Population Analysis (NPA) for 1. The calculated charge on the rhenium atom in 1 is considerable lower than the formal charge +5, corresponding d^2 configuration of the central ion. It results from charge donation from the oxo ligands, halide ions and PPh_3 molecule. The P atom is positively charged, and the charges on the terminal oxo, chloride and oxygen atom of *hquin-7-COOH* are significantly smaller than −2, −1 and −1, respectively. The terminal oxo ions are less negative in comparison with the oxygen atoms of *hquin-7-COOH* ligand. It confirms the higher electron density delocalization from the terminal ligand towards the rhenium center and corresponds to differences in the Re–O(1) and Re–O(2) bond lengths.

The molecular orbital diagram of I with several occupied and unoccupied molecular orbital contours is presented in Fig. 3. The local symmetry of the rhenium center has been considered in the discussion: *z* axis goes

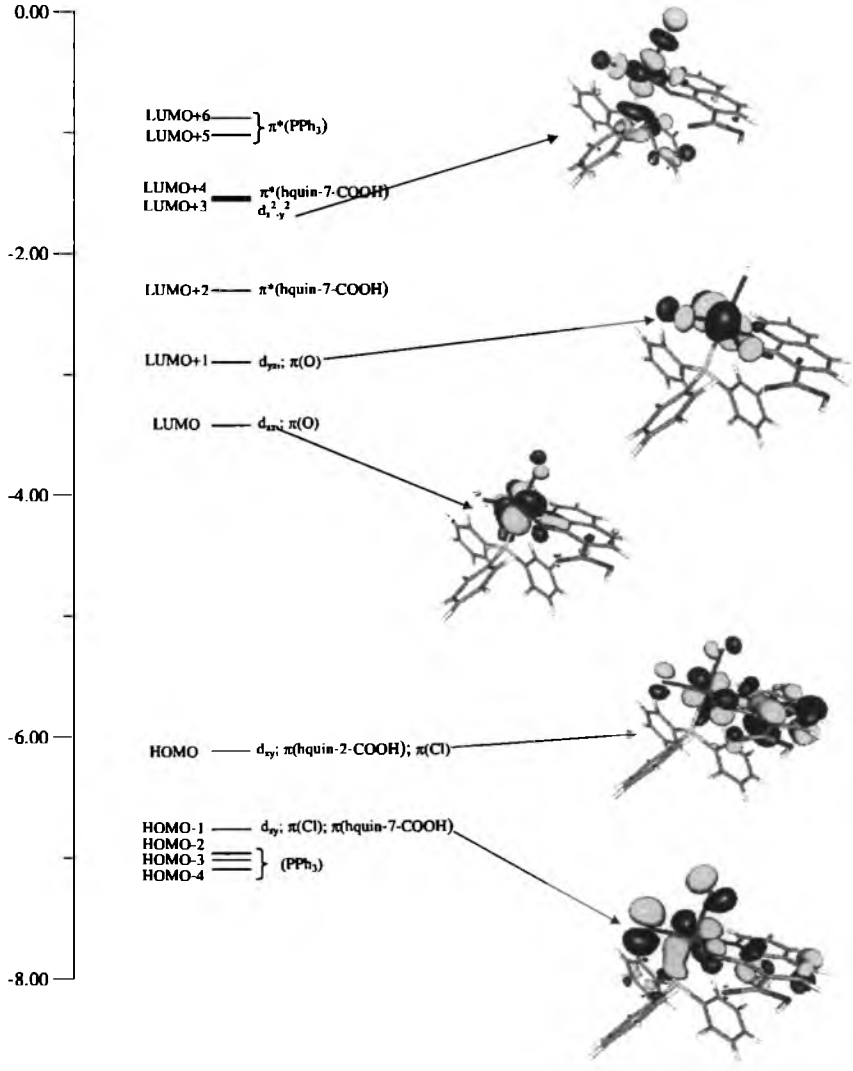

Fig. 3. The energy (eV), character and some contours of the occupied and unoccupied molecular orbitals of 1. Positive values of the orbital contour are represented in blue (0.04 au) and negative values – in yellow (−0.04 au). (For interpretation of the references in colour in this figure legend, the reader is referred to the web version of this article.)

along the O–Re–O linkage, and x axis – through the P–Re–Cl bonds.

The value of the energy separation between the highest occupied molecular orbital (HOMO) and the lowest unoccupied molecular orbital (LUMO) equals to 2.67 eV. This value is lower in comparison with the HOMO–LUMO gap calculated for the related Re(V)-oxo complexes with 8-quinolinolato or quinoline-2-carboxylate ligands [8,9]. The lower absolute value of the gap energies means lower stability and higher reactivity of the title complex.

Two highest occupied MOs are delocalized among d_{xy} rhenium orbital, chloride and *hquin-7-COOH* orbitals. The LUMO and LUMO + 1 are predominately localized on the rhenium atom (d_{xz} and d_{yz} orbitals) with some contribution of p_π oxygen orbitals. They can be ascribed as π-antibonding rhenium–oxygen molecular orbitals. The LUMO + 3 is of $d_{x^2-y^2}$ character, and d_{z^2} rhenium orbital contributes to the LUMO + 13.

Since the rhenium atom has d^2 electronic configuration, the empty $5d_{xz}$ and $5d_{yz}$ orbitals are available to overlap with $2p_x$ and $2p_y$ orbitals of the terminal oxygen to form an effective triple bond.

The nature of rhenium–terminal oxygen interaction in **1** has been studied by NBO analysis. The occupancy and composition of the calculated Re–O_t natural bond orbitals (NBOs) are given in Table 7. Two detected natural Re–O_t bond orbitals of **1** are of π character – they arise from overlap of the two occupied oxygen p_π orbitals with the empty d_{xz} and d_{yz} metal orbitals. Not detected σ_{Re-Ot} bond has character of predominant Coulomb-type interactions between the central ion and ligands [47]. The terminal oxo ligand of **1** has two lone pair orbitals, and electron density from one of them is strongly delocalized into non-Lewis rhenium orbital. Accordingly, NBO analysis confirms a triple bond between the rhenium and the terminal oxygen ligand.

4.4. Electronic spectra

The electronic spectra of [$ReOX_2$(hquin-7-COOH)(PPh_3)] and [$ReOX_2$(hmquin-7-COOH)(PPh_3)] complexes are very similar in terms of the position, intensity and shape of the bands in the whole region 1000–180 nm. The positions and molar absorption coefficients of electronic bands for [$ReOX_2$(hquin-7-COOH)(PPh_3)] and [$ReOX_2$(hmquin-7-COOH)(PPh_3)] complexes are given in Table 8.

The experimental and calculated electronic spectra of **1** are presented in Fig. 4. Each calculated transition is represented by a gaussian function $y = ce^{-bx^2}$ with the height (c) equal to the oscillator strength and b equal to 0.04 nm^{-2}. Table 9 presents the calculated singlet–singlet electronic transitions of **1** and their assignments to the experimental bands. For the high energy part of the spectrum, only transitions with oscillator strengths larger than 0.015 are listed in Table 9.

The assignment of the calculated transitions to the experimental bands is based on the criterion of the energy and oscillator strength of the calculated transitions. In the description of the electronic transitions the HOMO orbital is described as d_{Re} orbital, whereas the participation of d_{Re} in the H – 1 orbital is omitted.

Table 8
Band position (nm) and molar absorption coefficient [$dm^3\ mol^{-1}\ cm^{-1}$] (in brackets) of [$ReOX_2$(hquin-7-COOH)(PPh_3)] and [$ReOX_2$(hmquin-7-COOH)(PPh_3)] complexes

1	2	3	4
835.0 (125)	815.6 (170)	805.0 (150)	799.5 (175)
691.4 (335)	687.0 (360)	682.0 (350)	685.5 (360)
481.6 (920)	475.4 (1100)	456.3 (990)	456.3 (1050)
402.2 (8090)	405.5 (10160)	387.5 (9100)	392.0 (9500)
264.6 (48800)	264.0 (54600)	271.0 (47600)	262.5 (49200)
221.8 (94400)	225.1 (96700)	218.5 (89900)	221.6 (97800)
209.4 (122600)	208.0 (130900)	205.5 (115700)	204.5 (128400)

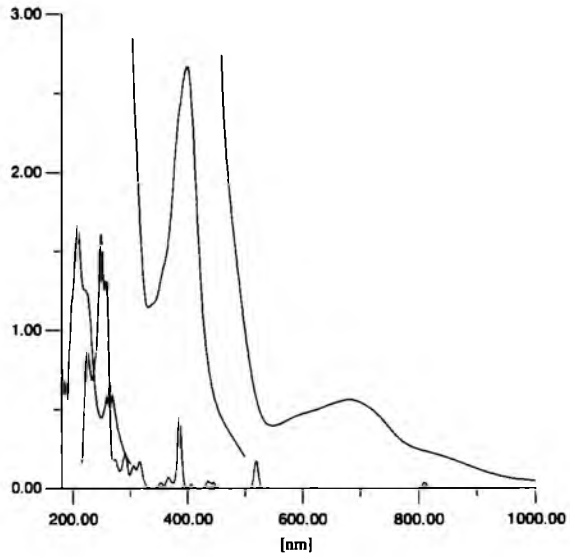

Fig. 4. The experimental (black) and calculated (red) electronic absorption spectra of **1**. (For interpretation of the references in colour in this figure legend, the reader is referred to the web version of this article.)

Table 7
The occupancy of the calculated natural bond orbitals (NBOs) between the rhenium and the oxo ligand for **1**

BD	Occupancy	BD	BD*	Occupancy
Re–O_t	1.993	$0.570(d)_{Re} + 0.821(p)_O$	$0.821(d)_{Re} - 0.570(p)_O$	0.316
Re–O_t	1.984	$0.583(d)_{Re} + 0.813(p)_O$	$0.813(d)_{Re} - 0.583(p)_O$	0.302

BD denotes 2-center bond, * – denotes antibond NBO.

Table 9
The energy and molar absorption coefficients of experimental absorption bands and the electronic transitions calculated with the TDDFT method for **1**

The most important orbital excitations	Character	λ (nm)	E (eV)	f	Experimental Λ (nm) (E (eV)) ε
H → L	d → d	810.2	1.53	*0.0093*	835.0 (1.48) 125
H → L + 1	d → d	619.6	2.00	*0.0028*	691.4 (1.79) 335
H − 1 → L	π(Cl)/π(hquin-7-COOH) → d	519.4	2.39	*0.0434*	481.6 (2.57) 920
H − 1 → L + 1	π(Cl)/π(hquin-7-COOH) → d	445.2	2.78	*0.0085*	402.2 (3.08) 8090
H − 2 → L	π(PPh_3) → d				
H − 2 → L	π(PPh_3) → d	435.6	2.85	*0.0112*	
H → L + 2	d → π*(hquin-7-COOH)	385.7	3.21	*0.1122*	
H → L	d → d	365.9	3.39	*0.0155*	
H → L + 4	d → π*(hquin-7-COOH)	316.6	3.92	*0.0331*	264.6 (4.69) 48800
H − 8 → L + 1	π(hquin-7-COOH) → d	305.8	4.05	*0.0228*	
H − 1 → L + 3	π(Cl)/π(hquin-7-COOH) → d	291.5	4.25	*0.0456*	
H − 10 → L + 1	π(Cl)/π(hquin-7-COOH) → d	284.9	4.35	*0.0228*	
H − 13 → L	π(Cl)/π(O)/π(hquin-7-COOH) → d	276.0	4.49	*0.0169*	
H − 10 → L + 2	π(Cl)/π(hquin-2-COOH) → π*(hquin-7-COOH)	260.9	4.75	*0.0419*	221.8 (5.59) 94400
H − 2 → L + 3	π(PPh_3) → d	259.5	4.78	*0.1535*	
H − 2 → L + 4	π(PPh_3) → π*(hquin-7-COOH)	257.4	4.82	*0.1065*	
H − 9 → L + 2	π(Cl) → π*(hquin-7-COOH)	252.6	4.91	*0.0188*	
H − 4 → L + 3	π(PPh_3) → d	252.0	4.92	*0.0205*	
H − 5 → L + 2	π(PPh_3) → d	250.5	4.95	*0.0293*	
H → L + 8	d → π*(PPh_3)				
H − 2 → L + 4	π(PPh_3) → π*(hquin-7-COOH)	249.7	4.97	*0.1939*	
H − 5 → L + 3	π(PPh_3) → d	247.4	5.24	*0.0359*	
H → L + 8	d → π*(PPh_3)				
H − 14 → L	π(Cl)/π(O)/π(hquin-7-COOH) → d	246.1	5.04	*0.0987*	
H − 3 → L + 4	π(PPh_3) → π*(hquin-7-COOH)				
H − 4 → L + 4	π(PPh_3) → π*(hquin-7-COOH)	243.7	5.09	*0.0627*	
H − 1 → L + 5	π(Cl)/π(hquin-7-COOH) → π*(PPh_3)				
H − 1 → L + 5	π(Cl)/π(hquin-7-COOH) → π*(PPh_3)	241.8	5.13	*0.0177*	
H − 6 → L + 3	π(PPh_3) → d				
H − 15 → L + 1	π(Cl)/π(O)/π(hquin-7-COOH) → d	239.1	5.19	*0.0343*	
H − 18 → L	π(PPh_3) → d	237.0	5.23	*0.0376*	
H − 1 → L + 6	π(Cl)/π(hquin-7-COOH) → π*(PPh_3)				
H − 1 → L + 6	π(Cl)/π(hquin-7-COOH) → π*(PPh_3)	236.6	5.24	*0.0323*	
H − 7 → L + 3	π(PPh_3) → d				
H − 2 → L + 5	π(PPh_3) → π*(PPh_3)	231.6	5.35	*0.0445*	
H − 2 → L + 5	π(PPh_3) → π*(PPh_3)	228.5	5.42	*0.0248*	
H − 2 → L + 5	π(PPh_3) → π*(PPh_3)	227.0	5.46	*0.0387*	
H − 12 → L + 2	π(Cl)/π(O)/π(hquin-7-COOH) → π*(hquin-7-COOH)	224.8	5.51	*0.0411*	
H − 5 → L + 5	π(PPh_3) → π*(PPh_3)	223.2	5.55	*0.0269*	
H − 1 → L + 7	π(Cl)/π(hquin-7-COOH) → π*(PPh_3)	222.2	5.58	*0.0293*	
H − 4 → L + 6	π(PPh_3) → π*(PPh_3)	220.8	5.61	*0.0235*	
					209.4 (5.92) 122600

ε – molar absorption coefficient ($dm^3\ mol^{-1}\ cm^{-1}$); f – oscillator strength; H – highest occupied molecular orbital; L – lowest unoccupied molecular orbital.

Two longest wavelength experimental bands at 835.0 and 691.4 nm are attributed to the transitions of d → d character. The *ligand–metal charge transfer* (π(Cl)/π(hquin-7-COOH) → d) transitions make the largest contribution into the experimental band at 481.6 nm.

The intense absorption band with maximum at 402.2 nm results mainly from *metal–ligand charge transfer* (d → π*(hquin-7-COOH)). However the contribution of the *ligand–metal charge transfer* excitations (π(Cl)/π(PPh_3)/π(hquin-7-COOH) → d) into this band is also confirmed by the calculations. The experimental band at 264.8 nm can be asigned the *ligand–metal charge transfer* (π(Cl)/π(hquin-7-COOH) → d) transitions. The absorption bands at 221.8 and 209.4 nm are assigned mainly to *ligand–ligand charge transfer* and interligand (*IL*) transitions. However some contribution of the *ligand–metal charge transfer* from the triphenylphosphine orbitals to the *d* rhenium orbitals in the band at 221.8 nm is also confirmed by the calculations.

As can be seen from Fig. 3 and Table 9, most occupied molecular orbitals are delocalized of the π(Cl)/π(hquin-7-COOH) unit. It seems to explain lack of any differences in the LMCT bands between Cl and Br complexes. Furthermore, the LMCT absorption bands of the examined complexes are broad and overlap.

5. Supplementary material

CCDC 665000, 665001 and 665002 contain the supplementary crystallographic data for $C_{46}H_{36}Cl_2NO_5P_2Re$, $C_{28}H_{21}Br_2NO_4PRe$ and $C_{29}H_{23}Cl_2NO_4PRe$. These data can be obtained free of charge via http://www.ccdc.cam.ac.uk/conts/retrieving.html, or from the Cambridge Crystallographic Data Centre, 12 Union Road, Cambridge CB2 1EZ, UK; fax: (+44) 1223-336-033; or e-mail: deposit@ccdc.cam.ac.uk.

Acknowledgements

The GAUSSIAN03 calculations were carried out in the Wrocław Centre for Networking and Supercomputing, WCSS, Wrocław, Poland.

References

[1] R.H. Holm, Chem. Rev. 87 (1987) 1401.
[2] C.C. Romao, F.E. Kühn, W.A. Hermann, Chem. Rev. 97 (1997) 3197.
[3] S.B. Seymore, S.N. Brown, Inorg. Chem. 39 (2000) 325.
[4] F.E. Kühn, A. Scherbaum, W.A. Herrmann, J. Organomet. Chem. 689 (2004) 4149.
[5] A.M. Kirillov, M. Haukka, M.V. Kirillova, A.J.L. Pombeiro, Adv. Synth. Catal. 347 (2005) 1435.
[6] W. Volkert, W.F. Goeckeler, G.J. Ehrhardt, A.R. Ketring, J. Nucl. Med. 32 (1991) 174.
[7] E.A. Deutsch, K. Libson, J.L. Vanderheyden, Technetium and Rhenium in Chemistry and Nuclear Medicine, Raven Press, New York, 1990.
[8] B. Machura, S. Michalik, R. Kruszynski, J. Kusz, Polyhedron 26 (2007) 2837.
[9] B. Machura, R. Kruszynski, Polyhedron 26 (2007) 3686.
[10] F. Zouhiri, J.-F. Mouscadet, K. Mekouar, D. Desmaele, D. Savoure, H. Leh, F. Subra, M.L. Bret, Ch. Auclair, J. d'Angelo, J. Med. Chem. 43 (2000) 1533.
[11] H. Chermette, Coord. Chem. Rev. 178–180 (1998) 699.
[12] M.C. Aragoni, M. Arca, T. Cassano, C. Denotti, F.A. Devillanova, F. Isaia, V. Lippolis, D. Natali, L. Niti, M. Sampietro, R. Tommasi, G. Verani, Inorg. Chem. Commun. 5 (2002) 869.
[13] P. Romaniello, F. Lelj, Chem. Phys. Lett. 372 (2003) 51.
[14] A. Voigt, U. Abram, R. Böttcher, U. Richter, J. Reinhold, R. Kirmse, Chem. Phys. 253 (2000) 171.
[15] M. Lipowska, L. Hansen, R. Cini, X. Xu, H. Choi, A.T. Taylor, L.G. Marzilli, Inorg. Chim. Acta 339 (2002) 327.
[16] J. Gancheff, C. Kremer, E. Kremer, O.N. Ventura, J. Mol. Struct. (Theochem) 580 (2002) 107.
[17] M.L. Kuznestov, E.A. Klestova-Nadeeva, A.I. Dement'ev, J. Mol. Struct. (Theochem) 671 (2004) 229.
[18] N. Psaroudakis, K. Mertis, D.G. Liakos, E.D. Simandiras, Chem. Phys. Lett. 369 (2003) 490.
[19] X.-Y. Liu, S. Bouherour, H. Jacobsen, H.W. Schmalle, H. Berke, Inorg. Chim. Acta 330 (2002) 250.
[20] É. Bencze, J. Mink, I. Pápai, I.S. Butler, D. Lafleur, D.F.R. Gilson, J. Organomet. Chem. 616 (2000) 1.
[21] W.-Y. Wong, S.-H. Cheung, X. Huang, Z. Lin, J. Organomet. Chem. 655 (2002) 39.
[22] B. Machura, R. Kruszynski, Polyhedron 25 (2006) 1985.
[23] G. Rouschias, G. Wilkinson, J. Chem. Soc. A (1966) 465.
[24] K. Mekouar, J. Med. Chem. 41 (1998) 2846.
[25] STOE & Cie, X-RED. Version 1.18, STOE & Cie GmbH, Darmstadt, Germany, 1999.
[26] G.M. Sheldrick, Acta Crystallogr., Sect. A 46 (1990) 467.
[27] G.M. Sheldrick, SHELXL97. Program for the Refinement of Crystal Structures, University of Göttingen, Germany, 1997.
[28] G.M. Sheldrick, shelxtl: Release 4.1 for Siemens Crystallographic Research Systems, Siemens Analytical X-ray Instruments Inc., Madison, Wisconsin, USA, 1990.
[29] A.D. Becke, J. Chem. Phys. 98 (1993) 5648.
[30] C. Lee, W. Yang, R.G. Parr, Phys. Rev. B 37 (1988) 785.
[31] M.J. Frisch, G.W. Trucks, H.B. Schlegel, G.E. Scuseria, M.A. Robb, J.R. Cheeseman, J.A. Montgomery, Jr., T. Vreven, K.N. Kudin, J.C. Burant, J.M. Millam, S.S. Iyengar, J. Tomasi, V. Barone, B. Mennucci, M. Cossi, G. Scalmani, N. Rega, G.A. Petersson, H. Nakatsuji, M. Hada, M. Ehara, K. Toyota, R. Fukuda, J. Hasegawa, M. Ishida, T. Nakajima, Y. Honda, O. Kitao, H. Nakai, M. Klene, X. Li, J.E. Knox, H.P. Hratchian, J.B. Cross, C. Adamo, J. Jaramillo, R. Gomperts, R.E. Stratmann, O. Yazyev, A.J. Austin, R. Cammi, C. Pomelli, J.W. Ochterski, P.Y. Ayala, K. Morokuma, G.A. Voth, P. Salvador, J.J. Dannenberg, V.G. Zakrzewski, S. Dapprich, A.D. Daniels, M.C. Strain, O. Farkas, D.K. Malick, A.D. Rabuck, K. Raghavachari, J.B. Foresman, J.V. Ortiz, Q. Cui, A.G. Baboul, S. Clifford, J. Cioslowski, B.B. Stefanov, G. Liu, A. Liashenko, P. Piskorz, I. Komaromi, R.L. Martin, D.J. Fox, T. Keith, M.A. Al-Laham, C.Y. Peng, A. Nanayakkara, M. Challacombe, P.M.W. Gill, B. Johnson, W. Chen, M.W. Wong, C. Gonzalez, and J.A. Pople, GAUSSIAN 03, Revision B.03, Gaussian, Inc., Pittsburgh, PA, 2003.
[32] P.J. Hay, W.R. Wadt, J. Chem. Phys. 82 (1985) 299.
[33] K. Eichkorn, F. Weigend, O. Treutler, R. Ahlrichs, Theor. Chem. Acc. 97 (1997) 119.
[34] P.C. Hariharan, J.A. Pople, Theor. Chim. Acta 28 (1973) 213.
[35] V.A. Rassolov, M.A. Ratner, J.A. Pople, P.C. Redfern, L.A. Curtiss, J. Comp. Chem. 22 (2001) 976.
[36] M.E. Casida, in: J.M. Seminario (Ed.), Recent Developments and Applications in Modern Density Functional Theory, Theoretical and Computational Chemistry, vol. 4, Elsevier, Amsterdam, 1996.
[37] J.E. Carpenter, F. Weinhold, J. Mol. Struct. (Theochem) 169 (1988) 41.
[38] A.E. Reed, L.A. Curtiss, F. Weinhold, Chem. Rev. 88 (1988) 899.
[39] K. Nakamoto, Infrared and Raman Spectra of Inorganic and Coordination Compounds, 4th ed., Wiley-Interscience, New York, 1986.
[40] L. Wei, J. Babich, J. Zubieta, Inorg. Chim. Acta 358 (2005) 2413.
[41] G.R. Desiraju, T. Steiner, The Weak Hydrogen Bond in Structural Chemistry and Biology, Oxford University Press, 1999.
[42] G.A. Jeffrey, W. Saenger, Hydrogen Bonding in Biological Structures, Springer-Verlag, 1994.
[43] C.A. Hunter, J.K.M. Sanders, J. Am. Chem. Soc. 112 (1990) 5525.
[44] J.M. Mayer, Inorg. Chem. 27 (1988) 3899.
[45] S.R. Fletcher, A.C. Skapski, J. Chem. Soc., Dalton Trans. (1972) 1073.
[46] E. Shuter, H.R. Hoveyda, V. Karunaratne, S.J. Retting, C. Orvig, Inorg. Chem. 35 (1996) 368.
[47] M.L. Kuznetsov, A.J.L. Pombeiro, J. Chem. Soc., Dalton Trans. (2003) 738.

Struct Chem (2008) 19:257–263
DOI 10.1007/s11224-007-9280-9

BRIEF COMMUNICATION

The reaction between $[RuCl_2(PPh_3)_3]$ and hydroxyquinoline carboxylic acid

J. G. Małecki · J. Kusz · R. Kruszynski · D. Tabak · Z. Mazurak

Received: 12 October 2007 / Accepted: 19 December 2007 / Published online: 12 January 2008

Abstract The reactions of $[RuCl_2(PPh_3)_3]$ with 8-hydroxy-2-methyl-quinoline-7-carboxylic acid was examined, and a novel ruthenium(II) complex—$[Ru(PPh_3)_2(C_5H_8NO)_2]$—was obtained. The compound was studied by IR, UV–vis spectroscopy, and X-ray crystallography. The molecular orbital diagram of the complex was calculated with the density functional theory (DFT) method. The spin-allowed singlet–singlet electronic transitions of the compound were calculated using the time-dependent DFT method, and the UV–vis spectrum of the compound was discussed, on this basis. The luminescence property of the $[Ru(PPh_3)_2(C_5H_8NO)_2]$was examined.

J. G. Małecki (✉)
Department of Crystallography, Institute of Chemistry, University of Silesia, 9th Szkolna Street, 40-006 Katowice, Poland
e-mail: gmalecki@us.edu.pl

J. Kusz
Institute of Physics, University of Silesia, 4th Uniwersytecka Street, 40-006 Katowice, Poland

R. Kruszynski
Department of X-Ray Crystallography and Crystal Chemistry, Institute of General and Ecological Chemistry, Lodz University of Technology, 116 Żeromski Street, 90-924 Lodz, Poland
e-mail: kruszyna@p.lodz.pl

D. Tabak
Department of Organic Chemistry, Institute of Chemistry, University of Silesia, 9th Szkolna St, 40-006 Katowice, Poland
e-mail: tapcio@interia.pl

Z. Mazurak
Polish Academy of Sciences, Centre of Polymer Chemistry, M. Sklodowskiej-Curie 34, Zabrze 41-819, Poland
e-mail: mazurka@cchp-pan.zabrze.pl

Keywords Ruthenium · Quinoline carboxylic acid · X-ray structure · TDDFT method · Luminescence

Introduction

Quinoline moiety is present in many classes of biologically active compounds. A number of them was clinically used as antifungal, antibacterial and antiprotozoic drugs [1, 2] as well as antituberculotic agents [3, 4]. Some quinoline based compounds showed also antineoplastics activity [5]. Several quinoline derivatives showed also antiasthmatic and antiplatelet activity [6–10]. Acetylcholinesterase inhibitory activity of various quinoline derivatives was tested for potential treatment of nervous diseases [11]. Styrylquinoline derivatives have gained strong attention recently due to their activity as perspective HIV integrase inhibitors [12–16]. The study dealing with styrylquinoline derivatives showed that they could also possess strong antifungal activity [17]. The compounds containing 8-hydroxyquinoline pharmacophore seem especially interesting. According to the results reported recently, some new 8-hydroxyquinoline derivatives possessed interesting antifungal and herbicidal activities [18, 19].

On the other hands, geometry of the $[RuL_2(PPh_3)_2]$ species, where L is a symmetrical or unsymmetrical bidentate ligand is very important for variable-valence transition metal chemistry [20].

The density functional theory (DFT) is a very popular computational method for calculations of a number of molecular properties. Due to its great computational efficiency, DFT has been applied extensively to inorganic and organometallic complexes [21–25]. The time-dependent generalization of DFT (TDDFT) offered a rigorous route to calculate the dynamic response of the charge density

[26–28]. The reliability of TDDFT approach in obtaining accurate predictions for excitation energies and oscillator strengths is well documented. The method has been successfully used to calculate the electronic spectra of transition metal complexes with variety of ligands [29–31]. It was found that TDDFT method gives fairly accurate results for valence excited states but incorrectly describes long-range excited states of CT character. This failure was ascribed to a self-interaction error in DFT or alternatively to an incorrect asymptotic behaviour of the approximate density functional [32]. The influence of the contribution of the HF exchange in hybrid functional on the calculated energies of CT states was studied for ruthenium complexes [33].

In this article, we present the synthesis and characterizations of a novel ruthenium(II) complex with the N-donor ligand.

Experimental

Physical measurements

Infrared spectra were recorded on a Nicolet Magna 560 spectrophotometer in the spectral range of 4,000–400 cm^{-1} with the sample in the form of KBr pellet. Electronic spectra were measured on a Lab Alliance UV–vis 8500 spectrophotometer in the range of 800–200 nm in acetonitrile solution. Elemental analyses (C, H, N) were performed on a Perkin–Elemer CHN-2400 analyzer. Luminescence measurements were made on a Jobin-Yvon (SPEX) FLUOROLOG-3.12 spectrofluorometer at room temperature.

All reagents except the 8-hydroxy-2-methylquinoline-7-carboxylic acid used for the synthesis of the complexes are commercially available and were used without further purification. The $[RuCl_2(PPh_3)_3]$ complex was synthesized using a literature method [34].

The 8-hydroxy-2-methylquinoline-7-carboxylic acid was synthesized as described in the literature [13].

Synthesis of $[Ru(PPh_3)_2(C_{10}H_8NO_3)_2]$

A suspension of $[RuCl_2(PPh_3)_3]$ (0.2 g) and 8-hydroxy-2-methyl-quinoline-7-carboxylic acid (0.1 g) in methanol (100 cm^{-3}) was magnetically stirred for 4 h and filtered. The crystals suitable for X-ray crystal analysis were obtained by slow evaporation the reaction mixture. The yield was 68%.

Anal. Calc. for $C_{62}H_{56}N_2O6P_2Ru$: C 68.44% H 5.19% N 2.57%. Found: C 67.01%; H 5.18% N 2.56%.

IR (KBr): **1**: 3055 ν_{CH}; 2925 $\nu_{CH-phenyl}$; 1620 ν_{CN}; 1591 asν_{COO}; 1482 $\delta_{(C-CH\ in\ the\ plane)}$; 1434 $\nu_{Ph(P-Ph)}$; 1358 sν_{COO};1121 $\delta_{(C-CH\ in\ the\ plane)}$; 996 $\delta_{(C-C\ out\ of\ the\ plane)}$; 756 $\delta_{(C-C\ out\ of\ the\ plane)}$; 697 $\delta_{(C-C\ in\ the\ plane)}$. UV–vis [nm] in acetonitrile (log ε): 422.0 (1.98); 269.4 (2.79); 205.8 (3.04).

DFT calculations

Gaussian-03 program [35] was used for the calculations. The geometry optimisation was carried out using the DFT method with the B3LYP functional [36]. The electronic transitions were calculated with the TDDFT method [37] with the PCM model [38] in the acetonitrile solution as the solvent. The calculation was performed using the DZVP basis set [39] using f functions with exponents 1.94722036 and 0.748930908 on ruthenium atom, and polarization functions for all other atoms: 6–31 g(2d,p)—chlorine, 6–31 g**—carbon, nitrogen, oxygen, and 6–31 g(d,p)—hydrogen. Natural bond orbital (NBO) calculations were performed using the NBO code [40] included in Gaussian03.

Crystal structures determination and refinement

A red needle of the studied compound was mounted on a KM-4-CCD automatic diffractometer equipped with CCD detector, and used for data collection. X-ray intensity data were collected with graphite monochromated MoK_α radiation (λ = 0.71073 Å) at temperature 150.0(2) K with ω scan mode. A 12 s exposure time was used and a whole Ewald sphere were collected up to 2θ = 65.92°. The unit cell parameters were determined from least-squares refinement of the setting angles of 2125 strongest reflections. Details concerning crystal data and refinement are given in Table 1. During the data reduction above, a decay correction coefficient was taken into account. Lorentz, polarization and numerical absorption [41] corrections were applied. The structure was solved by direct methods and subsequently completed using the difference Fourier recycling. All non-hydrogen atoms were refined anisotropically using full-matrix, least-squares technique on F^2. All hydrogen atoms were found from difference Fourier synthesis after four cycles of anisotropic refinement. H-atoms were then refined as "riding" on the adjacent carbon atom with individual isotropic temperature factor equal 1.2 times the value of equivalent temperature factor of the aromatic parent carbon atom and equal 1.5 times the value of equivalent temperature factor of the methyl parent carbon atom. SHELXS97 [42], SHELXL97 [43] and SHELXTL [44] programs were used for all the calculations. Atomic scattering factors were those incorporated in the computer programs.

Table 1 Crystal data and structure refinement details of $[Ru(PPh_3)_2(C_{10}H_8NO_3)_2] \cdot 0.5CH_3OH$

Empirical formula	C59H50N2O7P2Ru
Formula weight	1062.02
Temperature [K]	150.0(2) K
Crystal system	Monoclinic
Space group	$P2_1/n$
Unit cell dimensions	
a [Å]	10.808(10)
b [Å]	16.306(15)
c [Å]	14.285(13)
α [°]	101.633(9)
β [°]	
γ [°]	
Volume [Å^3]	2465.8(3)
Z	2
Calculated density [Mg/m^3]	1.430
Absorption coefficient [mm^{-1}]	0.441
F(000)	1096
Crystal dimensions [mm]	0.40 × 0.03 × 0.03
θ range for data collection [°]	2.89 to 32.96
Index ranges	$-8 \le h \le 16$
	$-24 \le k \le 24$
	$-21 \le l \le 21$
Reflections collected	23585
Independent reflections	8298 [$R_{(int)} = 0.0954$]
Data/restraints/parameters	8298/0/333
Goodness-of-fit on F^2	0.677
Final R indices [$I > 2\sigma(I)$]	$R_1 = 0.0404$
	$wR_2 = 0.0632$
R indices (all data)	$R_1 = 0.1457$
	$wR_2 = 0.0717$
Largest diff. peak and hole	0.858 and −0.669 e.Å^{-3}

Results and discussion

The reaction of the $[RuCl_2(PPh_3)_3]$ complex with 8-hydroxy-2-methyl-quinoline-7-carboxylic acid has been performed. Mixing the ruthenium(II) complex with the ligand in methanol leads to the $[Ru(PPh_3)_2(C_{10}H_8NO_3)_2]$ complex with a good yield. The elemental analysis of the complex is in good agreement with the compound's formulation. The IR spectrum of the complex is consistent with their molecular structures.

The band at 1,620 cm^{-1} is attributed to the CN stretching of the quinoline type ligand presents in the complex. The asymmetric and symmetric ν_{COO} stretching bands are visible at 1,591 and 1,358 cm^{-1}, respectively. The $\nu_{Ph(P-Ph)}$ absorption band at 1,434 cm^{-1} indicates the triphenylphosphine ligands.

Crystal structure

The studied complex $[Ru(PPh_3)_2(C_{10}H_8NO_3)_2]$ crystallises as a solvate in the monoclinic $P2_1/n$ group. The asymmetric unit includes a half of the complex molecule. The Ru(1) atoms lie on symmetry centre (special positions *a* at ½, ½, ½ [45]) and rest of the atoms lie in general position. The methanol molecules are disordered over two sites by symmetry centre located at ½, 0, ½ (special positions *c*), thus, $[Ru(PPh_3)_2(C_{10}H_8NO_3)_2] \cdot CH_3OH$ occupies two asymmetric units. The crystal data of the complex is given in the Table 1. The molecular structure of the studied compound is presented in Fig. 1. Relevant distances and angles are collected in the Table 2.

The ruthenium atom has an octahedral environment with the *trans* triphenylphosphine and quinoline ligands. The small distortions of the octahedral coordination are visible in the angles between phosphorus and nitrogen or oxygen donor atoms. The 8-hydroxy-2-methyl-quinoline-7-carboxylic acid substituent is close to planarity, most deviating N(1) atom derive 0.1790(18) Å form weighted least squares plane calculated through all non-hydrogen atoms of this substituent. The ruthenium atom derives 0.5348(17) Å from mentioned plane. The planar in the range of experimental error phenyl rings of triphenylphosphine substituent are inclined at 69.73(7), 48.57(9) and 85.72(7)°, respectively for pairs of rings indicated by C(1)/C(7), C(7)/C(13) and C(1)/C(13) atoms. The

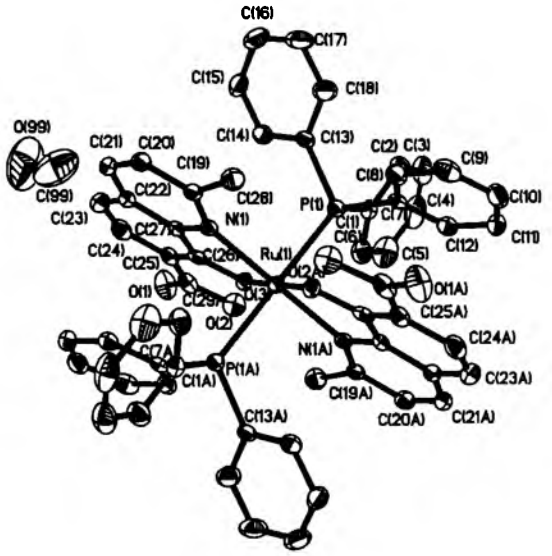

Fig. 1 ORTEP drawing of $[Ru(PPh_3)_2(C_{10}H_8NO_3)_2]$ with 50% probability displacement ellipsoids. The hydrogen atoms and disordered part of solvate molecule were omitted for clarity. The symmetry generated atoms are indicated by A letter

Table 2 Selected bond lengths [Å] and angles [°] for $[Ru(PPh_3)_2(C_{10}H_8NO_3)_2] \cdot 0.5CH_3OH$

	Experimental	Calculated
1		
Bond lengths [Å]		
Ru(1)–O(3)	2.101(16)	2.134
Ru(1)–N(1)	2.127(2)	2.204
Ru(1)–P(1)	2.402(7)	2.507
Angles [°]		
O(3)–Ru(1)–N(1)	77.79(7)	76.51
O(3)–Ru(1)–P(1)	91.68(5)	91.21
O(3A)–Ru(1)–N(1)	102.21(7)	103.48
N(1A)–Ru(1)–N(1)	180.00(11)	180.00
O(3)–Ru(1)–P(1A)	88.32(5)	88.77
N(1A)–Ru(1)–P(1A)	89.65(5)	89.85
N(1)–Ru(1)–P(1A)	90.35(5)	90.16

conformation of the molecule is stabilised by one medium strength O—H···O and two weak C—H···O [46] intramolecular hydrogen bonds (Table 3). The molecules are arranged in well shaped, separate piles along crystallographic *a* axis (Fig. 2).

Geometry optimisation

The geometry of the studied complex was optimised using the DFT method with the B3LYP functional. The optimised geometry parameters are given in Table 2. In general, the predicted bond lengths and angles are in good agreement with the values based upon the X-ray crystal structure data, and the general trends observed in the experimental data are well reproduced in the calculations. The calculated bond lengths and angles for the studied complex agree well with the experiment, the largest difference being found for the Ru–P bond (0.105 Å). The maximum difference between the calculated and experimental angles is visible for the angle O–Ru–N, and it is close to 1.3.

Table 3 Hydrogen bonds for $[Ru(PPh_3)_2(C_{10}H_8NO_3)_2] \cdot CH_3OH$ (Å and °)

D–H···A	d(D–H)	d(H···A)	d(D···A)	<(DHA)
O(2)–H(2O)···O(3)	0.93	1.66	2.547(2)	158.5
C(6)–H(6)···O(3)	0.93	2.57	3.256(3)	130.7
C(28)–H(28A)···O(3)#1	0.93	2.25	3.101(3)	147.8

#1 Symmetry transformations used to generate equivalent atoms: #1 −x + 1, −y + 1, −z + 1

Fig. 2 Part of molecular packing showing piles created along *a* axis

Charge distribution and electronic structure

The calculated charge on the ruthenium atom in the $[Ru(PPh_3)_2(C_{10}H_8NO_3)_2]$ complex is considerable lower than the formal charge +2; it is close to 0.50. The charges on the phosphine ligands are positive and close to 0.33. The occupancy of the ruthenium *d* orbitals, obtained from NBO analysis, is as follows: d_{xy}—1.08; d_{xz}—1.34; d_{yz}—1.26; $d_{x^2-y^2}$—1.84; d_{z^2}—1.70. Taking into account the maximum of stabilization energies ΔE_{ij} (kcal/mol) in the studied complex associated with delocalization, estimated by the second-order perturbative as:

$$\Delta E_{ij} = q_i(F(i,j)^2)/(\varepsilon_j - \varepsilon_i)$$

(where q_i is the donor orbital occupancy, ε_i, ε_j are diagonal elements (orbital energies) and F(i,j) is the off-diagonal NBO Fock or Kohn–Sham matrix element), this is visible in the donation from lone pair localised on phosphorus to antibonding *d* orbitals on ruthenium central ion (145.92 kcal/mol). The appropriate energies of quinoline oxygen and nitrogen atoms vary from about 40 kcal/mol to 61 kcal/mol.

The molecular orbitals are composed of AO's of ligands. The H − 8 (−6.653; 43%), H − 7 (−6.628; 63%) and H − 6 (−6.614; 41%) molecular orbitals are localized on the COOH groups of the quinoline ligands. Numbers in the round brackets show the energy values in eV and the percentage participation of oxygen in the molecular orbitals. The non-bonding lone pairs localized on the phosphorus atoms play significant role in the Homo − 5 (−6.424; 24% n_P) molecular orbital.

The Homo − 3 and Homo − 2 molecular orbitals in the complex are character of *d* ruthenium orbitals. Homo − 4 MO's are consisted of d_{yz} orbitals share with an antibonding contribution from π^*_{qu}. The Homo orbital is composed of d_{Ru} and π^*_O orbitals. In the virtual molecular

orbitals, the Lumo + 1; + 2 and Lumo + 11 are composed of $d_{x^2-y^2}$ and d_{z^2} ruthenium orbitals with π^*_{qu} and n_N orbitals or nitrogen lone pairs, respectively. The character and energy of frontier molecular orbitals of the complex are given in Table 4. The HOMO–LUMO gap is 3.19 eV.

Electronic spectrum

The investigated complex has large size, and the number of basis functions is equal to 1,102. Hundred electron transitions calculated by the TDDFT method with PCM model do not comprise all the experimental absorption bands. The UV–vis spectrum was calculated up to

Table 4 Energy and character of the frontier molecular orbitals of $[Ru(PPh_3)_2(C_{10}H_8NO_3)_2] \cdot 0.5CH_3OH$

MO	Energy [eV]	Character
H − 20	−7,310	$\pi_{phosphine}$
H − 19	−7,286	$\pi_{phosphine}$
H − 18	−7,095	$\pi_{phosphine}$
H − 17	−7,043	$\pi_{phosphine}$
H − 16	−7,019	$\pi_{phosphine}$
H − 15	−6,984	$\pi_{phosphine}$
H − 14	−6,966	$\pi_{phosphine}$
H − 13	−6,941	$\pi_{phosphine}$
H − 12	−6,901	$\pi_{phosphine}$
H − 11	−6,736	$\pi_{phosphine}$
H − 10	−6,710	$\pi_{qu} + \pi_{phosphine}$
H − 9	−6,668	π_{qu}
H − 8	−6,653	π_{COOH}
H − 7	−6,628	π_{COOH}
H − 6	−6,614	$\pi_{qu} + \pi_{COOH}$
H − 5	−6,424	$\pi_{phosphine}$ (n_P)
H − 4	−6,271	$d_{yz} + \pi^*_{qu}$
H − 3	−5,684	d_{yz}
H − 2	−5,489	d_{xz}
H − 1	−5,447	$\pi_{qu} + \pi_o$
Homo	−4,914	$d_{xy} + \pi^*_o$
Lumo	−1,722	π^*_{qu}
L + 1	−1,538	$d_{x^2-y^2} + \pi^*_{qu}$
L + 2	−1,210	$d_{z^2} + \pi^*_{qu}$
L + 3	−0,924	π^*_{qu}
L + 4	−0,822	π^*_{qu}
L + 5	−0,785	$\pi^*_{phosphine}$
L + 6	−0,750	$\pi^*_{phosphine}$
L + 7	−0,591	$\pi^*_{phosphine}$
L + 8	−0,544	$\pi^*_{phosphine}$
L + 9	−0,541	$\pi^*_{phosphine}$
L + 10	−0,297	$\pi^*_{phosphine}$
L + 11	−0,251	$d_{x^2-y^2}-n_N$
L + 12	−0,242	$\pi^*_{phosphine}$
L + 13	−0,205	$\pi^*_{phosphine}$
L + 14	−0,104	$\pi^*_{phosphine}$

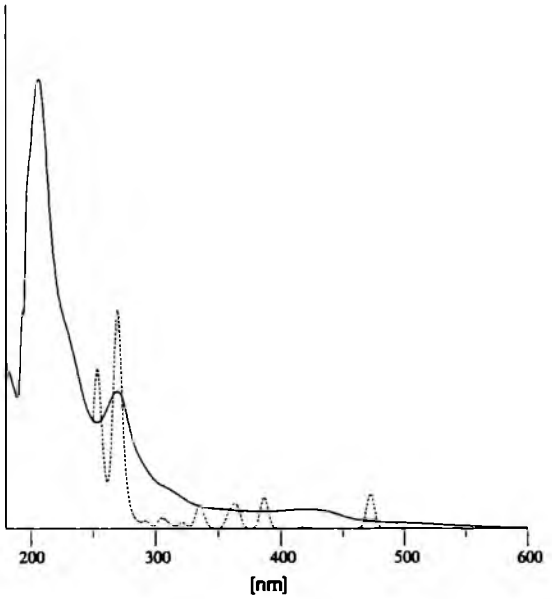

Fig. 3 The UV–vis spectra of $[Ru(PPh_3)_2(C_{10}H_8NO_3)_2]$; solid line—experimental; dashed line—calculated

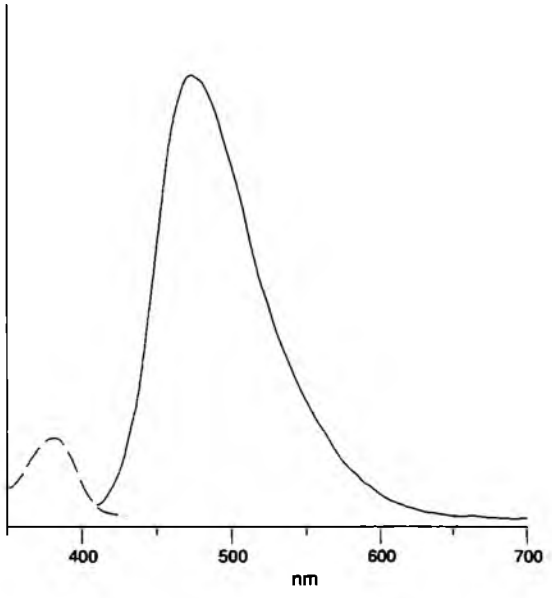

Fig. 4 The emission spectrum of $[Ru(PPh_3)_2(C_{10}H_8NO_3)_2]$; solid line—emission; dashed line—excitation

~250 nm, so the shortest wavelength experimental bands cannot be assigned to the calculated transitions. However, considering that the solution spectra of PPh_3 and quinoline moiety exhibit intense absorption bands in 260–200 nm region, some additional intraligand and interligand transitions are expected to be found at higher energies in the calculations.

The experimental and calculated spectra of $[Ru(PPh_3)_2(C_{10}H_8NO_3)_2]$ are depicted in Fig. 3. Each calculated transition in Fig. 3 was represented by a Gaussian function with the height equal to the oscillator strength and width equal to 0.05. The lowest energy experimental band with the maximum at 422.0 nm consists of $d \rightarrow \pi^*_{hq}$ MLCT (Metal–Ligand Charge Transfer) transitions (H − 3/H − 2/H → LUMO). In the range between 400 nm and 300 nm, the d → d (H − 2 → L + 2) LF (Ligand Field) transitions with contributions of MLCT excitation between ruthenium *d* and $\pi^*_{phosphine/qu}$ orbitals are calculated. For higher energy band (maximum at 269 nm) of the complex, mainly MLCT transitions are observed with the contributions of intra- and inter-ligand transitions ($\pi_{qu} \rightarrow \pi^*_{Ph}$; $\pi_{qu} \rightarrow \pi^*_{qu}$). The band at 205 nm was not calculated but in this energy region some additional intraligand and interligand transitions are expected.

An emission property of the studied complex has been examined in the acetonitrile solution at room temperature. The luminescence spectrum was presented in Fig. 4. On the excitation at 398 nm, the emission peak was observed at 473 nm and it was independent of concentration of the solution. The emission originates from the lowest energy metal to ligand charge transfer (MLCT) state, derived from the excitation involving a $d_\pi \rightarrow \pi^*_{hq}$ transition.

Supplementary data

CCDC 653305 contains the supplementary crystallographic data for the studied complex. The data can be obtained free of charge via http://www.ccdc.cam.ac.uk/conts/retrieving.html, or from the Cambridge Crystallographic Data Centre, 12 Union Road, Cambridge CB2 1EZ, UK; fax: (+44) 1223-336-033; or e-mail: deposit@ccdc.cam.ac.uk.

References

1. Roth HJ, Fenner H (2000) In: Arzneistoffe 3rd ed. Deutscher Apotheker Verlag, Stuttgart, pp 51–114
2. Harris CR, Thorarensen A (2004) Curr Med Chem 11:2213
3. Andries K, Verhasselt P, Guillemont J, Gohlmann HW, Neefs JM, Winkler H, Van Gestel J, Timmerman P, Zhu M, Lee E, Williams P, de Chaffoy D, Huitric E, Hoffner S, Cambau E, Truffot-Pernot C, Lounis N, Jarlier V (2005) Science 307:223
4. Vangapandu S, Jain M, Jain R, Kaur S, Singh PP (2004) Bioorg Med Chem 12:2501
5. Sissi C, Palumbo M (2003) Curr Med Chem Anti-Canc Agents 3:439
6. Bossu E, Agliano AM, Desideri N, Sestili I, Porra R, Grandilone M, Quaglia MG (1999) J Pharm Biomed Anal 19:539
7. Ko TC, Hour MJ, Lien JC, Teng CM, Lee KH, Kuo SC, Huang LJ (2001) Bioorg Med Chem Lett 11:279
8. Jampilek J, Dolezal M, Kunes J, Vichova P, Jun D, raich I, ÓConnor R, Clynes M (2004) J Pharm Pharmacol 56:783
9. Jampilek J, Dolezal M, Kunes J, Vichova P, Jun D, raich I, ÓConnor R, Clynes M (2004) Curr Org. Chem 8:1235
10. Jampilek J, Dolezal M, Opletalova V, Hartl J (2006) Curr Med Chem 13:117
11. Marco JL, Carmo CM (2003) Mini Rev Med Chem 3:518
12. Mekouar K, Mouscadet JF, Desmaele D, Subra F, Leh H, Savoure D, Auclair C, d'Angelo J (1998) J Med Chem 41:2846
13. Polanski J, Zouhiri F, Jeanson L, Desmaele D, d'Angelo J, Mouscadet J, Gieleciak R, Gasteiger J, Le Bret M (2002) J Med Chem 45:4647
14. Polanski J, Niedbala H, Musiol R, Tabak D, Podeszwa B, Gieleciak R, Bak A, Palka A, Magdziarz T (2004) Acta Poloniae Pharm. Drug Res 61:3
15. Pommier Y, Johnson AA, Marchand C (2005) Nat Rev Drug Discov 4:236
16. Zouhiri F, Danet M, Bernard C, Normand-Bayle M, Mouscadet JF, Leh H, Thomas CM, Mbemba G, J. d'Angelo, Desmaele D (2005) Tetrahedron Lett 46:2201
17. Musiol R, Jampilek J, Buchta V, Silva L, Niedbala H, Podeszwa B, Palka A, Majerz-Maniecka KA, Oleksyn B, Polanski J (2006) Bioorg Med Chem 14:3592
18. Jampilek J, Dolezal M, Kunes J, Buchta V, Kralova K (2005) Med Chem 1:591
19. Musiol R, Jampilek J, Kralova K, Podeszwa B, Finster J, Niedbala H, Palka A, Polanski J (2005) ECSOC-9. http://www.usc.es/congresos/ecsoc/9/BOCNP/c005/index.htm. Accessed 1 Nov 2005
20. Menon M, Pramanik A, Bag N, Chakravorty A (1995) J Chem Soc Dalton Trans 1417
21. Hohenberg PC, Kohn W, Sham LJ (1990) Adv Quantum Chem 21:7
22. Kohn W, Becke AD, Parr RG (1996) J Phys Chem 100:12974
23. Parr RG, Yang W (1995) Ann Rev Phys Chem 46:701
24. Baerends EJ, Gritsenko OV (1997) J Phys Chem A 101:5383
25. Ziegler T (1991) Chem Rev 91:651
26. Casida ME (1995) In: Chong DP (ed) Recent advances in density functional methods, vol 1. World Scientific, Singapore
27. Casida ME (1996) In: Seminario JM (ed) Recent developments and applications of modern density functional theory, theoretical and computational chemistry, vol 4. Elsevier, Amsterdam, p 391
28. Casida ME, Jamorski C, Casida KC, Salahub DR (1998) J Chem Phys 108:4439
29. Adamo C, Barone V (2000) Theor Chem Acta 105:169
30. van Gisbergen SJA, Groeneveld JA, A.Rosa, Snijders JG, Baerends EJ (1999) J Phys Chem A 103:6835
31. Rosa A, Baerends EJ, van Gisbergen SJA, van Lenthe E, Groeneveld JA, Snijders JG (1999) J Am Chem Soc 121:10356
32. Dreuw A, Head-Gordon M (2004) J Am Chem Soc 126:4007; Dreuw A, Weisman JL, Head-Gordon M (2003) J Chem Phys 119:2943; Gritsenko O, Baerends EJ (2004) J Chem Phys 121:655
33. Záliš S, Ben Amor N, Daniel C (2004) Inor Chem 43:7978
34. Stephenson TA, Wilkonson G (1966) J Inorg Nucl Chem 28:945
35. Gaussian 03, Revision B.03,Frisch MJ, Trucks GW, Schlegel HB, Scuseria GE, Robb MA, Cheeseman JR, Montgomery JA Jr., Vreven T, Kudin KN, Burant JC, Millam JM, Iyengar SS, Tomasi

J, Barone V, Mennucci B, Cossi M, Scalmani G, Rega N, Petersson GA, Nakatsuji H, Hada M, Ehara M, Toyota K, Fukuda R, Hasegawa J, Ishida M, Nakajima T, Honda Y, Kitao O, Nakai H, Klene M, Li X, Knox JE, Hratchian HP, Cross JB, Adamo C, Jaramillo J, Gomperts R, Stratmann RE, Yazyev O, Austin AJ, Cammi R, Pomelli C, Ochterski JW, Ayala PY, Morokuma K, Voth GA, Salvador P, Dannenberg JJ, Zakrzewski VG, Dapprich S, Daniels AD, Strain MC, Farkas O, Malick DK, Rabuck AD, Raghavachari K, Foresman JB, Ortiz JV, Cui Q, Baboul AG, Clifford S, Cioslowski J, Stefanov BB, Liu G, Liashenko A, Piskorz P, Komaromi I, Martin RL, Fox DJ, Keith T, Al-Laham MA, Peng CY, Nanayakkara A, Challacombe M, Gill PMW, Johnson B, Chen W, Wong MW, Gonzalez C, and Pople JA, Gaussian, Inc., Pittsburgh, 2003

36. Becke D (1993) J Chem Phys 98:5648
37. Lee C, Yang W, Parr RG (1988) Phys Rev B 37:785
38. Mennucci B, Tomasi J (1997) J Chem Phys 106:5151
39. Eichkorn K, Weigend F, Treutler O, Ahlrichs R (1997) Theor Chim Acc 97:119
40. Glendening D, Reed AE, Carpenter JE, Weinhold F, NBO (version 3.1)
41. X-RED. Version 1.18. STOE & Cie GmbH, Darmstadt, Germany (1999)
42. Sheldrick GM (1990) Acta Cryst A46:467
43. Sheldrick GM, SHELXL97 (1997) Program for the solution and refinement of crystal structures. University of Göttingen, Germany
44. Sheldrick GM, SHELXTL: release 4.1 for Siemens Crystallographic Research Systems (1990)
45. International Tables for Crystallography (1983) In: Hahn T (ed) Space-group symmetry, vol A. Reidel Publishing Company, Dordrecht, Holland, pp 174–181
46. Jeffrey GA, Saenger W (1994) Hydrogen bonding in biological structures. Springer-Verlag; Desiraju GR, Steiner T (1999) The weak hydrogen bond in structural chemistry and biology. Oxford University Press

Struct Chem
DOI 10.1007/s11224-008-9390-z

ORIGINAL RESEARCH

Synthesis, spectroscopic characterization, X-ray structure, and DFT calculations of $[ReOBr_2(hmquin\text{-}7\text{-}COOH)(AsPh_3)]$

B. Machura · J. Kusz · D. Tabak

Received: 9 September 2008 / Accepted: 12 November 2008

Abstract The reaction of $[ReOBr_3(AsPh_3)_2]$ with 8-hydroxy-2-methylquinoline-7-carboxylic acid (Hhmquin-7-COOH) has been examined and the $[ReOBr_2(hmquin\text{-}7\text{-}COOH)(AsPh_3)]$ complex has been obtained. It was characterized by IR, UV–vis spectroscopy, and single crystal X-ray analysis. The nature of the frontier orbitals and the electronic transitions involved in the absorption spectrum have been studied by means of density functional and time-dependent density functional calculations.

Keywords Rhenium oxo complexes · 8-hydroxy-2-methylquinoline-7-carboxylic acid · X–ray and electronic structure · DFT calculations · NBO analysis

Introduction

For many years inorganic compounds containing an oxygen atom bonding to a transition metal have been the center of interest to those scientists engaged in basic research and to those trying to employ these complexes in catalytic processes. Oxygen atom transfer chemistry has been implicated in various reactions of industrial and biological importance, including olefin epoxidation and catalysis by cytochrome P-450 [1–3].

The chemistry of oxo rhenium complexes arouses particular interest among these compounds. Methyltrioxorhenium and its derivatives are among the most versatile oxidation catalysts known to date [4]. The oxorhenium(V) chelates $[ReOCl_2(O\text{–}N)(PPh_3)]$ with pyridinecarboxylate ligands exhibit a remarkable catalytic activity for the conversion of ethane, under relatively mild conditions, to a mixture of propionic and acetic acids in a single-pot process with various advantages over the industrial ones [5].

Furthermore, the favorable nuclear properties of ^{186}Re and ^{188}Re nuclides make the compounds with these radioisotopes useful for applications in radioimmunotherapy [6, 7]. Consequently, the inorganic chemistry studies with the naturally occurring non-radioactive rhenium isotopes are very attractive in order to clearly establish the molecular structure of ^{99m}Tc- and $^{186/188}$Re-based radiopharmaceuticals. In this context, the design, synthesis, and reactivity of novel rhenium oxocomplexes has become the aim of several laboratories, including ours.

Previously, we investigated structural and spectroscopic properties of $[ReOX_2(hqn)(AsPh_3)_2]$ and $[ReOX_2(quin\text{-}2\text{-}c)(AsPh_3)]$ (Hhqn = 8-hydroxyquinoline, quin-2-cH = quinoline-2-carboxylic acid) [8, 9]. As an extension of this work, we chose 8-hydroxy-2-methylquinoline-7-carboxylic acid (Hhmquin-7-COOH) as a ligand. Potentially, Hhmquin-7-COOH can act as a bidentate, tridentate, or bridging ligand. As a chelate 8-hydroxy-2-methylquinoline-7-carboxylic acid can bind to the metal center through the pyridine nitrogen and the deprotonated hydroxyl group (N,O-chelation) or through the carboxylate group and the deprotonated hydroxyl group (O,O-chelation).

B. Machura (✉)
Department of Crystallography, Institute of Chemistry, University of Silesia, 9th Szkolna St., 40-006 Katowice, Poland
e-mail: basia@ich.us.edu.pl

J. Kusz
Institute of Physics, University of Silesia, 4th Uniwersytecka St., 40-006 Katowice, Poland

D. Tabak
Department of Organic Chemistry, Institute of Chemistry, University of Silesia, 9th Szkolna St., 40-006 Katowice, Poland

Published online: 26 November 2008

X-ray and spectroscopic studies for [$ReOBr_2$(hmquin-7-COOH)($AsPh_3$)] confirm N,O-chelation of the hydroxy-2-methylquinoline-7-carboxylic acid. The COOH group of the Hhmquin-7-COOH in the examined complexes is available for further conjugation.

For complex [$ReOBr_2$(hmquin-7-COOH)($AsPh_3$)] the nature of the frontier orbitals and the electronic transitions involved in the absorption spectrum have been studied by means of density functional and time-dependent density functional calculations. Gancheff et al. [10] have performed extended tests of the ability of the B3LYP method in LANL2DZ basis set for rhenium compounds in a geometry optimization and calculation of spectral properties. Although this is not a very extended basis set, its use with DFT has shown to be sufficient for the geometry optimization and calculation of spectral properties. The correctness of B3LYP method with LANL2DZ basis set for rhenium complexes has been also proven in this paper. The experimental geometry of [$ReOBr_2$(hmquin-7-COOH)($AsPh_3$)] is well reproduced and the calculated electronic spectrum is in good accordance with the experimental one.

Experimental

General procedure

The [$ReOBr_3(AsPh_3)_2$] complex was synthesized according to the literature method [11]. 8-hydroxy-2-methylquinoline-7-carboxylic acid was prepared as reported previously [12].

All the solvents used in the synthesis were commercially available and were used without further purification.

IR spectra were recorded on a Nicolet Magna 560 spectrophotometer in the spectral range 4000–400 cm^{-1} with the samples in the form of KBr pellets. Electronic spectra were measured on a spectrophotometer Lab Alliance UV–VIS 8500 in the range 1000–180 nm in acetonitrile solution. Elemental analyses (C H N) were performed on a Perkin-Elmer CHN-2400 analyzer.

Preparation of [$ReOBr_2$(hmquin-7-COOH)(APh_3)]

[$ReOBr_3(AsPh_3)_2$] (0.5 g, 0.47 mmol) was added to 8-hydroxy-2-methylquinoline-7-carboxylic acid (0.10 g, 0.53 mmol) in acetonitrile (50 mL), and the reaction mixture was refluxed for 2 h. The resulting solution was allowed to cool to room temperature and reduced in volume to ~10 mL. A dark green crystalline precipitate of [$ReOBr_2$(hmquin-7-COOH)(APh_3)] was filtered off and dried in the air. Yield was 65%.

Single crystals of [$ReOBr_2$(hmquin-7-COOH)(APh_3)] were obtained by recrystallization from acetonitrile.

Anal. Calc. for $C_{29}H_{23}Br_2NO_4AsRe$: C, 40.02; H, 2.66; N, 1.61%. Found: C, 40.90; H, 2.48; N, 1.76%.

IR (KBr; ν/cm^{-1}): 3370(m) ν_{O-H}(COOH); 1660(s) $\nu_{C=O}$(COOH); 1616 (m), 1549 (m), 1511 (m), ν_{CN} and $\nu_{C=C}$; 975(s) $\nu_{Re=O}$.

Crystal structure determination and refinement

The X-ray intensity data of [$ReOBr_2$(hmquin-7-COOH)(APh_3)] were collected on a KM-4-CCD automatic diffractometer equipped with CCD detector and graphite monochromated MoK_α radiation (λ = 0.71073 Å) at room temperature. Details concerning crystal data and refinement are given in Table 1. Lorentz, polarization, and empirical absorption correction using spherical harmonics implemented in SCALE3 ABSPACK scaling algorithm [13] were applied. The structures were solved by the Patterson method and subsequently completed by different Fourier recycling. All the non-hydrogen atoms were refined anisotropically using full-matrix, least-squares technique. The hydrogen atoms were treated as "riding" on their adjacent atoms and assigned isotropic temperature factors equal to 1.2 times the value of equivalent temperature factor of the aromatic parent atoms and equal to 1.5 times the value of equivalent temperature factor of the methyl parent carbon atom and oxygen atom (OH). SHELXS97 [14], SHELXL97 [15], and SHELXTL [16] programs were used for all the calculations. Atomic scattering factors were those incorporated in the computer programs.

Computational details

Gaussian03 program [17] was used in the calculations. The geometry optimization of [$ReOBr_2$(hmquin-7-COOH)(APh_3)] in a singlet state was carried out with the DFT method using B3LYP functional [18, 19]. The electronic spectrum of [$ReOBr_2$(hmquin-7-COOH)(APh_3)] was calculated with the TDDFT method [20], and the solvent effect was simulated using the polarizable continuum model with the integral equation formalism (IEF-PCM). The calculations were performed by using ECP basis set on the rhenium atom, the standard 6-31 + G** basis for bromine, arsenic, oxygen, and nitrogen; 6-31G* for carbon and 6–31G for hydrogen atoms [21, 22]. The Xe core electrons of Re were replaced by an effective core potential and DZ quality Hay and Wadt Los Alamos ECP basis set (LANL2DZ) [23] was used for the valence electrons. Additional *d* function with exponent α = 0.3811 and *f* function with exponent α = 2.033 on the rhenium atom were added [24]. The optimized geometry of [$ReOBr_2$(hmquin-7-COOH)(APh_3)] was verified by performing a frequency calculation. All the vibrations in the calculated vibrational spectrum of

Table 1 Crystal data and structure refinement for [$ReOBr_2$(hmquin-7-COOH)($AsPh_3$)]

Empirical formula	$C_{29}H_{23}AsNO_4Br_2Re$
Formula weight	870.42
Temperature	293(2) K
Wavelength	0.71073 Å
Crystal system	Monoclinic
Space group	$P2_1/c$
Unit cell dimensions	a = 16.6800(9) Å,
	b = 10.6030(4) Å,
	β = 115.332(6)°
	c = 17.5609(9) Å
Volume	2807.1(2) $Å^3$
Z	4
Density (calculated)	2.060 Mg/m^3
Absorption coefficient	8.381 mm^{-1}
$F(000)$	1656
Crystal size	0.024 × 0.14 × 0.36 mm^3
θ range for data collection	2.94–25.00°
Index ranges	$-19 \le h \le 17$
	$-12 \le k \le 12$
	$-15 \le l \le 20$
Reflections collected	16994
Independent reflections	4929 (R_{int} = 0.0431)
Completeness to $2\theta = 50°$	99.4%
Data/restraints/parameters	4929/0/345
Goodness-of-fit on F^2	0.966
Final R indices [$I > 2\sigma(I)$]	R_1 = 0.0214 wR_2 = 0.0476
R indices (all data)	R_1 = 0.0293 wR_2 = 0.0488
Largest diff. peak and hole	0.939 and −0.766 $eÅ^{-3}$

[$ReOBr_2$(hmquin-7-COOH)(APh_3)] were real, thus the optimized geometry corresponds to true energy minimum.

Natural bond orbital (NBO) calculations were performed with the NBO code [25, 26] included in Gaussian03.

Results and discussion

Preparation and infrared data

The [$ReOBr_2$(hmquin-7-COOH)($AsPh_3$)] complex was prepared in high yields by a route analogous to that used for the synthesis of the [$ReOX_2$(hqn)($AsPh_3$)$_2$] and [$ReOX_2$(-quin-2-c)($AsPh_3$)], namely by ligand exchange reactions starting from [$ReOX_3$($AsPh_3$)$_2$] complexes and 8-hydroxy-2-methylquinoline-7-carboxylic acid in acetonitrile:

$$[ReOBr_3(AsPh_3)_2] + \text{Hhmquin-7-COOH} \rightarrow [ReOBr_2(\text{hmquin-7-COOH})(AsPh_3)] + HBr + AsPh_3$$

The complex is air stable and soluble in common organic solvents. The elemental analysis of the complex is in good agreement with its formulation. The selected frequencies observed in the IR spectrum of [$ReOBr_2$(hmquin-7-COOH)($AsPh_3$)] are given in the Experimental part. The carboxylic acid group of the *hmquin-7-COOH* ligand is characterized by the $\nu_{C=O}$ absorption at 1660 cm^{-1} and ν_{O-H} at 3370 cm^{-1} [27, 28]. The strong ν(Re=O) stretching band of [$ReOBr_2$(hmquin-7-COOH)($AsPh_3$)] appears at 975 cm^{-1}, in the range typical of six-co-ordinate complexes with a phenolic oxygen *trans* to Re=O [29].

Crystal structure

The crystallographic data for [$ReOBr_2$(hmquin-7-COOH)($AsPh_3$)] are given in Table 1, and molecular structures of the [$ReOBr_2$(hmquin-7-COOH)($AsPh_3$)] complex are presented in Fig. 1. The intermolecular interactions found in the examined structure are shown in the Table 2 [30, 31].

The rhenium atom is coordinated by terminal oxygen atom (O_t), two bromide ions in *cis* arrangement, $AsPh_3$ molecule, and the N,O donors of the *hmquin-7-COOH* ligand. The oxygen atom of the quinoline derivative lies in *trans* position to the terminal oxo ion. The geometry of [$ReOBr_2$(hmquin-7-COOH)($AsPh_3$)] compound reveals typical features of quasi-octahedral oxorhenium(V)complexes with oxygenated bidentate ligands. The deformation of the octahedron is caused by the presence multiple bonding ligand (terminal oxo) and narrow bite angle of the chelating ligand. The high concentration of electronic density along the Re–O_t axis strongly influences the positions of the adjacent halogen atoms, which are pushed away.

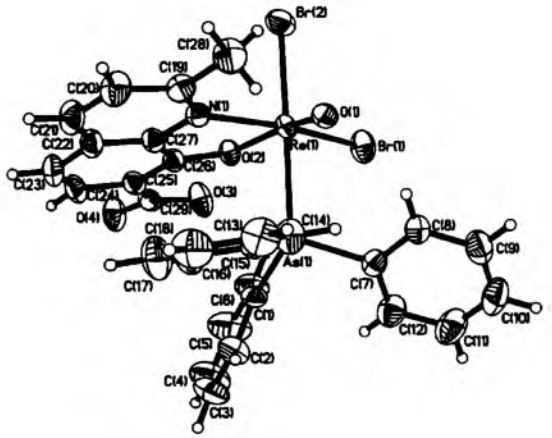

Fig. 1 The molecular structure of [$ReOBr_2$(hmquin-7-COOH)($AsPh_3$)]. Displacement ellipsoids are drawn at 50% probability

Table 2 Hydrogen bonds for [$ReOBr_2$(hmquin-7-COOH)($AsPh_3$)]

D	A	H···A (Å)	D···A (Å)	D–H···A (°)
C(8)	O(1)	2.50	3.177(4)	130.0
O(3)	O(4)#1	1.83	2.648(4)	172.9
C(2)	O(4)#2	2.59	3.386(5)	143.5
C(11)	O(4)#3	2.39	3.316(5)	174.8

#1 −x + 2,−y+1,−z + 1; #2 −x,−y + 3/2, z − 1/2; #3 −x + 2, y−1/2,−z + 1/2

The selected bond distances and angles of [$ReOBr_2$(hmquin-7-COOH)($AsPh_3$)] are collected in Table 3.

The Re–O_t bond length of [$ReOBr_2$(hmquin-7-COOH)($AsPh_3$)] falls in the range 1.639–1.76 Å, typical of mononuclear complexes of rhenium(V) having $[ReO]^{3+}$ core, and indicates the presence of a triple bond Re≡O [32]. The interatomic distance between the rhenium atom and the oxygen atom of bidentate ligand are somewhat shorter in comparison with an ideal single Re–O bond length (*ca.* 2.04 Å) [33], and indicates small delocalization in the O(2)–Re(1)–O(1) moiety. The similar trend is observed for many Re(V)–oxo complexes with an mono-anionic oxygen *trans* to the oxo group [34].

Table 3 The experimental and optimized bond lengths (Å) and angles (°) for [$ReOBr_2$(hmquin-7-COOH)($AsPh_3$)]

	Experimental	Optimized
Bond lengths		
Re(1)–O(1)	1.671(2)	1.684
Re(1)–O(2)	1.991(2)	2.024
Re(1)–N(1)	2.180(3)	2.221
Re(1)–Br(1)	2.4805(4)	2.543
Re(1)–Br(2)	2.5218(4)	2.574
Re(1)–As(1)	2.5662(4)	2.654
Bond angles		
O(1)–Re(1)–O(2)	163.53(11)	161.68
O(1)–Re(1)–N(1)	92.72(11)	93.63
O(2)–Re(1)–N(1)	75.74(10)	74.69
O(1)–Re(1)–Br(1)	102.79(8)	103.31
O(2)–Re(1)–Br(1)	88.65(7)	89.31
N(1)–Re(1)–Br(1)	164.34(7)	162.97
O(1)–Re(1)–Br(2)	100.05(8)	102.20
O(2)–Re(1)–Br(2)	91.70(7)	90.92
N(1)–Re(1)–Br(2)	89.61(7)	84.81
Br(1)–Re(1)–Br(2)	89.770(15)	89.79
O(1)–Re(1)–As(1)	81.13(8)	83.85
O(2)–Re(1)–As1)	87.13(7)	83.25
N(1)–Re(1)–As(1)	90.27(7)	95.14
Br(1)–Re(1)–As(1)	90.031(14)	88.54
Br(2)–Re(1)–As(1)	178.814(13)	173.95

The Re(1)–Br(2) distance *trans* to the $AsPh_3$ molecule is slightly longer than the Re(1)–Br(1) bond *trans* to the nitrogen atom of the *hmquin-7-COOH* ligand. It is a consequence of *structural trans* effect of the $AsPh_3$ ligand.

Geometry optimization, charge distribution, electronic structure, and NBO analysis

The geometry of [$ReOBr_2$(hmquin-7-COOH)($AsPh_3$)] was optimized in a singlet state by the DFT method with the B3LYP functional. The optimized geometric parameters of [$ReOBr_2$(hmquin-7-COOH)($AsPh_3$)] are presented in Table 3. In general, the predicted bond lengths and angles are in agreement with the values based upon the X-ray crystal structure data, and the general trends observed in the experimental data (discussed above) are well reproduced in the calculations.

Table 4 presents the atomic charges from the natural population analysis (NPA) for [$ReOBr_2$(hmquin-7-COOH)($AsPh_3$)]. The calculated charge on the rhenium atom in [$ReOBr_2$(hmquin-7-COOH)($AsPh_3$)] is considerably lower than the formal charge +5, corresponding to d^2 configuration of the central ion. It results from charge donation from the oxo ligands, halide ions, and $AsPh_3$ molecule. The As atom is positively charged, and the charges on the terminal oxo, bromide, and oxygen atom of *hmquin-7-COOH* are significantly smaller than −2, −1, and −1, respectively. The terminal oxo ions are less negative in comparison with the oxygen atoms of *hmquin-7-COOH* ligand. It confirms the higher electron density delocalization from the terminal ligand toward the rhenium center and corresponds to differences in the Re–O(1) and Re–O(2) bond lengths.

The complex [$ReOBr_2$(hmquin-7-COOH)($AsPh_3$)] is a closed-shell structure. Its partial molecular orbital diagram with several highest occupied and lowest unoccupied molecular orbital contours is presented in Fig. 2. In discussion of the orbital character, the local symmetry of the rhenium center has been considered: *z* axis goes along the O–Re–O linkage, and *x* axis through the As–Re–Br bonds. The value of the energy separation between the highest occupied molecular orbital (HOMO)

Table 4 Atomic charges from the natural population analysis (NPA) for [$ReOBr_2$(hmquin-7-COOH)($AsPh_3$)]

Atom	Charge
Re(1)	1.092
O(1)	−0.476
O(2)	−0.659
N(1)	−0.476
Br(1)	−0.288
Br(2)	−0.344
As(1)	1.384

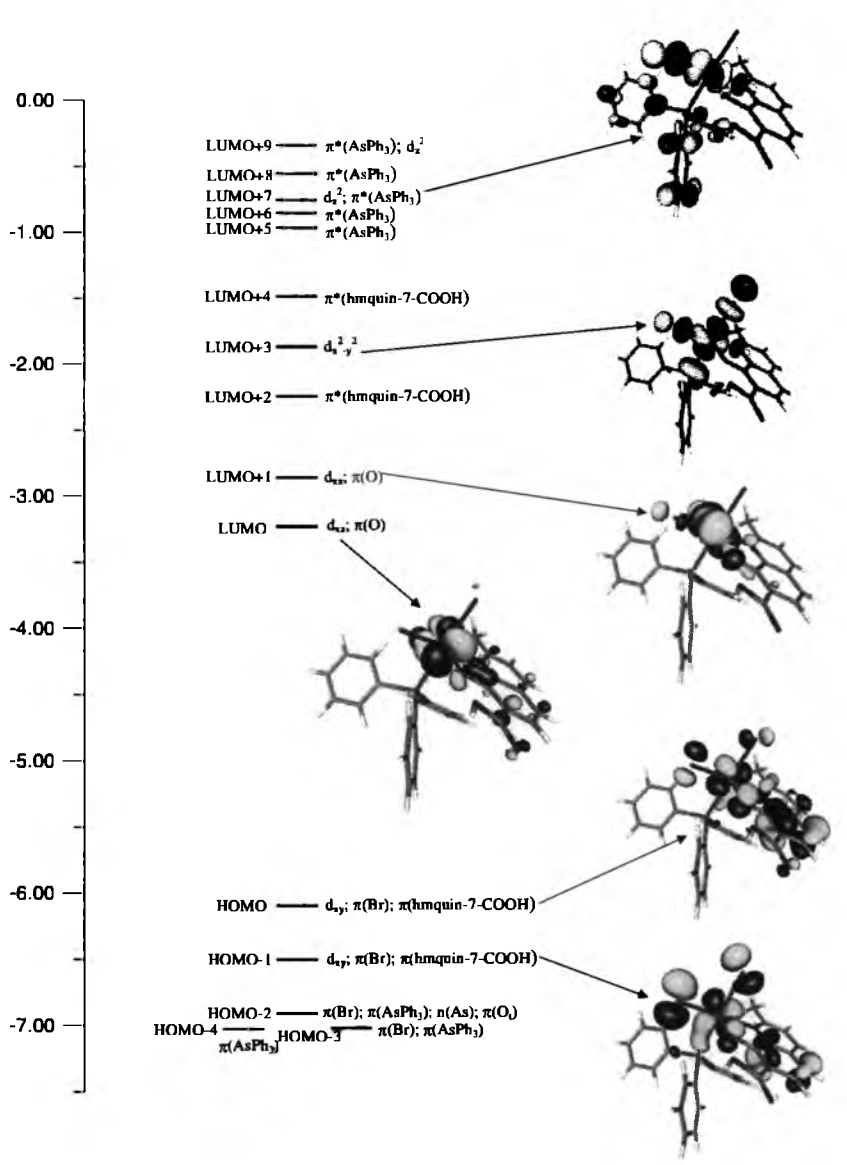

Fig. 2 The energy (eV), character and some contours of the occupied and unoccupied molecular orbitals of [$ReOBr_2$(hmquin-7-COOH)($AsPh_3$)]. Positive values of the orbital contour are represented in yellow (0.04 au) and negative values—in blue (−0.04 au)

Table 5 The occupancy of the calculated natural bond orbitals (NBOs) between the rhenium and the oxo ligand for [$ReOBr_2$(hmquin-7-COOH)($AsPh_3$)]

BD	Occupancy	BD	BD*	Occupancy
Re–O_t	1.991	$0.560(d)_{Re} + 0.828(p)_O$	$0.828(d)_{Re} - 0.560(p)_O$	0.286
Re–O_t	1.984	$0.572(d)_{Re} + 0.821(p)_O$	$0.821(d)_{Re} - 0.572(p)_O$	0.294

BD denotes 2-center bond, * denotes antibond NBO

and the lowest unoccupied molecular orbital (LUMO) equals to 2.89 eV. Two highest occupied MOs are delocalized among d_{xy} rhenium orbital, p_π bromide, and π-bonding of hmquin-7-COOH orbitals. The LUMO and LUMO + 1 are predominately localized on the rhenium atom (d_{xz} and d_{yz} orbitals) with some contribution of p_π oxygen orbitals. They can be ascribed as π-antibonding rhenium–oxygen molecular orbitals. The LUMO + 3 is of $d_{x^2-y^2}$ character, and d_{z^2} rhenium orbital contributes to the LUMO + 7.

Table 6 The energy and molar absorption coefficients of experimental absorption bands and the electronic transitions calculated with the TDDFT method for [$ReOBr_2$(hmquin-7-COOH)($AsPh_3$)]

The most important orbital excitations	Character	λ (nm)	E (ev)	f	Experimental Λ (nm) (E (eV))ε
H → L	d → d	759.6	1.63	0.0061	740.4 (1.67) 250
H → L + 1	d → d	630.5	1.97	0.0036	
H-1 → L	π(Br)/π(hmquin-7-COOH)/d → d	516.4	2.40	0.0458	480.0 (2.58) 740
H-1 → L + 1	π(Br)/π(hmquin-7-COOH) → d	462.1	2.68	0.0386	
H → L + 3	d → d	430.3	2.88	0.0069	
H-2 → L + 1	π(Br)/π($AsPh_3$)/n(As) → d	387.9	3.20	0.0183	402.7 (3.08) 5600
H → L + 2	d → π*(hmquin-7-COOH)	385.3	3.22	0.0562	
H-9 → L	π(hmquin-7-COOH) → d	345.1	3.59	0.0114	
H-1 → L + 2	π(Br)/π(hmquin-7-COOH) → π*(hmquin-7-COOH)				
H-1 → L + 3	π(Br)/π(hmquin-7-COOH) → d	329.9	3.76	0.0469	
H-10 → L + 1	π(Br)/π(O_t) → d	324.1	3.83	0.0266	
H-9 → L + 1	π(hmquin-7-COOH) → d	319.1	3.89	0.0142	
H → L + 4	d → π*(hmquin-7-COOH)	307.7	4.03	0.0688	
H-11 → L + 1	π(Br)/π(O_t) → d	301.0	4.12	0.0236	
H-13 → L + 1	π(Br)/n(As)/π(hmquin-7-COOH) → d	288.4	4.30	0.0615	267.1 (4.69) 55600
H-2 → L + 3	π(Br)/π($AsPh_3$)/n(As) → d				
H-14 → L	π(hmquin-7-COOH)/π(Br) → d	282.1	4.40	0.0219	
H-6 → L + 2	π($AsPh_3$) → π*(hmquin-7-COOH)	277.7	4.46	0.0287	
H-6 → L + 2	π($AsPh_3$) → π*(hmquin-7-COOH)	277.6	4.47	0.0389	
H-10 → L + 2	π(Br)/π(O_t) → π*(hmquin-7-COOH)	265.3	4.67	0.0469	
H-9 → L + 2	π(hmquin-7-COOH) → π*(hmquin-7-COOH)	263.6	4.70	0.1891	
H-7 → L + 3	π(Br)/π($AsPh_3$) → d	261.7	4.74	0.0623	
H-9 → L + 3	π(hmquin-7-COOH) → d	251.7	4.93	0.0419	
H-2 → L + 4	π(Br)/π($AsPh_3$)/n(As) → π*(hmquin-7-COOH)	251.4	4.93	0.0805	
H-1 → L + 5	π(Br)/π(hmquin-7-COOH) → π*($AsPh_3$)				
H-1 → L + 5	π(Br)/π(hmquin-7-COOH) → π*($AsPh_3$)	251.1	4.94	0.0372	
H-11 → L + 2	π(Br)/π(O_t) → π*(hmquin-7-COOH)	250.7	4.96	0.0227	
H-9 → L + 3	π(hmquin-7-COOH) → d	250.3	4.95	0.0914	
H-2 → L + 5	π(Br)/π($AsPh_3$)/n(As) → π*($AsPh_3$)	231.5	5.36	0.0330	204.8 (6.05) 88600
H → L + 11	d → π*($AsPh_3$)				
H-2 → L + 6	π(Br)/π($AsPh_3$)/n(As) → π*($AsPh_3$)	226.8	5.47	0.0586	
H-2 → L + 7	π(Br)/π($AsPh_3$)/n(As) → π*($AsPh_3$)/d	226.5	5.47	0.0488	
H-4 → L + 5	π($AsPh_3$) → π*($AsPh_3$)				
H-5 → L + 5	π($AsPh_3$) → π*($AsPh_3$)	225.3	5.50	0.0688	
H-9 → L + 4	π(hmquin-7-COOH) → π*(hmquin-7-COOH)				
H-5 → L + 5	π($AsPh_3$) → π*($AsPh_3$)	224.8	5.52	0.0390	
H-15 → L + 2	σ(Br)/π(hmquin-7-COOH)/π(O_t) → π*(hmquin-7-COOH)				
H-10 → L + 4	π(Br)/π(O_t) → π*(hmquin-7-COOH)	224.1	5.53	0.0211	
H-4 → L + 6	π($AsPh_3$) → π*($AsPh_3$)	223.8	5.54	0.0230	

ε, molar absorption coefficient ($dm^3\ mol^{-1}\ cm^{-1}$); f oscillator strength; H highest occupied molecular orbital; L lowest unoccupied molecular orbital

The nature of rhenium-terminal oxygen interaction in [$ReOBr_2$(hmquin-7-COOH)($AsPh_3$)] has been studied by NBO analysis. The occupancy and composition of the calculated Re–O_t natural bond orbitals (NBOs) are given in Table 5. Each natural bond orbital (NBO) σ_{AB} can be written in terms of two directed valence hybrids (NHOs) h_A and h_B on atoms A and B:

$$\sigma_{AB} = c_A h_A + c_B h_B$$

where c_A and c_B are polarization coefficients. Each valence bonding NBO must in turn be paired with a corresponding valence anti-bonding NBO:

$$\sigma^*_{AB} = c_B h_A - c_A h_B$$

to complete the span of the valence space. The Lewis-type (donor) NBOs are thereby complemented by the non-Lewis-type (acceptor) NBOs that are formally empty in an idealized Lewis picture. The interactions between 'filled' Lewis-type NBOs and 'empty' non-Lewis NBOs lead to loss of occupancy from the localized NBOs of the idealized Lewis structure into the empty non-Lewis orbitals, and they are referred to as 'delocalization' corrections to the zeroth-order natural Lewis structure [25, 26].

The two detected natural Re–O_t bond orbitals of [$ReOBr_2$(hmquin-7-COOH)($AsPh_3$)] are of π character—they arise from overlap of the two occupied oxygen p_π orbitals with the empty d_{xz} and d_{yz} metal orbitals. Not detected σ_{Re-Ot} bond has character of predominant Coulomb-type interactions between the central ion and ligands [35]. The terminal oxo ligand of [$ReOBr_2$(hmquin-7-COOH)($AsPh_3$)] has two lone pair orbitals, and electron density from one of them is strongly delocalized into non-Lewis rhenium orbital. Accordingly, NBO analysis confirms a triple bond between the rhenium and the terminal oxygen ligand.

Electronic spectra

The positions and molar absorption coefficients of electronic bands for [$ReOBr_2$(hmquin-7-COOH)($AsPh_3$)] complex are given in Table 6. The experimental and calculated electronic spectra of [$ReOBr_2$(hmquin-7-COOH)($AsPh_3$)] are presented in Fig. 3. Each calculated transition is represented by a gaussian function $y = ce^{-bx^2}$ with the height (c) equal to the oscillator strength and b equal to 0.04 nm^{-2}. Table 6 presents also the calculated singlet–singlet electronic transitions of [$ReOBr_2$(hmquin-7-COOH)($AsPh_3$)] and their assignments to the experimental bands. For the high energy part of the spectrum, only transitions with oscillator strengths larger than 0.020 are listed in Table 6. The assignment of the calculated transitions to the experimental bands is based on the criterion of the energy and oscillator strength of the calculated transitions.

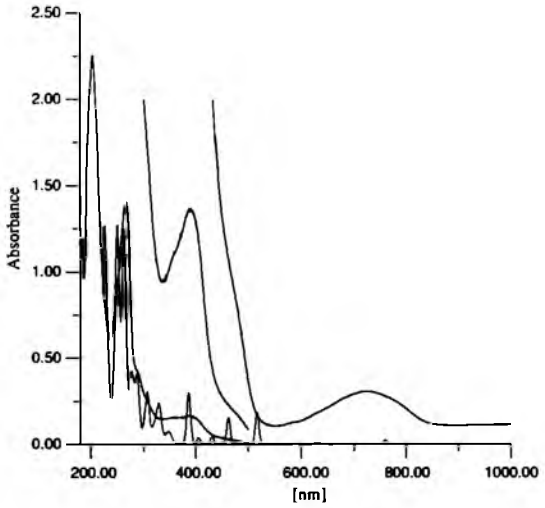

Fig. 3 The experimental (black) and calculated (red) electronic absorption spectra of [$ReOBr_2$(hmquin-7-COOH)($AsPh_3$)]

The TDDFT/PCM calculations show that the longest wavelength experimental bands of [$ReOBr_2$(hmquin-7-COOH)($AsPh_3$)] originates in the HOMO → LUMO and HOMO → LUMO + 1 transitions. As d_{Re} orbitals take main part in the HOMO, LUMO, and LUMO + 1 orbitals, the HOMO → LUMO and HOMO → LUMO + 1 transitions may be attributed to the transitions of d → d character. However, as it can be seen from the Fig. 2, the HOMO, LUMO, and LUMO + 1 orbitals are delocalized among rhenium ion, bromide, oxo, and hmquin-7-COOH ligands so a delocalized *MLLCT* (metal–ligand-to-ligand CT) description also can be used. In Table 6 the first type of description is used, the HOMO, LUMO, and LUMO + 1 are described as d_{Re} orbital, whereas the participation of d_{Re} in the H-1 orbital is omitted.

The intense absorption band with maximum at 402.7 nm results mainly from *Metal–Ligand Charge Transfer* (d → π^*(hmquin-7-COOH)). However the contribution of the *Ligand–Metal Charge Transfer* excitations (π(Br)/π($AsPh_3$)/π(hmquin-7-COOH) → d) into this band is also confirmed by the calculations.

The experimental bands below 300 nm are mainly assigned to *Ligand–Ligand Charge Transfer* and interligand (*IL*) transitions.

Supplementary data

Supplementary data for $C_{29}H_{23}AsNO_4Br_2Re$ are available from the CCDC, 12 Union Road, Cambridge CB2 1EZ, UK, on request, quoting the deposition numbers 701499.

Acknowledgments The Gaussian03 calculations were carried out in the Wrocław Centre for Networking and Supercomputing, WCSS, Wroclaw, Poland.

References

1. Holm RH (1987) Chem Rev 87:1401. doi:10.1021/cr00082a005
2. Romão CC, Kühn FE, Herrmann WA (1997) Chem Rev 97:3197. doi:10.1021/cr9703212
3. Seymore SB, Brown SN (2000) Inorg Chem 39:325. doi:10.1021/ic990851b
4. Kühn FE, Scherbaum A, Herrmann WA (2004) J Organomet Chem 689:4149. doi:10.1016/j.jorganchem.2004.08.018
5. Kirillov AM, Haukka M, Kirillova MV, Pombeiro AJL (2005) Adv Synth Catal 347:1435. doi:10.1002/adsc.200505092
6. Volkert W, Goeckeler WF, Ehrhardt GJ, Ketring AR (1991) J Nucl Med 32:174
7. Deutsch EA, Libson K, Vanderheyden JL (1990) Technetium and rhenium in chemistry and nuclear medicine. Raven Press, New York
8. Machura B, Michalik S, Kruszynski R, Kusz J (2007) Polyhedron 26:2837. doi:10.1016/j.poly.2007.01.054
9. Machura B, Kruszynski R (2007) Polyhedron 26:3686. doi:10.1016/j.poly.2007.03.058
10. Ganchеff J, Kremer C, Kremer E, Ventura ON (2002) J Mol Struct THEOCHEM 580:107. doi:10.1016/S0166-1280(01)00601-7
11. Rouschias G, Wilkinson G (1966) J Chem Soc A 465. doi:10.1039/j19660000465
12. Mekouar K (1998) J Med Chem 41:2846. doi:10.1021/jm980043e
13. STOE Cie (1999) X-RED. Version 1.18. STOE & Cie GmbH, Darmstadt, Germany
14. Sheldrick GM (1990) Acta Crystallogr A46:467
15. Sheldrick GM (1997) SHELXL97. Program for the refinement of crystal structures. University of Göttingen, Germany
16. Sheldrick GM (1990) SHELXTL: release 4.1 for Siemens crystallographic research systems
17. Frisch MJ, Trucks GW, Schlegel HB, Scuseria GE, Robb MA, Cheeseman JR, Montgomery JA Jr, Vreven T, Kudin KN, Burant JC, Millam JM, Iyengar SS, Tomasi J, Barone V, Mennucci B, Cossi M, Scalmani G, Rega N, Petersson GA, Nakatsuji H, Hada M, Ehara M, Toyota K, Fukuda R, Hasegawa J, Ishida M, Nakajima T, Honda Y, Kitao O, Nakai H, Klene M, Li X, Knox JE, Hratchian HP, Cross JB, Adamo C, Jaramillo J, Gomperts R, Stratmann RE, Yazyev O, Austin AJ, Cammi R, Pomelli C, Ochterski JW, Ayala PY, Morokuma K, Voth GA, Salvador P, Dannenberg JJ, Zakrzewski VG, Dapprich S, Daniels AD, Strain MC, Farkas O, Malick DK, Rabuck AD, Raghavachari K, Foresman JB, Ortiz JV, Cui Q, Baboul AG, Clifford S, Cioslowski J, Stefanov BB, Liu G, Liashenko A, Piskorz P, Komaromi I, Martin RL, Fox DJ, Keith T, Al-Laham MA, Peng CY, Nanayakkara A, Challacombe M, Gill PMW, Johnson B, Chen W, Wong MW, Gonzalez C, Pople JA (2003) Gaussian 03, Revision B.03. Gaussian, Inc., Pittsburgh PA
18. Becke AD (1993) J Chem Phys 98:5648. doi:10.1063/1.464913
19. Lee C, Yang W, Parr RG (1988) Phys Rev B 37:785. doi:10.1103/PhysRevB.37.785
20. Casida ME (1996) In: Seminario JM (ed) Recent developments and applications in modern density functional theory. Theoretical and computational chemistry, vol 4. Elsevier, Amsterdam
21. Hariharan PC, Pople JA (1973) Theor Chim Acta 28:213. doi:10.1007/BF00533485
22. Rassolov VA, Ratner MA, Pople JA, Redfern PC, Curtiss LA (2001) J Comput Chem 22:976. doi:10.1002/jcc.1058
23. Hay PJ, Wadt WR (1985) J Chem Phys 82:299. doi:10.1063/1.448975
24. Eichkorn K, Weigend F, Treutler O, Ahlrichs R (1997) Theor Chem Acc 97:119. doi:10.1007/s002140050244
25. Glendening ED, Reed AE, Carpenter JE, Weinhold F (1988) NBO (version 3.1). Theoetical Chemistry Institute, University of Wisconsin, Madison
26. Reed E, Curtiss LA, Weinhold F (1988) Chem Rev 88:899. doi:10.1021/cr00088a005
27. Nakamoto K (1986) Infrared and Raman spectra of inorganic and coordination compounds, 4th edn. Wiley-Interscience, New York
28. Wei L, Babich J, Zubieta J (2005) Inorg Chim Acta 358:2413. doi:10.1016/j.ica.2005.03.037
29. Mazzi U, Refosco F, Tisato F, Bandoli G, Nicolini M (1986) J Chem Soc Dalton Trans 1623. doi:10.1039/dt9860001623
30. Desiraju GR, Steiner T (1999) The weak hydrogen bond in structural chemistry and biology. Oxford University Press, Oxford
31. Jeffrey GA, Saenger W (1994) Hydrogen bonding in biological structures. Springer-Verlag, Berlin
32. Mayer JM (1988) Inorg Chem 27:3899. doi:10.1021/ic00295a006
33. Fletcher SR, Skapski AC (1972) J Chem Soc Dalton 1073
34. Shuter E, Hoveyda HR, Karunaratne V, Retting SJ, Orvig C (1996) Inorg Chem 35:368. doi:10.1021/ic9507528
35. Kuznetsov ML, Pombeiro AJL (2003) J Chem Soc Dalton Trans 738

VERSITA

Cent. Eur. J. Chem. • 7(3) • 2009 • 586-597
DOI: 10.2478/s11532-009-0059-2

Central European Journal of **Chemistry**

RP-HPLC determination of lipophilicity in series of quinoline derivatives

Research Article

Robert Musiol[a*], Josef Jampilek[b,c], Barbara Podeszwa[a], Jacek Finster[a], Dominik Tabak[a], Jiri Dohnal[b,c], Jaroslaw Polanski[a]

[a]*Institute of Chemistry, University of Silesia, 40007 Katowice, Poland*

[b]*Zentiva a.s., 10237 Prague 10, Czech Republic*

[c]*Department of Chemical Drugs, Faculty of Pharmacy, University of Veterinary and Pharmaceutical Sciences, 61242 Brno, Czech Republic*

Received 29 January 2009; Accepted 14 April 2009

Abstract: In the present paper we describe results on the synthesis and lipophilicity determination of a series of biologically active compounds based on their heterocyclic structure. For synthesis of styrylquinoline-based compounds we applied microwave irradiation and solid phase techniques. The correlation between RP-HPLC retention parameter log *k* (the logarithm of retention factor *k*) and log *P* data calculated in various ways is discussed, as well as, the relationships between the lipophilicity and the chemical structure of the studied compounds.

Keywords: *Lipophilicity • RP-HPLC • Microwave synthesis • Quinoline derivatives*

1. Introduction

The quinoline moiety is present in many classes of biologically active compounds. A number of them have been clinically used as antifungal, antibacterial and antiprotozoic drugs [1,2] as well as antituberculotic agents [3,4]. Some quinoline based compounds showed also antineoplastics, antiasthmatic and antiplatelet activity [5-10]. The acetylcholinesterase inhibitory activity of various quinoline derivatives has been tested for potential treatment of nervous diseases [11].

Styrylquinoline derivatives have gained great attention recently due to their activity as potential HIV integrase inhibitors [12-16]. Our previous study dealing with styrylquinoline derivatives showed that they could also possess also strong antifungal activity [17]. The compounds containing 8-hydroxyquinoline pharmacophore seem especially interesting.

According to the results reported recently some new 8-hydroxyquinoline derivatives possessed interesting antifungal and herbicidal activities [18,19].

Determination of the physico-chemical parameters of biologically active compounds has become more important with an age of rational thinking in drug design [20]. One of the major prerequisites for pharmacological screening and drug development is the prediction of absorption, *e.g.* the transport of a molecule through cellular membranes, *i.e.* bioavailability, fate in the biological system. Drugs cross biological barriers most frequently through passive transport, which strongly depends on their lipophilicity. Therefore hydrophobicity is one of the most important physical properties of biologically active compounds. This thermodynamic parameter describes the partitioning of a compound between an aqueous and an organic phase and can be characterized by the partition coefficient (log *P*) [21,22].

* *E-mail: robert.musiol@us.edu.pl*

With new computer methods for log *P* calculation, the possibility of high throughput screening of large combinatorial libraries is possible. However there is still a need for algorithms that are sensitive to various electronic effects and individual structural aspects.

Reversed-phase high performance liquid chromatography (RP-HPLC) methods have become popular and widely used for lipophilicity measurement [23-27]. The general procedure is the measurement of the directly accessible retention time under isocratic conditions with varying amounts of an organic modifier in the mobile phase. The lipophilicity index, log *k*, can be derived from the retention factor *k*.

Our investigation of the spectrum of biological activity of hydroxyquinoline derivatives showed that these compounds can be valuable antifungal and herbicidal agents [17-19]. Antifungal activity seems to be dependent on lipophilicity [17,19]. Some parameters influencing herbicidal activity are molecular size and position of the phenolic moiety in the quinoline nucleus. It is the interaction of the OH–N in the quinoline molecule and protonization the whole molecule that influences lipophilicity of compounds.

These facts inspired us to study the hydrophobic properties of quinoline derivatives prepared in our laboratory in great detail. The aim of this study was to determine the lipophilicity (log *k*) of a new series of biologically active quinoline derivatives. The general formulas of all evaluated quinoline derivatives are shown in Fig. 1. The results obtained are also discussed with lipophilicity (log *P*/Clog *P*) calculated using available computer programs.

2. Experimental Procedures

2.1 Lipophilicity HPLC determination (retention factor *k*/calculated log *k*)

The HPLC separation module Waters Alliance 2695 XE and Waters Photodiode Array Detector 2996 (Waters Corp., Milford, MA, U.S.A.) were used. The chromatographic column Symmetry® C_{18} 5 µm, 4.6×250 mm, Part No. WAT054275, (Waters Corp., Milford, MA, U.S.A.) was used. The HPLC separation process was monitored by Millennium32® Chromatography Manager Software, Waters 2004 (Waters Corp., Milford, MA, U.S.A.). The mixture of MeOH p.a. (55.0%) and H_2O-HPLC – Mili-Q Grade (45.0%) was used as a mobile phase for compounds **1-21** and **25-49**. The mixture of MeOH p.a. (50.0%) and H_2O-HPLC – Mili-Q Grade (50.0%) was used as a mobile phase for compounds **22-24**. H_2O-HPLC, pH = 7.02 (Mili-Q Grade) The total flow rate of the column was 0.9 mL min^{-1}, injection volume of 30 µL, column temperature 30°C and sample temperature 10°C. The detection wavelength was 210 nm. The KI methanolic solution was used for the hold-up time (t_0) determination. Retention times (t_R) were measured in minutes.

The capacity factors *k* were calculated using the Millennium32® Chromatography Manager Software according to the formula $k = (t_R-t_0)/t_0$, where t_R is the retention time of the solute, whereas t_0 denotes the hold-up time obtained *via* an unretained analyte. The log *k* values of the individual compounds, calculated from the retention factor *k*, are shown in Tables 1-4.

2.2 Lipophilicity calculations

Log *P* was calculated using the programs CS ChemOffice Ultra ver. 9.0 (CambridgeSoft, Cambridge, MA, U.S.A.) and ACD/LogP ver. 1.0 (Advanced Chemistry Development Inc., Toronto, Canada). Clog *P* values were generated by means of CS ChemOffice Ultra ver. 9.0 (CambridgeSoft, Cambridge, MA, U.S.A.) software. The miLog *P* values were calculated using free tool available at Molinspiration Property Calculation Service website [28-32]. The results are shown in Tables 1-4.

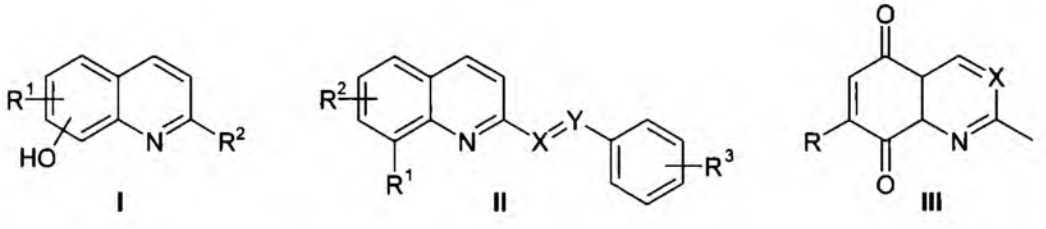

Figure 1. General formulas of all the quinoline/quinazoline derivatives

Table 1. Comparison of the calculated lipophilicities (log *P*/Clog *P*) with the determined log k of compounds **1-21**.

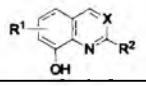

Comp.	R^1	R^2	X	log k	log P/Clog PChemOffice	log P ACD/LogP	miLog P
1				0.1580	1.64 / 1.523	1.88 ± 0.23	1.263
2				0.8233	1.91 / 1.079	1.02 ± 0.22	0.929
3				0.2443	2.03 / 2.076	2.04 ± 0.33	1.778
4				0.6649	2.82 / 2.528	2.54 ± 0.20	1.996
5	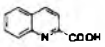			0.7125	2.10 / 2.603	2.17 ± 0.25	1.585
33				0.3629	2.38 / 2.579	2.22 ± 0.72	1.823
6				0.0029	0.62 / 0.781	1.18 ± 0.23	2.394
7				0.0996	0.93 / 1.722	2.34 ± 0.38	3.131
8				0.6061	2.43 / 2.577	1.91 ± 0.21	2.032
9	8-OH	CH_3	C	0.6838	2.43 / 2.577	2.33 ± 0.23	1.728
10	5-Br	CH_3	C	1.3142	3.26 / 3.562	3.54 ± 0.38	2.793
11	7-Br	CH_3	C	1.0759	3.26 / 3.282	3.38 ± 0.38	2.490
12	5,7-Br	CH_3	C	1.8054	4.09 / 4.188	4.55 ± 0.43	3.530
13	5-NO_2	H	C	0.5695	1.69 / 2.0836	2.00 ± 0.32	1.942
14	5,7-NO_2	H	C	0.7154	1.80 / 1.919	2.18 ± 0.34	1.776
15	5,7-NO_2	CH_3	C	0.7292	2.50 / 2.418	2.64 ± 0.35	1.829
16	5,7-NO_2	CH_3	N	0.5687	1.67 / 1.486	0.66 ± 1.27	1.829
17	5,7-NH_2	H	C	0.0522	0.12 / 1.344	-0.84 ± 0.34	0.824
18	5,7-NH_2	CH_3	C	0.2707	0.83 / 1.843	-0.38 ± 0.35	0.878
19	5-SO_3H-7-NO_2	H	C	0.1479	0.37 / -0.703	1.70 ± 0.88	-1.191
20	5-SO_3H-7-Br	H	C	0.3786	1.72 / -0.004	2.39 ± 0.91	-0.341
21	5-N=N-2,6-Cl-Ph	H	C	0.9633	5.28 / 5.570	4.72 ± 0.79	5.382

Table 2. Comparison of the calculated lipophilicities (log *P*/Clog *P*) with the determined log *k* of compounds **22-24**. (Different conditions MeOH/H_2O : 50/50).

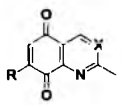

Comp.	R	X	log k	log P/Clog P ChemOffice	log P ACD/LogP	miLog P
22	-$NHCOCH_3$	C	0.2227	-0.91 / 0.939	1.09 ± 0.75	-0.875
23	-$NHCOCH_3$	N	0.0167	-1.07 / -1.250	0.69 ± 0.75	-0.706
24	-OCH_3	C	0.0907	-0.10 / 1.224	1.60 ± 0.75	-0.037

Table 3. Comparison of the calculated lipophilicities (log *P*/Clog *P*) with the determined log *k* of compounds **25-32**.

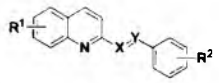

Comp.	R^1	R^2	X	Y	log k	log P/Clog P ChemOffice	log P ACD/ LogP	miLog P
25	8-OH	3-Cl	CH	CH	1.5395	4.90 / 5.483	5.08 ± 0.32	4.778
26	8-OH	4-Cl	CH	CH	1.5558	4.90 / 5.483	5.08 ± 0.32	4.802
27	8-OH	4-Br	CH	CH	1.5802	5.17 / 5.633	5.26 ± 0.38	4.934
28	8-OH	4-OH	N	CH	0.8353	3.92 / 3.569	1.24 ± 1.05	3.071
29	8-OH	2-OH	CH	N	0.4308	3.63 / 2.432	1.09 ± 0.79	3.012
30	8-OH	3-OH	CH	N	0.8860	3.63 / 2.432	1.51 ± 0.79	2.776
31	8-OH	4-OH	CH	N	1.0911	3.63 / 2.432	1.32 ± 0.79	2.80
32	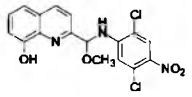				1.1766	4.08 / 4.661	4.44 ± 0.43	4.328
34	5-COOH	4-Cl	CH	CH	1.3976	4.85 / 5.485	4.97 ± 0.73	4.897
35	6-COOH	2-Cl	CH	CH	1.4787	4.85 / 5.485	5.02 ± 0.32	4.729
36	7-COOH	3-Cl	CH	CH	1.2858	4.85 / 5.485	4.97 ± 0.73	4.932
37	8-COOH	2-OCH_3	CH	CH	1.1922	4.16 / 4.691	3.62 ± 0.35	3.745
38	5,8-COOH	3-Br	CH	CH	1.2171	4.67 / 5.650	4.49 ± 0.80	4.528

Table 4. Comparison of the calculated lipophilicities (log *P*/Clog *P*) with the determined log k of compounds **39-49**.

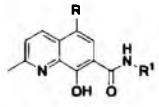

Comp.	R	R^1	log k	log P/Clog P ChemOffice	log P ACD/ LogP	miLog P
39	H	-CH_2Ph	0.2812	3.31 / 4.840	3.75 ± 0.80	2.821
40	H	-CH_2Ph-4-F	0.3389	3.47 / 4.983	3.80 ± 0.85	2.984
41	H	-$CH(CH_3)$Ph-4-F	0.3720	3.78 / 5.2918	4.15 ± 0.85	3.544
42	-NO_2	-$CH(CH_3)$Ph-4-F	0.4283	3.42 / 5.2237	4.47 ± 0.85	3.733
43	H	-CH_2Ph-4-CH_3	0.3903	3.79 / 5.339	4.21 ± 0.80	3.269
44	H	-CH_2Ph-4-OCH_3	0.2843	3.18 / 4.759	3.67 ± 0.81	2.877
45	H	-CH_2CH_2Ph	0.2404	3.59 / 4.969	4.17 ± 0.80	3.226
46	H	-CH_2CH_2Ph-4-F	0.3342	3.74 / 5.112	4.22 ± 0.84	3.390
47	H	-$CH_2CH_2CH_2CH_2$Ph	0.5075	4.00 / 5.348	5.06 ± 0.79	4.015
48	H	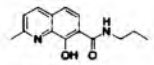	0.1109	2.91 / 5.991	4.04 ± 1.13	2.532
49	H	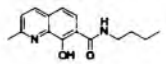	0.1208	3.01 / 6.303	4.26 ± 1.12	2.802

3. Results and Discussion

3.1 Chemistry

All of the synthesized compounds were derived from quinoline.

The chemistry and physico-chemical properties of quinoline have been described very well [33]. The synthesis of compounds **1-12** is shown in Scheme 1. New and/or more advantageous preparations of some compounds were described recently [18]. The main starting material **1** was obtained by means of condensation between but-3-en-2-one with 3-aminocyclohex-2-enone. Ketone **1** was reduced with Synhydride® to give racemic secondary alcohol **2**.

Radical oxidative bromination of ketone **1** using N-bromosuccinimide (NBS) yielded compounds **3** and **8**, nevertheless compound **8** was also obtained also by means of oxidation with 2,3-dichloro-5,6-dicyano-1,4-benzoquinone (DDQ).

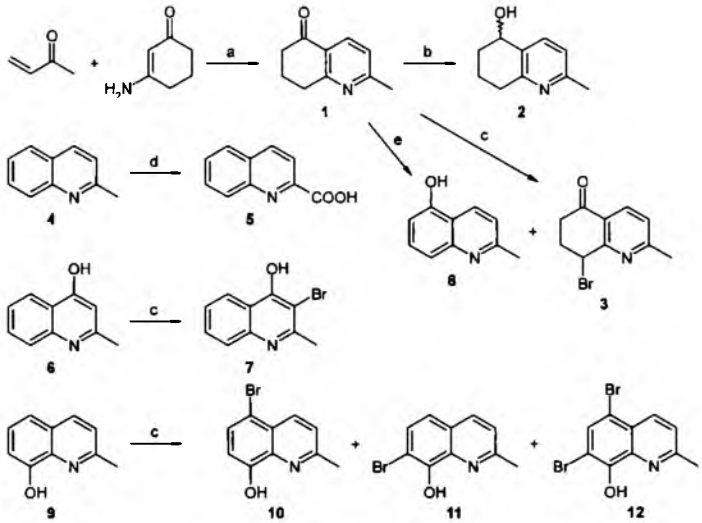

Scheme 1. Synthesis of compounds **1-12**: (a) DMF; (b) Synhydride, toluene; (c) NBS, dibenzoyl peroxide, CCl_4; (d) SeO_2, dioxan; (e) DDQ, dioxan.

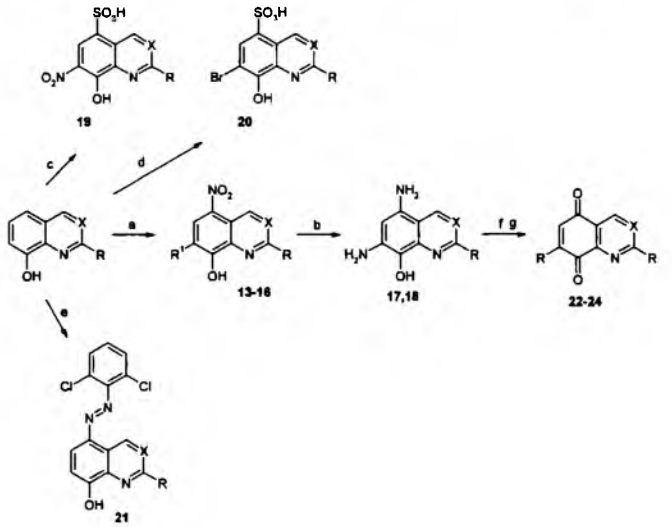

Scheme 2. Synthesis of compounds **13-24**: (a) HNO_3/H_2SO_4, 0°C; (b) H_2/Pd; (c) AcOH/NHO_3; (d) Br_2/MeOH; (e) 2,6-dichloroaniline/$NaNO_2$/HCl, 5°C; (f) AcOH; (g) $K_2Cr_2O_7$; (h) MeOH, heat.

Compounds **4**, **6** and **9** were further starting materials. Quinaldine (**4**) was oxidized using SeO_2 to acid **5**. Compounds **6** and **9** were oxidatively brominated using NBS and dibenzoyl peroxide to give compounds **7**, **10-12** [18].

8-Hydroxyquinoline, 8-hydroxyquinaldine and 8-hydroxyquinazoline were used as starting compounds in synthesis of drugs **13-24**, see Scheme 2. Nitration of these compounds yielded **13-16**. Subsequent hydrogenation yielded diamino derivatives **17**, **18**. These compounds in the next steps gave quinolinediones derivatives **22-24**. Methanolysis of **22** performed in hot MeOH generated compound **24**. Compounds **19**, **20** were obtained from 5-sulfo-8-hydroxyquinoline by gentle nitration or bromination respectively. The direct introduction of a diazonium salt derived from 2,6-dichloroaniline in 8-hydroxyquinaldine resulted in compound **21** [17,19]. A more comprehensive study on quinolinedione derivatives has been recently described [34,35].

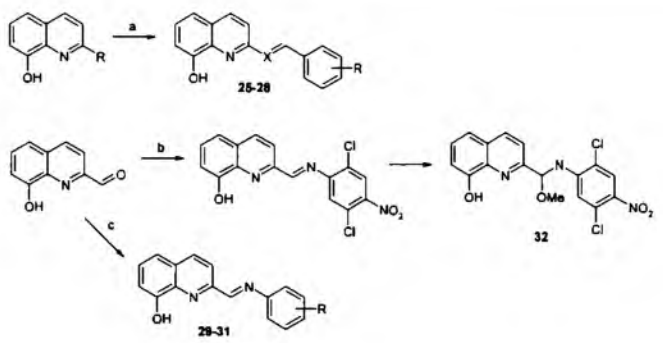

Scheme 3. Synthesis of compounds **25-32**: (a) aldehydes, SiO_2, microwave irradiation (R=NH_2: 4-hydroxybenzaldehyde, benzene, reflux 2 h. (b) 2,5-dichloro-4-nitro-aniline, MeOH, piperidine; (c) aniline, benzene, reflux 2 h.

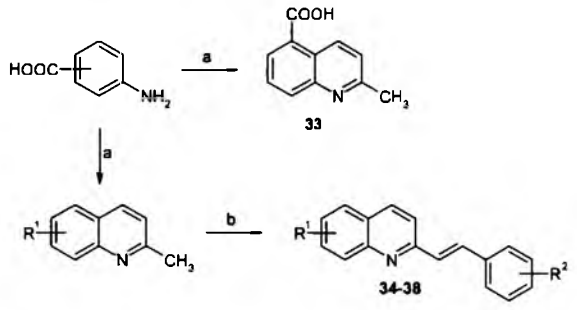

Scheme 4. Preparation of styrylquinoline derivatives **33-38**: (a) crotonaldehyde, HCl; (b) aldehyde, microwave irradiation.

Compounds **25-27** were obtained from 8-hydroxyquinaldine and the appropriate aldehydes using microwave assisted methods [14]. Azaanalogues of styrylquinolines **29-31** were obtained by means of condensation of 8-hydroxyquinoline-2-carbaldehyde with the appropriate aniline in dry benzene. Compound **28** was obtained according to this procedure from 2-amino-8-hydroxyquinoline and 4-hydroxybenzaldehyde. 8-Hydroxyquinoline-2-carbaldehyde with 2,5-dichloro-4-nitroaniline in methanol generated a Schiff base, which was transformed to compound **32**, see Scheme 3 [17,19,36].

Microwave assisted organic synthesis was used to obtain the group of styrylquinoline-like compounds **34-38**, see Scheme 4, while necessary quinaldines were synthesized from aromatic amines according to the Scraup synthesis *e.g.* compound **33** [19,37].

Compounds **39-49** were synthesized according to the procedure showed below [38,39]. The Kolbe-Schmidt reaction was used to generate the carboxylic acids which further reacted with the appropriate amine in presence of ethyldimethylaminopropyl carbodiimide (EDCI) to afford an amide. In case of **48**, **49** diamine and twofold of quinaldic acid were used, see Scheme 5.

3.2 Lipophilicity

Chromatographic behaviour and hydrophobicity of quinoline derivatives have not been previously studied to a large extent. Only some QSAR or RP-TLC studies of variously substituted quinolines or substituted 4(1H)-quinolinones have been reported [40,41]. A number of chromatographic studies of diazine hydrophobicity were found. Some groups used a C_{18} chromatographic column with a methanol–water mobile phase to obtain log k_w, *i.e.* the retention factor extrapolated to 0% organic modifier, as an alternative to log *P* [42]. The log k_w is obtained by performing several measurements varying the ratio of water to organic solvent. Nevertheless, determination of log k_w has some disadvantages. Determination of log k_w is time consuming due to a number of measurements before the calculation of log k_w [43]. The conditions (non-buffered mobile phase) were chosen with respect to conditions of biological systems, which are performed mostly under neutral (pH ~ 7) or weakly acidic conditions. Molecules are transported through cellular membranes in organisms in similar environments. The lipophilicity data can be strongly influenced by intramolecular interactions under the applied chromatographic conditions [44-47].

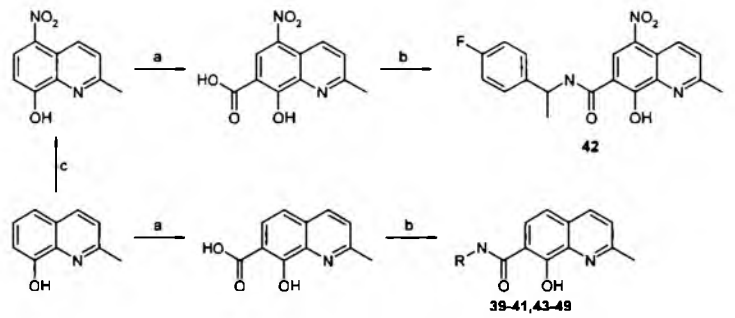

Scheme 5. Synthesis of compounds **39-49**: (a) KOH, CO_2; (b) amine, EDCI; (c) HNO_3/H_2SO_4, 0°C.

Therefore, in this study, the measurements were performed using methanol to water (55:45) as the mobile phase. Log *k* derived from RP-HPLC retention factors and computational log *P* values are given in Tables 1-4.

Hydrophobicities (log *P*/Clog *P* values) of all the studied compounds were calculated using available programs and measured by means of RP-HPLC determined retention factors *k* (log *k*). The results are shown in Tables 1-4. All of the hydrophobicity data of the individual compounds are illustrated in Figs. 2-4 and they are ordered according to increasing experimental log *k* values.

Log *P* is the logarithm of the partition coefficient in a biphasic system (*e.g.* *n*-octanol/water), defined as the ratio of a compound concentration in both organic/inorganic phases. The log *P* is, according to definition determined for the uncharged species of the drug. Clog *P* values represent the logarithm of the n-octanol/water partition coefficient based on established chemical interactions. Log *k* is the logarithm of the retention factors (*e.g.* capacity factor *k*) in chromatographic approaches, which is related to the partitioning of a compound between a mobile and a (pseudo-) stationary phase. The procedure is most frequently performed under isocratic conditions with an organic modifier in the mobile phase using an end-capped non-polar C_{18} stationary RP column. Log *k* can be used as the lipophilicity index converted to log *P* scale [24]. An excellent review on the effect of the stationary and mobile phase has been published by van der Waterbeemd *et al.* [22] and, more recently, by Claessens *et al.* [25].

Lipophilicity computing software can usually calculate log *P* and Clog *P* Log *P* is calculated for the uncharged molecules. Note that compounds presented in this work may exist preferably in the ionic or zwitterionic form(s). In these cases traditional methods of computing log *P* can provide errors and misleading values. The software calculates log *P* as lipophilicity contributions/increments of individual atoms, fragments and pair of interacting fragments in the chemical structure, *i.e.* increments of carbon and hetero atoms, aromatic systems and functional groups. Every software calculates lipophilicity contributions according to different internal databases/ libraries. Therefore values of computed lipophilicities are dependent on the used software, and the values for individual compounds may be different. This fact as well as various ionic/zwitterionic forms and intramolecular interactions may cause differences between computed and experimentally determined lipophilicities. It should be noted that for compounds discussed in this paper with values of log *P* obtained using different software, the log *P* values correlate to each other with r^2=0.6. With this in mind, it is very difficult to perform any SAR predictions on the basis of such data.

The results obtained for the compounds **1-49** show that the experimentally determined lipophilicities (log *k* values) are lower than those indicated by the calculated log *P*/Clog *P*, see Tables 1-4 and Schemes 2-4. The program ChemOffice has not resolved various lipophilicity values of individual positional isomers, *e.g.* compounds **10**, **11** or **29-31**, respectively. The program calculating the miLog *P* values did not resolve hydrophobicities of individual isosters, see compounds **15** and **16**.

All compounds showed differences between experimental and calculated lipophilicity values which are probably caused by interactions of the substituents with heteroatoms in the individual compounds. The lipophilicity of all the discussed 8-hydroxyquinoline derivatives may be modified by an intramolecular hydrogen bond between the quinoline nitrogen and the phenolic moiety. The lipophilicity of further hydroxyquinoline derivatives may be modified by the keto-enol tautomerism, see Schemes 3, 4 [48].

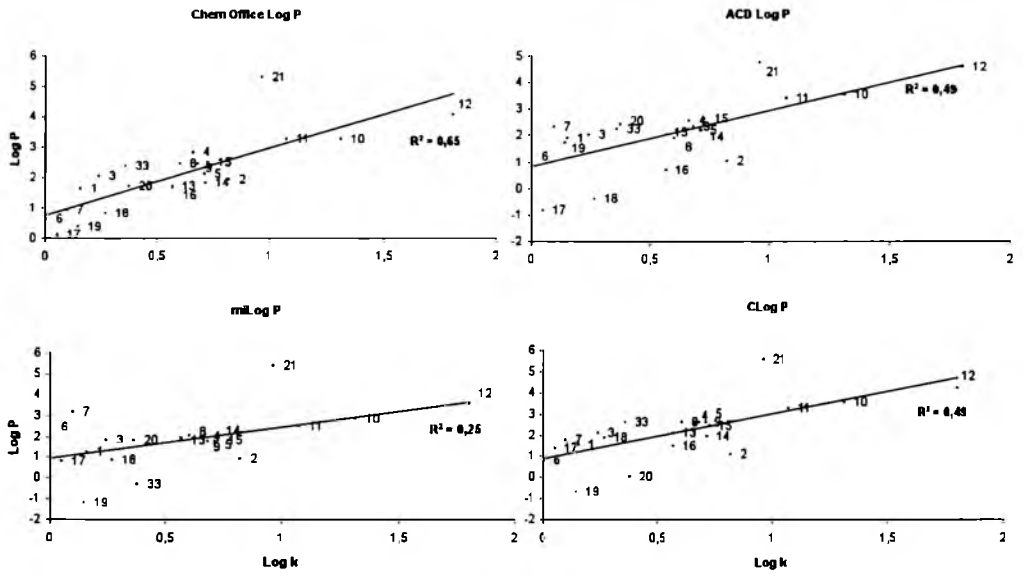

Figure 2. Comparison of the calculated log *P*/Clog *P* data using the three programs with the experimentally found log k values of compounds **1-21.** The compounds are ordered according to increasing experimental log *k* values.

Low hydrophobicity of quinolinediones derivatives **22-24** (Table 2) forced us to use different lipophilicity measurement conditions (MeOH/H_2O : 50/50). When conditions of MeOH to H_2O : 55/45 were used, the compounds were eluted from the column within hold-up time. The lowest lipophilicity was expected for these compounds of all the quinoline derivatives. This fact is probably caused by the presence of the diketone moiety as well as the second nitrogen atom in the quinoline ring.

The results of the compounds **1-21** (Fig. 2) show that the experimentally determined log *k* values correlate best with the lipophilicity data (log *P*) computed using ChemOffice software (r^2=0.65). In This set of compounds **21** is an anomaly and correlation without this structure can be improved (r^2=0.77 for ChemOffice). Other programs did not give reasonable data for this compound (correlation below 0.5) and miLog *P* provided the worst result (r^2=0.2).

As expected, compound **12** possessed the highest hydrophobicity, while unexpectedly compound **6** showed the lowest lipophilicity. This compound exists as 2-methyl-1H-quinolin-4-one, see Scheme 4. This fact corresponds with the following results, keto derivative **1** possesses lower lipophilicity than hydroxy derivative **2**. As expected, bromo derivatives **3** and **7** showed higher hydrophobicity than the unsubstituted compounds **1** and **6**. A large difference between all the experimental and calculated lipophilicity parameters could be observed for the compounds **2** and **8**. Hydroxy derivative **2** shows higher lipophilicity according to log *k* than 2-methyl-quinolin-5-ol (**8**) but according to the calculated data compound **8** seems to be much more hydrophobic.

According to all the calculated and experimental data a carboxylic acid moiety in position $C_{(5)}$, compound **33**, decreases the lipophilicity much more than carboxylic acid moiety in position $C_{(2)}$, compound **5**. Quinaldine (**4**) is less hydrophobic than quinaldine acid (**5**) according to experimental log *k*, contrary to all the calculated data.

The quinaldine phenolic derivatives **6** and **8** showed lower lipophilicity than quinaldine (**4**), only 8-hydroxyquinaldine (**9**) possessed higher hydrophobicity. Unsubstituted 8-hydroxyquinaldine (**9**) showed a log *k* value in the middle of the series of the compounds **9-21**. Compound **17** showed the lowest lipophilicity within this series.

Compounds substituted by bromine atoms or azoderivatives showed the highest lipophilicity in the series of the discussed compounds. Diamino substituted compounds **17** and **18** possess lower lipophilicity than dinitro substituted compounds **14** and **15**, as expected. Quinoline derivatives **14** and **16** show lower hydrophobicity than quinaldine derivatives **15** and **18**. Subsequent substitution by the second nitrogen atom

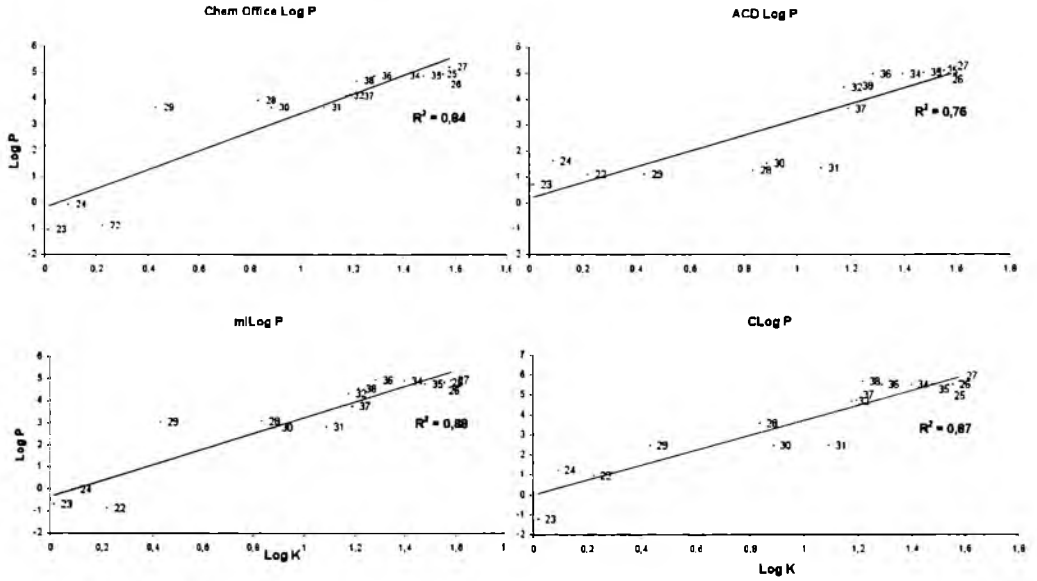

Figure 3. Comparison of the calculated log *P*/Clog *P* data using the three programs with the experimentally found log k values of compounds **25-38.** The compounds are ordered according to increasing experimental log *k* values.

in the position $C_{(3)}$ causes a decrease in lipophilicity, see compounds **15** and **16**. The sulfonic moiety in compounds **19** and **20** causes significant decrease in hydrophobicity, as expected.

7-Bromo-2-methylquinolin-8-ol (**11**) shows lower lipophilicity than 5-bromo-2-methylquinolin-8-ol (**10**). This fact may be probably caused by an interaction of the $C_{(7)}$-bromine substitution with $C_{(8)}$-phenolic moiety.

The electronic effects from the bromine atom in the $C_{(7)}$ position compared to the electronic effects of bromine in the $C_{(5)}$ position differ in their influence on the vicinal phenolic oxygen [45-46] and influence the resultant lipophilicity of compound **11**. These differences cannot be explained more precisely on the basis of the results presented here. Similarly the differences observed for compounds **6, 8** and **9** seem to be the effect of hydrogen bonding (**8** *vs.* **9**) or tautomeric forms (**6** *vs.* **8, 9**).

A large difference between the experimental and calculated lipophilicity parameters could be observed for compound **21**. Azoderivative **21** according to all the calculated data seems to be the most hydrophobic within this series which is in contrary with log *k*. This can be only explained by a strong tendency to form a less hydrophobic 5,8-diene- tautomeric structure, as we reported recently [17].

The results of compounds **25-38** (Scheme 2) show that the experimentally determined log *k* values correlate best with milog *P* values calculated according to the molinspiration service. ACD/LogP provided the poorest results for this set of compounds. Structure **29** is an anomaly and correlation without this compound gives and R^2 = 0.95 for miLogP and an R^2 = 0.92 for ChemOffice.

The experimental lipophilicity parameters specify lipophilicity within individual series of compounds **25-27** (3-Cl, 4-Cl, 4-Br), as well as **29-31** (2-OH, 3-OH, 4-OH). Compounds **29-31** possess much less lipophilicity than other styrylquinoline derivatives. This fact is caused by the presence of the nitrogen atom in the olefinic linker. 2-[(2-Hydroxyphenylimino)methyl]quinolin-8-ol (**29**) is much less lipophilic than indicated by the calculated lipophilicity. This fact is probably caused by the interaction of the imine nitrogen with the phenolic moiety in the styryl part of the molecule. Log *k* of **29** equals half of the values of compound **28** or **30** while their calculated log *P* are approximately the same. From this point it can be assumed, that the difference between calculated and measured lipophilicity is caused by two intramolecular hydrogen bonding centres in **29**.

As expected, carboxylic acids of the styrylquinoline derivatives showed lower lipophilicity than

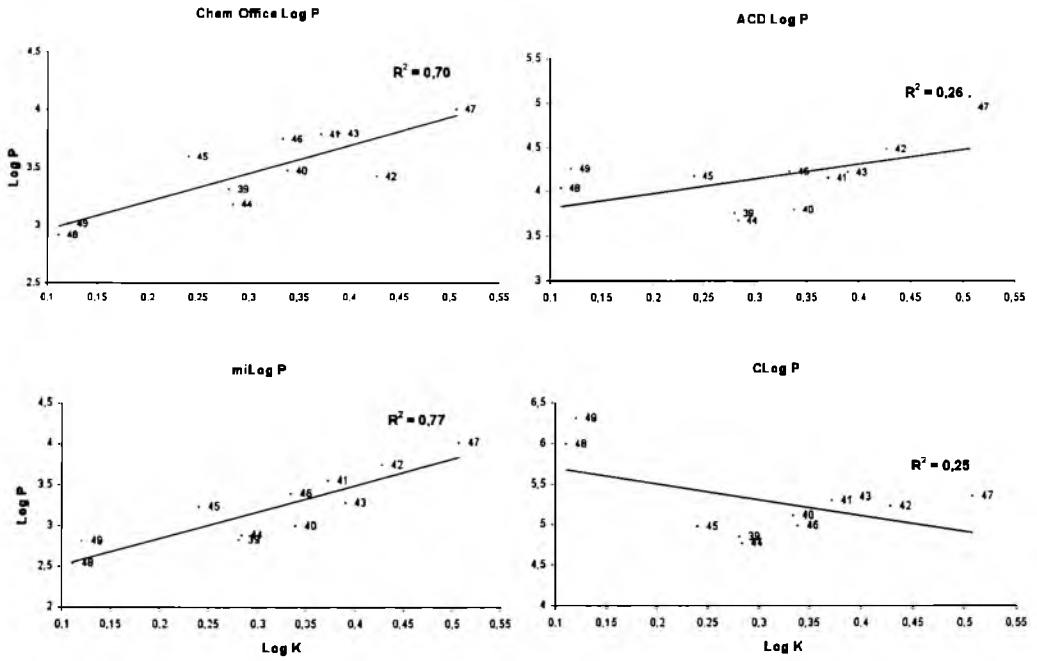

Figure 4. Comparison of the calculated log *P*/Clog *P* data using the three programs with the experimentally found log k values of compounds **39-49.** The compounds are ordered according to increasing experimental log *k* values.

styrylquinolines **25-27**. Compounds **37** and **38** showed the lowest hydrophobicity than other carboxylic acid derivatives due to substitution by a methoxy moiety in the phenyl ring (compound **36**) or the presence of two carboxylic acid groups in quinoline (compound **38**).

The structure-lipophilicity relationships of compound **32** cannot be discussed in connection with other compounds due to large differences in its substituents.

The results of compounds **39-49** (Fig. **4**) show that the experimentally determined log *k* values correlate approximately with the computed miLog *P* (R^2=0.77) data and log *P* values using ChemOffice software (R^2=0.7). Clog *P* values calculated by ChemOffice software and ACD/LogP program do not agree with the target compounds **39-49** (r^2 <<0.5). It is notewothy that in the results from ACD and ClogP, compounds **48** and **49** can be regarded as anomalies. Especially the Clog *P* values for those structures which are much higher than the measured lipophilicity.

The lipophilicity (log *k* data) of the substituents in the amide part of the molecules increases from benzyl (**45**) < phenyl (**39**) < n-propylphenyl (**47**), as expected. Lower lipophilicity of the benzyl substituent than the phenyl substituent was also described in [49]. Compound **47** possessed the highest hydrophobicity within this series.

Lipophilicity (log *k* data) of phenyl substituents increases H < OCH_3 < F < CH_3. Great differences between the experimental and calculated lipophilicity parameters could be observed for compounds **45** and **44**. Compound **45** (benzyl derivative) showed low lipophilicity, but according to the calculated data it seems to be much more hydrophobic. The compound **44** (4-methoxyphenyl derivative) possesses higher lipophilicity than derived from the calculated data.

Low lipophilicity of both dimers 48 and 49 is interesting. Both dimers showed the lowest hydrophobicity (log *k* data) contrary to the calculated data. However it is noteworthy here that for compounds **39-47** differences between measured and calculated lipophilicities are roughly the same. This suggests that one major effect plays a crucial role for all compounds in this group. This is likely due to hydrogen bonding between $C_{(8)}$-OH and the carbonyl C=O and consequently keto-enol tautomerism as should be expected [50-52]. For compounds **48** and **49**, where two such groups exist, the discussed differences are nearly twofold (**39** and **45** *vs.* **48** and **49**).

4. Conclusions

Forty-nine quinoline based compounds possessing significant antifungal and herbicidal activities as well as interesting HIV-integrase inhibiting activity were prepared. Hydrophobicity (log *k*) of all the target compounds was determined by means of RP-HPLC methods for lipophilicity measurement. All the compounds can be divided into four groups according to their structure. Lipophilicity of hydroxyquinoline derivatives may be modified by keto-enol tautomerism. The keto-form of the hydroxyquinolines resulted in a decrease of lipophilicity compared with enol-form. The lipophilicity of all the discussed 8-hydroxyquinoline derivatives is modified by an intramolecular hydrogen bond between the quinoline nitrogen and the phenolic moiety. As was shown, log *k* correlates relatively poorly with calculated lipophilicity of compounds within each series. Nevertheless, it can be assumed that the calculated values of log *P* correlate best within congeneric series of structurally similar compounds. For styrylquinolines correlation of log *k* and calculated lipophilicity reach reasonable levels (r^2 above 0.9). The more diverse the set of compounds, the worse the correlation. This can be seen in the first series. Intramolecular effects such as hydrogen bonding and tautomeric forms can also affect lipophilicity. Popular computer programs that provide tool for calculating log *P* cannot recognize specific strutural features and generate poor results. In quinoline based hydroxylated compounds these effects play a crucial role. The lipophilicity data we have obtained confirm strong influence of intramolecular interactions. All the discussed compounds show relatively low lipophilicity. General structures of small 8-hydroxyquinoline derivatives and styrylquinolines substituted by bromine atoms possess the highest hydrophobicity, compared with the compounds substituted by sulfonic or amino moieties. N-substituted carbamoyl groups show low lipophilicity as well. An introduction of the second nitrogen atom to the position $C_{(3)}$ of the quinoline ring (quinazoline isoster) or the presence of the nitrogen atom in the olefinic linker of styrylquinolines or the quinone moeity itself, causes a decrease in lipophilicity. Experimentally determined log *k* data determine lipophilicity within the series of compounds.

References

[1] H.J. Roth, H. Fenner Iarzneistoffe, 3rd edition (Deutscher Apotheker Verlag, Stuttgart, 2000) 51
[2] C.R. Harris, A. Thorarensen, Curr. Med. Chem. 11, 2213 (2004)
[3] K. Andries, P. Verhasselt, J. Guillemont, H.W. Gohlmann, J.M. Neefs, H. Winkler, J. Van Gestel, P. Timmerman, M. Zhu, E. Lee, P. Williams, D. de Chaffoy, E. Huitric, S. Hoffner, E. Cambau, C. Truffot-Pernot, N. Lounis, V. Jarlier, Science 307, 223 (2005)
[4] S. Vangapandu, M. Jain, R. Jain, S. Kaur, P.P. Singh, Bioorg. Med. Chem. 12, 2501 (2004)
[5] C. Sissi, M. Palumbo, Curr. Med. Chem. Anti-Canc. Agents 3, 439 (2003)
[6] E. Bossu, A.M. Agliano, N. Desideri, I. Sestili, R. Porra, M. Grandilone, M.G. Quaglia, J. Pharm. Biomed. Anal. 19, 53 (1999)
[7] T.C. Ko, M.J. Hour, J.C. Lien, C.M. Teng, K.H. Lee, S.C. Kuo, L.J. Huang, Bioorg. Med. Chem. Lett. 11, 279 (2001)
[8] J. Jampilek, M. Dolezal, J. Kunes, P. Vichova, D. Jun, I. Raich, R. O´Connor, M. Clynes, J. Pharm. Pharmacol. 56, 783 (2004)
[9] J. Jampilek, M. Dolezal, J. Kunes, P. Vichova, D. Jun, I. Raich, R. O´Connor, M. Clynes. Curr. Org. Chem. 8, 1235 (2004)
[10] J. Jampilek, M. Dolezal, V. Opletalova, J. Hartl. Curr. Med. Chem. 13, 117 (2006)
[11] J.L. Marco, C.M. Carmo, Mini Rev. Med. Chem. 3, 518 (2003)
[12] K. Mekouar, J.-F. Mouscadet, D. Desmaele, F. Subra, H. Leh, D. Savoure, C. Auclair, J. d'Angelo, J. Med. Chem. 41, 2846 (1998)
[13] J. Polanski, F. Zouhiri, L. Jeanson, D. Desmaele, J. d'Angelo, J-F. Mouscadet, R. Gieleciak, J. Gasteiger, M. Le Bret. J. Med. Chem. 45, 4647 (2002)
[14] J. Polanski, H. Niedbala, R. Musiol, D. Tabak, B. Podeszwa, R. Gieleciak, A. Bak, A. Palka, T. Magdziarz, Acta Polonia Pharm. Drug Res. 61, 3 (2004)
[15] Y. Pommier, A.A. Johnson, C. Marchand, Nat. Rev. Drug. Discov. 4, 236 (2005)
[16] F. Zouhiri, D. Danet, C. Bernard, M. Normand-Bayle, J. F. Mouscadet, H. Leh, C.M. Thomas, G. Mbemba, J. d'Angelo, D. Desmaele, Tetrahedron Lett. 46, 2201 (2005)

[17] R. Musiol, J. Jampilek, V. Buchta, L. Silva, H. Niedbala, B. Podeszwa, A. Palka, K.A. Majerz-Maniecka, B. Oleksyn, J. Polanski, Bioorg. Med. Chem. 14, 3592 (2006)
[18] J. Jampilek, M. Dolezal, J. Kunes, V. Buchta, K. Kralova, Med. Chem. 1, 591 (2005)
[19] R. Musiol, J. Jampilek, K. Kralova, D.R. Richardson, D. Kalinowski, B. Podeszwa, J. Finster, H. Niedbala, A. Palka, J. Polanski, Bioorg. Med. Chem. 15, 1280 (2007)
[20] C.A. Lipinski, F. Lombardo, B.W. Dominy, P.J. Feeney, Adv. Drug. Delivery Rev. 23, 4 (1997)
[21] A. Avdeef, Curr. Topics Med. Chem. 1, 277 (2001)
[22] V. Pliska, In V. Pliska, B. Testa, H. van der Waterbeemd (Eds.), Lipophilicity in Drug Action and Toxicology (Wiley-VCH, New York, 1996) 1
[23] S. Gocan, G. Cimpan, J. Comer, Adv. Chromatogr. 44, 79 (2006)
[24] K. Valko, C.M. Du, C. Bevan, D.P. Reynolds, M.H. Abraham, Curr. Med. Chem. 8, 1137 (2001)
[25] G. Cimpan, F. Irimie, S. Gocan, H.A. Claessens, J. Chromatogr. B 714, 247 (1998)
[26] T. Hartmann, J. Schmitt, Drug Disc. Today Technol. 1, 431 (2004)
[27] A. Nasal, D. Siluk, R. Kaliszan, Curr. Med. Chem. 10, 381 (2003)
[28] www.molinspiration.com
[29] J.A. Rothwell, A.J. Day, M.R.A. Morgan, J. Agric. Food Chem. 53, 4355 (2005)
[30] P. Ertl, P. Selzer, J. Muehlbacher, Drug Discov. Today 2, 201 (2004)
[31] G.G. Nys, R.F. Rekker, Chim. Ther. 8, 521 (1973)
[32] G.G. Nys, R.F. Rekker, Chim. Ther. 9, 361 (1974)
[33] J. Cioslowski, A.Szarecka, D.Moncrieff, Molecular Physics 101, 1221 (2003)
[34] B. Podeszwa, R. Musiol, D. Tabak, J. Finster, J. Polanski, H. Niedbala, A. Palka, Polish Patent Application P 380818 (2006)
[35] B. Podeszwa, H. Niedbala, J. Polanski, R. Musiol, D. Tabak, J. Finster, K. Serafin, M. Milczarek, J. Wietrzyk, S. Boryczka, W. Mol, J. Jampilek, J. Dohnal, D. Kalinowski, D.R. Richardson, Bioorg. Med. Chem. Let. 17, 6138 (2007)
[36] K.A. Majerz-Maniecka, R. Musiol, W. Nitek, B.J. Oleksyn, J. Polanski, Bioorg. Med. Chem. Lett. 16, 1005 (2005)
[37] R. Musiol, B. Podeszwa, J. Finster, H. Niedbala, J. Polanski, Monatsh. Chem. 137, 1211 (2006)
[38] R. Musiol, D. Tabak, H. Niedbala, B. Podeszwa, J. Jampilek, K. Kralova, J. Dohnal, J. Finster, A. Mencel, J. Polanski, Bioorg. Med. Chem. 16, 4490 (2008)
[39] J. Polanski, H. Niedbala, R. Musiol, B. Podeszwa, D. Tabak, A. Palka, A. Mencel, J.-F. Mouscadet, M. Le Bret, Letters in Drug Design and Discovery 4, 99 (2007)
[40] M. Yoshimoto, C. Hansch, J. Med. Chem. 19, 71 (1976)
[41] W.D. Warner, J.D. Musto, J.N. Sane, K.H. Kim, G.L. Grunewald, J. Med. Chem. 20, 92 (1977)
[42] G. Piraprez, M.F. Herent, S. Collin, Flavour Fragr. J. 13, 400 (1998)
[43] K. Valko, J. Chromatogr. A 1037, 299 (2004)
[44] C. Yamagami, N. Takao, Chem. Express. 6, 113 (1991)
[45] C. Yamagami, K. Iwasaki, A. Ishikawa. Chem. Pharm. Bull. 45, 1953 (1997)
[46] C. Yamagami, K. Araki, K. Ohnishi, K. Hanasato, H. Inaba, M. Aono, A. Ohta, J. Pharm. Sci. 88, 1299 (1999)
[47] C. Yamagami, K. Kawase, K. Iwaki, Chem. Pharm. Bull. 50, 1578 (2002)
[48] M.H. Palmer, The Structure and Reactions of Heterocyclic Compounds (Edward Arnold Publisher Ltd., London, 1967) 105
[49] J. Jampilek, J. Vinsova, J. Dohnal, In J.A. Seijas, M.P. Vázquez-Tato (Eds.), Electronic Conference on Synthetic Organic Chemistry, November 1-30, 2005 (MDPI, Basel, Switzerland, 2005) A008
[50] J.D. Geerlings, C.A.G.O. Varma, J. Photochem. Photobiol. A. 129, 129 (1999)
[51] M. Albrecht, K. Witt, R. Frohlich, O. Kataeva, Tetrahedron 58, 561 (2002)
[52] A. Koll, A. Karpfen, P. Wolschann, J. Mol. Struct. 790, 55 (2006)

Polyhedron 28 (2009) 493–500

Contents lists available at ScienceDirect

Polyhedron

journal homepage: www.elsevier.com/locate/poly

Synthesis, spectroscopic characterization, crystal and molecular structure of [ReOBr(hmquin-7-COOH)$_2$] and [ReOCl(hmquin-7-COOH)$_2$] · MeCN complexes. DFT and TD-DFT calculations for [ReOBr(hmquin-7-COOH)$_2$]

B. Machura [a,*], J. Kusz [b], D. Tabak [c], R. Kruszynski [d]

[a] Department of Crystallography, Institute of Chemistry, University of Silesia, 9th Szkolna St., 40-006 Katowice, Poland
[b] Institute of Physics, University of Silesia, 4th Uniwersytecka St., 40-006 Katowice, Poland
[c] Department of Organic Chemistry, Institute of Chemistry, University of Silesia, 9th Szkolna St., 40-006 Katowice, Poland
[d] Department of X-ray Crystallography and Crystal Chemistry, Institute of General and Ecological Chemistry, Lodz University of Technology, 116 Żeromski St., 90-924 Łódź, Poland

ARTICLE INFO

Article history:
Received 21 August 2008
Accepted 26 November 2008
Available online 2 January 2009

Keywords:
Rhenium oxo complexes
Quinoline ligands
X-ray and electronic structure
DFT calculations
NBO analysis

ABSTRACT

Novel [ReOBr(hmquin-7-COOH)$_2$] (**1**) and [ReOCl(hmquin-7-COOH)$_2$] · MeCN (**2** · MeCN) complexes have been prepared by treatment of [ReOX$_3$(AsPh$_3$)$_2$] with an excess of 8-hydroxy-2-methylquinoline-7-carboxylic acid in acetonitrile. The compounds were characterized structurally and spectroscopically. The electronic structure of **1** has been calculated with the density functional theory (DFT) method, and additional information about binding has been obtained by NBO analysis. The UV–Vis spectrum of **1** has been discussed on the basis of TDDFT calculations.

1. Introduction

There is considerable interest in the chemistry of inorganic compounds containing an oxygen atom that is multiply bonding to a transition metal in a high oxidation state. These compounds can transfer an oxygen atom to reductants such as phosphines, sulfides, and alkenes. For many years they have been in the centre of interest to those scientists engaged in basic research and to those trying to employ these complexes in catalytic processes. Oxygen atom transfer chemistry has been implicated in various reactions of industrial and biological importance, including olefin epoxidation and catalysis by cytochrome P-450 [1–3].

The chemistry of oxo rhenium complexes arouses particular interest among these compounds. Methyltrioxorhenium and its derivatives are among the most versatile oxidation catalysts known to date [4]. The oxorhenium(V) chelates [ReOCl$_2$(O–N)(PPh$_3$)] with pyridinecarboxylate ligands exhibit a remarkable catalytic activity for the conversion of ethane, under relatively mild conditions, to a mixture of propionic and acetic acids in a single-pot process with various advantages over the industrial ones [5]. The [CH$_3$ReO(pic)$_2$] complex is an active precursor in olefin oxidation and forms epoxides in a two-phase H_2O_2–H_2O/CH_2Cl_2 system [6].

Furthermore, favourable nuclear properties of ^{186}Re and ^{188}Re nuclides make the compounds with these radioisotopes useful for applications in radioimmunotherapy [7,8].

In this context, the design, synthesis and reactivity of novel rhenium oxocomplexes has become the aim of several laboratories, including ours.

Previously, we investigated structural and spectroscopic properties of [ReOX(hqn)$_2$] and [ReOX(quin-2-c)$_2$] (Hhqn = 8-hydroxyquinoline, quin-2-cH = quinoline-2-carboxylic acid) [9,10]. As an extension of this work, we chose 8-hydroxy-2-methylquinoline-7-carboxylic acid (Hhmquin-7-COOH) as a ligand. Potentially, Hhmquin-7-COOH can act as a bidentate, tridentate or bridging ligand. As a chelate 8-hydroxy-2-methylquinoline-7-carboxylic acid can bind to the metal centre through the pyridine nitrogen and the deprotonated hydroxyl group (N,O-chelation) or through the carboxylate group and the deprotonated hydroxyl group (O,O-chelation).

X-Ray and spectroscopic studies for [ReOBr(hmquin-7-COOH)$_2$] (**1**) and [ReOCl(hmquin-7-COOH)$_2$]·MeCN (**2** · MeCN) confirm N,O-chelation of the hydroxy-2-methylquinoline-7-carboxylic acid. The COOH group of the Hhmquin-7-COOH in the examined complexes is available for further conjugation.

For complex **1** the nature of the frontier orbitals and the electronic transitions involved in the absorption spectrum have been

* Corresponding author.
E-mail addresses: basia@ich.us.edu.pl (B. Machura), rafal.kruszynski@p.lodz.pl (R. Kruszynski).

0277-5387/$ - see front matter © 2008 Elsevier Ltd. All rights reserved.
doi:10.1016/j.poly.2008.11.053

studied by means of density functional and time-dependent density functional calculations. Gancheff and co-workers [11] have performed extended tests of the ability of the B3LYP method in LANL2DZ basis set for rhenium compounds in a geometry optimization and calculation of spectral properties. Although this is not a very extended basis set, its use with DFT has shown to be sufficient for the geometry optimization and calculation of spectral properties. The correctness of B3LYP method with LANL2DZ basis set for rhenium complexes has been also proven in this paper. The experimental geometry of [ReOBr(hmquin-7-COOH)$_2$] is well reproduced and the calculated electronic spectrum is in good accordance with the experimental one.

2. Experimental

2.1. General procedure

The [ReOX$_3$(AsPh$_3$)$_2$] (X = Cl, Br) complexes were synthesised according to the literature methods [12]. 8-hydroxy-2-methylquinoline-7-carboxylic acid was prepared as reported previously [13].

IR spectra were recorded on a Nicolet Magna 560 spectrophotometer in the spectral range 4000–400 cm^{-1} with the samples in the form of KBr pellets. Electronic spectra were measured on a spectrophotometer Lab Alliance UV–Vis 8500 in the range 1000–180 nm in acetonirile solution. Elemental analyses (C H N) were performed on a Perkin–Elmer CHN-2400 analyzer.

2.2. Preparation of [ReOBr(hmquin-7-COOH)$_2$](1)

[ReOBr$_3$(AsPh$_3$)$_2$] (0.5 g, 0.47 mmol) was added to 8-hydroxy-2-methylquinoline-7-carboxylic acid (0.28 g, 1.38 mmol) in acetonitrile (50 ml) and the reaction mixture was refluxed for 6 h. The resulting solution was allowed to cool to room temperature and reduced in volume to ~10 ml. A greenish-brown crystalline precipitate of **1** was filtered off and dried in the air. Yield 75%.

Single crystals of **1** were obtained by recrystallization from acetonitrile.

Anal. Calc. for $C_{22}H_{16}N_2O_7BrRe$: C, 38.49; H, 2.35; N, 4.08. Found: C, 38.35; H, 2.43; N, 4.37%.

2.3. Preparation of [ReOCl(hmquin-7-COOH)$_2$] · MeCN (2 · MeCN)

A procedure similar to that for **1** was used with [ReOCl$_3$(AsPh$_3$)$_2$] (0.5 g, 0.54 mmol) and 8-hydroxy-2-methylquinoline-7-carboxylic acid (0.28 g, 1.38 mmol). Crystalline precipitate of **2** · MeCN was collected in 70% yield.

Anal. Calc. for $C_{24}H_{19}N_3O_7ClRe$: C, 42.20; H, 2.80; N, 6.15. Found: C, 42.98; H, 2.68; N, 6.81%.

2.4. Crystal structures determination and refinement

The X-ray intensity data of **1** and **2** · MeCN were collected on a KM-4-CCD automatic diffractometer equipped with CCD detector and graphite monochromated Mo Kα radiation (λ = 0.71073 Å) at temperature of 293(2) K. Details concerning crystal data and refinement are given in Table 1. Lorentz, polarization and empirical absorption correction using spherical harmonics implemented in SCALE3 ABSPACK scaling algorithm [14] were applied. The structures were solved by the Patterson method and subsequently completed by the difference Fourier recycling. All the non-hydrogen atoms were refined anisotropically using full-matrix, least-squares technique. The hydrogen atoms were treated as 'riding' on their adjacent atoms and assigned isotropic temperature factors equal 1.2 times the value of equivalent temperature factor of the aromatic parent atoms and equal 1.5 times the value of equivalent temperature factor of the methyl parent carbon atom and oxygen atom (OH). SHELXS97 [15], SHELXL97 [16] and SHELXTL [17] programs were used for all the calculations. Atomic scattering factors were those incorporated in the computer programs.

Table 1
Crystal data and structure refinement for **1** and **2** · MeCN complexes.

	1	2 · MeCN
Empirical formula	$C_{22}H_{16}N_2O_7BrRe$	$C_{24}H_{19}N_3O_7ClRe$
Formula weight	686.48	683.07
Temperature	293(2) K	293(2) K
Wavelength	0.71073 Å	0.71073 Å
Crystal system	triclinic	triclinic
Space group	$P\bar{1}$	$P\bar{1}$
Unit cell dimensions	a = 7.5564(5) Å,	a = 7.5538(3) Å
	b = 9.8626(7) Å,	b = 10.3044(2) Å,
	c = 15.8327(11) Å	c = 16.3587(2) Å
	α = 92.417(6)°	α = 71.695(4)°
	β = 102.129(6)°	β = 77.391(4)°
	γ = 106.571(6)°	γ = 88.826(4)°
Volume	1099.11(13) Å^3	1178.14(5) Å^3
Z	2	2
D_{calc}	2.074 Mg/m^3	1.926 Mg/m^3
Absorption coefficient	7.393 mm^{-1}	5.322 mm^{-1}
F(000)	656	664
Crystal size	0.02 × 0.04 × 0.22 mm	0.03 × 0.15 × 0.48 mm
Θ range for data collection	2.89–25.00°	3.31–25.00°
Index ranges	$-5 \leqslant h \leqslant 8$	$-6 \leqslant h \leqslant 8$
	$-11 \leqslant k \leqslant 11$	$-12 \leqslant k \leqslant 12$
	$-18 \leqslant l \leqslant 18$	$-19 \leqslant l \leqslant 19$
Reflections collected	6981	7373
Independent reflections (R_{int})	3766 (0.0277)	4012 (0.0214)
Completeness to 2θ = 50°	97.4%	97.1%
Data/restraints/parameters	3766/0/302	4012/0/330
Goodness-of-fit on F^2	1.014	0.986
Final R indices [$I > 2\sigma(I)$]	R_1 = 0.0335	R_1 = 0.0209
	wR_2 = 0.0883	wR_2 = 0.0521
R indices (all data)	R_1 = 0.0468	R_1 = 0.0257
	wR_2 = 0.0994	wR_2 = 0.0533
Largest difference in peak and hole e Å^{-3}	0.982 and −1.516	1.017 and −0.880

2.5. Computational details

GAUSSIAN 03 program [18] was used in the calculations. The geometry optimization of [ReOBr(hmquin-7-COOH)$_2$] in a singlet state was carried out with the DFT method with the use of B3LYP functional [19,20]. The electronic spectrum of [ReOBr(hmquin-7-COOH)$_2$] was calculated with the TDDFT method [21], and the solvent effect was simulated using the polarizable continuum model with the integral equation formalism (IEF-PCM). The calculations were performed by using ECP basis set on the rhenium atom, the standard 6-31+G** basis for bromine, oxygen and nitrogen, 6-31G* for carbon and 6-31G for hydrogen atoms [22,23]. The Xe core electrons of Re were replaced by an effective core potential and DZ quality Hay and Wadt Los Alamos ECP basis set (LANL2DZ) [24] was used for the valence electrons. Additional d function with exponent α = 0.3811 and f function with exponent α = 2.033 on the rhenium atom were added [25]. The optimized geometry of **1** was verified by performing a frequency calculation. The vibrations in the calculated vibrational spectrum of **1** were real, thus the optimized geometry corresponds to true energy minimum.

Natural bond orbital (NBO) calculations were performed with the NBO code [26] included in GAUSSIAN 03.

3. Results and discussion

3.1. Preparation and infrared data

The [ReOX(hmquin-7-COOH)$_2$] (X = Cl, Br) complexes were prepared in high yields by a route analogous to that used for the

Table 2
Selected IR frequencies [cm^{-1}] values of [ReOBr(hmquin-7-COOH)$_2$] complexes.

Complex	ν(O–H)$_{COOH}$	ν(C=O)$_{COOH}$	ν(N=C)	ν(C–O)$_{COOH}$	ν(C–O)$_{OH}$	ν(Re=O)
[ReOBr(hmquin-7-COOH)$_2$]	3467	1660	1616	1368	1245	976
	3372		1550			
[ReOCl(hmquin-7-COOH)$_2$]	3467	1716	1620	1378	1235	978
	3358		1549			

synthesis of the [ReOX(hqn)$_2$] and [ReOX(quin-2-c)$_2$], namely by ligand exchange reactions starting from [ReOX$_3$(AsPh$_3$)$_2$] complexes and 8-hydroxy-2-methylquinoline-7-carboxylic acid in acetonitrile:

$$[ReOX_3(AsPh_3)_2] - 2Hhmquin - 7 - COOH \rightarrow [ReOX(hmquin - 7 - COOH)_2] + 2HX + 2AsPh_3$$

Table 3
Hydrogen bonds for **1** and **2** · MeCN complexes.

D	H	A	H···A (Å)	D···A (Å)	D–H···A (°)
1					
O3	H3	O2	0.82	2.589(8)	143.1
O6	H6A	O7#1	0.82	2.629(8)	160.2
C2	H2	O4#2	0.93	3.391(10)	169.8
C10	H10A	O1	0.96	2.882(11)	103.9
C10	H10B	O3#2	0.96	3.460(10)	170.9
C17	H17	O6	0.93	2.729(10)	101.1
2 · MeCN					
O4	H4	O7#3	0.82	2.724(4)	173.4
O6	H6A	O5	0.82	2.552(4)	152.8
C6	H6	O4	0.93	2.716(5)	100.0
C10	H10A	O1	0.96	2.884(5)	101.0
C13	H13	O3#4	0.93	3.263(5)	155.7
C14	H14	O3#5	0.93	3.317(5)	156.8
C98	H98C	O7#6	0.96	3.413(7)	147.8

Symmetry codes: #1 $-x, -y+1, -z+1$; #2 $x+1, y+1, z$; #3 $-x+2, -y+1, -z+2$; #4 $x-1, y, z$; #5 $-x+1, -y+1, -z+2$; #6 $x-1, y-1, z$.

They were isolated as greenish-brown microcrystalline solids, soluble in common organic solvents.

The selected frequencies observed in the IR spectra of [ReOX(hmquin-7-COOH)$_2$] complexes are collected in Table 2. The assignments are based on those found in the literature for related species [27,28]. Similar to the [ReOX(hqn)$_2$] complexes, the strong ν(Re=O) stretching bands of [ReOX(hmquin-7-COOH)$_2$] appear at ~975 cm^{-1}, in the range typical of six-co-ordinate complexes with a phenolic oxygen *trans* to Re=O [29]. A significant difference between complexes **1** and **2** can be noticed for ν(C=O)$_{COOH}$ stretching frequency. The ν(C=O)$_{COOH}$ stretching vibration of **1** is downshifted in comparison with ν(C=O)$_{COOH}$ for complex **2**. It is a result of delocalisation of CO bonds of the carboxylic group, observed for complex **1** and discussed in detail in crystal structure part (Table 3).

3.2. Crystal structures

The crystallographic data for **1** and **2** · MeCN are given in Table 1. The intermolecular interactions found in the examined structures are shown in the Table 2 [30,31] and Figs. 1 and 2.

The packing of molecules in crystal and in consequence hydrogen bonding scheme of compound **1** distinctly differ from these of compound **2** · MeCN. In compound **1** the medium strength intermolecular O–H···O bond create typical $N_1R_2^2(8)$ motif, but in **2** · MeCN $N_1R_2^2(24)$ motif is created. The intermolecular bonding scheme in both compound is identical (S(6) motif of O–H···O interactions) due to similarity of inner coordination spheres.

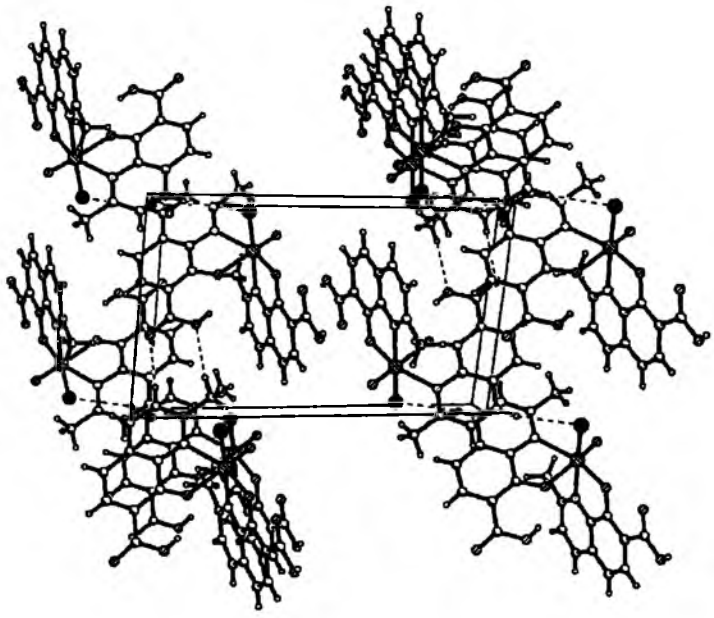

Fig. 1. Packing diagram of **1** showing the shortest intermolecular interactions.

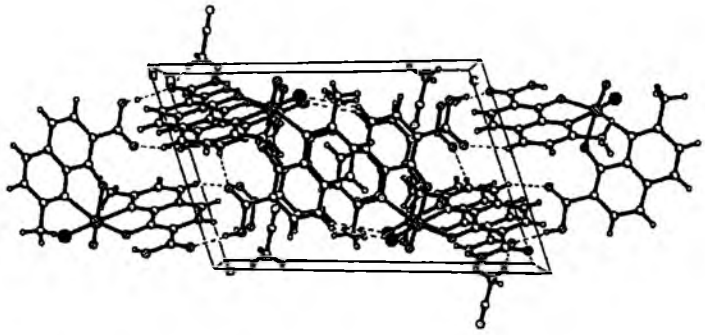

Fig. 2. Packing diagram of **2** · MeCN showing the shortest intermolecular interactions.

The molecular structure of $[ReOBr(hmquin\text{-}7\text{-}COOH)_2]$ is presented in Fig. 3, and the selected bond distances and angles of $[ReOX(hmquin\text{-}7\text{-}COOH)_2]$ complexes are collected in Tables 4 and 5, respectively.

The geometry of $[ReOX(hmquin\text{-}7\text{-}COOH)_2]$ compounds reveals typical features of quasi-octahedral oxorhenium(V)complexes with oxygenated bidentate ligands. For complex **1** the rhenium atom is displaced 0.3240 (28) Å from the equatorial plane formed by the two nitrogens, one oxygen and one bromide atoms (plane A) and 0.0730(30) and 0.0249(25) Å from the axial planes formed respectively by the three oxygen, one nitrogen atoms (plane B) and two oxygens, one bromide and one nitrogen atoms (plane C). Least squares plane A is inclined at 88.90(13)° to the plane B and at 89.81(12)° to the plane C. The planes B and C are inclined at 85.50(14)°. These values for chloride analogue are respectively 0.2916 (13), 0.0773 (13), and 0.0292(12) Å, 89.92(7) 89.25(5) and 83.92(7)°. Clear distortions of the pseudooctahedral environment of Re center in $[ReOX(hmquin\text{-}7\text{-}COOH)_2]$ is induced by the multiple bonding ligand (terminal oxo ligand $-O_t$) and narrow bite angles of the chelating ligands. The last ones are similar to those observed for $[ReOX(hqn)_2]$ (75.9(3)° and 80.1(3)°) [9].

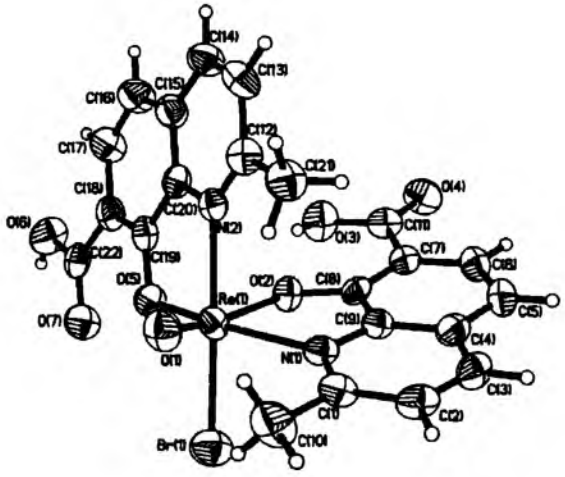

Fig. 3. The molecular structure of $[ReOBr(hmquin\text{-}7\text{-}COOH)_2]$. Displacement ellipsoids are drawn at 50% probability.

The $Re\text{–}O_t$ bond lengths fall in the range typical of mononuclear complexes of rhenium(V) having $[ReO]^{3+}$ core, and indicates the presence of a triple bond Re≡O [32]. The interatomic distance between the rhenium atom and the oxygen atom of hmquin-7-COOH in *trans* position to the terminal oxo ion is somewhat longer than the corresponding Re–O bond in the equatorial plane. This structural *trans* influence is common in mononuclear six-coordinate oxo Re(V) complexes with an monoanionic oxygen *trans* to the oxo group [33]. Noteworthy is fact that CO bonds of indicated by C(22) atom –COOH group of **1** are delocalised and they have can be considered as bonds with multiplicity of 1.5 (all other –COOH groups have localised double C=O and single C–O–H bonds). Such effect should be explained by O–H.O hydrogen bond creating symmetric 8-membered rings ($N_1R_2^2(8)$ motifs).

Table 4
The experimental and optimized bond lengths [Å] and angles [°] for $[ReOBr(hmquin\text{-}7\text{-}COOH)_2]$.

Bond lengths	Experimental	Optimized	Bond angles	Experimental	Optimized
Re(1)–O(1)	1.660(6)	1.687	O(1)–Re(1)–O(2)	163.3(2)	159.22
Re(1)–O(2)	2.068(5)	1.965	O(1)–Re(1)–O(5)	107.7(3)	109.38
Re(1)–O(5)	1.962(5)	1.929	O(2)–Re(1)–O(5)	82.2(2)	85.91
Re(1)–N(1)	2.176(6)	2.202	O(1)–Re(1)–N(1)	95.6(3)	90.44
Re(1)–N(2)	2.166(6)	2.144	O(2)–Re(1)–N(1)	75.5(2)	75.49
Re(1)–Br(1)	2.4773(10)	2.562	O(5)–Re(1)–N(1)	156.6(2)	190.06
O(3)–C(11)	1.335(10)	1.334	O(1)–Re(1)–N(2)	91.1(3)	87.28
O(4)–C(11)	1.201(10)	1.213	O(2)–Re(1)–N(2)	77.1(2)	81.60
O(6)–C(22)	1.269(10)	1.358	O(5)–Re(1)–N(2)	79.8(2)	79.66
O(7)–C(22)	1.264(10)	1.208	N(1)–Re(1)–N(2)	101.7(2)	104.20
			O(1)–Re(1)–Br(1)	101.6(2)	101.46
			O(2)–Re(1)–Br(1)	92.22(15)	92.53
			O(5)–Re(1)–Br(1)	87.03(16)	89.07
			N(1)–Re(1)–Br(1)	86.90(16)	84.70
			N(2)–Re(1)–Br(1)	163.97(17)	167.60

Table 5
The experimental bond lengths [Å] and angles [°] for [ReOCl(hmquin-7-COOH)$_2$].

Bond lengths	Experimental	Bond angles	Experimental
Re(1)–O(1)	1.666(3)	O(1)–Re(1)–O(2)	162.36(12)
Re(1)–O(2)	2.017(2)	O(1)–Re(1)–O(5)	105.96(12)
Re(1)–O(5)	1.993(2)	O(5)–Re(1)–O(2)	83.53(11)
Re(1)–N(1)	2.172(3)	O(1)–Re(1)–N(1)	96.01(13)
Re(1)–N(2)	2.171(3)	O(2)–Re(1)–N(1)	75.80(10)
Re(1)–Cl(1)	2.3345(9)	O(5)–Re(1)–N(1)	157.94(11)
C(11)–O(3)	1.201(5)	O(1)–Re(1)–N(2)	88.42(13)
C(11)–O(4)	1.330(5)	O(2)–Re(1)–N(2)	78.68(11)
O(6)–C(22)	1.323(5)	O(5)–Re(1)–N(2)	79.02(11)
O(7)–C(22)	1.211(5)	N(2)–Re(1)–N(1)	103.98(12)
		O(1)–Re(1)–Cl(1)	102.54(10)
		O(2)–Re(1)–Cl(1)	92.49(7)
		O(5)–Re(1)–Cl(1)	87.85(7)
		N(1)–Re(1)–Cl(1)	85.44(8)
		N(2)–Re(1)–Cl(1)	164.86(9)

3.3. Geometry optimization, charge distribution, electronic structure and NBO analysis

The geometry of **1** was optimized in a singlet state by the DFT method with the B3LYP functional. The optimized geometric parameters of **1** are gathered in Table 4. In general, the predicted bond lengths and angles are in agreement with the values based upon the X-ray crystal structure data, and the general trends observed in the experimental data are well reproduced in the calculations.

Table 6 presents the atomic charges from the Natural Population Analysis (NPA) for **1**. The calculated charge on the rhenium atom is considerable lower than the formal charge +5, corresponding d^2 configuration of the central ion. It results from significant charge donation from the ligands. The charges on the terminal oxo, bromide and oxygen donor atoms of hmquin-7-COOH are significantly smaller than −2, −1 and −1, respectively. The terminal oxo ion is less negative in comparison with the oxygen atom of hmquin-7-COOH ligand. It indicates the higher electron density delocalization from the O_t ligand towards the central ion and corresponds to differences in the Re–$O_{hydroxy}$ and Re–$O_{terminal}$ bond lengths. Similarly, the oxygen atom of hmquin-7-COOH in *trans* position to the bromide ion is less negative in comparison with the corresponding Re–O bond opposite the terminal oxo ligand.

A comparison of the NPA analysis for [ReOBr(hqn)$_2$] and [ReOBr(hmquin-7-COOH)$_2$] allows to notice less efficient ligand-to-metal donation from the bromide ion in the case [ReOBr(hqn)$_2$], resulting in a significantly elongation of the Re–Br bond length in this complex.

The complex [ReOBr(hmquin-7-COOH)$_2$] is a closed-shell structure. Its partial molecular orbital diagram with several highest occupied and lowest unoccupied molecular orbital contours is presented in Fig. 4. In discussion of the orbital character the local symmetry of the rhenium centre has been considered: *z* axis goes along the O–Re–O linkage, and *x* axis – through the N(1)–Re–O(5) bonds.

Table 6
Atomic charges from the natural population analysis (NPA) for [ReOBr(hmquin-7-COOH)$_2$].

Atom	Charge
Re(1)	1.441
O(1)	−0.498
O(2)	−0.722
O(5)	−0.619
N(1)	−0.487
N(2)	−0.486
Br(1)	−0.349

The value of the energy separation between the highest occupied molecular orbital (HOMO) and the lowest unoccupied molecular orbital (LUMO) equals to 2.80 eV. This value is somewhat higher in comparison with the HOMO–LUMO gap calculated for [ReOBr(hqn)$_2$] [9]. The bigger absolute value of the gap energies means better stability of the title complex.

The highest occupied MO of **1** is of d_{xy} type with some contributions from p_π bromide and π-bonding of hmquin-7-COOH. Four lowest virtual orbitals are delocalized among Re, O_t and π-antibonding orbitals of hmquin-7-COOH. As d_{xz} and d_{yz} rhenium orbitals take main part in the LUMO and LUMO+1 orbitals, they are indicated in Table 8 by d_{Re} orbitals, whereas LUMO+1 and LUMO+2 were treated as π-antibonding orbitals of hmquin-7-COOH. The LUMO+6 is of $d_{x-y}^2{}^2$ character, and d_z^2 rhenium orbital contributes to the LUMO+12.

The nature of rhenium–terminal oxygen interaction in **1** has been studied by NBO analysis. The occupancy and composition of the calculated Re–O_t natural bond orbitals (NBOs) are given in Table 7. Each natural bond orbital (NBO) σ_{AB} can be written in terms of two directed valence hybrids (NHOs) h_A and h_B on atoms A and B:

$$\sigma_{AB} = c_A h_A + c_B h_B$$

where c_A and c_B are polarization coefficients. Each valence bonding NBO must in turn be paired with a corresponding valence *anti*-bonding NBO:

$$\sigma^*_{AB} = c_B h_A - c_A h_B$$

to complete the span of the valence space. The Lewis-type (donor) NBOs are thereby complemented by the non-Lewis-type (acceptor) NBOs that are formally empty in an idealized Lewis picture. The interactions between 'filled' Lewis-type NBOs and 'empty' non-Lewis NBOs lead to loss of occupancy from the localized NBOs of the idealized Lewis structure into the empty non-Lewis orbitals, and they are referred to as 'delocalization' corrections to the zeroth-order natural Lewis structure [26].

The detected natural Re–O_t bond orbitals of **1** are π orbitals – the p_x and p_y oxygen orbitals and d_{xz} and d_{yz} rhenium orbitals are involved in their formation. Not detected σ_{Re-Ot} bond has character of predominant Coulomb-type interactions between the central ion and ligands [34]. The terminal oxo ligand of **1** has two lone pair orbitals, and electron density from one of them is strongly delocalized into non-Lewis rhenium orbital. Accordingly, NBO analysis confirms a triple bond between the rhenium and the terminal oxygen ligand.

3.4. Electronic spectra

The experimental and calculated electronic spectra of **1** are presented in Fig. 5. Each calculated transition is represented by a gaussian function $y = ce^{-bx^2}$ with the height (c) equal to the oscillator strength and b equal to 0.04 nm $^{-2}$. In order to examine the effect of adding additional basis functions on the heavy atoms, the TDDFT/PCM calculations were performed by using LANL2DZ basis set on the rhenium atom (blue curve) and by using LANL2DZ basis set with additional d function with exponent $\alpha = 0.3811$ and f function with exponent $\alpha = 2.033$ (red curve). As seen in the Fig. 5, the effect of additional d functions for TDDFT calculations is very small. The B3LYP method in LANL2DZ basis set is sufficient for calculation of spectral properties of rhenium compounds.

The spin-allowed singlet–singlet electronic transitions calculated with the TDDFT method for **1** are gathered in Table 8. For the high energy part of the spectrum, only transitions with oscillator strengths larger than 0.030 are listed in Table 8.

The TDDFT/PCM calculations show that the two longest wavelength experimental bands of **1** originate in the HOMO → LUMO

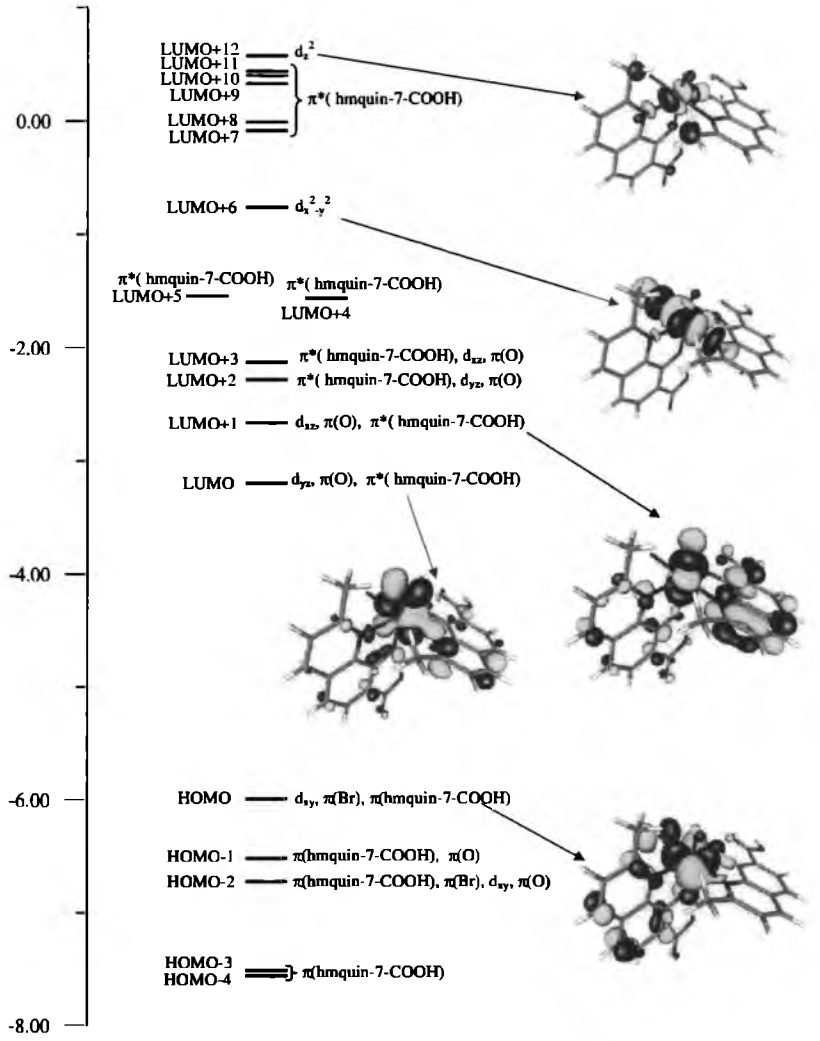

Fig. 4. The energy (eV), character and some contours of the occupied and unoccupied molecular orbitals of [ReOBr(hmquin-7-COOH)$_2$]. Positive values of the orbital contour are represented in blue (0.04 au) and negative values – in yellow (−0.04 au). (For interpretation of the references to colour in this figure legend, the reader is referred to the web version of this article.)

Table 7
The occupancy of the calculated natural bond orbitals (NBOs) between the rhenium and the oxo ligand for [ReOBr(hmquin-7-COOH)$_2$].

BD	Occupancy	Composition of NBO	BD*	Occupancy
Re–O_t	1.993	$0.552(d)_{Re} + 0.834(p)_O$	$0.834(d)_{Re} - 0.552(p)_O$	0.274
Re–O_t	1.983	$0.568(d)_{Re} + 0.823(p)_O$	$0.823(d)_{Re} - 0.568(p)_O$	0.301

BD denotes 2-center bond; * denotes antibond NBO.

and HOMO → LUMO+1 transitions, respectively. As d_{Re} orbitals take main part in the HOMO, LUMO and LUMO+1 orbitals, the HOMO → LUMO and HOMO → LUMO+1 transitions may be attributed to the transitions of d → d character. However, as it can be seen from the Fig. 4, the HOMO, LUMO and LUMO+1 orbitals are delocalized among rhenium ion, bromide, oxo and hmquin-7-COOH ligands so a delocalized *MLLCT* (metal-ligand-to-ligand CT) description can also be used.

The broad absorption band with maximum at 397.8 nm results from the *ligand-metal charge transfer* and *metal-ligand charge transfer* transitions.

The experimental bands below 300 nm nm result mainly from *ligand-ligand charge transfer* and interligand (*IL*) transitions.

The shape of the UV–Vis spectrum of **2** is the same as for the bromo analogue; the absorption bands of the chloro complex were recorded at 802.1, 678.9, 575.9, 398.5, 263.4 and 203.7 nm.

Table 8
The energy and molar absorption coefficients of experimental absorption bands and the electronic transitions calculated with the TDDFT method for [ReOBr(hmquin-7-COOH)$_2$].

The most important orbital excitations	Character	λ (nm)	E(eV)	f	Experimental Λ (nm) (E[eV])ε
H → L	d → d	831.4	1.49	0.0067	807.0 (1.54) 65
H → L+1	d → d	593.2	2.09	0.0037	685.7 (1.81) 170 587.2(2.11)100
H-1 → L	π(hmquin-7-COOH)/π(O$_t$) → d	473.7	2.62	0.0519	397.8 (3.12) 6380
H → L+3	d → π*(hmquin-7-COOH)	429.4	2.89	0.0491	
H → L+2	d → π*(hmquin-7-COOH)	410.7	3.02	0.1011	
H-1 → L+1	π(hmquin-7-COOH)/π(O) → d	381.3	3.25	0.0950	
H-2 → L+1	π(hmquin-7-COOH)/π(Br)/π(O) → d	371.5	3.34	0.0305	
H → L+5	d → π*(hmquin-7-COOH)	322.7	3.84	0.0540	
H-1 → L+4	π(hmquin-7-COOH) → π*(hmquin-7-COOH)	274.5	4.52	0.2056	263.0 (4.71) 38300
H-4 → L	π(hmquin-7-COOH) → d				
H-10 → L	π(hmquin-7-COOH) → d	264.9	4.68	0.0372	
H-6 → L+2	π(Br)/π(O$_t$)/π(hmquin-7-COOH) → π*(hmquin-7-COOH)/d	262.7	4.72	0.0385	
H-6 → L+2	π(Br)/π(O$_t$)/π(hmquin-7-COOH) → π*(hmquin-7-COOH)/d	259.2	4.78	0.0396	
H-8 → L+1	π(hmquin-7-COOH) → d	252.8	4.91	0.0378	
H-11 → L	π(hmquin-7-COOH)/σ(Br)/π(O$_t$) → d	252.2	4.92	0.2296	
H-3 → L+2	π(hmquin-7-COOH) → π*(hmquin-7-COOH)/d				
H-4 → L+3	π(hmquin-7-COOH) → π*(hmquin-7-COOH)/d	251.6	4.93	0.5531	
H-7 → L+3	π(Br)/π(hmquin-7-COOH) → π*(hmquin-7-COOH)/d	248.8	4.98	0.1090	
H-9 → L+1	π(hmquin-7-COOH)/σ(Br)/π(O$_t$) → d	244.2	5.08	0.0386	
H-9 → L+2	π(hmquin-7-COOH)/σ(Br)/π(O$_t$) → π*(hmquin-7-COOH)/d	226.0	5.49	0.0353	206.3 (6.01) 28090
H-3 → L+4	π(hmquin-7-COOH) → π*(hmquin-7-COOH)				
H-3 → L+5	π(hmquin-7-COOH) → π*(hmquin-7-COOH)	224.7	5.52	0.0340	
H-6 → L+4	π(Br)/π(O$_t$)/π(hmquin-7-COOH) → π*(hmquin-7-COOH)	221.5	5.60	0.0571	
H-4 → L+4	π(hmquin-7-COOH) → π*(hmquin-7-COOH)				
H-6 → L+5	π(Br)/π(O$_t$)/π(hmquin-7-COOH) → π*(hmquin-7-COOH)	220.8	5.62	0.0419	
H-12 → L+1	π(hmquin-7-COOH) → d	212.0	5.85	0.0603	
H-10 → L+3	π(hmquin-7-COOH) → π*(hmquin-7-COOH)/d	210.7	5.88	0.0422	
H-1 → L+7	π(hmquin-7-COOH)/π(O$_t$) → π*(hmquin-7-COOH)				
H-1 → L+7	π(hmquin-7-COOH)/π(O$_t$) → π*(hmquin-7-COOH)	208.7	5.94	0.0420	
H-2 → L+7	π(hmquin-7-COOH)/π(O$_t$) → π*(hmquin-7-COOH)	205.6	6.03	0.0621	
H-11 → L+3	π(hmquin-7-COOH)/σ(Br)/π(O$_t$) → π*(hmquin-7-COOH)/d	205.1	6.04	0.0443	

ε – molar absorption coefficient [dm^3 mol^{-1} cm^{-1}]; f – oscillator strength; H – highest occupied molecular orbital; L – lowest unoccupied molecular orbital.

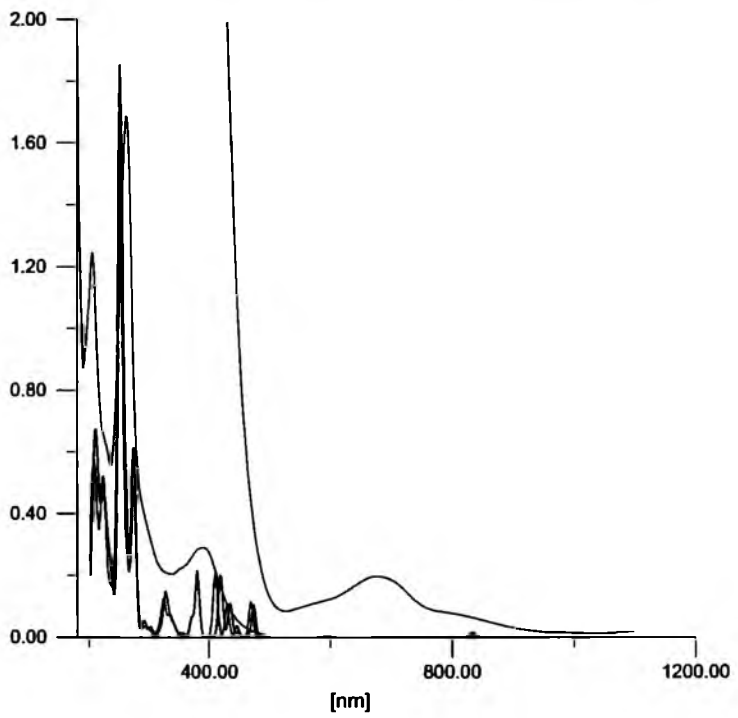

Fig. 5. The experimental (black) and calculated (red and blue) electronic absorption spectra of [ReOBr(hmquin-7-COOH)$_2$]. Red line: spectrum calculated with B3LYP functional and LANL2DZ basis set with additional d and f functions on the rhenium atom. Blue line: spectrum calculated with B3LYP functional and LANL2DZ basis set on the rhenium. (For interpretation of the references to colour in this figure legend, the reader is referred to the web version of this article.)

Supplementary data

CCDC 699353 and 699354 contain the supplementary crystallographic data for $C_{22}H_{16}N_2O_7BrRe$ and $C_{24}H_{19}N_3O_7ClRe$. These data can be obtained free of charge via http://www.ccdc.cam.ac.uk/conts/retrieving.html, or from the Cambridge Crystallographic Data Centre, 12 Union Road, Cambridge CB2 1EZ, UK; fax: (+44) 1223-336-033; or e-mail: deposit@ccdc.cam.ac.uk.

Acknowledgements

The GAUSSIAN 03 calculations were carried out in the Wrocław Centre for Networking and Supercomputing, WCSS, Wrocław, Poland.

References

[1] R.H. Holm, Chem. Rev. 87 (1987) 1401.
[2] C.C. Romão, F.E. Kühn, W.A. Hermann, Chem. Rev. 97 (1997) 3197.
[3] S.B. Seymore, S.N. Brown, Inorg. Chem. 39 (2000) 325.
[4] F.E. Kühn, A. Scherbaum, W.A. Herrmann, J. Organomet. Chem. 689 (2004) 4149.
[5] A.M. Kirillov, M. Haukka, M.V. Kirillova, A.J.L. Pombeiro, Adv. Synth. Catal. 347 (2005) 1435.
[6] A. Deloffre, S. Halut, L. Salles, J.-M. Brégeault, J.R. Gregorio, B. Denise, H. Rudler, J. Chem. Soc., Dalton Trans. (1999) 2897.
[7] W. Volkert, W.F. Goeckeler, G.J. Ehrhardt, A.R. Ketring, J. Nucl. Med. 32 (1991) 174.
[8] E.A. Deutsch, K. Libson, J.L. Vanderheyden, Technetium and Rhenium in Chemistry and Nuclear Medicine, Raven Press, New York, 1990.
[9] B. Machura, R. Kruszynski, Polyhedron 26 (2007) 2957.
[10] B. Machura, J. Kusz, Polyhedron 27 (2008) 187.
[11] J. Gancheff, C. Kremer, E. Kremer, O.N. Ventura, J. Mol. Struct. (Theochem) 580 (2002) 107.
[12] G. Rouschias, G. Wilkinson, J. Chem. Soc. A (1966) 465.
[13] K. Mekouar, J. Med. Chem. 41 (1998) 2846.
[14] CrysAlis RED, Oxford Diffraction Ltd., Version 1.171.29.2.
[15] G.M. Sheldrick, Acta Cryst. A46 (1990) 467.
[16] G.M. Sheldrick, SHELXL97. Program for the Refinement of Crystal Structures, University of Gttingen, Germany, 1997.
[17] G.M. Sheldrick, SHELXTL: release 4.1 for Siemens Crystallographic Research Systems, 1990.
[18] GAUSSIAN 03, Revision B.03, M.J. Frisch, G.W. Trucks, H.B. Schlegel, G.E. Scuseria, M.A. Robb, J.R. Cheeseman, J.A. Montgomery, Jr., T. Vreven, K.N. Kudin, J.C. Burant, J.M. Millam, S.S. Iyengar, J. Tomasi, V. Barone, B. Mennucci, M. Cossi, G. Scalmani, N. Rega, G.A. Petersson, H. Nakatsuji, M. Hada, M. Ehara, K. Toyota, R. Fukuda, J. Hasegawa, M. Ishida, T. Nakajima, Y. Honda, O. Kitao, H. Nakai, M. Klene, X. Li, J.E. Knox, H.P. Hratchian, J.B. Cross, C. Adamo, J. Jaramillo, R. Gomperts, R. E. Stratmann, O. Yazyev, A.J. Austin, R. Cammi, C. Pomelli, J.W. Ochterski, P.Y. Ayala, K. Morokuma, G.A. Voth, P. Salvador, J.J. Dannenberg, V.G. Zakrzewski, S. Dapprich, A.D. Daniels, M.C. Strain, O. Farkas, D.K. Malick, A. D. Rabuck, K. Raghavachari, J.B. Foresman, J.V. Ortiz, Q. Cui, A.G. Baboul, S. Clifford, J. Cioslowski, B.B. Stefanov, G. Liu, A. Liashenko, P. Piskorz, I. Komaromi, R.L. Martin, D.J. Fox, T. Keith, M.A. Al-Laham, C.Y. Peng, A. Nanayakkara, M. Challacombe, P.M. W. Gill, B. Johnson, W. Chen, M.W. Wong, C. Gonzalez, J.A. Pople, Gaussian, Inc., Pittsburgh PA, 2003.
[19] A.D. Becke, J. Chem. Phys. 98 (1993) 5648.
[20] C. Lee, W. Yang, R.G. Parr, Phys. Rev. B 37 (1988) 785.
[21] M.E. Casida, in: J.M. Seminario (Ed.), Recent Developments and Applications in Modern Density Functional Theory Theoretical and Computational Chemistry, vol. 4, Elsevier, Amsterdam, 1996.
[22] P.C. Hariharan, J.A. Pople, Theor. Chim. Acta 28 (1973) 213.
[23] V.A. Rassolov, M.A. Ratner, J.A. Pople, P.C. Redfern, L.A. Curtiss, J. Comput. Chem. 22 (2001) 976.
[24] P.J. Hay, W.R. Wadt, J. Chem. Phys. 82 (1985) 299.
[25] K. Eichkorn, F. Weigend, O. Treutler, R. Ahlrichs, Theor. Chem. Acc. 97 (1997) 119.
[26] E.D. Glendening, A.E. Reed, J.E. Carpenter, F. Weinhold, NBO (version 3.1). E. Reed, L.A. Curtiss, F. Weinhold, Chem. Rev. 88, 1988, 899.
[27] W.P. Griffith, H.I.S. Nogueira, B.C. Parkin, R.N. Sheppard, A.J.P. White, D.J. Williams, J. Chem. Soc., Dalton Trans. (1995) 1775.
[28] S.M.O. Quintal, H.I.S. Nogueira, V. Félix, M.G.B. Drew, New J. Chem. 24 (2000) 511.
[29] U. Mazzi, F. Refosco, F. Tisato, G. Bandoli, M. Nicolini, J. Chem. Soc., Dalton Trans. (1986) 1623.
[30] G.A. Jeffrey, W. Saenger, Hydrogen Bonding in Biological Structures, Springer-Verlag, 1994.
[31] G.R. Desiraju, T. Steiner, The Weak Hydrogen Bond in Structural Chemistry and Biology, Oxford University Press, 1999.
[32] J.M. Mayer, Inorg. Chem. 27 (1988) 3899.
[33] F.H. Allen, Acta Crystallogr., Sect. B 58 (2002) 380.
[34] M.L. Kuznetsov, A.J.L. Pombeiro, J. Chem. Soc., Dalton Trans. (2003) 738.

Polyhedron 28 (2009) 3774–3780

Contents lists available at ScienceDirect

Polyhedron

journal homepage: www.elsevier.com/locate/poly

Synthesis, spectroscopic characterization, X-ray structure and magnetic properties of [Cu(hmquin-7-COOH)$_2$(MeOH)] complex

B. Machura [a,*], A. Świtlicka [a], J. Mroziński [b], J. Kłak [b], R. Kruszynski [c], J. Kusz [d], D. Tabak [e]

[a] Department of Crystallography, Institute of Chemistry, University of Silesia, 9th Szkolna St., 40-006 Katowice, Poland
[b] Faculty of Chemistry, Wroclaw University, F. Joliot-Curie 14 St., 50-383 Wrocław, Poland
[c] Department of X-ray Crystallography and Crystal Chemistry, Institute of General and Ecological Chemistry, Lodz University of Technology, 116 Żeromski St., 90-924 Łódź, Poland
[d] Institute of Physics, University of Silesia, 4th Uniwersytecka St., 40-006 Katowice, Poland
[e] Department of Organic Chemistry, Institute of Chemistry, University of Silesia, 9th Szkolna St., 40-006 Katowice, Poland

ARTICLE INFO

Article history:
Received 8 July 2009
Accepted 29 July 2009
Available online 5 August 2009

Keywords:
Copper(II)
8-Hydroxy-2-methylquinoline-7-carboxylic acid
X-ray structure
Magnetic properties and TDDFT calculations

ABSTRACT

The reaction of copper(II) chloride dihydrate and 8-hydroxy-2-methylquinoline-7-carboxylic acid (Hhmquin-7-COOH) leads to [Cu(hmquin-7-COOH)$_2$(MeOH)]. The compound has been studied by IR, UV–Vis, EPR spectroscopy and X-ray crystallography. X-ray studies confirm bidentate coordination mode of the hmquin-7-COOH anions *via* the pyridine nitrogen atom and deprotonated hydroxyl group. The COOH groups of the hmquin-7-COOH ligands are potentially available for further conjugation. The title complex has been additionally studied by magnetic measurement. The TDDFT/PCM calculations have been employed to discuss the electronic spectrum of [Cu(hmquin-7-COOH)$_2$(MeOH)] in more detail.

1. Introduction

The structure and bond properties of copper(II) compounds are of continuous interest in inorganic chemistry [1,2]. Recently, considerable attention has been paid to the copper(II) complexes of multifunctional ligands, especially of those with an aromatic nitrogen donors and carboxylato groups. The ligand multifunctionality offers interesting possibilities in crystal engineering, owing to its chelating properties along with additional, not involved in the coordination, binding sites as potential linkers [3–6].

The incorporation of carboxylic acid groups into coordination compounds is particularly attractive since different coordination modes of carboxylate groups can lead to the formation of both mononuclear and polynuclear structures [7,8]. The polynuclear copper(II) compounds are extensively studied in view of their interesting magnetic properties. It is well known that the carboxylate group is able to create hydrogen bonds leading to the formation of supramolecular networks which play an important role in the transmission of magnetic interactions. Furthermore a lot of carboxylic acids and their derivatives play an important role in biological processes [3–8].

The ligand used in this study, 8-hydroxy-2-methylquinoline-7-carboxylic acid (Hhmquin-7-COOH), is one of the most attractive multifunctional ligands (Scheme 1).

It can act as a bidentate, tridentate or bridging ligand. As a chelate 8-hydroxy-2-methylquinoline-7-carboxylic acid can bind to the metal center through the pyridine nitrogen and deprotonated hydroxyl group (N,O-chelation) or through the carboxylate group and deprotonated hydroxyl group (O,O-chelation) and the third group is potentially available for further conjugation.

Additionally, 8-hydroxy-2-methylquinoline-7-carboxylic acid as a derivative of 8-hydroxyquinoline belongs to the important class of compounds in the search of the potential inhibitors of HIV-1 integrase [9].

Here, we present the synthesis, spectroscopic data, crystal and molecular structure of the [Cu(hmquin-7-COOH)$_2$(MeOH)] complex. X-ray studies confirm bidentate coordination mode of two hmquin-7-COOH anions *via* the pyridine nitrogen atom and deprotonated hydroxyl group. The COOH groups of the hmquin-7-COOH ligands in [Cu(hmquin-7-COOH)$_2$(MeOH)] are potentially available for further conjugation. The complex [Cu(hmquin-7-COOH)$_2$(MeOH)] has been additionally studied by magnetic measurement. The TDDFT/PCM calculations have been employed to discuss the electronic spectrum of [Cu(hmquin-7-COOH)$_2$(MeOH)] in more detail.

* Corresponding author.
E-mail addresses: basia@ich.us.edu.pl (B. Machura), jmroz@wchuwr.chem.uni.wroc.pl (J. Mroziński), rafal.kruszynski@p.lodz.pl (R. Kruszynski).

0277-5387/$ - see front matter © 2009 Elsevier Ltd. All rights reserved.
doi:10.1016/j.poly.2009.07.057

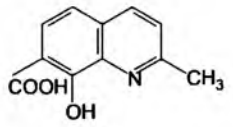

Scheme 1. Structure of Hhmquin-7-COOH ligand.

2. Experimental

2.1. General procedure

8-Hydroxy-2-methylquinoline-7-carboxylic acid was synthesised according to the literature method [10]. All the other reagents used to the synthesis were commercially available and were used without further purification.

Elemental analyses (C H N) were performed on a Perkin–Elmer CHN-2400 analyzer. IR spectrum was recorded on a Nicolet Magna 560 spectrophotometer in the spectral range 4000–400 cm^{-1} with the samples in the form of KBr pellets. Electronic spectrum was measured on a spectrophotometer Lab Alliance UV–VIS 8500 in the range 1100–180 nm in methanol solution. EPR spectra were recorded at room temperature and 77 K on a Bruker ESP 300 spectrometer operating at X-band equipped with an ER 035 M Bruker NMR gaussmeter and HP 5350B Hewlett–Packard microwave frequency counter. The spectra at 4.5 K temperature were measured with a X-band Radiopan SE/X 2543 Spectrometer.

2.2. Preparation of [Cu(hmquin-7-COOH)$_2$(MeOH)]

A solution of 8-hydroxy-2-methylquinoline-7-carboxylic acid (1.2 mmol, 024 g) in methanol (15 ml) was added to 0.1 g (0.6 mmol) of $CuCl_2 2H_2O$ in 15 ml of methanol and stirred for 6 h. The resulting brown crystalline precipitate of [Cu(hmquin-7-COOH)$_2$(MeOH)] was filtered off and dried. Yield 80%. The crystals suitable for X-ray investigation were obtained by recrystallization from methanol.

IR (KBr; ν/cm^{-1}): 3324(m) (ν(O–H)$_{COOH}$); 1733(vs), 1682(vs) (ν_{as}(C=O)$_{COOH}$), 1608(s), 1557(s) (ν(C=C), ν(C=N)), 1418(s) (ν_{as}(C=O)$_{COOH}$).

Anal. Calc. for [Cu(hmquin-7-COOH)$_2$(MeOH)]: C, 55.25; H, 4.03; N, 5.60. Found: C, 55.87; H, 4.19; N, 5.76%.

Table 1
Crystal data and structure refinement for [Cu(hmquin-7-COOH)$_2$(MeOH)].

Empirical formula	$C_{23}H_{20}N_2O_7Cu$
Formula weight	499.95
T (K)	150(2)
λ (Å)	0.71073
Crystal system	monoclinic
Space group	$P2_1/c$
Unit cell dimensions (Å, °)	
a	16.5739(14)
b	7.2421(7)
c	17.2437(14)
β	106.100(8)
V (Å^3)	1988.6(3)
Z	4
D_{calc} (Mg/m^3)	1.670
Absorption coefficient (mm^{-1})	1.151
F(0 0 0)	1028
Crystal size (mm)	0.07 × 0.26 × 0.26
θ Range for data collection (°)	3.02–25.00
Index ranges	$-14 \leqslant h \leqslant 19$ $-8 \leqslant k \leqslant 8$ $-20 \leqslant l \leqslant 18$
Reflections collected	10848
Independent reflections	3437 (R_{int} = 0.0302)
Completeness to 2θ = 25.00°	97.8%
Minimum and maximum transmission.	0.752 and 0.921
Data/restraints/parameters	3437/0/302
Goodness-of-fit (GOF) on F^2	0.944
Final R indices ($I > 2\sigma(I)$)	R_1 = 0.0322; wR_2 = 0.0780
R indices (all data)	R_1 = 0.0574; wR_2 = 0.0836
Largest difference in peak and hole (e Å^{-3})	0.552 and −0.566

2.3. X-ray diffraction study

A brown crystal of [Cu(hmquin-7-COOH)$_2$(MeOH)] was mounted on a KM-4-CCD automatic diffractometer equipped with a CCD detector, and used for data collection. X-ray intensity data were collected with graphite monochromated Mo Kα radiation (λ = 0.71073 Å) at 150(2) K. Details concerning crystal data and refinement are given in Table 1. Lorentz, polarization and empirical absorption correction using spherical harmonics implemented in SCALE3 ABSPACK scaling algorithm [11] were applied. The structure was solved by direct methods and subsequently completed by the difference Fourier recycling. All the non-hydrogen atoms were refined anisotropically using full-matrix, least-squares technique. The hydrogen atoms were treated as "riding" on their adjacent atoms and assigned isotropic temperature factors equal 1.2 times the value of equivalent temperature factor of the aromatic parent atoms and equal 1.5 times the value of equivalent temperature factor of the methyl parent carbon atom and oxygen atom (OH). SHELXS97 [12], SHELXL97 [13] and SHELXTL [14] programs were used for all the calculations. Atomic scattering factors were those incorporated in the computer programs.

2.4. Magnetic measurement

The magnetization of the powdered samples was measured over the temperature range 1.8–300 K using a Quantum Design SQUID-based MPMSXL-5-type magnetometer. The superconducting magnet was generally operated at a field strength ranging from 0 to 5 Tesla. Measurements sample of compounds were made at magnetic field 0.5 Tesla.

The SQUID magnetometer was calibrated with the palladium rod sample. Corrections are based on subtracting the sample-holder signal and contribution χ_D estimated from the Pascal constants [15] and equal -129×10^{-6} cm^3 mol^{-1} for complex. The effective magnetic moment was calculated from the equation, $\mu_{eff} = 2.83(\chi_M T)^{1/2}$(B.M.)

2.5. Computational

The electronic spectrum of [Cu(hmquin-7-COOH)$_2$(MeOH)] was calculated starting from the crystallographic coordinates with the TDDFT method using the hybrid B3LYP functional of GAUSSIAN-03 [16–18]. The calculations were performed by using the standard 6-311+G(d,p) basis for Cu atom, 6-31+G** basis for nitrogen, 6-31G* for carbon and 6-31G for hydrogen atoms. The solvent

Table 2
Inter- and intra-molecular hydrogen bonding contacts detected in the structure of [Cu(hmquin-7-COOH)$_2$(MeOH)].

D–H	A	H···A (Å)	D···A (Å)	D–H···A (°)
O(7)–H(O7)	O(3)#1	1.75	2.719(2)	171.2
O(2)–H(2O)	O(1)	1.65	2.499(2)	154.8
O(6)–H(6)	O(4)	1.79	2.523(3)	148.7
C(13)–H(13)	O(3)#2	2.55	3.429(3)	158.3
C(23)–H(23A)	O(3)#3	2.39	3.352(3)	177.1

Symmetry transformations used to generate equivalent atoms: #1 − x, 2 − y, 1 − z #2 − x, 0.5 + y, 0.5 − z #3 1 − x, 2 − y, 1 − z.

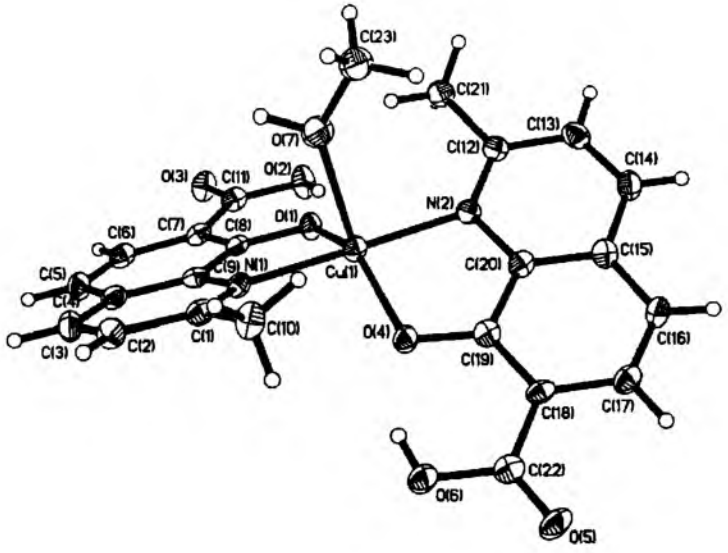

Fig. 1. The molecular structure of $[Cu(hmquin\text{-}7\text{-}COOH)_2(MeOH)]$. Displacement ellipsoids are drawn at 50% probability.

Table 3
The experimental bond lengths (Å) and angles (°) for $[Cu(hmquin\text{-}7\text{-}COOH)_2(MeOH)]$.

Bond lengths	Experimental	Bond angles	Experimental
Cu(1)–N(1)	2.067(2)	N(1)–Cu(1)–N(2)	177.51(9)
Cu(1)–N(2)	2.063(2)	N(1)–Cu(1)–O(4)	93.34(8)
Cu(1)–O(4)	1.8986(17)	N(2)–Cu(1)–O(4)	86.02(8)
Cu(1)–O(7)	2.289(2)	N(1)–Cu(1)–O(7)	82.65(8)
Cu(1)–O(1)	1.9419(17)	N(2)–Cu(1)–O(7)	95.59(8)
		O(4)–Cu(1)–O(7)	120.07(8)
		N(1)–Cu(1)–O(1)	85.11(7)
		N(2)–Cu(1)–O(1)	96.95(8)
		O(4)–Cu(1)–O(1)	138.69(8)
		O(7)–Cu(1)–O(1)	100.71(7)

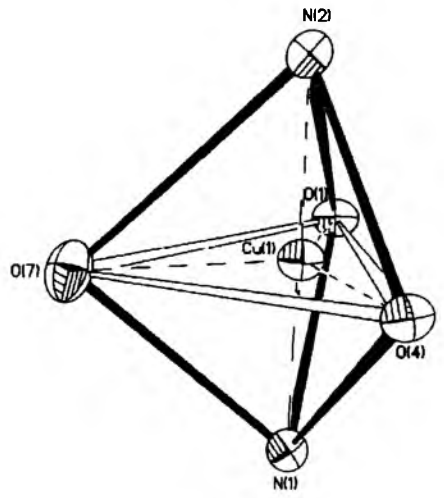

Scheme 2. Coordination polyhedron of $[Cu(hmquin\text{-}7\text{-}COOH)_2(MeOH)]$.

(methanol) effect was simulated using the polarizable continuum model with the integral equation formalism (IEF-PCM) [19].

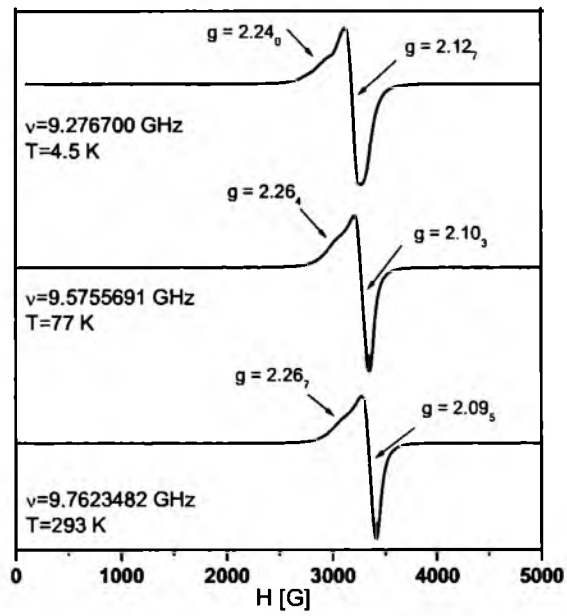

Fig. 2. EPR (X-band) spectrum of powdered sample of $[Cu(hmquin\text{-}7\text{-}COOH)_2(MeOH)]$ at room temperature, 77 K and 4.5 K.

3. Results and discussion

3.1. Synthesis

The complex $[Cu(hmquin\text{-}7\text{-}COOH)_2(MeOH)]$ was prepared in good yield by the reaction of 8-hydroxy-2-methylquinoline-7-carboxylic acid (Hhmquin-7-COOH) with copper(II) chloride dihydrate in molar ratio 2:1. The formation of $[Cu(hmquin\text{-}7\text{-}COOH)_2(MeOH)]$ has been also observed at 1:1 ratio of ligand to metal, but the complex yield has been considerable lower.

3.2. Crystal structure

The crystallographic data of [Cu(hmquin-7-COOH)$_2$(MeOH)] are summarized in Table 1. The complex molecule core consisting of [Cu(hmquin-7-COOH)$_2$(O)] moiety has an internal twofold rotation axis going through Cu(1) and O(2) atoms thus the structure can be solved also in *C2/c* space group (with the 20.3355, 7.2421, 16.5739 Å, 90.000°, 125.442°, 90.000° unit cell parameters after application of [1 0 1; 0 1 0; −1 0 0] transformation matrix), with MeOH non-oxygen atoms disordered equally over two positions. The pseudosymmetry generates fake systematic absences of C centering with mean I/σ 3.2 (I/σ for other centered cells is about 10). A summary of intra- and inter-molecular hydrogen bonding contacts detected in [Cu(hmquin-7-COOH)$_2$(MeOH)] structure is given in Table 2 [20,21]. The two intra-molecular O–H···O hydrogen bonds create classic S(6) motif, however there is COOH → CO^- interaction instead of most typical COH → COO^- interaction. The inter-molecular O–H···O hydrogen bond link molecules to the cyclic dimer, and N_1 motif can be described as $R_2^2(16)$. Additionally, in the structure can be found some intermolecular short C–H···O contacts (Table 2), which can be considered as weak hydrogen bonds [20].

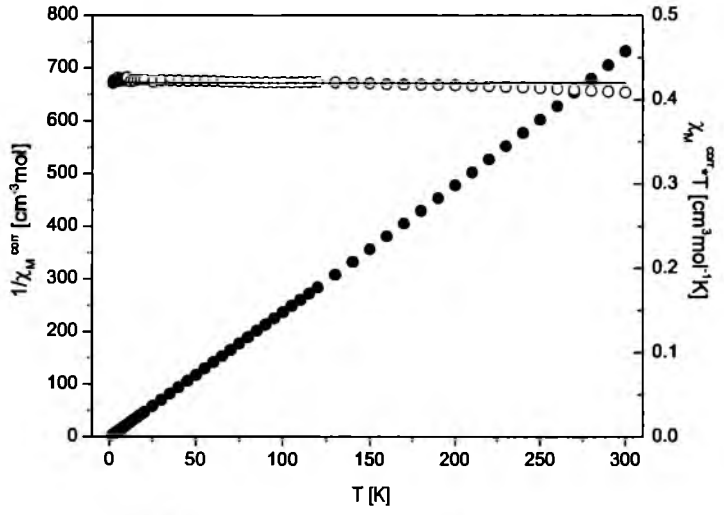

Fig. 3. Temperature dependence of experimental χ_M^{-1} (●) and $\chi_M T$ (○) for complex [Cu(hmquin-7-COOH)$_2$(MeOH)]. The solid line is the calculated curve for $\chi_M T$.

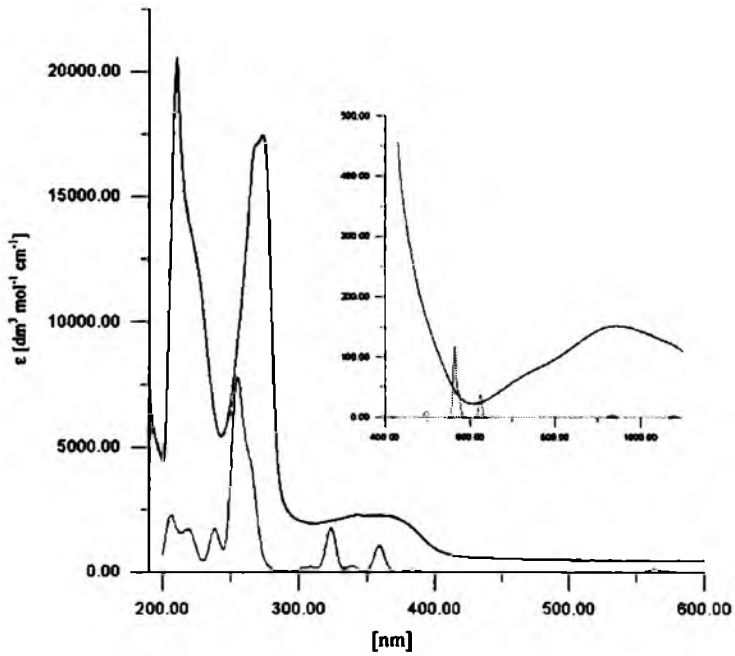

Fig. 4. The experimental (black) and calculated (red) electronic absorption spectra of methanolic solution of [Cu(hmquin-7-COOH)$_2$(MeOH)]. (For interpretation of the references to color in this figure legend, the reader is referred to the web version of this article.)

The molecular structure of the [Cu(hmquin-7-COOH)$_2$(MeOH)] is presented in Fig. 1, and the selected bond distances and angles of [Cu(hmquin-7-COOH)$_2$(MeOH)] are collected in Table 3.

The Cu(II) center of [Cu(hmquin-7-COOH)$_2$(MeOH)] is bound to the methanol molecule and two hmquin-7-COOH anions through the pyridine nitrogen atoms and deprotonated hydroxyl groups, forming two five-membered rings. The COOH groups of the hmquin-7-COOH ligands in the examined complex are almost parallel to the quinoline plane and they are available for further conjugation. For comparison, the related ligand 8-hydroxyquinoline-2-carboxylic acid acts as a dibasic tridentate ligand and coordinates to copper(II) center through two O and one N atoms [22].

The angular structural index parameter τ [23] expressed here as the difference between the bond angles N(1)–Cu(1)–N(2) and O(4)–Cu(1)–O(1) divided by 60 has a value of 0.65. Compared with the ideal values of 1 for an equilateral bipyramid and 0 for a square pyramid, the τ descriptor of the examined structure suggests a stereochemistry intermediate between equilateral-bipyramidal and squarepyramidal, but on the basis of coordination geometry considerations in terms of scalene bipyramid it can be stated that coordination polyhedron is slightly distorted trigonal bipyramid with three O atoms in the basal coordination positions and two N atoms in the apical positions (Scheme 2).

The Cu–O and Cu–N distances fall within the normal range, corresponding to the bond lengths in other five-coordinated Cu complexes. Similar to the related five-coordinated Cu complexes the Cu–O(7) bond is significantly longer than the equatorial Cu–O distances [24–26].

3.3. Spectroscopic properties

The IR spectrum of [Cu(hmquin-7-COOH)$_2$(MeOH)] shows asymmetric stretching vibrations ν_{as}(OCO) at 1733 and 1682 cm^{-1}. The broad ν_s(OCO) is found at 1418 cm^{-1}. The medium intensity band assigned to ν(OH) vibrations occurs at 3324 cm^{-1}, and the characteristic C=C and C=N stretching modes are observed in the range 1620–1540 cm^{-1} [27].

The EPR powder spectra of the complex [Cu(hmquin-7-COOH)$_2$-(MeOH)] recorded in the X-band at room temperature, 77 K and 4.5 K (Fig. 2) indicate two poorly resolved lines. They are in accordance with the existence around the Cu(II) ion of the distorted trigonal-bipyramidal symmetry Cu(1)N$_2$O$_3$ [28,29].

3.4. Magnetic properties

The magnetic properties of the complex were determined over the temperature range 1.8–300 K. Plots of magnetic susceptibility χ_M and χ_M^{-1} product versus T are given in Fig. 3.

The value $\chi_M T$ of at 300 K for complex equals 0.409 cm^3 mol^{-1} K (1.81 B.M.). The value of $\chi_M T$ product is constant in whole temperature range and reaches 0.421 cm^3 mol^{-1} K (1.84 B.M.) at 1.8 K.

The values Curie and Weiss constants determined from the relation $1/\chi_M T = f(T)$ over temperature range 1.8–300 K are equal to 0.414 cm^3 mol^{-1} K and 0.64 K.

On such situation the magnetic data were fitted using the susceptibility equation for $S = {}^1/_2$, (Eq. (1)). To elucidate the significance of exchange between copper(II) ions in the crystal lattice, a molecular field correction term was also included, Eq. (2) [30].

Table 4
The spin-allowed doublet-doublet electronic transitions calculated with the TDDFT method and the assignments of the calculated transitions to the experimental absorption bands of [Cu(hmquin-7-COOH)$_2$(MeOH)].

The most important orbital excitations	Character	λ (nm)	E (eV)	*f*	Experimental *λ* (nm) (E(eV))
H(β) → L(β)	π(hmquin-7-COOH) → d	1077.65	1.1505	0.0003	946.0 (1.31)
H-4(β) → L(β)	$\pi(O_{MeOH})/\pi$(hmquin-7-COOH)/d → d				
H-1(β) → L(β)	π(hmquin-7-COOH) → d	934.64	1.3266	0.0005	
H-5(β) → L(β)	d/π(hmquin-7-COOH)/$\pi(O_{MeOH})$ → d				
H(β) → L(β)	π(hmquin-7-COOH) → d	623.87	1.9873	0.0038	
H-11(β) → L(β)	π(hmquin-7-COOH)/d/$\pi(O_{MeOH})$ → d				
H-1(β) → L(β)	π(hmquin-7-COOH) → d	579.76	2.1385	0.0001	503.8 (2.46)
H-20(β) → L(β)	d/π(hmquin-7-COOH) → d				
H-20(β) → L(β)	d/π(hmquin-7-COOH) → d	573.34	2.1625	0.0038	
H-1(β) → L(β)	π(hmquin-7-COOH) → d				
H(β) → L(β)	π(hmquin-7-COOH) → d	563.48	2.2003	0.0118	
H(β) → L+1(β)	π(hmquin-7-COOH) → π^*(hmquin-7-COOH)	358.79	3.4556	0.1051	349.4 (3.55)
H(α) → L(α)	π(hmquin-7-COOH) → π^*(hmquin-7-COOH)				
H(β) → L+3(β)	π(hmquin-7-COOH) → π^*(hmquin-7-COOH)	323.59	3.8315	0.0820	
H(α) → L+2(α)	π(hmquin-7-COOH) → π^*(hmquin-7-COOH)				
H(β) → L+4(β)	π(hmquin-7-COOH) → π^*(hmquin-7-COOH)	322.76	3.8414	0.0945	
H(α) → L+3(α)	π(hmquin-7-COOH) → π (hmquin-7-COOH)				
H-11(β) → L(β)	π(hmquin-7-COOH)/d/$\pi(O_{MeOH})$ → d	266.47	4.6528	0.2522	266.7 (4.65)
H-13(β) → L(β)	π(hmquin-7-COOH)/d/$\pi(O_{MeOH})$ → d				
H-2(β) → L+1(β)	π(hmquin-7-COOH) → π^*(hmquin-7-COOH)	264.15	4.6938	0.0590	
H-2(α) → L(α)	π(hmquin-7-COOH) → π^*(hmquin-7-COOH)	260.34	4.7624	0.1584	
H-3(α) → L(α)	π(hmquin-7-COOH) → π^*(hmquin-7-COOH)	259.59	4.7762	0.0624	
H-2(α) → L+1(α)	π(hmquin-7-COOH) → π^*(hmquin-7-COOH)	256.19	4.8395	0.0840	
H-3(α) → L+1(α)	π(hmquin-7-COOH) → π^*(hmquin-7-COOH)	254.09	4.8795	0.5913	
H-3(β) → L+2(β)	π(hmquin-7-COOH) → π (hmquin-7-COOH)				
H-3(α) → L+2(α)	π(hmquin-7-COOH) → π^*(hmquin-7-COOH)	237.94	5.2107	0.0717	206.3 (6.01)
H-3(β) → L+4(β)	π(hmquin-7-COOH) → π^*(hmquin-7-COOH)				
H-2(α) → L+3(α)	π(hmquin-7-COOH) → π^*(hmquin-7-COOH)				
H(β) → L+6(β)	π(hmquin-7-COOH) → π^*(hmquin-7-COOH)	221.09	5.6079	0.0506	
H(α) → L+5(α)	π(hmquin-7-COOH) → π^*(hmquin-7-COOH)				
H(β) → L+8(β)	π(hmquin-7-COOH) → π (hmquin-7-COOH)	205.44	6.0349	0.1272	

f – oscillator strength.
H – highest occupied molecular orbital.
L – lowest unoccupied molecular orbital.

$$\chi_M = \frac{N\beta^2 g^2}{3kT} S(S+1) \quad (1)$$

$$\chi_M^{corr} = \frac{\chi_M}{1 - \frac{2zJ'}{N\beta^2 g^2} \cdot \chi_M} \quad (2)$$

where N is the Avogadro's number, g – the spectroscopic splitting factor, β – the Bohr magneton, k – the Boltzmann constant, zJ' – intermolecular exchange parameter and z is the number of the nearest neighbors of Cu(II) center. The least-squares fit of the experimental data using these equations were limited to the temperature range from 1.8 K up to 300 K and leads to $zJ' = 0.03\ cm^{-1}$ and $g = 2.12$, as indicated by the solid curve in Fig. 3. The agreement factor R is equal 6.57×10^{-5}. The criterion used in determination of the best fit was based on minimization of the sum of squares of the deviation: $R = \sqrt{\sum_{i=1}^{n} \frac{1}{(\chi_i^{exp})} \left(\chi_i^{exp} - \chi_i^{calc^2}\right)} \Big/ \sqrt{\sum_{i=1}^{n} \frac{1}{(\chi_i^{exp^2})}}$. The result of calculations may be indicative of lack of interactions between metallic centers for reason of large distance Cu···Cu in the crystal lattice (9.017 Å). This fact is expected in mononuclear magnetically diluted Cu(II) compounds (1.7–2.2 B.M.) [31].

3.5. Electronic spectrum

The nature of the transitions observed in the UV–Vis spectrum of the title complex has been studied by the time-dependent density functional (TDDFT) method starting from the crystallographic coordinates. The calculated electronic spectrum of [Cu(hmquin-7-COOH)$_2$(MeOH)] in comparison with the experimental one is presented in Fig. 4. Each calculated transition is represented by a Gaussian function $y = ce^{-bx^2}$ with the height (c) equal to the oscillator strength and b equal to 0.04 nm^{-2}. As can be seen from the Fig. 4, the TDDFT calculated results are consistent well with the experimental ones.

Table 4 presents the most important electronic transitions calculated with the TDDFT method for [Cu(hmquin-7-COOH)$_2$(MeOH)] and their assignments to the observed absorption bands

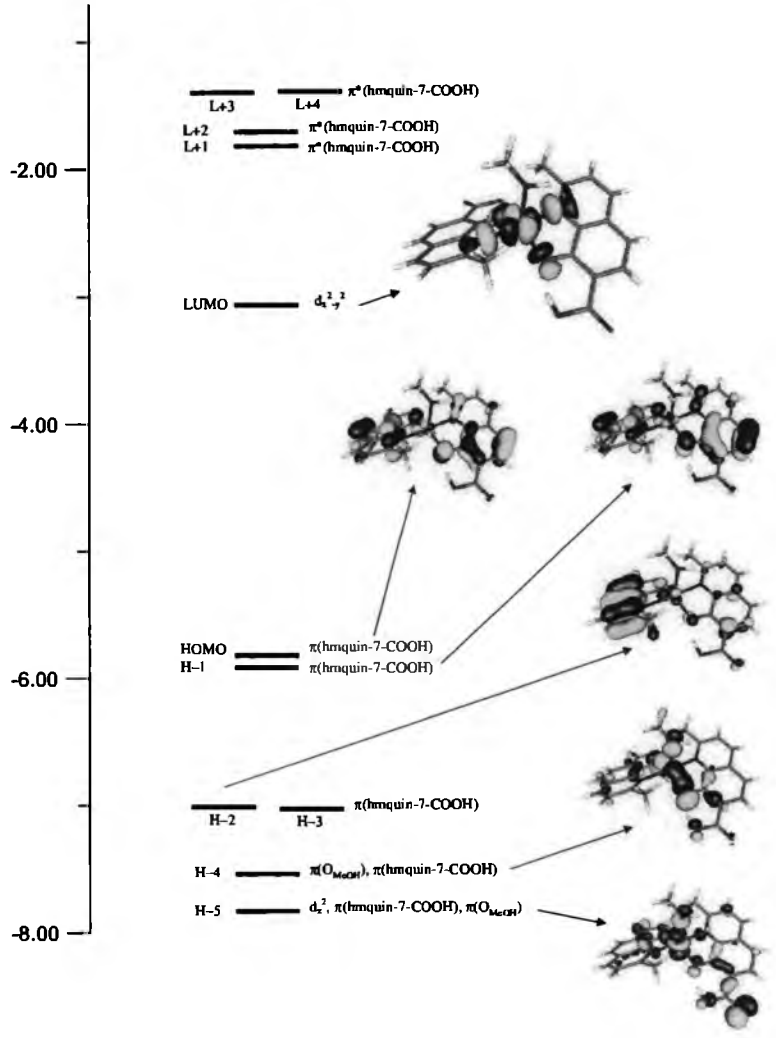

Fig. 5. The β-spin frontier molecular orbital energy (eV) level diagram of [Cu(hmquin-7-COOH)$_2$(MeOH)]. Positive values of the orbital contour are represented in blue (0.04 au) and negative values in yellow (−0.04 au). (For interpretation of the references to color in this figure legend, the reader is referred to the web version of this article.)

of the complex. For the high energy part of the spectrum, only transitions with oscillator strengths larger than 0.0300 are listed in Table 4. The TDDFT/PCM calculations show that the calculated absorption maxima involve mainly the β-spin frontier molecular orbital energy. Fig. 5 presents the β-spin frontier molecular orbital energy (eV) level diagram of [Cu(hmquin-7-COOH)$_2$(MeOH)]. The assignment of the calculated orbital excitations to the experimental bands was based on an overview of the contour plots and relative energy of occupied (HOMO) and unoccupied (LUMO) molecular orbitals involved in the electronic transitions.

The weak experimental bands in the visible region (at 946.0, 720.6 and 503.8 nm) originate from the HOMO(β) → LUMO(β), HOMO-4(β) → LUMO(β), HOMO-1(β) → LUMO(β), HOMO-5(β) → LUMO(β), HOMO-11(β) → LUMO(β) and HOMO-20(β) → LUMO(β) transitions. As can be seen from the Fig. 4, the LUMO orbital with β-spin is $d_{x^2-y^2}$ copper orbital in character. The HOMO(β) is mainly localized on the hmquin-7-COOH ligands. The β-spin HOMO-5 orbital is composed of d_{z^2} copper orbital with some contribution of the π-bonding orbitals of hmquin-7-COOH MeOH, whereas the d_{xy} copper orbital contributes mainly into the HOMO-20. The HOMO-4 and HOMO-11 are delocalized among the copper ion and π-bonding orbitals of ligands (MeOH and hmquin-7-COOH). Accordingly, the transitions assigned to the three longest wavelength experimental bands can be seen as mixed hmquin-7-COOH/O_{MeOH} → Cu (*Ligand–Metal Charge Transfer*; *LMCT*) and d → d (*Ligand Field; LF*) transitions. Similar to the previously studied copper complexes [Cu(pybzim)$_2$(NO_3)](NO_3) and [Cu(pdm)$_2$] [32,33], no 'clear' d–d transition bands occur in the low-lying energy region for [Cu(hmquin-7-COOH)$_2$(MeOH)]. The reason for this is probably due to the fact that the hmquin-7-COOH ligand (similar to other coordinated heterocyclic molecules) provides high-lying occupied π-bonding orbitals, and as a result the high-lying occupied orbitals are composed of the π-bonding orbitals of hmquin-7-COOH ligand.

The experimental bands at 349.4, 266.7 and 206.3 nm originate predominately in the *intraligand* (IL) and *ligand–ligand charge transfer* (*LLCT*) transitions. However some contribution of the hmquin-7-COOH/O_{MeOH} → Cu (*Ligand–Metal Charge Transfer*) in the band at 266.7 nm has been also confirmed by the calculations.

Supplementary data

CCDC 739242 contains the supplementary crystallographic data for this paper. These data can be obtained free of charge via http://www.ccdc.cam.ac.uk/conts/retrieving.html, or from the Cambridge Crystallographic Data Centre, 12 Union Road, Cambridge CB2 1EZ, UK; fax: (+44) 1223-336-033; or e-mail: deposit@ccdc.cam.ac.uk.

Acknowledgement

The GAUSSIAN03 calculations were carried out in the Wrocław Centre for Networking and Supercomputing, WCSS, Wrocław, Poland under calculational Grant No. 51/96.

References

[1] B.P. Murphy, B.J. Hathaway, Coord. Chem. Rev. 124 (1993) 63.
[2] B.J. Hathaway, in: G. Wilkinson, R.D. Gillard, J.A. McCleverty (Eds.), Comprehensive Coordination Chemistry, vol. 5, Pergamon Press, Oxford, 1987. p. 553.
[3] D. Min, S.S. Yoon, D.-Y. Jung, Ch.Y. Lee, Y. Kim, W.S. Han, S.W. Lee, Inorg. Chim. Acta 324 (2001) 293.
[4] B.O. Patrick, C.L. Stevens, A. Storr, R.C. Thompson, Polyhedron 22 (2003) 3025.
[5] S.-I. Noro, S. Kitagawa, T. Wada, Inorg. Chim. Acta 358 (2005) 423.
[6] L. Xue, F. Luo, Y.-X. Che, J.-M. Zheng, J. Mol. Struct. 832 (2007) 132.
[7] B. Żurowska, J. Mroziński, Z. Ciunik, Polyhedron 26 (2007) 1251.
[8] B. Żurowska, J. Mroziński, K. Ślepokura, Polyhedron 26 (2007) 3379.
[9] F. Zouhiri, J.-F. Mouscadet, K. Mekouar, D. Desmaele, D. Savoure, H. Leh, F. Subra, M.L. Bret, Ch. Auclair, J. d'Angelo, J. Med. Chem. 43 (2000) 1533.
[10] K. Mekouar, J. Med. Chem. 41 (1998) 2846.
[11] CRYSALIS RED, Oxford Diffraction Ltd., Version 1.171.29.
[12] G.M. Sheldrick, Acta Crystallogr., A 46 (1990) 467.
[13] G.M. Sheldrick, SHELXL97. Program for the Refinement of Crystal Structures, University of Gottingen, Germany, 1997.
[14] G.M. Sheldrick, SHELXTL: Release 4.1 for Siemens Crystallographic Research Systems, 1990.
[15] E. König, Magnetic Properties of Coordination and Organometallic Transition Metal Compounds, Springer-Verlag, Berlin, 1966.
[16] M.J. Frisch, G.W. Trucks, H.B. Schlegel, G.E. Scuseria, M.A. Robb, J.R. Cheeseman, J.A. Montgomery Jr., T. Vreven, K.N. Kudin, J.C. Burant, J.M. Millam, S.S. Iyengar, J. Tomasi, V. Barone, B. Mennucci, M. Cossi, G. Scalmani, N. Rega, G.A. Petersson, H. Nakatsuji, M. Hada, M. Ehara, K. Toyota, R. Fukuda, J. Hasegawa, M. Ishida, T. Nakajima, Y. Honda, O. Kitao, H. Nakai, M. Klene, X. Li, J.E. Knox, H.P. Hratchian, J.B. Cross, C. Adamo, J. Jaramillo, R. Gomperts, R.E. Stratmann, O. Yazyev, A.J. Austin, R. Cammi, C. Pomelli, J.W. Ochterski, P.Y. Ayala, K. Morokuma, G.A. Voth, P. Salvador, J.J. Dannenberg, V.G. Zakrzewski, S. Dapprich, A.D. Daniels, M.C. Strain, O. Farkas, D.K. Malick, A.D. Rabuck, K. Raghavachari, J.B. Foresman, J.V. Ortiz, Q. Cui, A.G. Baboul, S. Clifford, J. Cioslowski, B.B. Stefanov, G. Liu, A. Liashenko, P. Piskorz, I. Komaromi, R.L. Martin, D.J. Fox, T. Keith, M.A. Al-Laham, C.Y. Peng, A. Nanayakkara, M. Challacombe, P.M.W. Gill, B. Johnson, W. Chen, M.W. Wong, C. Gonzalez, J.A. Pople, GAUSSIAN 03, Revision B.03, Gaussian, Inc., Pittsburgh, PA, 2003.
[17] A.D. Becke, J. Chem. Phys. 98 (1993) 5648.
[18] C. Lee, W. Yang, R.G. Parr, Phys. Rev. B 37 (1988) 785.
[19] M.E. Casida, in: J.M. Seminario (Ed.), Recent Developments and Applications in Modern Density Functional Theory, Theoretical and Computational Chemistry, vol. 4, Elsevier, Amsterdam, 1996.
[20] G.R. Desiraju, T. Steiner, The Weak Hydrogen Bond in Structural Chemistry and Biology, Oxford University Press, 1999.
[21] G.A. Jeffrey, W. Saenger, Hydrogen Bonding in Biological Structures, Springer-Verlag, 1994.
[22] M. Nakamura, Ch. Kitamura, H. Ueyama, K. Yamana, A. Yoneda, Anal. Sci.: X-ray Struct. Anal. Online 21 (2005) x115.
[23] A.W. Addison, T.N. Rao, J. Reedijk, J. Rijn, G.C. Verschoor, J. Chem. Soc., Dalton Trans. (1984) 1349.
[24] S.P.S. Rao, H. Manohar, K. Aoki, H. Yamazaki, J. Chem. Soc., Dalton Trans. (1987) 1009.
[25] S.P.S. Rao, H. Manohar, K. Aoki, H. Yamazaki, R. Bau, J. Chem. Soc., Chem. Commun. (1986) 4.
[26] F. Jian, Y. Wang, L. Lu, X. Yang, X. Wang, S. Chantrapromma, H.-K. Fun, I.A. Razak, Acta Crystallogr., C 57 (2001) 714.
[27] K. Nakamoto, Infrared and Raman Spectra of Inorganic and Coordination Compounds, 4th ed., Wiley-Interscience, New York, 1986.
[28] J.R. Pilbrow, Transition Ion Electron Paramagnetic Resonance, Oxford Science Publications, Oxford, 1990.
[29] B.J. Hathaway, D.E. Billing, Coord. Chem. Rev. 5 (1970) 143.
[30] J. Samuel Smart, Effective Field Theories of Magnetism, W.B. Saunders Comp., Philadelphia and London, 1966.
[31] R.L. Carlin, Magnetochemistry, Springer-Verlag, Berlin, 1986.
[32] B. Machura, A. Świtlicka, M. Wolff, J. Kusz, R. Kruszynski, Polyhedron 26 (2007) 3379.
[33] Y.-P. Tong, S.-L. Zheng, J. Mol. Struct. 841 (2007) 34.

Bioorganic & Medicinal Chemistry 19 (2011) 1606–1612

Contents lists available at ScienceDirect

Bioorganic & Medicinal Chemistry

journal homepage: www.elsevier.com/locate/bmc

X-ray and molecular modelling in fragment-based design of three small quinoline scaffolds for HIV integrase inhibitors

Katarzyna Majerz-Maniecka [a,*], Robert Musiol [b,*], Agnieszka Skórska-Stania [a], Dominik Tabak [b], Pawel Mazur [b], Barbara J. Oleksyn [a], Jaroslaw Polanski [b]

[a] Faculty of Chemistry, Jagiellonian University, ul. R. Ingardena 3, 30-060 Kraków, Poland
[b] Institute of Chemistry, University of Silesia, ul. Szkolna 9, 40-007 Katowice, Poland

ARTICLE INFO

Article history:
Received 23 November 2010
Revised 20 January 2011
Accepted 21 January 2011
Available online 27 January 2011

Keywords:
HIV integrase
Quinolines
Fragment-based drug design
Crystal structure

ABSTRACT

Crystal structures of three small molecular scaffolds based on quinoline, 2-methylquinoline-5,8-dione, 5-hydroxy-quinaldine-6-carboxylic acid and 8-hydroxy-quinaldine-7-carboxylic acid, were characterised. 5-Hydroxy-quinaldine-6-carboxylic acid was co-crystallized with cobalt(II) chloride to form a model of divalent metal cation–ligand interactions for potential HIV integrase inhibitors. Molecular docking into active site of HIV IN was also performed on 1WKN PDB file. Selected ligand–protein interactions have been found specific for active compounds. Studied structures can be used as scaffolds in fragment-based design of new potent drugs.

1. Introduction

Recently the fragment-based approach (F-BA) to drug discovery has gained stronger attention than ever before. During the last 10 years this methodology has been intensively developing and now it can be successfully used as an alternative for poorly effective HTS.[1,2] However, it should be remembered that the molecules used as fragments do not possess high activity, but they are much more druggable than huge, sophisticated structures usually pointed out in HTS. Thus, in F-BA we are looking rather for possibility of creating a new drug than for activity. Successful molecular scaffolds should be easily accessible and transferable into real drug. Probably the best way to achieve this aim is to explore the so-called privileged structures as a scaffold.[3] Unfortunately there are no simple rules that specify which structure is really privileged. On the other hand quinoline and its derivatives such as quinolone antibiotics can be the most spectacular examples of the potential efficiency of this system.[4] Quinine molecule, which also contains a quinoline moiety, proves the Nature preference for this system. Quinoline scaffold can also be found in many classes of other biologically active compounds used as antifungals, antibacterials and antiprotozoic drugs[5–8] as well as antituberculotic agents.[9] Some quinoline analogues showed also antineoplastic activity. Thorough knowledge of all interactions which occur in solutions or crystals of molecules proposed as scaffolds is very important for better understanding its fate in biological systems and for (Q)SAR studies. Certain specific interactions are able to change crucial parameters of molecules or even to change the structure via shift of tautomeric equilibrium.[10] Here we wish to report our findings concerning intermolecular interactions in the crystal structures of three quinoline-based scaffolds that are promising in design of new antiviral and anticancer agents (Fig. 1). In the next stage, we applied molecular docking to correlate data derived from crystal structure and biological activity.

Quinoline-5,8-dione is a substantial molecular fragment of lavendomycin and related compounds (Fig. 2). Lavendomycin was originally isolated from the fermented broth of *Streptomyces lavendulae* and the compounds of this class were identified in the 1970's as anti-tumour agents. Although the toxicity of lavendomycin makes it unsuitable for clinical use, its activity has inspired several investigations.[11–14] This scaffold was found to be very

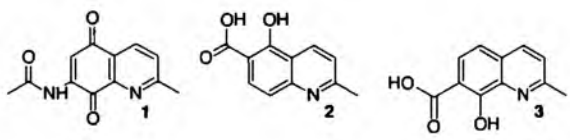

Figure 1. Three molecular scaffolds as fragments of HIV integrase inhibitors.

* Corresponding authors.
E-mail addresses: majerz.maniecka@gmail.com (K. Majerz-Maniecka), robert.musiol@us.edu.pl (R. Musiol).

0968-0896/$ - see front matter © 2011 Elsevier Ltd. All rights reserved.
doi:10.1016/j.bmc.2011.01.045

Figure 2. Quinolinone-based antibiotics show the importance of quinoline as molecular fragment.

promising in our recent investigation of anticancer agents with activity against P-388 leukaemia cells twice as high as that of cisplatin.[15]

5-Hydroxy-quinaldine-6-carboxylic acid (Fig. 1(2)) proved its applicability in design of novel HIV integrase inhibitors[16,17] and herbicidal agents.[18] Its isomer, 8-hydroxy-quinalidne-7-carboxylic acid, is a well-known scaffold used in synthesis of potent HIV integrase inhibitors (e.g., FZ41), antifungal and anticancer agents.[19–22]

Most of HIV integrase inhibitors are believed to interact with divalent metal cations such as magnesium or manganese, located at the protein active site.[23] Recently retroviral intasome has been elucidated by mean crystal structure of IN from PFV virus.[24,25] This can also confirmed importance of this mechanism. Elvitegravir and raltegravir two known potent inhibitors of HIV integrase were found engaging two Mg cations in the active site of the intasome.[26] It seems obvious that knowledge of interactions between an inhibitor molecule and cations is crucial for better understanding its mode of action and explaining its activity and/or selectivity.[27] Furthermore they can also be useful in elucidation the problem of drug resistance caused by small mutations.[28]

2. Results and discussion

2.1. Chemistry

Synthesis of studied scaffolds is depicted in Scheme 1.

Compound **1** was obtained from 2-methyl-8-hydroxyquinoline through nitration, reduction and finally oxidation to give crude product (purified by crystallization from EtOH) as yellow solid, 80% yield, mp 258 °C (lit. mp 260.5 °C[29]). Compound **2** was obtained from 2-hydroxy-4-aminobenzoic acid and crotonaldehyde in Skraup reaction.[16] 8-Hydroxy-2-methylquinoline-7-carboxylic acid **3** was obtained in Kolbe–Schmidt reaction from 8-hydroxyquinaldine as described earlier.[21]

2.2. Crystal structures

Single crystals of compound **1** (CCDC 752663) were obtained from ethanol solution, while compound **2** (CCDC 752665) was co-crystallized with cobalt dichloride hexahydrate also from ethanol. Single crystals of compound **3** (CCDC 795948) developed in dimethyl sulfoxide and ethanol solution (1 v/1 v). All the crystals were grown by slow evaporation of the solvent, at a temperature of about 293 K. X-ray data were collected on a Bruker-Nonius KappaCCD diffractometer using MoKα radiation. The phase problem was solved by direct methods using SIR[30] and refined by full matrix least-squares method using SHELX97.[31] Hydrogen atoms were located in difference Fourier maps and refined isotropically, using riding model.

The details of the crystal data, data collection and refinement are listed in Table 1, while the asymmetric units of these structures together with atom numbering are shown in Figure 3. All projections were generated using ORTEP.[32]

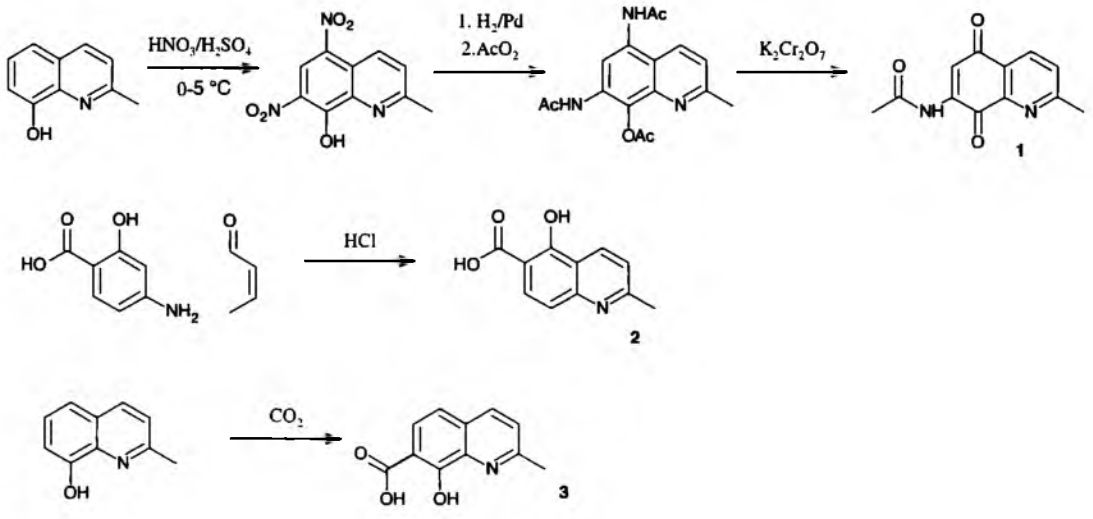

Scheme 1. Synthesis of quinolines **1–3**.

Table 1
Crystal data, measurement and calculation details

Chemical formula	Structure 1 $C_{12}H_{10}N_2O_3$	Structure 2 $2[C_{11}H_8NO_3{\cdot}HCl]\cdot[Co(H_2O)_4]^{2+}$	Structure 3 $[C_{11}H_{10}NO_3]^+{\cdot}Cl$
Crystal data			
M (g mol^{-1})	230.339	304.14	239.759
Crystal system	Triclinic	Triclinic	Triclinic
Space group	$P\bar{1}$	$P\bar{1}$	$P\bar{1}$
a [Å]	3.864(3)	7.274(3)	7.207(1)
b [Å]	11.545(1)	7.413(3)	9.470(2)
c [Å]	14.049(1)	11.874(6)	9.639(2)
α [°]	104.33(3)	91.38(2)	97.21(1)
β [°]	94.16(2)	103.40(2)	109.52(1)
γ [°]	92.45(5)	94.75(2)	108.12(1)
V [Å^3]	604.43(9)	620.10(5)	569.64(2)
Z	2	2	2
D [g cm^{-3}]	1.265	1.629	1.502
F (0 0 0)	240	313	268
μ [mm^{-1}]	0.093	0.968	0.338
Data collection			
h_{min}, h_{max}	−5, 5	−9, 9	−9, 9
k_{min}, k_{max}	−15, 15	−9, 9	−12, 12
l_{min}, l_{max}	−15, 18	−15, 15	−12, 12
Θ range [°]	3.58–27.67	2.76–27.51	1.00–27.48
Unique reflns	3665	4855	5054
Reflns $F_0 > 4\delta(F_0)$	2667	2825	2615
Refinement			
R_1 for $F_0 > 2\delta(F_0)$	0.0847	0.0605	0.0376
R_1 for all data	0.1790	0.0893	0.0462
wR_2 for $F_0 > 2\delta(F_0)$	0.2539	0.1324	0.1084
GOOF on F^2	1.032	1.020	1.059

2.2.1. Molecule 1

The asymmetric unit of **1** consists of one molecule (Fig. 3(1)). The bond lengths C7–C8 and C5–C10 are 1.354(5) Å and 1.377(5) Å, respectively, and they are shorter than typical C_{Ar}–C_{Ar} distances.[33] The C6–O1 and C9–O2 bonds demonstrate double character, which suggest electron localisation of quinolinedione arrangement of the ring. The valence angles C5–C6–C7 = 118.4(3)° and C8–C9–C10 = 118.5(3)° are smaller than 120°, which can be ascribed, according to VSEPR theory, to the influence of oxygen free electron pairs and C–O double bonds. The high values of the atomic displacement parameters for the methyl group and for oxygen can be explained by the rotational freedom (O3) and certain possibility of disorder (O1, O2). The ring system of the molecule **1** is almost planar and coplanar with the substituents, the greatest distortion, 0.107(5) Å, being that of the O3 atom. Also torsion angles, C10–C5–C6–O1 = 177.8(4)°, C7–C8–C9–O2 = −179.6(4)°, C7–C8–N2–C11 = −3.3(7)°, C8–N2–C11–O3 = −1.2(7)°, C8–N2–C11–C12 = −179.6(4)°, confirm planarity of the whole molecule. The packing of the molecules in the unit cell is dominated mainly by hydrogen bonds and π–π interactions. The details of hydrogen bond geometry are given in Table 2. The proton of N2 atom is shared by two oxygen atoms with formation of a bifurcated hydrogen bond. The intermolecular contact N2–H2···O2 represents rather a weak hydrogen bond interaction as shown by the donor–acceptor distance (Table 2).

This situation is most probably caused by the steric hindrance introduced by methyl groups. Intramolecular N2–H2···O2 hydrogen bond is another example of weak interaction because it leads to formation of a strained pentagonal ring. There are also π–π interactions in structure of **1** as shown by the distance between centroids of neighbouring rings, which is 3.864(3) Å. This distance is equal to the unit cell parameter a, which shows that the 'sheets' of molecules **1**, parallel to (1 0 0) planes, are densely stacked in the crystal.

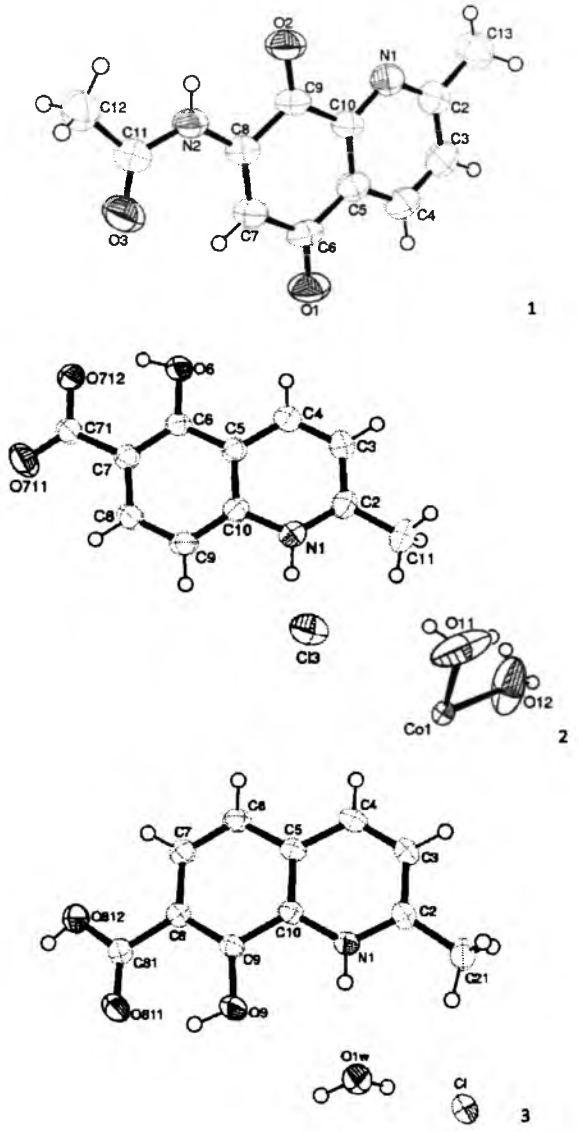

Figure 3. ORTEP projection of the asymmetric units of structures **1–3**.

Table 2
Hydrogen bonds geometry in the crystal structure of **1**

D–H	A	d(D–H) [Å]	d(H···A) [Å]	∠ DHA [°]	d(D···A) [Å]
N2–H2	O2i	0.83(4)	2.33(4)	176(3)	3.15(4)
N2–H2	O2	0.83(4)	2.33(4)	102(3)	2.63(1)

Symmetry codes (i) $-x+3, -y, -z+1$.

2.2.2. Molecule 2

The asymmetric unit of **2** consists of one molecule **2**, protonated at N1, one chloride anion, the cobalt cation and two water molecules (Fig. 3(2)). Since the Co^{2+} position is that of the inversion centre (1/2, 1/2, 1/2), this ion is present at half-occupancy. Water molecules linked with the cobalt cation show the highest atomic displacement parameters because of their disorder.

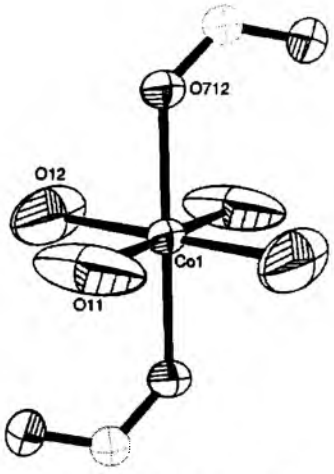

Figure 4. Cobalt cation environment.

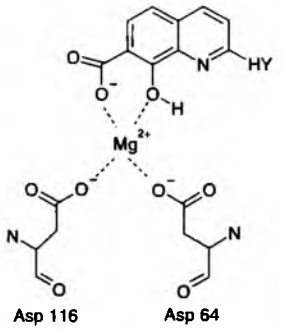

Figure 5. Hypothetical mechanism of quinoline derivative–magnesium cation interaction[35] at the active site of HIV integrase. HY-hydrophobic moiety.

Table 3
Hydrogen bonds geometry in the crystal structure of **2**

D–H	A	d(D–H) [Å]	d(H···A) [Å]	∠ DHA [°]	d(D···A) [Å]
O11–H111	O712i	0.88(2)	2.42(4)	113(3)	2.88(5)
O11–H111	O711i	0.88(2)	2.52(7)	120(6)	3.06(6)
O12–H121	O711i	0.91(2)	2.56(8)	133(9)	3.25(7)
O12–H122	O711ii	0.89(2)	2.11(6)	129(6)	2.75(6)
O11–H112	O12	0.89(2)	2.42(4)	118(3)	2.94(1)
N1–H1	Cl3	0.91(4)	2.21(4)	168(4)	3.11(4)
O6–H61	O712	0.87(5)	1.70(5)	151(5)	2.49(4)

i = −x, −y, −z; ii = x, y + 1, z + 1.

The bond lengths, bond angles and torsion angles are comparable to those typical for similar compounds.[23]

The relatively high value of C2–N1–C10 angle, equal to 123.9(3)°, is most probably the result of N1 protonation.

The coordination sphere of the cobalt cation is occupied by the oxygen atoms belonging to four water molecules and two molecules **2** (Fig. 4).

The O–Co–O angles are approximately equal to 90°, which leads to octahedral environment of Co. Crystal structure of **2** is stabilized by seven hydrogen bonds. The details of their geometry are given in Table 3.

Intramolecular O6–H61···O712 hydrogen bond is a weak interaction because it is strained by its participation in the six-membered ring which consist of C6, O6, H61, O72, C71 and C7. Intermolecular O11–H111···O712i and O11–H11···1O711i interactions are bifurcated, and similar situation can be observed for

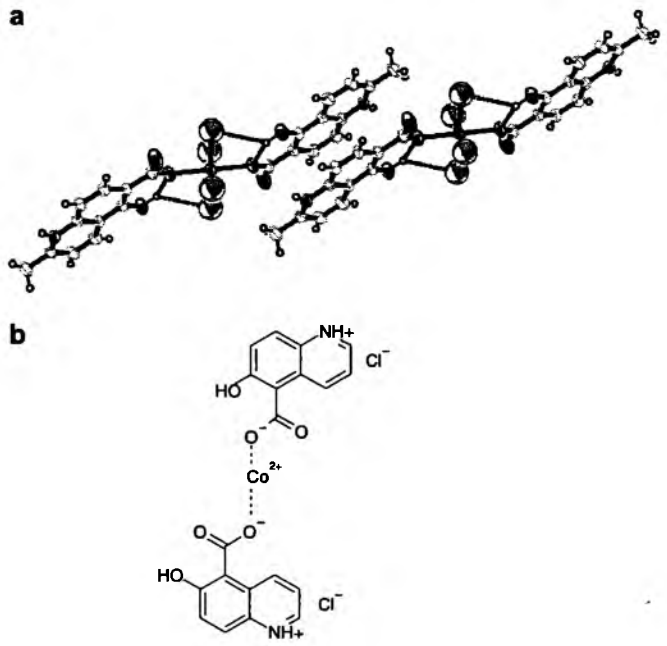

Figure 6. (a) Fragment of the crystal structure of **2** showing the coordination of Co cation and mutual π–π interactions between quinoline moieties of two complexes. (b) Scheme of cobalt cation interactions with carboxyl oxygen atoms.

Table 4
Hydrogen bonds geometry in the crystal structure of **3**

D–H	A	d(D–H) [Å]	d(H···A) [Å]	∠ DHA [°]	d(D···A) [Å]
N1–H1	O1 W	0.83(2)	2.01(2)	2.830(2)	166(2)
O9–H9	O811	0.89(2)	1.81(2)	2.590(2)	146(2)
O812–H812	Cli	0.87(2)	2.13(2)	2.965(1)	161(2)
O1W–H1W1	Cl	0.86(2)	2.31(2)	3.168(1)	177(2)
O1 W–H1W2	Clii	0.90(2)	2.39(2)	3.282(1)	170(2)

i = x + 1, y + 1, z + 1; ii = −x − 1, −y + 1, −z + 2.

O711i oxygen atom, which is an acceptor for two hydrogen atoms, H111 and H121. The strongest interaction is N1–H1···Cl3, where the chloride anion is the hydrogen acceptor.

Two molecules **2**, that coordinate cobalt cation, form a dimer, which is stabilized by the π–π interactions. The distance between centroids of quinoline ring is 4.00(3)Å.

Since the crystal structure of the salt $2[C_{11}H_8NO_3{\cdot}HCl]^{-}{\cdot}[Co(H_2O)_4]^{2+}$ is very interesting from the viewpoint of its inhibitory behaviour towards HIV integrase, it is described below in greater detail.

There are two hypotheses about magnesium cation–quinoline derivatives interactions at the active site of HIV integrase. According to the first of them one molecule of the inhibitor is in contact with two metal cations,[25–27,34] while according to the second hypothesis one quinoline interacts with one Mg cation.[23]

In the pattern shown in Figure 5 one molecule of inhibitor is in contact with magnesium cation via carboxyl and hydroxyl group, in position 7 and 8 of the quinoline ring, respectively. There are also two aspartic acid moieties (Asp 64 and Asp 116) and two water molecules in the octahedral Mg cation environment.

The model of interactions between the metal atom at the integrase active site and the quinoline inhibitor, which we can deduce from the Co-model inhibitor interactions in the crystal structure of molecule **2** (Fig. 6) is different.

The cobalt cation interacts with the oxygen atoms, which belong to the deprotonated carboxyl groups of two quinoline moieties, with Co–O distance equal 2.072(3) Å. The hydroxyl group is a proton donor in the intramolecular hydrogen bond, which stabilizes the orientation of substituents coplanar with the quinoline plane. It is interesting that, in spite of these differences, the Co–O distance is equal to those characteristic for Mg–O (2.073(2) Å) in magnesium–quinoline complex.[34] In this context we postulate that the cobalt cation might be a suitable model for prediction of the magnesium cation interactions with its environment.

2.2.3. Molecule 3

The asymmetric unit of the third structure contains one molecule **3**, in the hydrochloride form, and one water molecule (Fig. 3(3)). The bond lengths, bond angles and torsion angles are comparable to those typical for similar organic compounds.[33] The hydroxyl and methyl group are coplanar with the quinoline ring, the torsion angles C7–C8–C9–O9 and C4–C3–C2–C21 being −179.8(1)° and −178.5(1)°, respectively. The carboxyl group is deviated from planarity as shown by the C6–C7–C8–C81 angle value, −175.5(1)°. The packing of the molecules **3** in the crystal is dominated mainly by hydrogen bonds, see Table 4 for details. Intermolecular hydrogen bonds are formed between molecule **3** and water molecules, molecule **3** and the chloride anion and also between the water molecule and chloride anion. Intramolecular bond, O9–H9···O811, is weak because it leads to formation of strained hexagonal ring.

Crystal structure of **3** is also stabilized by π–π interactions between two quinolines, which are related via inversion centre. The distance between C10 atom of one molecule to the centroid of the neighbouring ring is 3.461(3) Å.

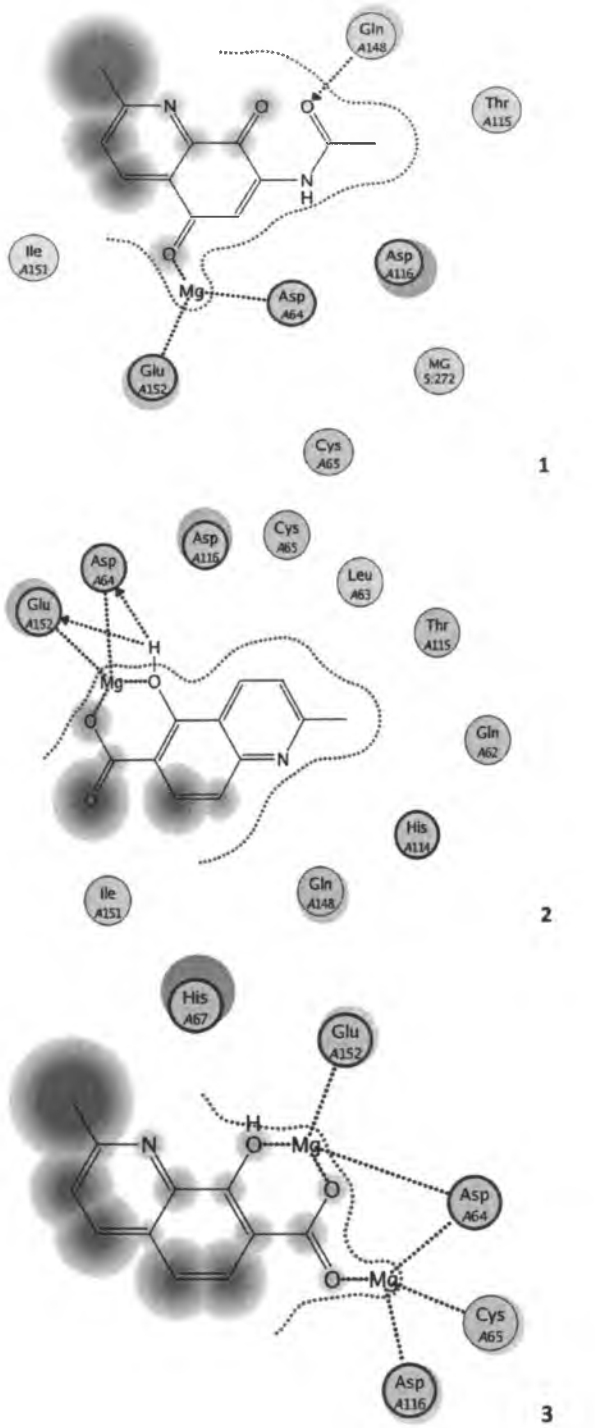

Figure 7. Compounds **1–3** docked into HIV IN active site.

2.3. Molecular docking simulations

Molecular modelling and molecular mechanics simulations were performed using the CCG MOE software packages running

Table 5
Selected interactions between studied compounds and HIV IN

Compound	IC_{50}[41] [μM]	LdG[a] [kcal/mol]	Interactions with Mg^{2+}	Interactions with aminoacids		
				Through Mg^{2+}	Hydrogen bonding	Indirect (allosteric)
1	77	−9, 67	O1–Mg	AspA64 GluA152	O3–GlnA148	AspA116
2	47[16]	−18, 75	O6–Mg–O711	AspA64 GluA152	O6H–AspA64 O6H–GluA152	AspA116
3	>100[21]	−14, 66	O9–Mg1–O812 O811–Mg	GluA152 AspA64 AspA116 CysA65	–	HisA67

[a] Calculated for the best docked pose of each structure.

on an Intel Pentium based machines with the GNU/Linux Debian operating system. Molecules **1–3** were collected in the input set and prepared for docking by standard procedure including the structure optimisation using the MMFF94x forcefield and calculation of the partial atomic charges using PM1 algorithm. Protomers and tautomers for these compounds were generated. Protein structure of HIV-1 integrase (full length DNA–integrase complex) was obtained from 1WKN PDB entry containing two aminoacid chains and two Mg^{2+} ions per each chain, bonded to ASP64, ASP116 and GLU152 residues. Additionally into the enzyme two strands of the viral DNA, segments: 1–25 and 26–52[36] has been docked. The integrase structure was prepared for docking by addition of missing hydrogen atoms, protein desolvatation, the calculation of the atomic partial charges (AMBER99 forcefield) and the protonation of the protein at physiological pH 7.4 using the PROPKA related method.[37] During docking a series of poses (ligand–protein complexes of particular conformation and mutual orientation) was generated for each molecule. The used alpha triangle docking algorithm consisted in alignment of triplets of ligand atoms on triplets of protein site points which are the centres of alpha spheres[38] created in the potential binding sites. During the simulation the poses were generated in sequence from a single conformer (protomer, tautomer) by applying a collection of preferred torsion angles to the rotatable bonds. The last stage of docking procedure was the energy minimisation and geometry optimisation of each docked pose in the binding site conditions. Classification of docking results was realized using London dG (LdG) scoring function (SF) which estimates the free energy of the ligand binding. A set of the highest scored poses were chosen for each molecule (pose) docked.[39]

According to some reports the scoring functions assessing molecular docking simulations should not be quantitatively correlated with activity.[40] Thus, in Figure 7 we present the two-dimensional ligand–receptor interaction diagrams which allows us to qualitatively observe binding in the presence of ligands.

This depicts relatively strong connections or hydrogen bonds as well as electrostatic or charge-transfer interactions between the ligand and the respective aminoacid residues. In Table 5 we have shown the interactions between ligand and protein in complex along with scoring functions and biological activities of the studied compounds. Activities are relatively low when compared to the leading structures described in literature. However, in case of fragment-based design this level of activity is quite promising for further optimisation. Nevertheless compound **3** can be regarded as inactive while **1** and **2** are moderately active. Further insight into the data collected in Table 5 provides some interesting remarks.

When compared only by scoring function, the scaffold **2** was docked at the active site with the lowest energy which can be ascribed to its high affinity, no doubt influencing the activity. Then 8-hydroxy-2-methylquinoline-7-carboxylic acid (**3**) seems to be favourably docked into the active site of HIV IN with strong interactions with two metal cations. On the other hand, it does not bind directly to aminoacids. Furthermore, the pattern of allosteric interactions in case of **1** and **2** is different from that observed in case of **3**. At the same time, compound **2** binds very efficiently and interacts with two aminoacids AspA64 and GluA152 by means of hydrogen bonding. Compound **1** binds relatively weakly to one Mg^{2+} cation and interacts with GlnA148. On this basis we can suggest different interactions pattern for structures **2** and its isomer **3**.

3. Conclusions

Three small molecular scaffolds used for fragment-based design of new HIV IN inhibitors were synthesized. Their crystal structures and in vitro activities were collected and molecular docking of studied compounds was performed. Some differences in the molecular interactions between inhibitors and enzyme seem to elucidate the activity pattern. Most active scaffold of 5-hydroxyquinaldine-6-carboxylic acid was found to be more efficient in hydrogen bonding interactions with enzyme active site than other two compounds. Further optimisation of this scaffold may lead to new interesting inhibitors.

Acknowledgements

This work was supported in part by KBN Grant PB1942/H03/2006/31 to K.M.-M. Molecular modelling was supported from PB N519 575638.

Supplementary data

Supplementary data associated with this article can be found, in the online version, at doi:10.1016/j.bmc.2011.01.045. These data include MOL files and InChiKeys of the most important compounds described in this article.

References and notes

1. Rees, D. C.; Congreve, M.; Murray, C. W.; Carr, R. *Nat. Rev. Drug Disc.* **2004**, *3*, 660.
2. Hajduk, P. J.; Greer, J. *Nat. Rev. Drug Disc.* **2007**, *6*, 211.
3. Kubinyi, H. Privileged Structures and Analogue-based Drug Discovery. In *Analogue-based Drug Discovery, IUPAC*; Fischer, J., Ganellin, C. R., Eds.; Wiley-VCH: Weinheim, 2006; pp 53–68.
4. Petersen, U. Quinolone Antibiotics: The Development of Moxifloxacin. In *Analogue Based Drug Discovery*; Fischer, J., Ganellin, C. R., Eds.; VCH-Wiley Verlag GmbH & Co., 2006; pp 315–370.
5. Fostel, J. M.; Lartey, P. A. *Drug Discovery Today* **2000**, *5*, 25.
6. Zainaba, D.; Meryem, L.; Abdelmejid, B.; Abdelfatah, A.; Mohammed, H.; Said, K.; Mohammed, B.; Mohammed, B. *Farmaco* **2004**, *59*, 195.
7. Musiol, R.; Serda, M.; Hensel-Bielowka, S.; Polanski, J. *Curr. Med. Chem.* **2010**, *17*, 1960.
8. Majerz-Maniecka, K.; Oleksyn, B.; Musiol, R.; Podeszwa, B.; Polanski, J. *Abstracts of Papers*, Joint Meeting on Medicinal Chemistry, Vienna, Austria, June 20–23, 2005. In Sci. Pharm. 2005; 73, 194.
9. Urbina, J.; Cortes, J.; Palma, A.; Lopez, S.; Kouznetsov, V. V.; Zacchino, S. A.; Enriz, R. D.; Ribas, J. C. *Bioorg. Med. Chem.* **2000**, *8*, 691.
10. Majerz-Maniecka, K.; Musiol, R.; Nitek, W.; Oleksyn, B. J.; Mouscadet, J.; Le Bret, M.; Polanski, J. *Bioorg. Med. Chem. Lett.* **2006**, *16*, 1005.

11. Doyle, T. W.; Balitz, D. M.; Grulich, R. E.; Nettleton, D. E.; Gould, S. J.; Tann, C.-H.; Meows, A. E. *Tetrahedron Lett.* **1981**, *22*, 4595.
12. Hackethal, C. A.; Golbey, R. B.; Tan, C. T. C.; Karnofsky, D. A.; Burchenal, J. H. *Antibiot. Chemother.* **1961**, *11*, 178.
13. Boger, D. L.; Mitscher, Y. M.; Drake, S. D.; Kitos, P. A.; Thompson, S. C. *J. Med. Chem.* **1987**, *30*, 1918.
14. Wilson, W. L.; Labra, C.; Barrist, E. *Antibiot. Chemother.* **1961**, *11*, 147.
15. Podeszwa, B.; Niedbala, H.; Polanski, J.; Musiol, R.; Tabak, D.; Finster, J.; Serafin, K.; Milczarek, M.; Wietrzyk, J.; Boryczka, S.; Mól, W.; Jampilek, J.; Dohnal, J.; Kalinowski, D. S.; Richardson, D. R. *Bioorg. Med. Chem. Lett.* **2007**, *17*, 6138.
16. Polanski, J.; Niedbala, H.; Musiol, R.; Podeszwa, B.; Tabak, D.; Palka, A.; Mencel, A.; Finster, J.; Mouscadet, J.-F.; Le Bret, M. *Lett. Drug Des. Disc.* **2006**, *3*, 175.
17. Polanski, J.; Niedbala, H.; Musiol, R.; Podeszwa, B.; Tabak, D.; Palka, A.; Mencel, A.; Mouscadet, J.-F.; Le Bret, M. *Lett. Drug Des. Disc.* **2007**, *4*, 99.
18. Musiol, R.; Tabak, D.; Niedbala, H.; Podeszwa, B.; Jampilek, J.; Kralova, K.; Dohnal, J.; Finster, J.; Mencel, A.; Polanski, J. *Bioorg. Med. Chem.* **2008**, *16*, 4490.
19. Musiol, R.; Jampilek, J.; Buchta, V.; Niedbala, H.; Podeszwa, B.; Palka, A.; Majerz-Maniecka, K.; Oleksyn, B.; Polanski, J. *Bioorg. Med. Chem.* **2006**, *14*, 3592.
20. Musiol, R.; Jampilek, J.; Kralova, K.; Richardson, D. R.; Kalinowski, D. S.; Podeszwa, B.; Finster, J.; Niedbala, H.; Palka, A.; Polanski, J. *Bioorg. Med. Chem.* **2007**, *15*, 1280.
21. Mekouar, K.; Mouscadet, J. F.; Desmaele, D.; Subra, F.; Leh, H.; Savoure, D.; Auclair, C.; d'Angelo, J. *J. Med. Chem.* **1998**, *41*, 2846.
22. Bonnenfant, S.; Thomas, C. M.; Vita, C.; Subra, F.; Deprez, E.; Zouhiri, F.; Desmaele, D.; d'Angelo, J.; Mouscadet, J. F.; Leh, H. *J. Virol.* **2004**, *78*, 5728.
23. Ma, X. H.; Zhang, X. Z.; Tan, J. J.; Chen, W. Z.; Wang, C. X. *Acta Pharmacol. Sin.* **2004**, *25*, 950.
24. Hare, S.; Gupta, S. S.; Valkov, E.; Engelman, A.; Cherepanov, P. *Nature* **2010**, *464*, 232.
25. Maertens, G. N.; Hare, S.; Cherepanov, P. *Nature* **2010**, *468*, 326.
26. Cherepanov, P. *EMBO Rep.* **2010**, *11*, 328.
27. Li, X.; Krishnan, L.; Cherepanov, P.; Engelman, A. *Virology* **2011** in press, doi:10.1016/j.virol.2010.12.008.
28. Hare, S.; Vos, A. M.; Clayton, R. F.; Thuring, J. W.; Cummings, M. D.; Cherepanov, P. *PNAS* **2010**, *107*, 20057.
29. Behforouz, M.; Haddad, J.; Cai, W.; Arnold, M. B.; Mohammadi, F.; Sousa, A. C.; Horn, M. A. *J. Org. Chem.* **1996**, *61*, 6552.
30. Altomare, A.; Cascarano, G.; Giacovazzo, C.; Guagliardi, A.; Moliterni, A.; Burla, M.; Polidori, G.; Camalli, M.; Spagna, R. *J. Appl. Crystallogr.* **1994**, *27*, 436.
31. Sheldrick, G. M. SHELXL97. Program For Crystal Structure Refinement, University of Göttingen, 1997.
32. Farrugia, L. J. *J. Appl. Crystallogr.* **1997**, *30*, 565.
33. Burgi, H.-B.; Dunitz, J. *Structure Correlation*; VCH, 1994.
34. Courcot, B.; Firley, D.; Fraisse, B.; Becker, P.; Gillet, J.-M.; Pattison, P.; Chernyshov, D.; Sghaier, M.; Zouhiri, F.; Desmaele, D.; d'Angelo, J.; Bonhomme, F.; Geiger, S.; Ghermani, N. E. *J. Phys. Chem. B* **2007**, *111*, 6042.
35. Zouhiri, F.; Mouscadet, J.-F.; Mekouar, K.; Desmaële, D.; Savouré, D.; Leh, H.; Subra, F.; Le Bret, M.; Auclair, C.; d'Angelo, J. *J. Med. Chem.* **2000**, *43*, 1533.
36. De Luca, L.; Pedretti, A.; Vistoli, G.; Letizia Barreca, M.; Villa, L.; Monforte, P.; Chimirri, A. *Biochem. Biophys. Res. Commun.* **2003**, *310*, 1083.
37. Li, H.; Robertson, A. D.; Jensen, J. H. *Proteins* **2005**, *61*, 704.
38. Edelsbrunner, H.; Facello, M.; Fu, R.; Liang, J. *Proceedings of the 28th Hawaii International Conference on Systems Science*. 1995, p 256.
39. Molecular Operating Environment (MOE 2008.10) CCG Inc. 1255 University St., Suite 1600, Montreal, Quebec, Canada H3B 3X3, http://www.chemcomp.com/.
40. Zentgraf, M.; Steuber, H.; Koch, C.; La Motta, C.; Sartini, S.; Sotriffer, C. A.; Klebe, G. *Angew. Chem. Int. Ed.* **2007**, *46*, 3575.
41. Polanski, J.; Zouhiri, F.; Jeanson, L.; Desmaele, D.; d'Angelo, J.; Mouscadet, J.; Gieleciak, R.; Gasteiger, J.; Le Bret, M. *J. Med. Chem.* **2002**, *45*, 4647.

Journal of Organometallic Chemistry 696 (2011) 731–738

Contents lists available at ScienceDirect

Journal of Organometallic Chemistry

journal homepage: www.elsevier.com/locate/jorganchem

Novel tricarbonyl rhenium complexes of 5,8-quinolinedione derivatives – Synthesis, spectroscopic characterisation, X-ray structure and DFT calculations

B. Machura [a,*], A. Świtlicka [a], M. Wolff [a], D. Tabak [b], R. Musioł [b], J. Polański [b], R. Kruszynski [c]

[a] Department of Crystallography, Institute of Chemistry, University of Silesia, 9th Szkolna Street, 40-006 Katowice, Poland
[b] Department of Organic Chemistry, Institute of Chemistry, University of Silesia, 9th Szkolna Street, 40-006 Katowice, Poland
[c] Department of X-ray Crystallography and Crystal Chemistry, Institute of General and Ecological Chemistry, Technical University of Lodz, 116 Żeromski Street, 90-924 Łódź, Poland

ARTICLE INFO

Article history:
Received 12 May 2010
Received in revised form
21 September 2010
Accepted 26 September 2010
Available online 11 November 2010

Keywords:
Rhenium(I) carbonyl complexes
5,8-Quinolinedione derivatives
X-ray structure
UV–vis spectra
DFT calculations

ABSTRACT

The molecular structure of 7-acetamido-2-methyl-quinoline-5,8-dione has been determined and the reactivity of 7-acetamido-2-methyl-quinoline-5,8-dione (**1**) and 6-acetamido-2-methyl-quinoline-5,8-dione (**2**) towards $Re(CO)_5Cl$ has been examined. Two novel tricarbonyl rhenium complexes, *fac*-[$Re(CO)_3$(7-acetamido-2-methyl-quinoline-5,8-dione)Cl]·$CHCl_3$ (**3**·$CHCl_3$) and *fac*-[$Re(CO)_3$(6-acetamido-2-methyl-quinoline-5,8-dione)Cl]$_2$·$CHCl_3$ (**4**·$CHCl_3$), have been synthesized and characterized spectroscopically and structurally. The electronic spectrum of **3** was investigated at the TDDFT level employing B3LYP functional in combination with LANL2DZ.

1. Introduction

5,8-Quinolinediones are important and frequently studied class of compounds. The still growing interest in quinolinediones results from their wide spectrum of biological activities such as antifungal, antibacterial, antimalarial, antineoplastic and antitumor agents [1,2]. As ligands they usually bind to the central ion through the N–O chelating site. This coordination produces a five-membered ring containing an unsaturated α-iminoketo function which can act as a π acceptor towards a bound π electron-rich metal center such as rhenium(I). The α-iminoketo chelation plays an important role in the biosynthesis of the pterins, lumazines, flavins coenzymes [3, 4]. However, the number of structurally characterized of transition metal complexes incorporating such ligands is relatively rare [5].

Continuing our researches on the tricarbonyl rhenium complexes, we have examined the reactivity of two 5,8-quinolinedione derivatives, namely 7-acetamido-2-methyl-quinoline-5,8-dione (**1**) and 6-acetamido-2-methyl-quinoline-5,8-dione (**2**) (Scheme 1) towards $Re(CO)_5Cl$ in order to study of their coordination modes in dependence of the position of the acetamido group.

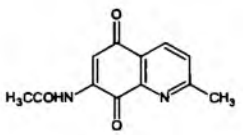

1

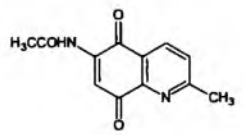

2

The still growing interest in the Re(I) complexes of heteroaromatic ligands results mainly from their unique photophysical and photochemical properties, crucial for numerous potential and already introduced practical applications. The most frequently studied compounds of this type are complexes of general formula *fac*-[$Re(CO)_3(L–L)(E)]^{0/+}$, where E stands for a halogen atom or other ligand approximately axial to the heteroaromatic rings plane. The photobehaviour of such complexes may be discussed in terms of three types of excited states: (i) metal-to-ligand charge transfer (MLCT) states, (ii) ligand-to-ligand charge transfer (LLCT) states, (iii) intraligand (IL)

* Corresponding author.
E-mail addresses: basia@ich.us.edu.pl (B. Machura), rafal.kruszynski@p.lodz.pl (R. Kruszynski).

0022-328X/$ – see front matter © 2010 Elsevier B.V. All rights reserved.
doi:10.1016/j.jorganchem.2010.09.058

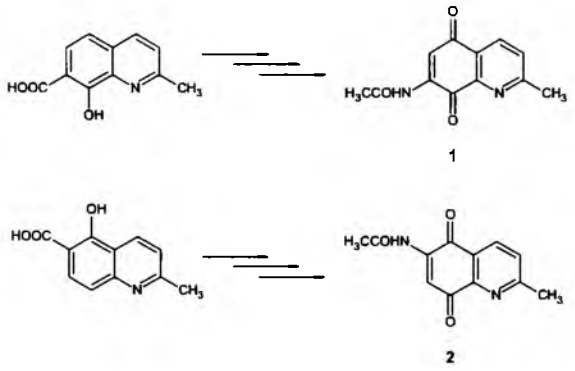

Scheme 1. Synthesis of the compounds **1** and **2**.

states. The latter one appears to lie at rather high energies in the *fac*-$[Re(CO)_3(L\text{-}L)(E)]^{0/+}$ complexes, and they are of little photochemical importance. The excited states of $[Re(CO)_3(L\text{–}L)(E)]^{0/+}$ complexes are often sufficiently long-lived to become engaged in energy transfer reactions. Currently, several *fac*-$Re(CO)_3^+$ complexes are used as electroluminescent materials in OLED-type devices [6–15]. The spectroscopic and redox behaviour of the Re(I) complexes are ligand dependent and can be tuned by varying the identity of their chelate ligands, so there is a clear need to synthesize and investigate novel species of this type.

The recent application of the *fac*-$Re(CO)_3^+$ complexes as diagnostic and therapeutic radiopharmaceuticals has resulted in an added increase in the interest of this group compounds [16].

Here, we present the synthesis, spectroscopic characterisation, crystal and molecular structures of *fac*-$[Re(CO)_3$(7-acetamido-2-methyl-quinoline-5,8-dione)Cl]·$CHCl_3$ (**3**·$CHCl_3$) and *fac*-$[Re(CO)_3$(6-acetamido-2-methyl-quinoline-5,8-dione)$Cl]_2$·$CHCl_3$ (**4**·$CHCl_3$) complexes, as well as the molecular structure of **1** (Fig. 1).

The experimental studies on the tricarbonyl rhenium complexes of quinoline-5,8-diones have been accompanied computationally by the density functional theory (DFT) and time-dependent DFT calculations. Currently density functional theory (DFT) is commonly used to examine the electronic structure of transition metal complexes. It meets with the requirements of being accurate, easy to use and fast enough to allow the study of relatively large molecules of transition metal complexes [17,18].

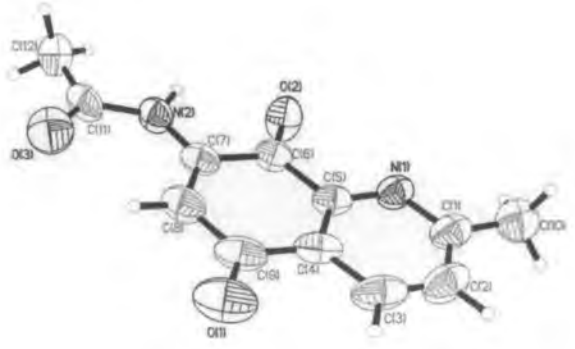

Fig. 1. Molecular structure of **1**.

2. Experimental

2.1. General procedure

All the reagents were purchased from Aldrich. 7-Acetamido-2-methyl-quinoline-5,8dione (**1**) and 6-acetamido-2-methyl-quinoline-5,8-dione (**2**) were synthesized according to the literature methods [19,20]. The reactions of $Re(CO)_5Cl$ with 7-acetamido-2-methyl-quinoline-5,8-dione and 6-acetamido-2-methyl-quinoline-5,8-dione were performed under an argon atmosphere.

The IR spectra were recorded on a Nicolet Magna 560 spectrophotometer in the spectral range 4000–400 cm^{-1} with the samples in the form of KBr pellets. The electronic spectra were measured on a spectrophotometer Lab Alliance UV–vis 8500 in the range 1000–180 nm in methanol. ^1H NMR spectra were obtained in $CDCl_3$ or DMSO-d_6 using Bruker Avance 400 spectrometer. Elemental analyses (C H N) were performed on a Perkin–Elmer CHN-2400 analyzer.

2.2. 7-Acetamido-2-methyl-quinoline-5,8-dione (1)

Yellow needles, mp 244–247 °C (decomp.). ^1H NMR (400 MHz, DMSO-d_6) δ: 2.24 (s, 3H), 2.64 (s, 3H), 7.69 (s, 1H), 7.70 (d, $J = 8.1$ Hz, 1H), 8.20 (d, $J = 8.1$ Hz, 1H), 10.00 (br s, 1H). ^{13}C NMR (100 MHz, DMSO-d_6) δ: 24.5, 24.6, 115.0, 126.5, 128.1, 133.7, 142.0, 145.8, 163.4, 171.4, 178.6, 184.8. ^{14}N NMR (400 MHz, $CDCl_3$, reference compound 90% CH_3NO_2 in $CDCl_3$) δ: 310 (pyridine N), 80 (amine N). IR (KBr, cm^{-1}) ν: 3332 (s), 1719 (s), 1687 (vs), 1641 (vs), 1618 (s), 1589 (s), 1510 (vs), 1373 (m), 1317 (s), 1216 (s), 1137 (s). EI-MS, 70 eV, *m/z*: 230 (M^+), 188, 161 (100), 132, 119, 104, 93, 68, 43. Anal. Calc. for $C_{12}H_{10}N_2O_3$: C, 62.60; H, 4.38; N, 12.17. Found: C, 62.91; H, 4.06; N, 12.30.

2.3. 7-Acetamido-2-methyl-quinoline-5,8-dione (2)

Yellow needles, mp 232–234 °C (decomp.). ^1H NMR (400 MHz, DMSO-d_6) δ: 2.25 (s, 3H), 2.65 (s, 3H), 7.69 (d, $J = 8.1$ Hz, 1H), 7.75 (s, 1H), 8.31 (d, $J = 8.0$ Hz, 1H), 9.97 (br s, 1H). ^{13}C NMR (100 MHz, DMSO-d_6) δ: 25.0, 25.1, 117.1, 126.1, 127.6, 135.0, 141.5, 147.0, 164.9, 171.9, 181.0, 184.3. IR (KBr, cm^{-1}) ν: 3346 (s), 1715 (s), 1665 (vs), 1617 (s), 1587 (s), 1505 (vs), 1376 (m), 1331 (vs), 1301 (s), 1224 (m), 1198 (s). ESI-MS (−), 100 eV, *m/z*: 230 (100, M^+), 215, 200, 190, 178, 160. Anal. Calc. for $C_{12}H_{10}N_2O_3$: C, 62.60; H, 4.38; N, 12.17. Found: C, 62.88; H, 4.19; N, 12.26.

2.4. fac-[Re(CO)$_3$(7-acetamido-2-methyl-quinoline-5,8-dione)Cl]·$CHCl_3$ (3·$CHCl_3$)

$Re(CO)_5Cl$ (0.1 g, 0.28 mmol) and 7-acetamido-2-methyl-quinoline-5,8-dione (0.07 g, 0.30 mmol) in chloroform (60 cm^3) were refluxed for 5 h. The resulting solution was reduced in volume to ~10 ml and allowed to cool to room temperature. X-ray quality red crystals of **3**·$CHCl_3$ were filtered off and dried in the air.

Yield 80%. IR (KBr, cm^{-1}): $\nu_{NH} = 3264$ and 3215 cm^{-1}; $\nu_{CO} = 2026$, 1928, 1893, 1721 and 1646 cm^{-1}; ν_{CN} and $\nu_{C=C} = 1592$, 1563 and 1512 cm^{-1}. ^1H NMR (400 MHz,$CDCl_3$) δ: 2.44 (s, 3H), 3.14 (s, 3H), 8.00 (d, 1H), 8.11 (s1H), 8.26 (br s, 1H), 8.53 (d, 1H). Anal. Calc. for $C_{16}H_{11}Cl_4N_2O_6Re$: C, 29.33; H, 1.69; N, 4.27%. Found: C, 29.57; H, 1.56; N, 4.34%.

2.5. fac-[Re(CO)$_3$(6-acetamido-2-methyl-quinoline-5,8-dione)Cl]$_2$·$CHCl_3$ (4·$CHCl_3$)

The complex **4**·$CHCl_3$ was obtained using a procedure similar to that for **3**·$CHCl_3$. Red crystals of **4**·$CHCl_3$ were collected in 85%, respectively. IR (KBr, cm^{-1}): $\nu_{NH} = 3339$ and 3291 cm^{-1}; $\nu_{CO} = 2023$, 1920, 1898, 1727 and 1681 cm^{-1}; ν_{CN} and $\nu_{C=C} = 1618$, 1594, 1558 and 1495 cm^{-1}. UV–vis of **4**·$CHCl_3$ (MeOH; λ_{max} [nm] (ε

Table 1
Crystal data and structure refinements for **1**, **3**·$CHCl_3$ and **4**·$CHCl_3$.

	1	**3**·$CHCl_3$	**4**·$CHCl_3$
Empirical formula	$C_{12}H_{10}N_2O_3$	$C_{16}H_{11}Cl_4N_2O_6Re$	$C_{31}H_{21}Cl_5N_4O_{12}Re_2$
Formula weight	230.22	655.27	1190.16
Temperature	293(2) K	291.0(3) K	293(2) K
Wavelength	0.71073 Å	0.71073 Å	0.71073 Å
Crystal system	Monoclinic	Triclinic	Triclinic
Space group	$P2_1/n$	$P\bar{1}$	$P\bar{1}$
Unit cell dimensions	$a = 3.8985(3)$ Å $b = 10.5426(12)$ Å, $\beta = 91.696(8)°$ $c = 26.749(2)$ Å	$a = 10.4441(18)$, $\alpha = 92.780(8)$ $b = 10.7079(12)$, $\beta = 112.740(9)$ $c = 10.9281(14)$, $\gamma = 109.699(11)$	$a = 7.6872(2)$, $\alpha = 98.555(2)$ $b = 11.0368(3)$, $\beta = 94.007(2)$ $c = 22.6413(5)$, $\gamma = 90.608(2)$
Volume	1098.91(15) Å^3	1038.4(3) Å^3	1894.49(8)
Z	4	2	2
Density (calculated)	1.392 mg/m^3	2.096 mg/m^3	2.086 mg/m^3
Absorption coefficient	0.102 mm^{-1}	6.402	6.802
$F(000)$	480	624	1130
Crystal size	0.039 × 0.039 × 0.445 mm	0.084 × 0.074 × 0.061 mm	0.030 × 0.057 × 0.192 mm
θ range for data collection	3.61–25.00°	2.06–25.01°	3.52–25.00°
Index ranges	$-4 \le h \le 4$, $-12 \le k \le 12$, $-31 \le l \le 31$	$-12 \le h \le 12$, $-12 \le k \le 12$, $-12 \le l \le 12$	$-9 \le h \le 9$, $-13 \le k \le 13$, $-26 \le l \le 26$
Reflections collected	10053	9214	34720
Independent reflections	1948 [R(int) = 0.0572]	3634 [R(int) = 0.0655]	6643 [R(int) = 0.0327]
Completeness to 2θ	99.7%	99.3%	99.7%
Max. and min. transmission	1.000 and 0.425	0.682 and 0.586	1.000 and 0.239
Data/restraints/parameters	1948/0/156	3634/0/264	6643/0/519
Goodness-of-fit on F^2	1.055	1.100	1.063
Final R indices [$I > 2\sigma(I)$]	$R1 = 0.0542$, $wR2 = 0.1389$	$R1 = 0.0671$, $wR2 = 0.1796$	$R1 = 0.0189$, $wR2 = 0.0426$
R indices (all data)	$R1 = 0.0827$, $wR2 = 0.1497$	$R1 = 0.0760$, $wR2 = 0.1844$	$R1 = 0.0236$, $wR2 = 0.0433$
Largest diff. peak and hole	0.154 and −0.204 eÅ^{-3}	1.327 and 1.071 eÅ^{-3}	1.188 and −1.224 eÅ^{-3}

[dm^3 mol^{-1} cm^{-1}]): 521.0 (2080), 356.6 (1860), 294.4 (29940), 257.6 (31970), 216.5 (36700), 184.7 (29860). ^{1}H NMR (400 MHz,$CDCl_3$) δ: 2.39 (s, 3H), 3.12 (s, 3H), 7.90 (d, 1H), 8.32 (s1H), 8.48 (br s, 1H), 8,52 (d, 1H). Anal. Calc. for $C_{21}H_{22}Cl_5N_4O_{12}Re_2$: C, 31.26; H, 1.78; N, 4.70%. Found: C, 31.79; H, 1.82; N, 4.59%.

2.6. Crystal structures determination and refinement

The X-ray intensity data of **3**·$CHCl_3$ were collected on a KM-4-CCD automatic diffractometer equipped with CCD detector and graphite monochromated MoKα radiation ($\lambda = 0.71073$ Å) at room temperature. Data collections of **1** and **4**·$CHCl_3$ were carried out on an Gemini A Ultra Oxford Diffraction four-circle kappa geometry diffractometer with Atlas CCD detector and graphite monochromated MoKα radiation ($\lambda = 0.71073$ Å) by applying the CrysAlis software system. Details concerning crystal data and refinement are given in Table 1. Lorentz, polarization and absorption correction [21] were applied. The structure of **1** was solved by direct methods, the structures of **3**·$CHCl_3$ and **4**·$CHCl_3$ – by the Patterson method, and then subsequently completed by the difference Fourier recycling. All the non-hydrogen atoms were refined anisotropically using full-matrix, least-squares technique. The hydrogen atoms were treated as "riding" on their parent carbon atoms and assigned isotropic temperature factors equal 1.2 (non-methyl) and 1.5 (methyl) times the value of equivalent temperature factor of the parent atom. The methyl groups were allowed to rotate about their local threefold axis. The solvent of compound **4** is disordered over two positions with 61:39 participation of domains. Some terminal atoms of the carbonyl groups of compound **4** show also signs of disordered exhibiting in relatively large displacement ellipsoids directed perpendicularly to the direction of terminal bonds. Because these atoms' electron density distribution shows no internal separated maxima, thus it can be supposed that the disorder is dynamical in character. SHELXS97 and SHELXL97 [22] programs were used for all the calculations. Atomic scattering factors were those incorporated in the computer programs.

Table 2
Short intra- and intermolecular contacts detected in **1**, **3**·$CHCl_3$ and **4**·$CHCl_3$.

D–H···A	D–H	H···A	D···A	D–H···A
1				
N2–H2N···O2	1.02	2.24	2.624(2)	104.9
N2–H2N···O2_$1	1.02	2.22	3.125(2)	169.7
C2–H1···O1_$2	0.93	2.49	3.246(3)	139.1
C8–H7···O3	0.93	2.25	2.845(3)	120.9
C12–H12B···O2_$1	0.96	2.48	3.368(3)	154.7
3·$CHCl_3$				
N2–H2···O4	0.86	2.33	2.702(14)	106.5
N2–H2···Cl1_$3	0.86	2.67	3.490(12)	159.6
C5–H5···O1_$4	0.93	2.58	3.303(15)	135.0
C9–H9···O6	0.93	2.20	2.795(18)	121.2
C99–H99···O5_$5	0.98	2.52	3.32(2)	138.9
C99–H99···Cl1_$6	0.98	2.80	3.595(16)	138.7
4·$CHCl_3$				
N2–H2N···O5	0.93	2.21	2.674(4)	110.0
N2–H2N···O14_$7	0.93	2.27	3.125(4)	153.5
N4–H4N···Cl89_$5	1.00	2.80	3.495(4)	127.5
N4–H4N···O2_$5	1.00	2.49	3.220(4)	129.9
N4–H4N···O12	1.00	2.10	2.666(4)	113.8
C10–H10···O6	0.93	2.25	2.831(4)	119.7
C13–H13B···Cl1_$8	0.96	2.70	3.641(3)	167.3
C25–H26···O14	0.93	2.26	2.850(4)	121.2
C28–H29B···Cl2_$5	0.96	2.74	3.695(4)	177.1

Symmetry transformations used to generate equivalent atoms: #1 1 − x, −y, −z; #2 −1/2 − x, 1/2 + y, 1/2 − z; #3 1 − x, 1 − y, −z; #4 x, y, 1 + z; #5 1 + x, y, z, #6 2 − x, 1 − y, 1 − z; #7 1 − x, 1 − y, −1 − z; #8 −1 + x, y, z.

2.7. Computational details

The gas phase geometry of **3** was optimized without any symmetry restrictions in singlet ground-states with the DFT method using the hybrid B3LYP functional of GAUSSIAN-03 [23–26]. The calculations were performed using ECP LANL2DZ basis set [27] with an additional d and f function with the exponent $\alpha = 0.3811$ and $\alpha = 2.033$ [28] for the rhenium and the standard 6-31G basis set for the other atoms. For chlorine, oxygen and nitrogen atoms, diffuse and polarization functions were added. All vibrations in the calculated vibrational spectrum of **3** were real, thus the geometry of **3** corresponds to true energy minimum.

The electronic spectrum of **3** was calculated with the TDDFT method [29], and the solvent effect (methanol) was simulated using

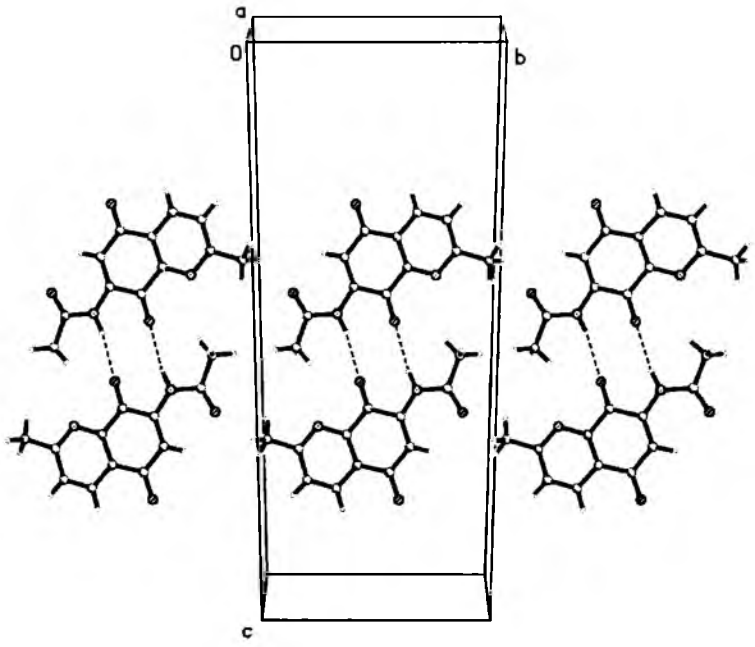

Fig. 2. The molecular packing of **1**.

the polarizable continuum model with the integral equation formalism (IEF-PCM) [29].

3. Results and discussion

3.1. Preparation and infrared data

Both 7-acetamido-2-methyl-quinoline-5,8dione (**1**) [19] and 6-acetamido-2-methyl-quinoline-5,8-dione (**2**) [20] were prepared in multistep synthesis (Scheme 1) described by us previously. Compound **2** characterized in this publication as **2a**, after NMR and especially X-ray studies, was definitely specified to have a structure **2**. The title compounds were unexpected products resulted in a reaction course initiated by decarboxylation within the 5,8-quinolinedione system.

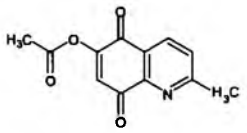

2a

Table 3
The experimental bond lengths [Å] and angles [°] for **1**.

Bond lengths		Bond angles	
O(1)–C(9)	1.226(3)	C(11)–N(2)–C(7)	128.1(2)
O(2)–C(6)	1.215(2)	C(2)–C(3)–C(4)	119.3(2)
N(2)–C(11)	1.375(3)	C(3)–C(2)–C(1)	120.6(3)
N(2)–C(7)	1.380(3)	N(1)–C(1)–C(2)	121.2(3)
C(12)–C(11)	1.478(4)	N(1)–C(1)–C(10)	116.7(2)
C(3)–C(2)	1.356(4)	C(2)–C(1)–C(10)	122.1(2)
C(3)–C(4)	1.396(4)	C(1)–N(1)–C(5)	117.7(2)
C(2)–C(1)	1.387(4)	N(1)–C(5)–C(4)	124.6(2)
C(1)–N(1)	1.338(3)	N(1)–C(5)–C(6)	116.2(2)
C(1)–C(10)	1.489(4)	C(4)–C(5)–C(6)	119.2(2)
N(1)–C(5)	1.341(3)	O(2)–C(6)–C(7)	119.9(2)
C(5)–C(4)	1.381(3)	O(2)–C(6)–C(5)	121.5(2)
C(5)–C(6)	1.489(3)	C(7)–C(6)–C(5)	118.6(2)
C(6)–C(7)	1.488(3)	C(8)–C(7)–N(2)	126.9(2)
C(7)–C(8)	1.349(3)	C(8)–C(7)–C(6)	120.8(2)
C(8)–C(9)	1.455(4)	N(2)–C(7)–C(6)	112.3(2)
C(9)–C(4)	1.475(4)	C(7)–C(8)–C(9)	121.3(2)
C(11)–O(3)	1.210(3)	O(1)–C(9)–C(8)	120.3(3)
		O(1)–C(9)–C(4)	120.5(3)
		C(8)–C(9)–C(4)	119.2(2)
		C(5)–C(4)–C(3)	116.6(3)
		C(5)–C(4)–C(9)	121.0(2)
		C(3)–C(4)–C(9)	122.5(2)
		O(3)–C(11)–N(2)	120.9(2)
		O(3)–C(11)–C(12)	124.0(2)

The complexes **3**·$CHCl_3$ and **4**·$CHCl_3$ were prepared by refluxing of [Re$(CO)_5Cl$] with a small excess of 7-acetamido-2-methyl-quinoline-5,8-dione and 6-acetamido-2-methyl-quinoline-5,8-dione in

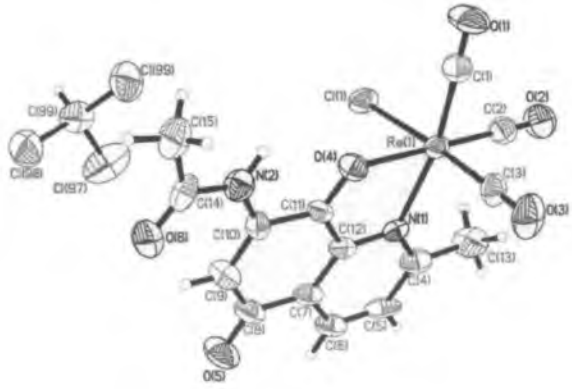

Fig. 3. Molecular structure of **3**·$CHCl_3$.

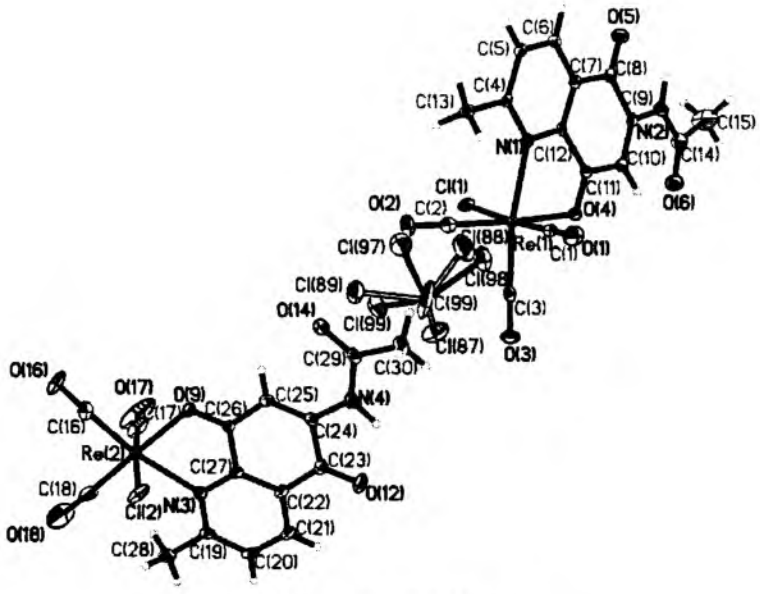

Fig. 4. Molecular structure of 4·$CHCl_3$.

chloroform, respectively. They were isolated as red solids, stable in air at room temperature, soluble in common organic solvents.

The infrared spectra of 3·$CHCl_3$ and 4·$CHCl_3$ display three bands in the carbonyl stretching region – a sharp intense band at ~2025 cm^{-1} and two lower-energy bands at 1928 and 1893 cm^{-1} for **3** and 1920 and 1898 cm^{-1} for **4**. This pattern corresponds to three CO units in a *fac* isomer arrangement [30]. The bands due to the ν(C=O) vibrations of the quinoline-5,8-dione ligands appear at 1721 and 1646 cm^{-1} for **3** and 1726 and 1681 cm^{-1} for **4**. The characteristic bands corresponding to the C=C and C=N stretching modes of the coordinated quinoline-5,8-diones are observed in the range 1620–1490 cm^{-1}. The medium intensity bands at 3264 and 3215 cm^{-1} for **3** and 3339 and 3291 cm^{-1} for **4** are assignable to ν(NH) vibration of the coordinated 7-acetamido-2-methyl-quinoline-5,8-dione and 6-acetamido-2-methyl-quinoline-5,8-dione, respectively [30].

Table 4
The experimental bond lengths [Å] and angles [°] for 3·$CHCl_3$.

Bond lengths			Bond angles		
	Experimental	Optimized		Experimental	Optimized
Re(1)–C(3)	1.920(13)	1.925	C(3)–Re(1)–C(2)	90.3(6)	90.90
Re(1)–C(2)	1.929(14)	1.919	C(3)–Re(1)–C(1)	89.8(6)	90.63
Re(1)–C(1)	1.933(14)	1.926	C(2)–Re(1)–C(1)	86.4(6)	88.74
Re(1)–O(4)	2.164(8)	2.167	C(3)–Re(1)–O(4)	93.2(5)	95.63
Re(1)–N(1)	2.247(10)	2.268	C(2)–Re(1)–O(4)	175.8(4)	173.10
Re(1)–Cl(1)	2.466(3)	2.510	C(1)–Re(1)–O(4)	95.9(4)	93.41
			C(3)–Re(1)–N(1)	94.8(5)	95.08
			C(2)–Re(1)–N(1)	103.6(5)	103.32
			C(1)–Re(1)–N(1)	168.9(5)	166.53
			O(4)–Re(1)–N(1)	73.8(3)	73.92
			C(3)–Re(1)–Cl(1)	176.2(4)	176.12
			C(2)–Re(1)–Cl(1)	92.7(4)	91.19
			C(1)–Re(1)–Cl(1)	92.6(4)	92.68
			O(4)–Re(1)–Cl(1)	83.7(3)	82.16
			N(1)–Re(1)–Cl(1)	82.4(3)	81.25
			O(1)–C(1)–Re(1)	178.5(13)	177.58
			O(2)–C(2)–Re(1)	179.7(13)	179.16
			O(3)–C(3)–Re(1)	177.3(13)	179.57

3.2. X-ray studies

The crystallographic data of **1**, 3·$CHCl_3$ and 4·$CHCl_3$ are summarized in Table 1. The short intra- and intermolecular contacts [31] detected in these structures are shown in Table 2.

Table 5
The experimental bond lengths [Å] and angles [°] for 4·$CHCl_3$.

Bond lengths		Bond angles	
Re(1)–C(2)	1.924(4)	C(2)–Re(1)–C(3)	87.47(14)
Re(1)–C(3)	1.939(4)	C(2)–Re(1)–C(1)	91.34(14)
Re(1)–C(1)	1.939(4)	C(3)–Re(1)–C(1)	86.38(13)
Re(1)–O(4)	2.161(2)	C(2)–Re(1)–O(4)	171.90(11)
Re(1)–N(1)	2.233(3)	C(3)–Re(1)–O(4)	95.22(11)
Re(1)–Cl(1)	2.4989(8)	C(1)–Re(1)–O(4)	96.44(12)
Re(2)–C(18)	1.909(4)	C(2)–Re(1)–N(1)	102.83(12)
Re(2)–C(17)	1.915(4)	C(3)–Re(1)–N(1)	169.69(12)
Re(2)–C(16)	1.925(4)	C(1)–Re(1)–N(1)	92.93(12)
Re(2)–O(9)	2.156(2)	O(4)–Re(1)–N(1)	74.62(9)
Re(2)–N(3)	2.242(3)	C(2)–Re(1)–Cl(1)	88.97(10)
Re(2)–Cl(2)	2.5044(9)	C(3)–Re(1)–Cl(1)	97.89(9)
		C(1)–Re(1)–Cl(1)	175.73(10)
		O(4)–Re(1)–Cl(1)	83.10(6)
		N(1)–Re(1)–Cl(1)	82.85(7)
		C(18)–Re(2)–C(17)	86.6(2)
		C(18)–Re(2)–C(16)	86.51(17)
		C(17)–Re(2)–C(16)	87.49(15)
		C(18)–Re(2)–O(9)	177.27(17)
		C(17)–Re(2)–O(9)	95.99(17)
		C(16)–Re(2)–O(9)	94.37(12)
		C(18)–Re(2)–N(3)	104.15(15)
		C(17)–Re(2)–N(3)	94.05(14)
		C(16)–Re(2)–N(3)	169.29(13)
		O(9)–Re(2)–N(3)	74.93(9)
		C(18)–Re(2)–Cl(2)	94.61(17)
		C(17)–Re(2)–Cl(2)	174.84(12)
		C(16)–Re(2)–Cl(2)	97.58(10)
		O(9)–Re(2)–Cl(2)	82.72(7)
		N(3)–Re(2)–Cl(2)	80.79(7)
		C(12)–N(1)–Re(1)	113.2(2)
		C(4)–N(1)–Re(1)	129.7(2)

3.3. 7-Acetamido-2-methyl-quinoline-5,8-dione

7-Acetamido-2-methyl-quinoline-5,8-dione (**1**) is crystallized in the monoclinic space group $P2_1/n$. The crystal structure of the compound comprises of one molecule per asymmetric unit. The molecules of **1** are linked by N–H···O intermolecular hydrogen bonds to dimers (Fig. 2). Additionally the dimers are connected by short intermolecular C–H···O contacts which can be classified as weak hydrogen bonds, to the hydrogen bonded chain along crystallographic [−311] axis. The existence of intramolecular N–H···O and C–H···O hydrogen bonds provides additional conformational stabilization to the side acetamide chain.

The selected bond distances and angles of **1** are shown in Table 3. All the distances and bond angles are unexceptional and fall within the normal range expected for this type of compounds.

3.4. *fac*-[Re(CO)$_3$(7-acetamido-2-methyl-quinoline-5,8-dione)Cl]·CHCl$_3$ and *fac*-[Re(CO)$_3$(7-acetamido-2-methyl-quinoline-5,8-dione)Cl]·CHCl$_3$ complexes

The both complexes **3**·CHCl$_3$ and **4**·CHCl$_3$ crystallize in *P*-1 space group. The crystal structure of **3**·CHCl$_3$ comprises of one complex and chloroform molecules per asymmetric unit, whereas the asymmetric unit of the second Re(I) carbonyl (**4**) consists of two complex molecules and one disordered CHCl$_3$ molecule (Figs. 3 and 4 respectively). The complex molecules of **3** are connected by Cl–H···O hydrogen bonds to dimers, where as the complex molecules of **4** are connected by N–H···O hydrogen bonds to tetramers. In **4** the solvent molecules are linked to complex molecules by Cl–H···O hydrogen bonds and such connection does not exist in **3**. The existence of weak hydrogen bonds (Table 2) in **3** and **4** expands the molecules to the three-dimensional nets. Additionally in both structures can be found some intramolecular hydrogen bonds (Table 2). The selected bond distances and angles of **3**·CHCl$_3$ and **4**·CHCl$_3$ are shown in Tables 4 and 5, respectively.

X-ray studies of **3** and **4** confirm bidentate coordination mode of 7-acetamido-2-methyl-quinoline-5,8dione and 6-acetamido-2-methyl-quinoline-5,8-dione. The both quinoline-5,8-dione derivatives are coordinated to the central ion through the N–O chelating site. The complexes **3** and **4** can be considered as distorted octahedrons with the largest deviations from the expected 90° bond angles coming from the bite angle of the quinoline-5,8-dione ligands. They are equal to ~74°, and they are similar to that reported for the related [Re(CO)$_3$(6-ATML)Cl]·

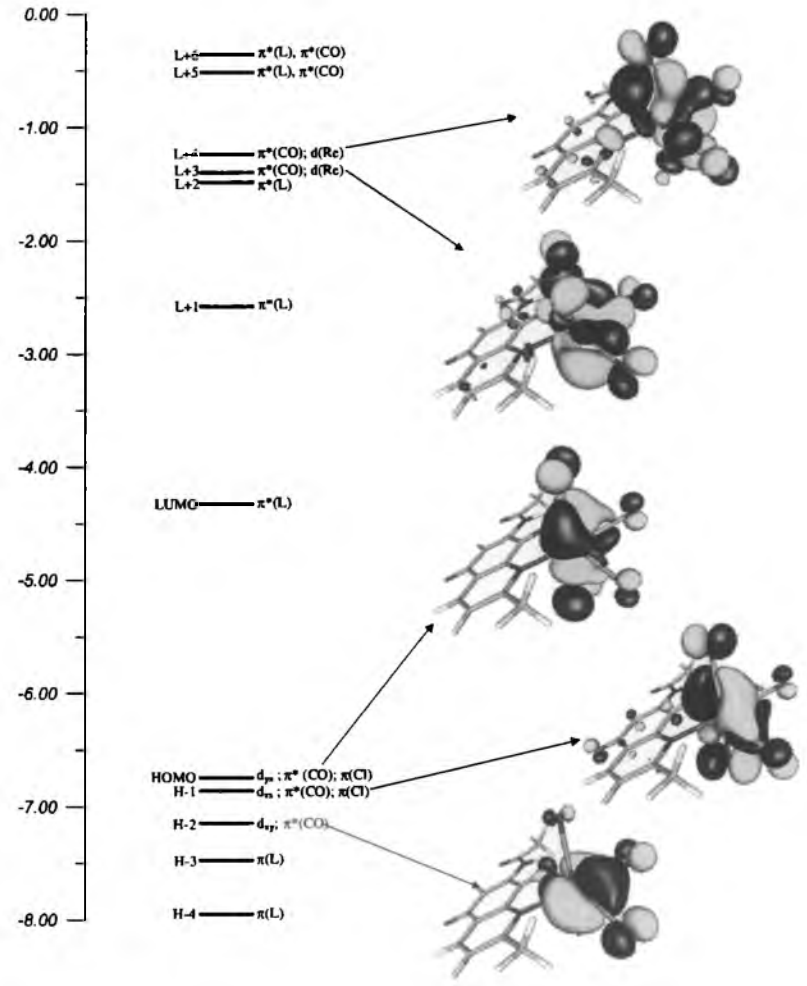

Fig. 5. The energy (eV), character and some contours of the occupied and unoccupied molecular orbitals of **3**·CHCl$_3$ (L = 7-acetamido-2-methyl-quinoline-5,8dione).

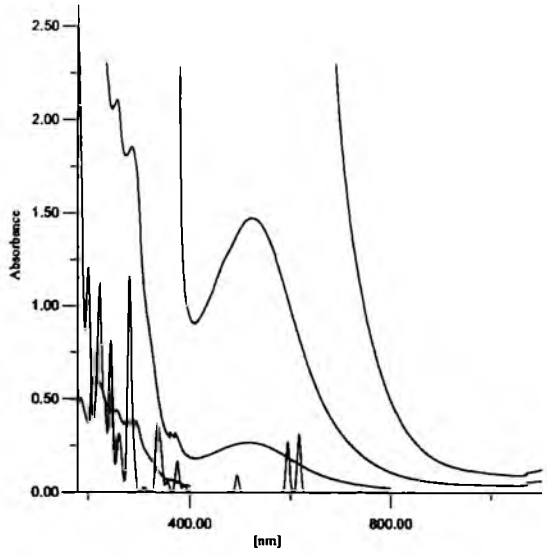

Fig. 6. The experimental (black) and calculated (red) electronic absorption spectra of **3**·$CHCl_3$.

$3C_6H_6$ (6-ATML = 6-acetyl-1,3,7-trimethyllumazine) [75.2(1)°]. The bite angles O–M–N in the structures with α-iminoketo chelate ligands bounded to transition metals depend mainly on the size of the metal center, the smallest values (down to 67°) were found for Ag^{I} complexes and the largest angles (up to 85°) were observed for compounds with Cu^{II} [3].

The electron-rich central ions of **3** and **4** show larger affinity towards the less basic but strongly π accepting carbonyl oxo atom, and the Re–O distances are slightly shorter than the Re–N bonds (Tables 2 and 4). The values Δ = d(M–N) – d(M–O), reflecting the symmetry of the chelate arrangement in such structures, are equal to 0.083 Å for **3** and 0.072 and 0.086 Å for **4**. It can be assumed that the Re center is situated symmetrically between N and O donor atoms of the quinoline-5,8-dione ligands.

3.5. Optimized geometry

The geometry of **3** was optimized in a singlet state by the DFT method with the B3LYP functional. The optimized geometric parameters are shown in Table 5. The calculated bond lengths and angles are in agreement with the values based upon the X-ray crystal structure data, and the general trends observed in the experimental data are well reproduced in the calculations.

Table 6
The energy and molar absorption coefficients of experimental absorption bands and the electronic transitions calculated with the TDDFT method for **3**·$CHCl_3$.

The most important orbital excitations	Character	λ [nm]	*E* [eV]	*f*	Experimental, λ [nm] (*E* [eV]) ε
H-1 → L	d/π(Cl) → π*(N–O)	616.68	2.0105	0.0783	525.6 (2.36)2820
H-2 → L	d → π*(N–O)	594.19	2.0866	0.0685	
H-3 → L	π(N–O) → π*(N–O)	493.66	2.5115	0.0236	
H-7 → L	π(Cl)/π(N–O)/d → π*(N–O)	374.79	3.3081	0.0421	365.8 (3.39)2880
H-1 → L+1	d/π(Cl) → π*(N–O)	342.79	3.6169	0.0517	
H-8 → L	π(N–O)/π(Cl)/d → π*(N–O)	336.09	3.6890	0.0801	
H-3 → L+1	π(N–O) → π*(N–O)	281.68	4.4016	0.2772	293.7 (4.22)22 700
H-2 → L+4	d → π*(CO)/d	263.38	4.7073	0.0324	
H-1 → L+3	d/π(CO)/π(Cl) → π*(CO)/d				
H-13 → L	π(N–O) → π*(N–O)				
H-1 → L+2	d/π(Cl) → π*(N–O)				
H-6 → L+1	π(Cl)/π(N–O)/d → π*(N–O)	246.71	5.0254	0.0557	257.6 (4.81)26 570
H-7 → L+1	π(Cl)/π(N–O)/d → π*(N–O)	244.81	5.0646	0.0967	
H-12 → L	π(N–O) → π*(N–O)	244.20	5.0771	0.0454	
H-8 → L+1	π(N–O)/π(Cl)/d → π*(N–O)	233.84	5.3020	0.0903	210.7 (5.88)31 250
H-3 → L+2	π(N–O) → π*(N–O)	224.85	5.5145	0.0694	
H-3 → L+3	π(N–O) → d/π*(CO)	223.63	5.5443	0.1227	
H-1 → L+7	d/π(Cl) → d/π*(CO)	221.32	5.6020	0.0358	
H → L+5	d//π(Cl) → π*(N–O)/π*(CO)				
H-9 → L+1	π(Cl)/π(N–O) → π*(N–O)	213.53	5.8064	0.0397	
H-14 → L	π(N–O) → π*(N–O)	202.31	6.1285	0.0326	183.7 (6.75)30 740
H-2 → L+8	d → π*(CO)/π*(N–O)/d	200.82	6.1738	0.0483	
H-6 → L+2	π(Cl)/π(N–O)/d → π*(N–O)				
H-2 → L+10	d → π*(CO)/d				
H-5 → L+4	π(Cl)/π(N–O) → d/π*(CO)	200.33	6.1889	0.0680	
H-2 → L+5	d → π*(N–O)/π*(CO)				
H-3 → L+5	π(N–O) → π*(N–O)/π*(CO)				
H-3 → L+6	π(N–O) → π*(N–O)/π*(CO)	187.99	6.5954	0.0586	
H-3 → L+6	π(N–O) → π*(N–O)/π*(CO)	187.04	6.6288	0.1338	
H-9 → L+3	π(Cl)/π(N–O) → π*(CO)/d	183.76	6.7471	0.0423	
H → L+13	d/π(Cl) → d/π*(CO)				
H → L+14	d/π(Cl) → d/π*(CO)				
H → L+12	d/π(Cl) → d/π*(CO)	182.65	6.7880	0.1395	
H-2 → L+9	d → d/π*(CO)				
H-6 → L+6	π(Cl)/π(N–O)/d → π*(N–O)/π*(CO)				
H-7 → L+5	π(Cl)/π(N–O)/d → π*(N–O)/π*(CO)	180.74	6.8599	0.1345	
H → L+15	d/π(Cl) → d/π*(CO)				

3.6. Electronic structure

The complex **3** is a closed-shell structure. Its molecular orbital diagram with several occupied and virtual molecular orbital contours is presented in Fig. 5. The HOMO–LUMO gap equals to 2.42 eV. The low-lying virtual orbitals correspond mainly to π-antibonding orbitals of 7-acetamido-2-methyl-quinoline-5,8-dione and carbonyl ligands. The LUMO, LUMO + 1 and LUMO + 2 are centered on the 7-acetamido-2-methyl-quinoline-5,8-dione ligand. The higher virtual orbitals are delocalized among Re and carbonyls or among Re, carbonyls and quinoline-5,8-dione derivative.

The three highest occupied molecular orbitals are predominately localized on the rhenium atom, corresponding to the $(5d_{xy})^2$ $(5d_{xz})^2$ $(5d_{yz})^2$ occupation of the central ion. However, ligand contributions are also important. All these orbitals have a relatively considerable CO character. The HOMO and HOMO-1 orbitals contain also an admixture of chloride p_π orbitals.

3.7. Electronic spectrum

The electronic absorption spectrum of **3** was measured in methanol, and the experimental absorption bands were assigned using the singlet excited states calculated with the time-dependent DFT method. The assignment of the calculated orbital excitations to the experimental bands was based on an overview of the contour plots and relative energy to the occupied and unoccupied orbitals involved in the electronic transitions. The experimental and calculated electronic spectra of **3** are compared in Fig. 6. Each calculated transition is represented by a Gaussian function $y = ce^{-bx^2}$ with the height (c) equal to the oscillator strength and b equal to 0.04 nm^{-2}. As seen in the Fig. 6, TDDFT/PCM calculations well reproduce the absorption spectrum of **3** measured in methanol.

Table 6 shows the spin-allowed singlet–singlet electronic transitions calculated with the TDDFT method for **3**. For the high energy part of the spectrum, only transitions with oscillator strengths larger than 0.030 are listed in Table 6. The assignment of the calculated orbital excitations to the experimental bands was based on an overview of the contour plots and relative energy to the occupied and unoccupied orbitals involved in the electronic transitions.

The longest wavelength experimental bands of **3** at 527.1 nm originate in the HOMO-1 → LUMO, HOMO-2 → LUMO and HOMO-2 → LUMO transitions, respectively. As it can be seen from Fig. 5, the LUMO orbital is completely centered on the chelate ligand, the HOMO-1 and HOMO-2 orbitals are delocalized among rhenium ion, chloride and carbonyl ligands, whereas the HOMO-3 is formed of π-bonding orbitals of the quinoline-5,8-dione ligand. Accordingly, the transitions assigned to the longest wavelength experimental bands can be seen as mixed $d_{Re} \rightarrow \pi^*(N{-}O)$ (MLCT) and $\pi Cl/\pi(N{-}O) \rightarrow \pi^*(N{-}O)$ (LLCT) or a delocalized MLLCT (metal–ligand-to-ligand CT) description can be used.

The transitions leading to the experimental bands at 365.8, 293.7, 257.6, 210.7 and 183.7 nm are attributed to *Metal-to-Ligand Charge Transfer* (occurring from the rhenium ion to the π-antibonding orbitals of the chelate ligand or π-antibonding orbitals of the carbonyl group), *Ligand–Ligand Charge Transfer* and intraligand (IL) transitions.

Acknowledgements

The GAUSSIAN-03 calculations were carried out in the Wroclaw Centre for Networking and Supercomputing, WCSS, Wroclaw, Poland, http://www.wcss.wroc.pl, under calculational Grant No. 51/96.

Appendix. Supplementary data

CCDC 776523, 776524 and 776525 contain the supplementary crystallographic data for this paper. These data can be obtained free of charge from The Cambridge Crystallographic Data Centre via www.ccdc.cam.ac.uk/data_request/cif.

References

[1] M. Behforouz, W. Cai, F. Mohammadi, M.G. Stocksdale, Z. Gu, M. Ahmadian, D.E. Baty, M.R. Etling, H. ChAl-Anzi, T.M. Swiftney, L.R. Tanzer, R.L. Merrimanb, N.C. Behforouz, Bioorg. Med. Chem. 15 (2007) 495.
[2] R. Hargreaves, C.L. David, L. Whitesell, E.B. Skibo, Bioorg. Med. Chem. Lett. 13 (2003) 3075.
[3] W. Kaim, B. Schwederski, O. Heilmann, F.M. Hornung, Coord. Chem. Rev. 182 (1999) 323.
[4] S.B. Jiménez-Pulido, M. Sieger, A. Knödler, O. Heilmann, M. Wanner, B. Schwederski, J. Fiedler, M.N. Moreno-Carretero, W. Kaim, Inorg. Chim. Acta 325 (2001) 65.
[5] Y. Prieto, M. Muñoz, V. Arancibia, M. Valderrama, F.J. Lahoz, M.L. Martin, Polyhedron 26 (2007) 5527.
[6] D.J. Stufkens, A. Vlček Jr., Coord. Chem. Rev. 177 (1998) 127.
[7] I.R. Farrell, A. Vlček Jr., Coord. Chem. Rev. 208 (2000) 87.
[8] A. Vogler, H. Kunkely, Coord. Chem. Rev. 200–202 (2000) 991.
[9] D.R. Striplin, G.A. Crosby, Coord. Chem. Rev. 211 (2001) 163.
[10] A. Vlček Jr., M. Busby, Coord. Chem. Rev. 250 (2006) 1755.
[11] S. Ranjan, S.-Y. Li, K.-C. Hwang, W.-L. Ching, C.-S. Liu, Y.-T. Tao, C.-H. Chien, S.-M. Peng, G.-H. Lee, Inorg. Chem. 42 (2003) 1248.
[12] F. Li, G. Cheng, Y. Zhao, J. Feng, S. Liu, M. Zhang, Y. Ma, J. Shen, Appl. Phys. Lett. 83 (2003) 4716.
[13] H. Hori, F.P.A. Johnson, K. Koike, K. Takeuchi, T. Ibusuki, O. Ishitani, J. Chem. Soc., Dalton Trans. (1997) 1019.
[14] S.S. Jurisson, J.D. Lydon, Chem. Rev. 99 (1999) 2205.
[15] W.A. Volkert, T.J. Hoffman, Chem. Rev. 99 (1999) 2269.
[16] B. Coutinho, D. Dawson, J.R. Dilworth, J.R. Miller, M. Rosser, C.M. Archer, J.D. Kelly, in: M. Nicolini, G. Bandoli, U. Mazzi, S.G. Editoriali Padova (Eds.), Technetium and Rhenium in Chemistry and Nuclear Medicine, 4, vol. 3, 1995; W. Koch, M.C. Holthausen, A Chemist's Guide to Density Functional Theory. Wiley-VCH, 2000.
[17] C.J. Cramer, D.G. Truhlar, Phys. Chem. Chem. Phys. 11 (2009) 10757.
[18] M. Behforouz, Z. Gu, W. Cai, M. Horn, M. Ahmadian, J. Org. Chem. 58 (1993) 7089.
[19] M. Behforouz, Z. Gu, L.S. Stelzer, M. Ahmadian, J. Haddad, J.A. Scherschel, Tetrahedron Lett. 38 (1997) 2210.
[20] A. Mrozek-Wilczkiewicz, D.S. Kalinowski, R. Musiol, J. Finster, A. Szurko, K. Serafin, M. Knas, S.K. Kamalapuram, Z. Kovacevic, J. Jampilek, A. Ratuszna, J. Rzeszowska-Wolny, Des R. Richardson, J. Polanski, Bioorg. Med. Chem. 18 (2010) 2664.
[21] (a) CrysAlis RED, Oxford Diffraction Ltd., Version 1.171.33.46. (b) STOE & Cie, X-RED. Version 1.18. STOE & Cie GmbH, Darmstadt, Germany, 1999.
[22] G.M. Sheldrick, Acta Cryst. A64 (2008) 112.
[23] M.J. Frisch, G.W. Trucks, H.B. Schlegel, G.E. Scuseria, M.A. Robb, J.R. Cheeseman, J.A. Montgomery Jr., T. Vreven, K.N. Kudin, J.C. Burant, J.M. Millam, S.S. Iyengar, J. Tomasi, V. Barone, B. Mennucci, M. Cossi, G. Scalmani, N. Rega, G.A. Petersson, H. Nakatsuji, M. Hada, M. Ehara, K. Toyota, R. Fukuda, J. Hasegawa, M. Ishida, T. Nakajima, Y. Honda, O. Kitao, H. Nakai, M. Klene, X. Li, J.E. Knox, H.P. Hratchian, J.B. Cross, C. Adamo, J. Jaramillo, R. Gomperts, R.E. Stratmann, O. Yazyev, A.J. Austin, R. Cammi, C. Pomelli, J.W. Ochterski, P.Y. Ayala, K. Morokuma, G.A. Voth, P. Salvador, J.J. Dannenberg, V.G. Zakrzewski, S. Dapprich, A.D. Daniels, M.C. Strain, O. Farkas, D.K. Malick, A.D. Rabuck, K. Raghavachari, J.B. Foresman, J.V. Ortiz, Q. Cui, A.G. Baboul, S. Clifford, J. Cioslowski, B.B. Stefanov, G. Liu, A. Liashenko, P. Piskorz, I. Komaromi, R.L. Martin, D.J. Fox, T. Keith, M.A. Al-Laham, C.Y. Peng, A. Nanayakkara, M. Challacombe, P.M.W. Gill, B. Johnson, W. Chen, M.W. Wong, C. Gonzalez, J.A. Pople, Gaussian 03, Revision B.03. Gaussian, Inc., Pittsburgh PA, 2003.
[24] A.D. Becke, J. Chem. Phys. 98 (1993) 5648.
[25] C. Lee, W. Yang, R.G. Parr, Phys. Rev. B 37 (1988) 785.
[26] P.J. Hay, W.R. Wadt, J. Chem. Phys. 82 (1985) 299.
[27] K. Eichkorn, F. Weigend, O. Treutler, R. Ahlrichs, Theor. Chem. Acc. 97 (1997) 119.
[28] M.E. Casida, in: J.M. Seminario (Ed.), Recent Developments and Applications in Modern Density Functional Theory, Theoretical and Computational Chemistry, vol. 4, Elsevier, Amsterdam, 1996.
[29] M. Cossi, G. Scalmani, N. Rega, V. Barone, J. Chem. Phys. 117 (2002) 43.
[30] K. Nakamoto, Infrared, Raman Spectra of Inorganic and Coordination Compounds, 4th ed. Wiley-Interscience, New York, 1986.
[31] G.A. Jeffrey, W. Saenger, Hydrogen Bonding in Biological Structures. Springer-Verlag, 1994.

RZECZPOSPOLITA POLSKA

Urząd Patentowy Rzeczypospolitej Polskiej

(12) **OPIS PATENTOWY** (19) **PL** (11) **207140**

(13) **B1**

(21) Numer zgłoszenia: **374130**

(22) Data zgłoszenia: **04.04.2005**

(51) Int.Cl.
C07D 215/20 (2006.01)
C07D 215/16 (2006.01)
C07B 63/00 (2006.01)
B01D 11/00 (2006.01)

(54) **Sposób oczyszczania amidów kwasów chinaldynokarboksylowych**

(43) Zgłoszenie ogłoszono:
16.10.2006 BUP 21/06

(45) O udzieleniu patentu ogłoszono:
30.11.2010 WUP 11/10

(73) Uprawniony z patentu:
UNIWERSYTET ŚLĄSKI, Katowice, PL

(72) Twórca(y) wynalazku:
HALINA NIEDBAŁA, Dąbrowa Górnicza, PL
ROBERT MUSIOŁ, Częstochowa, PL
ANNA PAŁKA, Sosnowiec, PL
BARBARA PODESZWA, Mikołów, PL
AGNIESZKA MENCEL, Pszów, PL
DOMINIK TABAK, Dąbrowa Górnicza, PL
JAROSŁAW POLAŃSKI, Katowice, PL
JACEK FINSTER, Pszczyna, PL

PL 207140 B1

Opis wynalazku

Przedmiotem wynalazku jest sposób oczyszczania pochodnych chinaldyny zawierających wiązanie amidowe. Wiele związków o podobnej budowie wykazuje właściwości hamujące integrazę wirusa HIV.

Wirus HIV, uważany za główną przyczynę nabytego zespołu upośledzenia odporności (AIDS), jest retrowirusem atakującym komórki układu immunologicznego limfocyty T. Do prawidłowego przebiegu cyklu życiowego wirusa potrzebuje on trzech enzymów: integrazy, proteazy i odwrotnej transkryptazy. Dotychczasowe metody terapii polegają głównie na hamowaniu aktywności proteazy i odwrotnej transkryptazy.

Integraza (IN) HIV jest enzymem, który katalizuje włączanie wirusowego DNA w genom komórki gospodarza. Proces ten przebiega dwuetapowo i polega na oderwaniu dwóch nukleotydów z każdego 3' końca wirusowego DNA i pozostawieniu wolnych grup hydroksylowych, po czym następuje przeniesienie i właściwa integracja nici wirusowego DNA z genomem zarażonej komórki gospodarza jak opisano w: Zouhiri, F., Mouscadet, J. F., Mekouar, K., Desmaele, D., Savoure, D., Leh, H., Subra, F., Le Bret, M., Auclair, C, d'Angelo, J., *J. Med. Chem.* 2000, 4, 8, 1533, Chen, J. C. Krucinski, J. Miercke, L. J. Finer-Moore, J. S. Tang, A. H. Leavitt, A. D. Stroud, R. M. *Proc. Natl. Acad. Sci. U.S.A.* 2000, *97*, 8233.

W pierwszym etapie integraza do pełnej aktywności potrzebuje obecności dwudodatnich jonów metali np.; Mg^{2+}, Mn^{2+} i cząsteczek wody lub innego czynnika nukleofilowego na przykład małych cząsteczek alkoholi, glicerolu lub aminokwasów (Vink, C. Yeheskiely, E. van der Marel, G. A. van Boom, J. H. Plasterk, R. H. *Nucleic Acids Res.* 1991, *19*, 6691.) W drugim etapie utworzone wcześniej grupy 3'-OH atakują grupy fosforanowe w DNA gospodarza. Tak zaatakowana komórka rozpoczyna proces namnażania potomnych wirionów.

Dotychczasowe metody terapii przeciwwirusowej stosowanej w leczeniu AIDS polegają na podawaniu inhibitorów transkryptazy i proteazy oraz związków hamujących wnikanie lub uwalnianie wirusów. Wciąż brak jest skutecznych inhibitorów integrazy HIV.

Dużą aktywność wykazują związki oparte na strukturze chinoliny, zwłaszcza pochodne posiadające wiązanie amidowe stanowią obiecujące cele badań. W polskim zgłoszeniu patentowym P-371824 przedstawiono strukturę i zastosowanie pochodnych należących do tej grupy i wykazujących aktywność względem integrazy wirusa HIV. Niestety dotychczasowe metody syntezy takich związków są długotrwałe i nieefektywne. Najczęściej stosowane metody polegają na reakcji bezwodników odpowiednich kwasów karboksylowych z aminami. Problemem jest konieczność długotrwałego izolowania i oczyszczania otrzymanego produktu. Wykorzystanie metod opisanych w literaturze wiąże się z koniecznością zastosowania znacznego nadmiaru rozpuszczalników i wielokrotną krystalizacją, co zmniejsza wydajność i wpływa na koszty otrzymania związków. Jedną z metod, którą można stosować w syntezie amidów jest reakcja tworzonego in situ bezwodnika w obecności dicykloheksylokarbodiimidu (DCC) i odpowiedniej aminy (Sheehan, Hess, *J. Am. Chem. Soc.* 77, 1067, **1955**). Także w tym wypadku problemem jest konieczność wyizolowania i oczyszczenia otrzymywanego amidu od produktów rozkładu DCC.

Zadaniem wynalazku jest wyeliminowanie wad znanych metod przez opracowanie sposobu umożliwiającego szybką i skuteczną metodę oczyszczenia strukturalnie różnorodnych analogów związków opisanych wzorem (2) o szerokim znaczeniu medycznym.

Istota sposobu oczyszczania amidów kwasów chinaldynokarboksylowych powstałych w reakcji tworzonego in situ bezwodnika kwasu karboksylowego i odpowiedniej aminy w obecności dicykloheksylokarbodiimidu (DCC) polega na oczyszczaniu surowego produktu przez wymywanie wodnym roztworem węglanu sodu w ilościach od 0,1 ml do 100 ml na 1 mg surowego produktu korzystnie 2 ml, a następnie ekstrakcję wrzącym chloroformem w ilościach od 0,1 do 500 ml na 1 mg surowego produktu, korzystnie 1 ml na 1 mg.

Przebieg syntezy jest uwidoczniony na schemacie według wzoru 1. Podstawniki we wzorze 1 oznaczają:

A - grupę zawierającą układ chinolinowy, przedstawioną według wzoru 2,

R - podstawiony i niepodstawiony układ alkilowy, arylowy lub heterocykliczny,

przy czym R może oznaczać zarówno układ zawierający jedną jak i więcej grup aminowych.

Odpowiednie substraty, wśród których wiele jest dostępnych handlowo, można ewentualnie łatwo otrzymać na drodze syntezy. Rozpuszczalniki i związki stosowane jako katalizatory są tanie i łatwo dostępne.

Opracowany sposób umożliwia oczyszczanie wielu, strukturalnie rozbudowanych związków wykazujących aktywność względem integrazy wirusa HIV. Ponadto produkty syntezy stanowiąc bardzo silne bioefektory, mogą stanowić składniki leków antyretrowirusowych (Mekouar, Mouscadet, Desmaele, Subra, Leh Savoure, Auclair, d'Angelo, J. Med. Chem. 1998, 41, 2846). Mogą być wykorzystywane korzystnie jako inhibitory enzymów, pestycydy, związki kompleksujące dwudodatnie jony metali, takie jak: Mg^{2+}, Mn^{2+}.

P r z y k ł a d 1. 8-hydroksychinaldyno-7-karboksylo-benzylo-amid

A=chinolina podstawiona grupą OH w pozycji 8 i grupą COOH w pozycji 7 R=Ph. Związek ten może być otrzymany z kwasu 8-hydroksy-chinaldyno-7-karboksylowego i benzyloaminy zgodnie z procedurą opisaną w European Patent Application No 02701583.3. Do roztworu DCC w dichlorometanie dodaje się równomolowe ilości kwasu i aminy, a po przereagowaniu osad po odsączeniu przemywa się czterokrotnie 2 ml roztworu węglanu sodu i poddaje się ekstrakcji ciągłej wrzącym chloroformem stosując 6 ml czystego, suchego chloroformu. Związek ten może być korzystnie stosowany do leczenia AIDS w formie leku działającego na integrazę HIV Ttop=225°C.

P r z y k ł a d 2. 8-hydroksy-chinaldyno-7-karboksy-(4-fluoro-benzylo)-amid

A=chinolina podstawiona grupą OH w pozycji 8 i grupą COOH w pozycji 7 R=4-fluorofenyl. Związek ten może być otrzymany z kwasu 8-hydroksy-chinaldyno-7-karboksylowego i 4-fluorobenzyloaminy tak jak w przykładzie 1. Ttop=182°C. Związek ten wykazuje aktywność względem integrazy wirusa HIV in vivo i przez to może być korzystnie stosowany jako inhibitor tego enzymu.

P r z y k ł a d 3. 1,2-etylodiamid kwasu 7-karboksylo-8-hydroksy-2-metylochinolinowego

A=chinolina podstawiona grupą OH w pozycji 8 i karboksylową w pozycji 7, R=2-aminoetan. Związek ten może być otrzymany z kwasu 8-hydroksy-chinaldyno-7-karboksylowego i 1,2-diaminoetanu tak jak w przykładzie 1. Do 10 ml roztworu DCC w dichlorometanie dodaje się kwasu 8-hydroksy-chinaldyno-7-karboksylowego. Następnie osad po odsączeniu przemywa się 3 ml roztworu węglanu sodu i poddaje się ekstrakcji ciągłej wrzącym chloroformem stosując 8 ml rozpuszczalnika.

Zastrzeżenie patentowe

Sposób oczyszczania amidów kwasów chinaldynokarboksylowych powstałych w reakcji tworzonego in situ bezwodnika kwasu karboksylowego i odpowiedniej aminy w środowisku dicykloheksylokarbodiimidu (DCC), **znamienny tym**, że osad poreakcyjny przemywa się wodnym roztworem węglanu sodu w ilościach od 0,1 ml do 100 ml na 1 mg surowego produktu korzystnie 2 ml, a następnie ekstrahuje wrzącym chloroformem w ilościach od 0,1 do 500 ml na 1 mg surowego produktu, korzystnie 1 ml na 1 mg.

Rysunki

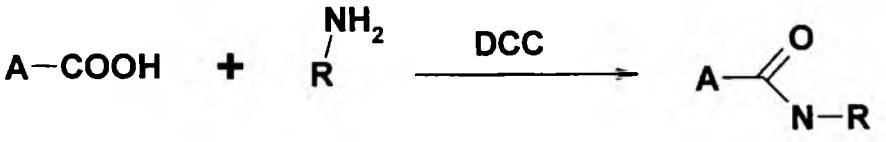

Wzór 1.

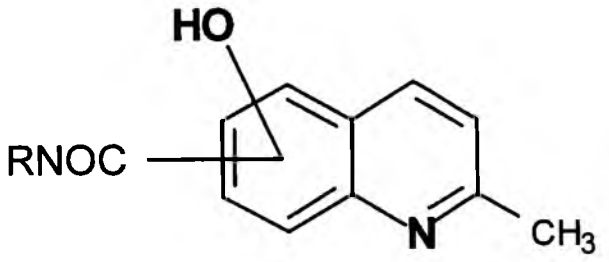

Wzór 2.

Departament Wydawnictw UP RP
Cena 2,00 zł.

10th International Electronic Conference on Synthetic Organic Chemistry (ECSOC-10). 1-30 November 2006. http://www.usc.es/congresos/ecsoc/10/ECSOC10.htm & http://www.mdpi.org/ecsoc-10/

[c007]

ZENTIVA

Substituted Amides of Quinoline Derivatives: Preparation and Their Photosynthesis-inhibiting Activity

Robert Musiol[1]*, Josef Jampilek[2], Katarina Kralova[3], Dominik Tabak[1] Barbara Podeszwa[1], Jacek Finster[1], Jaroslaw Polanski[1]

[1] Institute of Chemistry, University of Silesia, Szkolna 9, 40007 Katowice, Poland; e-mail: rmusiol@us.edu.pl, tel: +48-32-3591206, fax: +48-32-2599978

[2] Zentiva a.s., U kabelovny 130, 102 37 Prague 10, Czech Republic

[3] Institute of Chemistry, Faculty of Natural Sciences, Comenius University, Mlynska dolina Ch-2, 84215 Bratislava, Slovakia

* Author to whom correspondence should be addressed.

Abstract: The series of nine amides of substituted 8-hydroxyquinolines were prepared. The synthetic procedures of compounds are presented. All the prepared quinoline derivatives were analyzed using RP-HPLC method for the lipophilicity measurement and their lipophilicity were determined. The prepared compounds were tested for the reduction of chlorophyll content in *Chlorella vulgaris* Beij. Several compounds showed biological activity comparable with or higher than the standard 3-(3,4-dichlorophenyl)-1,1-dimethylurea (DCMU). The relationships between the lipophilicity and the chemical structure of the studied compounds are discussed as well as structure-activity relationships (SAR) between the chemical structure and the biological activities of the evaluated compounds.

Keywords: Quinoline derivatives; Lipophilicity; Reduction of chlorophyll content; *Chlorella vulgaris*; Structure-activity relationships.

INTRODUCTION

Quinoline moiety is present in many classes of biologically active compounds. A number of them have been clinically used as antifungal, antibacterial and antiprotozoic drugs [1,2] as well as antituberculotic agents [3,4]. Some quinoline based compounds showed also

antineoplastics activity [5]. Styrylquinoline derivatives have gained strong attention recently due to their activity as perspective HIV integrase inhibitors [6,7,8,9,10].
Our previous study dealing with styrylquinoline derivatives showed that they could possess also strong antifungal activity [11], the compounds containing 8-hydroxyquinoline pharmacophore seem especially interesting. According to the results reported recently some new 8-hydroxyquinoline derivatives possessed interesting antifungal and herbicidal activities [12,13,14,15].
The chemistry of quinoline has been described very well. On the other hand synthetic routes of quinoline derivatives are time consuming. Thus new efficient methods of microwave assisted organic synthesis for discussed quinoline derivatives were applied [16,17,18]. This interesting route to structurally diverse quinoline derivatives is now under optimisation. Wider discussion will be subsequently published. During our preliminary studies we have found that some up-to-date synthesized structures could be interesting to wider forum.
Various compounds possessing -NHCO- moiety were found to inhibit photosynthetic electron transport. Amides of the substituted pyridine-4-carboxylic acids [19] as well as anilides of the substituted pyrazine-2-carboxylic acids [20,21,22,23] inhibited oxygen evolution rate in *Chlorella vulgaris* and they showed some antialgal properties. Therefore a new series of amides of 8-hydroxyquinoline derivatives were prepared by means of the above-discussed pathways [16,17,18] and evaluated as potential herbicides. Synthesis, lipophilicity as well as structure-activity relationships are discussed in this paper.

RESULTS AND DISCUSSION

The compounds **1-9** were synthesized according to the procedure showed below. Kolbe-Schmidt reaction was leading to carboxylic acids which further reacted with the appropriate amine in presence of DCC or ethyldimethylaminopropyl carbodiimid (EDCI) to afford an amide. In case of **8, 9** diamine and twofold of quinaldic acid were used, see Scheme 1.

Scheme 1. Synthesis of compounds **1-9**: (a) KOH, CO_2; (b) amine, DCC or EDCI.

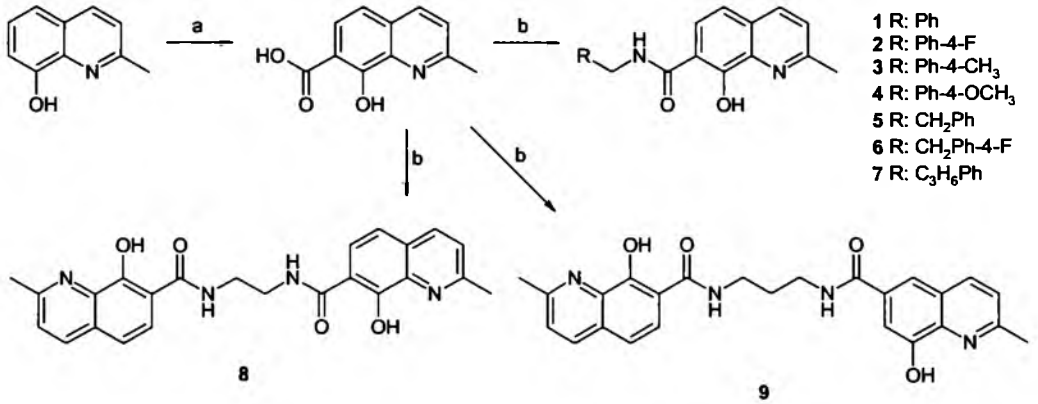

Hydrophobicities of the studied compounds **1-9** were measured by means of the reversed phase high performance liquid chromatography (RP-HPLC) method for the lipophilicity measurement. The procedure was performed under isocratic conditions with methanol as an organic modifier in the mobile phase using end-capped non-polar C_{18} stationary RP column.

The capacity factors *K* were determined and subsequent log *K* values were calculated. The results are shown in Table 1.

The total lipophilicity of the studied compounds is affected by the lipophilicity of the substituents on the aromatic rings as well as by the lipophilicity of the CH_2 and other function groups (e.g. –NH– or –C=O) in the linker. Using the π-parameter the lipophilicity of the substituents on the benzene rings can be expressed [24]. On the other hand the lipophilicity of CH_2, –NH– and –C=O groups can be expressed by aliphatic lipophilic fragment constants (f) whereas for the lipophilicity of the substituents on aromatic ring, aromatic lipophilic fragment constants (π) can be used [25]. The lipophilicity of phenyl substituents in position 4 increased in the following order: H (**1**, $\pi = 0$) < OCH_3 (**4**, $\pi = -0.03$) < F (**2**, $\pi = 0.15$) < CH_3 (**3**, $\pi = 0.60$), which corresponds to the experimentally determined log *K* values (Table 1). The lipophilicity of substituents in amide part of molecules expressed by log *K* values increased in the following order: benzyl (**5**) < phenyl (**1**) < *n*-propylphenyl (**7**). Lower lipophilicity of benzyl substituent than that of phenyl substituent was also described in ref [26]. The compound **7** possessed the highest hydrophobicity within this series. Low lipophilicity of both dimmers **8** and **9** is connected with hydrophilic 8-hydroxy substituents, on both 2-methylquinoline rings as well as by two carbonyl and –NH– groups in the spacer linking of these two ring structures (the corresponding lipophilic fragment constants (f) are -0.44 for –OH, -1.09 for –C=O and -2.15 for –NH– [25]).

All the studied compounds were handed over for herbicidal evaluation. The compound **5** was not tested due to low solubility in the testing medium. Two studied compounds (**3**, **7**) inhibited chlorophyll production in *C. vulgaris* comparable with the standard DCMU and the inhibitory activity of compound **4** evenly exceeded the activity of DCMU (Table 1). The interesting IC_{50} values varied in the range from 4.8 (**4**) to 17.2 μmol/l (**1**). Compound **4** (IC_{50} = 4.8 μmol/l) was the most efficient inhibitor.

Figure 1. Dependence of IC_{50} values (log $1/IC_{50}$ [mol/l]) related to the reduction of chlorophyll content in the suspension of *Chlorella vulgaris* on the σ constants of R substituent of 8-hydroxy-2-methylquinoline-7-carboxylic acid 4-R-benzylamides (**1-4**).

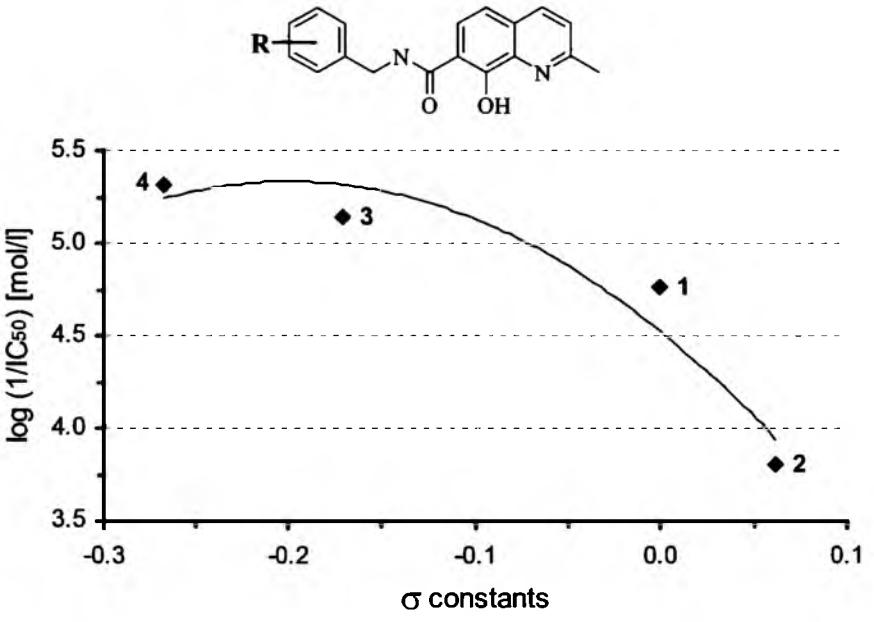

The inhibitory activity of 8-hydroxy-2-methylquinoline-7-carboxylic acid 4-R-benzylamides (**1-4**) depended on the Hammett constants σ of R substituent (Fig. 1). The σ constants of the R substituent were taken from Hansch and Leo: 0 (H, **1**); 0.062 (4-F, **2**); -0.17 (4-CH_3, **3**) and -0.268 (4-OCH_3, **4**) [25]. From Fig. 1 it is evident that the biological activity decreased with increasing σ value, *i.e.* with the electron accepting the power of the substituent.
The compounds **1** and **7**, **2** and **6** as well as **8** and **9** differ from each other by the number of CH_2 groups in the linker connecting two ring structures in the molecule. According to Hansch and Leo the hydrophobic fragment constant (f) for CH_2 group (corresponding to the contribution of CH_2 group to the compound lipophilicity) is 0.66 [25]. The comparison of compound **1** and **7** showed that the increase of the compound lipophilicity caused by prolongation of the linker by two CH_2 groups led to moderate increase of inhibitory activity. On the other hand, the prolongation of the spacer in 8-hydroxy-2-methylquinoline-7-carboxylic acid 4-fluorobenzylamide (**2**) by one CH_2 group (**6**) did not practically affect the biological activity of the compound. The addition of one CH_2 group to the spacer of bis-[8-hydroxy-2-methylquinoline-7-carboxylic acid]-1,2-etylamide (**8**) led to moderately lower activity of (**9**).
It can be assumed that the biological activity of the studied compounds depends not only on the lipophilicity but also on the electron-releasing or electron-withdrawing power of the substituent on the benzene ring. Using suitable electron-withdrawing substituent on the benzene ring and/or choosing suitable lipophilicity of the linker by addition of CH_2 group(s) the biological activity of the compounds could be optimised.

EXPERIMENTAL

General

All reagents were purchased from Aldrich. Kieselgel 60, 0.040-0.063 mm (Merck, Darmstadt, Germany) was used for column chromatography. TLC experiments were performed on alumina-backed silica gel 40 F254 plates (Merck, Darmstadt, Germany). The plates were illuminated under UV (254 nm) and evaluated in iodine vapour. Melting points were determined on Boetius PHMK 05 (VEB Kombinat Nagema, Radebeul, Germany) and are uncorrected. Elemental analyses were carried out on an automatic Perkin-Elmer 240 microanalyser (Boston, USA). All ^1H NMR spectra were recorded on a Bruker AM-500 (499.95 MHz for ^1H), Bruker BioSpin Corp., Germany. Chemicals shifts are reported in ppm (δ) to internal $Si(CH_3)_4$, when diffused easily exchangeable signals are omitted.

Synthesis of compounds **1-9**

General procedure for synthesis discussed compounds is as follows. 8-hydroxy-quinaldine-7-carboxylic acid, starting material for all synthesized amides was obtain according to known procedure.
To solution 8-hydroksyquinaldine-7-carboxylic acid (1.02 g, 5 mmol) in dry CH_2Cl_2 with 0.6 mmol of DCC was added 5.3 mmol of appropriate amine in dry CH_2Cl_2 during 4 h. After the reaction was completed, white solid was filtered, washed with 5% $NaHCO_3$, water and diethyl ether.

8-Hydroxy-2-methylquinoline-7-carboxylic acid benzylamide (**1**). Product was obtained with 86.4% yield as white solid mp 215-218 °C, ^1H NMR (DMSO-d_6, 500MHz) δ: 2.57 (s, 3H), 6.94 (d, 1H, *J*=8.4Hz), 7.3 (d, 1H, *J*=8.4Hz), 7.35-7.37 (m, 5H), 7.45 (d, 2H, *J*=7.3Hz), 7.74 (d, 1H, *J*=8.3Hz), 8.0 (d, 1H, *J*=8.3Hz).

8-Hydroxy-2-methylquinoline-7-carboxylic acid 4-fluorobenzylamide (**2**). Product was obtained according to ref [27].

8-Hydroxy-2-methylquinoline-7-carboxylic acid 4-methylbenzylamide (**3**). Product was obtained with 36.4% yield, as white solid mp 192-200°C (decomp.); ^{1}H NMR (DMSO-d_6, 500MHz) δ: 2.3 (s, 3H), 2.6(s, 3H), 4.02 (s, 2H), 6.9 (d, 1H, *J*=8.4Hz), 7.2 (d, 2H, *J*=7.5Hz), 7.31-7.35 (m, 3H), 7.75 (d, 1H, *J*=8.3Hz), 8.04 (d, 1H, *J*=8.2Hz).

8-Hydroxy-2-methylquinoline-7-carboxylic acid 4-methoxybenzylamide (**4**). Product was obtained with 34.5% yield as white solid, mp 180-190°C (decomp.); ^{1}H NMR (DMSO-d_6, 500MHz) δ: 2.6 (s, 3H), 3.7 (s, 3H), 3.9 (s, 2H), 6.93-694 (m, 3H), 7.3 (d, 1H, *J*=8.3Hz), 7.4 (d, 2H, *J*=8.3Hz), 7.7 (d, 1H, *J*=8.3Hz), 8.0 (d, 1H, *J*=8.3Hz).
21. ^{1}H NMR (DMSO-d_6, 500MHz) δ: 7.08 (d, 1H, *J*=7.3Hz), 7.71 (d, 2H, *J*=8.44Hz), 7.75 (d, 1H, *J*=8.54), 7.33-7.4 (m, 2H), 7.46-7.49 (m, 3H), 8.1 (d, 1H, *J*=16.1Hz), 8.27 (d, 1H, *J*=8.54).

8-Hydroxy-2-methylquinoline-7-carboxylic acid phenethylamide (**5**).
8-Hydroxy-2-methylquinoline-7-carboxylic acid [2-(4-fluorophenyl)-ethyl]-amide (**6**).
8-Hydroxy-2-methylquinoline-7-carboxylic acid (3-phenylpropyl)-amide (**7**).
Detailed discussion on synthesis and biological activity of compounds **5-7** will be published elsewhere.
bis-[8-Hydroxy-2-methylquinoline-7-carboxylic acid]-1,2-etylamide (**8**). Product was obtained according to ref [27].
bis-[8-Hydroxy-2-methylquinoline-7-carboxylic acid]-1,3-propylamide (**9**). Product was obtained according to ref [27].

Lipophilicity HPLC determination (capacity factor K / calculated log K)
The HPLC separation module Waters Alliance 2695 XE and Waters Photodiode Array Detector 2996 (Waters Corp., Milford, MA, U.S.A.) were used. The chromatographic column Symmetry® C_{18} 5 μm, 4.6×250 mm, Part No. WAT054275, (Waters Corp., Milford, MA, U.S.A.) was used. The HPLC separation process was monitored by Millennium32® Chromatography Manager Software, Waters 2004 (Waters Corp., Milford, MA, U.S.A.). The mixture of MeOH p.a. (50.0%) and H_2O-HPLC – Mili-Q Grade (50.0%) was used as a mobile phase. The total flow of the column was 0.9 ml/min, injection 30 μl, column temperature 30 °C and sample temperature 10 °C. The detection wavelength 210 nm was chosen. The KI methanolic solution was used for the dead time (T_D) determination. Retention times (T_R) were measured in minutes.
The capacity factors *K* were calculated using the Millennium32® Chromatography Manager Software according to the formula $K = (T_R - T_D) / T_D$, where T_R is the retention time of the solute, whereas T_D denotes the dead time obtained via an unretained analyte. Log *K*, calculated from the capacity factor *K*, is used as the lipophilicity index converted to log *P* scale. The log *K* values of the individual compounds are shown in Table 1.

Study of chlorophyll content reduction in Chlorella vulgaris Beij.
The green algae *C. vulgaris* Beij. was cultivated statically at room temperature according to Kralova et al. [28] (photoperiod 16 h light/8 h dark; photosynthetic active radiation 80 μmol/m^2.s; pH 7.2). The effect of the compounds on algal chlorophyll (Chl) content was determined after 4-day cultivation in the presence of the tested compounds. The Chl content in the algal suspension was determined spectrophotometrically (Kontron Uvikon 800, Kontron, Muenchen, Germany) after extraction into methanol according to Wellburn [29].

The Chl content in the suspensions at the beginning of the cultivation was 0.1 mg/l. Because of the low solubility of the studied compounds in water, these were dissolved in DMSO. DMSO concentration in the algal suspensions did not exceed 0.25% and the control samples contained the same DMSO amount as the suspensions treated with the tested compounds. The antialgal activity of compounds was expressed as IC_{50}. Comparable IC_{50} value for a selective herbicide 3-(3,4-dichlorophenyl)-1,1-dimethylurea, DCMU (DIURON) was about 7.3 μmol/l. The results are summarized in Table 1.

Table 1. Experimentally found hydrophobicity (log *K*) and IC_{50} values related to reduction of chlorophyll content in *C. vulgaris* of the compounds **1-9** in comparison with standard (DCMU).

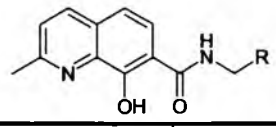

Compound	R	log *K*	IC_{50} [μmol/l]
1	-Ph	0.3019	17.2
2	-Ph-4-F	0.3603	158
3	-Ph-4-CH_3	0.3983	7.2
4	-Ph-4-OCH_3	0.3142	4.8
5	-CH_2Ph	0.2954	*a*
6	-CH_2Ph-4-F	0.3721	15.9
7	-C_3H_6Ph	0.6021	8.5
8	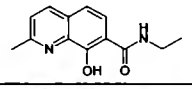	0.2151	93.7
9	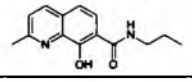	0.2388	149
DCMU	–	–	7.3

[a] not tested due to precipitation of a dissolved drug.

Acknowledgements. This study was supported by the KBN Warsaw 4T09A 088 25, and the Slovak Scientific Grant Agency VEGA No. 1/0089/03.

REFERENCES

[1] Roth, H.J.; Fenner, H. In *Arzneistoffe* 3rd ed.; Deutscher Apotheker Verlag: Stuttgart, **2000**; pp. 51-114.
[2] Harris, C.R.; Thorarensen, A. *Curr. Med. Chem.*, **2004**, *11*, 2213.
[3] Andries, K.; Verhasselt, P.; Guillemont, J.; Gohlmann, H.W.; Neefs, J.M.; Winkler, H.; Van Gestel, J.; Timmerman, P.; Zhu, M.; Lee, E.; Williams, P.; de Chaffoy, D.; Huitric, E.; Hoffner, S.; Cambau, E.; Truffot-Pernot, C.; Lounis, N.; Jarlier, V. *Science* **2005**, *307*, 223.
[4] Vangapandu, S.; Jain, M.; Jain, R.; Kaur, S.; Singh, P.P. *Bioorg. Med. Chem.* **2004**, *12*, 2501.
[5] Sissi, C.; Palumbo, M. *Curr. Med. Chem. Anti-Canc. Agents*, **2003**, *3*, 439.

[6] Mekouar, K.; Mouscadet, J. F.; Desmaele, D.; Subra, F.; Leh, H.; Savoure, D.; Auclair, C.; d'Angelo, J. *J. Med. Chem.* **1998**, *41*, 2846.
[7] Polanski, J.; Zouhiri, F.; Jeanson, L.; Desmaele, D.; d'Angelo, J.; Mouscadet, J.; Gieleciak, R.; Gasteiger, J.; Bret, M. L. *J. Med. Chem.* **2002**, *45*, 4647.
[8] Polanski, J.; Niedbala, H.; Musiol, R.; Tabak, D.; Podeszwa, B.; Gieleciak, R.; Bak, A.; Palka, A.; Magdziarz, T. *Acta Poloniae Pharm. Drug Res.* **2004**, *61*, 3.
[9] Pommier, Y.; Johnson, A. A.; Marchand, C. *Nat. Rev. Drug. Discov.* **2005**, *4*, 236.
[10] Zouhiri, F.; Danet, M.; Bernard, C.; Normand-Bayle, M.; Mouscadet, J. F.; Leh, H.; Thomas, C. M.; Mbemba, G.; d'Angelo, J.; Desmaele, D. *Tetrahedron Lett.* **2005**, *46*, 2201.
[11] Musiol, R.; Jampilek, J.; Buchta, V.; Silva, L.; Niedbala, H.; Podeszwa, B.; Palka, A.; Majerz-Maniecka, K.; Oleksyn, B.; Polanski, J. *Bioorg. Med. Chem.* **2006**, *14*, 3592.
[12] Jampilek, J.; Dolezal, M.; Kunes, J.; Buchta, V. *ECSOC-8* **2004**, November 1-30, http://www.lugo.usc.es/%7Eqoseijas/ECSOC-8/BOCNP/005/index.htm.
[13] Jampilek, J.; Dolezal, M.; Kunes, J.; Buchta, V.; Kralova, K. *Med. Chem.* **2005**, *1*, 591.
[14] Musiol, R.; Jampilek, J.; Kralova, K.; Podeszwa, B.; Finster, J.; Niedbala, H.; Palka, A.; Polanski, J. *ECSOC-9* **2005**, November 1-30, http://www.usc.es/congresos/ecsoc/9/BOCNP/c005/index.htm.
[15] Musiol, R.; Jampilek, J.; Kralova, K.; Richardson, D.R.; Kalinowski, D.; Podeszwa, B.; Finster, J.; Niedbala, H.; Palka, A.; Polanski, J. *Bioorg. Med. Chem.* **2006**, submitted.
[16] Polanski, J.; Niedbala, H.; Musiol, R.; Tabak, D.; Podeszwa, B.; Gieleciak, R.; Bak, A.; Palka, A.; Magdziarz, T. *Acta Poloniae Pharm. Drug Res.* **2004**, *61*, 3.
[17] Musiol, R.; Niedbala, H.; Polanski, J. *Monatsh. Chem.* **2006**, *137*, 1211.
[18] Majerz-Maniecka, K. A.; Musiol, R.; Nitek, W.; Oleksyn, B. J.; Polanski, J. *Bioorg. Med. Chem. Lett.* **2005**, *16*, 1005.
[19] Miletin, M.; Hartl, J.; Dolezal, M.; Odlerova, Z.; Kralova, K.; Machacek, M. *Molecules*, **2000**, *5*, 208 (http://www.mdpi.org/molecules/papers/50300208.pdf).
[20] Dolezal, M.; Miletin, M.; Kunes, J.; Kralova, K. *Molecules* **2002**, *7*, 363 (http://www.mdpi.net/molecules/papers/70300363.pdf).
[21] Jampilek, J.; Dolezal, M.; Osicka, Z.; Kunes, J.; Kralova, K. *ECSOC-7* **2003**, November 1-30, http://www.mdpi.net/ec/ec_article.php?id=81&file=papers/ecsoc-7/C001/C001.htm.
[22] Dolezal, M.; Cmedlova, P.; Palek, L.; Kunes, J.; Buchta, V.; Jampilek, J.; Kralova, K. *ECSOC-9* **2005**, November 1-30, http://www.usc.es/congresos/ecsoc/9/BOCNP/c010/index.htm.
[23] Dolezal, M.; Palek, L.; Vinsova, J.; Buchta, V.; Jampilek, J.; Kralova, K. *Molecules* **2006**, *11*, 242, http://www.mdpi.org/molecules/papers/11040242.pdf.
[24] Norrington, F.E.; Hyde, R.M.; Williams, G.G.; Wooton, R. *J. Med. Chem.* **1975**, *18*, 604.
[25] Hansch, C.; Leo, A.J. *Substituent Constants for Correlation Analysis in Chemistry and Biology*; John Wiley: New York, **1979**.
[26] Jampilek, J.; Vinsova, J.; Dohnal, J. *ECSOC-9* **2005**, November 1-30, http://www.usc.es/congresos/ecsoc/9/GOS/a008/index.htm.
[27] Polanski, J.; Niedbala, H.; Musiol, R.; Podeszwa, B.; Tabaka, D.; Palka, A.; Mencel, A.; Mouscadet, J-F.; Le Bret, M. Fragment based approach for the investigation of HIV-1 integrase inhibitors, *Lett. Drugs Des. Disc.* **2006** submitted.
[28] Kralova, K.; Sersen, F.; Melnik, M. *J. Trace Microprobe Techn.*, **1998**, *16*, 491.
[29] Wellburn, A.R. *J. Plant. Physiol.*, **1994**, *144*, 307.

ANALOGUES OF THE STYRYLQUINOLINE AND STYRYLQUINAZOLINE HIV-1 INTEGRASE INHIBITORS: DESIGN AND SYNTHETIC PROBLEMS

J. POLAŃSKI*, H. NIEDBAŁA, R. MUSIOŁ, D. TABAK, B. PODESZWA, R. GIELECIAK, A. BĄK, A. PAŁKA and T. MAGDZIARZ

Department of Organic Chemistry, Institute of Chemistry, University of Silesia, PL 40-006 Katowice, Poland,

Abstract: In our work, leading to new styrylquinoline and styrylquinazoline inhibitors of HIV integrase, we analyzed virtual combinatorial library that includes these compounds. Using this method we were able to find interesting synthetic targets. We optimized synthetic procedure yielding such compounds and obtained a couple of new analogues. Their activity will be evaluated in the near future.

Keywords: HIV integrase inhibitors; styrylquinolines; styrylquinazolines

HIV integrase (IN) is a specific enzyme that catalyzes important process in HIV life cycle: the insertion of viral DNA into host genome (1, 2). This implicates hypothesis that integrase blocking is essential for the suppression of the HIV virus in human body cells. Because divalent metal cations such as: Mg^{2+}, Mn^{2+} are needed for the integrase activity, our investigations on the potent IN inhibitors are focused on styrylquinolines analogues, as these compounds are well known complexing agents for these ions (3–6). Some potent styrylquinoline (**1**) and styrylquinazoline (**2**) *in vitro* and *in vivo* IN inhibitors have been described previously (Scheme 1) (7, 8).

EXPERIMENTAL

Melting points were determined in a Boetius apparatus (VEB Analityk) and are uncorrected. Nuclear magnetic resonance spectra for proton (^{1}H NMR) were recorded on a 500 MHz spectrometer. The chemical shifts are expressed in ppm relative to tetramethylsilane as an internal standard.

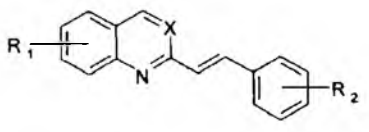

Scheme 1. R_1, R_2=COOH, OH, OMe; **1.** X=C, **2.** X=N.

Styrylquinoline compounds

2-(2-Phenylethenyl)-8-hydroxyquinoline 1a (Scheme 2: R_1=8-OH, R_2=H, X=C) quinaldine (10 mmole) and benzaldehyde (20 mmole) were mixed with silica gel (50–100 mesh, 3.5 g), and placed in an open vessel in domestic microwave oven for 6 minutes (pulsed irradiation 2 min with 20 s intervals; 900 W). Then, the content of the reactor was extracted with dichloromethane and evaporated. The solid residue was purified by crystallization to afford pure product, mp 98–100°C (lit. mp 96–100°C (9)).

2-2-(3-chlorophenyl)-ethenyl-6-quinolinecarboxylic acid 2a (Scheme 2: R_1=6-COOH, R_2=3-Cl, X=C), m.p. 273-274°C, yield 55%.

^{1}H NMR (DMSO-$_{d6}$, 500 MHz) d: 7.42–7.48 (m, 2H); 7.62 (d, *J*=16.5 Hz, 1H); 7.75 (d, *J*=7.2 Hz, 1H); 7.86–7.95 (m, 3H); 8.06 (d, *J*=9 Hz, 1H); 8.21 (d, *J*=8.7 Hz, 1H); 8.56 (d, J= 8.7 Hz, 1H); 8.64 (s, 1H); 13.2 bs. Calcd for $C_{18}H_{12}ClNO_2$*1/3H_2O: C, 68.47; H, 4.04. Found C, 68.50; H, 4.04.

2-2-(2-chlorophenyl)-ethenyl-8-quinolinecarboxylic acid 3a (Scheme 2: R_1=8-COOH, R_2=2-Cl, X=C), m.p. 190-195°C, yield 47%.

^{1}H NMR (DMSO-$_{d6}$, 500 MHz) d: 7.42–7.48 (m, 2H); 7.54–7.6 (m, 1H); 7.7 (d, *J*=16.5 Hz, 1H); 7,8 (t, 1H); 8.06–8.14 (m, 3H); 8.34 (d, *J*=8.1 Hz, 1H); 8.58 (d, *J*=7,2Hz, 1H); 8.71 (d, *J*=8.7 Hz, 1H); 16.4 bs. Calcd for $C_{18}H_{12}ClNO_2$*1/3H_2O: C, 68.47; H, 4.04. Found C, 68.36; H, 4.12.

The reference reaction yielding styrylquinolines in acetic anhydride was performed as follows (10–14):

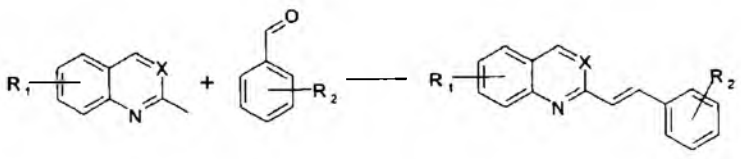

Scheme 2. R_1, R_2=COOH, OH, OMe; X=C, N.

* Corresponding author: e-mail – polanski@us.edu.pl

ANALOGUES OF THE STYRYLQUINOLINE AND STYRYLQUINAZOLINE HIV-1 INTEGRASE INHIBITORS: DESIGN AND SYNTHETIC PROBLEMS.

J. Polański, H. Niedbała, R. Musioł, D. Tabak, B. Podeszwa, R. Gieleciak, A. Bąk, A. Pałka, T. Magdziarz.

Department of Organic Chemistry, Institute of chemistry, University of Silesia, PL 40-006 Katowice, Poland, e-mail: polanski@us.edu.pl

Abstract: In our work leading to obtain new styrylquinolie and styrylquinazoline inhibitors of HIV integrase we analyzed virtual combinatorial library that include these compounds. Using this method we were able to find interesting synthetic targets. We optimized synthetic procedure yielding such compounds and obtained few analogs. Their activity will be evaluated in the near future.

Keywords: HIV integrase inhibitors, styrylquinolines, styrylquinazolines

INTRODUCTION

HIV Integrase (IN) is a specific enzyme that catalyzed important process in HIV life cycle: the insertion of viral DNA into host genome [1, 2]. That implicates hypothesis that integrase blocking is essential for the suppression of the HIV virus in human body cells. Because divalent metal cations such as: Mg^{2+}, Mn^{2+} are needed for the integrase activity, our investigations on the potent IN inhibitors are focused on styrylquinolines analogs, as these compounds are well known complexing agent for these ions [3]. Some potent styrylquinoline (**1**) and styrylquinazoline (**2**) in vitro and in vivo IN inhibitors have been described previously (Scheme 1) [4].

Scheme 1.

EXPERIMENTAL

Melting points were determined in a Kofler's apparatus and are uncorrected. Nuclear magnetic resonance spectra for proton (^{1}HNMR) were recorded on a 500 MHz spectrometer. The chemical shifts are expressed in ppm relative to tetramethylsilane as an internal standard.

Scheme 2.

Styrylquinoline compounds

A1. 2-(2-Phenylethenyl)-8-hydroxyquinoline. (scheme 2: R_1=8-OH, R_2=H, X=C) 10 mmol of quinaldine and 20 mmol benzlaldehyde were mixed with 3.5 g of silica gel(50-100 mesh), and placed in an open vessel in domestic microwave oven for 6 minutes (pulsed irradiation 2 min with 20 s intervals) at power 900 W. After this, the content of reactor was extracted with dichloromethane and evaporated. The solid residue was purified by crystallization to afford a pure product, mp 98-100°C (lit. mp 96-100°C [5]).

A2. 2-[2-(3-chlorophenyl)-ethenyl]-6-quinolinecarboxylic acid (scheme 2: R_1=6-COOH, R_2=3-Cl, X=C) mp 273-274°C, yield 55%.

^{1}H NMR (DMSO-$_{d6}$, 500MHz) δ: 7,42-7,48 (m, 2H); 7,62 (d, *J*=16,5Hz, 1H); 7,75 (d, *J*=7,2Hz, 1H); 7,86-7,95 (m, 3H); 8,06 (d, *J*=9Hz, 1H); 8,21 (d, *J*=8,7Hz, 1H); 8,56 (d, J= 8,7Hz, 1H); 8,64 (s, 1H); 13,2 bs. Calcd for $C_{18}H_{12}ClNO_2$*1/3H_2O: C, 68.47; H, 4.04. Found C, 68.5; H, 4.04.

A3. 2-[2-(2-chlorophenyl)-ethenyl]-8-quinolinecarboxylic acid scheme 2: R_1=8-COOH, R_2=2-Cl, X=C) mp 190-195°C, yield 47%.

^{1}H NMR (DMSO-$_{d6}$, 500MHz) δ: 7,42-7,48 (m, 2H); 7,54-7,6 (m, 1H); 7,7 (d, *J*=16,5Hz, 1H); 7,8 (t, 1H); 8,06-8,14 (m, 3H); 8,34 (d, *J*=8,1Hz, 1H); 8,58 (d, *J*=7,2Hz, 1H); 8,71 (d, *J*=8,7Hz, 1H); 16,4 bs. Calcd for $C_{18}H_{12}ClNO_2$*1/3H_2O: C, 68.47; H, 4.04. Found C, 68.36; H, 4.12.

The reference reaction yielding styrylquinolines in acetic anhydride was performed as follows [6-9]: To a solution of 1.0 equiv of appropriate quinaldine in acetic anhydride (50ml) was added 4.0 equiv of aldehyde. The mixture was heated under reflux for 24 h and evaporated in vacuo. The residue was dissolved in pyridine (40ml), water (10ml) was added and the reaction mixture was refluxed for 3 h and concentrated in vacuo. To the

residue CH_2Cl_2 was added and a mixture is left for 8 h at 0°C, then filtered, washed with boiling propanol, ether and crystallized to give product in 34% yield.

RESULTS AND CONCLUSIONS

We built a virtual combinatorial library (VCL) shown in scheme 3, to design promising synthetic targets. A comparison of the molecular surfaces by Comparative Molecular Surface Analysis (CoMSA) and Principal Clustering Analysis (PCA) or Kohonen mapping as described elsewhere [5] indicated several interesting compounds.

Scheme 3.

Therefore, we aimed at synthesis of these compounds. Existing methods for the direct introduction of alkyl substituent into quinoline nuclei depend on reactions of parent heterocycles or their N-oxides with organometallic [10] compounds, reaction of chloro-derivatives with active methylene compound salts, or with Wittig reagents [11, 12]. The most convenient method is probably the reaction of appropriate quinaldine with aldehydes in acetic anhydride. This requires, however, long reaction duration and the usage of a large excess of reagents. On the other hand the resulting reaction products are difficult to purify. Therefore, we performed a complex study aimed at the optimization of the reaction conditions. We have found that both the compounds having the -C=C- and -C=N- central linker, as shown in schemes 3 and 4, can be efficiently synthesized using microwave reactor [13]. The yields are much better that those for standard synthetic procedures, and the reactions are significantly faster in such conditions. In a series of experiments we applied silica gel as a carrier and pulse irradiation for solid phase synthesis. We successfully used microwave assisted organic synthesis (MAOS) to obtain structures of our interest, as shown for compounds A1, A2, A3. Further survey on wider spectrum of structures will help improve this method.

ACKNOWLEDGEMENTS

We would like to thank for the financial support of Polish State Committee for Scientific Research (KBN) grant No. 4 T09 A 008 25 to A. Bąk.

REFERENCES

[1] Ho D. D., Neumann A. U., Perelson A. S., Chen W., Leonard J. M., Markowitz M., *Nature,* **373**, 123 (1995).

[2] De Clerq E., *J. Med. Chem.,* **38**, 2491(1995); Brown P. O., *Curr. Top. Microbiol. Immunol.,* **19**, 157 (1990).

[3] Phillips, P. Merrit, L. L. *J. Am. Chem. Soc.* **71**, 3984 (1949); Phillips, P. Merrit, L. L. *J. Am. Chem. Soc.* **70**, 410 (1948); Phillips, P. Elbinger, R. L. Merrit, L. L. *J. Am. Chem. Soc.,* **71**, 3986 (1949); Irving, H. Butler, E. J. Ring, M. F. *J. Chem. Soc.* **1949**, 1489.

[4] Ouali M., Laboulais C., Leh H., Gill D., Desmaele D., Mekouar Kh., Zouhiri F., Auclair C., d'Angelo J., Mouscadet J. F., Le Bret M., *J. Med. Chem.,* **43**, 1949 (2000); Polanski, J. Zouhiri, F. Jeanson, L. Desmaele, D. d'Angelo, J. Mouscadet, J. F. Gieleciak, R. Gasteiger, J. Le Bret, M. *J. Med. Chem.*, **45**, 4647 (2002).

[5] Polanski J., Gieleciak R., Niedbala H., Musiol R., Tabak D., Bak A., Palka A., Gasteiger J., Le Bret M., Comparative molecular surface analysis: Application to the study of molecular diversity for styrylquinoline HIV-1 blocking agents, *J. Comb. Chem.*, (2004) under preparation.

[6] Mekouar Kh., Mouscadet J. F., Desmaele D., Subra F., Leh H., Savoure D., Auclair C., d'Angelo J., *J. Med. Chem.,* **41**, 2846 (1998).

[7] Dyda F., Hickman A. B., Jenkins T., Engelman A., Craigie E., Davies D., *Science,* **266**, 1981 (1994).

[8] Phillips J. P., Breese R., Barrall E. M., *J. Org. Chem.*, **1959**, 1104.

[9] Vass A., Dudas J., Varma R. S., *Tetrahedron Lett.*, **40**, 4951 (1999); Patonay T., Varma R. S., Vass A., Levai A., Dudas J., *Tetrahedron Lett.*, **42**, 1403 (2001).

[10] Ochiai E., Aromatic Amine Oxides Elsevier, New York , N. Y., 1967; Katritzky A. R., Lagowski J. M., Chemistry of the heterocyclic N-oxides Academic Press, New York, N. Y., 1971; Scalzi F. V., Golob N. F., *J. Org. Chem.,* **36**, 2541 (1971); Giam C. S., Stout J. L., *J. Chem Soc. D,* **1969**,142.

[11] Ochiai E., Kuniyoshi I., *Pharm. Bull.,* **5**, 292 (1957); Higashino T., Hayashi E., *Chem. Pharm., Bull.,* **18**, 1457 (1970); Cooper G. G., Rickard R. L., *J. Chem. Soc. C.*, **1971**, 772.

[12] Arnold D. R. , Bolton J. R., Pedersen J. A., *J. Am. Chem. Soc.*, **94**, 2874 (1972).

[13] Musiol R., Niedbala H., Polanski J., Polish Patent Application P 363 409.

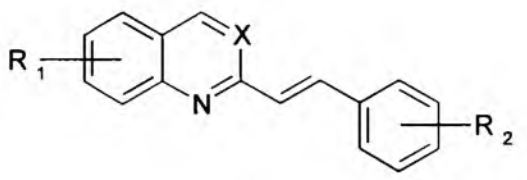

Scheme 1. R_1, R_2= COOH, OH, OMe; **1.** X=C, **2.** X=N.

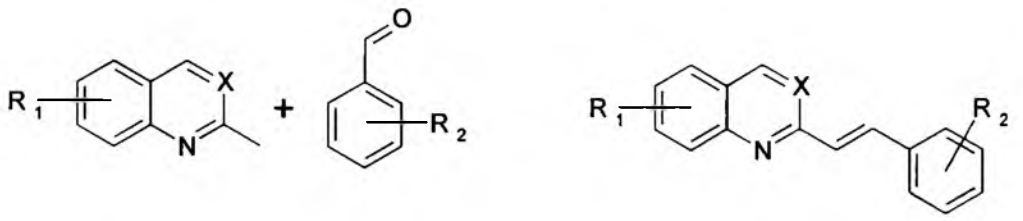

Scheme 2. R_1, R_2= COOH, OH, OMe; X=C, N.

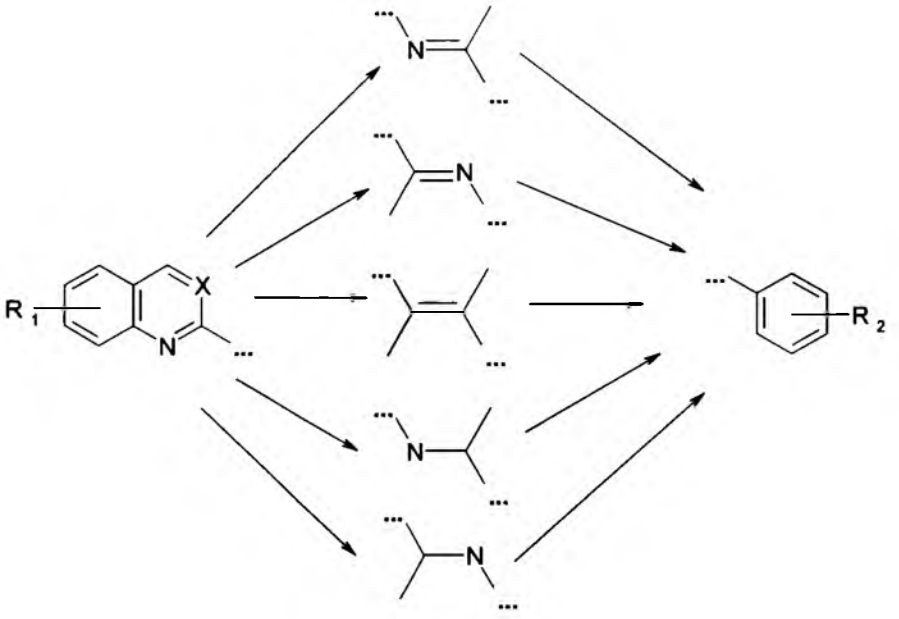

Scheme 3. R_1, R_2=COOH,OH, OMe, Cl, Br; X=C, N.

Molecules **2009**, *14*, 1145-1159; doi:10.3390/molecules14031145

OPEN ACCESS

molecules

ISSN 1420-3049

www.mdpi.com/journal/molecules

Article

Ring-substituted 4-Hydroxy-1*H*-quinolin-2-ones: Preparation and Biological Activity ‡

Josef Jampilek [1,2,*], Robert Musiol [3], Matus Pesko [4], Katarina Kralova [4], Marcela Vejsova [5], James Carroll [6], Aidan Coffey [6], Jacek Finster [3], Dominik Tabak [3], Halina Niedbala [3], Violetta Kozik [3], Jaroslaw Polanski [3], Jozef Csollei [2] and Jiri Dohnal [1,2]

[1] Zentiva k.s., U kabelovny 130, 102 37 Prague 10, Czech Republic

[2] Department of Chemical Drugs, Faculty of Pharmacy, University of Veterinary and Pharmaceutical Sciences, Palackeho 1/3, 61242 Brno, Czech Republic

[3] Institute of Chemistry, University of Silesia, Szkolna 9, 40007 Katowice, Poland; E-mail: robert.musiol@us.edu.pl (R.M.), polanski@us.edu.pl (J.P.)

[4] Institute of Chemistry, Faculty of Natural Sciences, Comenius University, Mlynska dolina Ch-2, 84215 Bratislava, Slovakia; E-mail: kralova@fns.uniba.sk (M.P.)

[5] Department of Biological and Medical Sciences, Faculty of Pharmacy in Hradec Kralove, Charles University in Prague, Heyrovskeho 1203, 500 05 Hradec Kralove, Czech Republic; E-mail: marcela.vejsova@faf.cuni.cz (M.V.)

[6] Department of Biological Sciences, Cork Institute of Technology, Bishopstown, Cork, Ireland; E-mail: james.carroll@cit.ie (J.C.), aidan.coffey@cit.ie (A.C.)

‡ Preliminary results were presented at The Twelfth Electronic Conference on Synthetic Organic Chemistry (ECSOC-12, http://www.usc.es/congresos/ecsoc/12/ECSOC12.htm), November 1-30, 2008 (paper C0012).

* Author to whom correspondence should be addressed; E-mail: josef.jampilek@zentiva.cz; Tel.: +42026724695; Fax: +420272701331.

Received: 4 February 2009; in revised form: 3 March 2009 / Accepted: 11 March 2009 / Published: 13 March 2009

Abstract: In the study, a series of twelve ring-substituted 4-hydroxy-1*H*-quinolin-2-one derivatives were prepared. The procedures for synthesis of the compounds are presented. The compounds were analyzed using RP-HPLC to determine lipophilicity and tested for their photosynthesis-inhibiting activity using spinach (*Spinacia oleracea* L.) chloroplasts.

All the synthesized compounds were also evaluated for antifungal activity using *in vitro* screening with eight fungal strains. For all the compounds, the relationships between the lipophilicity and the chemical structure of the studied compounds are discussed, as well as their structure-activity relationships (SAR).

Keywords: Quinolinone derivatives; Lipophilicity; OER inhibition; Spinach chloroplasts; *In vitro* antifungal activity; Structure-activity relationships.

I. Introduction

The quinoline scaffold is present in many classes of biologically-active compounds [1]. A series of compounds derived from 8-hydroxyquinoline and styrylquinoline derivatives were recently synthesized as potential HIV-1 integrase inhibitors [2,3]. These compounds show a significant similarity to some novel antifungal agents, namely homoallylamines, and therefore possess potential antifungal activity [4]. Our previous study dealing with 8-hydroxyquinoline and styrylquinoline derivatives showed that they could also possess a strong antifungal activity [5-7]. According to the results reported recently, some new hydroxyquinoline derivatives also possess interesting herbicidal activities [6,8-13]. Some investigated compounds also showed antineoplastic activity [14].

Photosystem II (PS II) is a multisubunit membrane protein complex, which uses light energy to oxidize water and reduce plastoquinone. Binding of herbicides to photosystem II inhibits the electron transfer from Q_A to Q_B due to competition of herbicides with plastoquinone bound at the Q_B site. Thus, the Q_B quinone-binding site of photosystem II is an important target for herbicides, including herbicides based on phenylurea moieties. It was found that a tail can be attached to the *para* position of phenylurea-type herbicides without any loss of binding, provided that the tail is hydrophobic. This indicates that the herbicides must be oriented in the Q_B site so that these positions point toward the natural isoprenyl tail-binding pocket that extends out of the Q_B site. In turn, the requirement that the tail must extend out of the Q_B site constrains the size of the other herbicide substituents in the pocket [15]. In addition to phenylurea-type herbicides, various other compounds possessing an amide -NHCO- moiety were also found to inhibit the photosynthetic electron transport [16-21]. Better understanding of these SAR relationships are not only important for the design of modern agricultural agents, but can also provide remarkable insights into the photosynthetic mechanisms of green cells.

Over the last three decades there has been a dramatic increase in the incidence of fungal infections, and the discovery of new drugs for the treatment of systemic mycoses is a major challenge in infectious disease research. There is an intensified need for new antifungal remedies with novel modes of action due to the rapid growth of the immunocompromised patient population, the development of resistance to the present azole therapies, and high toxicity of polyenes [22-24].

Compounds bearing a quinoline moiety are well known due to their broad biological activity [6]. In particular, hydroxyquinoline and its derivatives were introduced as antifungal agents in clinical practice and the novel compounds of this type are still investigated [25,26]. This paper deals with synthesis, herbicidal and antifungal activity of ring-substituted 4-hydroxy-1*H*-quinolin-2-one derivatives. All the compounds were tested for their photosynthesis-inhibiting activity (the inhibition

of photosynthetic electron transport in spinach chloroplasts (*Spinacia oleracea* L.). Primary *in vitro* screening of all synthesized compounds was evaluated against eight fungal strains by means of the broth microdilution test in RPMI 1640 medium [27]. Lipophilicity (log *k*) of the compounds was determined using RP-HPLC. The procedure was performed under isocratic conditions with methanol as an organic modifier in the mobile phase using end-capped non-polar C_{18} stationary RP column. The structure-activity relationships of the compounds are also discussed.

2. Results and Discussion

2.1. Chemistry

In most of the synthesis protocols, aniline derivatives were used as the starting materials due to their convenient availability from chemical providers. Microwave assisted synthesis with malonic acid or its esters, was used to make compounds **1-4**. Further nitration and reduction according to established procedures were used to make compounds **5** and **6**. Acylation of **6** with cinnamoyl chloride provided compound **7**. Diazo derivative **8** was made by means of a two-step synthesis from 4-aminobenzoic acid and diethyl malonate and gave 4-hydroxy-2-oxo-1,2-dihydroquinoline-6-carboxylic acid, which was coupled with the freshly prepared diazo salt derived from 4-nitro-2,5-dichloroaniline. Quinolines functionalized with carboxylic acid groups at $C_{(3)}$ 9-12 were obtained in neat microwave assisted synthesis in moderate or good yield. Synthesis of all the above compounds is depicted in Scheme 1.

Scheme 1. General preparation of quinoline derivatives 1-12: (a) PPA, microwave irradiation; (b) HNO_3; (c) Sn, HCl; (d) cinnamoyl chloride; (e) (2,5-dichloro-4-nitrophenyl)diazonium chloride; (f) microwave irradiation; (g) hydrolysis.

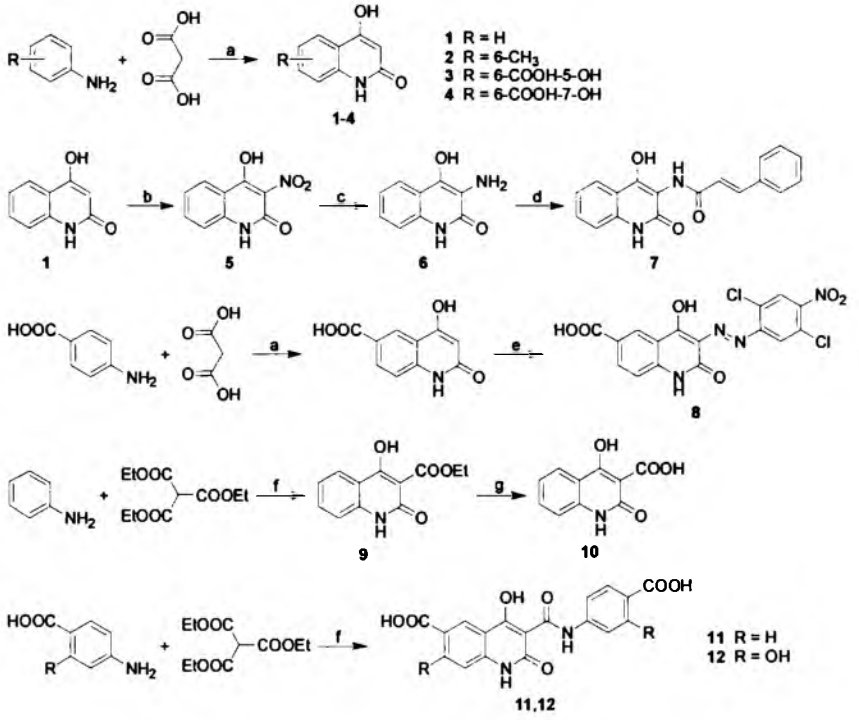

2.2. Lipophilicity

Hydrophobicities (log *P*/Clog *P* values) of the compounds **1-12** were calculated using two commercially available programs and also measured by means of the reversed phase high performance liquid chromatography (RP-HPLC) method for lipophilicity measurement. The procedure was performed under isocratic conditions with methanol as an organic modifier in the mobile phase using an end-capped non-polar C_{18} stationary RP column. The capacity factors *k* were determined and subsequent log *k* values were calculated.

The results are summarized in Table 1 and illustrated in Figure 1. The results obtained with all the compounds show that the experimentally-determined lipophilicities (log *k* values) are lower than those indicated by the calculated log *P*/Clog *P*, as shown in Figure 1, indicating relatively poor correlation between the experimentally-determined log *k* values and the calculated values. As expected, compound **8** showed the highest lipophilicity, while compound **3** possessed the lowest hydrophobicity, which was unexpected. Compound **7** showed less hydrophobicity contrary to all the results of the lipophilicity calculated by software. Comparing the lipophilicity data log *k* of both position analogues **3** and **4**, it can be stated that the 7-hydroxy derivative **4** possessed higher hydrophobicity than 5-hydroxy analogue **3**. The salicylic acid derivative **12** showed higher lipophilicity than benzoic derivative **11**. These facts are caused by intramolecular interactions [28].

Figure 1. Comparison of the computed log *P*/Clog *P* values using the two programs with the calculated log *k* values. The discussed compounds 1-12 are ordered according to the log *k* values increase.

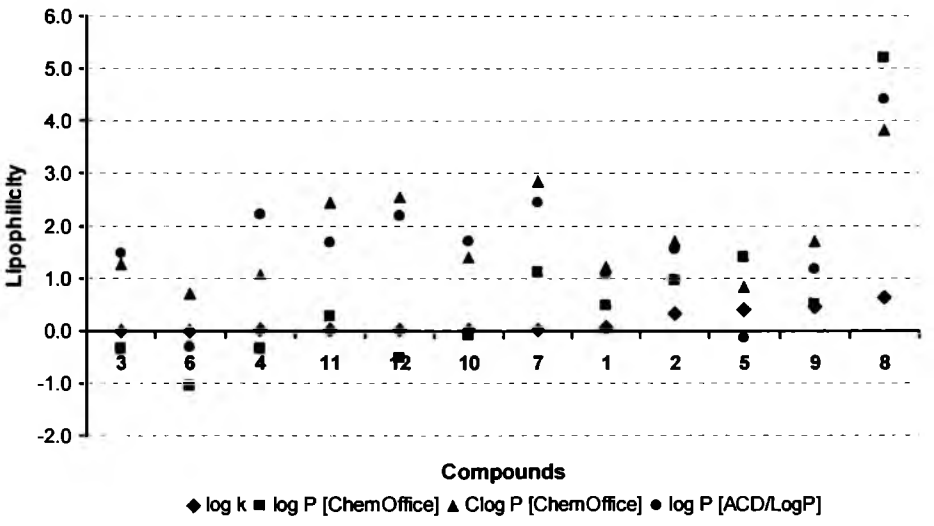

Table 1. Comparison of the calculated lipophilicities (log *P*/Clog *P*) with the determined log *k* values.

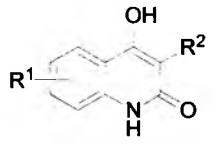

Comp.	R^1	R^2	log *k*	log *P*/Clog *P* ChemOffice	log *P* ACD/LogP
1	H	H	0.0664	0.49 / 1.216	1.10 ± 0.75
2	6-CH_3	H	0.3307	0.97 / 1.715	1.56 ± 0.75
3	6-COOH-5-OH	H	0.0002	-0.34 / 1.261	1.47 ± 0.75
4	6-COOH-7-OH	H	0.0080	-0.34 / 1.070	2.22 ± 0.75
5	H	-NO_2	0.4052	1.39 / 0.836	-0.14 ± 1.00
6	H	-NH_2	0.0004	-1.06 / 0.719	-0.32 ± 1.00
7	H	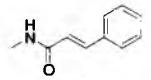	0.0128	1.11 / 2.848	2.45 ± 1.00
8	6-COOH	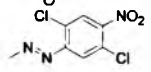	0.6394	5.22 / 3.840	4.41 ± 1.00
9	H	-$COOC_2H_5$	0.4595	0.51 / 1.694	1.17 ± 0.75
10	H	-COOH	0.0118	-0.09 / 1.409	1.71 ± 0.35
11	6-COOH	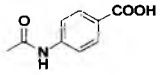	0.0081	0.27 / 2.445	1.67 ± 1.00
12	6-COOH-5-OH	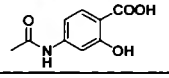	0.0093	-0.51 / 2.543	2.20 ± 1.00

2.3. Oxygen evolution rate inhibition in spinach chloroplasts

All compounds were evaluated for their *in vitro* herbicidal efficiency. The results are listed in Table 2. Quinoline derivatives **1-12** showed a wide range of activity related to inhibition of oxygen evolution rate (OER) in spinach chloroplasts. Two compounds showed interesting IC_{50} (half maximal inhibitory concentration) values: 126 μmol/L (**8**) and 157 μmol/L (**2**); nevertheless the studied activity of all the other compounds was very low.

Due to the moderate and/or low activity of compounds **1-12**, it is difficult to determine simple structure-activity relationships. However some interesting observations can be made: in the case of compound **1**, an unsubstituted structure did not have any effect on OER in chloroplasts. The remaining compounds could be divided into two groups according to their chemical structure. Group 1 includes compounds **2-4**, **8**, **11** and **12**, and Group 2 compounds **5-7**, **9** and **10**.

Group 1 showed higher biological activity than Group 2. The activity related to OER inhibition seems to be positively influenced by substitution of ring B: especially the $C_{(6)}$ position (see compounds **2-4**, **11**, **12**). Comparison of the OER-inhibiting activities of compounds **2-4**, **8**, **11** and **12** also indicated that the lipophilicity increase is connected with the quasi-parabolic increase of biological activity (Figure 2).

Table 2. IC_{50} values related to OER inhibition in spinach chloroplasts in comparison with 3-(3,4-dichlorophenyl)-1,1-dimethylurea (DCMU) standard and *in vitro* antifungal activity (IC_{80}) of compounds **1-12** compared with fluconazole (FLU) standard.

Comp.	OER inhibition IC_{50} [μmol/L]	MIC/IC_{80} [μmol/L]							
		CA	CT	CK	CG	TB	AF	AC	TM
		24h	*24h*	*24h*	*24h*	*24h*	*24h*	*24h*	*72h*
		48h	*48h*	*48h*	*48h*	*48h*	*48h*	*48h*	*120h*
1	925	>500	>500	>500	>500	>500	>500	>500	>500
		>500	>500	>500	>500	>500	>500	>500	>500
2	157	>500	>500	>500	>500	>500	>500	>500	>500
		>500	>500	>500	>500	>500	>500	>500	>500
3	346	125	500	>500	250	250	>500	>500	>500
		125	>500	>500	250	>500	>500	>500	>500
4	538	15.62	500	>500	62.50	62.50	500	>500	>500
		62.50	>500	>500	250	>500	>500	>500	>500
5	510	>500	>500	>500	>500	>500	>500	>500	>500
		>500	>500	>500	>500	>500	>500	>500	>500
6	775	>500	>500	>500	>500	>500	>500	>500	>500
		>500	>500	>500	>500	>500	>500	>500	>500
7	916	>125	>125	>125	>125	>125	>125	>125	>125
		>125	>125	>125	>125	>125	>125	>125	>125
8	126	31.25	250	250	250	250	125	62.50	62.50
		125	>250	250	>250	>250	250	250	125
9	494	>500	>500	>500	>500	>500	>500	>500	>500
		>500	>500	>500	>500	>500	>500	>500	>500
10	567	>500	>500	>500	>500	>500	>500	>500	>500
		>500	>500	>500	>500	>500	>500	>500	>500
11	380	>500	>500	>500	>500	>500	>500	>500	>500
		>500	>500	>500	>500	>500	>500	>500	>500
12	321	62.50	500	>500	125	125	500	500	500
		125	>500	>500	250	>500	>500	>500	>500
DCMU	1.9	-	-	-	-	-	-	-	-
FLU	-	0.06	0.12	3.91	0.98	0.24	>125	>125	1.95
		0.12	>125	15.62	3.91	0.48	>125	>125	3.91

It is noteworthy that there are great differences in OER inhibition levels caused by positional isomers **3** (6-COOH-5-OH) and **4** (6-COOH-7-OH). Introducing a further phenolic moiety in compound **12** (salicylic derivative) positively influenced OER inhibition. The higher inhibitory effect of compound **8** compared with compound **2** may have resulted from higher lipophilicity (easier penetration of the compound through cell walls) and/or redox properties of the nitro moiety of the 2,5-dichloro-4-nitrophenyldiazenyl substituent.

Figure 2. Relationships between the OER inhibition log ($1/IC_{50}$) [mmol/L] in spinach chloroplasts and lipophilicity (log *k*) of the studied compounds **1-12**.

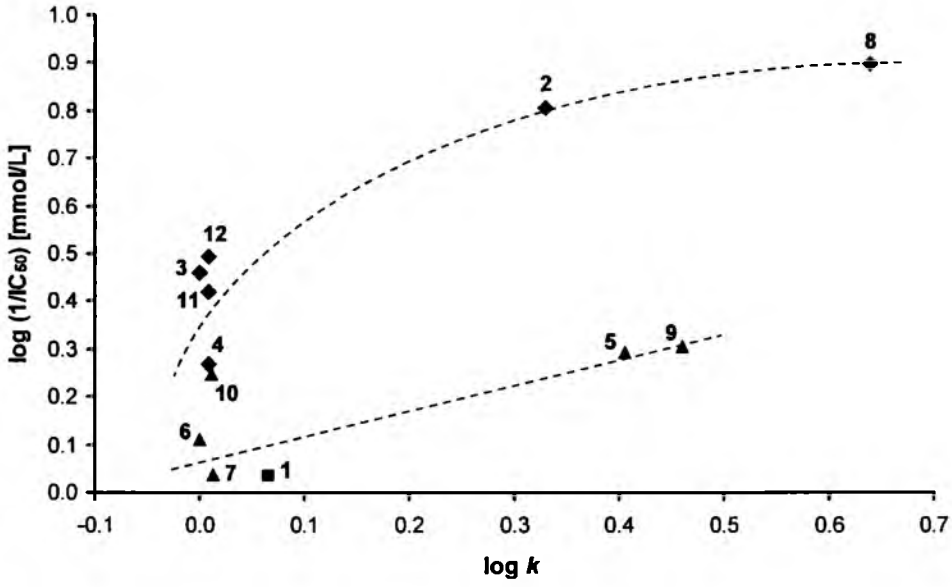

Generally, Group 2 compounds only caused slight inhibition of OER; nevertheless compounds **5** and **9** were approximately twice as effective as compound **1**. All these compounds possess the substituted position $C_{(3)}$ of ring A, which caused the decrease in OER inhibition compared with Group 1 compounds. The most active compound from Group 2 was the ester **9**.

2.4. In vitro antifungal susceptibility testing

All the compounds were tested for their *in vitro* antifungal activity. Compounds **1-3, 5-7, 9-11** did not show any activity and compounds **4, 8** and **12** showed only a moderate activity, especially against *Candida albicans* ATCC 44859. Compound **4** showed medium activity against *Candida glabrata* 20/I, and compound **8** against *Trichophyton mentagrophytes* 445. The activities of the compounds are shown in Table 2.

Generally, it can be stated that *in vitro* antifungal activity depends on heteroaromatic ring A. Hydrogenation of ring A and introduction of keto group resulted in the loss of the antifungal effect compared with hydroxyquinoline derivatives [6,7]. Substitution of the $C_{(3)}$ position by various moieties did not have a significant influence on the activity. Nevertheless salicylic acid derivative **12** showed a higher activity compared with benzoic derivative **11**, probably due to the substitution of the $C_{(3)}'$ position by phenolic moiety.

Unsubstituted ring B or $C_{(6)}$ substitution by a methyl moiety did not results in any activity. Substitution of phenyl ring B by 6-COOH (compounds **3**, **4**, **8** and **11**, **12**) caused the activity to increase. Position of the phenolic moiety seems to be a very important parameter for antifungal activity. While a 6-COOH-5-OH substitution pattern (compound **3**) did not show any activity increase, introduction of 6-COOH along with a 7-OH moiety (compound **4**) increased the activity significantly. The antifungal activity of compounds **8** and **12** was connected with 2,4-dichloro-4-nitrophenyldiazenyl

and 3-(4-carboxy-3-hydroxyphenylcarbamoyl) substituents, respectively. According to the results, it can be assumed that lipophilicity is only of secondary importance for antifungal activity.

3. Conclusions

A series of twelve ring-substituted 4-hydroxy-1*H*-quinolin-2-one derivatives were prepared and characterized. All the prepared quinoline derivatives were analyzed using a RP-HPLC method for the lipophilicity measurement and their lipophilicity was determined. The prepared compounds were tested for their photosynthesis-inhibiting activity (the inhibition of photosynthetic electron transport in spinach chloroplasts (*Spinacia oleracea* L.) and for their antifungal activity. (*E*)-3-[(2,5-Dichloro-4-nitrophenyl)diazenyl]-4-hydroxy-2-oxo-1,2-dihydroquinoline-6-carboxylic acid (**8**) showed the highest OER inhibition activity and 4,7-dihydroxy-2-oxo-1,2-dihydroquinoline-6-carboxylic acid (**4**) and compound **8** possessed the highest *in vitro* antifungal activity within the series.

4. Experimental

4.1. General

All reagents were purchased from Aldrich. Kieselgel 60, 0.040-0.063 mm (Merck, Darmstadt, Germany) was used for column chromatography. TLC experiments were performed on alumina-backed silica gel 40 F254 plates (Merck, Darmstadt, Germany). The plates were illuminated under UV (254 nm) and evaluated in iodine vapour. The melting points were determined on Boetius PHMK 05 (VEB Kombinat Nagema, Radebeul, Germany) and are uncorrected. Elemental analyses were carried out on an automatic Perkin-Elmer 240 microanalyser (Boston, USA). The purity of the final compounds was checked by the HPLC separation module Waters Alliance 2695 XE (Waters Corp., Milford, MA, U.S.A.). The detection wavelength 210 nm was chosen. The peaks in the chromatogram of the solvent (blank) were deducted from the peaks in the chromatogram of the sample solution. The purity of individual compounds was determined from the area peaks in the chromatogram of the sample solution. UV spectra (λ, nm) were determined on a Waters Photodiode Array Detector 2996 (Waters Corp., Milford, MA, U.S.A.) in ca 6×10^{-4} mol methanolic solution and log ε (the logarithm of molar absorption coefficient ε) was calculated for the absolute maximum λ_{max} of individual target compounds. Infrared spectra were recorded in a Smart MIRacle™ ATR ZnSe for Nicolet™ 6700 FT-IR Spectrometer (Thermo Scientific, U.S.A.). Spectra are corrigated. All ^{1}H NMR spectra were recorded on a Bruker AM-500 (499.95 MHz for ^{1}H), Bruker BioSpin Corp., Germany. Chemicals shifts are reported in ppm (δ) to internal $Si(CH_3)_4$, when diffused easily exchangeable signals are omitted.

4-Hydroxyquinolin-2(1H)-one (**1**). Preparation of PPA: P_2O_5 (287.9 g) was added to 85% phosphoric acid (200 g, 118.4 mL) under stirring and microwave heating. The mixture was then heated for 15 min. Aniline (7 mL, 5 mmol) and malonic acid (5.2 g, 5 mmol) were thoroughly mixed with 20 g PPA and heated under stirring in microwave reactor at 400 W during 2×20 min with 5 min interval. The temperature reached 210 °C. Then the mixture was poured into crushed ice and the beige solid was filtered and purified by extraction with EtOH and a white crystalline compound was obtained [29].

Yield 35%; Mp 340 °C; HPLC purity 97.12%; UV (nm), λ_{max}/log ε: 231.3/3.51; IR (cm^{-1}): 3618, 1180 (OH), 3043 (=CH-), 1670 (lactam), 1650 (C=O), 1593 (Ph), 1522 (NH).

4-Hydroxy-6-methylquinolin-2(1H)-one (**2**). The product was obtained according to the previously described procedure [30,31] as a light brown crystalline compound. Yield 35%; Mp 320 °C; HPLC purity 97.72%; UV (nm), λ_{max}/log ε: 232.4/3.55; IR (cm^{-1}): 3618, 1180 (OH), 3044 (=CH-), 2965, 1379 (CH_3), 1668 (lactam), 1652 (C=O), 1592 (Ph), 1522 (NH).

4,5-Dihydroxy-2-oxo-1,2-dihydroquinoline-6-carboxylic acid (**3**). Naphthalene (15.4 g, 0.12 mol) and malonic acid (18.7 g, 0.18 mol) were melted with stirring under temperature control (<150 °C) to avoid decarboxylation of the acid. $POCl_3$ (32.9 g, 0.36 mol) was then added dropwise over 30 min and *p*-aminosalicylic acid (15.3 g, 0.1 mol) was then added. The resulting mixture was heated for 30 min and allowed to cool. Water (100 mL) was added to the warm mixture and the solution was made alkaline to pH 9 with 20% NaOH. After cooling on ice precipitated naphthalene, it was filtered and the filtrate was acidified to pH 2. The product was filtered again and crystallized from acetic acid as a bright yellow crystalline compound. Yield 36%; Mp 250 °C; Anal. calc. for $C_{10}H_7NO_5$ (221.16): C 54.31%, H 3.19%; found: C 54.51%, H 4.11%; HPLC purity 98.74%; UV (nm), λ_{max}/log ε: 244.2/3.54; IR (cm^{-1}): 3620, 1180 (OH), 3045 (=CH-), 2950, 1690 (acid), 1672 (lactam), 1650 (C=O), 1598 (Ph), 1523 (NH), 1329, 1198 (OH_{phenol}); ^{1}H-NMR (DMSO-d_6) δ: 5.65 (s, 1H), 6.60 (d, *J*=8.3 Hz, 1H), 7.80 (d, *J*=8.3 Hz, 1H), 11.3 (bs, 1H), 12.20 (bs, 1H).

4,7-Dihydroxy-2-oxo-1,2-dihydroquinoline-6-carboxylic acid (**4**). The product was obtained as an isomer of **3** during its synthesis. Isolated by fractional crystalization as a white crystalline compound. Yield 36%; Mp 250 °C; Anal. calc. for $C_{10}H_7NO_5$ (221.16): C 54.31%, H 3.19%; found: C 54.09%, H 3.52%; HPLC purity 98.51%; UV (nm), λ_{max}/log ε: 243.0/3.54; IR (cm^{-1}): 3618, 1181 (OH), 3043 (=CH-), 2948, 1693 (acid), 1670 (lactam), 1651 (C=O), 1599 (Ph), 1521 (NH), 1328, 1200 (OH_{phenol}); ^{1}H-NMR (DMSO-d_6) δ: 5.60 (s, 1H), 6.67 (s, 1H), 8.25 (s, 1H).

4-Hydroxy-3-nitroquinolin-2(1H)-one (**5**). The product was obtained according to the described nitration procedure [32] as a yellow crystalline compound. Yield 71%; Mp 252-255 °C; HPLC purity 99.72%; UV (nm), λ_{max}/log ε: 336.8/3.57; IR (cm^{-1}): 3620, 1181 (OH), 1712 (C=O), 1682 (lactam), 1622 ($C=C_{cycle}$), 1595 (Ph), 1547 (NO_2), 1525 (NH).

3-Amino-4-hydroxyquinolin-2(1H)-one (**6**). Compound **6** (2.0 g, 0.0097 mol) and tin powder (3.8 g, 0.032 mol) were stirred with 36% HCl (8.1 mL). The mixture was warmed at 80-90 °C for 30 min. The brown solution was cooled to room temperature and filtered. The filtrate was alkalized with $NH_{3(aq)}$ and warmed for 20 min. Then Celite (1.3 g) was added and filtered. The solid was washed thoroughly with hot water (80 °C). The combined filtrates were concentrated and acidified. After cooling a white crystalline compound was obtained. Yield 85%; Mp 300 °C [33]; HPLC purity 91.99%; UV (nm), λ_{max}/log ε: 232.8/3.53; IR (cm^{-1}): 3620, 1181 (OH), 3312, 1618 (NH_2), 1670 (lactam), 1650 (C=O), 1625 ($C=C_{cycle}$), 1598 (Ph), 1523 (NH).

(2E)-N-(4-Hydroxy-2-oxo-1,2-dihydroquinolin-3-yl)-3-phenylprop-2-enamide (7). Compound **7** (0.018 g, 0.001 mol) was mixed with water (5 mL), Et_2O (5 mL) and sodium bicarbonate (0.3 g). The resulted mixture was stirred in an ice bath (-3 °C) and 10 mL of Et_2O solution of cinamoyl chloride (0.017 g, 0.001 mol) was added slowly. The resulting mixture was stirred at room temperature for 2 days, cooled in fridge and filtered. Et_2O was added to the solid and dried. A white crystalline compound was obtained. Yield 50%; Mp 145 °C; Anal. calc. for $C_{18}H_{14}N_2O_3+H_2O$ (324.33): C 66.66%, H 4.97%; found: C 66.54%, H 5.27%; HPLC purity 99.79%; UV (nm), λ_{max}/log ε: 263.1/3.51; IR (cm^{-1}): 3620, 1180 (OH), 3035 (CH_{arom}), 1670 (lactam), 1650 (C=O), 1648 (amide), 1628 ($C=C_{cycle}$), 1618, 974 (C=C), 1599 (Ph), 1525 (NH); ^{1}H-NMR (DMSO-d_6) δ: 3.30 (s, 1H), 6.50 (d, *J*=16.2 Hz, 2H), 7.10 (s, 1H), 7.38 (m, 9H), 7.5 (s, 1H).

(E)-3-[(2,5-Dichloro-4-nitrophenyl)diazenyl]-4-hydroxy-2-oxo-1,2-dihydroquinoline-6-carboxylic acid (**8**). 4-Hydroxy-2-oxo-1,2-dihydroquinoline-6-carboxylic acid was obtained as compound **3** from 4-aminobenzoic acid and used without thorough purification in further synthesis as follows. IR (cm^{-1}): 3618, 1179 (OH), 3043 (=CH-), 2948, 1686 (acid), 1677 (lactam), 1650 (C=O), 1599 (Ph), 1523 (NH); ^{1}H-NMR (DMSO-d_6) δ: 7.7 (s, 1H), 7.9 (m, 3H), 10.43 (s, 1H), 10.47 (s, 1H), 12.7 (s, IH). 2,5-Dichloro-4-nitroaniline (0.92 g) was dissolved in 2:1 Et_2O/EtOH , then 15% HCl (0.91 mL) was added to this solution and the mixture was cooled to 5 °C. $NaNO_2$ (0.4 g, 5.7 mmol) and 4-hydroxy-2-oxo-1,2-dihydroquinoline-6-carboxylic acid (1.0 g, 5.7 mmol) was added slowly under the temperature of 5 °C and pH<7 (15% HCl). The resulting mixture was left in ice overnight. The precipitated solid was then filtered and crystallized from Et_2O/EtOH. A reddish crystalline compound was obtained. Yield 64%; Mp 340 °C; Anal. calc. for $C_{16}H_8Cl_2N_4O_6$ (423.16): C 45.41%, H 1.91%; found: C 45.26%, H 2.24%; HPLC purity 96.39%; UV (nm), λ_{max}/log ε: 271.4/3.61; IR (cm^{-1}): 3616, 1180 (OH), 3030 (CH_{arom}), 2950, 1680 (acid), 1670 (lactam), 1655 (C=O), 1630 ($C=C_{cycle}$), 1614 (N=N), 1598 (Ph), 1543 (NO_2), 1520 (NH); ^{1}H-NMR (DMSO-d_6) δ: 5.70 (s, 1H), 7.10-7.60 (m, 3H), 11.10 (s, 1H), 11.30 (s, 1H).

Ethyl 4-hydroxy-2-oxo-1,2-dihydroquinoline-3-carboxylate (**9**). Aniline (0.46 mL, 0.005 mol) and triethyl methanetricarboxylate (2.12 mL, 0.01 mol) were heated in microwave reactor for 8 min at 60% power level. The mixture was then cooled to room temperature and 7 mL of Et_2O was added. The crude product was crystallized from MeOH. A white crystalline compound was obtained. Yield 50%; Mp 116-120 °C; Anal. calc. for $C_{12}H_{11}NO_4$ (233.22): C 61.80%, H 4.75%; found: C 61.65%, H 4.39%; HPLC purity 95.01%; UV (nm), λ_{max}/log ε: 244.2/3.59; IR (cm^{-1}): 3620, 1180 (OH), 2958 (CH_3), 2925 (CH_2), 1680 (lactam), 1638 (C=O), 1630 ($C=C_{cycle}$), 1598 (Ph), 1520 (NH), 1191 ($C=O_{ester}$); ^{1}H-NMR (DMSO-d_6) δ: 1.19 (t, 3H), 4.17 (q, 2H), 4.70 (s, 1H), 7.09 (t, 2H), 7.32 (t, 1H), 7.52 (d, *J*=8.5 Hz, 1H), 10.30 (t, IH).

4-Hydroxy-2-oxo-1,2-dihydroquinoline-3-carboxylic acid (**10**). The product was obtained according to the described procedure [34,35] as a white crystalline compound. Yield 99%; Mp 225 °C; HPLC purity 99.51%; UV (nm), λ_{max}/log ε: 250.1/3.52; IR (cm^{-1}): 3621, 1182 (OH), 2965, 1670 (acid), 1679 (lactam), 1646 (C=O), 1629 ($C=C_{cycle}$), 1599 (Ph), 1525 (NH).

3-(4-Carboxyphenylcarbamoyl)-4-hydroxy-2-oxo-1,2-dihydroquinoline-6-carboxylic acid (**11**). 4-Aminobenzoic acid (0.7 g, 0.005 mol) was mixed with triethyl methanetricarboxylate (2.12 mL, 0.01 mol) and heated in microwave reactor at 50% of power during 15 min and 3 min at 90%. The temperature reached 231 °C during heating. Et_2O was added to the cooled mixture and the precipitate was washed with hot (55 °C) MeOH to obtain the pure product as a yellow crystalline compound. Yield 62%; Mp 340-350 °C; Anal. calc. for $C_{18}H_{12}N_2O_7$ (368.29): C 58.70%, H 3.28%; found: C 58.09%, H 3.54%; HPLC purity 97.52%; UV (nm), λ_{max}/log ε: 251.3/3.53; IR (cm^{-1}): 3621, 1180 (OH), 3034 (CH_{arom}), 2970, 1689 (acid), 1680 (lactam), 1642 (C=O), 1635 ($C=C_{cycle}$), 1630 (amide), 1599 (Ph), 1520 (NH); ^{1}H-NMR (DMSO-d_6) δ: 7.41 (d, *J*=8.5 Hz, 1H), 7.70 (d, *J*=9.1 Hz, 2H), 7.90 (d, *J*=9.1 Hz, 2H), 8.15 (d, *J*=8.5 Hz, 1H), 8.50 (s, 1H), 12.40 (s, 1H), 12.95 (s, 1H), 16 (s, 1H).

3-(4-Carboxy-3-hydroxyphenylcarbamoyl)-4-hydroxy-2-oxo-1,2-dihydroquinoline-6-carboxylic acid (**12**). 4-Aminosalicylic acid (0.7 g, 0.005 mol) was mixed with triethyl methanetricarboxylate (2.12 mL, 0.01 mol) and heated in microwave reactor at 50% of power for 15 min and 3 min at 90%. The temperature reached 230 °C during heating. Et_2O was added to the cooled mixture and the precipitate was washed with hot (55 °C) MeOH to obtain the pure product as a yellow crystalline compound. Yield 20%; Mp 350 °C; Anal. calc. for $C_{18}H_{12}N_2O_9$ (400.29): C 54.01%, H 3.02%; found: C 54.05%, H 9.94%; HPLC purity 96.42%; UV (nm), λ_{max}/log ε: 256.0/3.53; IR (cm^{-1}): 3620, 1179 (OH), 3035 (CH_{arom}), 2972, 1688 (acid), 1680 (lactam), 1640 (C=O), 1633 ($C=C_{cycle}$), 1632 (amide), 1600 (Ph), 1521 (NH), 1329, 1199 (OH_{phenol}); ^{1}H-NMR (DMSO-d_6) δ: 7.43 (d, *J*=8.5 Hz, 2H), 7.7 (s, IH), 7.9 (m, 3H), 10.43 (s, 1H), 10.47 (s, 1H), 12.7 (s, 1H) 16.0 (s, 1H).

4.2. Lipophilicity HPLC determination (capacity factor k / calculated log k)

The HPLC separation module Waters Alliance 2695 XE and Waters Photodiode Array Detector 2996 (Waters Corp., Milford, MA, U.S.A.) were used. A Symmetry® C_{18} 5 μm, 4.6 × 250 mm, Part No. WAT054275, (Waters Corp., Milford, MA, U.S.A.) chromatographic column was used. The HPLC separation process was monitored by Millennium32® Chromatography Manager Software, Waters 2004 (Waters Corp., Milford, MA, U.S.A.). The mixture of MeOH p.a. (55.0%) and H_2O-HPLC – Mili-Q Grade (45.0%) was used as a mobile phase. The total flow of the column was 0.9 mL/min, injection 30 μL, column temperature 30 °C and sample temperature 10 °C. The detection wavelength 210 nm was chosen. The KI methanolic solution was used for the dead time (T_D) determination. Retention times (t_R) were measured in minutes. The capacity factors *k* were calculated using the Millennium32® Chromatography Manager Software according to formula $k = (t_R - t_D) / t_D$, where t_R is the retention time of the solute, whereas t_D denotes the dead time obtained via an unretained analyte. Log *k*, calculated from the capacity factor *k*, is used as the lipophilicity index converted to log *P* scale. The log *k* values of the individual compounds are shown in Table 1.

4.3. Lipophilicity calculations

Log *P*, *i.e.* the logarithm of the partition coefficient for *n*-octanol/water, was calculated using the programs CS ChemOffice Ultra ver. 9.0 (CambridgeSoft, Cambridge, MA, U.S.A.) and ACD/LogP ver. 1.0 (Advanced Chemistry Development Inc., Toronto, Canada). Clog *P* values (the logarithm of

n-octanol/water partition coefficient based on established chemical interactions) were generated by means of CS ChemOffice Ultra ver. 9.0 (CambridgeSoft, Cambridge, MA, U.S.A.) software. The results are shown in Table 1.

4.4. Study of inhibition of oxygen evolution rate (OER) in spinach chloroplasts

Chloroplasts were prepared from spinach (*Spinacia oleracea* L.) according to Masarovicova and Kralova [36]. The inhibition of photosynthetic electron transport (PET) in spinach chloroplasts was determined spectrophotometrically (Genesys 6, Thermo Scientific, U.S.A.) using an artificial electron acceptor 2,6-dichlorophenol-indophenol (DCPIP) according to Kralova *et al.* [37] and the rate of photosynthetic electron transport was monitored as a photoreduction of DCPIP. The measurements were carried out in phosphate buffer (0.02 mol/L, pH 7.2) containing sucrose (0.4 mol/L), $MgCl_2$ (0.005 mol/L) and NaCl (0.015 mol/L). The chlorophyll content was 30 mg/L in these experiments and the samples were irradiated (~100 W/m^2) from 10 cm distance with a halogen lamp (250 W) using a 4 cm water filter to prevent warming of the samples (suspension temperature 22 °C). The studied compounds were dissolved in DMSO due to their limited water solubility. The applied DMSO concentration (up to 4%) did not affect the photochemical activity in spinach chloroplasts. The inhibitory efficiency of the studied compounds was expressed by IC_{50} values, *i.e.* by molar concentration of the compounds causing 50% decrease in the oxygen evolution rate relative to the untreated control. The comparable IC_{50} value for a selective herbicide 3-(3,4-dichlorophenyl)-1,1-dimethylurea, DCMU (Diurone®) was about 1.9 μmol/L [38]. The results are summarized in Table 2.

4.4. In vitro antifungal susceptibility testing

The broth microdilution test [27,39] was used for the assessment of *in vitro* antifungal activity of the synthesized compounds against *Candida albicans* ATCC 44859 (CA), *Candida tropicalis* 156 (CT), *Candida krusei* ATCC 6258 (CK), *Candida glabrata* 20/I (CG), *Trichosporon beigelii* 1188 (TB), *Aspergillus fumigatus* 231 (AF), *Absidia corymbifera* 272 (AC), and *Trichophyton mentagrophytes* 445 (TM). Fluconazole (FLU) was used as the standard of a clinically used antimycotic drug. The procedure was performed with twofold dilution of the compounds in RPMI 1640 (Sevapharma a.s., Prague, Czech Republic) buffered to pH 7.0 with 0.165 mol of 3-morpholino-propane-1-sulfonic acid (MOPS, Sigma, Germany). The final concentrations of the compounds ranged from 500 to 0.975 μmol/l. Drug–free controls were included. The MIC was defined as an 80% or greater (IC_{80}) reduction of growth in comparison with the control. The values of MICs were determined after 24 and 48 h of static incubation at 35 °C. For *T. mentagrophytes*, the final MICs were determined after 72 and 120 h of incubation. The results are summarized in Table 2.

Acknowledgements

This study was supported by the Polish Ministry of Science N405 178735, by the Ministry of Education of the Czech Republic MSM 6215712403, by the Slovak Scientific Grant Agency VEGA 1/0089/03, and by the Irish Department of Education and Science TSR Strand1-06/CR08.

References

1. Roth, H.J.; Fenner, H. *Arzneistoffe,* 3rd Ed.; Deutscher Apotheker Verlag: Stuttgart, Germany, 2000; pp. 51-114.
2. Polanski, J.; Niedbala, H.; Musiol, R.; Podeszwa, B.; Tabak, D.; Palka, A.; Mencel, A.; Finster, J.; Mouscadet, J.F.; Le Bret, M. 5-Hydroxy-8-nitro-6-quinaldic Acid as a Novel Molecular Scaffold for HIV-1 Integrase Inhibitors. *Lett. Drugs Des. Disc.* **2006**, *3*, 175-178.
3. Polanski, J.; Niedbala, H.; Musiol, R.; Podeszwa, B.; Tabak, D.; Palka, A.; Mencel, A.; Mouscadet, J.F.; Le Bret, M. Fragment Based Approach for the Investigation of HIV-1 Integrase Inhibition. *Lett. Drugs Des. Disc.* **2007**, *4*, 99-105.
4. Vargas, L.Y.; Castelli, M.V.; Kouznetsov, V.V.; Urbina, J.M.; Lopez, S.N.; Sortino, M.; Enriz, R.D.; Ribas, J.C.; Zacchino, S. *In vitro* Antifungal Activity of New Series of Homoallylamines and Related Compounds with Inhibitory Properties of the Synthesis of Fungal Cell Wall Polymers. *Bioorg. Med. Chem.* **2003**, *11*, 1531-1550.
5. Jampilek, J.; Dolezal, M.; Kunes, J.; Buchta, V. Quinaldine derivatives preparation and their antifungal activity. *ECSOC-8* **2004**, c005, http://www.lugo.usc.es/%7Eqoseijas/ECSOC-8/BOCNP/005/index.htm.
6. Jampilek, J.; Dolezal, M.; Kunes, J.; Buchta, V.; Kralova, K. Quinaldine Derivatives: Preparation and Biological Activity. *Med. Chem.* **2005**, *1*, 591-599.
7. Musiol, R.; Jampilek, J.; Buchta, V.; Niedbala, H.; Podeszwa, B.; Palka, A.; Majerz-Maniecka, K.; Oleksyn, B.; Polanski, J. Antifungal Properties of New Series of Quinoline Derivatives. *Bioorg. Med. Chem.* **2006**, *14*, 3592-3598.
8. Musiol, R.; Jampilek, J.; Kralova, K.; Podeszwa, B.; Finster, J.; Niedbala, H.; Palka, A.; Polanski, J. New quinoline derivatives possessing herbicidal activity. *ECSOC-9* **2005**, c005, http://www.usc.es/congresos/ecsoc/9/BOCNP/c005/index.htm.
9. Musiol, R.; Jampilek, J.; Kralova, K.; Tabak, D.; Podeszwa, B.; Finster, J.; Polanski, J. Substituted amides of quinoline derivatives: preparation and their photosynthesis-inhibiting activity. *ECSOC-10* **2006**, c007, http://www.usc.es/congresos/ecsoc/10/ECSOC10.htm.
10. Musiol, R.; Jampilek, J.; Kralova, K.; Richardson, D.R.; Kalinowski, D.; Podeszwa, B.; Finster, J.; Niedbala, H.; Palka, A.; Polanski, J. Investigating Biological Activity Spectrum for Novel Quinoline Analogues. *Bioorg. Med. Chem.* **2007**, *15*, 1280-1288.
11. Musiol, R.; Jampilek, J.; Kralova, K.; Tabak, D.; Finster, J.; Podeszwa, B.; Kozik, V.; Dohnal, J.; Polanski, J. Preparation and Herbicidal Activities of Substituted Amides of Quinoline Derivatives. *ECSOC-11* **2007**, a011, http://www.usc.es/congresos/ecsoc/11/hall_aGOS/a011/index.htm.
12. Musiol, R.; Tabak, D.; Niedbala, H.; Podeszwa, B.; Jampilek, J.; Kralova, K.; Dohnal, J.; Finster, J.; Mencel, A.; Polanski, J. Investigating Biological Activity Spectrum for Novel Quinoline Analogues 2: Hydroxyquinolinecarboxamides with Photosynthesis Inhibiting Activity. *Bioorg. Med. Chem.* **2008**, *16*, 4490-4499.
13. Musiol, R.; Jampilek, J.; Kralova, K.; Finster, J.; Tabak, D.; Niedbala, H.; Csollei, J.; Dohnal, J.; Polanski, J. Ring-substituted 4-hydroxy-1*H*-quinolin-2-ones: Preparation and Their Photosynthesis-inhibiting Activity. *ECSOC-12* **2008**, c0012, http://www.usc.es/congresos/ecsoc/12/ECSOC12.htm.

14. Podeszwa, B.; Niedbala, H.; Polanski, J.; Musiol, R.; Tabak, D.; Finster, J.; Serafin, K.; Wietrzyk, J.; Boryczka, S.; Mol, W.; Jampilek, J.; Dohnal, J.; Kalinowski, D.; Richardson, D.R. Investigating the Antiproliferative Activity of Quinoline-5,8-dione Analogues on Tumour Cell Lines. *Bioorg. Med. Chem. Lett.* **2007**, 17, 6138-6141.
15. Reifler, M.J.; Szalai, V.A.; Peterson, C.N.; Brudvig, G.W. Effects of Tail-like Substituents on the Binding of Competitive Inhibitors to the Q_B Site of Photosystem II. *J. Mol. Recognit.* **2001**, *14*, 157-165.
16. Moreland D.E. Research on Biochemistry of Herbicides – an Historical Overview. *Z. Naturforsch. C-A J. Biosci.* **1993**, *48*, 121-131.
17. Zakarya, D.; Larfaoui, E.M.; Boulaamail, A.; Tollabi, M.; Lakhlifi, T. QSARs for a Series of Inhibitory Anilides. *Chemosphere* **1998**, *36*, 2809-2818.
18. Kralova, K.; Sersen, F.; Kubicova, L.; Waisser, K. Inhibitory Effects of Substituted Benzanilides on Photosynthetic Electron Transport in Spinach Chloroplasts. *Chem. Pap.* **1999**, *53*, 328-331.
19. Dolezal, M.; Miletin, M.; Kunes, J.; Kralova, K. Synthesis and Biological Evaluation of Some Amides of Pyrazine-2-carboxylic acids *Molecules* **2002**, *7*, 363-373.
20. Dolezal, M.; Palek, L.; Vinsova, J.; Buchta, V.; Jampilek, J.; Kralova, K. Substituted Pyrazinecarboxamides: Synthesis And Biological Evaluation. *Molecules* **2006**, *11*, 242-256.
21. Dolezal, M.; Cmedlova, P.; Palek, L.; Vinsova, J.; Kunes, J.; Buchta, V.; Jampilek, J.; Kralova, K. Synthesis and Antimycobacterial Evaluation of Substituted Pyrazinecarboxamides. *Eur. J. Med. Chem.* **2008**, *43*, 1105-1113.
22. Polak, A. The past, Present and Future of Antimycotic Combination Therapy. *Mycoses* **1999**, *42*, 355-370.
23. Fostel, J.M.; Lartey, P.A. Emerging Novel Antifungal Agents. *Drug Discov. Today* **2000**, *5*, 25-32.
24. http://www.doctorfungus.org/ , accessed on January 30, 2009.
25. Gershon, H; Gershon, M; Clarke, D.D. Synergistic Mixtures of Fungitoxic Monochloro- and Dichloro-8-quinolinols against Five Fungi. *Mycopathologia* **2004**, *158*, 131-135.
26. Dardari, Z.; Lemrani, M.; Bahloul, A.; Sebban, A.; Hassar, M.; Kitane, S.; Berrada, M.; Boudouma, M. Antileishmanial Activity of a New 8-Hydroxyquinoline Derivative Designed 7-[5'-(3'-phenylisoxazolino)methyl]-8-hydroxyquinoline: preliminary study. *Farmaco* **2004**, *59*, 195-199.
27. Sheehan, D.J.; Espinel-Ingroff, A.; Steele, M.; Webb, C.D. Antifungal Susceptibility Testing of Yeasts: a Brief Overview. *Clin. Infect. Dis.* **1993**, *17*, 494-500.
28. Dolezal, M.; Jampilek, J.; Osicka, Z.; Kunes, J.; Buchta, V.; Vichova, P. Substituted 5-aroylpyrazine-2-carboxylic Acid Derivatives: Synthesis and Biological Activity. *Farmaco* **2003**, *58*, 1105-1111.
29. Collins, J.F.; Donnelly, W.J.; Grundon, M.F.; James, K.J. Biosynthesis of Aromatic Isoprenoids. Part I. The role of 3-Prenylquinolines and of Platydesmine in the Biosnthesis of the Furuquinoline Alkaloid, Dictamnine. *J. Chem. Soc., Perkin Trans.* **1974**, *1*, 2177-2181.
30. Buckle, D.R.; Cantello, B.C.C.; Smith, H.; Spicer, B.A. 4-Hydroxy-3-nitro-2-quinolones and Related Compounds as Inhibitors of Allergic Reactions. *J. Med. Chem.* **1975**, *18*, 726-732.

31. Ziegler, E.; Wolf, R.; Kappe, T. Synthesen von Heterocyclen, 66. Mitt.: Eine Einfache Synthese des 4-Hydroxycarbostyrils und seiner Derivate. *Monatsh. Chem.* **1965**, *96*, 418-422.
32. Dolle, V.; Fan, E.; Nguyen, C.H.; Aubertin, A.M.; Kirn, A.; Andreola, M.L.; Jamieson, G.; Tarrago-Litvak, L.; Bisagni, E. A New Series of Pyridinone Derivatives as Potent non-Nucleoside Human Immunodeficiency Virus Type 1 Specific Reverse Transcriptase Inhibitors. *J. Med. Chem.* **1995**, *38*, 4679-4686.
33. Ukrainets, I.V.; Taran, S.G.; Sidorenko, L.V.; Gorokhova, O.V.; Ogirenko, A.A.; Turov, A.V.; Filimonova, N.I. 4-Hydroxy-2-quinolones. 3-Amino-1-R-2-oxo-4-hydroxyquinolines and Their Acyl Derivatives. *Chem. Heterocycl.Compd.* **1996**, *32*, 960-970.
34. Ukrainets, I.V.; Gorokhova, O.V.; Sidorenko, L.V. 4-Hydroxyquinol-2-ones. 85. Synthesis of 2-Chloro-4-hydroxyquinoline-3-carboxylic Acid Ethyl Ester. *Chem. Heterocycl. Compd.* **2005**, *41*, 1019-1021.
35. Detsi, A.; Bardakos, V.; Markopoulos, J.; Igglessi-Markopoulou, O. Reactions of 2-Methyl-3,1-benzoxazin-4-one with Active Methylene Compounds: a New Route to 3-Substituted 4-Hydroxyquinolin-2(1*H*)-ones. *J. Chem. Soc., Perkin Trans. 1* **1996**, *24*, 2909-2913.
36. Masarovicova, E.; Kralova, K. *Approaches to Measuring Plant Photosynthesis Activity.* In *Handbook of Photosynthesis* 2nd Ed.; Pessarakli, M., Ed.; Taylor & Francis Group: Boca Raton, London-New York-Singapore, 2005; pp. 617-656.
37. Kralova, K.; Sersen, F.; Sidoova, E. Photosynthesis Inhibition Produced by 2-Alkylthio-6-R-benzothiazoles *Chem. Pap.* **1992**, *46*, 348-350.
38. Fedke, C. *Biochemistry and Physiology of Herbicide Action.* Springer Verlag: Berlin-Heidelberg-New York, USA, 1982.
39. National Committee for Clinical Laboratory standards. Reference *Method for Broth Dilution Antifungal Susceptibility Testing of Yeast: Approved Standard, NCCLS document M27-A*; NCCLS: Villanova, PA, USA, **1997**.

Sample Availability: Samples of the compounds are available from the authors.

Polyhedron 39 (2012) 76–84

Contents lists available at SciVerse ScienceDirect

Polyhedron

journal homepage: www.elsevier.com/locate/poly

Novel *trans*-dioxorhenium complex with imidazo[1,2a]pyridine ligand – Synthesis, spectroscopic and electrochemical characterization, X-ray crystal structure and DFT calculations

B. Machura [a], M. Wolff [a,*], D. Tabak [b], Y. Ikeda [c], K. Hasegawa [c]

[a] Department of Crystallography, Institute of Chemistry, University of Silesia, 9th Szkolna St., 40-006 Katowice, Poland
[b] Department of Organic Chemistry, Institute of Chemistry, University of Silesia, 9th Szkolna St., 40-006 Katowice, Poland
[c] Research Laboratory for Nuclear Reactors, Tokyo Institute of Technology, 2-12-1-N1-34 O-okayama, Meguro-ku, Tokyo 152-8550, Japan

ARTICLE INFO

Article history:
Received 23 February 2012
Accepted 16 March 2012
Available online 24 March 2012

Keywords:
Dioxorhenium(V) complex
X-ray crystal structure
DFT calculations
Electrochemistry
Cyclic voltammetry

ABSTRACT

The reaction of $[ReO_2(py)_4]Cl$ with imidazo[1,2a]pyridine has been examined and a novel dioxorhenium(V) complex – $[ReO_2(impy)_4]Cl{\cdot}MeCN{\cdot}2H_2O$ with *trans*-$[O{=}Re{=}O]^+$ core has been obtained. The X-ray crystal structure of the complex has been determined and the electronic structure has been examined using the density functional theory (DFT) method. The UV–Vis absorption spectrum of the complex has been interpreted on the basis of the results of time-dependent DFT (TDDFT) calculations. Electrochemical reaction of $[ReO_2(impy)_4]^+$ in CH_3CN solution containing tetra-*n*-butylammonium perchlorate as a supporting electrolyte has been studied using cyclic voltammetry at 25 °C. Cyclic voltammograms show one redox couple around 0.156 (E_{pa}) and 0.080 V (E_{pc}) [versus ferrocene/ferricenium ion redox couple, (Fc/Fc^+)]. Potential differences between two peaks (ΔE_p) at scan rates (v) in the range from 0.04 to 0.20 $V s^{-1}$ are ca. 75 mV, which is almost consistent with the theoretical ΔE_p value (59 mV) for the reversible one electron transfer reaction at 25 °C. The ratios of anodic peak currents to cathodic ones are in the range from 4.76 ($v = 0.04 V s^{-1}$) to 3.11 ($v = 0.20 V s^{-1}$) and the $(E_{pa} + E_{pc})/2$ value is constant, 0.118 ± 0.001 V versus Fc/Fc^+, regardless of the scan rate. Spectroelectrochemical experiments have also been carried out by applying potentials from 0.009 to 0.159 V versus Fc/Fc^+ with an optically transparent thin layer electrode. It was found that the UV–Vis absorption spectra show clear isosbestic points at 218.9, 248.3 and 292.8 nm, and that the electron stoichiometry is evaluated as 1.04 from the Nernstian plot. These results indicate that the $[ReO_2(impy)_4]^+$ complex is oxidized quasi-reversibly to the $[ReO_2(impy)_4]^{2+}$ complex.

1. Introduction

The widespread contemporary interest in the coordination chemistry of rhenium arises mainly from the introduction of β^- emitting isotopes ^{188}Re and ^{186}Re in radiotherapy and its similarity with technetium, whose metastable γ-emitting isotope ^{99m}Tc plays important role in diagnostic nuclear medicine [1]. Depending on the target organ or tissue to be reached by the radiopharmaceutical, different characteristics of the complex (redox properties, thermodynamic stability, stereochemistry, charge, lipophilicity) are needed. Furthermore, complexes, specifically designed to reach a certain organ, can undergo in vivo reactions that considerably affect their biodistribution patterns [2]. Thus, there is a still need for a fundamental knowledge about the structural and spectroscopic properties, redox activities, and mechanism of ligand substitution reactions to develop new and improved Re and Tc radiopharmaceuticals. Among Tc and Re complexes currently used in nuclear medicine, those incorporating $[M{=}O]^{3+}$, $[MO_2]^+$ and $[M(CO)_3]^+$ cores are the most common [3].

Oxorhenium complexes are also interesting due to their application as catalysts, particularly in oxidation [4–6] and oxygen atom transfer reactions (OAT) [7–9]. Methyltrioxorhenium(VII) is one of the most versatile and highly efficient transition metal catalysts known to date [10], and some oxorhenium(V) complexes were found to be highly successful in OAT reactions.

Another area of investigations of rhenium compounds is connected with their unique electrochemical, photophysical and photochemical properties, crucial for numerous potential and already introduced practical applications. The most frequently studied compounds of this type are complexes containing the $[Re(CO)_3]^+$ and *trans*-$[ReO_2]^+$ fragment [11–15].

This work stems from our interest in the design and characterization of novel oxorhenium(V) compounds incorporating biologically relevant N-donor ligands. Here, we present synthesis, spectroscopic (IR, NMR, UV–Vis), structural (single crystal X-ray

* Corresponding author. Tel.: +48 32 3591886.
E-mail address: mwolff@us.edu.pl (M. Wolff).

0277-5387/$ - see front matter © 2012 Elsevier Ltd. All rights reserved.
http://dx.doi.org/10.1016/j.poly.2012.03.026

analysis) and electrochemical studies for novel complex $[ReO_2(impy)_4]Cl{\cdot}MeCN{\cdot}2H_2O$, being the product of reaction $[ReO_2(py)_4]Cl$ with imidazo[1,2a]pyridine (Scheme 1).

Imidazo[1,2-a]pyridines are a very important class of pharmaceutical compounds. They exhibit a wide spectrum of biological activities, including antibacterial and fungicidal. It has been also reported that they significantly inhibit gastric acid secretion and act as cardiostimulators [16–18].

The experimental studies on the dioxo Re(V) complex have been accompanied computationally by the density functional theory (DFT) calculations. Currently density functional theory (DFT) is commonly used to examine the electronic structure of transition metal complexes. It meets with the requirements of being accurate, easy to use and fast enough to allow the study of relatively large molecules of transition metal complexes. Ganchieff et al. [19,20] have performed extended tests of the ability of different DFT methods, including B3LYP with LANL2DZ basis set, for rhenium compounds in a geometry optimization and calculation of spectral properties. Although LANL2DZ is not a very extended basis set, its use with B3LYP has shown to be sufficient for the geometry optimization and calculation of spectral properties. It gives good agreement with the experimental data and its use is justified in the case of large molecules.

2. Experimental

2.1. General procedure

All synthetic manipulations were carried out open to the atmosphere. The solvents were of reagent grade quality and purchased commercially. Ammonium perrhenate, triphenylphosphine, pyridine, and imidazo[1,2a]pyridine were purchased from Sigma Aldrich and used without further purification. The $[ReO_2(py)_4]Cl$ complex was prepared according to the literature method [21].

2.2. Physical measurements

The IR spectrum was recorded on a Perkin–Elmer 1600 FTIR spectrophotometer in the spectral range 4000–400 cm^{-1} with the samples in the form of KBr pellets. The electronic spectrum was measured on a spectrophotometer Lab Alliance UV–VIS 8500 in the range 1100–180 nm in CH_3CN solution. The emission spectrum was measured by Hitachi F-2500 spectrofluorimeter in methanol solution at room temperature. The ^1H and ^{13}C NMR spectra were obtained in $CDCl_3$ at room temperature on a Bruker AM 400 spectrometer. Chemical shifts (δ, ppm) are relative to internal TMS. Measurements of electrospray ionization mass spectrometry (ESI-MS) were performed on a Varian 500-MS IT Mass Spectrometer ion trap apparatus. The instrument was operating in the positive ion mode with a capillary voltage of 20 V, needle voltage of 5 kV and a spray shield voltage of 600 V. Drying gas (N_2) temperature was 150 °C. Elemental analyses (C, H, N) were performed on a Perkin–Elmer CHN-2400 analyzer. Measurements of CV were performed at 25 ± 1 °C under Ar atmosphere with a BAS CV-50 W voltammetric analyzer and a BAS CV cell as reported previously [22]. A three-electrode system was utilized, i.e., a BAS 11-2013 Pt working electrode (surface area: S = 0.02 cm^2), a BAS 11-2025 reference electrode (Ag/$AgNO_3$ in TBAP/acetonitrile solution), and a BAS 51-2222 Pt auxiliary electrode. The ferrocene/ferricenium (Fc/Fc^+) couple was used as the reference redox system and its redox potential is 0.081 V versus Ag/$AgNO_3$ reference electrode. All potentials reported here are versus Fc/Fc^+. All sample solutions were deoxygenated by passing Ar gas into solutions for at least 10 min before starting CV measurements.

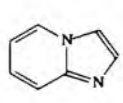

Scheme 1. Structure of imidazo[1,2a]pyridine (impy) ligand.

Spectroelectrochemical measurements were carried out using Shimadzu UV-3150 spectrophotometer equipped with optically transparent thin layer electrode (OTTLE) cell [22], which has a Pt minigrid electrode as the optically transparent working electrode. The optical path length of OTTLE cell for measuring UV–Vis spectra was calibrated as 2.20×10^{-2} cm spectrophotometrically. The UV–Vis spectral changes during the electrochemical reaction were observed with spectropotentiostatic technique, in which the spectrum at each applied potential was measured after equilibrium was achieved. In the present experiments, the equilibrium was evidenced by cessation of absorbance changes and required at least 2 min.

2.3. Preparation of trans-$[ReO_2(impy)_4]Cl{\cdot}MeCN{\cdot}2H_2O$ (1)

$[ReO_2(py)_4]Cl$ (0.5 g, 0.88 mmol) and imidazo[1,2a]pyridine (0.42 g, 3.56 mmol) were refluxed in the mixture of methanol (50 ml) and tetrahydrofuran (50 ml) for 2 h. The reaction mixture was cooled to room temperature, and the solvents were removed by rotatory evaporation resulting in a reddish-brown precipitate. Recrystallization from acetonitrile gave a reddish-brown microcrystalline solid. Suitable crystals for X-ray diffraction studies were obtained by slow diffusion of an aqueous solution into acetonitrile. Yield: 90%. *Anal.* Calc. for $C_{30}H_{31}N_9O_4ClRe$: C, 44.86; H, 3.89; N, 15.69. Found: C, 43.09; H, 3.66; N, 15.59%. IR (KBr, cm^{-1}) 3352(m) $\upsilon_{CH(im)}$; 3108(m), 3078(m), 3026(m) $\upsilon_{CH(py)}$; 1635(m) $\upsilon_{CC(py)}$, $\upsilon_{CN(im)}$, $\delta_{CCH(py)}$; 1546 (w) υ_{CC}, $\upsilon_{CN(im+py)}$, $\delta_{CCH(im+py)}$; 1505(s) $\delta_{CCH(py)}$, $\delta_{NCH(py)}$, $\upsilon_{CC(py)}$, $\upsilon_{CN(im)}$; 1447(w) $\delta_{CCH(py)}$, $\delta_{NCH(py)}$, $\upsilon_{CN(py)}$; 1379(w) $\delta_{CCH(im)}$, $\upsilon_{CN(im)}$; 1341(w) $\delta_{CCH(py)}$, $\upsilon_{CN(im)}$; 1318(m) $\upsilon_{CN(im+py)}$, $\upsilon_{CC(im+py)}$; 1292(w), 1235(w), 1158(m), 1147(m) $\delta_{CCH(py)}$ $\delta_{NCH(py+im)}$, $\upsilon_{CN(im)}$; 1087(w) $\delta_{NCH(im)}$; 1012(w) $\delta_{CCH(py)}$, $\upsilon_{CC(py)}$; 957(w) $\gamma_{CH(py)}$; 905(w) $\gamma_{CH(py)}$, $\delta_{CNCH(im)}$; 854(w) $\gamma_{CH(py+im)}$; 802(s) $\upsilon_{asO=Re=O}$; 762(s) $\delta_{CH(py)}$; 753(s) $\gamma_{CH(py+im)}$, $\gamma_{CNCH(py)}$; 633(w) $\delta_{ring(py)}$, $\delta_{HCCH(py)}$; 568(w) $\gamma_{HCCH(py)}$, $\gamma_{HCNC(im)}$. ^1H NMR (400 MHz, $CDCl_3$): δ = 8.46 (d, J_{34} = 6.7 Hz, 4H, C(3)), 7.99 (d, J_{56} = 9.3 Hz, 4H, C(6)), 7.91 (s, 4H, C(1)), 7.71 (d, J_{12} = 1.3 Hz, 4H, C(2)), 7.06–7.02 (m, 4H, C(5)), 6.88 (t, J_{34} = 6.8 Hz, 4H, C(4)), 3.49 (s, 4H), 2.02 (s, 3H, C(98)). ^{13}C NMR (100 MHz, $CDCl_3$): δ = 144.98, 134.25, 128.41, 127.98, 127.66, 127.34, 126.46, 115.66, 115.47, 114.68, 114.53, 114.54, 113.75. ESI^+-MS (MeOH): *m/z* 119.42 $((impy)+H)^+$, 335.37 $([ReO_2(impy)])^+$, 455.35 $([ReO_2(impy)_2])^+$, 497.18 $([ReO_2(impy)_2]+CH_3CN)^+$, 573.18 $([ReO_2(impy)_3])^+$, 731.05 $([ReO_2(impy)_4]+CH_3CN)^+$.

2.4. Crystal structure determination and refinement

The X-ray intensity data of complex **1** were collected on a Gemini A Ultra diffractometer equipped with Atlas CCD detector and graphite monochromated Mo Kα radiation (λ = 0.71073 Å) at room temperature. Details concerning crystal data and refinement are given in Table 1. Lorentz, polarization and empirical absorption correction using spherical harmonics implemented in SCALE3 ABSPACK scaling algorithm [23] were applied. The structure was solved by the Patterson method and subsequently completed by the difference Fourier recycling. All the non-hydrogen atoms were refined anisotropically using full-matrix, least-squares technique. The hydrogen atoms were treated as "riding" on their parent carbon atoms and assigned isotropic temperature factors equal 1.2 (non-methyl) and 1.5 (methyl) times the value of equivalent temperature factor of the parent atom. The methyl groups were allowed to rotate about their local threefold axis. SHELXS97 and SHELXL97

Table 1
Crystal data and structure refinement for **1**.

Empirical formula	$C_{30}H_{31}ClN_9O_4Re$
Formula weight	803.29
Temperature (K)	293.0(2)
Wavelength (Å)	0.71073
Crystal system	monoclinic
Space group	$P2_1/n$
Unit cell dimensions	
a (Å)	13.1027(4)
b (Å)	14.8812(5)
c (Å)	17.2451(6)
β (°)	101.985(3)
Volume (Å^3)	3289.22(19)
Z	4
D_{Calc} (mg m^{-3})	1.622
Absorption coefficient (mm^{-1})	3.824
$F(000)$	1592
Crystal size (mm)	0.202 × 0.150 × 0.048
θ range for data collection (°)	3.44–25.00
Index ranges	$-15 \leqslant h \leqslant 15$ $-14 \leqslant k \leqslant 17$ $-20 \leqslant l \leqslant 20$
Reflections collected	18607
Independent reflections (R_{int})	5783 (0.0326)
Completeness to 2θ = 25.00° (%)	99.8
Minimum and maximum transmittance	0.4466–1.0000
Data/restraints/parameters	5783/0/411
Goodness-of-fit on F^2	1.072
Final R indices [$I > 2\sigma(I)$]	R_1 = 0.0302 wR_2 = 0.0642
R indices (all data)	R_1 = 0.0407 wR_2 = 0.0673
Largest difference in peak and hole (e Å^{-3})	1.152 and −0.488

[24,25] programs were used for all the calculations. Atomic scattering factors were those incorporated in the computer programs.

2.5. Computational details

The GAUSSIAN-09 program package was used for all the calculations [26]. The gas phase geometry of cation $[ReO_2(impy)_4]^+$ was fully optimized without any symmetry restrictions in singlet ground-states with the DFT method using the B3LYP hybrid exchange–correlation functional. The calculations were performed using LANL2DZ ECP basis set with additional d (with exponent α = 0.3811) and f (with exponent α = 2.033) functions for the rhenium and the standard 6-31G basis set for the other atoms. For oxygen and nitrogen atoms, diffuse and polarization functions were added [27,28]. All the calculated vibrational frequencies are real and positive, indicating that the optimized structure represents real minima of the ground state potential energy surface.

The electronic spectrum was calculated with the TDDFT method [29] and the solvent effect (acetonitrile) was simulated using the polarizable continuum model with the integral equation formalism (IEF-PCM) [30]. For cation $[ReO_2(impy)_4]^+$, 120 singlet–singlet spin-allowed excitations in solution were taken into account.

3. Results and discussion

3.1. Synthesis

The complex $[ReO_2(impy)_4]Cl{\cdot}MeCN{\cdot}H_2O$ (**1**) was prepared in good yield in the reaction of *trans*-$[ReO_2(py)_2]Cl$ with an excess of imidazo[1,2a]pyridine in a mixture of methanol–tetrahydrofuran. It was isolated as air stable reddish-brown microcrystalline solid, soluble in acetonitrile, methanol, dichloromethane and chloroform.

The IR spectrum of **1** displays a single O=Re=O asymmetrical stretching mode at 802 cm^{-1}, consistent with *trans*-dioxo geometry and within the range reported for dioxorhenium complexes [31–35]. For chloride and iodide salts $[ReO_2L_4]X$ with pyridines and aliphatic amines the strong ν_{as}(O=Re=O) band is found between 810 and 825 cm^{-1} [31], whereas for complexes containing imidazole ligands this vibration tends to appear at 765–794 cm^{-1}. The characteristic bands corresponding to ν(C=N), ν(C=C) modes of the impy ligand appear at 1650–1500 cm^{-1}. The strong bands at 762 and 753 cm^{-1} are attributable to the ring breathing and the CH stretching vibrations.

The calculated (non-scaled) vibrational spectrum of **1** stays in good agreement with experimental data (Fig. 1). The calculated ν(O=Re=O) value occurs at 807 cm^{-1} and correlates well with the experimental one 802 cm^{-1}. Similarly, the calculated absorptions due to ν(C=N), ν(C=C) modes of the impy, appearing at 1695–1497 cm^{-1}, fall in the experimental range.

The ^{1}H NMR spectrum of **1** in $CDCl_3$ shows sharp and clear peaks, which is typical of the diamagnetic nature of the d^2 system. Four coordinated imidazo[1,2a]pyridine ligands are magnetically equivalent and they are represented by six separate signals (multiplet, triplet, singlet and two doublets) in aromatic range. In comparison with free ligand the signals are downshifted. The singlets at δ = 3.49 and 2.02 ppm originate from non-coordinating solvents – water and acetonitrile.

3.2. Crystal structure

The complex $[ReO_2(impy)_4]Cl$ crystallizes as a solvate with one molecule of MeCN and two molecules of H_2O per asymmetric unit.

The crystallographic data of **1** are summarized in Table 1, and intra- and inter-molecular contacts [36,37] detected in the structure are given in Table 2. Four water molecules and two chloride ions form $[(H_2O)_4Cl_2]^{2-}$ moiety *via* O(98)–H(98B)···Cl(1), O(99)–H(99A)···O(98)_#1 and O(99)–H(99B)···Cl(1) hydrogen bonds, and two water molecules of $[(H_2O)_4Cl_2]^{2-}$ interact further with O(1) atoms of two complex cations $[[ReO_2(impy)_4]^+$, forming dimeric unit consisting of two cations $[ReO_2(impy)_4]^+$ and one $[(H_2O)_4Cl_2]^{2-}$ (Fig. 2). Additionally, the structure **1** is stabilized by C–H···O interactions, which can be considered as weak or very weak hydrogen bonds.

The molecular structure of **1** is depicted in Fig. 3, and selected bond lengths and angles are listed in Table 3.

The coordination environment around the central atom may be described as a distorted octahedron with oxo oxygen atoms in axial positions. Four imidazo[1,2a]pyridine ligands are bonded equatori-

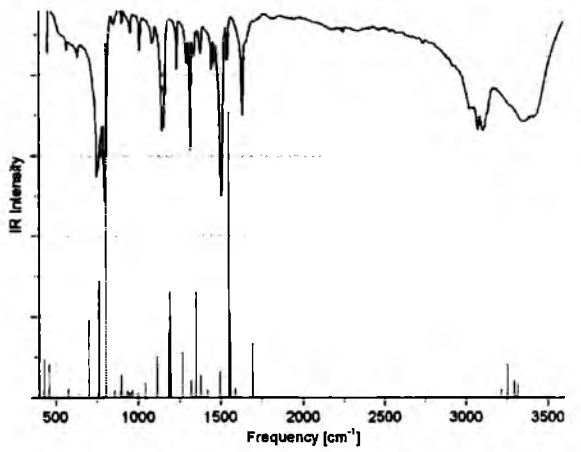

Fig. 1. The experimental (black) and calculated (red) vibrational spectrum (colour online).

Table 2
Hydrogen bonds for **1**.

D–A	D–H (Å)	H···A (Å)	D···A (Å)	D–H···A (°)
O(98)–H(98A)···O(1)	0.95	1.76	2.694(4)	165.8
O(98)–H(98B)···Cl(1)	1.00	2.10	3.096(3)	172.7
O(99)–H(99A)···O(98)_#1	1.00	1.73	2.724(5)	171.9
O(99)–H(99B)···Cl(1)	0.99	2.24	3.215(4)	167.6
C(6)–H(6)···O(1)	0.93	2.53	3.140(5)	123.6
C(9)–H(9)···O(2)_#2	0.93	2.41	3.334(6)	171.2
C(10)–H(10)···Cl(1)_#3	0.93	2.68	3.545(6)	154.5
C(13)–H(13)···O(1)	0.93	2.38	3.007(5)	124.4
C(16)–H(16)···Cl(1)_#4	0.93	2.81	3.665(5)	153.4
C(17)–H(17)···O(99)_#4	0.93	2.48	3.293(6)	146.4
C(23)–H(23)···O(98)_#5	0.93	2.36	3.280(6)	169.7
C(24)–H(24)···Cl(1)_#5	0.93	2.67	3.589(6)	167.9
C(27)–H(27)···O(1)	0.93	2.46	3.058(5)	122.0

#1: 1 − x, 2 − y, −z; #2: 2 − x, 1 − y, −z; #3: 1/2 + x, 3/2 − y, −1/2 + z; #4: 1 + x, y, z; #5: 1/2 + x, 3/2 − y, 1/2 + z.

ally in a paddle-wheel arrangement. The *trans*-oxo ligands are approximately linear with an O=Re=O angle of 177.89(13)°, and *cis*-N–Re–N and O–Re–N angles are close to 90°. The Re–O bond lengths (1.768(3) and 1.745(3) Å) fall in the range typical of rhenium(V) incorporating $[ReO_2]^+$ core [22,32–34,38,40–42], and reflect the expected double bond character [39]. In particular, the Re=O bonds lengths of **1** compare well with the values found for Re=O distances in $[ReO_2(4\text{-Me-py})_4]^+$ (1.74(2), 1.76(2) Å) and $[ReO_2(3\text{-}NH_2\text{-py})_4]^+$ (1.761(2), 1.771(2) Å) [40,41]. A slight difference between two axial Re=O bond lengths is probably due to involving O(1) atom in O(98)–H(98A)···O(1) hydrogen bond.

The Re–N (2.128–2.136 Å) distances are also unexceptional and compares well with distances of 2.060–2.170 Å for $[ReO_2(py)_4]^+$ [41] and 2.137–2.148 Å for $[ReO_2(2\text{-MeImH})_4]^+$ [32].

3.3. Geometry optimization

The optimized geometric parameters of the cation $[ReO_2(impy)_4]^+$ are gathered in Table 3. The B3LYP method in combination with the LANL2DZ basis gives a very good estimation of Re–O (with deviations equal to +0.009 to +0.0018 Å) and Re–N bond lengths (with errors ranging from 0.035 to +0.042 Å). The bond angles and general trends observed in the experimental data are also well reproduced in the calculations.

3.4. Electronic structure

A schematic representation of the energy and character of the frontier orbitals of cation $[ReO_2(impy)_4]^+$ is presented in Fig. 4. The energy gap from HOMO to LUMO is equal to 3.62 eV. The highest MO presents significant metallic character. It is predominantly of d_{xy} type with some contributions from impy orbitals. The high-lying occupied orbitals (HOMO−1 to HOMO−3) are mostly contributed by imidazo[1,2a]pyridine orbitals. The LUMO, LUMO+1, LUMO+4, LUMO+5 orbitals are composed of d_{xz} and d_{yz} rhenium orbitals in antibonding arrangement to *p* oxygen orbitals. All they contain admixture from two imidazo[1,2a]pyridine orbitals. To some extent they represent π-antibonding rhenium–oxygen molecular orbitals. Higher-energy virtual MOs correspond to π-antibonding impy orbitals. The LUMO+10 and LUMO+20 are mostly contributed by metal orbitals $d_{x^2-y^2}$ and d_{z^2}, respectively.

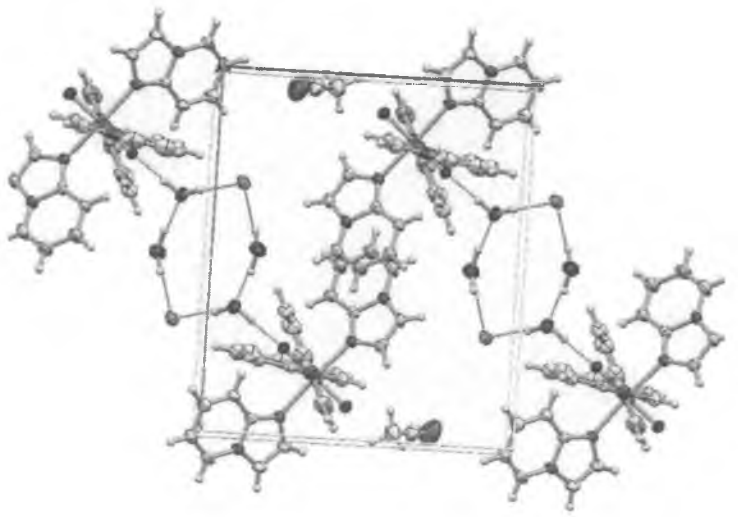

Fig. 2. Packing diagram of **1** showing the shortest intermolecular interactions.

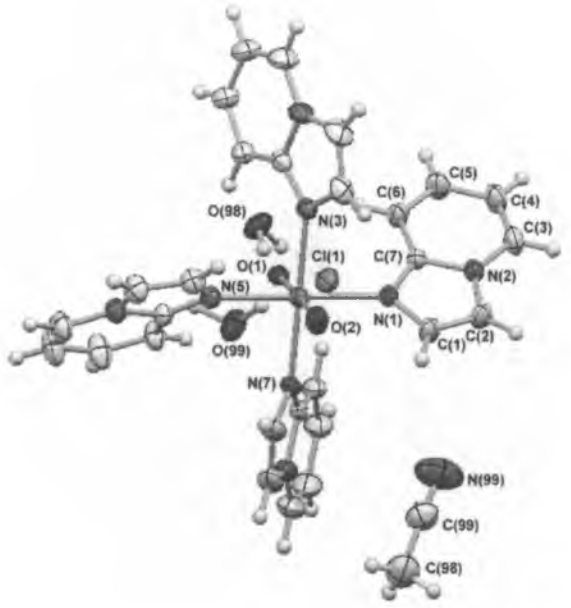

Fig. 3. The molecular structure of **1**. Displacement ellipsoids are drawn at 50% probability.

3.5. Electronic spectrum

The experimental and calculated electronic spectra of **1** in CH_3CN are presented in Fig. 5. Each calculated transition for cation $[ReO_2(impy)_4]^+$ is represented by a gaussian function $y = ce^{-bx^2}$ with the height (c) equal to the oscillator strength and b equal to 0.04 nm^{-2}. Table 4 present the most important electronic transitions calculated with the TDDFT method assigned to the observed absorption bands of **1**. For the high energy part of the spectrum, only transitions with oscillator strengths larger than 0.0400 are listed in Table 4. The assignment of the calculated orbital excitations to the experimental bands was based on an overview of the contour plots and relative energy to the occupied and unoccupied orbitals involved in the electronic transitions.

The electronic spectrum of **1** exhibit three absorptions (at 216.5, 273.5 and 367.0 nm) in UV region and one band in visible range (at 455.0 nm). This lowest-energy peak seems to be characteristic of *trans*-dioxorhenium(V) complexes and is generally assigned to the ligand field $^1A_{1g}[(b_{2g})^2] \rightarrow {}^1E_g[(b_{2g})^1(e_g)^1]$ transition. For compounds $[ReO_2(py)_4]^+$, $[ReO_2(3\text{-Cl-py})_4]^+$, $[ReO_2(3\text{-}SO_3\text{-py})_4]^+$ and $[ReO_2(4\text{-MeO-py})_4]^+$ this absorption appears at 440, 428, 431 and 448 nm, respectively [43].

The TDDFT/PCM calculations show that the two lowest-energy absorption bands of **1** (at 455.0 and 367.0 nm) originates from the excitations between the highest occupied orbital and LUMO, LUMO+1, LUMO+4 and LUMO+5. As can be seen from the Fig. 4, these orbitals are delocalized among rhenium ion and impy ligand. Due to their mixed character a delocalized *MLLCT* (metal–ligand-to-ligand CT) description can be used for the transitions assigned to the lowest-energy absorptions of **1**. On the other hand, taking into consideration significant metallic character of HOMO, LUMO, LUMO+1, LUMO+4 and LUMO+5 orbitals these transitions may be seen as *d–d* transitions.

The origin of the absorption bands at the highest-energy part of the spectrum (at 273.5 and 216.5 nm) is attributed to *Ligand–Ligand Charge Transfer*.

3.6. Emission spectrum

Emission properties of the title complex **1** have been examined in a methanol solution (with concentration of 1×10^{-3} mol dm^{-3}) at room temperature. The most intensive and representative emission spectrum was obtained with use 315 nm excitation wavelength (Fig. 6). Excitation of the complex led to the observation of emission with maximum at 402 nm.

3.7. Cyclic voltammetric measurements

The cyclic voltammograms of solution prepared by dissolving **1** (9.90×10^{-4} M) and TBAP (0.10 M) into CH_3CN were measured in the potential range from −0.08 to 0.32 V at the different scan rates (v = 0.04–0.20 $V s^{-1}$). The result is shown in Fig. 7, in which peaks of one redox couple are observed around 0.15 (E_{pa}) and 0.08 V (E_{pc}). The electrochemical data are listed in Table 5. The values of ΔE ($=E_{pa} - E_{pc}$) are almost constant without depending on the scan rate, i.e. 0.075 V (see Table 5), which is almost consistent with the theoretical value (0.059 V) for the reversible one-electron transfer process at 25 °C. The ratio of anodic peak currents to cathodic ones (i_{pa}/i_{pc}) is in the range of 4.8–3.1 and the value of $(E_{pa} + E_{pc})/2$ ($=E°$) is constant, 0.117 ± 0.002 V, without depending on the scan rate. Furthermore, a plot of i_{pa} versus $v^{1/2}$ gives a good linear relationship as shown in Fig. 8. These results suggest that $[ReO_2(impy)_4]^+$ is almost reversibly oxidized to $[ReO_2(impy)_4]^{2+}$.

Table 3
The experimental and optimized bond lengths (Å) and angles (°) for **1**.

Bond lengths	Experimental	Optimized	Bond angles	Experimental	Optimized
Re(1)–O(2)	1.746(3)	1.764	O(2)–Re(1)–O(1)	177.89(13)	179.94
Re(1)–O(1)	1.766(3)	1.775	O(2)–Re(1)–N(3)	90.06(14)	88.01
Re(1)–N(3)	2.129(3)	2.171	O(1)–Re(1)–N(3)	91.55(12)	91.92
Re(1)–N(5)	2.131(3)	2.171	O(2)–Re(1)–N(5)	87.47(13)	88.05
Re(1)–N(1)	2.134(3)	2.171	O(1)–Re(1)–N(5)	91.17(13)	91.96
Re(1)–N(7)	2.136(4)	2.171	N(3)–Re(1)–N(5)	89.90(13)	89.95
			O(2)–Re(1)–N(1)	89.49(13)	88.07
			O(1)–Re(1)–N(1)	91.91(12)	91.92
			N(3)–Re(1)–N(1)	88.70(13)	89.96
			N(5)–Re(1)–N(1)	176.65(13)	176.12
			O(2)–Re(1)–N(7)	88.72(15)	88.05
			O(1)–Re(1)–N(7)	89.67(13)	92.01
			N(3)–Re(1)–N(7)	178.72(13)	176.07
			N(5)–Re(1)–N(7)	89.67(13)	89.96
			N(1)–Re(1)–N(7)	91.66(13)	89.86

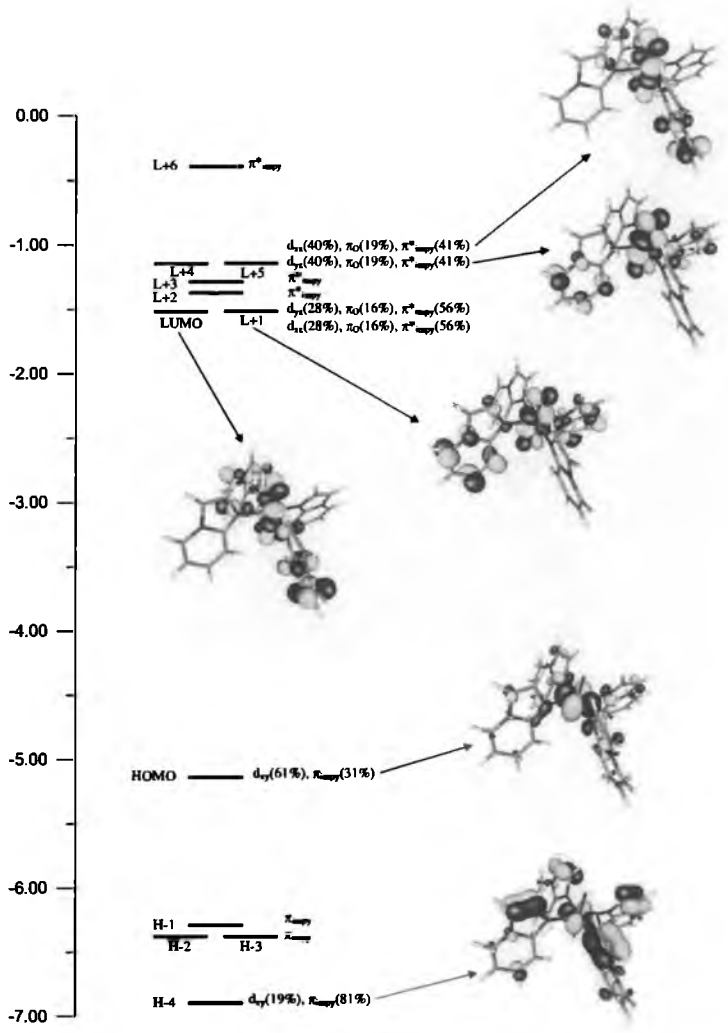

Fig. 4. The energy (eV), character and some contours of the unoccupied molecular orbitals of $[ReO_2(impy)_4]^+$. Positive values of the orbital contour are represented in blue (0.04 au) and negative values – in yellow (−0.04 au) (colour online).

3.8. Spectroelectrochemical measurements

The UV–Vis absorption spectra of CH_3CN solution dissolved **1** (1.02×10^{-3} M) and TBAP (0.10 M) were measured at each applied potential in the range from 0.009 to 0.159 V. The results are shown in Fig. 9. As seen from this figure, the absorption spectra change with the appearance of isosbestic points at 218.9, 248.3, 292.8 and 531.3 nm with increasing the potential. This indicates that only one equilibrium reaction exists in this system. The redox equilibrium of $[ReO_2(impy)_4]^+/[ReO_2(impy)_4]^{2+}$ mentioned above is proposed as the most probable candidate. Furthermore, the absorption spectral changes were found to converge around 0.159 V. This suggests that the absorption spectrum observed at 0.159 V correspond to that of $[ReO_2(impy)_4]^{2+}$. In order to confirm whether the redox equilibrium is $[ReO_2(impy)_4]^+/[ReO_2(impy)_4]^{2+}$, i.e., the electron stoichiometry (n value) is 1, the Nernstian plot was performed for the absorbencies at 277 nm in Fig. 9. The result is shown in Fig. 10. From an intercept and a slope of this plot, the E° and n values were evaluated as 0.082 V and 1.04 at 25 °C, respectively. Although the E° value is a little bit difference from that (0.117 ± 0.002 V) obtained from the CV measurement, the n value is nearly 1. Hence, it is concluded that the redox couple at E_{pa}/E_{pc} corresponds to the following redox reaction (1) and that the absorption spectrum measured at 0.159 V is assigned as that for pure $[ReO_2(impy)_4]^{2+}$

$$[ReO_2(impy)_4]^{2+} + e^- = [ReO_2(impy)_4]^+ \quad E^\circ = 0.117V \qquad (1)$$

As seen from Fig. 9, the characteristic absorption bands of $[ReO_2(impy)_4]^{2+}$ are observed around 276, 314(shoulder), and 616 nm. Their ε values were estimated to be 3.4×10^4, 4.4×10^3, and 8.9×10^2 M^{-1} cm^{-1}, respectively.

3.9. Reversibility of redox reaction of $[ReO_2(impy)_4]^+$

In order to evaluate the validity of assignment that the electrochemical reaction (1) is almost reversible, the standard rate constant (k^0) was estimated using Nicholson's equation [Eq. (2)] based on the assumption that diffusion coefficients of oxidant (D_O) and reductant (D_R) are equal

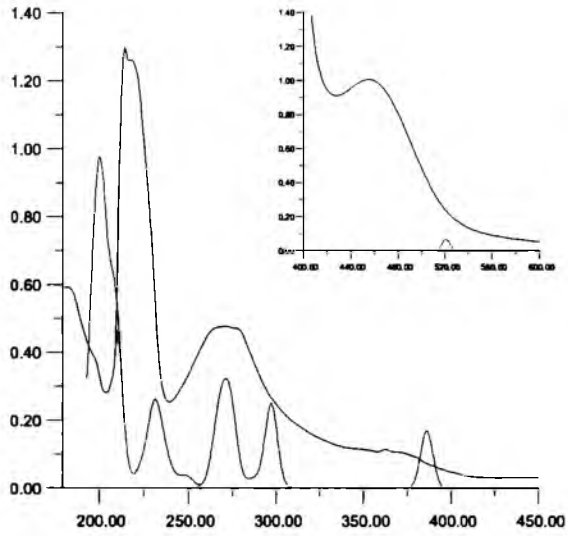

Fig. 5. The experimental (black) and calculated (red) electronic absorption spectra of 1 (colour online).

$$\psi = k^0/\{D_R\pi(nF/RT)v\}^{1/2} \quad (2)$$

where ψ is the kinetic parameter defined by Nicholson [44,45]. The D_R value was estimated from the value of slope (10.36) in Fig. 8 by using Eq. (3) [46]

$$i_{pa} = 0.4463 \times 10^{-3} n^{3/2} (F^3/RT)^{1/2} A C_R D_R^{1/2} v^{1/2} \quad (3)$$

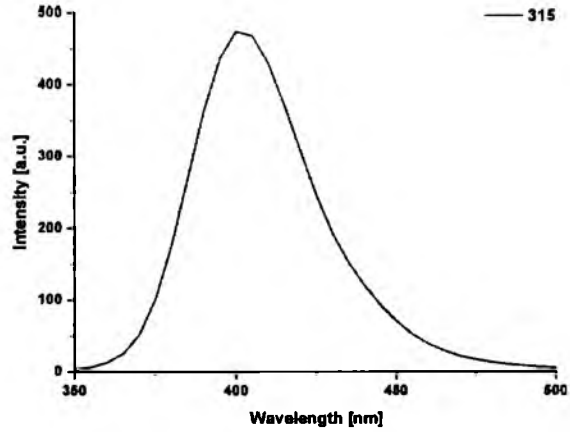

Fig. 6. The fluorescence spectrum of 1 in methanol obtained under excitation wavelength 315 nm.

where A (cm^2) and C_R^0 (M) are the surface area of working electrode and the concentration of reductant, i.e., $[ReO_2(impy)_4]^+$, respectively. The D_R value was estimated to be 3.44×10^{-6} $cm^2 s^{-1}$ at 25 °C. In the present study, the ΔE_p values are 0.078 and 0.069 V at $v = 0.04$ and 0.1 Vs^{-1}, respectively. Hence, the corresponding ψ values are obtained to be 1.6 and 2.7 on the basis of Nicholson's data [44]. From these ψ values and the estimated D_R value, the k^0 values of the electrochemical reaction (1) in the range of present scan rates were evaluated as $(0.66–1.10) \times 10^{-2}$ $cm\,s^{-1}$ at 25 °C by using Eq. (2).

Table 4
The energy and molar absorption coefficients of experimental absorption bands and the electronic transitions calculated with the TDDFT method for $[ReO_2(impy)_4]^+$.

The most important orbital excitations	Character	λ (nm)	E (eV)	f	Experimental λ (nm) (E (eV))ε
H → L	d/π(impy) → d/π*(impy)	520.6	2.38	*0.0088*	455.0 (2.72) 3240
H → L + 5	d/π(impy) → d/π*(impy)				
H → L + 1	d/π(impy) → d/π*(impy)	520.4	2.38	*0.0085*	
H → L + 4	d/π(impy) → d/π*(impy)				
H → L + 4	d/π(impy) → d/π*(impy)	386.0	3.21	*0.0836*	367.0 (3.38) 9000
H → L + 1	d/π(impy) → d/π*(impy)				
H → L + 5	d/π(impy) → d/π*(impy)	385.8	3.21	*0.0830*	
H → L	d/π(impy) → d/π*(impy)				
H − 1 → L	π(impy) → d/π*(impy)	297.2	4.17	*0.1229*	273.5 (4.53) 38060
H − 1 → L + 1	π(impy) → d/π*(impy)	297.1	4.17	*0.1213*	
H − 2 → L + 2	π(impy) → π*(impy)	274.9	4.51	*0.0730*	
H − 3 → L + 2	π(impy) → π*(impy)	274.8	4.51	*0.0729*	
H − 1 → L + 3	π(impy) → π*(impy)	272.2	4.55	*0.0527*	
H − 11 → L	d → d/π*(impy)	268.9	4.61	*0.0645*	
H − 11 → L + 1	d → d/π*(impy)	268.9	4.61	*0.0620*	
H − 2 → L + 5	π(impy) → d/π*(impy)	264.6	4.69	*0.0488*	
H − 7 → L + 3	π(impy) → π*(impy)	236.0	5.25	*0.0318*	
H → L + 15	d/π(impy) → π*(impy)	230.8	5.37	*0.0713*	
H → L + 16	d/π(impy) → π*(impy)	230.7	5.37	*0.0733*	
H − 4 → L + 7	d/π(impy) → π*(impy)	210.4	5.89	*0.0403*	216.5 (5.73) 102880
H − 4 → L + 9	d/π(impy) → π*(impy)	209.0	5.93	*0.4415*	
H − 4 → L + 6	d/π(impy) → π*(impy)	202.6	6.12	*0.1070*	
H − 4 → L + 7	d/π(impy) → π*(impy)	202.6	6.12	*0.1087*	
H − 4 → L + 9	d/π(impy) → π*(impy)	201.0	6.17	*0.4058*	
H − 5 → L + 6	π(O)/π(impy) → π*(impy)	198.7	6.24	*0.0281*	
H − 6 → L + 6	π(O)/π(impy) → π*(impy)				
H − 5 → L + 7	π(O)/π(impy) → π*(impy)	198.7	6.24	*0.0558*	
H − 5 → L + 8	π(O)/π(impy) → π*(impy)	197.9	6.26	*0.1375*	
H − 5 → L+	π(O)/π(impy) → π*(impy)				
H − 6 → L + 9	π(O)/π(impy) → π*(impy)	197.9	6.27	*0.1372*	
H − 7 → L + 6	π(impy) → π*(impy)	195.2	6.35	*0.0456*	
H − 7 → L + 7	π(impy) → π*(impy)	195.2	6.35	*0.0457*	
H − 7 → L + 8	π(impy) → π*(impy)	194.1	6.39	*0.0652*	

ε, molar absorption coefficient ($dm^3 mol^{-1} cm^{-1}$); f, oscillator strength; H, highest occupied molecular orbital; L, lowest unoccupied molecular orbital.

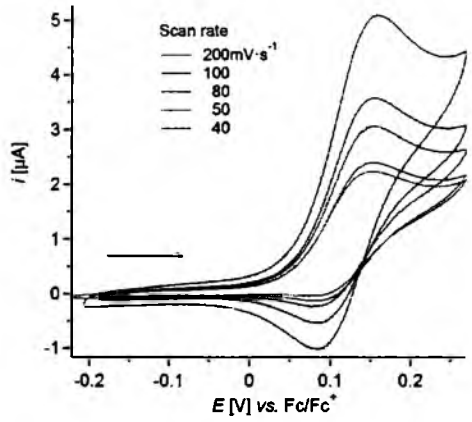

Fig. 7. Cyclic voltammograms of solution prepared by dissolving **1** (9.09×10^{-4} M) and TBAP (0.10 M) into CH_3CN measured at different scan rates in the range from 40 to 200 mV s^{-1}. Initial scan direction: anodic temperature = 25 °C.

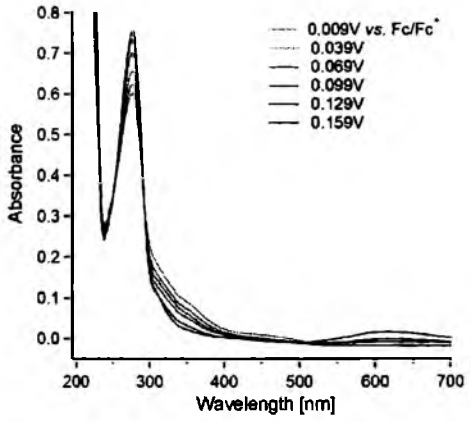

Fig. 9. UV–Vis absorption spectra measured at the applied potentials in the range from 0.009 to 0.159 V vs. Fc/Fc^+ for the solution prepared by dissolving **1** (1.02×10^{-3} M) and TBAP (0.10 M) into CH_3CN. Optical path length = 2.20×10^{-2} cm.

Table 5
Electrochemical data of **1** in CH_3CN.

v (V s^{-1})	E_{pa} (V)	E_{pc} (V)	ΔE_p (V)	$(E_{pa} + E_{pc})/2$ (V)
0.04	0.153	0.075	0.078	0.114
0.05	0.154	0.078	0.076	0.116
0.08	0.155	0.078	0.077	0.117
0.10	0.153	0.084	0.069	0.119
0.20	0.157	0.083	0.074	0.120

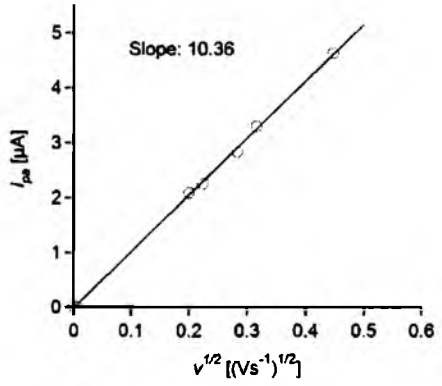

Fig. 8. A plot of i_{pa} vs. $v^{1/2}$ for the cyclic voltammograms shown in Fig. 7.

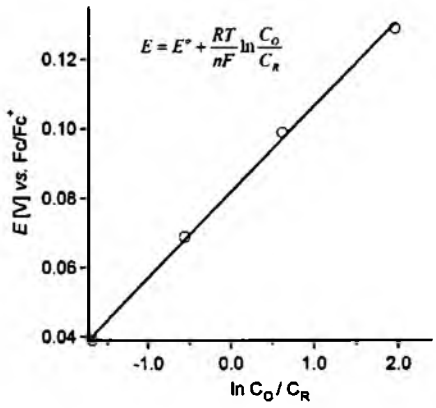

Fig. 10. Nernstian plot for the absorbencies at 277 nm in Fig. 9.

Matsuda et al. have proposed the reversibility factor (Λ) for electrochemical reactions [46,47]. The Λ value is defined by Eq. (4) for $D_O = D_R$

$$\Lambda = k^0/(D_R n F v/RT)^{1/2} \quad (4)$$

Reversible system : $\Lambda > 15$
Quasi-reversible system : $15 > \Lambda > 10^{-2(1+\alpha)}$
Irreversible system : $10^{-2(1+\alpha)} > \Lambda$

If the relation of $D_O = D_R = 3.44 \times 10^{-6}$ $cm^2 s^{-1}$ holds in the electrochemical reaction (1), the Λ equation is expressed as $\Lambda = 86k^0/v^{1/2}$. In α (transfer coefficient) = 0.5, the following relationships for the k^0 value are derived in the range of $v = 0.04$–0.20 V s^{-1}

Reversible system : $k^0 > (3.5 - 7.8) \times 10^{-2}$

Quasi-reversible system : $(3.5 - 7.8) \times 10^{-2} > k^0 > (2.3 - 5.2) \times 10^{-5}$

Irreversible system : $(2.3 - 5.2) \times 10^{-5} > k^0$

These classifications support that the electrochemical reaction (1) is quasi-reversible under the present experimental conditions, because the estimated k^0 value $[(0.66 - 1.10) \times 10^{-2}$ cm $s^{-1}]$ is compatible with the range of $(3.5 - 7.8) \times 10^{-2} > k^0 > (2.3 - 5.2) \times 10^{-5}$. As a result, it is concluded that the electrochemical oxidation of $[ReO_2(impy)_4]^+$ to $[ReO_2(impy)_4]^{2+}$ in CH_3CN is quasi-reversible.

Acknowledgements

The GAUSSIAN-09 calculations were carried out in the Wrocław Centre for Networking and Supercomputing, WCSS, Wrocław, Poland, http://www.wcss.wroc.pl, under under calculational Grant No. 18.

Appendix A. Supplementary material

CCDC 868406 contains the supplementary crystallographic data for C30H31N9O4ClRe. These data can be obtained free of charge via http://www.ccdc.cam.ac.uk/conts/retrieving.html; or from the Cambridge Crystallographic Data Center, 12 Union Road, Cambridge CB21EZ, UK; fax: +44 1223 336 033; or e-mail: deposit@ccdc.cam.ac.uk.

References

[1] U. Abram, R. Alberto, J. Braz. Chem. Soc. 17 (2006) 1486.
[2] P. Blower, Dalton Trans. (2006) 1705.
[3] Contrast agents III: Radiopharmaceuticals – from diagnostics to therapeutics. Springer, Berlin, Heidelberg, New York, 2005, p. 1.
[4] G.M. Lobmaier, G.D. Frey, D.E. Dewhurst, E. Herdtweck, W.A. Herrmann, Organometallics 26 (2007) 6290.
[5] A. Schröckeneder, P. Traar, G. Raber, J. Baumgartner, F. Belaj, N.C. Mösch-Zanetti, Inorg. Chem. 48 (2009) 11608.
[6] P. Traar, J.A. Schachner, L. Steiner, A. Sachse, M. Volpe, N.C. Mosch-Zanetti, Inorg. Chem. 50 (2011) 1983.
[7] J. Arias, C.R. Newlands, M.M. Abu-Omar, Inorg. Chem. 40 (2001) 2185.
[8] M.M. Abu-Omar, Chem. Commun. (2003) 2102.
[9] L.D. McPherson, M. Drees, S.I. Khan, T. Strassner, M.M. Abu-Omar, Inorg. Chem. 43 (2004) 4036.
[10] F.E. Kühn, A. Scherbaum, W.A. Herrmann, J. Organomet. Chem. 689 (2004) 4149.
[11] D.W. Pipes, T.J. Meyer, J. Am. Chem. Soc. 107 (1985) 7201.
[12] J.R. Winkler, H.B. Gray, J. Am. Chem. Soc. 105 (1983) 1373.
[13] D.W. Pipes, T.J. Meyer, Inorg. Chem. 25 (1986) 3256.
[14] H.H. Thorp, J. Van Houten, H.B. Gray, Inorg. Chem. 28 (1989) 889.
[15] V.W. Yam, K. Tam, M. Cheng, S. Peng, Y. Wang, J. Chem. Soc., Dalton Trans. (1992) 1717.
[16] M.H. Fischer, A. Lusi, J. Med. Chem. 15 (1972) 982.
[17] C. Sabalayrolles, G.H. Gros, J.C. Milhavet, E. Rechenq, J.P. Chapat, M. Boucard, J.H. McNeill, J. Med. Chem. 27 (1984) 206.
[18] J.J. Kaminski, B. Wallmark, C. Briving, B.M. Anderson, J. Med. Chem. 34 (1991) 533.
[19] J.S. Gancheff, P.A. Denis, F.E. Hahn, J. Mol. Struct.: THEOCHEM 941 (2010) 1.
[20] J.S. Gancheff, P.A. Denis, F.E. Hahn, Spectrochimica Acta A: Mol. Biomol. Spectroscopy 76 (2010) 348.
[21] M.S. Ram, J.T. Hupp, Inorg. Chem. 30 (1991) 130.
[22] A. Canlier, T. Kawasaki, S. Chowdhury, Y. Ikeda, Inorg. Chim. Acta 363 (2010) 1.
[23] Oxford Diffraction, CrysAlis PRO, Oxford Diffraction Ltd., Yarnton, England, 2011.
[24] G.M. Sheldrick, SHELXS-97. Program for Crystal Structure Resolution, Univ. of Göttingen, Göttingen, Germany, 1997.
[25] G.M. Sheldrick, SHELXL-97. Program for Crystal Structures Analysis, Univ. of Gottingen, Göttingen, Germany, 1997.
[26] M.J. Frisch, G.W. Trucks, H.B. Schlegel, G.E. Scuseria, M.A. Robb, J.R. Cheeseman, G. Scalmani, V. Barone, B. Mennucci, G.A. Petersson, H. Nakatsuji, M. Caricato, X. Li, H.P. Hratchian, A.F. Izmaylov, J. Bloino, G. Zheng, J.L. Sonnenberg, M. Hada, M. Ehara, K. Toyota, R. Fukuda, J. Hasegawa, M. Ishida, T. Nakajima, Y. Honda, O. Kitao, H. Nakai, T. Vreven, J.A. Montgomery, J.E. Peralta, F. Ogliaro, M. Bearpark, J.J. Heyd, E. Brothers, K.N. Kudin, V.N. Staroverov, R. Kobayashi, J. Normand, K. Raghavachari, A. Rendell, J.C. Burant, S.S. Iyengar, J. Tomasi, M. Cossi, N. Rega, J.M. Millam, M. Klene, J.E. Knox, J.B. Cross, V. Bakken, C. Adamo, J. Jaramillo, R. Gomperts, R.E. Stratmann, O. Yazyev, A.J. Austin, R. Cammi, C. Pomelli, J.W. Ochterski, R.L. Martin, K. Morokuma, V.G. Zakrzewski, G.A. Voth, P. Salvador, J.J. Dannenberg, S. Dapprich, A.D. Daniels, O. Farkas, J.B. Foresman, J.V. Ortiz, J. Cioslowski and D.J. Fox, Gaussian 09, Revision A.1, Gaussian, Inc., Wallingford CT (2009).
[27] P.J. Hay, W.R. Wadt, J. Chem. Phys. 82 (1985) 299.
[28] K. Eichkorn, F. Weigend, O. Treutler, R. Ahlrichs, Theor. Chem. Acc. 97 (1997) 119.
[29] P.M.W. Gill, B.G. Johnson, J.A. Pople, M.J. Frisch, Chem. Phys. Lett. 197 (1992) 499.
[30] M.E. Casida, in: J.M. Seminario (Ed.), Recent Developments and Applications in Modern Density Functional Theory, Theoretical and Computational Chemistry, vol. 4, Elsevier, Amsterdam, 1996.
[31] B. Jezowska-Trzebiatowska, J. Hanuza, M. Baluka, Spectrochim. Acta 27A (1971) 1753.
[32] A.M. Lebuis, J.M.C. Young, A.L. Beauchamp, Can. J. Chem. 71 (1993) 2070.
[33] S. Belanger, A.L. Beauchamp, Inorg. Chem. 35 (1996) 7836.
[34] A.M. Lebuis, A.L. Beauchamp, Can. J. Chem. 71 (1993) 2060.
[35] B.W. Tsang, J. Reibenspies, A.E. Martell, Inorg. Chem. 32 (1993) 988.
[36] G.A. Jeffrey, W. Saenger, Hydrogen Bonding in Biological Structures, Springer, Verlag, 1994.
[37] G.R. Desiraju, T. Steiner, The Weak Hydrogen Bond in Structural Chemistry and Biology, Oxford University Press, 1999.
[38] C. Kremer, E. Kremer, S. Dominguez, E. Chinea, A. Mederos, A. Castineiras, Polyhedron 15 (1996) 4341.
[39] J.M. Mayer, Inorg. Chem. 27 (1988) 3899.
[40] J.W. Johnson, J.F. Brody, G.B. Ansell, S. Zentz, Inorg. Chem. 23 (1984) 2415.
[41] A. Kochel, Acta Crystallogr., Sect. E: Struct. Rep. Online 62 (2006) m1740.
[42] C.J.L. Lock, G. Turner, Acta Crystallogr., Sect. B: Struct. Crystallogr. Cryst. Chem. 34 (1978) 923.
[43] M.S. Ram, L.M. Jones, H.J. Ward, Y.H. Wong, C.S. Johnson, P. Subramanian, J.T. Hupp, Inorg. Chem. 30 (1991) 2928.
[44] R.S. Nicholson, Anal. Chem. 37 (1965) 1351.
[45] J. Heinze, Angew. Chem., Int. Ed. Engl. 23 (1984) 831.
[46] A.J. Bard, L.R. Faulkner, Electrochemical Methods Fundamentals and Applications, John Wiley & Sons, New York, Chichester, Brisbane, Toronto, 1980.
[47] H. Matsuda, Y. Ayabe, Z. Elektrochem. 59 (1955) 494.

EurJIC European Journal of Inorganic Chemistry

DOI: 10.1002/ejic.201200277

Oxidorhenium(V) Complexes with Phenolate- and Carboxylate-Based Ligands: Structure and Catalytic Epoxidation

Barbara Machura,*[a] Mariusz Wolff,[a] Dominik Tabak,[b] Jörg A. Schachner,[c] and Nadia C. Mösch-Zanetti[c]

Keywords: Rhenium / Phenolate ligands / Carboxylate ligands / Epoxidation

Several oxidorhenium(V) complexes with phenolate- and carboxylate-based ligands were synthesized: $[ReOCl(hpbi)_2]\cdot THF$, $[ReOCl(hmpbta)_2]$, $[ReOBr(hmpbta)_2]$, $[ReOCl(hpbo)_2]$, $[ReOCl(hpbt)_2]\cdot 2MeCN$, $[ReO(OMe)(quin)_2]$, $[ReO(OMe)(pic)_2]$, $[ReO(OMe)(2,5\text{-dipic})_2]\cdot C_5H_5N$, $[ReOCl(pic)_2]$, and $[ReOCl(3\text{-ind})_2]$ [in which Hhpbi = 2-(2-hydroxyphenyl)-1*H*-benzimidazole, Hhmpbta = 2-(2-hydroxy-5-methylphenyl)-benzotriazole, Hhpbo = 2-(2-hydroxyphenyl)-2-benzoxazole, Hhpbt = 2-(2-hydroxyphenyl)benzothiazole, Hquin = quinaldic acid, picH = picolinic acid, 2,5-dipicH = 2,5-pyridinedicarboxylic acid, and 3-indH = indazole-3-carboxylic acid]. The compounds were characterized by spectroscopic methods and single-crystal X-ray diffraction analysis. Interestingly, the complex $[ReO(OMe)(quin)_2]$ is a rare *trans*-N,N and *trans*-O,O isomer of $[ReOX(N\text{–}O)_2]$ with two chelating quinoline-2-carboxylate ligands in the equatorial plane and a linear axial [O=Re–OMe] unit. The other disubstituted compounds were found to be the most common *cis*-N,N structure of $[ReOX(N\text{-}O)_2]$ with the oxygen atom of one of the chelating ligands in a *trans* position to the oxido ligand. All the complexes were tested in the epoxidation of cyclooctene with *tert*-butyl hydroperoxide (3 equiv.). The lowest conversion of only 3% has been confirmed for $[ReOCl(hpbi)_2]$. All other complexes reached yields of cyclooctane oxide between 58 and 75%.

Introduction

The widespread contemporary interest in the coordination chemistry of rhenium arises mainly from the introduction of β^--emitting isotopes ^{188}Re and ^{186}Re in radiotherapy and its similarity with technetium, the metastable γ-emitting isotope ^{99m}Tc, which plays an important role in diagnostic nuclear medicine. Thus, there is still a need for basic knowledge about the structural and spectroscopic properties, redox activities, and mechanism of ligand-substitution reactions to develop new and improved Re radiopharmaceuticals.[1–4]

Another area of growing interest for rhenium–oxido compounds is their application as catalysts, particularly in oxidation and oxygen-atom-transfer (OAT) reactions. This field is clearly highlighted by methyltrioxidorhenium(VII), one of the most versatile and highly efficient transition-metal catalysts known to date.[5–7]

Oxidorhenium(V) compounds have been far less explored, although straightforward preparation and high stability towards hydrolysis make them attractive options as catalysts. For this reason, some effort has been recently devoted to the investigation of Re^V complexes as catalysts in epoxidation reactions of olefins. Detailed studies have been performed for monosubstituded or disubstituted complexes of the type $[ReOX_2L(PPh_3)]$ and $[ReOXL_2]$ with β-ketiminate ligands, pyrazole phenolate and naphtholate ligands, acetylacetone-derived Schiff bases, and oxazolinylmethoxido ligands, as well as for $[ReOX_2L]$ and [ReOXL] with tridentate or tetradentate Schiff bases or pyridazine phenolate ligands. However, only limited success has been attained as the reported Re^V complexes showed lower activity or productivity than rhenium(VII) systems.[8–16] Therefore, there is a need for further investigations on furnishing novel rhenium(V) complexes with ligands that exhibit higher stability towards oxidation.

However, oxidorhenium(V) complexes were found to be highly successful in OAT reactions. Espenson and co-workers reported some rhenium(V) complexes to be efficient catalysts of oxygen-atom transfer from pyridine *N*-oxide to phosphanes.[17,18] Abu-Omar and co-workers developed a new class of molecular rhenium(V) oxotransferases that incorporate oxazoline-derivatized phenolates, which efficiently catalyze the reduction of perchlorate to chloride ions, one of the most challenging reactions due to its kinetic hindrance and environmental importance.[19–21]

The recent success of the rhenium(V) complexes and the need for novel catalytically active species prompted us to

[a] Department of Crystallography, Institute of Chemistry, University of Silesia,
9th Szkolna St., 40-006 Katowice, Poland
E-mail: basia@ich.us.edu.pl
[b] Department of Organic Chemistry, Institute of Chemistry, University of Silesia,
9th Szkolna St., 40-006 Katowice, Poland
[c] Institute of Chemistry, Karl-Franzens-University Graz,
Stremayrgasse 16, 8010 Graz, Austria
E-mail: nadia.moesch@uni-graz.at

synthesize a set of oxo compounds of the general formula $[ReOX(N–O)_2]$ and investigate their potential as catalysts in oxidation reactions. Depending on the type of chelating ligand, compounds investigated herein can be divided into two groups: those that incorporate ligands structurally related to oxazoline-derivatized phenolates investigated by Abu-Omar et al.,[19–21] namely, 2-(2-hydroxyphenyl)-1*H*-benzimidazole (Hhpbi), 2-(2-hydroxy-5-methylphenyl)benzotriazole (Hhmpbta), 2-(2-hydroxyphenyl)-2-benzoxazole (Hhpbo), and 2-(2-hydroxyphenyl)benzothiazole (Hhpbt), and those that include bidentate ligands based on an aromatic heterocycle and a carboxylic acid as second and charge-neutralizing coordinating functionality [quinaldic acid (quinH), picolinic acid (picH), 2,5-pyridinedicarboxylic acid (2,5-dipicH), and indazole-3-carboxylic acid (3-indH)]. Phenolate- and carboxylate-based ligands employed in this study are shown in Scheme 1. The use of various chelating ligands that incorporate different heterocycle rings and O-donor groups allows us to expect unusual electronic influences on the coordinating capability as well as on the catalytic activity.

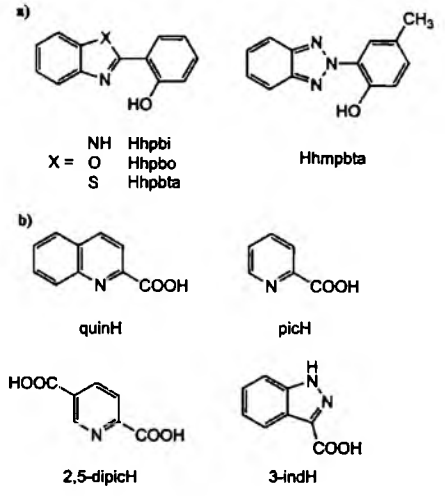

Scheme 1. (a) Phenolate- and (b) carboxylate-based ligands employed in this study.

Results and Discussion

Synthesis

Phenolate-disubstituted oxidorhenium(V) complexes $[ReOCl(N–O)_2]$ (**1–4**) were obtained by treatment of $[ReOCl_3(OPPh_3)(SMe_2)]$ with the corresponding ligand (2 equiv.) 2-(2-hydroxyphenyl)-1*H*-benzimidazole (Hhpbi), 2-(2-hydroxy-5-methylphenyl)benzotriazole (Hhmpbta), 2-(2-hydroxyphenyl)-2-benzoxazole (Hhpbo), and 2-(2-hydroxyphenyl)benzothiazole (Hhpbt) (Scheme 2).

To investigate the effect of the halide ion, the reaction of $[ReOBr_3(OPPh_3)(SMe_2)]$ with 2-(2-hydroxy-5-methylphenyl)benzotriazole was also examined and $[ReOBr(hmpbta)_2]$ (**5**) was isolated.

As expected, the metal precursors $[ReOX_3(OPPh_3)(SMe_2)]$ turned out to be an excellent starting material for preparation of these complexes. The yields obtained were comparable with those reported for alternative metal precursor $[NBu_4][ReOX_4]$[22] and significantly higher than $[ReOX_3(PPh_3)_2]$, which gave only minor amounts of $[ReOX_2(N–O)_2]$.[23] Complexes **1–5** show high stability toward air and moisture both in the solid state and in solution for several months at ambient temperature. They exhibit moderate solubility in strong polar solvents such as thf, acetonitrile, acetone, chloroform, methanol, and ethanol, and are insoluble in medium polar and apolar solvents.

The ^1H NMR spectra of these complexes confirmed the occurrence of only one isomer in solution, which was shown to contain nonequivalent N–O ligands. Particularly characteristic are protons of the N–H group of the imidazole ring in **1** and methyl groups attached to the phenolate ring in **2** and **5**, which gave nonequivalent chemical shifts (δ = 13.80 and 13.64 ppm for **1**, δ = 2.58 and 2.05 ppm for **2**, and δ = 2.58 and 2.04 ppm for **5**).

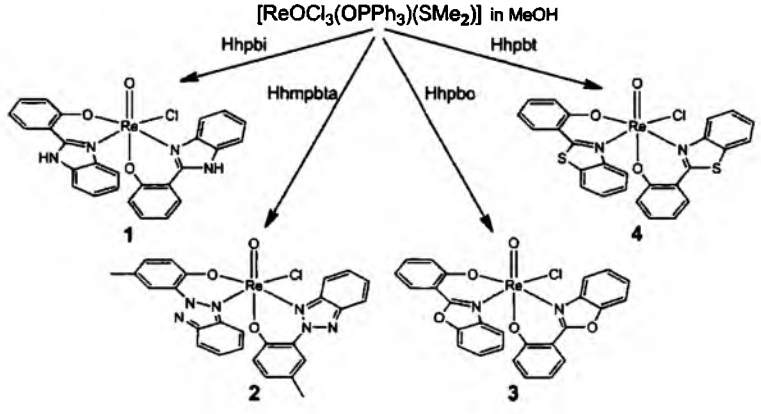

Scheme 2.

The IR spectra were characterized by strong absorptions at approximately 960 cm^{-1} that were assigned to the Re=O stretching frequencies. This value is in the range typical of neutral six-coordinate mono-oxidorhenium(V) complexes with an anionic phenolate oxygen coordinated *trans* to the oxo group.[13,14,24] The absorptions in the region 1630–1520 cm^{-1} were assigned to the ν(C=N) modes of the chelating ligands.

To synthesize carboxylate-disubstituted oxidorhenium(V) complexes, two metal precursors $[ReOCl_3(OPPh_3)(SMe_2)]$ and $[ReO_2(py)_4]Cl$ were used. The better results were achieved in the case of synthetic strategy based on the reaction of $[ReO_2(py)_4]Cl$ with carboxylic acids, which yielded the compounds $[ReO(OMe)(N–O)_2]$ (**6–8**; Scheme 3).

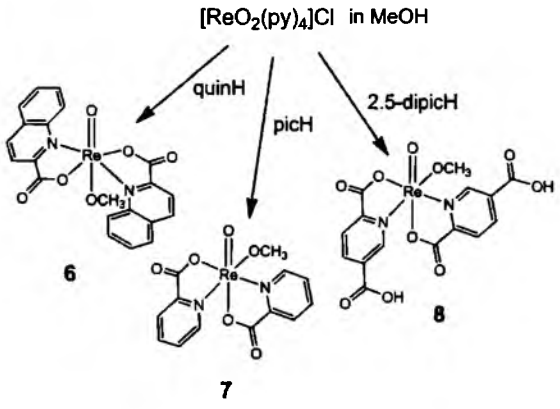

Scheme 3.

Apart from its high yield, this procedure has another important advantage: the desired complexes precipitate directly from the reaction mixture under prolonged reflux conditions and are easily isolated by simple filtration. Treatment of the alternative metal precursor $[ReOCl_3(OPPh_3)(SMe_2)]$ with the corresponding carboxylic acid (2 equiv.) in MeOH heated at reflux led to the disubstituted complexes $[ReOCl(N–O)_2]$ (**9**, **10**; Scheme 4), but the yields obtained were lower than $[ReO_2(py)_4]Cl$.

Most interestingly, the choice of metal precursor turned out to be crucial in the synthesis of the carboxylate-disubstituted rhenium(V) complexes. Attempts to synthesize the disubstituted rhenium complex of indazole-3-carboxylate ligand by employing $[ReO_2(py)_4]Cl$ failed. They yielded an insoluble pink powder, which prevented its further characterization. The desired complex $[ReOCl(3\text{-ind})_2]$ (**10**) was obtained by using $[ReOCl_3(OPPh_3)(SMe_2)]$.

In contrast, treatment of $[ReO_2(py)_4]Cl$ with 2,5-pyrazinedicarboxylic acid led to $[ReO(OMe)(2,5\text{-dipic})_2]$, whereas a synthetic procedure with $[ReOCl_3(OPPh_3)(SMe_2)]$ resulted in the formation of an unidentified reaction mixture as revealed by ^1H NMR spectroscopy. Pyridine-2-carboxylic and quinoline-2-carboxylic acids reacted with both metal precursors to give disubstituted Re^V–oxido complexes $[ReO(OMe)(N–O)_2]$ or $[ReOCl(N–O)_2]$.

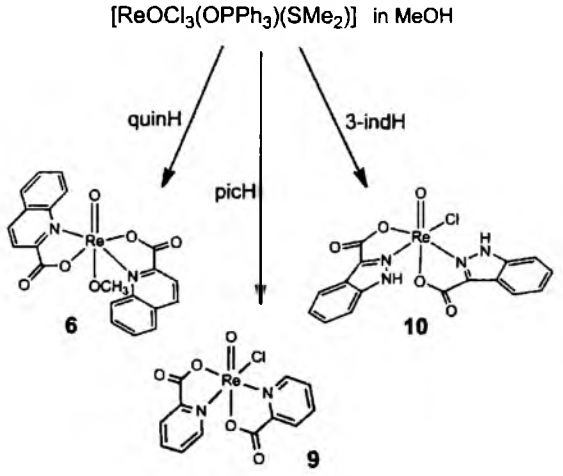

Scheme 4.

All carboxylate–rhenium(V)–oxido complexes **6–10** show high stability toward air and moisture both in the solid state and in solution, but compounds **7**, **8**, and **10** exhibit limited solubility in most common solvents, which prevented the recording of their ^{13}C NMR spectra.

The ^1H NMR spectrum of **6** revealed only one set of ligand resonances, thus indicating a higher symmetric species in contrast to complexes **7–10** with two sets of signals in the ^1H NMR spectra for the attached ligands.

In principle, there are several different possible orientations for the ligands in complexes of general formula $[ReOX(N–O)_2]$, as shown in Scheme 5.

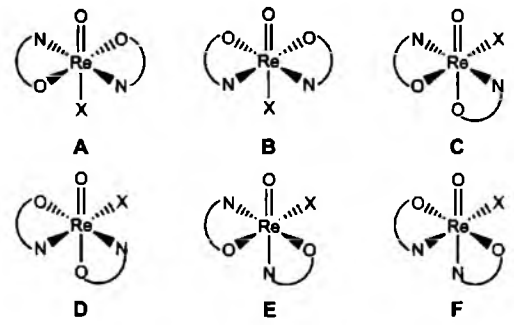

Scheme 5. Possible ligand orientations for $[ReOX(N–O)_2]$ complexes.

Generally, they can be divided into two subgroups: (i) with the X ligand coordinated *trans* to the Re=O group (types A and B), and (ii) with the X ligand *cis* to the Re=O moiety (types C–F). Moreover, five of the possible constitution isomers (types B–F) exist as a pair of enantiomers.

Unambiguous determination of the ligand arrangement around the metal center in **6–10** was possible by single-crystal X-ray diffraction, and structural studies are in good agreement with the NMR spectroscopic results. Complexes **7–10** adopt the most common structure of type D and dis-

play two sets of ^1H NMR spectroscopic signals for the attached ligands, which is in accordance with their nonequivalent coordination geometry. The ligands of **6** are arranged around the Re center as in isomer **A**, and two equivalent N–O ligands revealed only one set of ligand resonances in the NMR spectra.

For each carboxylato-rhenium(V) complex, IR spectroscopy confirmed the presence of an Re=O fragment. The strong Re=O stretching mode was found at 955 cm $^{-1}$ for **6** and approximately 985 cm^{-1} for **7–10**. The bathochromic shift of this vibration in complex **6**, which incorporates a *trans*-$[ReO(OMe)]^{2+}$ unit, is normal and results from the competition of the methoxide group for π bonding with the $d\pi$ orbitals of the metal, thereby leading to the weakness of the Re=O bond.[25] A higher wavenumber of **7–10** indicates that the Re–carboxylate bond *trans* to the oxido ligand is not very strong and does not compete effectively for the d_{Re} orbitals. Coordination of the carboxylate group was confirmed by absorptions in the regions 1730–1660 and 1330–1280 cm^{-1}, which are assigned to the asymmetric and symmetric stretching vibration of the COO^- group, respectively.

Molecular Structures of the Complexes $[ReOX(N–O)_2]$

The molecular structures of compounds **1** and **3–10** were determined by single-crystal X-ray diffraction analysis. The perspective molecular views of the complexes are shown in Figures 1, 2, and 3. Crystallographic data are presented in Tables 1 and 2, and selected bond lengths and angles are given in Tables 3, 4, and 5. The molecular structure of **2** was discussed in our previous paper.[23]

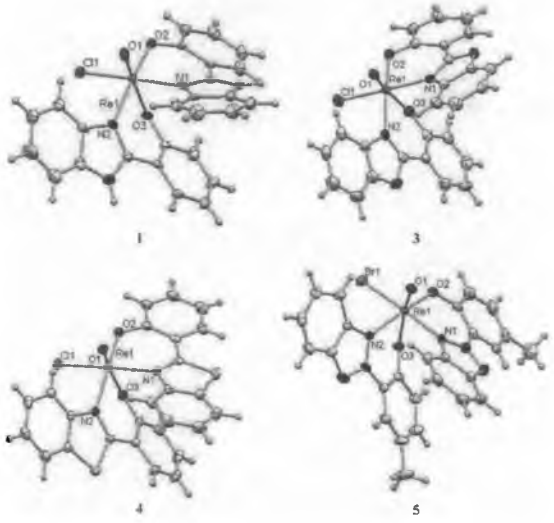

Figure 1. Molecular views of phenolate disubstituted compounds $[ReOCl(N–O)_2]$ with selected atom numbering.

All examined complexes show a six-coordinate rhenium atom with distorted octahedral geometries. Each phenolate or carboxylate ligand chelates to the oxidorhenium core through N and O atoms. In complex **6**, two quinoline-2-

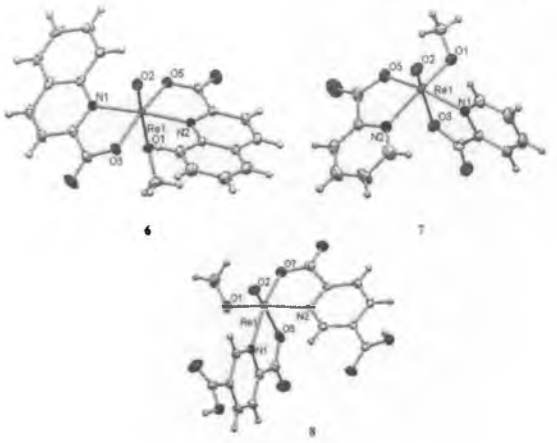

Figure 2. Molecular views of carboxylate disubstituted compounds $[ReO(OMe)(N–O)_2]$ with selected atom numbering.

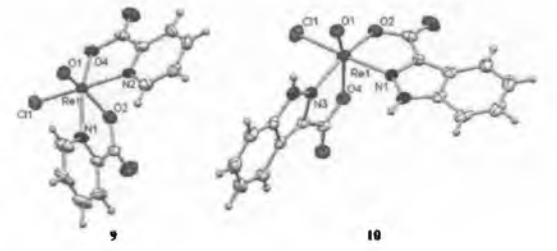

Figure 3. Molecular views of carboxylate disubstituted compounds $[ReOCl(N–O)_2]$ with selected atom numbering.

carboxylate ligands are situated in an equatorial plane with a *trans*-N,N *trans*-O,O arrangement, and the coordination site *trans* to the oxido ligand is occupied by the methoxy group. Such ligand arrangement around the central ion makes complex **6** a very rare example of $[ReOX(N–O)_2]$ complexes.

A related $[ReOCl(N–O)_2]$ compound with two symmetrically coordinated salen ligands in the equatorial plane and a linear [O=Re–X] moiety was isolated by Herrmann and co-workers in 2007 as a side product in the reaction of $[NBu_4][ReOCl_4]$ with the bis(alkyl/aryl)-2-pyridylalcoholate ligand.[8] A *trans* O=Re–X conformation has also been confirmed in a few other $[ReOXL_2]$ compounds, namely, $[ReOCl(o\text{-}C_6O_2Cl_4)(Ph_2PCH_2CH_2PPh_2)]$,[25] $[ReOCl(NH_2\text{-}CH_2CH_2S)_2]$,[26] $[ReOCl\{NH(o\text{-}C_6H_4)SCH_3\}_2]$,[27] and $[ReOCl(OPhsal)\{P(CH_3)_2Ph\}]$ [OPhsal = *N*-(2-oxidophenyl)salicylideneiminate].[28]

Complexes **1–5** and **7–10** were found to be the *cis*-N,N isomer of type D (Scheme 1). The equatorial plane of these compounds consists of the two nitrogen atoms, an oxygen atom from the chelating ligand, and the halide atom or methoxy group. The oxido ligand along the axial direction is *trans* to the phenol or carboxylic oxygen atom. This is due to a strong *trans* influence of the oxido group, which forces the harder oxygen atom of the N–O ligand into a *trans* position. Such stereochemistry is well documented in

Table 1. Crystal data and structure refinement for complexes **1**, **3**, **4**, and **5**.

	1	**3**	**4**	**5**
Empirical formula	$C_{30}H_{26}ClN_4O_4Re$	$C_{26}H_{16}ClN_2O_5Re$	$C_{30}H_{22}ClN_4O_4S_2Re$	$C_{26}H_{20}BrN_6O_3Re$
Formula weight	728.20	658.06	772.29	730.59
T [K]	293.0(2)	293.0(2)	293.0(2)	293.0(2)
Crystal system	monoclinic	monoclinic	monoclinic	orthorhombic
Space group	$P2_1/n$	$P2_1/n$	$P2_1/n$	$Pbca$
a [Å]	12.9021(10)	9.2556(13)	13.3205(4)	15.8338(6)
b [Å]	13.6136(8)	14.5250(3)	15.9693(5)	15.8517(8)
c [Å]	15.9407(16)	17.5280(2)	13.4978(4)	19.9989(9)
α [°]	90	90	90	90
β [°]	110.716(10)	104.320(12)	94.374(3)	90
γ [°]	90	90	90	90
V [Å^3]	2618.9(4)	2283.2(3)	2862.88(15)	5019.6(4)
Z	4	4	4	8
$\rho_{calcd.}$ [g cm^{-3}]	1.847	1.914	1.792	1.934
μ [mm^{-1}]	4.788	5.482	4.524	6.475
F(000)	1432	1272	1512	2816
Crystal size [mm]	0.851 × 0.203 × 0.011	0.158 × 0.054 × 0.028	1.318 × 0.504 × 0.424	0.346 × 0.092 × 0.086
θ range for data collection [°]	3.38 to 25.00	3.61 to 25.00	3.72 to 25.00	3.52 to 25.00
Reflections collected	23034	9935	14038	22712
Independent reflections	4568 (R_{int} = 0.0652)	3997 (R_{int} = 0.0593)	4980 (R_{int} = 0.0268)	4403 (R_{int} = 0.0437)
Completeness to 2θ = 25° [%]	99.1	99.7	98.8	99.7
Min. and max. transmission	0.511 to 1.000	0.505 to 1.000	0.362 to 1.000	0.475 to 1.000
Data / restraints / parameters	4568 / 0 / 361	3997 / 0 / 316	4980 / 0 / 372	4403 / 0 / 336
Goodness-of-fit on F_2	1.138	1.010	0.952	0.975
Final R indices [$I > 2\sigma(I)$]	R_1 = 0.0343	R_1 = 0.0541	R_1 = 0.0221	R_1 = 0.0207
	wR_2 = 0.1083	wR_2 = 0.1313	wR_2 = 0.0505	wR_2 = 0.0555
R indices (all data)	R_1 = 0.0498	R_1 = 0.0738	R_1 = 0.0331	R_1 = 0.0339
	wR_2 = 0.1507	wR_2 = 0.1422	wR_2 = 0.0521	wR_2 = 0.0572
Largest diff. peak / hole [e Å^{-3}]	1.568 and –1.650	3.835 and –1.976	0.744 and –0.809	0.700 and –0.539

Table 2. Crystal data and structure refinement for complexes **6**, **7**, **8**, **9**, and **10**.

	6	**7**	**8**	**9**	**10**
Empirical formula	$C_{21}H_{15}N_2O_6Re$	$C_{13}H_{11}N_2O_6Re$	$C_{20}H_{16}N_3O_{10}Re$	$C_{12}H_8ClN_2O_5Re$	$C_{17}H_{14}ClN_4O_6Re$
Formula weight	577.55	477.44	644.56	481.85	591.97
T [K]	293.0(2)	293.0(2)	293(2)	293.0(2)	293.0(2)
Crystal system	triclinic	monoclinic	monoclinic	monoclinic	triclinic
Space group	$P\bar{1}$	$P2_1/c$	$P2_1/n$	Cc	$P\bar{1}$
a [Å]	7.6615(15)	14.3597(6)	13.1896(5)	7.7249(3)	7.2256(7)
b [Å]	7.9952(16)	7.5279(2)	7.2002(2)	12.0684(5)	8.6703(8)
c [Å]	17.5095(4)	14.3971(6)	22.2021(8)	15.1121(6)	16.4617(16)
α [°]	83.332(4)	90	90	90	94.924(8)
β [°]	84.009(4)	113.328(5)	99.129(3)	99.368(4)	93.370(8)
γ [°]	61.519(6)	90	90	90	110.372(9)
V [Å^3]	934.89(8)	1429.08(9)	2081.78(12)	1390.07(10)	958.87(16)
Z	2	4	4	4	2
$\rho_{calcd.}$ [g cm^{-3}]	2.052	2.219	2.057	2.302	2.050
μ [mm^{-1}]	6.543	8.534	5.903	8.956	6.519
F(000)	556	904	1248	904	568
Crystal size [mm]	0.099 × 0.098 × 0.056	0.402 × 0.279 × 0.031	0.218 × 0.132 × 0.065	0.162 × 0.110 × 0.108	0.145 × 0.122 × 0.014
θ range for data collection [°]	3.41 to 25.00	3.39 to 25.00	3.38 to 25.00	3.38 to 25.00	3.73 to 25.00
Reflections collected	17400	25290	14891	10106	17532
Independent reflections	3279 (R_{int} = 0.0582)	2502 (R_{int} = 0.0878)	3668 (R_{int} = 0.0353)	2438 (R_{int} = 0.0359)	3374 (R_{int} = 0.0552)
Completeness to 2θ = 25° [%]	99.7	99.7	99.8	99.8	99.6
Min. and max. transmission	0.462 to 1.000	0.108 to 1.000	0.545 to 1.000	0.481 to 1.000	0.397 to 1.000
Data / restraints / parameters	3279 / 0 / 266	2502 / 0 / 200	3668 / 0 / 308	2438 / 2 / 190	3374 / 0 / 264
Goodness-of-fit on F_2	1.094	1.100	1.313	1.027	1.057
Final R indices [$I > 2\sigma(I)$]	R_1 = 0.0225	R_1 = 0.0334	R_1 = 0.0342	R_1 = 0.0201	R_1 = 0.0329
	wR_2 = 0.0525	wR_2 = 0.0881	wR_2 = 0.0824	wR_2 = 0.0384	wR_2 = 0.0826
R indices (all data)	R_1 = 0.0261	R_1 = 0.0397	R_1 = 0.0387	R_1 = 0.0221	R_1 = 0.0389
	wR_2 = 0.0537	wR_2 = 0.0918	wR_2 = 0.0836	wR_2 = 0.0390	wR_2 = 0.0843
Largest diff. peak / hole [e Å^{-3}]	0.548 and –1.216	0.916 and –1.295	1.129 and –0.905	0.624 and –0.413	2.259 and –0.794

EurJIC European Journal of Inorganic Chemistry

Table 3. Selected bond lengths [Å] and angles [°] of compounds **1**, **3**, **4**, and **5**.

	1	3	4	5
Re1–O1	1.682(6)	1.654(7)	1.673(2)	1.685(3)
Re1–O2	1.982(6)	1.977(6)	1.966(2)	1.968(3)
Re1–O3	2.019(6)	1.986(6)	1.984(2)	1.976(2)
Re1–N1	2.083(6)	2.111(7)	2.133(3)	2.112(3)
Re1–N2	2.109(7)	2.127(8)	2.140(3)	2.134(3)
Re1–X1	2.359(2)	2.353(3)	2.3633(9)	2.4856(5)
O1–Re1–O2	103.0(3)	105.2(3)	103.69(11)	102.71(13)
O1–Re1–O3	166.0(3)	165.6(3)	165.33(11)	162.33(12)
O2–Re1–O3	86.4(2)	82.7(3)	85.40(10)	88.49(11)
O1–Re1–N1	88.0(3)	85.1(3)	87.01(11)	86.64(13)
O2–Re1–N1	87.8(2)	88.3(3)	90.25(10)	87.63(12)
O3–Re1–N1	82.0(2)	83.0(3)	81.39(10)	80.14(12)
O1–Re1–N2	92.1(3)	91.9(3)	91.04(11)	89.73(13)
O2–Re1–N2	164.7(3)	162.8(3)	164.66(10)	167.41(12)
O3–Re1–N2	79.0(2)	81.2(3)	81.07(10)	79.90(11)
N1–Re1–N2	94.6(2)	95.5(3)	94.81(10)	95.12(12)
O1–Re1–X1	101.9(2)	99.7(2)	100.94(9)	102.10(10)
O2–Re1–X1	85.27(17)	87.27(19)	85.74(8)	87.57(9)
O3–Re1–X1	89.04(17)	92.7(2)	91.09(7)	91.86(8)
N1–Re1–X1	168.98(19)	174.2(2)	171.75(7)	170.77(8)
N2–Re1–X1	89.94(19)	87.7(2)	87.32(7)	87.93(9)

Table 4. Selected bond lengths [Å] and angles [°] of compounds **6**, **7**, and **8**.

	6	7	8
Re1–O2	1.696(3)	1.671(5)	1.683(5)
Re1–O1	1.893(3)	1.937(5)	1.927(5)
Re1–O5	2.037(3)	1.995(5)	–
Re1–O7	–	–	2.006(5)
Re1–O3	2.068(3)	2.081(4)	2.075(5)
Re1–N1	2.131(3)	2.121(5)	2.098(6)
Re1–N2	2.138(3)	2.132(6)	2.139(6)
O1–C1	1.388(5)	1.419(9)	1.409(10)
O2–Re1–O1	170.59(13)	104.4(3)	102.9(3)
O2–Re1–O5	99.94(14)	109.7(2)	–
O1–Re1–O5	86.15(13)	89.9(2)	–
O2–Re1–O7	–	–	108.6(3)
O1–Re1–O7	–	–	93.7(2)
O2–Re1–O3	91.38(14)	159.0(2)	160.9(2)
O1–Re1–O3	82.63(13)	86.1(2)	86.4(2)
O5–Re1–O3	168.69(12)	88.1(2)	–
O5–Re1–N1	100.64(12)	162.2(2)	–
O2–Re1–N1	95.86(14)	88.1(2)	89.6(3)
O1–Re1–N1	90.00(13)	85.8(2)	84.7(2)
O7–Re1–O3	–	–	87.1(2)
O7–Re1–N1	–	–	161.6(2)
O3–Re1–N1	77.96(12)	74.3(2)	74.5(2)
O2–Re1–N2	90.64(13)	94.7(3)	93.1(2)
O1–Re1–N2	83.51(12)	160.1(2)	163.8(2)
O5–Re1–N2	78.52(12)	78.5(2)	–
O7–Re1–N2	–	–	78.3(2)
O3–Re1–N2	101.57(12)	77.5(2)	79.1(2)
N1–Re1–N2	173.49(12)	100.3(2)	98.4(2)
C1–O1–Re1	141.2(3)	122.1(5)	123.0(6)

Table 5. Selected bond lengths [Å] and angles [°] of compounds **9** and **10**.

	9	10
Re1–O1	1.674(4)	1.681(4)
Re1–O4	1.986(6)	1.999(5)
Re1–O2	2.007(5)	2.059(4)
Re1–N2	2.092(5)	–
Re1–N3	–	2.076(5)
Re1–N1	2.120(7)	2.107(5)
Re1–Cl1	2.3482(18)	2.3711(18)
O1–Re1–O4	109.8(2)	109.9(2)
O1–Re1–O2	162.2(2)	159.8(2)
O4–Re1–O2	85.6(2)	89.84(18)
O1–Re1–N2	91.4(2)	–
O4–Re1–N2	79.93(19)	–
O2–Re1–N2	82.5(2)	–
O1–Re1–N3	–	96.2(2)
O4–Re1–N3	–	78.53(19)
O2–Re1–N3	–	83.44(18)
O1–Re1–N1	89.5(2)	86.7(2)
O4–Re1–N1	160.5(2)	163.26(19)
O2–Re1–N1	74.9(2)	73.42(17)
N2–Re1–N1	97.8(2)	–
N3–Re1–N1	–	99.0(2)
O1–Re1–Cl1	98.97(16)	97.42(17)
O4–Re1–Cl1	90.21(15)	87.74(15)
O2–Re1–Cl1	89.42(14)	87.12(13)
N2–Re1–Cl1	167.66(15)	–
N3–Re1–Cl1	–	163.30(14)
N1–Re1–Cl1	89.03(18)	91.46(15)

the literature and seems to be the most common structure type for $[ReOX(N–O)_2]$ complexes.[12,14,22,23,29] There is no clear explanation for the different ligand orientation of complex **6** relative to compounds **7**–**10**. The studies have shown that even small changes in the steric and electronic properties of the ligand can have a significant impact on the stereochemistry of the resulting compounds.

All compounds give bond lengths for Re=O [1.654(7)–1.996(3) Å; Tables 2, 3, and 4] within the expected range for six-coordinate monooxidorhenium(V) complexes.[8,12–16,22–28] The Re=O distance of **6** [1.696(3) Å] is slightly longer than Re=O bond lengths in **7** [1.671(5) Å] and in **8** [1.683(5) Å]. This elongation of Re=O in **6** is accompanied by a small shortening of the Re–O(methoxy) distance [1.893(3) Å in **6**, 1.937(5) Å in **7**, and 1.927(5) Å in **8**]. It seems to be a consequence of the competition of the methoxide with the oxido group in the interaction with the dπ orbitals of the metal and is a typical feature of complexes that incorporate a linear core $[O=Re–OR]^{2+}$.[29,30] However, the weakening of the Re=O bond in **6** is better illustrated by a significant bathochromic shift for ν(Re=O) in **6** discussed above. In all reported complexes, the O=Re–O_{trans} angles are significantly below the ideal of 180° for an octahedral complex, and the interatomic distances between the rhenium atom and phenolate or carboxylate oxygen atom in a *trans* position to the terminal oxido ligand are longer than the corresponding Re–O bonds in the equatorial plane, which seems to be a typical feature of *cis*-N,N isomers of $[ReOX(N–O)_2]$ of type D.

The nitrogen atoms of **6** are coordinated in a *trans* position to each other with comparable bond lengths of 2.131(3) and 2.138(3) Å. In compounds $[ReOCl(N–O)_2]$, the Re–N bond *trans* to the chloride ion is shorter than the Re–N bond *trans* to the oxygen atom of the chelating ligand. It seems to be due to the stronger π donation of the chloride ion. For all reported complexes the Re–N bonds are significantly longer than the Re–O distances.

Catalytic Epoxidation Experiments

All ten oxidorhenium(V) complexes **1**–**10** were tested in the epoxidation of cyclooctene (cyOct). Epoxidation experiments were done with 1 mol-% of the respective complex at 50 °C in $CHCl_3$ using *tert*-butyl hydrogenperoxide (TBHP; 3 equiv.) for a time between 20–27 h (Scheme 6).

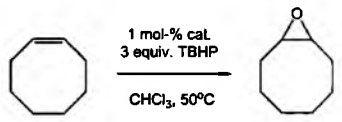

Scheme 6. Epoxidation of cyclooctene.

Out of the 10 complexes, **1**, which is equipped with benzimidazole ligands, showed the lowest conversion of only 3%, respectively, with a very long induction period (>3 h). All other complexes **2**–**10** reached yields of cyclooctane oxide (cyOxid) between 58 and 75% (Table 6).

Table 6. Catalytic performance of complexes **2**–**10** in the epoxidation of cyclooctene.

Cat.	*t* [h]	cyOxid [%]	Selectivity of epoxide [%]	Side product [%]
2	5	61	84	5[a]
	21	50		11[b]
3	0.5	16	97	3[a]
	3	36		
	20	62		
	27	74		
4	1	4	96	4[a]
	3	22		
	7.5	59		
	23	75		
5	1	16	95	5[a]
	4	33		
	24	61		
6	1	33	>99	–
	2.75	56		
	19	69		
	25	68		
7	0.5	4	>99	–
	5	26		
	21	62		
8	3	13	>99	–
	22	55		
9	0.5	4	98	2[a]
	5	21		
	21	58		
10	0.5	22	98	2[a]
	5	41		
	21	59		

[a] Side product: cyclooctane-1,2-diole (cyDiole). [b] Side product: *tert*-butoxycyclooctane (cyO*t*Bu).

The catalytic performances of the oxidorhenium(V) complexes that incorporate phenolate ligands were found to be strongly influenced by the heterocycle ring, most likely because of the different electronic properties. The carboxylate oxidorhenium(V) complexes gave comparable conversion of the alkene into the epoxide with a yield only slightly lower than the complexes that incorporate benzoxazole and the benzothiazole ligand (**3** and **4**), for which the best yield was observed. The highest selectivity (>99%) in catalytic epoxidation experiments was found with **7** and **8**, for which no side products could be detected (below the threshold of the GC–MS integration routine). Slightly higher catalytic performance with regard to substrate conversion was shown by **7** with a yield of cyOxide of 62% after 21 h in comparison to **8** with 55%. Furthermore, with catalyst **8**, an induction period was observed. All other complexes (**2**–**6**, **9**, and **10**) revealed variable amounts of side products (2–15%), usually the ring-opened product by water, cyclooctane-1,2-diole (cyDiole). Only with complex **2**, which contained a benzotriazole ligand, could the formation of an additional side product be observed (11% cyO*t*Bu after 21 h). Its mass spectrum is consistent with *tert*-butoxycyclooctane, presumably formed through a ring-opening by *tert*-butyl alcohol. This is in line with the observed 10% decrease of cyOxide with time (60% after 5 h and 50% after 21 h). In general, all observed yields are in a similar range, thereby impeding a detailed structure/activity correlation. Apparently, the electronic and steric environments imposed by the investigated ligands lead to similar rhenium centers. This is apparent when comparing compounds **7** and **9**, which differ only in one anionic ligand (methoxy versus chloro). However, the two complexes **2** and **6** display a superior initial activity (61% after 5 h for **2** and 56% after 2.75 h for **6**). It is worth noting that **2** is the only compound among the phenoxide group with an additional methyl substituent, and **6** is the only one with a *trans* MeO–Re=O orientation. With the rhenium(V) catalyst, no full conversion has been observed thus far, presumably due to both catalase activity and catalyst deactivation.[8–16] Apparently, the better donor properties of hmpbta in **2** and the *trans* orientation in **6** have a beneficial influence on the catalytic yield. Therefore, future complex design will include *trans*-oriented complexes with ligands that have superior donor properties.

Conclusion

A series of oxidorhenium(V) complexes that incorporate phenolate and carboxylate ligands were synthesized, characterized, and utilized as catalyst in the epoxidation of cyclooctene. The metal precursors $[ReO_2(py)_4]Cl$ turned out to be an excellent starting material for the preparation of $[ReOX(N–O)_2]$ complexes with carboxylate ligands. One of the reported $[ReOX(N–O)_2]$ complexes shows a very rare *trans*-N,N and *trans*-O,O ligand arrangement. Except for **1**, the compounds show good catalytic activity and selectivity in the epoxidation of cyclooctene with *tert*-butyl hydroperoxide. The yield of cyclooctane oxide varies between 58 and 75%, which is comparable to previously reported oxidorhenium(V) systems, but lower than rhenium(VII) compounds. Interestingly, the highest initial activity was displayed by an

unusual *trans*-N,N and *trans*-O,O isomer of [ReOX(N–O)$_2$], thus indicating that different region isomers might have a significant influence on catalyst activity.

Experimental Section

Materials: All chemicals were purchased from commercial sources and were used without further purification. [ReOCl$_3$(OPPh$_3$)(SMe$_2$)] and [ReO$_2$(py)$_4$]Cl were prepared according to previously published methods.[31–33]

Instrumentation: IR spectra were recorded with a Nicolet Magna 560 spectrophotometer in the spectral range 4000–400 cm^{-1} with the samples in the form of KBr pellets. The ^{1}H and ^{13}C NMR spectra were recorded (295 K) with a Bruker Avance 400 NMR spectrometer at a resonance frequency of 400 MHz for ^{1}H NMR spectra and 100 MHz for ^{13}C NMR spectra by using [D$_6$]DMSO or CDCl$_3$ as solvent and TMS as an internal solvent. ESI–MS was performed with a Varian 500-MS IT mass spectrometer ion trap apparatus. The instrument was operating in the positive-ion mode with a capillary voltage of 20 V, needle voltage of 5 kV, and a spray shield voltage of 600 V. The drying gas (N_2) temperature was 150 °C. The single-crystal X-ray diffraction measurement was carried out with a Gemini A Ultra diffractometer equipped with an Atlas CCD detector. Intensities of reflections were measured using graphite-monochromated Mo-K_α radiation (λ = 0.71073 Å) with ω scan mode at room temperature. During the data reduction, Lorentz, polarization, and empirical absorption correction using spherical harmonics, implemented in the SCALE3 ABSPACK scaling algorithm, were applied.[34] The structures were solved by Patterson synthesis using SHELXS-97[35] and refined on F_2 by full-matrix least-square techniques using the SHELXTL-97[36] program. The non-hydrogen atoms of the complexes were refined with anisotropic temperature parameters. The hydrogen atoms bound to carbon atoms were placed in calculated positions and treated as riding on their parent atoms with d(C–H) = 0.93 Å, U_{iso}(H) = 1.2 U_{eq}(C) (aromtic); and d(C–H) = 0.96 Å, U_{iso}(H) = 1.5 U_{eq}(C) (methyl). The methyl groups were allowed to rotate about their local threefold axis.

CCDC-858621 (for **1**), -858622 (for **3**), -858623 (for **4**), -858624 (for **5**), -858625 (for **6**), -858626 (for **7**), -858627 (for **8**), -858628 (for **9**), and -858629 (for **10**) contain the supplementary crystallographic data for this paper. These data can be obtained free of charge from The Cambridge Crystallographic Data Centre via www.ccdc.cam.ac.uk/data_request/cif.

General Epoxidation Procedure: Epoxidation experiments were carried out with 1 mol-% of the respective complex at 50 °C in CHCl$_3$ by using TBHP (3 equiv.) for a time between 20 and 27 h. Progress was analyzed by GC–MS using Mesitylene as internal standard. Yields were calculated in relation to cyclooctene (cyOct) conversion. In a typical experiment, the respective catalyst (1–1.5 mg) was dissolved in CHCl$_3$ (2 mL) in a Mininert vial, and the calculated amount of cyOct (which resulted in 1 mol-% catalyst loading) was added with a syringe, capped, and heated to 50 °C. Then TBHP (3 equiv. with respect to cyOct) was added through the septum and stirred. For GC–MS analysis, samples (10 μL) were withdrawn at different times and diluted to 1 mL with ethyl acetate that contained 50 ppb mesitylene as internal standard. All solvents as well as reagents were used as received. GC–MS measurements were performed with an Agilent 7890 A with an Agilent 19091J-433 column coupled to a mass spectrometer type Agilent 5975 C.

General Procedure for the Preparation of Rhenium Complexes 1–5: [ReOX$_3$(OPPh$_3$)(SMe$_2$)] (0.77 mmol) was suspended in methanol (80 mL) and phenol-based ligand (1.54 mmol) was added. The suspension was stirred at ambient temperature for 48 h and filtered, thus yielding a green solid, which was washed with ethanol and diethyl ether and then recrystallized.

[ReOCl(hpbi)$_2$]·THF (1): The compound was prepared according to the general procedure by employing hpbi (0.32 g, 1.54 mmol) and [ReOCl$_3$(OPPh$_3$)(SMe$_2$)] (0.50 g, 0.77 mmol) to give **1** (0.34 g, 61%). Recrystallization from methanol/tetrahydrofuran. ^{1}H NMR (400 MHz, [D$_6$]DMSO): δ = 13.80 (s, 1 H), 13.64 (s, 1 H), 8.08–8.00 (m, 2 H), 7.77 (d, J = 8.0 Hz, 1 H), 7.62–7.55 (m, 2 H), 7.49 (t, J = 7.6 Hz, 1 H), 7.42 (dd, J = 7.9, 1.4 Hz, 1 H), 7.35 (d, J = 8.0 Hz, 1 H), 7.24 (d, J = 7.4 Hz, 1 H), 7.07 (t, J = 7.5 Hz, 1 H), 7.04–6.96 (m, 2 H), 6.81 (t, J = 7.5 Hz, 1 H), 6.69 (t, J = 7.1 Hz, 1 H), 6.14 (d, J = 8.3 Hz, 1 H), 6.04 (d, J = 7.5 Hz, 1 H), 3.64–3.58 (m 4 H), 1.79–1.73 (m, 4 H) ppm. ^{13}C NMR (100 MHz, [D$_6$]-DMSO): δ = 167.5, 161.2, 154.3, 141.6, 140.4, 133.8, 133.7, 131.4, 131.3, 130.9, 130.4, 129.0, 128.9, 128.4, 127.7, 125.6, 124.7, 123.8, 123.2, 120.4, 119.6, 119.4, 119.0, 114.9, 112.9, 112.7, 49.08, 21.8 ppm. $C_{30}H_{26}Cl_1N_4O_4Re$ (728.20): calcd. C 49.44, H 3.57, N 7.69; found C 48.32, H 3.03, N 8.24. IR (KBr): $\tilde{\nu}$ = 3190 [ν(N–H)]; 1622, 1603, 1578 and 1538 ν(C=N) and ν(C=C); 960 ν(Re=O) cm^{-1}. ESI$^+$-MS (MeOH): m/z = 437.62 [{ReO(hpbi)} + Na + 2H]$^+$, 621.57 [{ReO(hpbi)$_2$}]$^+$, 643.63 [{ReO(hpbi)$_2$} + Na]$^+$, 655.65 [{ReOCl(hpbi)$_2$}]$^+$, 675.61 [{ReO(hpbi)$_2$} + Na + MeOH]$^+$, 728.10 [{ReOCl(hpbi)$_2$} + THF]$^+$.

[ReOCl(hmpbta)$_2$] (2): The compound was prepared according to the general procedure by employing hmpbta (0.35 g, 1.54 mmol) and [ReOCl$_3$(OPPh$_3$)(SMe$_2$)] (0.50 g, 0.77 mmol) to give **2** (0.34 g, 66%). Recrystallization from methanol/acetonitrile. ^{1}H NMR (400 MHz, CDCl$_3$): δ = 8.47 (d, J = 8.8 Hz, 1 H), 8.35 (d, J = 1.2 Hz, 1 H), 8.02 (d, J = 8.7 Hz, 1 H), 7.84–7.80 (m, 1 H), 7.76 (d, J = 8.6 Hz, 1 H), 7.60–7.55 (m, 3 H), 7.42–7.37 (m, 1 H), 7.35–7.31 (m, 1 H), 7.14–7.10 (m, 1 H), 6.75 (dd, J = 8.4, 1.6 Hz, 1 H) 6.34 (d, J = 8.8 Hz, 1 H), 6.22 (d, J = 8.4 Hz, 1 H), 2.58 (s, 3 H), 2.05 (s, 3 H) ppm. ^{13}C NMR (100 MHz, CDCl$_3$): δ = 160.0, 151.4, 146.0, 145.4, 143.3, 142.6, 132.8, 132.8, 132.6, 131.8, 130.7, 130.6, 128.1, 127.8, 127.2, 125.7, 125.2, 121.6, 121.4, 120.1, 119.3, 119.0, 118.6, 114.3, 20.6, 20.5 ppm. $C_{26}H_{20}Cl_1N_6O_3Re$ (686.13): calcd. C 45.47, H 2.91, N 12.24; found C 44.97, H 2.73, N 12.87. IR (KBr): $\tilde{\nu}$ = 1612, 1572 and 1504 ν(C=N) and ν(C=C); 957 ν(Re=O) cm^{-1}. ESI$^+$-MS (MeOH): m/z = 651.66 [{ReO(hmpbta)$_2$}]$^+$, 675.76 [{ReO(hmpbta)$_2$} + Na + H]$^+$, 709.54 [{ReOCl(hmpbta)$_2$} + Na]$^+$, 1394.16 [{ReOCl(hmpbta)$_2$}$_2$ + Na]$^+$.

[ReOCl(hpbo)$_2$] (3): The compound was prepared according to the general procedure by employing hpbo (0.33 g, 1.54 mmol) and [ReOCl$_3$(OPPh$_3$)(SMe$_2$)] (0.50 g, 0.77 mmol) to give **3** (0.33 g, 65%). Recrystallization from methanol/acetonitrile. ^{1}H NMR (400 MHz, CDCl$_3$): δ = 8.32–8.28 (m, 1 H), 8.16 (dd, J = 8.0, 1.6 Hz, 1 H), 7.81 (dd, J = 7.3, 1.5 Hz, 1 H), 7.73–7.66 (m, 3 H), 7.64–7.60 (m, 2 H), 7.44 (d, J = 8.2 Hz, 1 H), 7.25–7.20 (m, 1 H), 7.09–7.00 (m, 3 H), 6.83–6.79 (m, 1 H), 6.55 (d, J = 7.9 Hz, 1 H), 6.49 (d, J = 8.4 Hz, 1 H) ppm. ^{13}C NMR (100 MHz, CDCl$_3$): δ = 173.1, 166.8, 164.7, 164.5, 149.2, 149.1, 143.0, 140.2, 137.2, 136.2, 128.9, 128.0, 127.4, 126.9, 126.6, 126.1, 124.6, 121.2, 121.1, 119.1, 118.9, 115.7, 111.5, 111.3, 110.7, 108.9 ppm. $C_{26}H_{16}Cl_1N_2O_5Re$ (658.06): calcd. C 47.41, H 2.43, N 4.25; found C 49.70, H 2.93, N 3.61. IR (KBr): $\tilde{\nu}$ = 1607, 1567 and 1535 ν(C=N) and ν(C=C); 958 ν(Re=O) cm^{-1}. ESI$^+$-MS (MeOH): m/z = 623.47 [{ReO(hpbo)$_2$}]$^+$, 647.52 [{ReO(hpbo)$_2$} + Na]$^+$, 677.56 [{ReOCl(hpbo)$_2$} + NH$_4$]$^+$, 681.45 [{ReOCl(hpbo)$_2$} + Na]$^+$, 1333.69 [{ReOCl(hpbo)$_2$}$_2$ + NH$_4$]$^+$.

[ReOCl(hpbt)$_2$]·2MeCN (4): The compound was prepared according to the general procedure by employing hpbt (0.35 g, 1.54 mmol) and [ReOCl$_3$(OPPh$_3$)(SMe$_2$)] (0.50 g, 0.77 mmol) to give **4** (0.41 g, 68%). Recrystallization from methanol/acetonitrile. ^{1}H NMR (400 MHz, CDCl$_3$): δ = 8.79 (d, J = 8.1 Hz, 1 H), 7.99 (d, J = 7.8 Hz, 1 H), 7.80–7.68 (m, 3 H), 7.66–7.60 (m, 1 H), 7.57–7.54 (m, 2 H), 7.23–7.16 (m, 2 H), 7.08–7.01 (m, 2 H), 7.00–6.94 (m, 1 H), 6.92–6.87 (m, 1 H), 6.65 (t, J = 7.6 Hz, 1 H), 6.44 (d, J = 8.2 Hz, 1 H), 2.52 (s, 3 H), 2.50 (s, 3 H) ppm. ^{13}C NMR (100 MHz, CDCl$_3$): δ = 171.9, 168.0, 161.5, 155.0, 153.1, 136.0, 135.5, 130.8, 130.1, 129.5, 129.1, 129.0, 127.5, 127.1, 126.8, 126.6, 126.3, 124.9, 121.9, 121.5, 121.4, 120.8, 119.5, 119.3, 118.2, 117.6, 116.4, 114.8, 30.9, 2.1 ppm. $C_{30}H_{22}ClN_4O_3ReS_2$ (772.29): calcd. C 46.61, H 2.85, N 7.25; found C 42.51, H 2.03, N 3.66. IR (KBr): $\tilde{\nu}$ = 1599 and 1557 ν(C=N) and ν(C=C); 960 ν(Re=O) cm^{-1}. ESI$^+$-MS (MeOH): m/z = 655.45 [{ReO(hpbt)$_2$}]$^+$, 679.50 [{ReO(hpbt)$_2$} + Na + H]$^+$, 709.54 [{ReOCl(hpbt)$_2$} + NH$_4$ + H]$^+$, 713.43 [{ReOCl(hpbt)$_2$} + Na]$^+$, 1397.61 [{ReOCl(hpbt)$_2$}$_2$ + NH$_4$]$^+$.

[ReOBr(hmpbta)$_2$] (5): The compound was prepared according to the general procedure by employing hmpbta (0.29 g, 1.28 mmol) and [ReOBr$_3$(OPPh$_3$)(SMe$_2$)] (0.60 g, 0.64 mmol) to give **5** (0.32 g, 57%). Recrystallization from methanol/acetonitrile. ^{1}H NMR (400 MHz, CDCl$_3$): δ = 8.53 (d, J = 8.8 Hz, 1 H), 8.33 (s, 1 H), 8.00 (d, J = 8.7 Hz, 1 H), 7.85–7.79 (m, 1 H), 7.76 (d, J = 8.6 Hz, 1 H), 7.62–7.52 (m, 3 H), 7.41–7.35 (m, 1 H), 7.35–7.29 (m, 1 H), 7.14–7.07 (m, 1 H), 6.75 (d, J = 8.3 Hz, 1 H), 6.29 (d, J = 8.8 Hz, 1 H), 6.23 (d, J = 8.4 Hz, 1 H), 2.58 (s, 3 H), 2.04 (s, 3 H) ppm. ^{13}C NMR (100 MHz, CDCl$_3$): δ = 159.9, 151.1, 145.8, 145.6, 143.3, 142.5, 132.8, 132.7, 132.6, 131.8, 130.7, 130.6, 128.1, 127.8, 127.3, 125.6, 125.2, 121.5, 121.5, 120.1, 119.3, 119.1, 119.0, 114.1, 20.6, 20.5 ppm. $C_{26}H_{20}Br_1N_6O_3Re$ (730.59): calcd. C 42.70, H 2.74, N 11.50; found C 42.87, H 2.50, N 11.49. IR (KBr): $\tilde{\nu}$ = 1612, 1571 and 1504 ν(C=N) and ν(C=C); 956 ν(Re=O) cm^{-1}. ESI$^+$-MS (MeOH): m/z = 528.36 [{ReO(hmpbta)} + Na]$^+$, 621.32 [{ReO(hmpbta)$_2$} – 2CH$_3$]$^+$, 675.46 [{ReO(hmpbta)$_2$} + Na]$^+$, 752.21 [{ReOBr(hmpbta)$_2$} + Na]$^+$.

General Procedure for the Preparation of Rhenium Complexes 6–8: A mixture of [ReO$_2$(py)$_4$]Cl (0.90 mmol) and the corresponding carboxylic acid (1.80 mmol) in methanol (80 mL) was heated at reflux for 30 min and allowed to cool to ambient temperature. The resulting dark red suspension was filtered and the reddish-brown microcrystalline precipitate was washed with methanol and diethyl ether.

[ReO(OMe)(quin)$_2$] (6): The compound was prepared according to the general procedure by employing quin (0.31 g, 1.80 mmol) and [ReO$_2$(py)$_4$]Cl (0.50 g, 0.90 mmol) to give **6** (0.38 g, 75%). ^{1}H NMR (400 MHz, CDCl$_3$): δ = 9.76 (d, J = 8.9 Hz, 2 H), 8.83 (d, J = 8.3 Hz, 2 H), 8.73 (d, J = 8.3 Hz, 2 H), 8.27 (ddd, J = 8.6, 6.9, 1.5 Hz, 2 H), 8.12 (d, J = 7.0 Hz, 2 H), 7.99–7.90 (m, 2 H), 3.08 (s, 3 H) ppm. ^{13}C NMR (100 MHz, CDCl$_3$): δ = 182.3, 150.2, 150.0, 144.4, 134.9, 130.7, 130.2, 128.9, 128.4, 121.9, 57.6 ppm. $C_{21}H_{15}N_2O_6Re$ (577.55): calcd. C 43.62, H 2.60, N 4.85; found C 43.37, H 2.26, N 4.71. IR (KBr): $\tilde{\nu}$ = 1683 $\nu(COO)_{asym}$; 1617, 1595, 1569 and 1515 ν(C=N) and ν(C=C); 1323 $\nu(COO)_{sym}$; 955 ν(Re=O); 512 and 500 ν(Re–OMe) cm^{-1}. ESI$^+$-MS (MeOH): m/z = 428.45 [{ReO(OMe)(quin)} + Na]$^+$, 547.33 [{ReO(quin)$_2$}]$^+$, 571.34 [{ReO(quin)$_2$} + Na + H]$^+$, 601.31 [{ReO(OMe)(quin)$_2$} + Na]$^+$, 1176.69 [{ReO(OMe)(quin)$_2$}$_2$ + Na]$^+$.

[ReO(OMe)(pic)$_2$] (7): The compound was prepared according to the general procedure by employing pic (0.22 g, 1.80 mmol) and [ReO$_2$(py)$_4$]Cl (0.50 g, 0.90 mmol) to give **7** (0.29 g, 68%). ^{1}H NMR (400 MHz, [D$_6$]DMSO): δ = 8.74 (d, J = 5.6 Hz, 1 H), 8.67 (d, J = 5.3 Hz, 1 H), 8.54–8.48 (m, 2 H), 8.24–8.22 (m, 1 H), 8.23 (dd, J = 7.7, 0.7 Hz, 1 H), 8.09–8.05 (m, 1 H), 8.00–7.92 (m, 2 H), 4.55 (s, 3 H) ppm. $C_{13}H_{11}N_2O_6Re$ (477.44): calcd. C 32.67, H 2.30, N 5.86; found C 32.65, H 2.10, N 5.86. IR (KBr): $\tilde{\nu}$ = 1712 and 1676 $\nu(COO)_{asym}$; 1609 ν(C=N) and ν(C=C); 1317 and 1287 $\nu(COO)_{sym}$; 984 ν(Re=O); 573 ν(Re–OMe) cm^{-1}. ESI$^+$-MS (MeOH): m/z = 447.43 [{ReO(pic)$_2$}]$^+$, 501.36 [{ReO(OMe)(pic)$_2$} + Na]$^+$, 977.49 [{ReO(OMe)(pic)$_2$}$_2$ + Na]$^+$.

[ReO(OMe)(2,5-dipic)$_2$]·C$_5$H$_5$N (8): The compound was prepared according to the general procedure by employing 2,5-dipic (0.30 g, 1.80 mmol) and [ReO$_2$(py)$_4$]Cl (0.50 g, 0.90 mmol) to give **8** (0.42 g, 73%). ^{1}H NMR (400 MHz, [D$_6$]DMSO): δ = 9.15 (dd, J = 2.1, 0.7 Hz, 1 H), 8.74 (d, J = 4.9 Hz, 1 H), 8.43 (dd, J = 8.1, 2.1 Hz, 2 H), 8.15 (dd, J = 8.1, 0.7 Hz, 2 H), 7.74–7.66 (m, 1 H), 2.09 (s, 3 H) ppm. $C_{20}H_{16}N_3O_{10}Re$ (644.56): calcd. C 37.23, H 2.48, N 6.52; found C 36.30, H 2.17, N 6.37. IR (KBr): $\tilde{\nu}$ = 1716 and 1685 $\nu(COO)_{asym}$; 1565 ν(C=N) and ν(C=C); 1299 and 1289 $\nu(COO)_{sym}$; 980 ν(Re=O); 570 ν(Re–OMe) cm^{-1}. ESI$^+$-MS (MeOH + AcOH): m/z = 415.25 [{ReO(OMe)} + Na + 2C$_5$H$_5$N]$^+$, 437.37 [{ReO(OMe)(py)$_2$} + K]$^+$, 573.23 [{ReO(py)$_2$} + K]$^+$.

General Procedure for the Preparation of Rhenium Complexes 9 and 10: [ReOCl$_3$(OPPh$_3$)(SMe$_2$)] (0.77 mmol) was suspended in methanol or acetonitrile (80 mL) and the corresponding carboxylic acid (1.54 mmol) was added. The suspension was stirred at ambient temperature for 48 h and filtered, thereby yielding a blue solid, which was washed with ethanol and diethyl ether and then recrystallized.

[ReOCl(pic)$_2$] (9): The compound was prepared according to the general procedure by employing pic (0.19 g, 1.54 mmol) and [ReOCl$_3$(OPPh$_3$)(SMe)$_2$] (0.50 g, 0.77 mmol) to give **9** (0.28 g, 77%). ^{1}H NMR (400 MHz, [D$_6$]DMSO): δ = 9.02 (d, J = 5.5 Hz, 1 H), 8.69 (d, J = 5.4 Hz, 1 H), 8.64 (d, J = 3.6 Hz, 2 H), 8.30 (d, J = 7.6 Hz, 1 H), 8.19 (t, J = 6.0 Hz, 1 H), 8.12–8.02 (m, 2 H) ppm. ^{13}C NMR (100 MHz, [D$_6$]DMSO): δ = 180.7, 164.3, 158.2, 151.7, 148.6, 147.2, 146.2, 143.4, 132.4, 129.6, 127.4, 126.1 ppm. $C_{12}H_8ClN_2O_5Re$ (481.85): calcd. C 29.88, H 1.66, N 5.81; found C 29.98, H 1.44, N 5.92. IR (KBr): $\tilde{\nu}$ = 1712 and 1669 $\nu(COO)_{asym}$; 1609 and 1570 ν(C=N) and ν(C=C); 1317 and 1287 $\nu(COO)_{sym}$; 984 ν(Re=O) cm^{-1}. ESI$^+$-MS (MeOH): m/z = 447.48 [{ReO(pic)$_2$}]$^+$, 501.41 [{ReO(OMe)(pic)$_2$} + Na]$^+$, 977.35 [{ReO(OMe)(pic)$_2$}$_2$ + Na]$^+$.

[ReOCl(3-ind)$_2$]·CH$_3$OH (10): The compound was prepared according to the general procedure by employing pic (0.25 g, 1.54 mmol) and [ReOCl$_3$(OPPh$_3$)(SMe$_2$)] (0.50 g, 0.77 mmol) to give **10** (0.34 g, 74%). ^{1}H NMR (400 MHz, [D$_6$]DMSO): δ = 8.10 (d, J = 8.0 Hz, 1 H), 7.90 (d, J = 7.5 Hz, 1 H), 7.85 (d, J = 7.0 Hz, 1 H), 7.73 (d, J = 8.4 Hz, 1 H), 7.50–7.35 (m, 4 H), 3.62 (s, 1 H), 2.08 (s, 3 H) ppm. $C_{17}H_{14}Cl_1N_4O_6Re$ (591.97): calcd. C 34.46, H 2.36, N 9.46; found C 35.89, H 2.01, N 11.46. IR (KBr): $\tilde{\nu}$ = 3109 ν(N–H); 1725 and 1685 $\nu(COO)_{asym}$; 1630 and 1583 ν(C=N) and ν(C=C); 1388 and 1366 $\nu(COO)_{sym}$; 990 ν(Re=O) cm^{-1}. ESI$^+$-MS (MeOH + AcOH): m/z = 415.35 [{ReOCl(ind)} + NH$_4$]$^+$, 421.43 [{ReOCl(ind)} + Na]$^+$, 527.41 [{ReO(ind)$_2$}]$^+$.

Acknowledgments

M. W. thanks the Österreichischer Austauschdienst (ÖAD) for supporting his stay at the Institute of Chemistry, Karl-Franzens-University of Graz, Austria. This work was financed by the Polish National Science Centre (NCN), under Grant No. 2011/03/N/ST5/04522.

[1] W. T. Volkert, T. J. Hoffman, *Chem. Rev.* **1999**, *99*, 2269–2292.
[2] J. R. Dilworth, S. J. Parrot, *Chem. Soc. Rev.* **1998**, *27*, 43–55.
[3] R. Schibli, P. A. Schubiger, *Eur. J. Nucl. Med. Mol. Imaging* **2002**, *29*, 1529–1542.
[4] P. Blower, *Dalton Trans.* **2006**, 1705–1711.
[5] C. C. Romão, F. E. Kühn, W. A. Herrmann, *Chem. Rev.* **1997**, *97*, 3197–3246.
[6] F. E. Kühn, A. Scherbaum, W. A. Herrmann, *J. Organomet. Chem.* **2004**, *689*, 4149–4164.
[7] F. E. Kühn, A. M. Santos, W. A. Herrmann, *Dalton Trans.* **2005**, 2483–2491.
[8] G. M. Lobmaier, G. D. Frey, D. E. Dewhurst, E. Herdtweck, W. A. Herrmann, *Organometallics* **2007**, *26*, 6290–6299.
[9] A. Deloffre, S. Halut, L. Salles, J.-M. Brégeault, J. R. Gregorio, B. Denise, H. Rudler, *J. Chem. Soc., Dalton Trans.* **1999**, 2897–2898.
[10] A. Sachse, N. C. Mösch-Zanetti, G. Lyashenko, J. W. Wielandt, K. Most, J. Magull, F. Dall'Antonia, A. Pal, R. Herbst-Irmer, *Inorg. Chem.* **2007**, *46*, 7129–7135.
[11] S. Dinda, M. G. B. Drew, R. Bhattacharyya, *Catal. Commun.* **2009**, *10*, 720–724.
[12] A. Schröckeneder, P. Traar, G. Raber, J. Baumgartner, F. Belaj, N. C. Mösch-Zanetti, *Inorg. Chem.* **2009**, *48*, 11608–11614.
[13] P. Traar, A. Schröckeneder, M. Judmaier, F. Belaj, J. Baumgartner, A. Sachse, N. C. Mösch-Zanetti, *Eur. J. Inorg. Chem.* **2010**, *36*, 5718–5727.
[14] P. Traar, J. A. Schachner, L. Steiner, A. Sachse, M. Volpe, N. C. Mösch-Zanetti, *Inorg. Chem.* **2011**, *50*, 1983–1990.
[15] B. Terfassa, P. Traar, M. Volpe, N. C. Mösch-Zanetti, V. J. T. Raju, N. Megersa, N. Retta, *Eur. J. Inorg. Chem.* **2011**, *28*, 4434–4440.
[16] K. R. Grünwald, G. Saischek, M. Volpe, N. C. Mösch-Zanetti, *Inorg. Chem.* **2011**, *50*, 7162–7171.
[17] J. H. Espenson, *Coord. Chem. Rev.* **2005**, *249*, 329–341.
[18] X. Shan, A. Ellern, J. H. Espenson, *Inorg. Chem.* **2002**, *41*, 7136–7142.
[19] M. M. Abu-Omar, L. D. McPherson, J. Arias, V. M. Berreau, *Angew. Chem. Int. Ed.* **2000**, *39*, 4310–4313.
[20] J. Arias, C. R. Newland, M. M. Abu-Omar, *Inorg. Chem.* **2001**, *40*, 2185–2192.
[21] L. D. McPherson, M. Drees, S. I. Khan, T. Strassner, M. M. Abu-Omar, *Inorg. Chem.* **2004**, *43*, 4036–4050.
[22] E. Shuter, H. R. Hoveyda, V. Karunaratne, S. J. Rettig, Ch. Orvig, *Inorg. Chem.* **1996**, *35*, 368–372.
[23] B. Machura, M. Wolff, R. Kruszynski, J. Kusz, *Polyhedron* **2009**, *28*, 1211–1220.
[24] U. Mazzi, F. Refosco, F. Tisato, G. Bandoli, M. Nicolini, *J. Chem. Soc., Dalton Trans.* **1986**, 1623–1628.
[25] O. Sigouin, Ch. Reber, A. L. Beauchamp, *Inorg. Chim. Acta* **2006**, *359*, 2059–2066.
[26] K. T. Shimazaki, Y. Kawai, M. Hirotsu, *Inorg. Chem.* **2001**, *40*, 4250–4256.
[27] T. I. A. Gerber, E. Hosten, D. Luzipo, P. Mayer, *J. Coord. Chem.* **2006**, *59*, 1063–1068.
[28] U. Mazzi, F. Refosco, G. Bandoli, M. Nicolini, *Transition Met. Chem.* **1985**, *10*, 121–127.
[29] J. D. G. Correia, Â. Domingos, A. Paulo, I. Santos, *J. Chem. Soc., Dalton Trans.* **2000**, 2477–2482.
[30] S. Bolaño, J. Bravo, R. Carballo, E. Freijanes, S. García-Fontán, P. Rodríguez-Seoane, *Polyhedron* **2003**, *22*, 1711–1717.
[31] M. S. Ram, J. T. Hupp, *Inorg. Chem.* **1991**, *30*, 130–133.
[32] B. D. Sherry, R. N. Loy, F. D. Toste, *J. Am. Chem. Soc.* **2004**, *126*, 4510–4511.
[33] D. E. Grove, G. Wilkinson, *J. Chem. Soc. A* **1966**, 1224–1230.
[34] Oxford Diffraction, *CrysAlis PRO*, Oxford Diffraction Ltd, Yarnton, England, **2011**.
[35] G. M. Sheldrick, *SHELXS-97, Program for Crystal Structure Resolution*, University of Göttingen, Göttingen, Germany, **1997**.
[36] G. M. Sheldrick, *SHELXL-97, Program for Crystal Structures Analysis*, University of Göttingen, Göttingen, Germany, **1997**.

Received: March 19, 2012
Published Online: June 29, 2012

RZECZPOSPOLITA POLSKA

Urząd Patentowy Rzeczypospolitej Polskiej

(12) **OPIS PATENTOWY** (19) **PL** (11) **210315**

(13) **B1**

(21) Numer zgłoszenia: **379432**

(22) Data zgłoszenia: **10.04.2006**

(51) Int.Cl.
C07D 215/48 (2006.01)
C07D 215/16 (2006.01)
A61P 31/18 (2006.01)

(54) **Amidy heterocykliczne oraz ich zastosowanie**

(43) Zgłoszenie ogłoszono:
15.10.2007 BUP 00/07

(45) O udzieleniu patentu ogłoszono:
31.01.2012 WUP 01/12

(73) Uprawniony z patentu:
UNIWERSYTET ŚLĄSKI W KATOWICACH, Katowice, PL

(72) Twórca(y) wynalazku:
AGNIESZKA MENCEL, Pszów, PL
DOMINIK TABAK, Dąbrowa Górnicza, PL
JAROSŁAW POLAŃSKI, Katowice, PL
BARBARA PODESZWA, Mikołów, PL
JACEK FINSTER, Pszczyna, PL
HALINA NIEDBAŁA, Dąbrowa Górnicza, PL
ANNA PAŁKA, Sosnowiec, PL
KATARZYNA SERAFIN, Katowice, PL
ROBERT MUSIOŁ, Częstochowa, PL

PL 210315 B1

Opis wynalazku

Przedmiotem wynalazku są amidy heterocykliczne hamujące działanie integrazy wirusa HIV oraz ich zastosowanie jako składniki skutecznych leków w terapii AIDS.

Wirus HIV, uważany za główną przyczynę nabytego zespołu upośledzenia odporności (AIDS), jest retrowirusem atakującym komórki układu immunologicznego limfocyty T. Do prawidłowego przebiegu cyklu życiowego wirusa potrzebuje on trzech enzymów: integrazy, proteazy i odwrotnej transkryptazy. Dotychczasowe metody terapii polegają głównie na hamowaniu aktywności proteazy i odwrotnej transkryptazy.

Integraza (IN) HIV jest enzymem, który katalizuje włączanie wirusowego DNA w genom komórki gospodarza. Proces ten przebiega dwuetapowo i polega na oderwaniu dwóch nukleotydów z każdego 3' końca wirusowego DNA i pozostawieniu wolnych grup hydroksylowych, po czym następuje przeniesienie i właściwa integracja nici wirusowego DNA z genomem zarażonej komórki gospodarza jak opisano w: Zouhiri, F., Mouscadet, J. F., Mekouar, K., Desmaele, D., Savoure, D., Leh, H., Subra, F., Le Bret, M., Auclair, C., d'Angelo, J., J. Med. Chem. 2000, 4, 8, 1533, Chen, J. C., Krucinski, J., Miercke, L. J., Finer-Moore, J. S., Tang, A. H., Leavitt, A. D., Stroud, R. M., Proc. Natl. Acad. Sci. U.S.A. 2000, 97, 8233.

W pierwszym etapie działanie integrazy wymaga obecności dwudodatnich jonów metali np.; Mg^{2+} Mn^{2+} i cząsteczek wody lub innego czynnika nukleofilowego, na przykład małych cząsteczek alkoholi, glicerolu lub aminokwasów (Vink, C., Yeheskiely, E., van der Marel, G. A., van Boom, J. H., Plasterk, R. H., Nucleic Acids Res. 1991, 19, 6691). W drugim etapie utworzone wcześniej grupy 3'-OH atakują grupy fosforanowe w DNA gospodarza. Tak zaatakowana komórka rozpoczyna proces namnażania potomnych wirionów.

Dotychczasowe metody terapii przeciwwirusowej stosowane w leczeniu AIDS polegają na podawaniu inhibitorów transkryptazy i proteazy oraz związków hamujących wnikanie lub uwalnianie wirusów. Wciąż brak jest skutecznych inhibitorów integrazy HIV. Pomimo, że struktura integrazy jest znana, dotychczas nie udało się opracować skutecznych jej inhibitorów, które dostępne byłyby na rynku farmaceutycznym. Jednym z najbardziej aktywnych potencjalnych inhibitorów IN są analogi diketokwasów (DKA) opisanych w pracach: Hazuda, D. J.; Felock P, Witmer M., Wolfe A., Stillmock K., Grobler J. A., Espeseth A., Gabryelski L., Schleif W., Blau C., Miller M. D., Science, 2000, 28, 7646-7650, Long, Y-Q.; Jiang, X-H.; Dayam, R.; Sanchez, T.; Shoemaker, R.; Sei, S.; Neamati, N. J., Med. Chem. 2004, 47, 2561-2573. Obecnie w fazie testów klinicznych znajdują się dwa połączenia L870-810 oraz S-1360. (Johnson, A. A.; Marchand, Ch.; Pommier, Y. Curr. Topics in Med. Chem. 2004, 4, 671-686).

W związkach tych farmakofor DKA występuje w formie naftyrydyny. Z opisu patentowego nr WO 2002 030930 znane są aktywne układy naftyrydynowe zawierające farmakofor DKA jako pochodną hydroksykwasu 7-COOH, 8-OH oraz chinolinowe, zawierające analogiczny farmakofor w konfiguracji 7-COOH, 8-OH (EP nr 1 375 486). Kwas 7-hydroksy-8-chinalclynokarboksylowy nie wykazuje jednak aktywności względem integrazy wirusa HIV. W zgłoszeniu nr P 371 842 opisano inhibitory integrazy wirusa HIV oparte na strukturze chinoliny i zawierające farmakofor diketokwasu DKA. Działanie tych związków opiera się na kompleksowaniu jonów magnezu w miejscu aktywnym integrazy.

W wyniku przeprowadzonych badań okazało się, że będące przedmiotem niniejszego wynalazku heterocykliczne pochodne amidowe, w porównaniu z opisanymi dotychczas związkami, wykazują znacznie wyższe powinowactwo w stosunku do integrazy.

Amidy heterocykliczne według wynalazku mają strukturę chemiczną według wzoru 1:

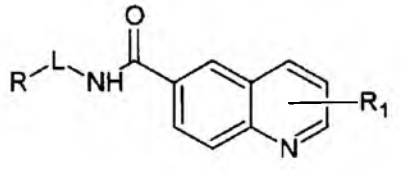

Wzór 1

gdzie:

L oznacza łącznik alkilowy również rozgałęziony, zawierający od 1 do 5 atomów węgla;

R oznacza grupę hydroksylową, metoksylową lub aminową,

R_1 oznacza jeden lub więcej podstawników w położeniach 2-5 oraz 7, 8, identycznych lub różnych, wybranych spośród: grupa metylowa, hydroksylowa, nitrowa, atom chlorowca lub atom wodoru.

Związki opisane wynalazkiem można korzystnie stosować w leczeniu choroby AIDS. Związki te hamują aktywności integrazy wirusa HIV1 lub HIV2 *in vitro* lub *in vivo*. Szczególnie korzystnie można stosować związki opisane wzorem 1, również w formie dopuszczalnych soli, jako składniki leków wieloskładnikowych stosowanych w terapii AIDS, co dodatkowo podnosi zalety wynalazku.

Poniżej przedstawiono przykłady związków opisanych wynalazkiem oraz ich zastosowanie.

P r z y k ł a d 1

5-hydroksy-2-metylo-8-nitro-chinolino-6-karboksylo(2-hydroksyetylo)amid według wzoru 1, gdzie R_1 = grupa nitrowa w położeniu 8, hydroksylowa w położeniu 5 i metylowa w położeniu 2 pierścienia chinoliny, L oznacza łącznik etylenowy, n = 2, R = OH. Związek może być otrzymany korzystnie w reakcji pomiędzy kwasem 5-hydroksy-2-metylo-8-nitrochinolino-6 karboksylowym i odpowiednią aminą, tak jak opisano w zgłoszeniu patentowym nr P 347 130 i może być korzystnie stosowany jako skuteczny inhibitor integrazy HIV.

^{1}H NMR (DMSO-d_6, 500 MHz) δ [ppm] 2,60 (s, 3H, CH3); 2,83 (t, 2H, CH2); 3,55 (t, 2H, CH2); 7,34-7,35 (d, J = 8,3 Hz, 1H, Ar); 8,51-8,53 (d, J = 8,35 Hz, 1H, Ar); 8,96 (s, 1H, Ar);

IR (KBr) [cm^{-1}]: 3512-2487 (OH rozc.); 1585 (C = O rozc.); 1516-1498 (def. C= N); 1445-1330 (szkieletowe pierść.); 1249-1203 (pasmo amidowe III); 1146-1114 (def. C-H w pł. pierść.); 1084-1034 (def. C-H w pł. pierść.); 789-705 (def. C-H poza pł. pierść.).

P r z y k ł a d 2

5-hydroksy-2-metylo-8-nitrochinolino-6-karboksylo(2-hydroksy-1,1-dimetyloetylo)amid, według wzoru 1 gdzie R_1 = grupa nitrowa w położeniu 8, hydroksylowa w położeniu 5 i metylowa w położeniu 2 pierścienia chinoliny, L oznacza łącznik 1,1-dimetyloetylowy, R = OH. Związek ten może być otrzymany podobnie jak w przykładzie 1 i stosowany korzystnie jako składnik leków wieloskładnikowych w terapii AIDS.

P r z y k ł a d 3

Oznaczanie aktywności badanych związków wobec integrazy. Pomiary hamowania integrazy wykonano wobec krótkich oligonukleotydów imitujących koniec DNA U5 wirusa w obecności 150 nM rekombinatu integrazy HIV-1 oraz 10 mM jonów Mg. Wartości IC_{50} obliczone metodą regresji nieliniowej krzywych zależności między aktywnością a stężeniem wynoszą poniżej 1 μM. Wartość IC_{50} związku opisanego w przykładzie 1 wynosi 0,5 μm.

Zastrzeżenia patentowe

1. Amidy heterocykliczne, **znamienne tym**, że mają strukturę chemiczną według wzoru 1:

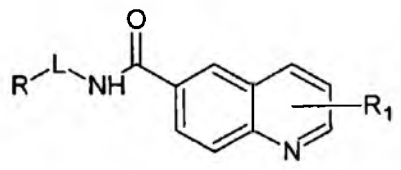

Wzór 1

gdzie: L oznacza łącznik alkilowy również rozgałęziony zawierający od 1 do 5 atomów węgla, R oznacza grupę hydroksylową, metoksylową lub aminową, R_1 oznacza jeden lub więcej podstawników w położeniach 2-5 oraz 7, 8, identycznych lub różnych, wybranych spośród: grupa metylowa, hydroksylowa, nitrowa, atom chlorowca lub atom wodoru.

2. Amidy heterocykliczne według zastrz. 1 do zastosowania w leczeniu choroby AIDS.

Departament Wydawnictw UP RP
Cena 2,46 zł (w tym 23% VAT)

RZECZPOSPOLITA POLSKA

Urząd Patentowy Rzeczypospolitej Polskiej

(12) **OPIS PATENTOWY** (19) **PL** (11) **210314**

(13) **B1**

(21) Numer zgłoszenia: **380818**

(22) Data zgłoszenia: **12.10.2006**

(51) Int.Cl.
C07D 215/48 (2006.01)
C07D 215/06 (2006.01)
A61P 31/18 (2006.01)

(54) **2-oksoamidy jako inhibitory integrazy HIV oraz ich zastosowanie**

(43) Zgłoszenie ogłoszono:
14.04.2008 BUP 00/08

(45) O udzieleniu patentu ogłoszono:
31.01.2012 WUP 01/12

(73) Uprawniony z patentu:
UNIWERSYTET ŚLĄSKI W KATOWICACH, Katowice, PL

(72) Twórca(y) wynalazku:
BARBARA PODESZWA, Mikołów, PL
ROBERT MUSIOŁ, Częstochowa, PL
DOMINIK TABAK, Dąbrowa Górnicza, PL
JACEK FINSTER, Pszczyna, PL
JAROSŁAW POLAŃSKI, Katowice, PL
HALINA NIEDBAŁA, Dąbrowa Górnicza, PL
ANNA PAŁKA, Sosnowiec, PL

PL 210314 B1

Opis wynalazku

Przedmiotem wynalazku są 2-oksoamidy jako nowe inhibitory integrazy HIV oraz ich zastosowanie do hamowania aktywności integrazy wirusa HIV.

Wirus HIV, uważany za główną przyczynę nabytego zespołu upośledzenia odporności (AIDS), jest retrowirusem atakującym komórki układu immunologicznego limfocyty T. Do prawidłowego przebiegu cyklu życiowego wirusa potrzebuje on trzech enzymów: integrazy, proteazy i odwrotnej transkryptazy. Dotychczasowe metody terapii polegają głównie na hamowaniu aktywności proteazy i odwrotnej transkryptazy.

Integraza (IN) HIV jest enzymem, który katalizuje włączanie wirusowego DNA w genom komórki gospodarza. Proces ten przebiega dwuetapowo i polega na oderwaniu dwóch nukleotydów z każdego 3' końca wirusowego DNA i pozostawieniu wolnych grup hydroksylowych, po czym następuje przeniesienie i właściwa integracja nici wirusowego DNA z genomem zarażonej komórki gospodarza, jak opisano w: Zouhiri, F., Mouscadet, J. F., Mekouar, K., Desmaele, D., Savoure, D., Leh, H., Subra, F., Le Bret, M., Auclair, C., d'Angelo, J., J. Med. Chem. 2000, 4, 8, 1533, Chen, J. C., Krucinski, J., Miercke, L. J., Finer-Moore, J. S., Tang, A. H., Leavitt, A. D., Stroud, R. M., Proc. Natl. Acad. Sci. U.S.A. 2000, 97, 8233.

W pierwszym etapie integraza do pełnej aktywności potrzebuje obecności dwudodatnich jonów metali np.; Mg^{2+}, Mn^{2+} i cząsteczek wody lub innego czynnika nukleofilowego, na przykład małych cząsteczek alkoholi, glicerolu lub aminokwasów (Vink, C., Yeheskiely, E., van der Marel, G. A., van Boom, J. H., Plasterk, R. H., Nucleic Acids Res. 1991, 19, 6691). W drugim etapie utworzone wcześniej grupy 3'-OH atakują grupy fosforanowe w DNA gospodarza. Tak zaatakowana komórka rozpoczyna proces namnażania potomnych wirionów.

Dotychczasowe metody terapii przeciwwirusowej stosowane w leczeniu AIDS polegają na podawaniu inhibitorów transkryptazy i proteazy oraz związków hamujących wnikanie lub uwalnianie wirusów.

Znanych jest także wiele związków hamujących integrazę HIV (omówione w pracy P. Cotelle, „Patented HIV-1 integrase inhibitors" Recent Patents on Anti-Infective Drug Discovery, 2006, 1, 1). Wciąż jednak brak dopuszczonych do obrotu leków o takim działaniu.

Znaczna liczba związków opisanych w literaturze niestety nie przekłada się na dostępność potencjalnych leków.

Związki, które poddawane są badaniom klinicznym okazują się nie spełniać pokładanych w nich nadziei. Aktywność *in vitro* nie jest równoznaczna z aktywnością *in vivo*, kolejnym problemem okazuje się wysoka toksyczność aktywnych układów.

Przykładem mogą służyć analogi diketokwasów (DKA), jedne z najbardziej aktywnych potencjalnych inhibitorów IN opisane w pracach: Hazuda, D. J.; Felock P., Witmer M., Wolfe A., Stillmock K., Grobler J. A., Espeseth A., Gabryelski L., Schleif W., Blau C., Miller M. D., Science, 2000, 28, 7646-7650, Long, Y-Q.; Jiang, X-H.; Dayam, R.; Sanchez, T.; Shoemaker, R.; Sei, S.; Neamati, N. J., Med. Chem. 2004, 47, 2561-2573.

W szczególności, dwa połączenia L870-810 oraz S-1360 pokazane na wzorach (Johnson, A. A.; Marchand, Ch.; Pommier, Y. Curr. Topics in Med. Chem. 2004, 4, 671-686) zostały wycofane z zaawansowanych badań klinicznych ze względu na znaczną toksyczność.

Znane są, według opisu w zgłoszeniu patentowym US 2006/0024330 A1, układy analogów oksoamidów, w których wiązanie amidowe stanowi część pierścienia niearomatycznego przedstawione na rysunku poniżej.

Związki te mogą stanowić inhibitory integrazy HIV.

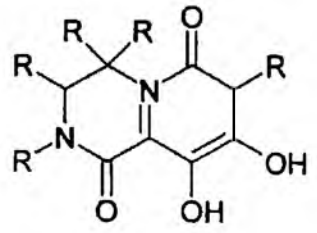

Dotychczas jednakże nie zostały opisane amidy lub ich analogi, w których możliwa byłaby wolna rotacja grupy amidowej, a przez to lepsze dopasowanie do miejsca działania leku.

Zadaniem niniejszego wynalazku jest zaproponowanie nowych inhibitorów integrazy HIV opartych na strukturze 2-oksoamidów, których struktura umożliwia wolną rotację grupy amidowej.

Związki będące przedmiotem wynalazku mogą być wysokoaktywnymi inhibitorami integrazy HIV w warunkach *in vitro* lub *in vivo*. W wyniku przeprowadzonych badań okazało się, że szczególnie aktywne są układy heterocykliczne 2-oksoamidów i/lub ich sole.

Istotą wynalazku są 2-oksoamidy jako inhibitory integrazy HIV posiadające strukturę chemiczną według wzoru 1:

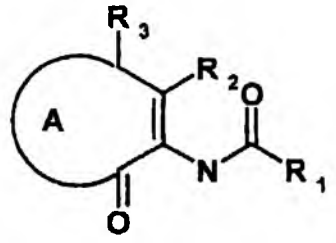

Wzór 1

gdzie:

A - oznacza dwupierścieniowy układ heterocykliczny chinoliny lub chinaldyny,

R_1 - oznacza pierścień fenylowy lub grupę styrylową, ewentualnie podstawioną przy pierścieniu fenylowym grupą hydroksylową, nitrową lub atomem chlorowca,

R_2 - oznacza atom wodoru, grupę OH lub OMe,

R_3 - oznacza atom wodoru, grupę OH, OMe lub OEt, przy czym w szczególnie korzystnym dla aktywności przypadku R_3 może oznaczać grupę okso (=O).

Związki opisane wynalazkiem można korzystnie stosować w leczeniu choroby AIDS.

Związki będące przedmiotem wynalazku przedstawione są poniższymi przykładami.

P r z y k ł a d 1. 2E-N-(5,8-dihydro-5,8-diokso-2-metylochinolin-7-yl)-3-fenyloprop-2-enamid

Wzór 1: A = układ chinaldyny, R_1 = grupa styrylowa, R_2 = H, R_3 = (=O).

Związek ten można otrzymać w reakcji 7-amino-5,8-chinaldynodionu i odpowiedniego chlorku kwasowego jedną ze znanych metod.

Ze względu na jego aktywność nadaje się on korzystnie do hamowania działania integrazy HIV w warunkach *in vitro* lub *in vivo*.

P r z y k ł a d 2. N-(5,8-dihydro-2-metylo-5,8-dioksochinolin-7-yl)-benzamid

Wzór 1: A = układ chinaldyny, R_1 = pierścień fenylowy, R_2 = H, R_3 = (=O).

Związek można otrzymać w reakcji: w kolbie kulistej zaopatrzonej w chłodnicę zwrotną oraz mieszadło magnetyczne umieszczono roztwór 0,06 g (0,32 mmola) 7-amino-2-metylochinolino-5,8-dionu w 2 ml suchej pirydyny.

Następnie, dodano chlorku 0,05 ml (0,42 mmola).

Zawartość kolby delikatnie chłodząc za pomocą łaźni lodowej mieszano, przez 2 h.

W trakcie prowadzenia reakcji wypadł żółty osad, który następnie odsączono i poddano krystalizacji z metanolu.

Otrzymano 0,055 g produktu, co stanowi 60% wydajności reakcji.

2-oksoamid otrzymany w ten sposób może być korzystnie stosowany jako składnik antywirusowych leków wieloskładnikowych stosowanych w terapii AIDS.

Zastrzeżenia patentowe

1. 2-oksoamidy jako inhibitory integrazy HIV, **znamienne tym**, że mają strukturę chemiczną według wzoru 1:

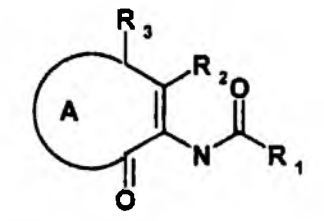

Wzór 1

gdzie:

A - oznacza dwupierścieniowy układ heterocykliczny chinoliny lub chinaldyny,

R_1 - oznacza pierścień fenylowy lub grupę styrylową, ewentualnie podstawioną przy pierścieniu fenylowym grupą hydroksylową, nitrową lub atomem chlorowca,

R_2 - oznacza atom wodoru, grupę OH lub OMe,

R_3 - oznacza atom wodoru, grupę OH, OMe lub OEt, przy czym w szczególnie korzystnym dla aktywności przypadku R_3 może oznaczać grupę okso (=O).

2. 2-oksoamidy według zastrz. 1 do zastosowania w leczeniu choroby AIDS.

Departament Wydawnictw UP RP
Cena 2,46 zł (w tym 23% VAT)

RZECZPOSPOLITA POLSKA

Urząd Patentowy Rzeczypospolitej Polskiej

(12) **OPIS PATENTOWY** (19) **PL** (11) **213476**

(13) **B1**

(21) Numer zgłoszenia: **382828**

(22) Data zgłoszenia: **03.07.2007**

(51) Int.Cl.
C07D 215/12 (2006.01)
A61K 31/47 (2006.01)
A61P 35/00 (2006.01)

(54) **Nowe pochodne styrylochinoliny**

(43) Zgłoszenie ogłoszono:
05.01.2009 BUP 01/09

(45) O udzieleniu patentu ogłoszono:
29.03.2013 WUP 03/13

(73) Uprawniony z patentu:
UNIWERSYTET ŚLĄSKI W KATOWICACH, Katowice, PL

(72) Twórca(y) wynalazku:
ROBERT MUSIOŁ, Będzin, PL
BARBARA PODESZWA, Mikołów, PL
DOMINIK TABAK, Dąbrowa Górnicza, PL
JACEK FINSTER, Pszczyna, PL
HALINA NIEDBAŁA, Dąbrowa Górnicza, PL
JAROSŁAW POLAŃSKI, Katowice, PL

PL 213476 B1

Opis patentowy

Przedmiotem wynalazku są niektóre pochodne styrylochinoliny wykazujące aktywność antyproliferacyjną.

Opracowanie nowych, skutecznych sposobów leczenia raka jest jednym z najważniejszych wyzwań dzisiejszej nauki. Dotychczasowe osiągnięcia medycyny i chemii leków sprawiły, że obecnie wiele nowotworów może być całkowicie wyleczonych. W dalszym ciągu jednak nie znamy skutecznej metody walki z wieloma innymi, również nieznanymi, odmianami tej choroby. Stosowane leki to w przeważającej liczbie związki o działaniu cytostatycznym lub cytotoksycznym. Mechanizmy działania oraz struktura chemiczna tych leków powodują, że niepożądane działanie uboczne staje się poważnym problemem w chemioterapii i ważną przyczyną niepowodzeń, dlatego wiele wysiłków skierowanych jest na projektowanie nowych związków o większej selektywności i niższej toksyczności. Szczególne zainteresowanie budzą związki oparte na szkielecie chinoliny oraz jej analogów, które często wykazują znaczne podobieństwo do naturalnie występujących związków o działaniu antyrakowym.

Dotychczasowe rozwiązania pozwalają przypuszczać, że pochodne chinoliny mogą uzupełnić arsenał leków stosowanych w terapii antyrakowej. W dalszym ciągu jednak brakuje konkretnych i skutecznych rozwiązań.

W opisie patentowym WO 2005/115145 z 8 grudnia 2005 opisano pochodne chinoliny i chinazoliny będące inhibitorami kinaz proteinowo-tyrozynowych (PTK) związanych z angiogenezą komórek rakowych. Aktywność opisywanych w tym zgłoszeniu związków polegała na hamowaniu czynników wzrostu receptorów kinaz, które regulują rozwój naczyń krwionośnych. Działanie opisanych układów jest nieodwracalne, a więc polega na silnym i trwałym wiązaniu do odpowiednich receptorów. Opis wynalazku zezwala na obecność podstawników w pozycji 2 szkieletu chinoliny lecz nie obejmuje pochodnych 2-styrylochinolinowych.

W opisie patentowym WO 2006/040522 opisano układy chinoliny modyfikowane w położeniu 4-podstawionym pirazolem. Według opisu związki mogą stanowić środki ograniczające proliferację komórek rakowych poprzez mechanizm hamowania PDGF receptorów kinaz. Wynalazek dotyczy również metod otrzymywania oraz stosowania opisywanych związków. Jednakże nie są omawiane inne układy oparte na strukturze chinoliny.

W opisie patentowym EP 0634170 opisano zastosowanie 8-hydroksychinoliny jako składnika leków wieloskładnikowych stosowanych w terapii łuszczycy. Opis patentowy dotyczy jedynie niepodstawionej 8-hydroksychinoliny oraz mieszanek zawierających 8-hydroksychinolinę. Zastosowanie opisane w wynalazku związane jest przede wszystkim z chorobami skórnymi.

Znany jest również szereg innych rozwiązań dotyczących zastosowania pochodnych chinoliny lub chinazoliny w hamowaniu proliferacji komórek rakowych np. WO 9850370, nie opisano dotychczas jednakże pochodnych opartych na strukturze styrylochinoliny o działaniu antyproliferacyjnym. Pochodne takie natomiast mogą być bardzo korzystnie stosowane do hamowania rozwoju komórek rakowych w badaniach *in vitro* oraz *in vivo*.

Badania skoncentrowane na poszukiwaniu nowych bioefektorów zawierających układ chinoliny doprowadziły do opracowania pochodnych wykazujących znaczną aktywność antyproliferacyjną. W porównaniu z dotychczas opisanymi związkami układy te mogą stanowić tanie, łatwe w otrzymywaniu aktywne środki antyproliferacyjne do zastosowań medycznych lub naukowych.

Istotę wynalazku stanowią nowe pochodne styrylochinoliny wykazujące aktywność antyproliferacyjną, posiadające strukturę chemiczną według wzoru 1:

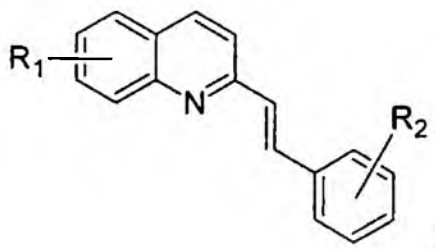

Wzór 1

gdzie:

R_1 oznacza grupę hydroksylową lub karboksylową w pozycjach 5, 6, 7, 8 pierścienia chinoliny, przy czym możliwe jest podstawienie jednocześnie w kilku pozycjach,

natomiast

R_2, oznacza atom chloru, bromu, grupę hydroksylową lub metoksylową w pozycjach 2, 3, 4 pierścienia fenylowego.

Poniżej przedstawiono przykłady związków opisanych wynalazkiem oraz ich zastosowanie.

Przykład 1.

Kwas 2-[2-(2-hydroksy-fenylo)-winylo]-chinolino-5-karboksylowy.

Związek otrzymano w reakcji 0,18 g kwasu chinaldyno-5-karboksylowego i 0,73 g aldehydu 2-hydroksybenzoesowego, oczyszczano przez krystalizację z metanolu uzyskując wydajność 0,14 g (49%) pomarańczowego osadu t.top=338-345°C. Strukturę związku potwierdzono na podstawie spektroskopii

^{1}H NMR (DMSO-d_6, 300MHz) δ: 6,9 (t, *J*=7,4 Hz, 1H); 7,04 (d, 1H, *J*=8,15 Hz), 7,3 (t, 1H), 7,62 (d, 1H, *J*=7,7 Hz), 7,94 (d, 1H, *J*=16,3 Hz), 8,05 (t, *J*=7,8 Hz, 1H), 8,32-8,35 (m, 2H), 8,48 (d, 1H, *J*=9,1 Hz), 8,55 (d, 1H, *J*=8,4 Hz), 9,61 (d, 1H, *J*=9,3 Hz), 10,7 (s, 1H), 13,7 (s, 1H).

Związek otrzymany w ten sposób nadaje się szczególnie korzystnie do dalszych modyfikacji na drodze syntezy chemicznej.

Przykład 2.

2-[2-(3-chloro-fenylo)-winylo]-8-hydroksychinolina.

Związek otrzymano w reakcji 1,6 g 8-hydroksychinaldyny i 2,8 g aldehydu 3-chlorbenzoesowego. Uzyskano 1,12 g (40%) żółtego, osadu t.top.=120-123°C. Strukturę związku potwierdzono na podstawie spektroskopii

^{1}H NMR (DMSO-d_6, 300MHz) δ 6,9 (t, *J*=7,4 Hz, 1H); 6,96 (d, *J*=7,4 Hz, 1H); 7,1 (d, *J*=7 Hz, 1H); 7,2 (t, *J*=7,1 Hz, 1H); 7,33-7,41 (m, 2H); 7,54 (d, *J*=16,5 Hz, 1H); 7,63 (d, *J*=7,9 Hz, 1H); 7,8 (d, *J*=8,7 Hz, 1H); 8,13 (d, *J*=16,4 Hz, 1H); 8,26 (d, *J*=8,5 Hz, 1H); 8,33 bs.

Ten związek jest aktywnym czynnikiem antyproliferacyjnym, który może być korzystnie stosowany do hamowania rozwoju komórek rakowych.

Przykład 3.

2-[(2-fenylo)-winylo]-8-hydroksychinolina.

Związek otrzymano w reakcji 1,6 g 8-hydroksy-chinaldyny i 2,12 g aldehydu benzoesowego. Zgodnie z opisem w J. Polanski, F. Zouhiri, L. Jeason, D. Desmaele, J. d'Angelo, J.F. Mouscadet, R. Gieleciak, J. Gastaiger, M. LeBert, *J. Med. Chem.*, 2002, **45**, 1949. Szczególnie korzystnie można ten związek wykorzystać do modyfikacji na drodze dalszej syntezy w celu otrzymania nowych pochodnych.

Przykład 4.

Kwas 2-[2-(3-metoksy-fenylo)-winylo]-chinolino-5,8-dikarboksylowy.

Związek otrzymano w reakcji 0,23 g kwasu chinaldyno-5,8-karboksylowego i 0,55 g aldehydu 3-metoksybenzoesowego, uzyskując 0,21 g (60%) żółtego produktu t.top. 258-264°C. Strukturę związku potwierdzono na podstawie spektroskopii

^{1}H NMR (DMSO-d_6, 500MHz) δ: 3,33 (s, 3H), 6,98 (t, *J*=7,8 Hz, 1H), 7,35-7,37 (m, 3H), 7,64 (d, *J*=16,4 Hz, 1H), 7,84 (d, *J*=16,4 Hz, 1H), 8,23 (d, *J*=9,2 Hz, 1H), 8,29 (d, *J*=7,6 Hz, 1H), 8,56 (d, *J*=7,6 Hz, 1H), 9,4 (d, *J*=9,1 Hz, 1H).

Związek ten można stosować do zatrzymania proliferacji komórek rakowych na przykład komórek mysiej białaczki P388 w badaniach *in vitro* lub *in vivo*.

Przykład 5.

Kwas 2-[2-(3-bromo-fenylo)-winylo]-8-hydroksychinolino-7-karboksylowy. Związek otrzymano w reakcji 0,19 g kwasu 8-hydroksychinaldyno-7-karboksylowego i 0,45 g aldehydu 3-bromobenzoesowego, uzyskując 0,07 g (30%) pomarańczowego produktu t.top 198-200°C. Strukturę związku potwierdzono na podstawie spektroskopii

^{1}H NMR (DMSO-d_6, 500MHz) δ: 7,3 (d, *J*= 8,5 Hz, 1H); 7,37 (t, *J*=6,5 Hz, 1H); 7,52 (d, *J*=6,8 Hz, 1H); 7,62 (d, *J*=16,2 Hz, 1H); 7,70 (d, *J*=7,7 Hz, 1H); 7,8 (d, *J*=8,5 Hz, 1H); 7,86 (d, *J*=16,4 Hz, 1H); 7,92 (s, 1H); 8,0 (d, *J*= 8,3 Hz, 1H); 8,38 (d, *J*=8,1 Hz, 1H).

Tak otrzymany związek może być składnikiem wieloskładnikowych leków przeciwnowotworowych korzystnie stosowanych do leczenia i profilaktyki antynowotworowej.

Zastrzeżenie patentowe

Nowe pochodne styrylochinoliny o działaniu antyproliferacyjnym, **znamienne tym**, że mają strukturę chemiczną według wzoru 1:

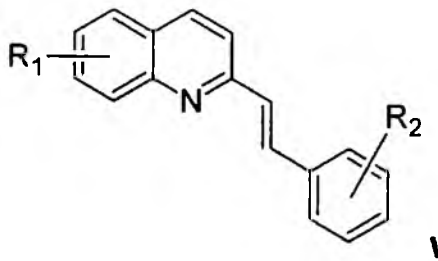

Wzór 1

gdzie R_1 oznacza grupę hydroksylową lub karboksylową w pozycjach 5, 6, 7, 8 pierścienia chinoliny, przy czym możliwe jest podstawienie jednocześnie w kilku pozycjach, natomiast R_2 oznacza atom chloru, bromu, grupę hydroksylową lub metoksylową w pozycjach 2, 3, 4 pierścienia fenylowego.

Departament Wydawnictw UP RP
Cena 2,46 zł (w tym 23% VAT)

11th International Electronic Conference on Synthetic Organic Chemistry (ECSOC-11), 1-30 November 2007. http://www.usc.es/congresos/ecsoc/11/ECSOC11.htm & http://www.mdpi.org/ecsoc-11/

[a011]

ZENTIVA

Preparation and Herbicidal Activities of Substituted Amides of Quinoline Derivatives

Robert Musiol[1]*, Josef Jampilek[2,3], Katarina Kralova[4], Dominik Tabak[1], Jacek Finster[1], Barbara Podeszwa[1], Violetta Kozik[1], Jiri Dohnal[2,3], Jaroslaw Polanski[1]

[1] Institute of Chemistry, University of Silesia, Szkolna 9, 40007 Katowice, Poland; e-mail: rmusiol@us.edu.pl, tel: +48-32-3591206, fax: +48-32-2599978

[2] Zentiva a. s., U kabelovny 130, 102 37 Prague 10, Czech Republic

[3] Department of Chemical Drugs, Faculty of Pharmacy, University of Veterinary and Pharmaceutical Sciences, Palackeho 1/3, 61242 Brno, Czech Republic

[4] Institute of Chemistry, Faculty of Natural Sciences, Comenius University, Mlynska dolina Ch-2, 84215 Bratislava, Slovakia

* Author to whom correspondence should be addressed.

Abstract: The series of eight substituted amides of 5-hydroxy-2-methylquinoline-7-carboxylic acid were prepared. The synthetic procedures of the compounds are presented. All the prepared quinoline derivatives were analyzed using RP-HPLC method for the lipophilicity measurement and their lipophilicity was determined. The prepared compounds were tested for their photosynthesis-inhibiting activity (the inhibition of photosynthetic electron transport in spinach chloroplasts (*Spinacia oleracea L.*) and the reduction of chlorophyll content in (*Chlorella vulgaris* Beij.). Several compounds showed the biological activity comparable with or higher than the standard 3-(3,4-dichlorophenyl)-1,1-dimethylurea (DCMU). The relationships between the lipophilicity and the chemical structure of the studied compounds are discussed as well as the structure-activity relationships (SAR) between the chemical structure and the biological activities of the evaluated compounds.

Keywords: Quinoline derivatives; Lipophilicity; OER inhibition; Spinach chloroplasts; Reduction of chlorophyll content; *Chlorella vulgaris*; Structure-activity relationships.

INTRODUCTION

Various compounds possessing an amide -NHCO- functionality were found to inhibit photosynthetic electron transport. Although this has been discovered more than fifty years ago [1], there are still many unanswered questions about structural requirements for the activity of these compounds. Better understanding of the SAR regularities are not only important for the design of modern agricultural agents but can also give the remarkable insight into the photosynthesis mechanisms of the green cells.

Quinoline scaffold is present in many classes of biologically active compounds [2]. A number of them showed antimicrobial activities [3-5]. Some quinoline analogues showed also antineoplastic activity [6,7]. Styrylquinoline derivatives have attracted strong attention recently due to their activity as prospective HIV integrase inhibitors [8,9].

As reported recently various quinoline derivatives inhibited oxygen evolution rate in spinach chloroplasts and they showed some antialgal properties [4,6,10-12]. In the current research, based on the analogy with the 8-hydroxy-2-methylquinoline-7-carboxamides (**I**) described in previous publications [11] we designed position isomers of the above mentioned derivatives – a series of 5-hydroxy-2-methylquinoline-6-carboxamides (**II**), which were evaluated as potential herbicides.

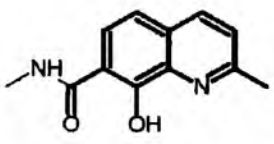

(I)

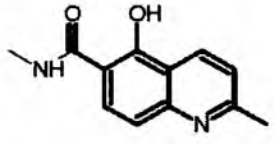

(II)

RESULTS AND DISCUSSION

The Skraup synthesis gave 5-hydroxy-2-methylquinoline-6-carboxylic acid that was nitrated to yield 5-hydroxy-2-methyl-8-nitroquinoline-6-carboxylic acid (**1**). 5-Hydroxy-2-methylquinoline-6-carboxylic acid further reacted with the appropriate amine in the presence of ethyldimethylaminopropyl carbodiimid (EDCI) or dicyclohexyl carbodiimid (DCC) to provide an amide. In case of compound **7** diamine and twofold of quinaldic acid were used. Compound **8** was prepared by reaction of twofold of 5-hydroxy-2-methyl-quinoline-6-carboxylic acid with urea. Synthetic pathways of all discussed quinoline derivatives **1-8** are shown in Scheme 1.

Scheme 1. Synthesis of compounds **1-8**: (a) Skraup synthesis; (b) HNO_3/H_2SO_4 5 °C; (c) amine, EDCI or DCC.

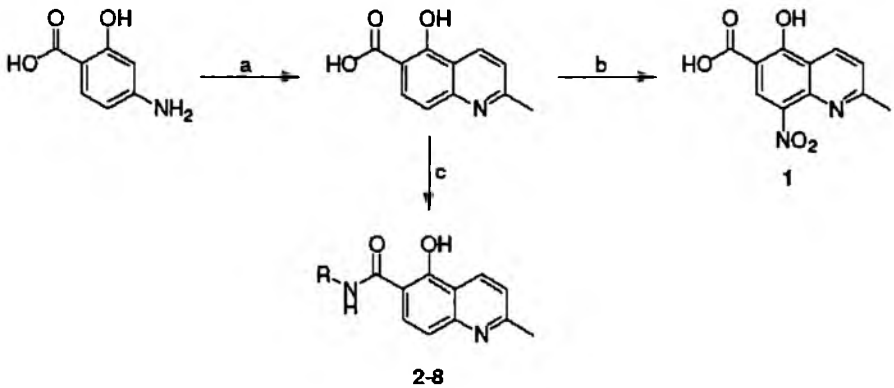

1

2-8

Hydrophobicities (log *P*/Clog *P* values) of the studied compounds **1-8** were calculated using two commercially available programs and also measured by means of the reversed phase high performance liquid chromatography (RP-HPLC) method for lipophilicity measurement. The procedure was performed under isocratic conditions with methanol as an organic modifier in the mobile phase using end-capped non-polar C_{18}

stationary RP column. The capacity factors K were determined and subsequent log K values were calculated. The results are shown in Table 1 and illustrated in Figure 1.

Table 1. Comparison of the calculated lipophilicities (log P/Clog P) with the determined log K values. IC_{50} values related to OER inhibition in spinach chloroplasts and reduction of chlorophyll content in C. *vulgaris* of compounds **1-8** in comparison with standard DCMU.

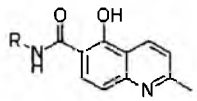

Comp.	R	log K	log P/Clog P ChemOffice	log P ACD/LogP	OER inhibition IC_{50} [µmol/L]	Chlorophyll reduction IC_{50} [µmol/L]
1	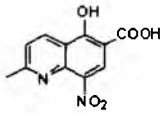	0.4072	1.95 / 3.235	2.47 ± 0.36	114.0	108.6 ± 11.3[a]
2	-Ph-4-Cl	0.3812	3.80 / 5.464	4.73 ± 0.42	265.0	23.8
3	$-CH_2Ph-4-CH_3$	0.3800	3.79 / 5.339	3.84 ± 0.41	468.0	97.2 ± 3.8
4	$-CH(CH_3)Ph-4-F$	0.3663	3.78 / 5.292	3.78 ± 0.47	426.0	100.0 ± 5.9[a]
5	$-C_2H_4Ph-4-OH$	0.3775	3.20 / 4.302	3.06 ± 0.40	16.0	102.5 ± 8.9[a]
6	$-C_4H_8Ph$	0.4173	4.42 / 5.877	4.68 ± 0.39	7.2	10.9
7	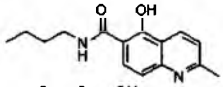	0.1203	3.01 / 6.303	3.51 ± 0.51	819.0	19.5
8	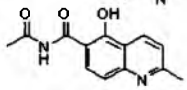	0.6120	3.20 / 6.223	3.31 ± 0.65	833.0	5.5
DCMU	-	-	2.76 / 2.691	2.78 ± 0.38	1.9	7.3

[a] IC_{50} was not determined for four compounds, an average decrease of Chl content related to the control for the concentration range of 0.83–100 µmol/L is indicated.

The results obtained with all the compounds show that the experimentally determined lipophilicities (log K values) are lower than those indicated by the calculated log P/Clog P, see Figure 1. The results show that experimentally determined log K values correlate relatively with calculated Clog P values, whereas log P data calculated using the ChemOffice software or ACD/Log P program do not agree with compounds **1-8**. As expected, dimmer **7** showed the lowest lipophilicity. Compound **8** possessed the highest hydrophobicity, which was unexpected. Acid **1** showed also high hydrophobicity contrary to all the results of the lipophilicity calculated softwares. If compared the lipophilicity results of position analogues presented in [11] it can be assumed, that 5-hydroxy derivatives **1-8** possessed higher hydrophobicity than 8-hydroxy analogues. This fact is caused by hydrogen bond between phenolic and carbonyl group [14] and/or ingeneration of hydrogen bond between phenolic and quinoline-nitrogen [4-6], due to their opposite positions.

Figure 1. Comparison of log P/Clog P values using the two programs with the calculated log K values of the compounds **1-8**.

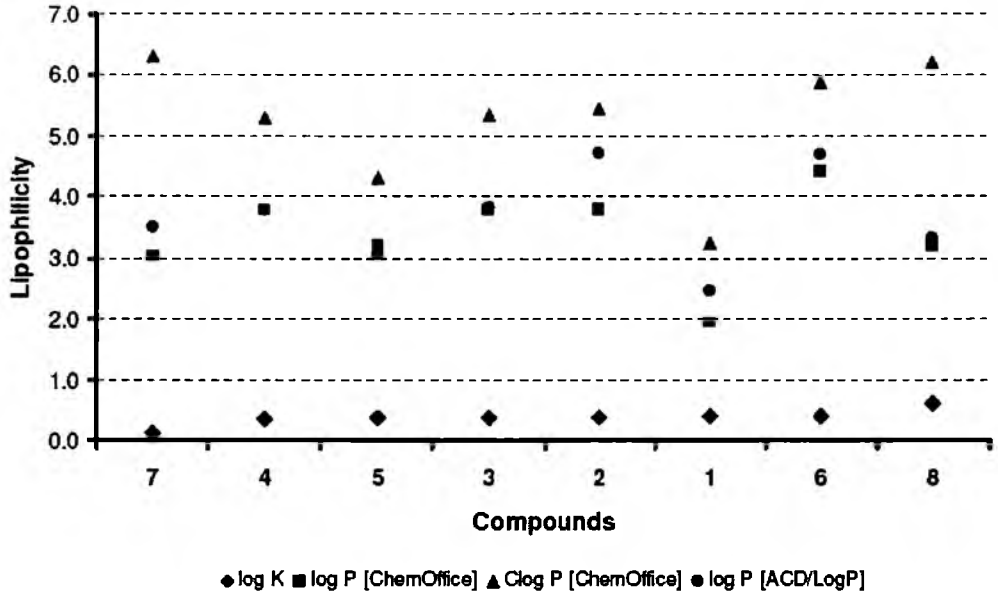

All compounds were evaluated for their *in vitro* herbicidal susceptibility. Some interesting results were obtained, see Table 1.

Derivatives of 5-hydroxy-2-methylquinoline-6-carboxylic acid **1-8** showed a wide range of OER-inhibiting activity in spinach chloroplasts activities. Two compounds showed interesting IC_{50} values: 7.2 μmol/L (**6**) and 16.0 μmol/L (**5**). The activity of compound **6** was comparable with DCMU. Both dimmers **7** and **8** possessed very low activity. Due to the small group and different structure types of the evaluated compounds **1-8** it is difficult to determine simple structure-activity relationships. However some observations seem to be interesting. It can be stated, that the lipophilicity is probably the secondary parameter for good activity as there is no good correlation between log *K* and the activity of compounds **1-8**. Poorly active compounds, when compared, showed some regularities between activity and structural properties, such as polarizability or molecular refraction, see Figure 2 and Figure 3.

Figure 2. OER inhibition {log (I/IC_{50} [mmol/L])} versus molecular mass of the studied compounds. The active compounds **5**, **6** and the poorly active compounds **1-4**, **7**, **8**.

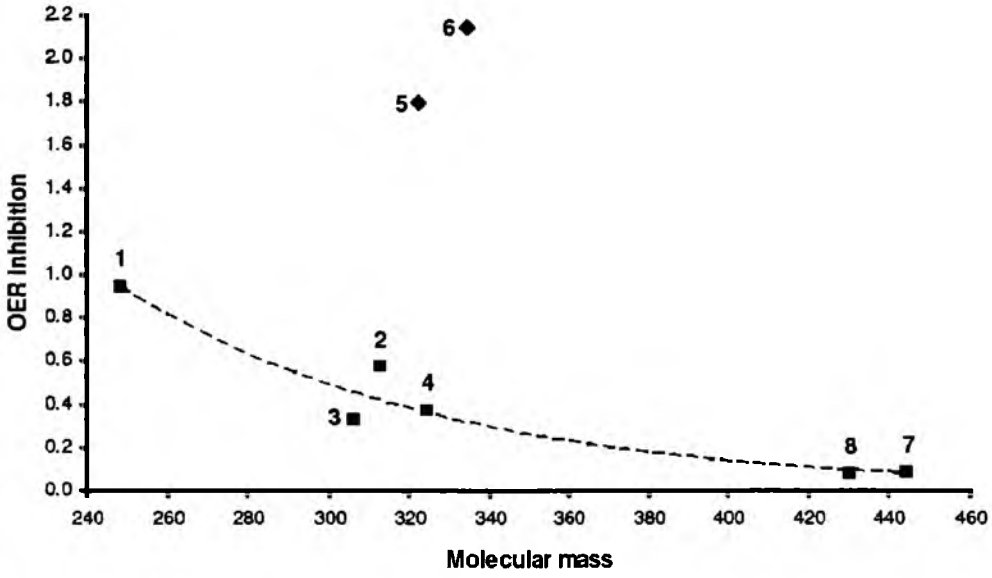

One can see that the activity dependence shown on Figure 2 is quite obvious as passive transport is important in fate of the active molecule in biological environment. Large molecules, usually highly lipophilic are less expected to achieve site of action. When compared molecular volume produces very similar changes in activity. Unfortunately the lack of compounds makes it difficult to predict the scope of preferable mass before further studies. Similar dependence can be observed for OER inhibition – polarizability/molecular refraction (Figure 3).

Figure 3. OER inhibition {log ($1/IC_{50}$ [mmol/L])} versus polarizability of compounds **1-4**, 7, **8**. The active compounds **5**, **6** and the poorly active compounds **1-4**, 7, **8**.

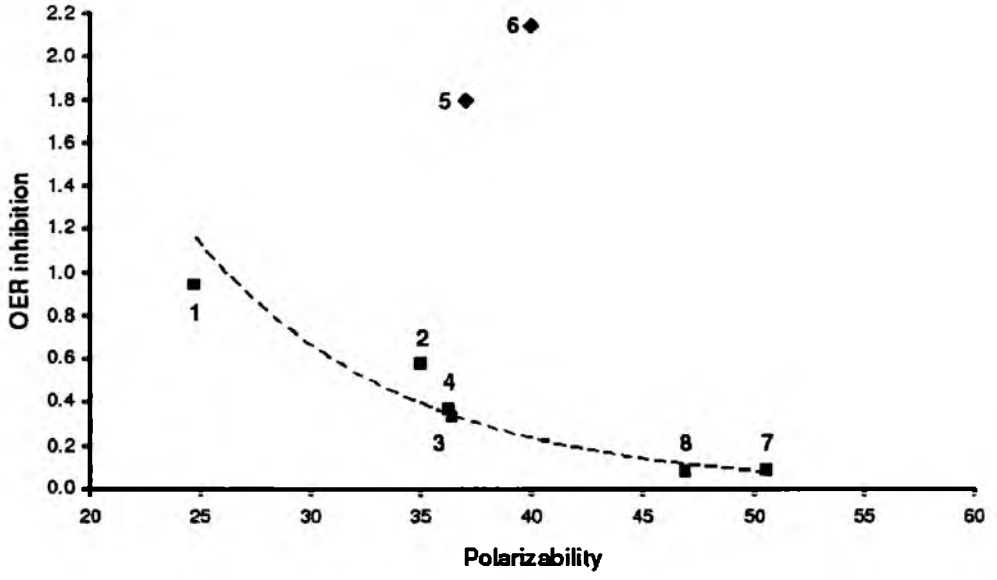

These regularities became even more important, if we compare them with two highly active compounds **5**, **6**. They are active despite the fact that all their properties suggest rather low OER activity. According to this we can guess that activity of two most active structures in OER measurements acts in different mechanism than the rest of the compounds.

Probably the more important parameter is the 2D distance between the quinoline nucleus and the $C_{(4)}$'-hydrogen/substituent in the phenyl ring.

5-Hydroxy-2-methylquinoline-6-carboxamides **2-8** possessed very interesting activity in reduction of chlorophyll content in *Chlorella vulgaris*. Compounds **2**, **6-8** (activity range 5.5-23.8 μmol/L) are potential herbicides with **8** the most active (IC_{50} = 5.5 μmol/L). According to Table 1 it seems, that there are better relationships between log *K* and the activity in series **1-8**. Anti-algal activity increased with the lipophilicity increase.

EXPERIMENTAL

General

All reagents were purchased from Aldrich. Kieselgel 60, 0.040-0.063 mm (Merck, Darmstadt, Germany) was used for column chromatography. TLC experiments were performed on alumina-backed silica gel 40 F254 plates (Merck, Darmstadt, Germany). The plates were illuminated under UV (254 nm) and evaluated in iodine vapour. The melting points were determined on Boetius PHMK 05 (VEB Kombinat Nagema, Radebeul, Germany) and are uncorrected. Elemental analyses were carried out on an automatic Perkin-Elmer 240 microanalyser (Boston, USA). The purity of the final compounds was checked by HPLC, see below. The detection wavelength 210 nm was chosen. The peaks in the chromatogram of the solvent (blank) were deducted from the peaks in the chromatogram of the sample solution. The

purity of individual compounds was determined from the area peaks in the chromatogram of the sample solution. UV spectra (λ, nm) were determined on a Waters Photodiode Array Detector 2996 (Waters Corp., Milford, MA, U.S.A.) in ca $6x10^{-4}$ mol methanolic solution and log ε (the logarithm of molar absorption coefficient ε) was calculated for the absolute maximum λ_{max} of individual target compounds. All ^{1}H NMR spectra were recorded on a Bruker AM-500 (499.95 MHz for ^{1}H), Bruker BioSpin Corp., Germany. Chemicals shifts are reported in ppm (δ) to internal $Si(CH_3)_4$, when diffused easily exchangeable signals are omitted.

5-Hydroxy-2-methyl-8-nitroquinoline-6-carboxylic acid (**1**). Product was obtained according to the described procedure [13]. Yield 53%. Mp 280 °C (decomp.). HPLC purity 94.25%. UV (nm), λ_{max}/log ε: 284.4 / 3.67.

General procedure of compounds 2-8

To solution prepared hydroxyquinaldinecarboxylic acids (1.02 g, 5.0 mmol) in dry CH_2Cl_2 with EDCI or DCC (0.6 mmol) was added of appropriate amine (5.3 mmol) in dry CH_2Cl_2 during 4 h. After the reaction was completed, solid was filtered, washed with 5% $NaHCO_3$, water and diethyl ether.

5-hydroxyquinaldine-6-carboxylic acid 4-chlorophenylamide (**2**). An orange crystalline compound. Yield 35%. Mp 176-178 °C. Anal. Calc. for $C_{17}H_{13}ClN_2O_2$+2H_2O (348.76): C 61.82%, H 4.55%; found: C 61.79%, H 4.21%. HPLC purity 94.13%. UV (nm), λ_{max}/log ε: 265.5 / 3.57. ^{1}H NMR (DMSO-d_6, 500 MHz) δ: 2.76 (s, 3H), 7.46 (d, *J*=8.45 Hz, 1H), 7.45 (d, *J*=7.5 Hz, 2H), 7.58 (d, *J*=8.4 Hz, 1H), 7.75 (d, *J*=7.5 Hz, 2H), 8.37 (d, *J*=9.2 Hz, 1H), 8.56 (d, *J*=8.8 Hz, 1H).

5-Hydroxyquinaldine-6-carboxylic acid 4-methylbenzylamide (**3**). A beige crystalline compound. Yield 50%. Mp 184-186 °C. Anal. Calc. for $C_{18}H_{18}N_2O_2$+2H_2O (342.37): C 65.80%, H 6.49%; found: C 65.85%, H 6.77%. HPLC purity 98.95%. UV (nm), λ_{max}/log ε: 257.2 / 3.57. ^{1}H NMR (DMSO-d_6, 500 MHz) δ: 2.28 (s, 3H), 2.65 (s, 3H), 3.95 (s, 2H), 7.10 (d, *J*=7.5 Hz 1H), 7.20 (d, *J*=8.5 Hz, 1H), 7.30 (d, *J*=8.5 Hz, 1H), 7.40 (d, *J*=7.6 Hz, 2H), 7.90 (d, *J*=7.6 Hz, 2H), 8.0 (bs, 1H), 8.60 (d, *J*=8.2 Hz, 1H).

5-Hydroxy-2-methylquinoline-6-carboxylic acid [1-(4-fluorophenyl)-ethyl]-amide (**4**). A bright brown solid. Yield 31%. Mp 240 °C (decomp). Anal. Calc. for $C_{19}H_{17}FN_2O_2$+H_2O (342.36): C 66.66%, H 5.59%; found: C 67.02%, H 5.39%. HPLC purity 81.13%. UV (nm), λ_{max}/log ε: 260.7 / 3.56. ^{1}H NMR (DMSO-d_6, 500 MHz) δ: 1.65 (d, 3H), 2.7 (d, 3H), 4.6 (q, 1H), 7.35-7.5 (m, 11H), $[\alpha]^{20}$=5 °.

5-hydroxyquinaldine-6-carboxylic acid 2-(4-hydroxyphenyl)-ethylamide (**5**). Product was obtained according to the described procedure [13]. Yield 47%. Mp 114-117 °C. HPLC purity 95.83%. UV (nm), λ_{max}/log ε: 258.4 / 3.54.

5-hydroxyquinaldine-6-carboxylic acid (4-phenylbuthyl)-amide (**6**). A beige crystalline compound. Yield 52%. Mp 156-159 °C. Anal. Calc. for $C_{21}H_{22}N_2O_2$+H_2O (352.42): C 71.60%, H 6.82%; found: C 71.38%, H 7.34%. HPLC purity 98.63%. UV (nm), λ_{max}/log ε: 257.2 / 3.52. ^{1}H NMR (DMSO-d_6, 500 MHz) δ: 1.48-1.60 (m, 4H), 2.60 (m, 5H); 2.75 (t, 2H), 6.95 (d, *J*=8.5 Hz, 1H), 7.15 (d, *J*=7.9 Hz, 1H), 7.20-7.30 (m, 5H), 760 (bs, 1H); 7.88 (d, *J*=8.5 Hz, 1H), 8.48 (d, *J*=8.6 Hz, 1H).

bis-(5-Hydroxy-2-methylquinoline-6-carboxylic acid)-1,3-propylamide (7). A light brown crystalline compound. Yield 24%. Mp 226 °C. Anal. Calc. for $C_{25}H_{24}N_4O_4$+2H_2O (480.49): C 61.35%, H 5.93%; found: C 61.65%, H 6.05%. HPLC purity 92.56%. UV (nm), λ_{max}/log ε: 248.9 / 3.56. ^{1}H NMR (DMSO-d_6, 500 MHz) δ: 1.85 (s, 2H), 2.35 (s, 6H), 2.90 (t, 4H), 6.95 (d, *J*=8.65 Hz, 2H), 7.10 (d, *J*=9.35 Hz, 2H), 7.85 (d, *J*=8.6 Hz, 2H), 7.94 (bs, 1H), 8.55 (d, *J*=7.5 Hz, 2H), 18.15 (s, 2H).

1,3-bis-(5-Hydroxyquinaldine-6-carboxyl)-urea (**8**). A yellow crystalline compound. Yield 29%. Mp 206 °C. Anal. Calc. for $C_{23}H_{18}N_4O_5$+H_2O (448.42): C 60.99%, H 4.53; found: C 60.84%, H 4.95%.HPLC purity 94.75%. UV (nm), λ_{max}/log ε: 263.1 / 3.55. ^{1}H NMR (DMSO-d_6, 500 MHz) δ: 2.63 (s, 6H), 7.15 (d, *J*=8.1 Hz, 2H), 7.35 (d, *J*=8.15 Hz, 2H), 8.05 (d, *J*=8.75 Hz, 2H), 8.70 (d, *J*=8.65 Hz, 2H).

Lipophilicity HPLC determination (capacity factor K / calculated log K)

The HPLC separation module Waters Alliance 2695 XE and Waters Photodiode Array Detector 2996 (Waters Corp., Milford, MA, U.S.A.) were used. The chromatographic column Symmetry® C_{18} 5 µm, 4.6x250 mm, Part No. WAT054275, (Waters Corp., Milford, MA, U.S.A.) was used. The HPLC separation process was monitored by Millennium32® Chromatography Manager Software, Waters 2004 (Waters Corp., Milford, MA, U.S.A.). The mixture of MeOH p.a. (55.0%) and H_2O-HPLC – Mili-Q Grade (45.0%) was used as a mobile phase. The total flow of the column was 0.9 mL/min, injection 30 µL, column temperature 30 °C and sample temperature 10 °C. The detection wavelength 210 nm was chosen. The KI methanolic solution was used for the dead time (T_D) determination. Retention times (T_R) were measured in minutes.

The capacity factors *K* were calculated using the Millennium32® Chromatography Manager Software according to formula $K = (T_R - T_D) / T_D$, where T_R is the retention time of the solute, whereas T_D denotes the dead time obtained via an unretained analyte. Log *K*, calculated from the capacity factor *K*, is used as the lipophilicity index converted to log *P* scale. The log *K* values of the individual compounds are shown in Table 1.

Lipophilicity calculations

Log *P*, *i.e.* the logarithm of the partition coefficient for *n*-octanol/water, was calculated using the programs CS ChemOffice Ultra ver. 9.0 (CambridgeSoft, Cambridge, MA, U.S.A.) and ACD/LogP ver. 1.0 (Advanced Chemistry Development Inc., Toronto, Canada). Clog *P* values (the logarithm of *n*-octanol/water partition coefficient based on established chemical interactions) were generated by means of CS ChemOffice Ultra ver. 9.0 (CambridgeSoft, Cambridge, MA, U.S.A.) software. The results are shown in Table 1.

Study of inhibition of oxygen evolution rate (OER) in spinach chloroplasts

Chloroplasts were prepared by the procedure of Walker from spinach (*Spinacia oleracea* L.) [15]. The inhibition of photosynthetic electron transport (PET) in spinach chloroplasts was determined spectrophotometrically (Kontron Uvikon 800, Kontron, Muenchen, Germany) using an artificial electron acceptor 2,6-dichlorophenol-indophenol (DCIPP) according to Kralova et al. [16] and the rate of photosynthetic electron transport was monitored as a photoreduction of DCPIP. The measurements were carried out in phosphate buffer (0.02 mol/L, pH 7.2) containing sucrose (0.4 mol/L), $MgCl_2$ (0.005 mol/L) and NaCl (0.015 mol/L). The chlorophyll content was 30 mg/L in these experiments and the samples were irradiated (~100 W/m^2) from 10 cm distance with a halogen lamp (250 W) using a 4 cm water filter to prevent warming of the samples (suspension temperature 22 °C). The studied compounds were dissolved in DMSO due to their limited water solubility. The applied DMSO concentration (up to 4%) did not affect the photochemical activity in spinach chloroplasts (PET). The inhibitory efficiency of the studied compounds has been expressed by IC_{50} values, *i.e.* by molar concentration of the compounds causing 50% decrease in the oxygen evolution relative to the untreated control. The comparable IC_{50} value for a selective herbicide 3-(3,4-dichlorophenyl)-1,1-dimethylurea, DCMU (Diurone®) was about 1.9 µmol/L [17]. The results are summarized in Table 1.

Reduction of chlorophyll content in the green algae Chlorella vulgaris Beij.

The green algae C. *vulgaris* Beij. was cultivated statically at room temperature according to Kralova et al. [18] (photoperiod 16 h light/8 h dark; photosynthetic active radiation 80 µmol/m^2.s; pH 7.2). The effect of the compounds on algal chlorophyll (Chl) content was determined after 7-day cultivation in the presence of the tested compounds. The Chl content in the algal suspension was determined spectrophotometrically (Kontron Uvikon 800, Kontron, Muenchen, Germany) after extraction into methanol according to Wellburn [19]. The Chl content in the suspensions at the beginning of the cultivation was 0.01 mg/L. The applied compound concentrations were as follows: 100, 75, 50, 25, 8.3, 4.2 and 0.83 µmol/L. Because of the low solubility of the studied compounds in water, these were dissolved in DMSO. DMSO concentration in the algal suspensions did not exceed 0.25% and the control samples contained the same DMSO amount as the suspensions treated with the tested compounds. The antialgal activity of the compounds was expressed as IC_{50} (the concentration of the inhibitor causing a 50% decrease in

content of chlorophyll as compared with the control sample) or as a percentage of the control determined for the studied concentration range (100-0.83 μmol/L) with a corresponding standard deviation (S.D.). Comparable IC_{50} value for a selective herbicide 3-(3,4-dichlorophenyl)-1,1-dimethylurea, DCMU (Diurone®) was about 7.3 μmol/L [17]. The results are summarized in Table 1.

Acknowledgements. This study was supported by KBN Warsaw 3T09A01127, by the Ministry of Education of the Czech Republic MSM 6215712403, and by the Slovak Scientific Grant Agency VEGA 1/0089/03.

REFERENCES

1. Roberts, D.H.; Hutson, T.R. (Eds.), *Herbicides*, Vol. 6, **1987**.
2. Roth, H.J.; Fenner, H. In *Arzneistoffe* 3rd ed.; Deutscher Apotheker Verlag: Stuttgart, **2000**; pp. 51-114.
3. Jampilek, J.; Dolezal, M.; Kunes, J.; Buchta, V. *ECSOC-8* **2004**, c005, http://www.lugo.usc.es/%7Eqoseiias/ECSOC-8/BOCNP/005/index.htm.
4. Jampilek, J.; Dolezal, M.; Kunes, J.; Buchta, V.; Kralova, K. *Med. Chem.* **2005**, *1*, 591.
5. Musiol, R.; Jampilek, J.; Buchta, V.; Silva, L.; Niedbala, H.; Podeszwa, B.; Palka, A.; Majerz-Maniecka, K.; Oleksyn, B.; Polanski, J. *Bioorg. Med. Chem.* **2006**, *14*, 3592.
6. Musiol, R.; Jampilek, J.; Kralova, K.; Richardson, D.R.; Kalinowski, D.; Podeszwa, B.; Finster, J.; Niedbala, H.; Palka, A.; Polanski, J. *Bioorg. Med. Chem.* **2007**, *15*, 1280.
7. Podeszwa, B.; Niedbala, H.; Polanski, J.; Musiol, R.; Tabak, D.; Finster, J.; Serafin, K.; Milczarek, M.; Wietrzyk, J.; Boryczka, S.; Mol, W.; Jampilek, J.; Dohnal, J.; Kalinowski, D.S.; Richardson, D.R. *Bioorg. Med. Chem. Lett.* **2007**, *17*, in press.
8. Polanski, J.; Zouhiri, F.; Jeanson, L.; Desmaele, D.; d'Angelo, J.; Mouscadet, J.; Gieleciak, R.; Gasteiger, J.; Bret, M. L. *J. Med. Chem.* **2002**, *45*, 4647.
9. Polanski, J.; Niedbala, H.; Musiol, R.; Tabak, D.; Podeszwa, B.; Gieleciak, R.; Bak, A.; Palka, A.; Magdziarz, T. *Acta Poloniae Pharm. Drug Res.* **2004**, *61*, 3.
10. Musiol, R.; Jampilek, J.; Kralova, K.; Podeszwa, B.; Finster, J.; Niedbala, H.; Palka, A.; Polanski, J. *ECSOC-9* **2005**, c005, http://www.usc.es/congresos/ecsoc/9/BOCNP/c005/index.htm.
11. Musiol, R.; Jampilek, J.; Kralova, K.; Tabak, D.; Podeszwa, B.; Finster, J.; Polanski, J. *ECSOC-10* **2006**, c007, http://www.usc.es/congresos/ecsoc/10/ECSOC10.htm.
12. Musiol, R.; Jampilek, J.; Kralova, K.; Tabak, D.; Finster, J.; Podeszwa, B.; Polanski, J. *Bioorg. Med. Chem.* **2007**, submitted.
13. Polanski, J.; Niedbala, H.; Musiol, R.; Podeszwa, B.; Tabak, D.; Palka, A.; Mencel, A.; Mouscadet, J.F.; Le Bret, M. *Lett. Drugs Des. Disc.* **2007**, *4*, 99.
14. Dolezal, M.; Jampilek, J.; Osicka, Z.; Kunes, J.; Buchta, V.; Vichova, P. *Farmaco* **2003**, *58*, 1105.
15. Walker, D. A. In *Methods in Enzymology* Part C; Colowick, S.P.; Kaplan, N.O. Ed.; Academic Press: New York, **1980**; Vol. 69, pp. 94-104.
16. Kralova, K.; Sersen, F.; Sidoova, E. *Chem. Pap.* **1992**, *46*, 348.
17. Fedke, C. *Biochemistry and Physiology of Herbicide Actio*n; Springer Verlag: Berlin-Heidelberg-New York, **1982**.
18. Kralova, K.; Sersen, F.; Melnik, M. *J. Trace Microprobe Techn.*, **1998**, *16*, 491.
19. Wellburn, A.R. *J. Plant. Physiol.*, **1994**, *144*, 307.

12th International Electronic Conference on Synthetic Organic Chemistry (ECSOC-12) 1-30 November 2008
http://www.usc.es/congresos/ecsoc/12/ECSOC12.htm & http://www.mdpi.org/ecsoc-12

[C0012]

Ring-substituted 4-Hydroxy-1*H*-quinolin-2-ones: Preparation and Their Photosynthesis-inhibiting Activity

Robert Musiol[1]*, Josef Jampilek[2*,3], Katarina Kralova[4], Jacek Finster[1], Dominik Tabak[1], Halina Niedbala[1], Jozef Csollei[3], Jiri Dohnal[2,3], Jaroslaw Polanski[1]

[1] Institute of Chemistry, University of Silesia, Szkolna 9, 40007 Katowice, Poland; e-mail: rmusiol@us.edu.pl, tel: +48-32-3591206, fax: +48-32-2599978

[2] Zentiva a.s., U kabelovny 130, 102 37 Prague 10, Czech Republic; e-mail: josef.jampilek@zentiva.cz, tel: +420-2-67243695, fax: +420-2-72701331

[3] Department of Chemical Drugs, Faculty of Pharmacy, University of Veterinary and Pharmaceutical Sciences, Palackeho 1/3, 61242 Brno, Czech Republic

[4] Institute of Chemistry, Faculty of Natural Sciences, Comenius University, Mlynska dolina Ch-2, 84215 Bratislava, Slovakia

* Authors to whom correspondence should be addressed.

Abstract: The series of twelve ring-substituted 4-hydroxy-1*H*-quinolin-2-one derivatives were prepared. The synthetic procedures of the compounds are presented. All the prepared quinoline derivatives were analyzed using RP-HPLC method for the lipophilicity measurement and their lipophilicity was determined. The prepared compounds were tested for their photosynthesis-inhibiting activity (the inhibition of photosynthetic electron transport in spinach chloroplasts (*Spinacia oleracea* L.). The relationships between the lipophilicity and the chemical structure of the studied compounds are discussed as well as the structure-activity relationships (SAR) between the chemical structure and the biological activities of the evaluated compounds.

Keywords: Quinolinone derivatives; Lipophilicity; OER inhibition; Spinach chloroplasts; Structure-activity relationships.

INTRODUCTION

The Q_B quinone-binding site of photosystem II is an important target for herbicides including herbicides based on phenylurea moieties. It was found that a tail can be attached to the *para* position of phenylurea-type herbicides without loss of binding, provided that the tail is hydrophobic. This indicates that the herbicides must be oriented in the Q_B site so that these positions point toward the natural isoprenyl tail-binding pocket that extends out of the Q_B site. In turn, the requirement that the tail must extend out of the Q_B site constrains the size of the other herbicide substituents in the pocket [1]. In addition to these herbicides various compounds possessing an amide -NHCO- functionality were found to inhibit photosynthetic electron transport as well [2-5]. Better understanding of the SAR regularities are not only important for the design of modern agricultural agents but can also give the remarkable insight into the photosynthesis mechanisms of the green cells.

Quinoline scaffold is present in many classes of biologically active compounds [6]. A series of compounds derived from 8-hydroxyquinoline and styrylquinoline derivatives as potential HIV-1 integrase inhibitors were synthesized recently [7-10]. Our study dealing with 8-hydroxyquinoline and styrylquinoline derivatives showed that they could possess also strong antifungal activity [11-13]. According to the results reported recently some new hydroxyquinoline derivatives possess interesting herbicidal activities as well [12,14-18]. Some investigated compounds showed also antineoplastic activity [19].

This paper deals with synthesis and herbicidal activity of ring-substituted 4-hydroxy-1*H*-quinolin-2-one derivatives. All the compounds were tested for their photosynthesis-inhibiting activity (the inhibition of photosynthetic electron transport in spinach chloroplasts (*Spinacia oleracea* L.). Lipophilicity (log *k*) of the compounds was determined using RP-HPLC. The procedure was performed under isocratic conditions with methanol as an organic modifier in the mobile phase using end-capped non-polar C_{18} stationary RP column. The structure-activity relationships of the studied compounds are discussed in the present study as well.

RESULTS AND DISCUSSION

Chemistry

In most of described synthesis aniline derivatives were used as starting materials for their great availability from chemical vendors. Microwave assisted synthesis with malonic acid or its esters provide us compounds **1**-**4**. Further nitration and reduction according to known procedures appeared to be succeful in obtaining compounds **6** and **7**. Diazo derivative **5** was synthesised from **3** with dichloroaniline. Acylation of **7** with cinnamoyl chloride provide us compound **8**. Quinolines functionalized with carboxylic group at $C_{(3)}$ **9**, **10** and **11** were obtained in neat microwave assisted synthesis with moderate or good yield. Structure **12** was obtained according to modified procedure from 4-Hydroxyquinolin-2(1H)-one (**1**).

Scheme 1. Synthesis of quinoline derivatives **1-12**: (a) PPA, microwave irradiation; (b) (2,5-dichloro-4-nitrophenyl)diazonium chloride; (c) HNO_3; (d) Sn, HCl; (e) cinnamoyl chloride; (f) microwave irradiation; (g) hydrolysis; (h) NaH.

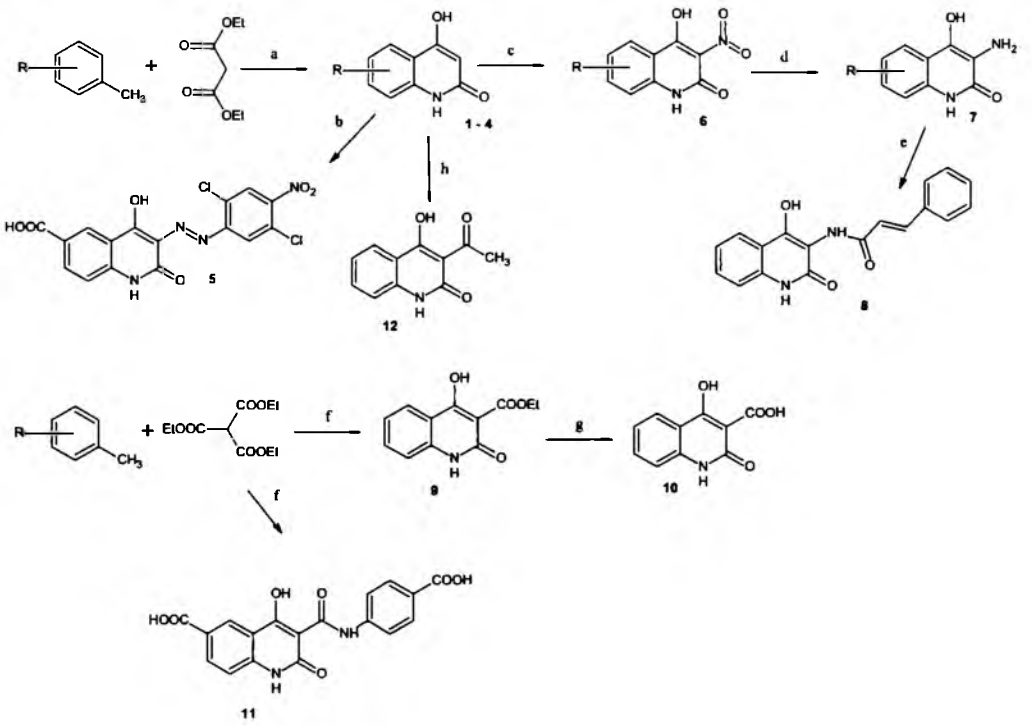

Hydrophobicities (log *P*/Clog *P* values) of the studied compounds **1-12** were calculated using two commercially available programs and also measured by means of the reversed phase high performance liquid chromatography (RP-HPLC) method for lipophilicity measurement. The procedure was performed under isocratic conditions with methanol as an organic modifier in the mobile phase using an end-capped non-polar C_{18} stationary RP column. The capacity factors *k* were determined and subsequent log *k* values were calculated. The results are shown in Table 1 and illustrated in Figure 1.

Table 1. Comparison of the calculated lipophilicities (log *P*/Clog *P*) with the determined log *k* values. IC_{50} values related to OER inhibition in spinach chloroplasts of compounds **1-12** in comparison with standard DCMU.

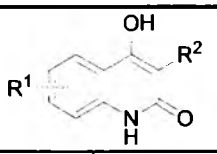

Comp.	R^1	R^2	log *k*	log *P*/Clog *P* ChemOffice	log *P* ACD/LogP	OER inhibition IC_{50} [μmol/L]
1	H	H	0.0664	0.49 / 1.216	1.10 ± 0.75	925
2	6-CH_3	H	0.3307	0.97 / 1.715	1.56 ± 0.75	157
3	6-COOH -5-OH	H	0.0002	-0.34 / 1.261	1.47 ± 0.75	346
4	6-COOH -7-OH	H	0.0080	-0.34 / 1.070	2.22 ± 0.75	538
5	6-COOH	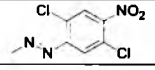	0.6394	5.22 / 3.840	4.41 ± 1.00	126
6	H	-NO_2	0.4052	1.39 / 0.836	-0.14 ± 1.00	510
7	H	-NH_2	0.0004	-1.06 / 0.719	-0.32 ± 1.00	775
8	H	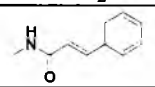	0.0128	1.11 / 2.848	2.45 ± 1.00	916
9	H	-$COOC_2H_5$	0.4595	0.51 / 1.694	1.17 ± 0.75	494
10	H	-COOH	0.0118	-0.09 / 1.409	1.71 ± 0.35	567
11	6-COOH	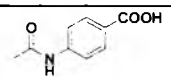	0.0081	0.27 / 2.445	1.67 ± 1.00	380
12	H	-$COCH_3$	0.0005	-0.24 / 1.012	-0.11 ± 1.00	[a]
DCMU	–	–	–	2.76 / 2.691	2.78 ± 0.38	1.9

[a] interacted with DCPIP.

The results obtained with all the compounds show that the experimentally determined lipophilicities (log *k* values) are lower than those indicated by the calculated log *P*/Clog *P*, see Figure 1. The results show that experimentally determined log *k* values correlate relatively poorly. As expected, compound **5** showed the highest lipophilicity, while compound **3** possessed the lowest hydrophobicity, which was unexpected. Compound **8** showed less hydrophobicity contrary to all the results of the lipophilicity calculated by software. If compared the lipophilicity data log *k* of both position analogues **3** and **4** it can be stated, that 7-hydroxy derivative **4** possessed higher hydrophobicity than 5-hydroxy analogue **3**. This fact is caused by intramolecular interactions [20].

Figure 1. Comparison of the computed log *P*/Clog *P* values using the two programs with the calculated log *k* values. The discussed compounds **1-12** are ordered according to the log *k* values increase.

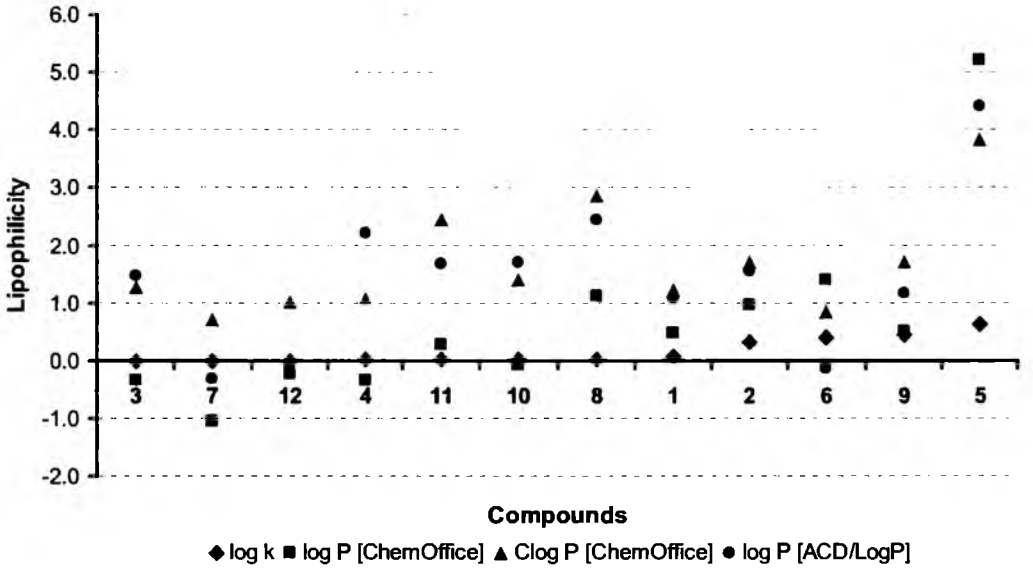

All compounds were evaluated for their *in vitro* herbicidal efficiency. The results are showed in Table 1.

Quinoline derivatives **1-11** showed a wide range of activity related to OER inhibition in spinach chloroplasts activities. Two compounds showed interesting IC_{50} values: 126 μmol/L (**5**) and 157 μmol/L (**2**); nevertheless the studied activity of all the other compounds was very low.

Due to the medium and/or moderate activity of all the evaluated compounds **1-11** it is difficult to determine simple structure-activity relationships. However some observations seem to be interesting.

Unsubstituted structure (compound **1**) did not practically affect OER in chloroplasts. The studied compounds could be divided into two groups according to their chemical structure. Group 1 includes compounds **2-5** and **11**, and Group 2 compounds **6-10**.

Group 1 showed higher biological activity than Group 2. The activity related to OER inhibition seems to be positively influenced by substitution of ring B – especially the $C_{(6)}$ position, see compounds **2-4**, **11**. Comparison of the OER-inhibiting activities of compounds **2-5** and **11** also indicated, that the lipophilicity increase is connected with the quasi-parabolic increase of biological activity, see Figure 2. Interesting are great differences in inhibition of OER of position analogues **3** (6-COOH-5-OH) and **4** (6-COOH-7-OH). Higher inhibiting effect of **5** compared with **2** may be caused by higher lipophilicity (easier penetration of compound to cell) and/or redox properties of nitro moiety of 2,5-dichloro-4-nitrophenyldiazenyl substituent.

Figure 2. Relationships between the OER inhibition log ($1/IC_{50}$) [mmol/L] in spinach chloroplasts and lipophilicity (log *k*) of the studied compounds **1-12**.

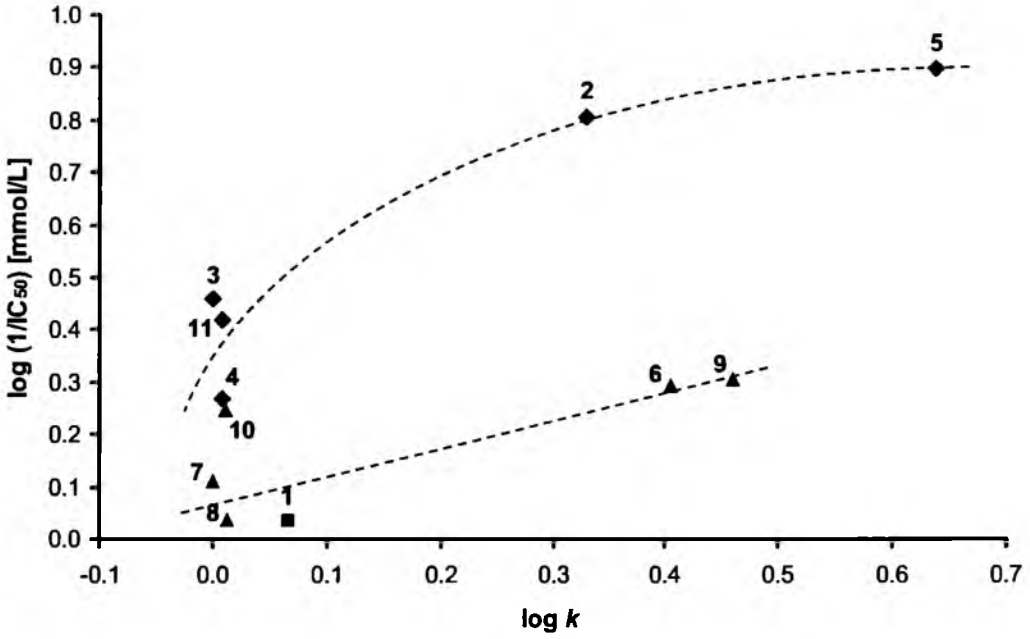

Generally, Group 2 inhibited OER only slightly; nevertheless the compounds **6** and **9** were approximately twice as efficient as the compound **1**. All these compounds possess the substituted position $C_{(3)}$ of ring A, that caused decrease of OER inhibition compared to Group 1. The most active compound from Group 2 was ester **9**.

EXPERIMENTAL

General

All reagents were purchased from Aldrich. Kieselgel 60, 0.040-0.063 mm (Merck, Darmstadt, Germany) was used for column chromatography. TLC experiments were performed on alumina-backed silica gel 40 F254 plates (Merck, Darmstadt, Germany). The plates were illuminated under UV (254 nm) and evaluated in iodine vapour. The melting points were determined on Boetius PHMK 05 (VEB Kombinat Nagema, Radebeul, Germany) and are uncorrected. Elemental analyses were carried out on an automatic Perkin-Elmer 240 microanalyser (Boston, USA). The purity of the final compounds was checked by HPLC, see section 4.3. The detection wavelength 210 nm was chosen. The peaks in the chromatogram of the solvent (blank) were deducted from the peaks in the chromatogram of the sample solution. The purity of individual compounds was determined from the area peaks in the chromatogram of the sample solution. UV spectra (λ, nm) were determined on a Waters Photodiode Array Detector 2996 (Waters Corp., Milford, MA, U.S.A.) in ca 6×10^{-4} mol methanolic solution and log ε (the logarithm of molar absorption coefficient ε) was calculated for the absolute maximum λ_{max} of individual target compounds. All ^{1}H NMR spectra were recorded on a Bruker AM-500 (499.95 MHz for ^{1}H), Bruker BioSpin Corp., Germany.

Chemicals shifts are reported in ppm (δ) to internal $Si(CH_3)_4$, when diffused easily exchangeable signals are omitted.

Synthesis

4-Hydroxyquinolin-2(1H)-one (1).
Aniline (7 mL, 5 mmol) and malonic acid (5.2 g, 5 mmol) was thoroughly mixed with 20 g PPA {P_2O_5 (287.9 g) was added to 85% phosphoric acid (200 g, 118.4 mL) with stirring and microwave heating. The mixture was then heated for next 15 min.} and heated with stirring in microwave reactor at 400 W during 2×20 min with 5 min interval. Temperature reached 210 °C. Then the mixture was pour into crushed ice and a cream solid was filtered and purified by extraction with EtOH and a white crystalline compound was obtained [21]. Yield 35%. Mp 340 °C. HPLC purity 97.12%. UV (nm), λ_{max}/log ε: 231.3 / 3.51.

4-Hydroxy-6-methylquinolin-2(1H)-one (2).
The product was obtained according to the described procedure [22, 23] as a light brown crystalline compound. Yield 54%. Mp 320 °C. HPLC purity 97.72%. UV (nm), λ_{max}/log ε: 232.4 / 3.55.

4,5-Dihydroxy-2-oxo-1,2-dihydroquinoline-6-carboxylic acid (3).
Naphthalene (15.4 g, 0.12 mol) and malonic acid (18.7 g, 0.18 mol) were melted with stirring at temperature control (<150 °C) to avoid decarboxylation of acid. $POCl_3$ (32.9 g, 0.36 mol) was then added dropwise during 30 min and *p*-aminosalicylic acid (15.3 g, 0.1 mol) was added. The resulted mixture was heated for next 30 min and left for cooling. Water (100 mL) was added to the warm mixture and the solution was alkalized with 20% NaOH to pH 9. After cooling on ice precipitated naphthalene was filtered and filtrate was acidified to pH 2. The product was filtered and crystallized from acetic acid as a bright yellow crystalline compound. Yield 36%. Mp 250 °C. Anal. Calc. for $C_{10}H_7NO_5$ (221.16): C 54.31%, H 3.19%; found: C 54.51%, H 4.11%. HPLC purity 98.74%. UV (nm), λ_{max}/log ε: 244.2 / 3.54. ^{1}H NMR (DMSO-d_6, 500 MHz) δ: 5.65 (s, 1H), 6.60 (d, *J*=8.3 Hz, 1H), 7.80 (d, *J*=8.3 Hz, 1H), 11.3 (bs, 1H), 12.20 (bs, 1H). IR [cm^{-1}] 3601, 2895, 1664, 1603, 1537, 1509, 1245

4,7-Dihydroxy-2-oxo-1,2-dihydroquinoline-6-carboxylic acid (4).
The product was obtained as isomer of **3** during its synthesis. Isolated by fractional crystalization as a white crystalline compound. Yield 36%. Mp 250 °C. Anal. Calc. for $C_{10}H_7NO_5$ (221.16): C 54.31%, H 3.19%; found: C 54.09%, H 3.52%. HPLC purity 98.51%. UV (nm), λ_{max}/log ε: 243.0 / 3.54. ^{1}H NMR (DMSO-d_6, 500 MHz) δ: 5.60 (s, 1H), 6.67 (s, 1H), 8.25 (s, 1H).

(E)-3-[(2,5-Dichloro-4-nitrophenyl)diazenyl]-4-hydroxy-2-oxo-1,2-dihydroquinoline-6-carboxylic acid (5).
2,5-Dichloro-4-nitroaniline (0.92 g) was dissolved in Et_2O/EtOH : 2/1, then 15% HCl (0.91 mL) was added to this solution and the mixture was cooled to 5 °C. $NaNO_2$ (0.39 g, 5.7 mmol) and compound **3** (1.0 g, 5.7 mmol) were added slowly with temperature still at 5 °C and pH<7 (15% HCl). The resulting mixture was standing overnight in ice. The precipitated solid was then filtered and crystallized from Et_2O/EtOH. A reddish crystalline compound was obtained. Yield 64%. Mp 340 °C. Anal. Calc. for $C_{16}H_8Cl_2N_4O_6$ (423.16): C 45.41%, H 1.91%; found: C 45.26%, H 2.24%. HPLC purity 96.39%. UV (nm), λ_{max}/log ε: 271.4 /

3.61.^{1}H NMR (DMSO-d_6, 500 MHz) δ: 5.70 (s, 1H), 7.10-7.60 (m, 3H), 11.10 (s, 1H), 11.30 (s, 1H).

4-Hydroxy-3-nitroquinolin-2(1H)-one (6).
The product was obtained according to the described nitration procedure [24] as a yellow crystalline compound. Yield 71%. Mp 252-255 °C. HPLC purity 99.72%. UV (nm), λ_{max}/log ε: 336.8 / 3.57.

3-Amino-4-hydroxyquinolin-2(1H)-one (7).
Compound **6** (2.0 g, 0.0097 mol) and tin powder (3.8 g, 0.032 mol) were stirred with 36% HCl (8.1 mL). The mixture was warmed at 80-90 °C during 30 min. The brown solution was cooled to room temperature and filtered. The filtrate was alkalized with $NH_{3(aq)}$ and warmed for 20 min. Then Celite (1.3 g) was added and filtered. The solid was washed thoroughly with hot water. The combined filtrates were concentrated and acidified. After cooling a white crystalline compound was obtained. Yield 85%. Mp 300 °C [25]. HPLC purity 91.99%. UV (nm), λ_{max}/log ε: 232.8 / 3.53.

(2E)-N-(4-Hydroxy-2-oxo-1,2-dihydroquinolin-3-yl)-3-phenylprop-2-enamide (8).
Compound **7** (0.018 g, 0.001 mol) was mixed with water (5 mL), Et_2O (5 mL) and sodium bicarbonate (0.3 g). The resulted mixture was stirred in an ice bath (-3 °C) and 10 mL of Et_2O solution of cynamoyl chloride (0.017 g, 0.001 mol) was added slowly. The resulted mixture was stirred in room temperature during 2 days, cooled in fridge and filtered. Et_2O was added to the solid and dried. A white crystalline compound was obtained. Yield 50%. Mp 145 °C. Anal. Calc. for $C_{18}H_{14}N_2O_3$+H_2O (324.33): C 66.66%, H 4.97%; found: C 66.54%, H 5.27%. HPLC purity 99.79%. UV (nm), λ_{max}/log ε: 263.1 / 3.51.^{1}H NMR (DMSO-d_6, 500 MHz) δ: 3.30 (s, 1H), 6.50 (d, J=16.2 Hz, 2H), 7.10 (s, 1H), 7.38 (m, 9H), 7.5 (s, 1H).

Ethyl 4-hydroxy-2-oxo-1,2-dihydroquinoline-3-carboxylate (9).
Aniline (0.46 mL, 0.005 mol) and triethyl methanetricarboxylate (2.12 mL, 0.01 mol) was heated in microwave reactor during 8 min at 60% power level. The mixture was then cooled to room temperature and 7 mL of Et_2O was added. The crude product was crystallized from MeOH. A white crystalline compound was obtained. Yield 50%. Mp 116-120 °C. TLC(SiO_2, R_f=0.71) Anal. Calc. for $C_{12}H_{11}NO_4$ (233.22): C 61.8%, H 4.75%; found: C 61.65%, H 4.39%. HPLC purity 95.01%. UV (nm), λ_{max}/log ε: 244.2 / 3.59.^{1}H NMR (DMSO-d_6, 500 MHz) δ: 1.19 (t, 3H), 4.17 (q, 2H), 4.70 (s, 1H), 7.09 (t, 2H), 7.32 (t, 1H), 7.52 (d, J=8.5 Hz, 1H), 10.30 (t, 1H).

4-Hydroxy-2-oxo-1,2-dihydroquinoline-3-carboxylic acid (10).
The product was obtained according to the described procedure [26,27] as a white crystalline compound. Yield 25%. Mp 225 °C. HPLC purity 99.51%. UV (nm), λ_{max}/log ε: 250.1 / 3.52.

3-(4-Carboxyphenylcarbamoyl)-4-hydroxy-2-oxo-1,2-dihydroquinoline-6-carboxylic acid(11).
4-Aminobenzoic acid (0.7 g, 0.005 mol) was mixed with triethyl methanetricaroxylate (2.12 ml, 0.01 mol) and heated in microwave reactor at 50% of power during 15 min and 3 min at 90%. Temperature reached 231 °C during heating. Et_2O was added to the cooled mixture and the precipitate was washed with hot MeOH to obtain the pure product as a yellow crystalline compound. Yield 62%. Mp 340-350 °C. Anal. Calc. for $C_{18}H_{12}N_2O_7$ (368.29): C 58.7%, H 3.28%; found: C 58.09%, H 3.54%. HPLC purity 97.52%. UV (nm), λ_{max}/log ε: 251.3 / 3.53.^{1}H NMR (DMSO-d_6, 500 MHz) δ: 7.41 (d, J=8.5 Hz, 1H), 7.70 (d, J=9.1 Hz,

2H), 7.90 (d, *J*=9.1 Hz, 2H), 8.15 (d, *J*=8.5 Hz, 1H), 8.50 (s, 1H), 12.40 (s, 1H), 12.95 (s, 1H), 16 (s, 1H). IR [cm^{-1}]: 3645, 1780, 1705, 1640, 1594, 1547, 1471, 1115

3-Acetyl-4-hydroxyquinolin-2(1H)-one (12).
NaH (2.4 g, 0.06 mol) was added to anhydrous benzene (180 mL) and then ethyl acetylacetate (7.6 mL, 0.06 mol) was added dropwise. The mixture was stirred for 1 h at ambient temperature and 2-methyl-3,1-benzoxazin-4-one (3.2 g, 0.02 mol) was added and stirred overnight. Water (180 mL) and Et_2O (150 mL) was added to the resulted mixture and the product was isolated from inorganic layer as a white crystalline compound. Yield 78%. Mp 254-257 °C. Anal. Calc. for $C_{11}H_9NO_3$ (203.19): C 65.12%, H 4.52%; found: C 65.02%, H 4.46%. HPLC purity 99.03%. UV (nm), λ_{max}/log ε: 252.5 / 3.57.^{1}H NMR (DMSO-d_6, 500 MHz) δ: 2.12 (s, 3H, CH_3), 7.13 (t, 1H, Ar-H), 7.56 (t, 1H, Ar-H), 7.95 (d, *J*=7.17 Hz, 1H, Ar-H), 8.44 (d, *J*=8.34 Hz, 1H, Ar-H), 11.04 (s, 1H, NH), 13.58 (s, 1H, OH).

Lipophilicity HPLC determination (capacity factor k / calculated log k)
The HPLC separation module Waters Alliance 2695 XE and Waters Photodiode Array Detector 2996 (Waters Corp., Milford, MA, U.S.A.) were used. The chromatographic column Symmetry® C_{18} 5 μm, 4.6×250 mm, Part No. WAT054275, (Waters Corp., Milford, MA, U.S.A.) was used. The HPLC separation process was monitored by Millennium32® Chromatography Manager Software, Waters 2004 (Waters Corp., Milford, MA, U.S.A.). The mixture of MeOH p.a. (55.0%) and H_2O-HPLC – Mili-Q Grade (45.0%) was used as a mobile phase. The total flow of the column was 0.9 mL/min, injection 30 μl, column temperature 30 °C and sample temperature 10 °C. The detection wavelength 210 nm was chosen. The KI methanolic solution was used for the dead time (T_D) determination. Retention times (T_R) were measured in minutes.
The capacity factors *k* were calculated using the Millennium32® Chromatography Manager Software according to formula $k = (T_R - T_D) / T_D$, where T_R is the retention time of the solute, whereas T_D denotes the dead time obtained via an unretained analyte. Log *k*, calculated from the capacity factor *k*, is used as the lipophilicity index converted to log *P* scale. The log *k* values of the individual compounds are shown in Table 1.

Lipophilicity calculations
Log *P*, *i.e.* the logarithm of the partition coefficient for *n*-octanol/water, was calculated using the programs CS ChemOffice Ultra ver. 9.0 (CambridgeSoft, Cambridge, MA, U.S.A.) and ACD/LogP ver. 1.0 (Advanced Chemistry Development Inc., Toronto, Canada). Clog *P* values (the logarithm of *n*-octanol/water partition coefficient based on established chemical interactions) were generated by means of CS ChemOffice Ultra ver. 9.0 (CambridgeSoft, Cambridge, MA, U.S.A.) software. The results are shown in Table 1.

Study of inhibition of oxygen evolution rate (OER) in spinach chloroplasts
Chloroplasts were prepared from spinach (*Spinacia oleracea* L.) according to Masarovicova and Kralova [28]. The inhibition of photosynthetic electron transport (PET) in spinach chloroplasts was determined spectrophotometrically (Kontron Uvikon 800, Kontron, Muenchen, Germany) using an artificial electron acceptor 2,6-dichlorophenol-indophenol (DCIPP) according to Kralova et al. [29] and the rate of photosynthetic electron transport was monitored as a photoreduction of DCPIP. The measurements were carried out in phosphate buffer (0.02 mol/L, pH 7.2) containing sucrose (0.4 mol/L), $MgCl_2$ (0.005 mol/L) and NaCl (0.015 mol/L). The chlorophyll content was 30 mg/L in these experiments and the samples were irradiated (~100 W/m^2) from 10 cm distance with a halogen lamp (250 W) using a 4 cm

water filter to prevent warming of the samples (suspension temperature 22 °C). The studied compounds were dissolved in DMSO due to their limited water solubility. The applied DMSO concentration (up to 4%) did not affect the photochemical activity in spinach chloroplasts (PET). The inhibitory efficiency of the studied compounds has been expressed by IC_{50} values, *i.e.* by molar concentration of the compounds causing 50% decrease in the oxygen evolution relative to the untreated control. The comparable IC_{50} value for a selective herbicide 3-(3,4-dichlorophenyl)-1,1-dimethylurea, DCMU (Diurone®) was about 1.9 μmol/L [30]. The results are summarized in Table 1.

Acknowledgements. This study was supported by Polish Ministry of Science: N405 178735, by the Ministry of Education of the Czech Republic MSM 6215712403, and by the Slovak Scientific Grant Agency VEGA 1/0089/03.

REFERENCES

1. Reifler, M.J.; Szalai, V.A.; Peterson, C.N.; Brudvig, G.W. *J. Mol. Recognit.* **2001**, *14*, 157.
2. Moreland D.E. *Z. Naturforsch. C-A J. Biosci.* **1993**, *48*, 121.
3. Zakarya, D.; Larfaoui, E.M.; Boulaamail, A.; Tollabi, M.; Lakhlifi, T. *Chemosphere* **1998**, *36*, 2809.
4. Kralova, K.; Sersen, F.; Kubicova, L.; Waisser, K. *Chem. Pap.* 1999, *53*, 328.
5. Dolezal, M.; Miletin, M.; Kunes, J.; Kralova, K. *Molecules* **2002**, *7*, 363.
6. Roth, H.J.; Fenner, H. In *Arzneistoffe* 3rd ed.; Deutscher Apotheker Verlag: Stuttgart, **2000**; pp. 51-114.
7. Polanski, J.; Zouhiri, F.; Jeanson, L.; Desmaele, D.; d'Angelo, J.; Mouscadet, J.; Gieleciak, R.; Gasteiger, J.; Le Bret, M. *J. Med. Chem.* **2002**, *45*, 4647.
8. Polanski, J.; Niedbala, H.; Musiol, R.; Tabak, D.; Podeszwa, B.; Gieleciak, R.; Bak, A.; Palka, A.; Magdziarz, T. *Acta Poloniae Pharm. Drug Res.* **2004**, *61*, 3.
9. Polanski, J.; Niedbala, H.; Musiol, R.; Podeszwa, B.; Tabak, D.; Palka, A.; Mencel, A.; Finster, J.; Mouscadet, J.F.; Le Bret, M. *Lett. Drugs Des. Disc.* **2006**, 3, 175.
10. Polanski, J.; Niedbala, H.; Musiol, R.; Podeszwa, B.; Tabak, D.; Palka, A.; Mencel, A.; Mouscadet, J.F.; Le Bret, M. *Lett. Drugs Des. Disc.* **2007**, 4, 99.
11. Jampilek, J.; Dolezal, M.; Kunes, J.; Buchta, V. *ECSOC-8* **2004**, c005, http://www.lugo.usc.es/%7Eqoseijas/ECSOC-8/BOCNP/005/index.htm.
12. Jampilek, J.; Dolezal, M.; Kunes, J.; Buchta, V.; Kralova, K. *Med. Chem.* **2005**, *1*, 591.
13. Musiol, R.; Jampilek, J.; Buchta, V.; Niedbala, H.; Podeszwa, B.; Palka, A.; Majerz-Maniecka, K.; Oleksyn, B.; Polanski, J. *Bioorg. Med. Chem.* **2006**, *14*, 3592.
14. Musiol, R.; Jampilek, J.; Kralova, K.; Podeszwa, B.; Finster, J.; Niedbala, H.; Palka, A.; Polanski, J. *ECSOC-9* **2005**, c005, http://www.usc.es/congresos/ecsoc/9/BOCNP/c005/index.htm.
15. Musiol, R.; Jampilek, J.; Kralova, K.; Tabak, D.; Podeszwa, B.; Finster, J.; Polanski, J. *ECSOC-10* **2006**, c007, http://www.usc.es/congresos/ecsoc/10/ECSOC10.htm.
16. Musiol, R.; Jampilek, J.; Kralova, K.; Richardson, D.R.; Kalinowski, D.; Podeszwa, B.; Finster, J.; Niedbala, H.; Palka, A.; Polanski, J. *Bioorg. Med. Chem.* **2007**, *15*, 1280.
17. Musiol, R.; Jampilek, J.; Kralova, K.; Tabak, D.; Finster, J.; Podeszwa, B.; Kozik, V.; Dohnal, J.; Polanski, J. *ECSOC-11* **2007**, a011, http://www.usc.es/congresos/ecsoc/11/hall_aGOS/a011/index.htm.
18. Musiol, R.; Tabak, D.; Niedbala, H.; Podeszwa, B.; Jampilek, J.; Kralova, K.; Dohnal, J.; Finster, J.; Mencel, A.; Polanski, J. *Bioorg. Med. Chem.* **2008**, *16*, 4490.

19. Podeszwa, B.; Niedbala, H.; Polanski, J.; Musiol, R.; Tabak, D.; Finster, J.; Serafin, K.; Wietrzyk, J.; Boryczka, S.; Mol, W.; Jampilek, J.; Dohnal, J.; Kalinowski, D.; Richardson, D.R. *Bioorg. Med. Chem. Lett.* **2007**, 17, 6138.
20. Dolezal, M.; Jampilek, J.; Osicka, Z.; Kunes, J.; Buchta, V.; Vichova, P. *Farmaco* **2003**, *58*, 1105.
21. Collins, J.F.; Donnelly, W.J.; Grundon, M.F.; James, K.J. *J. Chem. Soc., Perkin Trans. 1*, **1974**, 2177.
22. Buckle, D.R.; Cantello, B.C.C.; Smith, H.; Spicer, B.A. *J. Med. Chem.* **1975**, *18*, 726.
23. Ziegler, E.; Wolf, R.; Kappe, T. *Monatsh. Chem.* **1965**, *96*, 418.
24. Dolle, V.; Fan, E.; Nguyen, C.H.; Aubertin, A.M.; Kirn, A.; Andreola, M.L.; Jamieson, G.; Tarrago-Litvak, L.; Bisagni, E *J. Med. Chem.* **1995**, *38*, 4679.
25. Ukrainets, I.V.; Taran, S.G.; Sidorenko, L.V.; Gorokhova, O.V.; Ogirenko, A.A.; Turov, A.V.; Filimonova, N.I. *Chem. Heterocycl.Compd.* **1996**, *32*, 960.
26. Ukrainets, I.V.; Gorokhova, O.V.; Sidorenko, L.V. *Chem. Heterocycl. Compd.* **2005**, *41*, 1019.
27. Detsi, A.; Bardakos, V.; Markopoulos, J.; Igglessi-Markopoulou, O. *J. Chem. Soc., Perkin Trans. 1* **1996**, *24*, 2909.
28. Masarovicova, E.; Kralova, K. *Approaches to measuring plant photosynthesis activity.* In *Handbook of Photosynthesis* 2nd ed.; M. Pessarakli (Ed.), Taylor & Francis Group, Boca Raton: London-New York-Singapore, **2005**; pp. 617-656.
29. Kralova, K.; Sersen, F.; Sidoova, E. *Chem. Pap.* **1992**, *46*, 348.
30. Fedke, C. *Biochemistry and Physiology of Herbicide Action*; Springer Verlag: Berlin-Heidelberg-New York, **1982**.